THE GEOCHEMISTRY OF FLUID PROCESSES
IN THE EASTERN BRANCH OF
THE EAST AFRICAN RIFT SYSTEM

illiam

W. GEORGE DARLING

A thesis submitted in fulfilment of the
requirements of the Open University
for the degree of Doctor of Philosophy

February 1996

British Geological Survey

ABSTRACT

The East African Rift System is the world's major continental rift. While much geophysical and petrological attention has been paid to it, at least in the eastern branch ("Eastern Rift"), comparatively little research has been carried out into the geochemistry of rift fluids, despite the potential benefits to theoretical and practical studies. Hydrothermal activity provides the opportunity to sample a very wide range of waters and gases in the Eastern Rift. This thesis combines data from the literature with the results of the author's major investigation into Eastern Rift fluids carried out chiefly in Kenya, though with subsidiary investigations in Ethiopia and Djibouti. A synthetic approach has been adopted, whereby relationships and interactions are cross-referenced as far as possible to illuminate problems, thus demonstrating the usefulness of considering a wide range of fluids in the rift context.

After reviews of physiography, geology, geothermics and hydrology of the Eastern Rift, the following topics are considered in detail: (i) chemical and isotopic evidence for water origin, movement and evolution, (ii) chemical and isotopic evidence for gas origin, movement and evolution, and (iii) fluid geothermometry.

Within this context some specific aims have been pursued. The strong possibility of long-distance axial flows of groundwater has been shown by use of stable isotopic techniques. Further insights into alkaline hydrological discharge areas have been obtained by a combination of chemical and isotopic approaches. While carbon isotope ratios indicate an apparently homogeneous source of carbon dioxide, the existence of distinct mantle sources for volcanic rocks beneath different parts of the Eastern Rift has been comprehensively demonstrated by use of helium isotope ratios. Following the rather unsatisfactory performance of various gas geothermometers for evaluating geothermal system temperatures, a new relationship based on hydrocarbon breakdown has been developed. The possible use of oxygen isotopes in hydrothermal sinters as indicators of palaeoconditions has been investigated.

In conclusion, topics worthy of further research in the Eastern Rift are suggested where the study of fluids would be of benefit.

ACKNOWLEDGMENTS

CONTENTS

TABLES

FIGURES

CHAPTER 1

INTRODUCTION

This thesis is concerned with a comprehensive study of how the waters and gases in the crustal rocks of an important rift area originate and interact. The broadly geochemical approach adopted for this study includes the use of isotopic techniques, which are vital for a better understanding of the different parts of the hydrological and geochemical cycles of the East African rifts. The thesis is intended to be an investigation of fluids as a whole rather than a treatise on rift hydrogeology or geothermal energy, but inevitably contains data and arrives at conclusions which are applicable to both these and other subject areas.

1.1   Background

1.1.1   The East African Rift System

The East African Rift System (EARS) is a concatenation of rift zones with a total length on land of some 4000 km, making it by far the largest terrestrial rift system. The EARS is comprised of eastern and western branches, whose only apparent link is in the southern Tanzania-Malawi area (Fig 1.1). The style of these branches is quite different. For example, the eastern branch exhibits major hydrothermal activity, unlike the western branch which has much less of the volcanicity or extension that promotes such activity. Since it is the existence of this hydrothermalism which provides access to the deeper fluids of the EARS, this thesis is concerned with the eastern branch plus the related active rift in Djibouti.

Over much of its length, the eastern branch of the EARS forms a reasonably well-defined rift valley ("Eastern Rift") with fairly evenly-spaced late Quaternary volcanic centres along the axial line in between the numerous lakes occupying the floor (Fig 1.2). In the north, however, the Main Ethiopian Rift opens out into the Afar Triangle, a triple plate junction from which the active Djibouti rift heads off to the east. In the south, the Eastern Rift splays out in central Tanzania to form "riftlets" which die out within a relatively short distance.

The Eastern Rift consists of a series of separate, more-or-less aligned rift zones, the biggest offset occurring between the northernmost of the Kenya rifts and the Main Ethiopian Rift, coinciding roughly with the Kenya-Ethiopia border (Fig 1.2). For the purposes of this study,
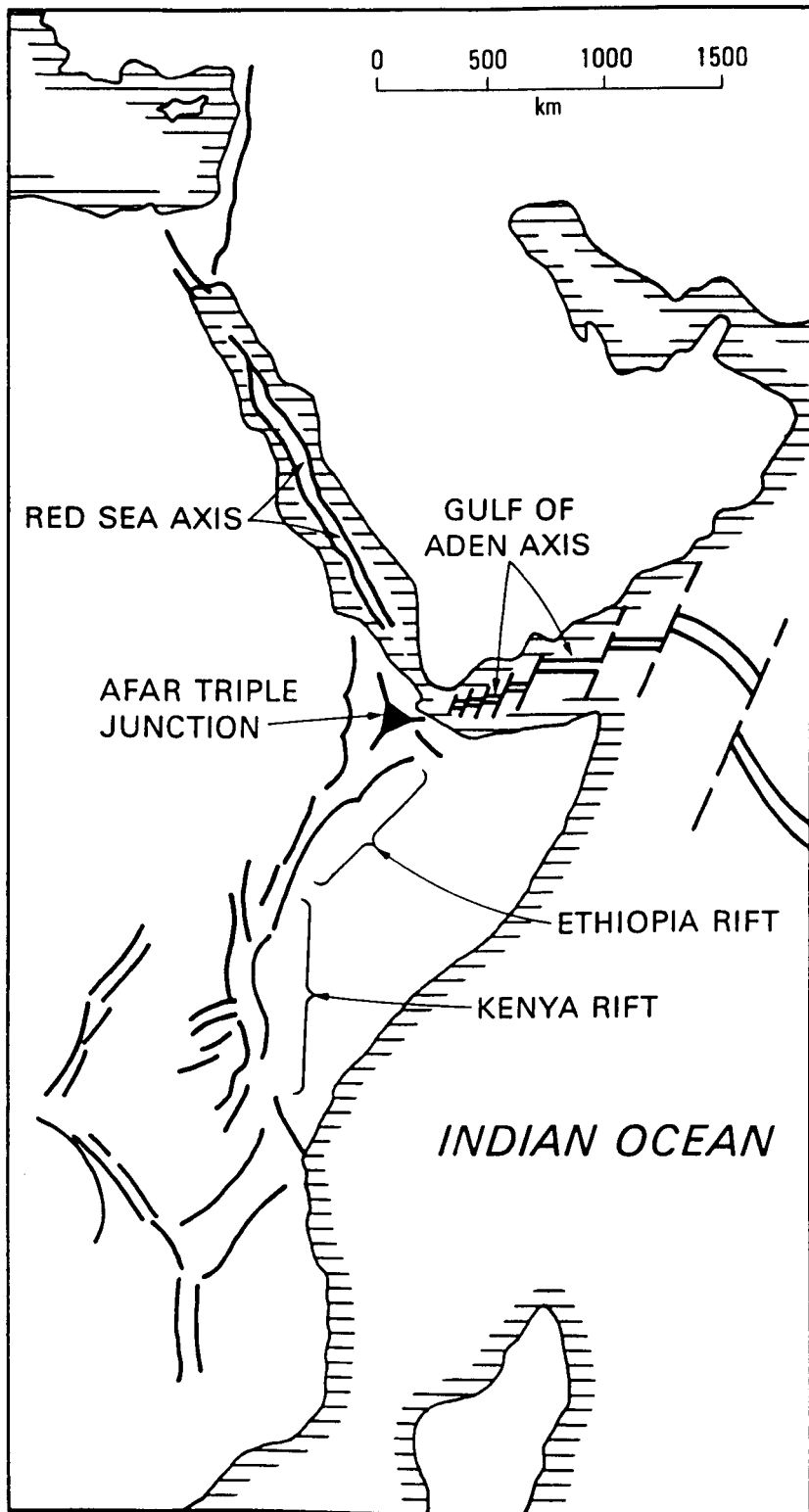
Fig 1.1   **The East African Rift System.**

three main areas are identified: the Kenya Rift Valleys (KRV), the Main Ethiopian Rift (MER), and southern Afar.

1.1.2   Previous studies

Previous studies of fluids in the Eastern Rift can be split into those concerned with water and those with geothermal resources. In practice, any consideration of the latter usually has to involve the former to some extent since water is the "working fluid" of hydrothermal systems. Few water resource studies have been carried out within the Eastern Rift because (certainly until recent years) resources of basically potable water have been adequate, particularly in the relatively wet MER. One of the few areas of concern has been Lake Naivasha in Kenya, principally because of the irrigation activity accompanying colonial and post-colonial agricultural development in the area. Research into the water balance of Naivasha commenced in the 1930s (Sikes, 1935) but was little followed up until the limnological studies of Ase et al (1986), except for a geothermally-directed assessment of the lake and neighbouring catchments in the southern Kenya Rift by McCann (1974). Further north in the KRV, WRAP (1987) worked on the resources of the Lake Baringo area. In the MER, hydrogeological surveying and mapping were carried out by the Ethiopian Institute of Geological Surveys (Chernet, 1988), while in Djibouti water resource studies were summarised by Verhagen et al (1991).

From a geothermal resource point of view, although minor use of thermal manifestations by the indigenous populations for washing, bathing, crop drying and (via condensation of steam) drinking water had been made for many years, intensive studies only began when the potential for electricity generation was recognised. This led to initial concentration of effort on areas judged to be most economically promising from a combination of amount of surface activity and proximity to areas of energy usage. The detailed investigation of the geothermal chemistry of waters and gases began with the work of Glover (1972, 1976) in Kenya and Ethiopia for the United Nations Development Programme (UNDP). Later, fluid samples were collected and measured during exploration in the Eastern Rift and Djibouti by the authorities and utilities of the countries concerned, variously aided by the Bureau de Recherches de Geologie et Minieres (BRGM, 1983), United Nations Development Programme (Armannsson, 1987), Geotermica Italiana Srl (1987a,b) and the British Geological Survey (Allen et al, 1989; Allen and Darling, 1992). An important but not specifically geothermal study of fluids in the MER and Afar was carried out by Craig et al (1977) for the UNDP. Appendix 1 lists the areas of the Eastern Rift in which the various teams have worked and gives details of the relevant work carried out.
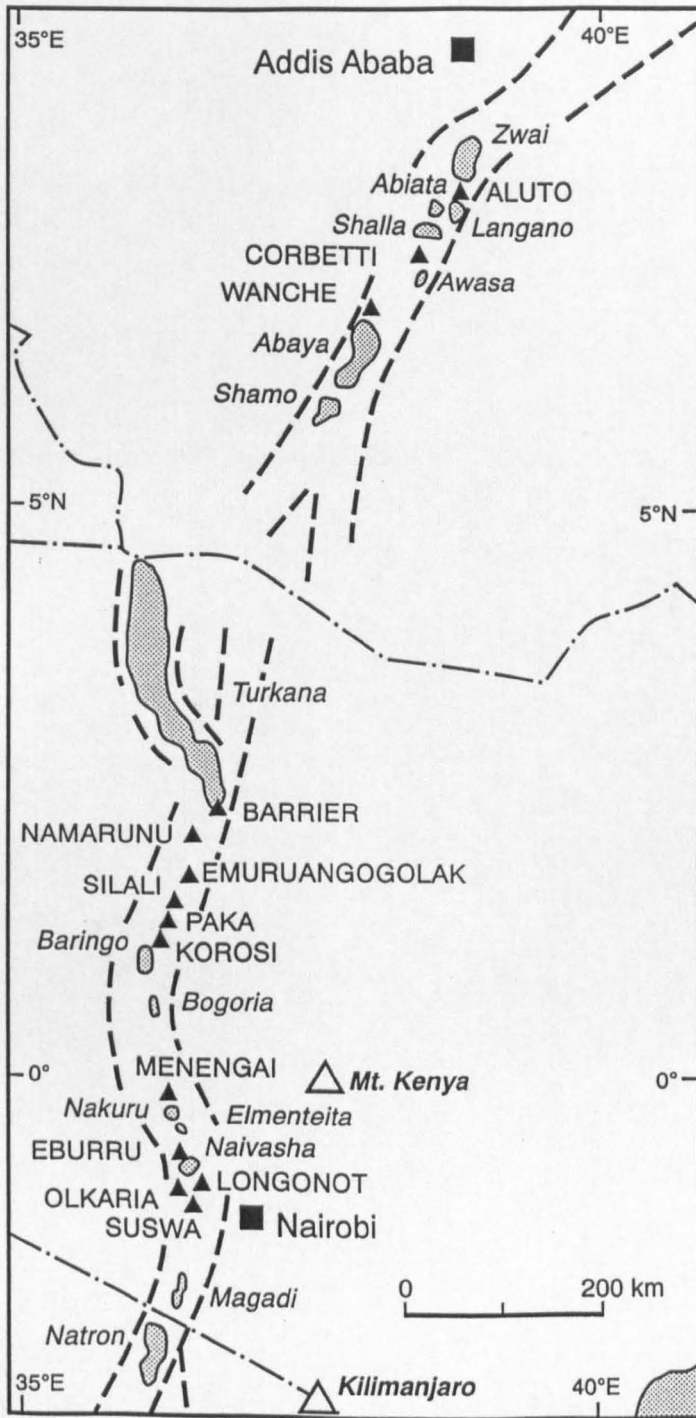
Fig 1.2 The rift valleys of Ethiopia and Kenya, showing the positions of lakes (names in italics) and late-Quaternary volcanic centres (names in upper case).

While two relatively deep wells were drilled on the Olkaria prospect (S Kenya) in the 1950s, methodical exploration in the Eastern Rift really began in the early 1970s. Large-scale drilling of deep geothermal wells commenced at Olkaria in 1973, followed by Asal (Djibouti) in 1974, Aluto-Langano (Ethiopia) in 1981, Hanle (Djibouti) in 1987, Eburru (Kenya) in 1989 and most recently at Tendaho (Ethiopia) in 1994. Fig 1.3 shows the location of the major fields. While not all these deep wells have been economically successful, there is in each drilled area some information about subsurface conditions, often including geochemical data. Away from these areas, all geothermal information has had to be gleaned from surface manifestations such as hot springs and fumaroles (steam jets).

Despite all the effort focused on geothermal exploration, rather few studies have been published in the open literature, and those that have are primarily concerned with resource assessment rather than fluid geochemistry.

1.2   The Present Study

1.2.1   Scope and aims of this work

While a considerable amount of geophysical and petrological information and overview is available for the Eastern Rift (particularly in the KRV), there has been a notable lack of data and interpretation for rift fluids, even though they are of considerable scientific and practical interest. This study has provided the opportunity to attempt such an overview of crustal fluids for a sizeable part of this geologically important area of the African continent.

The broad aim of the present work is to identify and characterise the nature of fluid sources and fluxes within the crustal rocks of the Eastern Rift, and to understand how they may interact, using geochemical (including isotopic) methods to achieve this goal. The results of such an understanding should be of considerable relevance in the context of hydrogeology, geothermal resources and rift structure. To quote from Olsen and Morgan (1995):

> Several economically important resources are often generated as a direct consequence of both thermal and structural processes of rift evolution. Some resources are formed within rifts, whereas others are created in earlier geological environments and are only later exposed or transported to the near-surface as a consequence of rifting. Largely thermally-associated resources include geothermal energy and mineral deposits of hydrothermal/magmatic origin, such as molybdenum, some hydrothermal copper, and magmatic copper-nickel deposits. Sedimentary rift basins provide near-ideal habitats (reservoirs) for hydrocarbon resources, and extensive evaporite deposits are characteristically found in basins associated with the late stages of rifting just prior to continental splitting (e.g., Afar). Increasingly groundwater is becoming

a critical resource, especially for developing large urban population centres. Rifts can affect or even control regional hydrology in very significant ways.

While not all of the foregoing is applicable to the EARS, clearly a review of rift fluids for this area is timely. To some extent this has required a synthesis of existing data from other sources, but original geochemical investigations form an important part of this thesis, particularly in the northern KRV where no studies of this kind had previously been carried out. The broadly synthetic approach of this work incorporates more specific aims, including the following:

Groundwater flow - How does groundwater move in the rift environment? Where does recharge originate, and what is the relationship between ground and surface waters?

Groundwater chemistry - How do the high bicarbonate waters of the Eastern Rift evolve? Why, for example, does the extreme case of Lake Magadi (southern KRV) differ from the rather similar area of the Suguta Valley (northern KRV)?

Palaeohydrology - Do geochemical techniques have the potential to reveal anything about hydrological conditions earlier in the Quaternary?

Outgassing - What is the origin of the carbon dioxide outgassed from the Eastern Rift? What can trace gases such as helium reveal about rift structure and the nature of the underlying mantle in different parts of the rift system?

Geothermal applications - What is the source of water for geothermal systems? How is geothermometry (the assessment of subsurface temperatures) affected by the distinctive chemistry of rift waters? Can gas geothermometry provide reasonably reliable temperature information and, if not, could isotopic methods be used for corrective purposes?

1.2.2   Fieldwork

The work described in this thesis is largely based on geothermal investigations in the Eastern Rift, supported by the British Overseas Development Administration and conducted mainly in Kenya, with subsidiary work in Ethiopia and Djibouti. Virtually all important geothermal manifestations in the Kenya rifts were visited and fluids sampled. In northern Kenya, fieldwork was partially carried out by helicopter; without this support a comprehensive investigation
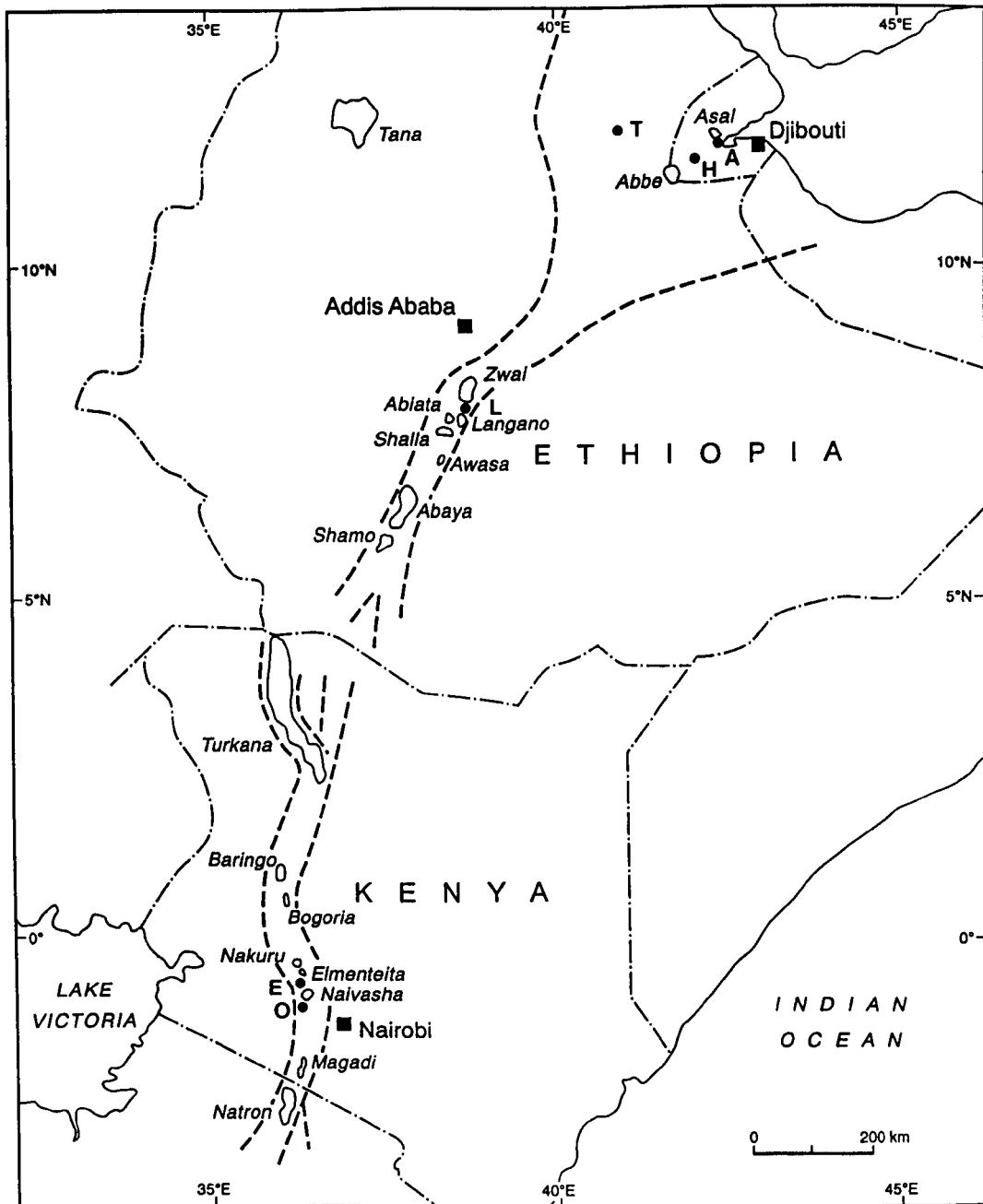
Fig 1.3 Location of areas in the Eastern Rift where geothermal exploration wells have been drilled. A - Asal, E - Eburru, H - Hanle, L - Aluto-Langano, O - Olkaria, T -Tendaho.

investigation would have been impracticable. In Ethiopia, representative sites in the MER were sampled between Lake Abaya in the south and the Awash National Park in the North. This latter area is generally taken to be the point at which the MER broadens to become Afar. Minor sampling was carried out in Djibouti between the Asal geothermal field and Lake Abbe. Apart from the Ministry of Energy in Kenya, three other governmental organisations assisted with logistical support: the Kenya Power and Light Company Ltd, the Ministry of Mines and Energy in Ethiopia, and the Institut Superieur d'Etudes et de Recherches Scientifiques (ISERST) of Djibouti.

1.2.3   Laboratory work

Most of the original chemical and isotopic data considered here were measured in the laboratories of the British Geological Survey Hydrogeology Group at Wallingford, Oxfordshire. Gas analyses (except those of noble gases) were carried out by the author, while stable isotopic measurements on waters and gases were made by the author or under his supervision. Hydrochemical analyses were performed by and under the supervision of the author's colleagues in the Hydrogeology Group.

Specialist gas and isotopic measurements were carried out at a variety of other institutions, on a collaborative basis unless otherwise indicated. Silica oxygen isotope ratios were measured at the Natural Environment Research Council's Isotope Geoscience Laboratory at Keyworth, Nottingham. Noble gas concentration and argon isotope analyses were performed at the University of Bath. Helium isotope ratios were measured at Cambridge University and the GSF Institute for Radiohydrometry, Munich. Radiocarbon was analysed via an allocation at the NERC Radiocarbon Laboratory, East Kilbride, Scotland. Tritium analyses were purchased from the DSIR Institute of Nuclear Sciences, New Zealand.

CHAPTER 2

PHYSIOGRAPHY AND GEOLOGY

The basic geology and physiography of the three main regions under consideration, the Kenya rifts, MER and Southern Afar, varies considerably from area to area. In Kenya, the position of the rifts, and to some extent their structure and volcanology, seem to be governed by variations in the underlying Precambrian basement. In the MER, such a relationship is much less apparent, probably because the nature of updoming in the two areas is very different. In southern Afar, the geology and physiography vary across the region from MER-like in the southwest to an apparently active rift in the southeast, the Asal Rift. In the KRV and MER rifting commenced in the Tertiary and was largely completed before the Quaternary, although the continuation of volcanism in parts of the rifts into historic times implies that the rifting is not yet completely over.

2.1   The Kenya Rifts

2.1.1   Background

The nomenclature adopted here for the Kenya rifts is that of Rosendahl (1987), who distinguishes between major *rift zones* and minor *rift units*. Rift zones tend to be built of rift units, but unlike the zones, the units are not generally given specific names unless found in relative isolation. Thus, Fig 2.1 shows the Gregory and Turkana rift zones, plus the Nyanza rift unit (referred to as Kavirondo Rift in some of the older geological literature). The Turkana rift zone is conveniently divided into northern and southern parts, the boundary approximately coinciding with the southern tip of Lake Turkana.

The Kenya rift valleys (KRV) are superimposed on (and indeed are probably partly caused by) an updoming presumably resulting from a convecting plume in the underlying mantle. The Gregory and Turkana rifts are by-and-large at their most "rift-like" in terms of physiography towards the centre of the dome, tending to spread out much more towards the north or south. There is a water divide in the Lake Naivasha area of the Gregory rift, though due to the general lack of surface watercourses this is not a particularly obvious feature.

Legend:
- >3000 metres
- 2000 - 3000 m
- 1000 - 2000 m
- 0 -1000 m

NORTH TURKANA RIFT ZONE

SOUTH TURKANA RIFT ZONE

GREGORY RIFT ZONE

NYANZA RIFT UNIT

Turkwel

Kerio

Suguta

Ewasongiro

0   200 km
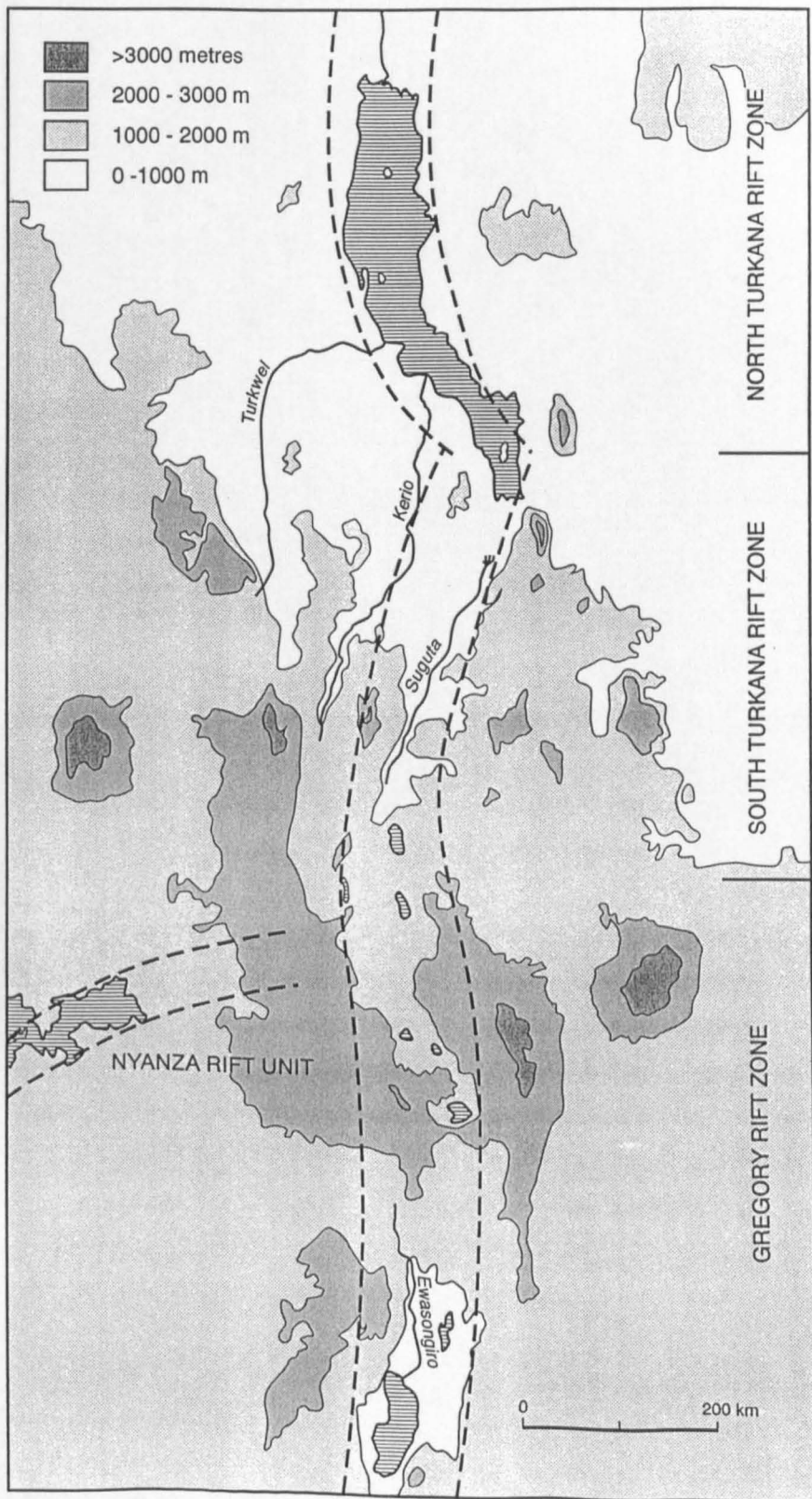
Fig 2.1   General physiography of the Kenya rift valleys.

2.1.2 Physiography

At present, the dome typically reaches an elevation of 3000 metres above sea level (asl) on the rift flanks, though locally up to 4000 m asl in the Nyandarua (Aberdare) Mountains to the immediate east of the Gregory rift. The rift floor reaches an elevation of about 2000 m in the Naivasha area, descending to 600 m in the Lake Magadi area to the south, and 300 m at Lake Turkana. The inner trough areas of the rift zones vary considerably in width, depending at least partly on where their boundaries are drawn, which in the case of multi-stepping escarpments is not always obvious. For example, while the inner trough is ~70 km wide at the latitude of Bogoria, it narrows to a mere 7 km at the northern end of the South Turkana rift, and then in the North Turkana zone splays out into a complex of faulted and tilted blocks ~250 km wide (Dunkley et al, 1993). Despite any surface indications to the contrary, the rift zones are not usually classic graben structures. Rather, they consist mainly of half-graben units, generally about 50 km in length and tilted down to the west (e.g. Rosendahl, 1987). Each half-graben tends to have its own late-Quaternary central volcano, and these are interspersed with relatively small lakes, except for Turkana which is the largest lake in the Eastern Rift. The volcanoes are presently dormant, though some have been active within historic times (Dunkley et al, 1993) and all have some fumarolic activity. On the other hand, high enthalpy hot-spring activity is very rare.

The Nyanza Rift slopes down in a roughly westerly direction towards and into Lake Victoria. The present sub-aerial length of the rift is some 130 km, while its width ranges from 25 km in the east to 50 km in the west (Pickford, 1982). The Nyanza unit has been viewed as the third arm of a tri-radial cracking pattern caused by updoming (eg Geotermica Italiana 1987), but there is little real evidence that this is so, since the Nyanza Rift fails by some way to join up with the Gregory rift (Fig 2.1). The notion that the adjacent Menengai area represents some kind of culmination of the updoming process is examined in more detail in 7.4.3 below.

2.1.3 General geology

The broadly sinusoidal shapes on a map of the Gregory and Turkana rift zones, together with their structure and volcanism, are primarily related to the underlying basement geology (summarised by Smith and Mosley, 1993, and Smith 1994). The more central parts of the rift zones (in terms of the updoming) are controlled by the suture between the low-grade metamorphic Archaeozoic Tanzanian cratonic block to the west and the younger, more highly-metamorphosed Proterozoic Mozambique mobile belt to the east. A shift from nephelinitic-

carbonatitic volcanism in the west to phonolitic volcanism in the centre and east has been identified (Fig 2.2). When the rift leaves the suture line and passes over one or other of the metamorphic terrains, it tends to splay out into "riftlets" as in Tanzania and the Turkana area.

Magmatism (presumably resulting from mantle plume impingement) predated rifting by some 10 Ma, and therefore rifting was a response to thermal stress in an area already subject to forces of shear which were otherwise too weak to cause rifting by themselves (Henry et al, 1990; Green et al, 1991). Since rifting started in the north at around 35 Ma and propagated to the south (e.g. Macdonald et al, 1994), more crustal thinning would be expected in the north; geophysical investigations indicate very thin crust (for a continental setting) around 20 km thick in the Turkana area extending to 35 km in the Naivasha area near the culmination of the dome, with an abrupt increase in thickness at the rift shoulders. However, while crustal thickness beneath the rifts varies in a predictable way with the estimated amount of extension, its geometry does not reflect the presently-known magmatic history in any simple way (Keller et al, 1994).

The volcanic rocks of the N-S Kenya rifts consist of an early (Oligocene) basaltic phase, followed by flood phonolites, largely in the Miocene, which in turn were succeeded by the various products of "central" eruptive centres, including trachytes, comendites and basalts, with large-scale ignimbritic deposits in addition to lavas and pumices etc. The ignimbrite events extended into the Pleistocene, and may in some cases be associated with the creation of the caldera structures which form a prominent feature of many of the most recent volcanoes. Other eruptive activity at these volcanoes has extended into the Holocene; this may have obscured evidence of possible early hydrothermal activity, but from the mid Pleistocene onwards, evidence in the form of hydrothermal sinters is preserved (Chapter 5).

Sediments have accumulated in the half-graben structures, and generally consist largely of volcaniclastics, with subsidiary lake sediments including muds, evaporites and diatomites. They nevertheless are likely to have a more important effect on fluid chemistry than the volcaniclastics.

The Nyanza Rift is a true graben for half its length, and its orientation is governed by the NE-SW fabric of the Nyanzian shield. Although once considered to have joined the Gregory Rift before being bridged at its eastern end by the Tinderet volcano, it is now known that this volcanic activity predates the main Pliocene fault activity and that the two rifts were never joined (Pickford, 1982). In the Nyanza Rift, voluminous Miocene phonolites were followed

	Trachytes, rhyolites & ignimbrites of caldera volcanoes (late Quaternary)
	Basalts (Quaternary)
	Trachytes, rhyolites & ignimbrites (Pliocene - Pleistocene)
	Phonolites (U. Miocene)
	Basalts (Eocene - Pliocene)
	Nephelinite - phonolite volcanoes (Miocene - Holocene)
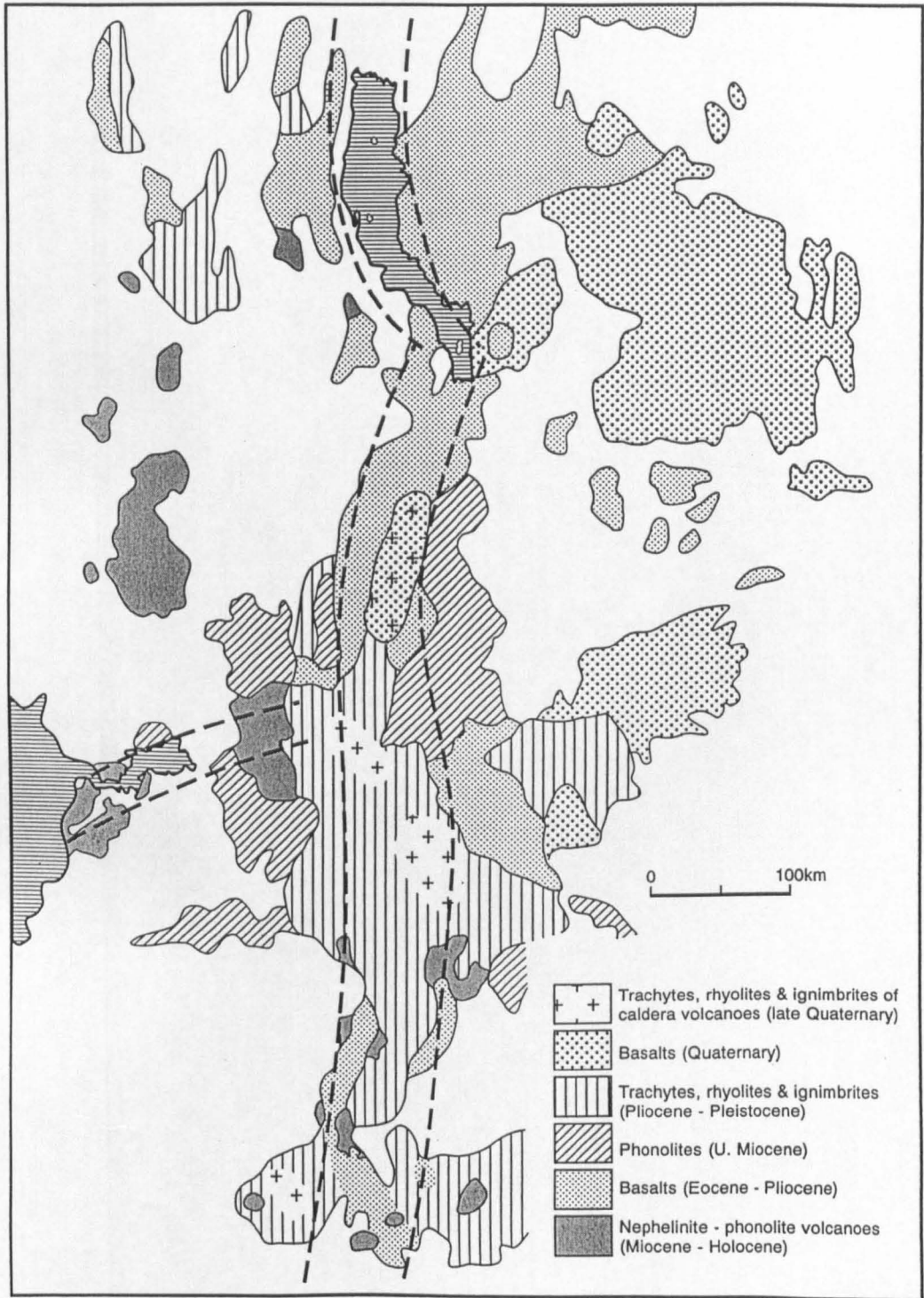
Fig 2.2   Volcanic geology of the Kenya rift valleys.

by Pliocene carbonatitic activity, with sediments accumulating from the beginning of the volcanic activity into Quaternary times. Though predominantly siliceous in nature, as there has been little lacustrine sedimentation, some of these sediments contain large amounts of carbonate material where the erosion of carbonatites has taken place. In the Nyanza Rift there is hot-spring activity in the roots of the eroded Homa Mountain carbonatite/ijolite complex (Clarke and Roberts, 1986).

2.2   The Main Ethiopian Rift

2.2.1   Background

The MER (Fig 2.3) has no obvious connection with the KRV. The Northern Turkana rift deflects to the west as it proceeds north and is responsible for the offset demonstrated by Lake Turkana. The Omo Valley rift may represent its prolongation into Ethiopia. A case could possibly be made for a rift trending northeastwards from the southern end of Lake Turkana to Lake Chew Bahir (Stephanie) in Ethiopia, though such a rift would have to be a comparatively old structure, now largely concealed by late-Tertiary lavas in the Marsabit area. The rifting in the Chew Bahir area itself is just part of the splaying effect seen at the southern end of the MER in a way analogous to the KRV. Unlike the Kenya rifts, however, the northern end of the MER is not splayed because it is terminated by the Afar triple plate junction area where a different set of conditions operates.

Like the KRV, the MER is set within a domal structure and presumably formed in a similar way, whereby a relatively weak regional shear force was assisted by thermal stress from the updoming. The Ethiopian dome, however, is considerably larger than the Kenyan dome and appears to be the result of the action of a large "hotspot"-type plume originating in the lower mantle. The thick, mid-Tertiary basalt plateau approximately bisected by the MER testifies to the size of this mantle plume; a volume in excess of 350,000 km^3 has been estimated (e.g. Davies et al, 1994). Four distinct stages of volcanism have occurred from 50 Ma ago, with uplift commencing after the earliest magmatism. Significant crustal extension occurred only in the final phase at 20-15 Ma ago. As in Kenya, therefore, volcanism did not result from lithospheric extension, but instead helped it to take place, albeit at a rather earlier date.

2.2.2   Physiography

The MER lies between latitudes 5 and 9° N and longitudes 37.5 to 40° E, and has been divided

14
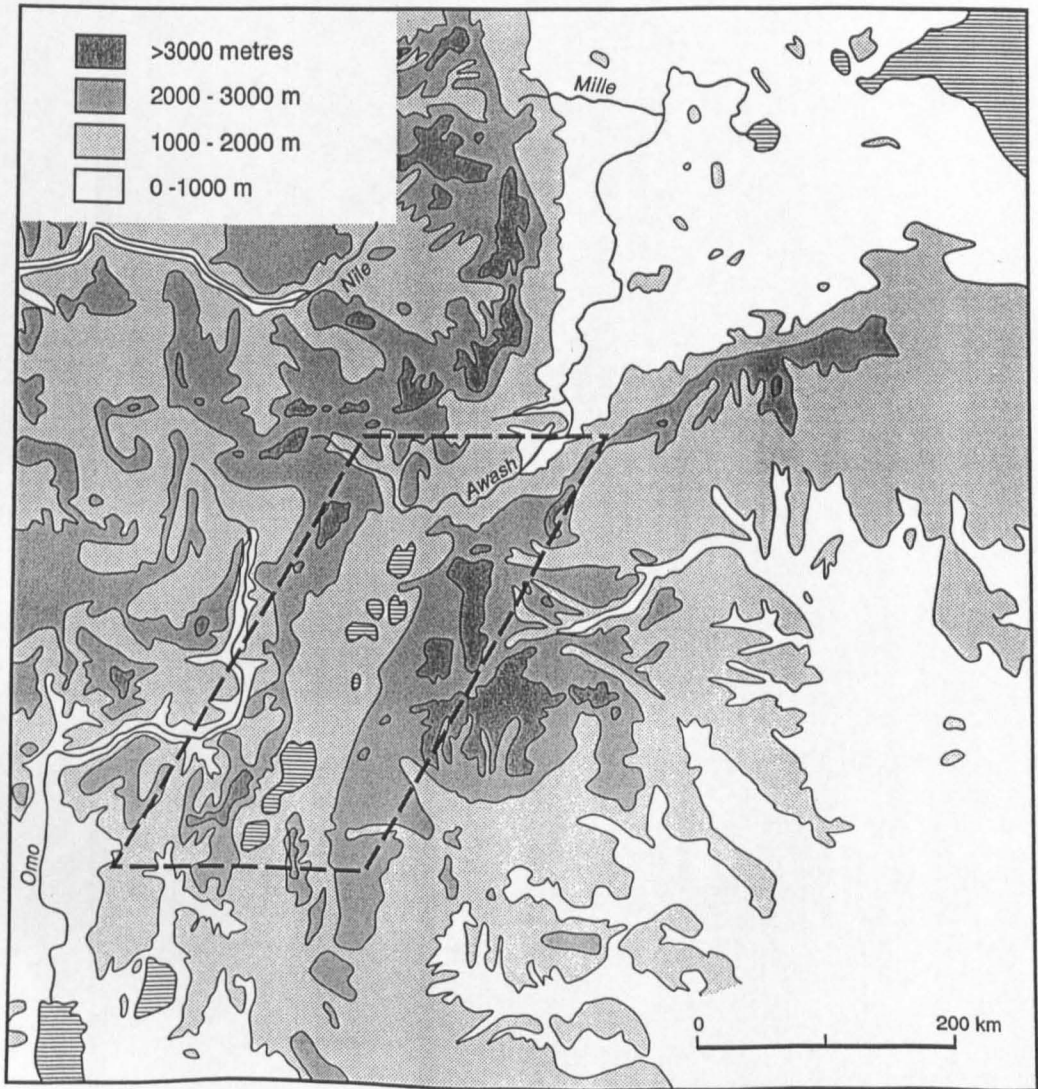
Fig 2.3   General physiography of the Main Ethiopian Rift (within the dashed lines) and the Somalian and southern Ethiopian plateaux to the east and west respectively. Southern Afar opens out to the north of the MER.

into northern, central and southern sectors, largely on physiographic grounds (Woldegabriel et al, 1990). The central sector is a classic graben rift structure, while the southern sector is where the MER becomes less well-defined and starts splaying out. The northern sector covers the zone where the MER turns from a generally NNE to a ENE trend, widening as it does so and merging into Afar.

From the southern sector, the rift floor rises steadily from an altitude of around 1200 m asl towards the northern end of the central sector at about 1700 m (Mohr, 1967). This is comparable to, but slightly lower than, the maximum elevation of the Gregory Rift floor in Kenya. Unlike the Gregory Rift, there is no counterpart to Lake Naivasha at the culmination of the MER; to the south lies the internal drainage basin occupied by Lakes Zwai, Langano and Abiata, while to the north the River Awash drains the catchment, ultimately to another closed basin in Afar. The MER becomes broader and rather less well-defined at the latitude of Addis Ababa, at least partly due to pre-Quaternary volcano-tectonic lineations, and the elevation of its floor declines steadily to the north, from 1350 m down to only 250 m in southern Afar.

In the more central parts of the MER, the rift flanks rise generally to around 2500 m asl, but locally reach around 3000 m where Pliocene volcanic edifices such as Guraghe are situated near the rift wall (Fig 2.3). Towards the northern and southern ends, the absolute altitudes fall, but similar heights above the rift floor tend to be maintained. In the south, the inner trough of the MER is around 75 km wide, narrowing to nearer 50 km in the central sector. In the north the rift widens to become southern Afar; at the latitude of the Fantale volcano (considered fairly arbitrarily to be the start of Afar) its width is approximately 100 km.

Like the KRV, the MER has a series of late-Quaternary central volcanoes interspersed by lakes (Fig 1.2). With the exception of Lake Turkana, itself fed largely from the Ethiopian plateau, the lakes of the MER are larger than their Kenyan counterparts because of the generally higher rainfall in Ethiopia. The central volcanoes are generally dissimilar to those of Kenya as relatively few have well-preserved calderas, and some of the calderas are much larger than those in Kenya. However, they tend to be in the same dormant phase with similar amounts of fumarolic activity. Presumably because of higher rainfall, high-enthalpy hot-spring activity is more common in the MER than in Kenya, but still rare when compared with many other geothermal areas of the world.

2.2.3 General geology

There is less evidence than for the KRV that the location of the MER is controlled by basement relationships, but Wolde (1989) postulated that the MER opened along a Precambrian plate margin. Comparisons drawn between Kenya and Ethiopia by Baker et al (1972) reveal that the superficial resemblances between the rifts in the two countries do not reflect a similar volcanology (Figs 2.2 and 2.4). There is, for example, no evidence for carbonatitic volcanism in the MER (though admittedly there is little or none in the main Kenya rifts either). More importantly, there is no Ethiopian equivalent of the flood phonolites of Kenya. Against this, basalts are more common in the Tertiary of the MER, and ignimbrites are more abundant in the Plio-Pleistocene. Also, trachytes and rhyolites are more abundant in the Quaternary of the MER.

Structurally, the MER appears to be more evolved than the KRV. By the late Oligocene - early Miocene, the MER had reached the state of a series of alternating half-grabens much like the present-day Kenya rifts. By late Miocene - early Pliocene times these half-grabens had been replaced by more symmetrical full graben structures (Woldegabriel et al, 1990). Present crustal thicknesses beneath the central MER are at around 50 km somewhat greater than for the Gregory Rift.

Most recent volcanic activity in the MER has occurred north of Lake Abaya (the largest Ethiopian rift valley lake in area), mostly in the central-to-eastern side of the floor in the Wonji Fault Belt (WFB) defined by Mohr (1963). Towards the northern sector the WFB bifurcates into two sub-parallel trends well defined by lines of scoria cones and a few major volcanic edifices such as Zuquala, Boseti Gudda, Kone and Fantale (Meyer et al, 1975).

As in the KRV, the extension of lakes under past pluvial episodes has given rise to areas of sediment cover on the floor of the MER. Although not usually thick, these sediments are quite extensive and consist of cemented volcaniclastics, silts, clays and diatomites, which have probably been laid down from the Pliocene onwards, judging by their relationships with volcanic deposits. In the floodplain of the River Awash alluvium has been deposited.
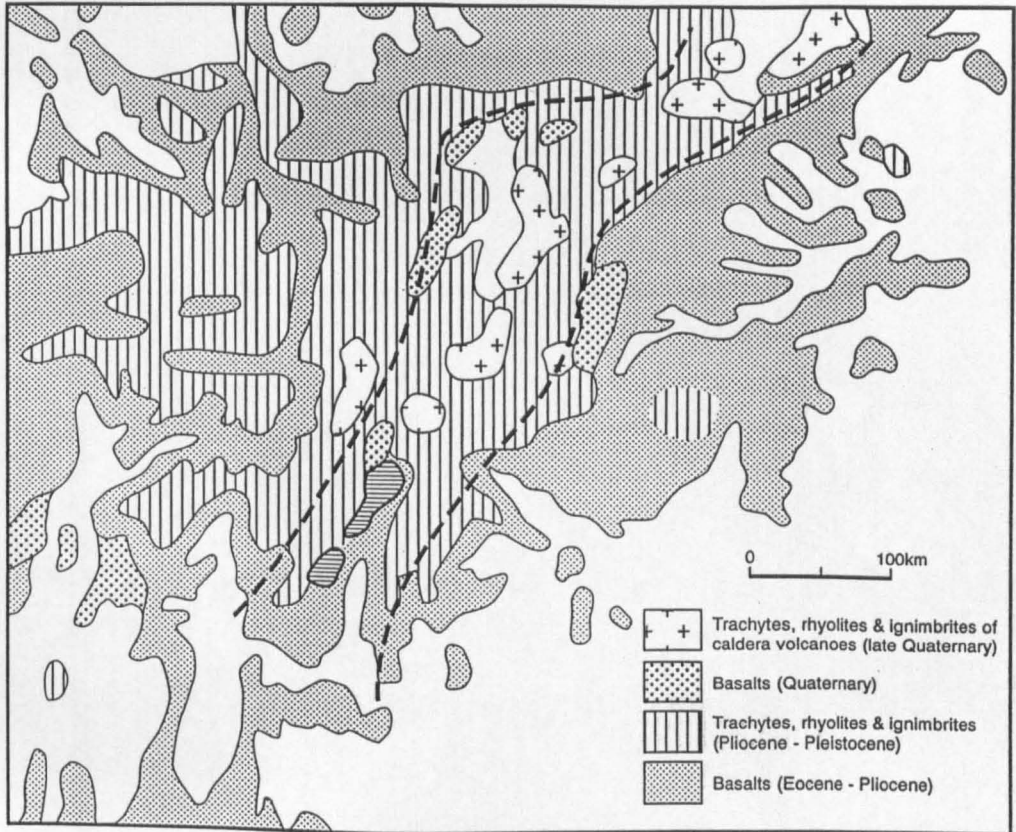
Fig 2.4   **Volcanic geology of the Main Ethiopian Rift, with rift boundaries shown.**

The legend reads:

- Trachytes, rhyolites & ignimbrites of caldera volcanoes (late Quaternary)
- Basalts (Quaternary)
- Trachytes, rhyolites & ignimbrites (Pliocene - Pleistocene)
- Basalts (Eocene - Pliocene)

Scale: 0 — 100km

2.3   Southern Afar

2.3.1   Background

The main Quaternary volcano-tectonic lineation represented by the Wonji Fault Belt (WFB) in the MER continues to run through southern Afar, until terminated against the Tendaho Graben (Fig 2.5), itself on a structural trend which curves round from an approximately E-W direction in the east of Afar to a northwesterly trend in central Afar. Coincidentally, this marks the northernmost point where comprehensive fluid chemical and isotopic data are available in Ethiopia (Glover, 1976; Craig et al, 1977), and therefore forms, along with some results from Djibouti at about the same latitude, the northern boundary for this study.

Afar is generally considered to start at the location of the Quaternary volcano Fantale, where the Oromo ethnic group of the MER region is largely replaced by the Afar peoples. There is little discernible geological change, apart from the River Awash entering at some prominent falls a gorge, in which it remains for much of its subsequent course before terminating in Lakes Gargon, Gamari, Afambo and Abbe.

2.3.2   Physiography

In Southern Afar, the altitude of the rift floor falls from around 1000 m asl in the Fantale area to some 250 m at Lake Abbe. However, if the spreading zone of Djibouti is included as part of the region, elevation declines to a depth of greater than 120 m below sea level at Lake Asal.

There is significant volcanicity in Southern Afar, although relief rarely exceeds 1000 m. However, there are high boundary escarpments to the west (Ethiopian plateau) and south (Somalian plateau) which rise to elevations of 3000 m and 2600 m respectively.

The area is extremely arid with significant "badland" areas (Mohr, 1978). All drainage is internal, with the River Awash representing the only permanent watercourse. One result of the area's dormant volcanism is fumarolic activity on most major volcanic centres, and also in the Tendaho graben where there is no obvious centre (c.f. the Arus area of the Gregory Rift). Like other parts of the Eastern Rift, the arid climatic conditions promote little in the way of high-enthalpy hot-spring activity.
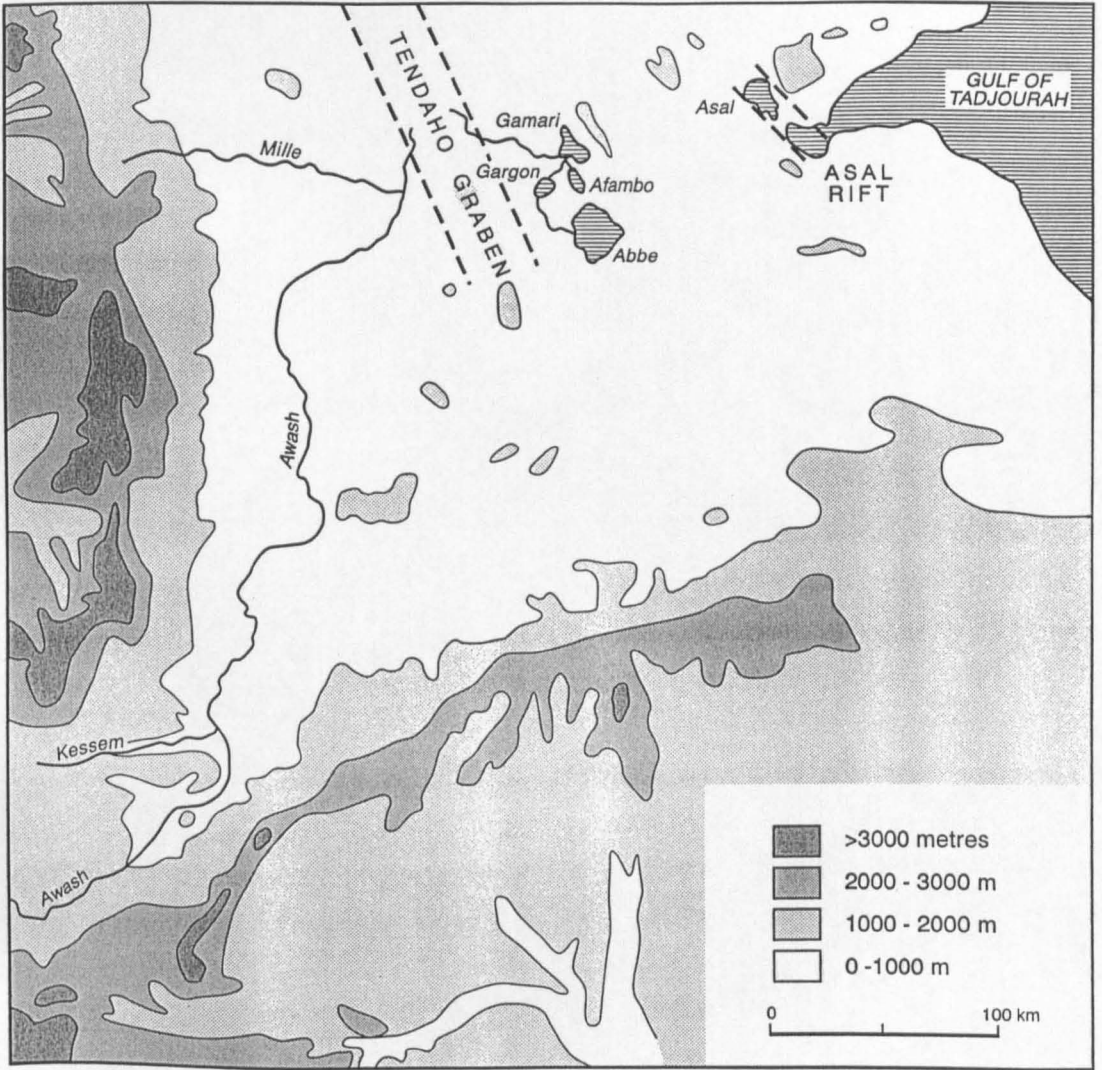
Fig 2.5 General physiography of Southern Afar, including the locations of the Tendaho Graben and the zone of active rifting at Asal in Djibouti.

2.3.3   General geology

This can be divided into two basic categories: the Southern Afar area *sensu stricto*, and the rifting in Djibouti apparently associated with the Gulf of Aden spreading axis (Fig 1.1). The geological development of Afar can be said to have begun contemporaneously with the start of rifting in the northern MER (Berhe, 1986) at around 25 Ma ago. Major rifting took place from 14 to 10 Ma, after which a number of rhyolite centres were emplaced in the MER and Afar up to about 5 Ma ago. The last important phase of rifting occurred at around 1.7 Ma in the southern-central part of the region, along the intersection of the WFB with a northwesterly-trending lineation (Berhe, 1986). Since then, faulting and volcanism have been concentrated along the WFB, with large amounts of rhyolite-trachyte and basaltic lavas erupted from Pleistocene to Recent times (Fig 2.6).

Whether the underlying crust of Afar is of oceanic or continental origin has not yet been fully resolved, but it looks increasingly unlikely that it can be regarded as oceanic because of the lack of resemblance between Afar and mid-ocean ridge basalts (e.g. Coleman, 1993), and because the crust seems too thick and may also be underplated (Keller et al, 1994).

By contrast, the rift zone of Djibouti is apparently the western extension of full oceanic rifting presently taking place in the Gulf of Aden. Activity in the Asal area resembles that occurring in the onshore rift zone of northeast Iceland. However, detailed examination of the evidence suggests that Asal is not (yet) a true extensional zone. Lepine and Hirn (1992) cite various pieces of evidence to support this view: there is no sign of the transform faulting accompanying "true" rifting; earthquake depths in the Gulf of Tadjoura currently extend to depths of 12 km and do not reflect the rheology of normal spreading ridges; and a 19 Ma basalt has been found at a depth of 2 km in a geothermal borehole in the Asal Rift. The last fact in particular is indicative of underplating due to the plume activity beneath the Afar region as a whole. However, stresses resulting from the Gulf of Aden rifting may be promoting the fissuring and dyke injection in the Asal area.

2.4   Implications of physiography and geology for rift fluids

Apart from "setting the scene" for the Eastern Rift areas studied, consideration of physiography and geology has certain implications for the study of fluids, their transport and interactions.
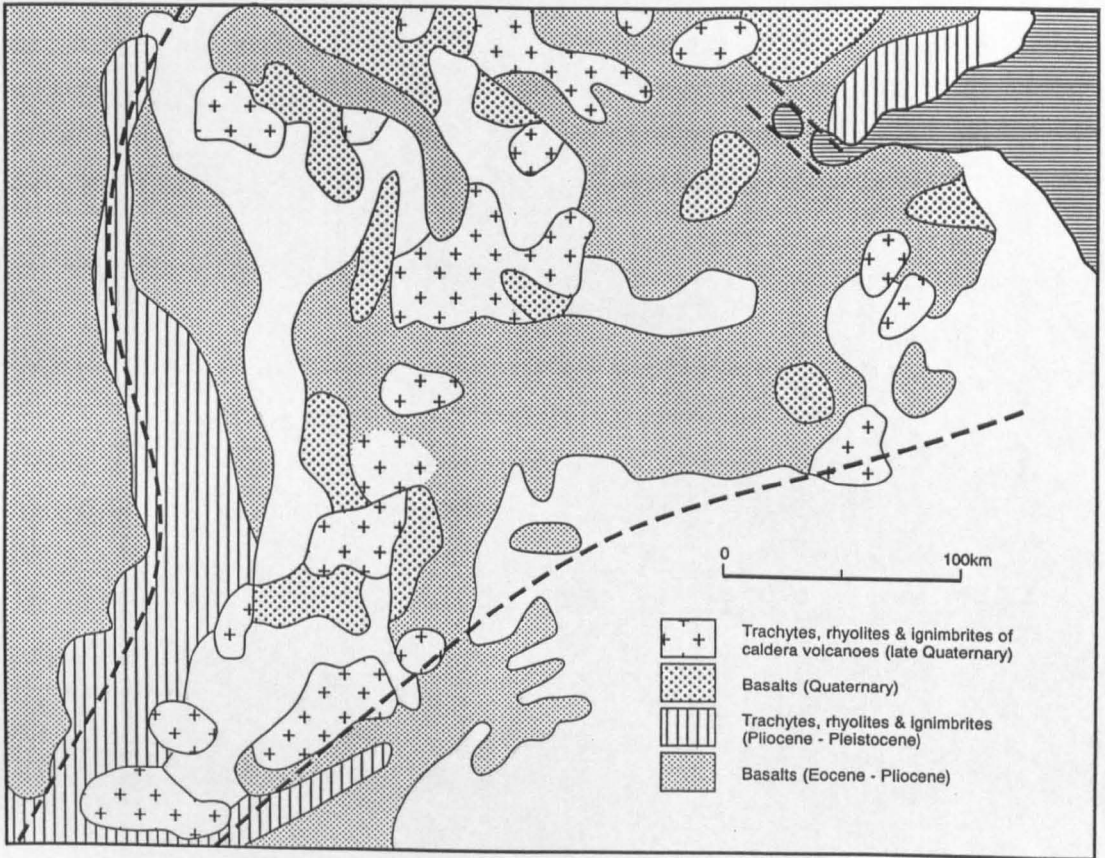
Fig 2.6 Volcanic geology of southern Afar, showing the rift boundaries.

The legend of the figure reads:

Trachytes, rhyolites & ignimbrites of caldera volcanoes (late Quaternary)

Basalts (Quaternary)

Trachytes, rhyolites & ignimbrites (Pliocene - Pleistocene)

Basalts (Eocene - Pliocene)

0   100km

2.4.1   Physiographical implications

These centre chiefly on water, its surface storage and movements. In most cases in the Eastern Rift, surface watersheds will coincide with subsurface water divides. The relief of the rift flanks is generally significant enough to provide stable isotopic signals enabling rift-wall recharge to be traced, whether in rivers or groundwater. The topography of the rift floor controls the existence of lakes, which may be sites of recharge (e.g. Lake Naivasha) but are more commonly discharge areas (e.g. Lake Abbe). In the case of the Asal basin, its depression below sea level promotes the inflow of both meteoric and marine waters.

2.4.2   Geological implications

Geology in its broadest sense is associated with the nature of rift fluids and also their movements within the crust. At a simple level, the chemistry of groundwaters depends to a large extent on water-rock interaction, though this work will show that water-rock-gas interaction is also important. The nature of these gases appears to depend largely on the existence of recent volcanism, and to a lesser extent on crustal thickness. Rift tectonic structures are of varying significance to the transport of fluids; they appear to be important for the deep circulation of groundwaters, but of less significance to the transport of gases.

CHAPTER 3

GEOTHERMICS

3.1 Background

Surface geothermal activity indicates that waters have circulated in the crust sufficiently to acquire varying amounts of heat. At the same time, these convective systems may have acquired a gaseous content resulting from crustal and/or mantle gas production in addition to any atmospheric component. For hot springs this can result in fluid compositions ranging from waters with no obvious outgassing, through to extremely effervescent waters which may have a gas content much higher in volume than the water, under surface conditions. Similarly, for fumaroles (steam jets) concentrations of gases accompanying steam range from extremely low to relatively high. In all cases, however, the water content is much higher than the gas content on a weight-for-weight basis.

Geothermal wells in the Eastern Rift commonly extend to depths of 1000 to 2500 m below ground level (bgl), and produce fluids from reservoirs with temperatures from 200 to over 300°C. The difference between surface and borehole sampling is that in the latter case fluids are brought much more rapidly to the surface, effectively in a closed system, and are therefore more likely to represent conditions at depth in the subsurface. Although the expense of drilling deep boreholes means that surface manifestations will always be important in geothermal exploration, the study of borehole fluids is important in showing the relative reliability of different determinands in surface samples as indicators of conditions at depth.

3.2 Surface manifestations

These are conveniently divided into two classes depending on their heat content, which is related to their presumed origin. The first category, *low enthalpy*, is reserved for waters which have been heated to <150°C and is thought to result primarily from the relatively deep circulation of groundwaters which acquire their heat from the "normal" geothermal gradient in the area. In the Kenya rifts this is often high, resulting in heat flows from 50 to over 100 mWm^{-2}, compared to the 40-60 Mwm^{-2} from the rift shoulders (Wheildon et al, 1994). Elsewhere in the Eastern Rift data are sparse, but there is no reason to believe that heat flows are significantly different. Rift flank hot springs often have temperatures in the range 40-80°C,

Temperature (°C)

Depth bgl (m)

Boiling-point curve

Low enthalpy typical curve
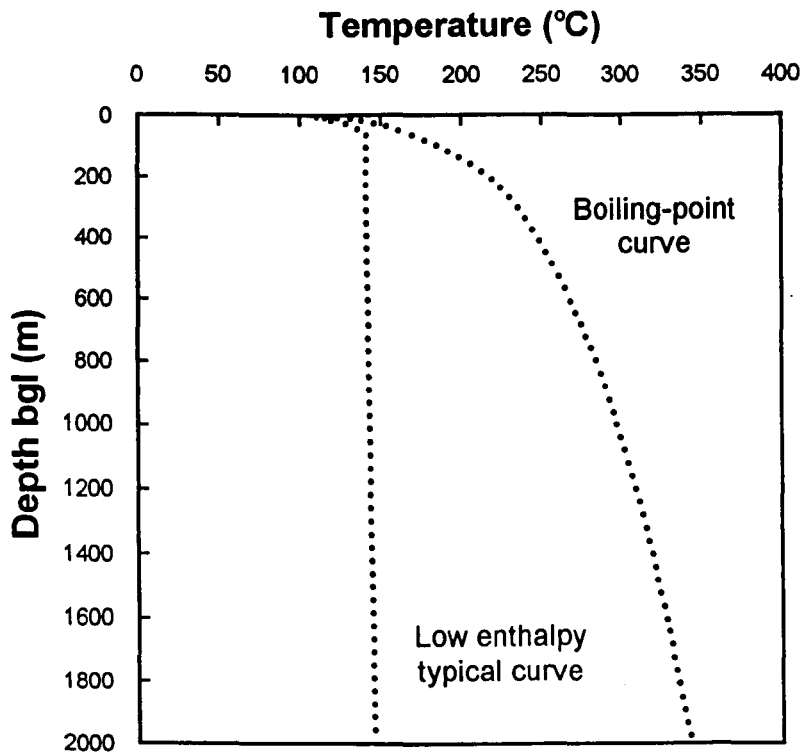
Fig 3.1   Temperature profiles for a typical low-enthalpy thermal water, and the boiling-point curve.   High-enthalpy thermal waters have a tendency to follow the latter, though specific conditions in individual geothermal fields can cause deviations from the curve.

which presupposes circulation to typical depths of 200-400 m bgl, though in some cases to perhaps twice these depths. As the term "low enthalpy" implies, the heat energy of these waters is such that only a small fraction of the water can be vaporised as steam when the surface is reached. The waters tend to reach a more-or-less stable temperature at a shallow depth (Fig 3.1).

The second category, *high enthalpy*, is applied to cases where there is enough heat input to cause extensive surface fumarolic activity, resulting from subsurface temperatures presumed to be well in excess of 150°C. These conditions only arise when geothermal gradients are very high, and are considered to originate from the presence of still hot or cooling magma chambers or smaller igneous bodies relatively close to the surface. Because of the high amount of heat energy stored in these waters, they tend to follow the boiling-point curve for water (Fig 3.1), at least over part of its course. This curve represents the temperature profile of the boiling point of water under hydrostatic pressure. There may be heat loss by conduction as a consequence of the low upflow rates that generally prevail in the Eastern Rift, but enough heat energy remains to vaporise a much higher proportion of the water than in the case of the low-enthalpy systems. Such boiling will occur when there is a release of pressure. This could simply be due to reaching the surface, but is just as likely to happen when fissures of varying depth intercept the rising water. Because of this, fumarolic steam sampled at the surface may have separated over a range of temperatures. This causes varying stable isotopic fractionations in the steam, the study of which is considered in more detail in Chapter 5.

While many Eastern Rift thermal manifestations can be easily assigned to one or other of the categories, some are more ambiguous, suggesting that "deep circulation" and "magmatic" categories are end-members of a continuum, as might be anticipated. Tables 3.1 and 3.2 give a list of geothermal manifestations in the study areas, with an estimate of the nature of their heat source. With very few exceptions, fumarolic areas are rated as high-enthalpy and of magmatic origin. By contrast, most hot springs are of low enthalpy and many of these probably result from deep circulation. The general absence of high-discharge boiling springs in the Eastern Rift suggests that there are few opportunities for apparently low-enthalpy waters to result from mixing processes. Equally, steam heating of waters is rare, although a few cases of drowned fumaroles or "frying pans" exist, such as at Arus in the KRV and Abaya in the MER.

Despite this, there are cases where surface steam is not associated with any obvious volcanic centre — for example Arus and Bogoria in Kenya, Tendaho in Ethiopia and Hanle in Djibouti.

Table 3.1 Characterisation of typical hydrothermal systems in the rifts of Kenya, Ethiopia and Djibouti: 1, hot spring areas, with details of discharge, apparent enthalpy and heat source. (Sources of 40°C and above).

Hot spring area	Site No	Max T °C	Discharge	Enthalpy	Heat source
K Bala	K53	72	large	low	deep circ
K Magadi	K03	85	large	low	?
K Kijabe	K26	43	small	low	deep circ
K Elmenteita	K41	42	small	low	?
K Kariandusi	K35	40	small	low	deep circ
K Bogoria	K69,260	96	large	high	?
K Kureswa	K256	62	medium	low	deep circ
K Ol Kokwe	K71	96	small	high	magmatic
K Kapedo	K48	51	large	low	deep circ
K Lorusio	K45	82	medium	low	?
K Suguta Valley	K185	68	medium	low	deep circ
K Kamuge	K187	50	small	low	deep circ
K Kageinya	K188	68	small	low	?
K Namarunu	K189	66	medium	low	?
K Elboitong	K236,237	95	large	low	?
K Logipi	K190,238	70	medium	low	?
K Loyangalani	K242	40	medium	low	deep circ
K Central Island	K239	71	small	high	magmatic
E Nech Sar[1]	-	58	large	low	deep circ
E Abaya	E12	95	large	high	magmatic
E Bilate[1]	-	51	medium	low	?
E Graha Que[1]	-	86	small	high	?
E Wondo Genet	E14	65	large	low	deep circ
E Bodicho[1]	-	89	-	low	deep circ
E Chitu[1]	-	60	-	low	?
E Shalla NE	E15	96	medium	low	?
E Langano	E11	97	large	high	magmatic
E Imba Koto[1]	-	49	small	low	deep circ
E Sodere	E16	65	large	low	?
E Awash Filwoha	E20	42	large	low	?
E Meteka[1]	-	86	small	low	?
E Allallobeda[1]	-	95	small	low	?
D Abbe SE	D06,07	90	medium	low	deep circ
D Korilli[2]	D05	79	large	low	?

K - Kenya   E - Ethiopia   D - Djibouti
[1] Data of Craig et al (1977)   [2] Data of Fontes et al (1980)
? - heat source not clear

Table 3.2 Characterisation of typical hydrothermal systems in Kenya, Ethiopia and Djibouti: 2, fumarolic areas, with details of apparent enthalpy and heat source.

Fumarolic area	Site No	Max T °C	Enthalpy	Heat source
K Suswa	K126,258,501	94	high	magmatic
K Longonot	K29,128	90	high	magmatic
K Domes	K31,127	95	high	magmatic
K Olkaria-Domes	K123,261-267	95	high	magmatic
K Eburru	K119	92	high	magmatic
K Menengai	K260	76	high	magmatic
K Arus	K257	95	high	?
K Bogoria	-	97	high	magmatic
K Ol Kokwe	K152	96	high	magmatic
K Korosi	K153-162	96	high	magmatic
K Paka	K163-182	96	high	magmatic
K Silali	K218-225	97	high	magmatic
K Emuruangogolak	K226-234	96	high	magmatic
K Barrier	K235,248-251	96	high	magmatic
K Central Island	K254,255	96	high	magmatic
K North Island	K252,253	97	high	magmatic
E Wanche	-	-	high	magmatic
E Corbetti	E06-08	95	high	magmatic
E Aluto	E04-06	93	high	magmatic
E Tulu Moye[1]	-	-	high	magmatic
E Gedemsa[1]	E10	73	high	magmatic
E Boseti[1]	-	-	high	magmatic
E Fantale[1]	-	-	high	magmatic
E Dofan[2]	-	-	high	magmatic
E Tendaho[2]	-	99	high	?
D Hanle	D04	-	?	?
D Asal	D02	99	high	magmatic
D Nord Ghoubet	D03	-	high	magmatic

K - Kenya   E - Ethiopia   D - Djibouti
[1] Evidence of Di Paola (1973)   [2] Data of Glover (1976)
? - heat source not clear

These may have "intermediate" heat sources, explained in 3.4 below. Nevertheless, the distinction between the deep circulation and magmatic categories is on the whole useful, and will be retained as appropriate during further discussions of fluid geochemistry.

3.3   Geothermal wells

The exploration and production boreholes in geothermal fields of the Eastern Rift (Fig 1.3) are typically of the order of 1000 to 2000 m deep in Kenya and Djibouti (Bodvarsson et al, 1987; Zan et al, 1990), and up to 2500 m in Ethiopia (Gizaw, 1993). Some of the feed zones in these wells may be significantly closer to the surface, but all are at least several hundreds of metres below ground level. Geothermal wells therefore provide the opportunity to sample fluids in the absence of atmospheric contamination and with a circumvention of the (usually) thick unsaturated zone. In this respect, they provide a "window" onto hydrothermal conditions away from the surface. This is important for several reasons. Firstly, the composition of deep thermal waters may be different from the local meteoric waters. This for example is the case at Olkaria, where it is demonstrated that some two-thirds of the deep fluid has been derived from infiltrating lake water (see Chapter 5). Secondly, the more reactive or diffusive gases (H_2S and H_2) are present in significantly greater amounts in geothermal wells than in the surrounding fumaroles (see Chapter 7). Thirdly, wells provide a way of checking the performance of gas geothermometers (see Chapter 8) and also serve to demonstrate that isotopic parameters (e.g. $\delta^{13}C$-CO_2 and $^3He/^4He$) are not significantly different between borehole and surface samples.

While the geothermal wellfields cover only a small fraction of the high-enthalpy geothermal areas of the Eastern Rift, the volcanic centres drilled in the Gregory Rift (Olkaria, Eburru) and the MER (Aluto-Langano) are fairly typical of most of the other centres in the continental rifts. In Afar, the Tendaho graben, which has recently been drilled, may simply have a very high heat flow without direct magmatic heating, and this could also be the case at Hanle in Djibouti. Further east of this at Asal, magmatic heating is certainly involved but the situation is, at least superficially, more like an area of active rifting such as northeast Iceland, where magmatic activity is likely to be in dyke form rather than central chambers.

3.4   Schematic of systems and manifestations

Fig 3.2 attempts to represent the nature of Eastern Rift hydrothermal systems and how they may control surface manifestations. This takes the form of a hypothetical cross-section across

Low enthalpy
(hot springs)

Intermediate
(fumaroles,
springs)

High enthalpy
(fumaroles)

Normal
circulation

Cross-section through
half-graben rift basin
with axial intrusion
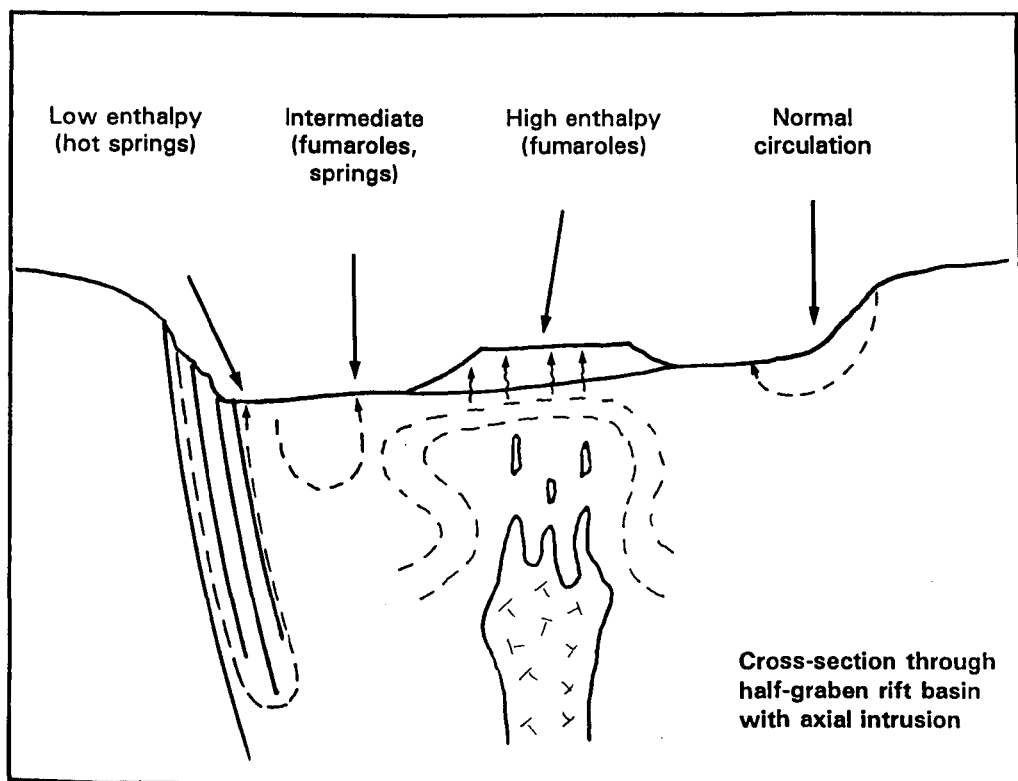
Fig 3.2   Schematic diagram of heat source occurrences in the Eastern Rift. Many
systems can be readily assigned to either the high- or low-enthalpy
categories, but some have more equivocal characteristics and may have
elements of both types.

a "typical" rift unit. On the eastern side, activity is confined to relatively shallow circulation resulting in spring temperatures rarely above 40°C (e.g. Kariandusi in the Gregory Rift). More centrally, a magma chamber causes a convective plume which results in fumarolic activity on the overlying volcanic edifice (e.g. most late-Quaternary centres in the KRV and MER). On the western side in this schematic, for structural reasons circulation to a greater depth is able to take place, resulting in higher temperatures than in the east (e.g. Kamuge, S Turkana Rift, and Imba Koto, northern MER). Generally low water tables mean that the waters heated magmatically are unable to reach local surface discharge in the liquid phase (notable exceptions would be the N Abaya and N Langano springs of the somewhat wetter MER). However, circulating waters from the rift wall may mix with these and acquire quite high temperatures and in a few cases may find a surface discharge (e.g. Lorusio in the S Turkana Rift, Graha Que in the MER). Alternatively, a sufficiently high heat flow may exist in certain places between the magmatic axial line and the rift wall, permitting relatively high temperatures for only moderate depths of circulation.

CHAPTER 4

HYDROLOGY AND HYDROGEOLOGY

This chapter provides an account of the movement of waters in the various rifts. This is necessary to provide a context in which to interpret the geochemical aspects to be covered in Chapters 5 to 9.

4.1   Rainfall and evaporation

Any discussion of hydrology and hydrogeology must begin with some consideration of the meteoric inputs to the Eastern Rift. Rainfall is primarily derived from the Indian Ocean by way of atmospheric circulation associated with the monsoon system. In Kenya the main wet season occurs from March to May, while in the MER it is rather later, from June to September. In Djibouti the concept of a wet season becomes invalid because rainfall is so light, but what rain there is usually falls between October and April.

In all the rift areas there is a relatively sharp transition between low amounts of rainfall on the rift floors and significantly greater amounts on the rift margins. Superimposed on this is the general variation of rainfall due to changes in absolute altitude. Thus in Kenya the low-lying Magadi area has a average rainfall of 430 mma^{-1}, while the Naivasha area at the culmination of the rift floor has some 630 mma^{-1}. However, the relationship with altitude is distorted by other physiographic factors which mean that the maximum rift-floor precipitation in Kenya is 980 mma^{-1} at Nakuru, some distance north of the culmination. North of this, rainfall starts to decline again, from around 800 mma^{-1} in the Bogoria area to below 200 mma^{-1} in the northern Suguta Valley and Turkana basin. These valley-floor rainfall figures are accompanied by antithetic amounts of potential evapotranspiration: over 2500 mma^{-1} at Magadi, 1700 mma^{-1} at Naivasha, 3000 mma^{-1} in the southern Suguta, and over 3500 mma^{-1} in the northern Suguta and Turkana areas.

By contrast, on the rift escarpments amounts of rainfall are usually much higher, ranging from up to 1250-1500 mma^{-1} in the central Gregory Rift down to 300-400 mma^{-1} on the eastern side of the South Turkana Rift. On the western side of this rift and in the Turkana basin, however, rainfall is more similar to rift-floor amounts, partly because of smaller altitude differences. As with the rift floor, potential evapotranspiration varies more or less antithetically, with

1400 mma^{-1} in the Naivasha area, 2000 mma^{-1} at Bogoria, 2500 mma^{-1} east of the Suguta Valley and up to 3000 mma^{-1} to the west (Allen et al, 1989; Allen and Darling, 1992).

Over most of the floor of the MER, average rainfall is in the range 500-1000 mma^{-1} (Chernet, 1988). This is accompanied by potential evapotranspiration rates of 1100 mma^{-1} to the south of Lake Shamo, 1250 mma^{-1} in the Lake Awasa area, and 1550 at Awash Station on the northern boundary of the area. On the rift escarpments rainfall rises to between 1000 and 1500 mma^{-1}, while potential evapotranspiration falls to around 1000 mma^{-1}.

In southern Afar and Djibouti, rainfall varies from around 450 mma^{-1} north of Fantale to 150 mma^{-1} in the centre and east of the region (Chernet, 1988; Verhagen et al, 1991). In locally mountainous areas this may rise to 300 mma^{-1}, but otherwise a major increase only occurs at the rift margins where the rapidly increasing altitude raises amounts to over 500 mma^{-1}. Typical transpiration rates for the drier areas are from 1800 mma^{-1} west of Lake Abbe to 3000 mma^{-1} at Lake Asal. At the rift margins these rates fall to below 1500 mma^{-1}.

4.2   Kenya Rifts

4.2.1   Surface hydrology

Lakes are the dominant surface hydrological feature of the Kenya rifts. There are no major permanent rivers, with the partial exception of the Kerio (Fig 2.1), which although it contributes in a small way to the water balance of Lake Turkana, flows for most of its length outside the South Turkana Rift proper.

The character of these lakes is partially governed by their position relative to the Kenya Dome, and partially by more local topographic and geological features. (Fig 4.1 shows the lakes in schematic form, with details of altitude, TDS and stable isotopic characteristics.) Thus Naivasha, at ~1880 m asl and the culmination of the rift floor, is fundamentally an infiltration reservoir for local stream and river waters to provide underflow to both the north and south. At the south end of the Gregory Rift and the north end of the South Turkana Rift, lie terminal lakes (Magadi, ~570 m and Logipi, ~270 m) which form sumps to surface and groundwater drainage. Although there is no surface water between Naivasha and Magadi, to the north of Naivasha lies a series of lakes of varying character. Elmenteita (~1780 m) and Nakuru (~1760 m) can be considered as occupying a single lake basin, from which there is no surface egress due to the damming effect of the Menengai volcanic shield. Both lakes are highly
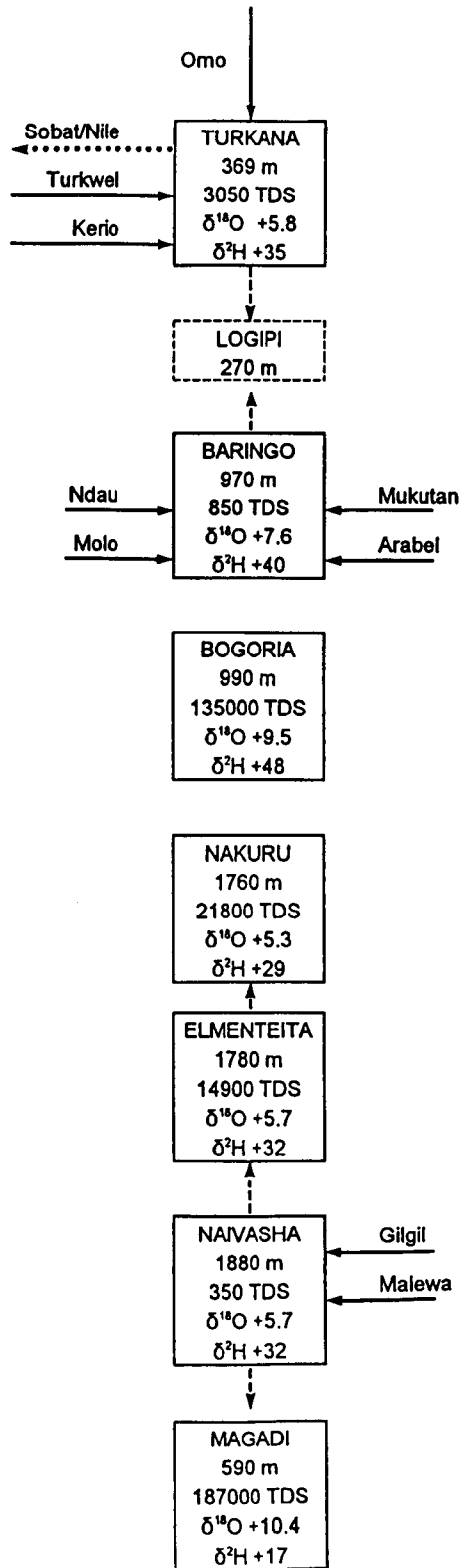
Fig 4.1   Schematic diagram of lakes in the Kenya rift valleys, giving basic information on altitude, total dissolved solids and stable isotopic values. Solid lines - rivers; dotted lines - occasional or palaeo river flow; dashed lines - underflow.

alkaline with a high TDS content. Much of the inflow to the lakes is by leakage from Naivasha (Allen et al, 1989), probably supplemented by subsurface outflow from the Eburru volcanic centre (Arusei, 1992). Thus waters already "pre-concentrated" by evaporation or water-rock interaction are further concentrated in Elmenteita and Nakuru.

Lake Bogoria at ~990 m is fed by small streams and hot springs, the latter having a high TDS content. Because there is no surface outlet and probably very little or no subsurface leakage, the lake is alkaline and has the highest TDS next to the "sump" lakes of Logipi and Magadi. On account of its greater depth and volume of water compared to Elmenteita and Nakuru, which are otherwise quite similar lakes, Bogoria has more consistent TDS and stable isotopic contents. Baringo (~970 m) has a hydrological situation similar to Naivasha, inasmuch as it is a "reservoir" lake from which water leaks out in the subsurface, though in this case only to the north. Baringo is slightly larger than Naivasha and has a greater inflow from minor rivers which, in the south particularly, have a high suspended solids load which is probably responsible for the characteristic coppery colour of the lake. The higher TDS content of Baringo is related to the higher potential evaporation in the area (2600 mma^{-1} as opposed to 1600 mma^{-1} at Naivasha; Allen et al, 1989, Allen and Darling, 1992), and perhaps the input of hot springs. However, the output of these springs, at least where exposed above lake level, is only small.

Apart from Victoria at the western end of the Nyanza Rift, the largest lake in Kenya is Turkana (~369 m). A terminal lake for probably the last 3.5 ka (Butzer et al, 1972), Turkana has had insufficient time to build up a high TDS content, though the water is alkaline and concentrated considerably relative to its main input, the River Omo, which rises in the Ethiopian Plateau to the north. Minor inputs to the lake include the Turkwel, with a flow large enough to provide some hydro-electric power, and the Kerio as previously mentioned.

Apart from the streams and rivers feeding Naivasha, Elmenteita, Bogoria and Baringo, the only significant river system in the rift south of Turkana is that of the Suguta (Fig 2.1). In its upper reaches (principally the Nginyang and Cheptopokwo rivers) there is a seasonal flow. However, below Kapedo a combination of thermal and sub-thermal springs means that the Suguta flows perennially, though at the cost of a high TDS content. The river generally terminates in the vicinity of the Namarunu volcano, where the water infiltrates before appearing again in the seasonal Lake Logipi (to which minor leakage from Turkana may also contribute). In the area of infiltration, a temporary lake (Alablab) sometimes appears during flood conditions.

In the Nyanza Rift, the River Nyando collects stream drainage, mainly from the southern rift wall, and proceeds to drain through a marshy area into the southeastern corner of the Winam Gulf of Lake Victoria.

Some idea of the catchment areas for the KRV can be gained from data in McCann (1974) concerning several Gregory Rift lakes. Where the rift walls form relatively sharp topographic highs, catchments are relatively small, such as Bogoria with an area of 752 km^2 (excluding the lake). By contrast, the catchment of Naivasha at 3128 km^2 includes the Nyandarua (Aberdare) Mountains which lie above and beyond the local rift wall to the northeast of the lake. To a large extent, therefore, knowledge of catchment area is of rather little importance for rift water balance assessments, since the nature of the catchments varies considerably. Thus, for example, the catchment immediately to the north of Naivasha (Elmenteita-Nakuru) has an area two-thirds that of Naivasha, but only one-third of the water supply. Similar or larger discrepancies are likely to occur in other parts of the Eastern Rift.

4.2.2 Hydrogeology

The hydrogeology of the main KRV can to some extent be understood from consideration of borehole physical data. These however are only available in significant number for the more central parts of the KRV (approximately from the Naivasha to Baringo areas), with the result that direct knowledge of subsurface flow tends to diminish rapidly to the north and south of this sector.

In simple terms, it would be expected that the main KRV, as a trough superimposed on a dome, would have a lateral inflow of groundwater towards the axial region of the floor, where the water would then be diverted to the north or south depending on the regional gradient. Although this basic pattern is observed, local factors can cause some disruption on the smaller scale. Fig 4.2 shows the hydrogeological situation for the central Gregory Rift as inferred by Allen et al (1989). Directions of flow are based on piezometric contours derived for the most part from borehole water level records. The confidence level of these equipotential lines varies; where there were judged to be sufficient data the lines are shown as solid, elsewhere as broken. In areas where water level data are scarce or absent, no attempt has been made to draw contours. Instead, Fig 4.2 shows the elevation of the bottom of dry boreholes to give an indication of the great depth to water table in the south of the region.

Borehole rest water levels in the vicinity of Lake Naivasha show that the water table is flat or

37
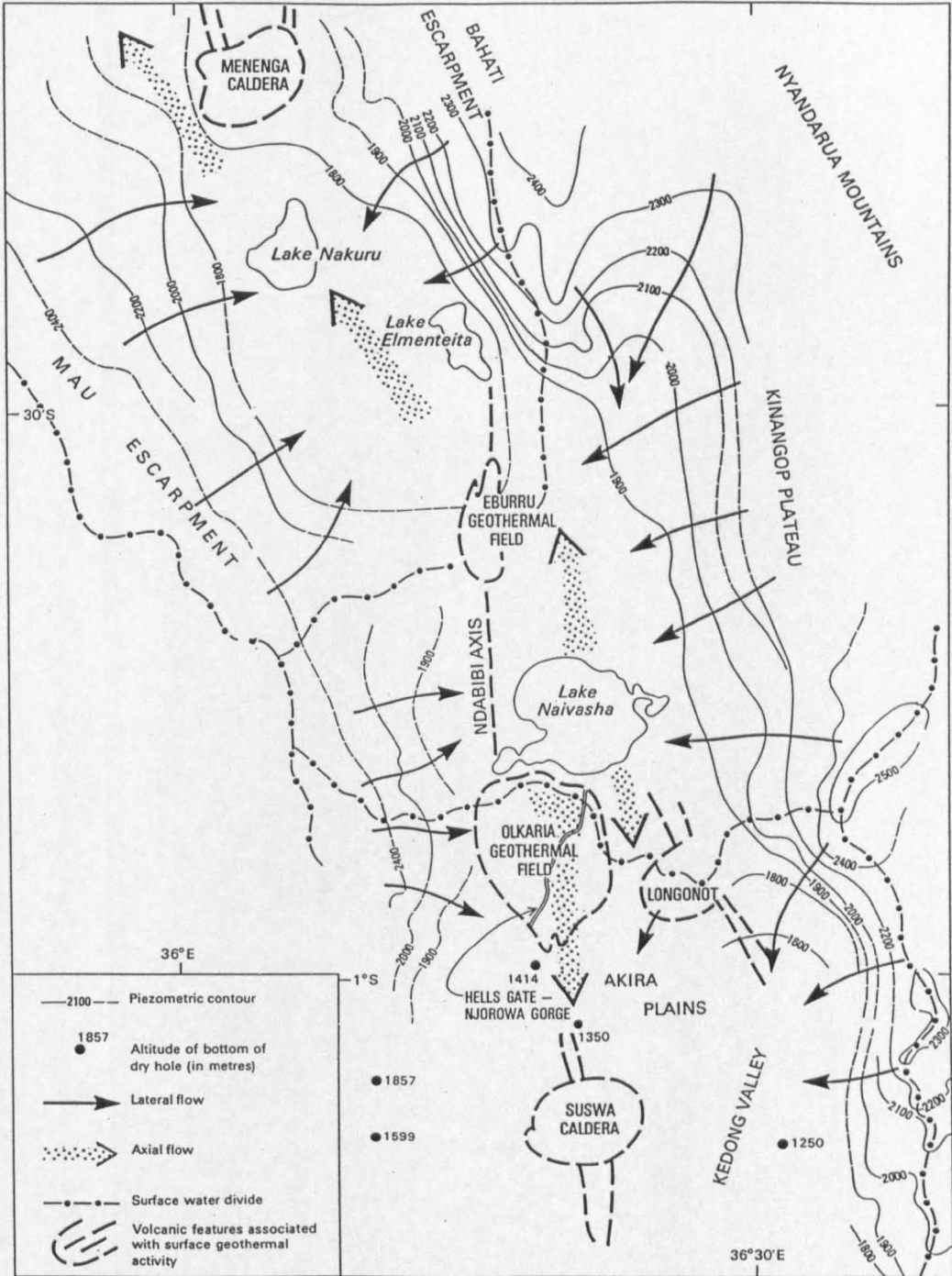
Fig 4.2 Hydrogeological map of the Lake Naivasha area of the Gregory Rift, Kenya. The altitudes of piezometric contours and dry hole bottoms are given in metres above sea level. (Modified from Allen et al, 1989.)

falling away to the north and south of the lake, which is therefore acting as a kind of recharging reservoir fed by the Malewa and Gilgil rivers. The lake is very shallow (a few metres deep over most of its area), and because of this exhibits fairly marked continuous changes in level (Ase et al, 1986) in response to changes in input volumes.

Available data show no great decline in aquifer permeability in the region to the north of Naivasha. However to the south of the lake, deep but dry boreholes (Fig 4.2) indicate that the piezometric surface must drop away at a rate of at least 0.05 m/m. A deep, north-south pressure gradient in the Olkaria geothermal field corresponding to a pressure gradient of 0.1 m/m was reported by Bodvarsson et al (1987). Such steep gradients are indicative of very low permeabilities.

Even in the Naivasha-Nakuru sector, which is probably the best-represented area of the whole Eastern Rift in terms of borehole data, good information about the aquifer properties of different rock types is scarce. Usually, aquifers are formed in fractured or reworked volcanics, and along the weathered contacts between different units. Typical hydraulic conductivities are 0.1 md^{-1} for tuffs and 1.1 md^{-1} for trachytes, two dominant rock types in this and other parts of the Eastern Rift. At depths greater than ~ 250 m below ground level (bgl), permeabilities are likely to fall as a result of overburden stress. At Olkaria, for example, an average hydraulic conductivity of only 3×10^{-3} md^{-1} was calculated by Allen et al (1989) from the data of Bodvarsson et al (1986).

The anisotropy in the rock "fabric" of the rift floor, due to faulting sub-parallel to the rift axis, affects groundwater flow in the Naivasha area (and probably much of the remainder of the Eastern Rift) in two main ways. Firstly, it tends to force water from the rift walls down to greater depths and hence over longer flowpaths than would occur in a more isotropic aquifer sequence. Secondly, when water has reached the axial area it tends to be channelled into flow to the north or south as appropriate.

Despite the combination of low permeability and increased length of flowpath due to faulting, there is no evidence that groundwater residence times are excessively long. Allen et al (1989) used an analytical model to show that even over horizontal distances of ~ 15 km and circulation depths of ~ 5 km, and under conditions of low permeability and porosity, residence times were unlikely to exceed around 100 years (Fig 4.3).

The question of whether separate aquifers exist in the melange of volcanic, volcaniclastic and
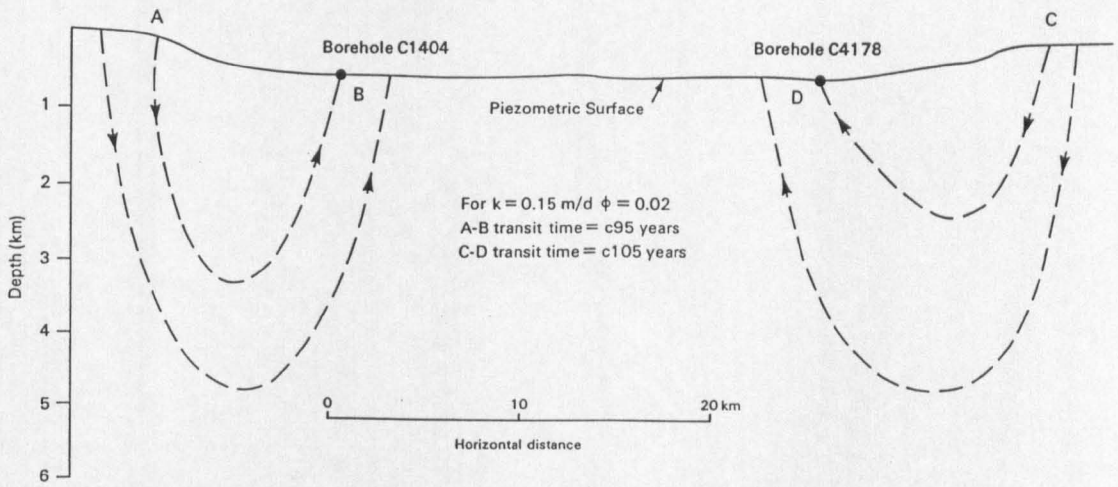
Fig 4.3   Section across the Gregory Rift showing possible flowpaths and transit times. (From Allen et al, 1989.)

40

other sedimentary rocks that fills this and most other parts of the Eastern Rift is not easy to answer. There is evidence from Olkaria that the upper, cooler aquifers are separated from the hotter geothermal reservoir(s) by a confining basaltic caprock (e.g. Bodvarsson et al, 1986), and self-sealing by mineral deposition may also be transiently important. However, away from the high-enthalpy areas there is little evidence from the shallower groundwaters that separate aquifer units exist, and therefore the model of a relatively simple fractured igneous rock aquifer seems most appropriate.

In the South Turkana Rift the situation is similar to the Gregory Rift, but with some local differences (Allen and Darling, 1992). The chief of these is that the tilt of the rift floor in the southern part of the area results in a displacement of the axial flow towards the western side of the rift floor (Fig 4.4). Very few boreholes occur on the valley floor, and therefore there is little information on permeabilities, but there is no reason to believe that they are any higher than further south. The north-south fabric of the rift appears to have similar effects on groundwater flow as in the south, except that there may be more axial dyke injection in the South Turkana Rift (Dunkley et al, 1993), which might act as more of a barrier to lateral flow. Allen and Darling (1992) cited a case from the Baringo-Paka area where there were extreme differences in water level between wells only a few kilometres apart.

The very scarce borehole data from the rest of the main KRV necessitate the assumption that similar hydrogeological conditions obtain there. Whether they apply to the Nyanza Rift too is doubtful because of the importance of carbonatites and related rocks in that rift. The more rapid chemical alteration of these rocks may have given rise to higher hydraulic conductivities, but supporting data are not available.

Catchment water balances are known too imprecisely to gain more than a very approximate idea of the volume of axial groundwater flows in the KRV. Effectively these equate to the underflows from Naivasha and Baringo. McCann (1974) estimated a groundwater recharge of 34×10^6 m^3 per year for Naivasha, while WRAP (1987) arrived at the almost identical figure of 33×10^6 m^3 per year for Baringo. However, other methods have suggested sometimes considerably different figures for underflows from these two lakes (see Chapter 5).
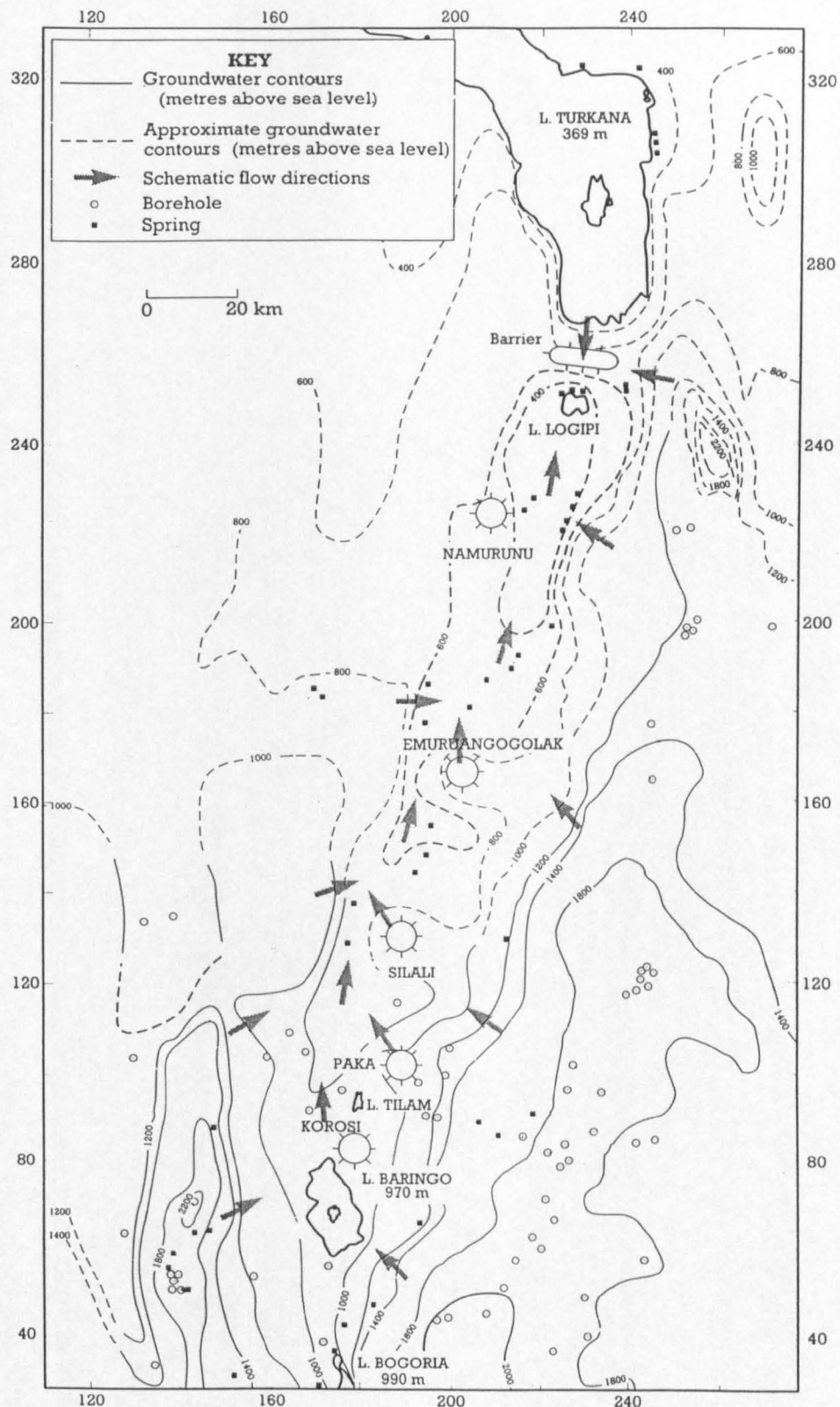
Fig 4.4   Potentiometric map of the South Turkana Rift, showing the effect of the
            westerly tilt of the rift floor on groundwater flowpaths. The positions of
            the central volcanoes from Korosi northwards to the Barrier are also
            shown. (From Dunkley et al, 1993.)

42

4.3   The Main Ethiopian Rift

4.3.1   Surface hydrology

North of the rift floor culmination between Lakes Zwai and Koka, there are no important natural surface water bodies in the northern MER (Koka is largely the result of a hydro-electric power dam built on the Awash river). The only surface hydrological feature of note is therefore the Awash itself (Fig 2.3). Conversely, from Lake Zwai southwards there are no major rivers in the MER. There are however lakes of varying size which can be regarded as northern and southern hydrological groups, separated by Lake Awasa (Fig 2.3). The northern group consists of Zwai, Langano, Abiata and Shalla, while the southern group is comprised of Abaya and Shamo. A schematic of the lakes is shown in Fig 4.5, which also includes details of palaeo-drainage to the presently desiccated Lake Chew Bahir and onwards to Turkana, thus linking up with the Kenya rifts.

In the north, Zwai ($\sim$ 1636 m), Langano ($\sim$ 1582 m) and Abiata ($\sim$ 1578 m) are all shallow lakes whose TDS contents are governed by the amount of outflow from each lake. Zwai has a surface outflow *via* the Bulbula stream directly to Abiata. There may also be an underflow to Langano (see Chapter 5), which might go some way to explaining the apparently anomalous chloride balance of the lake discussed in Street (1979) and Von Damm and Edmond (1984). There is possibly some underflow from Langano to Shalla ($\sim$ 1558 m), but otherwise outflow is on the surface *via* the Horocallo stream into Abiata. Abiata itself, though a high-TDS lake, is not as saline as Shalla, and underflow may occur to Shalla, although there is no direct evidence for this. Shalla is volumetrically by far the largest lake in the MER, and is also unique among lakes of the Eastern Rift in that it occupies a very large caldera structure. Because of this it is deep, with a maximum depth of 266 m. Since it is the true terminal lake of the four, it has the highest TDS content ($\sim$ 190000 mgl^{-1}) compared with Zwai (300 mgl^{-1}), Langano (1400 mgl^{-1}) or Abiata (14500 mgl^{-1}).

Awasa ($\sim$ 1680 m) is the Naivasha equivalent among the lakes of the MER, insofar as it has a topographic position which suggests that outflow could occur to the north or south (although unlike Naivasha, the lake is nowhere near the culmination of the rift floor, which occurs north of Zwai). Like Naivasha, the lake is fresh despite a lack of surface egress; isotopic techniques indicate that outflow occurs towards the north (Chapter 5), but as yet there is no evidence for southerly outflow.
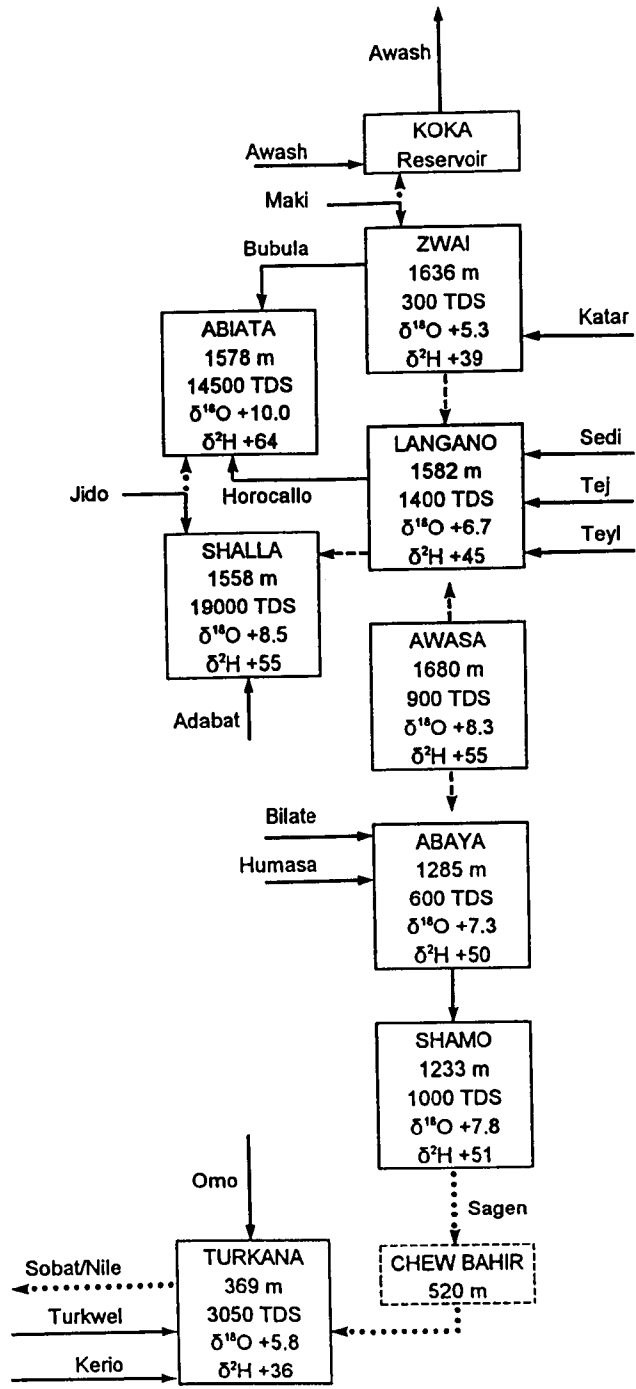
Fig 4.5 Schematic diagram of lakes in the Main Ethiopian Rift, giving basic information on altitude, total dissolved solids and stable isotopic values (based on the concept of Von Damm and Edmond, 1985). Solid lines - rivers; dotted lines - occasional or palaeo river flow; dashed lines - underflow.

Despite its size, Abaya ($\sim$ 1285 m) is a shallow lake with a maximum depth of only 13 m. With its high sediment content it resembles Langano to the north and also Baringo in Kenya, but unlike these lakes it has a surface outlet, to Shamo ($\sim$ 1233 m), which keeps the water fresher. The numerous springs between Abaya and Shamo suggest that there may be an underflow, though the limited stable isotope evidence indicates a relatively insignificant amount (Chapter 5). The Sagen River drains Shamo intermittently, ultimately to Chew Bahir ($\sim$ 520 m), a periodically dry alkaline lake. This drainage must occur frequently enough to keep the TDS content of Shamo relatively low.

During high lakestands of the late Quaternary, Chew Bahir (Stephanie) would have overflowed to Lake Turkana, thus linking the lake systems of the MER and Kenya rifts. At such high water levels there would also have been a linkage to the Nile drainage system (Butzer, 1971).

4.3.2   Hydrogeology

There is little published material concerning the physical hydrogeology of the MER. The main source of information is the hydrogeological map of Ethiopia (Chernet, 1988). However, the scale of the map (1:2,000,000) is such that only the broader details can be shown.

Fig 4.6 is a map of the MER and southern Afar with the hydrogeological information extracted from the 1:2,000,000 map for Ethiopia, and from Verhagen et al (1991) for Djibouti. Information is restricted to the position of major surface water divides, estimated flow directions, and some borehole depths and yields. The results are largely as would be expected from the example of the Kenya rifts: sub-parallel water divides on each side for most of the southern and central MER, with a divide crossing the rift floor between Zwai and Koka (though it appears that under wetter palaeoconditions, the Maki River may have fed both lakes - Street, 1979). This surface water divide is likely to coincide fairly closely with the groundwater divide, as in the Naivasha area for the Gregory Rift. North of this, there is a considerable salient in the western water divide around the Addis Ababa area; the topography which causes this is thought to have a tectonic origin (see Chapter 2). The distance between eastern and western divides closes again towards Awash Station, but almost immediately starts to open up again as the MER opens out into the Afar "funnel".

North of the Zwai-Koka divide, groundwater flow appears to be directed simply towards the River Awash as a linear zone of discharge. South of the divide, the situation is only slightly more complicated. Flow arrows are generally sub-perpendicular to the rift walls as in Kenya;

45
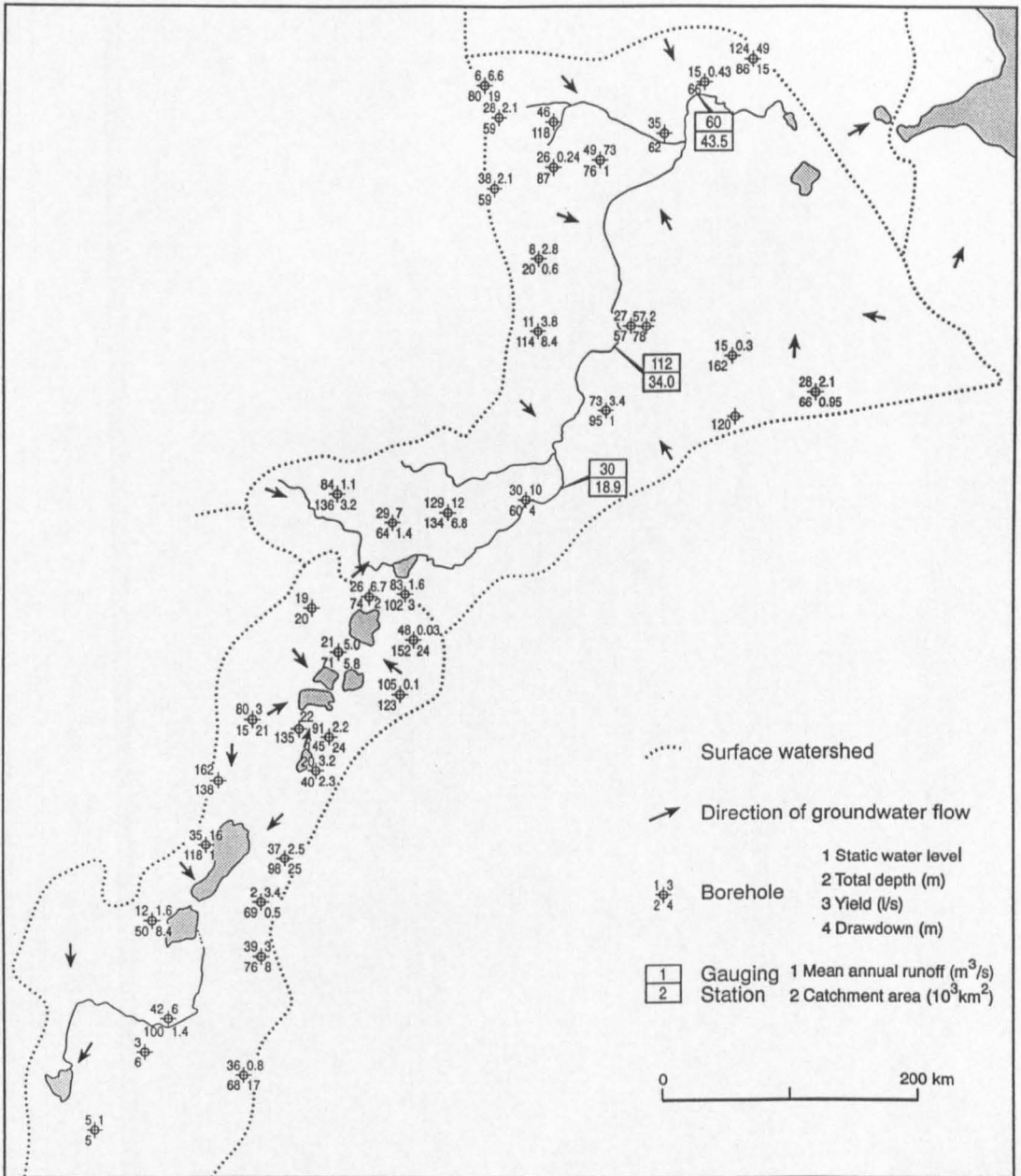
Fig 4.6   Hydrogeological map of the Main Ethiopian Rift and southern Afar (after Chernet, 1988 and Verhagen et al, 1991).

the only major exception to this is Lake Awasa which appears to give rise to an underflow to the north (backed by evidence to be considered in Chapter 5), i.e. against the general trend of this part of the MER to become lower towards the south.

Borehole information reveals that yields are generally restricted to a few litres per second, indicative in the context of water level and total depth of low transmissivities, and very similar to many rift floor boreholes in the KRV (Allen et al, 1989; Allen and Darling, 1992). There is therefore no reason to believe that the rocks underlying the MER behave hydrogeologically in a significantly different way to those in Kenya, and the simple fractured igneous rock aquifer therefore remains the preferred model for shallow to moderately deep groundwaters. As far as the deep thermal groundwaters are concerned, rates of circulation loss during the drilling of geothermal wells at Aluto-Langano have shown evidence of separate aquifer units, though these are by no means uniform across the geothermal field (Gizaw, 1993).

Some axial groundwater flow probably occurs in the MER, though the only area for which there is good evidence (north of Lake Awasa) is unusual, because flow is directed counter to the general southerly fall of the rift floor in the southern MER (see Fig 4.6 and Chapter 5). Little reliable information appears to exist concerning the volume of subsurface outflows.

4.4   Southern Afar

4.4.1   Surface hydrology

From the northern MER into southern Afar, surface hydrology is dominated by the River Awash. This is fed by tributaries mainly draining the flanks of the plateau to the west; the chief of these are the Kessem in the south and the Mille in the north of the area (Fig 2.5). For much of its course below the vicinity of Fantale, the Awash is incised in a gorge, though there are also some swampy areas where lakes existed during the late Quaternary highstands. Eventually in the Tendaho area, the Awash turns from a northward course to meander to the southeast through a number of small lakes (Gargon, Gamari and Afambo) before terminating in Lake Abbe ($\sim$230 m). These four lakes are rapidly shrinking as a result of the increasing abstraction of irrigation water from the Awash.

The only other lake of significant size in the region is Asal ($\sim$-156 m) in Djibouti. Although there are indications that this lake receives a groundwater contribution, the greater part of its inflow is provided by seawater which infiltrates for several kilometres along the active rift zone

in the Fiale area between the lake and the Gulf of Ghoubet. The lake maintains its water balance through an extremely high evaporation rate (of the order of 3000 mma^{-1}) which has resulted in the formation of an NaCl crust over much of the lake.

4.4.2   Hydrogeology

Southern Afar is a region in which the hydrogeology is very poorly known. However, since the Ethiopian part is a flat-lying area with only relatively isolated volcanic cones rising above the plain, it can be predicted that (away from the vicinity of the Ethiopian and Somalian plateaux) there will only be a low head driving regional flows, which will mostly be directed towards the Awash or Lake Abbe. Coupled to this, groundwater recharge is far from abundant owing to the arid climate. Borehole information on the hydrogeological map (Fig 4.6) reflects this in the form of deep water levels, and also shows from the yields that permeabilities are generally low, as elsewhere in the Eastern Rift. To some extent this is supported by the results of deep geothermal drilling at Tendaho, which so far has resulted in only low yields of steam (EIGS, pers. comm.)

In southwestern Djibouti, groundwater presumably flows to discharge in Lake Abbe. Further towards the east, the Asal depression is likely to act as a local sump for groundwaters, which in places appear to mix with seawater infiltrating from the Gulf of Ghoubet. Southeast of Asal, in the general area of Djibouti City, groundwater flow is assumed to be driven by the head resulting from recharge on the higher ground towards the border with Somalia, with discharge ultimately to the Gulf of Tadjourah.

Geothermal exploration in Djibouti has had mixed results. In the Hanle plain east of Abbe, two deep boreholes showed only minor loss of circulation during drilling and later gave water temperature profiles which showed little evidence of large-scale lateral flows (Zan et al, 1990). In the active rift zone to the northeast, on the other hand, there is evidence for circulation of cooler waters to considerable depths (for example to ~1000 m in Well A-5). There is prominent surface fissuring in this area, but temperature inversions of similar magnitude and depth are known from Olkaria and Aluto-Langano. Therefore the fissuring is unlikely to extend to great depth, and the deep circulation is more likely to be due to the higher enthalpy heat source beneath the Asal area compared to Hanle.

4.5   The hydrological and hydrogeological perspective

Mostly the surface hydrology of the Eastern Rift is straightforward in outline, with only minor complications resulting from some of the Ethiopian rivers which during floods can bifurcate to supply more than one lake. There is however an urgent need for better river gauging data in order that a more quantitative understanding of the water balance can be obtained for many of the lakes, and thereby the magnitude of any contribution they may be making to groundwater recharge.

Hydrogeological conditions in the rifts are clearly of relevance to the existence and manifestations of hydrothermal activity. The presence of the off-axis warm and hot springs can probably be attributed to the deep circulation promoted by the axially parallel faulting, especially the more major rift boundary faults. On the other hand, the often very deep water levels towards the rift axes, coupled with low permeabilities, means that high-enthalpy hydrothermal circulation is seldom able to discharge water at the surface. Hence the signs of classic geothermal areas such as geysering and sinter terraces are largely absent from the Eastern Rift.

CHAPTER 5

ISOTOPIC EVIDENCE
FOR WATER ORIGIN, MOVEMENT AND EVOLUTION

The rift valley environment, with lakes and altitude differences between rift flank and valley floor, provides a highly suitable opportunity for the use of oxygen and hydrogen isotopic techniques in the determination of subsurface hydrological processes. Ratios of $^{18}O/^{16}O$ and $^{2}H/^{1}H$ (normally expressed on the δ-scale: see Appendix B) are primarily affected by physical factors such as the temperature in the area of infiltration, and evaporation from surface water bodies. This makes O and H isotopes very effective tracers of groundwater origin and flowpaths. The presence or absence of the radioactive isotope tritium (^{3}H) indicates whether or not "young" (<30 years) water is present in groundwater sampled from springs or boreholes.

Carbon stable isotope ratios ($^{13}C/^{12}C$, also expressed on the δ-scale, see Appendix B) can reveal little about physical processes, but are much more important in terms of the geochemical evolution of groundwaters. In the EARS the copious flux of CO_2 has an important influence on groundwater chemistry, which requires an understanding of the carbon isotope systematics. Radiocarbon (^{14}C) can in principle be used as a residence time indicator for waters with ages from a few thousand to 40,000 years old, but its use is constrained in parts of the Eastern Rift by inputs of "dead" carbon of magmatic origin.

In Kenya the most comprehensive isotope work was carried out as part of the present research. In Ethiopia, much of the work was performed by the Scripps Institute of Oceanography and was originally reported and to some extent interpreted by Craig et al (1977). In Djibouti various workers have measured and interpreted isotopic data, principally Fontes et al (1980) and Verhagen et al (1992). The subject of isotopes in general will be considered primarily by topic and secondarily by area.

5.1 Oxygen and Hydrogen Stable Isotopes

5.1.1 Rainfall in the Eastern Rift

5.1.1.1   Kenya rift valleys

Rainfall samples were collected from 21 meteorological stations along the main KRV in January/February 1986. The station locations range from Magadi in the south to Lodwar near Lake Turkana in the north. $\delta^{18}O$ and δ^2H values are given in Table 5.1 and are plotted in Fig 5.1.   Data from three rainfall samples collected in 1985 in the Gregory Rift are also included in the figure.   A linear regression on the data revealed the following line:

$$\delta^2H = 5.56\ \delta^{18}O + 2.04 \quad (r^2 = 0.88) \tag{5.1}$$

This KRV meteoric line has a lower slope than that of the world meteoric line of Craig (1961), which has a slope of 8; this is probably because the rain evaporates as it falls. Additional support for the lower KRV slope is provided by other studies in Kenya. At Kericho between the main KRV and the Nyanza Rift a rainfall relationship with the following form was found based on 20 monthly samples (IAEA, 1971, 1973):

$$\delta^2H = 5.43\ \delta^{18}O + 7.30 \quad (r^2 = 0.71) \tag{5.2}$$

while in the Chyulu Hills of southeast Kenya a similar relationship was observed for 35 samples (Wright and Gunston, 1988):

$$\delta^2H = 5.68\ \delta^{18}O + 6.04 \quad (r^2 = 0.89) \tag{5.3}$$

This indicates that rather low slopes of the meteoric line for δ^2H versus $\delta^{18}O$ are found in Kenya as a whole and are not confined to rainfall within the rift valleys. However, rather depleted water from the Malewa River which rises in the ~4000 m Nyandarua (Aberdare) Mountains would actually plot on the world meteoric line (Fig 5.3). This implies that the modifying influences are restricted to lower altitudes, as might be expected because of the hotter conditions.

The high topographic relief of the KRV makes it likely that significant variations with altitude in the mean isotopic composition of rainfall will occur. This was investigated for the rainfall

Table 5.1   Results of stable isotopic analysis of rainfall samples collected from meteorological stations in the KRV.

Station	Coords	Alt. masl	Date	Amt. mm	δ^2H ‰	$\delta^{18}O$ ‰
Lodwar	35°36′E,3°7′N	550	4/3/86	28.9	+19	+1.9
"	"	"	24/4/86	33.4	-21	-4.6
Lockichar	35°40′E,2°23′N	880	5/3/86	32.3	-7	-2.0
"	"	"	7/3/86	23.3	-1	-1.6
Maralal	BM 43 21	2000	18/3/86	4.4	-31	-4.2
"	"	"	21/4/86	10.2	-16	-2.2
Nginyang	AM 69 05	900	7/3/86	16.1	-1	+0.3
"	"	"	22/3/86	5.4	0	-0.2
Kabarnet	ZR 05 54	2050	7/3/86	10.1	-4	-1.6
"	"	"	10/4/86	16.8	-47	-7.9
Bogoria	AL 76 38	1000	10/4/86	17.0	-19	-4.0
"	"	"	20/4/86	19.2	-5	-2.6
Chemogock	ZR 30 06	1550	18/3/86	8.0	-20	-5.3
"	"	"	7/4/86	25.0	-5	+0.9
Majimoto	AL 72 79	1150	20/3/86	10.7	+2	+0.7
"	"	"	10/4/86	39.7	-11	-0.3
Eldama Ravine	ZR 04 04	2100	18/3/86	23.3	0	-2.0
"	"	"	?	?	+3	-1.9
Mabroukie	BJ 41 79	2340	21/3/86	13.7	-14	-3.9
"	"	"	23/4/86	18.4	-41	-7.2
Nakuru	AK 73 69	1850	20/3/86	2.0	-4	-1.4
"	"	"	18/4/86	11.0	-5	-1.3
Gilgil	BK 02 45	2000	12/4/86	4.2	-3	-0.3
"	"	"	23/4/86	34.7	-53	-8.2
Naivasha	BK 14 20	1920	10/3/86	22.2	-7	-4.2
"	"	"	10/4/86	16.1	-39	-6.4
S Kinangop	AK 42 21	2550	10/3/86	8.8	-4	-2.3
"	"	"	22/4/86	49.0	-23	-4.9
Kijabe Stn	BJ 31 98	2200	7/3/86	8.4	-39	-5.8
"	"	"	23/4/86	7.6	-36	-5.6
Ohokurto	ZQ 16 36	2760	18/4/86	21.5	-47	-9.0
"	"	"	20/4/86	22.2	-18	-4.8
Narok	ZP 20 80	1900	5/3/86	14.3	+5	-0.2
"	"	"	11/4/86	6.6	-30	-6.8
Naroosura	ZP 18 30	1900	6/4/86	?	-10	-3.2
"	"	"	10/4/86	-	-64	-10.2
Kisames	BJ 37 37	1800	18/3/86	3.2	+12	+1.7
Olorgesailie	BJ 16 26	1000	21/3/86	8.4	-8	-0.3
"	"	"	7/4/86	11.4	-14	-2.1
Magadi	AH 98 91	600	21/3/86	16.3	-7	+0.8
"	"	"	31/3/86	2.6	+22	+5.2

$$\delta^2H = 5.56 \; \delta^{18}O + 2.04$$
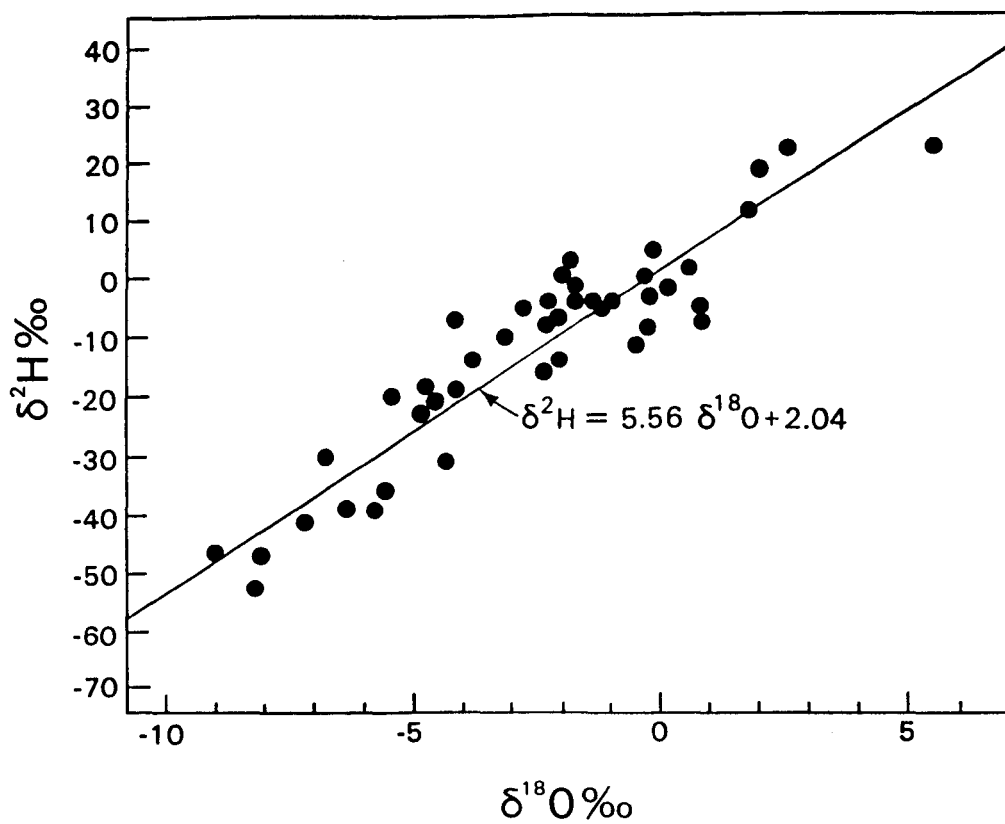
Fig 5.1 Plot of δ^2H vs $\delta^{18}O$ for rainfall from collection stations in the main KRV.

samples by plotting $\delta^{18}O$ and δ^2H against altitude. Taking altitude as the controlled variable in each case the following regression lines were obtained:

$$\delta^{18}O = -0.0029 \text{ x altitude (m)} + 1.99 \qquad (r^2 = 0.32) \qquad (5.4)$$

$$\delta^2H = -0.0148 \text{ x altitude (m)} + 10.82 \qquad (r^2 = 0.24) \qquad (5.5)$$

The rather poor correlations are considered to be due largely to the limited number of samples obtained from each station. Individual rainfall events at a given station can give widely differing isotopic results, as shown in Table 5.1, because evaporation and temperature effects will be different for different rainfall events. Many samples from a given station would however be expected to have isotopic compositions which fall around a mean, dependent mainly on the altitude.

The change in $\delta^{18}O$ is estimated as $-0.29‰$ for every 100 m of ascent from equation 5.4. This can be compared with values obtained elsewhere: $-0.2‰$ (Sweden), $-0.4‰$ (French Alps), -0.28 (Czechoslovakia), $-0.26‰$ (Nicaragua), $-0.18‰$ (Cameroon), and $-0.16‰$ for Greece (data from sources quoted in Darling and Lardner, 1985). Few studies of deuterium variation with height are available but it is assumed that if the figure for oxygen is accepted, then the estimated variation of $-1.5‰$ per 100 m for δ^2H from the above regression can also be accepted because of the close correlation between $\delta^{18}O$ and δ^2H demonstrated by the KRV meteoric line.

5.1.1.2 *Main Ethiopian Rift*

Very few rainfall samples have been collected in the MER, and no systematic records exist. However, the IAEA collection station at Addis Ababa has been operating intermittently since 1961 and a sizeable database now exists. The Addis Ababa meteoric line has the following form based on 93 months' data (IAEA, 1992):

$$\delta^2H = 6.95\ \delta^{18}O + 11.51 \qquad (r^2 = 0.92) \qquad (5.6)$$

A database of this size also means that the annual weighted mean values of $+2‰$ δ^2H and $-1.3‰$ $\delta^{18}O$ are likely to be highly representative for the area around the station. However, the altitude of Addis Ababa at 2360 m asl is significantly above the level of the MER floor and lower flanks, and it may be questioned how appropriate the figures are for use in the MER.

5.1.1.3   Southern Afar

As with the MER, no rainfall isotopic data appear to exist for the Ethiopian part of this area.
In Djibouti there is also a lack of published data, though on consideration of the available
evidence from groundwaters, Fontes et al (1980) arrived at a meteoric line with the following
form:

$$\delta^2H = 8 \, \delta^{18}O + 0 \qquad\qquad\qquad\qquad (5.7)$$

However, it is far from clear that this slope represents the true situation for rainfall in Afar.

5.1.1.4   Rainfall - general comment

Rainfall isotope data for all the rift areas is scant. Even in the KRV, where the slope of the
meteoric line is probably best-defined, information is lacking on long-term weighted means.
Elsewhere, even the meteoric slopes are not necessarily representative. Fortunately, despite
the fact that evaporative processes are of considerable importance in the modification of EARS
waters, there is sufficient "internal" evidence from the ground and surface waters themselves
to justify the use of stable isotopes in tracing their relationships without needing to know the
exact details of their meteoric origins.

5.1.2   Ground and surface waters in the Gregory Rift

The Gregory Rift is regarded here as including the area stretching from Lake Magadi in the
south to Lake Bogoria in the north. Analytical results are included in Tables 5.2a (wells and
boreholes), 5.2b (cool springs), 5.2c (hot springs), 5.2d (rivers and streams), 5.2e (lakes), 5.2f
(deep geothermal waters) and 5.2g (fumarole steam condensates). These tables also include
data from the Turkana and Nyanza Rifts. Gregory Rift sampling locations are shown in Figs
5.2a-e.

Fig 5.3 provides an overview δ-plot of Gregory Rift waters, though it does not include high-
enthalpy geothermal waters or fumarole steam condensates, which would complicate the
diagram considerably. Despite this there is a wide range of waters, from highly depleted as
in the case of the Malewa River (K79) to highly enriched, as shown by Lakes Bogoria and
Magadi in particular. A clustering of waters around the composition -4‰ $\delta^{18}O$, -20‰ δ^2H
reflects the average meteoric input, with the more depleted waters representing some of the

Table 5.2a Stable isotopic composition of water collected from boreholes and wells in the Kenya Rifts. Results in permil with respect to SMOW (H & O) and PDB (C).

Site Name	Site No.	Temp °C	δ^2H	$\delta^{18}O$	$\delta^{13}C$-DIC
Oltepesi[a]	K22	-	-25	-4.2	- 7.4
C4635, RVA[a]	K25	35	-20	-5.3	- 7.4
Suswa, S.Slope[a]	K30	-	+ 8	+0.6	-
Emerit[b]	K72	37	-24	-4.8	-
C4989[b]	K80	21	+18	+3.7	-
C567[b]	K81	22	+22	+4.5	- 0.4
C4178[b]	K82	20	-24	-4.1	-13.5
C563[b]	K83	26	+32	+5.6	-
C1487[b]	K84	21	-11	-1.9	-
C5002[b]	K85	20	-22	-4.4	-
C1063[b]	K86	26	+19	+3.7	-
C1488[b]	K87	26	-29	-3.7	-
C467[b]	K88	24	-11	-1.9	-
C580[b]	K89	25	+ 6	+0.3	-
C814[b]	K90	18	-20	-4.2	-
C570, Kanyamwi[b]	K92	22	-17	-4.7	- 2.5
C3784[c]	K93	23	-17	-3.5	-
C307[b]	K94	19	- 8	-1.1	-
C1190[b]	K95	24	-16	-3.6	-
P65, Kinangop[c]	K96	23	-24	-4.7	-12.0
C3955[b]	K97	23	-18	-4.0	-
C4179[b]	K99	26	-24	-4.1	-
C1404, Ndabibi[c]	K100	26	-28	-4.6	-10.6
Nakuru No.7[c]	K118	28	-18	-2.8	- 8.7
C431, ADC Fm[c]	K121	37	-27	-5.0	- 0.5
C1798, ADC Fm[c]	K122	35	-28	-4.8	-
DEL, Soysambu[c]	K124	32	-24	-3.8	- 2.7
C1990, Soysambu[c]	K125	28	-23	-3.5	0.0
C3525, Mosiro[c]	K129	-	-28	-4.6	-
Kampi Ya Samaki[d]	K131	-	+27	+5.5	-
Kampi Ya Samaki[g]	K131	-	+25	+4.9	- 6.2
C6364, Chesirimion[d]	K132	-	-11	-2.6	-14.9
C6364, Chesirimion[e]	K132	34	-10	-2.3	-13.8
C3437, Tangulbei[d]	K133	30	-11	-2.0	-13.7
D7, Kokwo Toto[d]	K134	28	- 9	-1.8	-14.6
D4b, Orus solar[d]	K135	28	-12	-1.9	-15.8
D4a, Orus hand[d]	K136	28	-10	-1.9	-15.4
D1, Katangora[d]	K137	36	-10	-2.1	- 9.6
Napeiton[d]	K198b	-	-18	-3.3	- 8.2
Napeiton[g]	K198b	37	-23	-3.7	-
Kositei Proj[d]	K200	-	+ 9	+0.5	-
Kositei Miss[d]	K201	-	-12	-2.7	-
C6363, Kositei[d]	K202	36	-15	-2.9	-11.6
C3868, Nginyang Sch[e]	K203	-	-11	-2.5	- 9.9
Nginyang Poly[e]	K204	36	-11	-2.3	-10.0
Nginyang Poly[g]	K204	34	-12	-2.8	-10.6
C3470, Chemolingot[e]	K205	38	-17	-2.9	-11.7
Parkati[g]	K243	-	-22	-3.9	-
Kanukurdio[b]	K08U*	33	-12	-2.8	-

Year of sampling: [a] - 1985; [b] - 1986; [c] - 1987; [d] - 1988; [e] - 1989; [g] - 1991
*UNDP data

Table 5.2b Stable isotopic composition of waters collected from cool (<40°C) springs in the Kenya Rifts. Results in permil with respect to SMOW (H & O) and PDB (C).

Site Name	Site No.	Temp °C	δ^2H	$\delta^{18}O$	$\delta^{13}C$-DIC
Mayers Farm[a]	K28	28	-28	-4.8	-16.5
Kariandusi[a]	K36	23	-24	-3.7	-
Meroronyi[a]	K37	30	-19	-3.7	-
Chamuka[a]	K39	29	-20	-4.5	-
Kanyamwi[b]	K91	24	-13	-3.9	-
Kokot[c]	K26	-	-35	-5.3	-
Hell's Gate seep 1[c]	K103	-	+ 1	+4.0	-
Hell's Gate seep 2[c]	K104	20	+ 7	+4.1	-11.0
Hell's Gate seep 3[c]	K105	-	+ 8	+2.5	-
Hell's Gate seep 6[c]	K108	23	+ 2	+3.5	-
Bala	K57	36	-17	-3.6	-
Kapedo[b]	K50	27	+ 4	-0.7	-
Nginyang-Kapedo[d]	K138	36	- 2	-0.3	-
Churo[d]	K139	28	-15	-3.0	-11.6
Churo[e]	K139	-	-15	-3.1	-12.5
Ebirisat[d]	K140	38	-16	-3.1	-14.9
Nangarwa[e]	K191	-	-16	-3.3	-11.7
Amaya[e]	K192	-	-15	-3.2	-10.6
N. Samburu Gates[e]	K193	-	-10	-1.3	- 6.6
Kachurkolh[e]	K194	31	+ 9	+1.6	- 0.5
Kalnangi[e]	K195	32	- 4	-0.9	- 2.7
Amakat[e]	K196	-	+54	+12.0	- 9.3
S. Nangarabat[e]	K197	31	0	-0.5	- 2.8
Napeiton[e]	K198a	33	-17	-3.0	-
Nasaken[e]	K199	31	-10	-1.7	- 8.7
Eliye[b]	K09U	32	-14	-2.9	-
Eliye[g]	K240	35	-13	-3.2	-10.1
Eliye N[g]	K241	37	-11	-2.9	-10.6
Tum[g]	K244	-	-25	-5.2	-

Year of sampling: [a] - 1985; [b] - 1986; [c] - 1987; [d] - 1988; [e] - 1989; [g] - 1991

Table 5.2c   Stable isotopic composition of waters collected from hot springs in the Kenya Rifts. Results in permil with respect to SMOW (H and O) and PDB (C).

Site Name	Site No.	Temp. °C	δ^2H	$\delta^{18}O$	$\delta^{13}C$-DIC
Little Magadi[a]	K3	85	- 6	-0.9	-
Little Magadi[e]	K3	83	- 3	-0.7	- 3.3
Magadi NW[a]	K9	45	-17	-3.1	+ 0.9
Magadi N[b]	K73	63	- 2	-0.1	-
Magadi NE[a]	K11	67	- 7	-1.0	-
Magadi E[a]	K13	40	-16	-2.4	-
Bird Rock [a]	K16	41	-14	-2.4	-
Magadi S[a]	K18	45	-23	-2.5	-
Majiyamoto[a]	K34	52	-27	-5.2	-
Hell's Gate seep 4[c]	K106	52	+10	+3.2	-
Hell's Gate seep 7[c]	K109	72	+11	+3.9	-
Kijabe[c]	K26	43	-19	-4.2	-12.6
Kariandusi[c]	K35	40	-14	-3.7	- 8.0
Elmenteita[a]	K41	43	- 7	-1.1	-
Bala[a]	K53	72	-16	-3.0	- 1.7
Bala[a]	K55	58	-18	-2.5	- 3.3
Bala[a]	K56	75	- 14	-3.7	-
Kureswa[g]	K256	62	-19	-4.5	- 6.7
Bogoria W[b]	K86	96	- 3	-1.1	-
Bogoria W[d]	K86	96	- 4	-0.6	-
Bogoria SW[b]	K64	45	- 7	-3.5	-
Bogoria SE[b]	K61	97	+ 1	+0.6	-
Bogoria SE[g]	K26	97	0	-2.6	- 1.5
Lorusio[b]	K45	81	-23	-3.1	-
Lorusio[d]	K45	82	-16	-3.4	- 2.6
Lorusio[g]	K45	81	-15	-3.6	-
Kapedo[b]	K48a	50	- 7	-3.5	-
Kapedo[d]	K48a	50	+ 2	-0.5	- 4.1
Kapedo[e]	K48a	50	- 2	-0.9	- 3.3
Kapedo[d]	K48b	50	- 3	-0.6	-
Kapedo[d]	K48c	50	- 1	-0.5	-
Ol Kokwe Island[d]	K71a	96	+15	+5.9	-
Ol Kokwe Island[b]	K71b	94	+ 7	+1.3	-
Ol Kokwe Island[d]	K71b	96	+ 4	+3.5	-
Ol Kokwe Island[d]	K71b	96	+11	+3.7	-
SL26/2[e]	K183	45	- 3	-0.7	-
SL27/5[e]	K184	45	- 2	-0.9	-
Suguta SV3a[e]	K185	68	-13	-2.7	- 4.2
Suguta SV3b[e]	K186	64	-14	-2.8	-
Kamuge[e]	K187	50	-19	-3.7	- 4.7
Kageinya[e]	K188	68	+ 9	+1.7	- 4.0
Namarunu[e]	K189	66	+14	+3.0	- 0.9
Logipi NW[e]	K190	61	+15	+2.2	- 1.2
Elboitong S[g]	K236	95	+21	+3.6	- 1.6
Elboitong N[g]	K237	92	+20	+3.7	- 1.5
Logipi NE[g]	K238	70	+14	+2.3	- 2.0
Central Island[g]	K239	71	+36	+5.8	-
Loyangalani[g]	K242	40	-21	-4.0	-12.3

Year of sampling: [a] - 1985;   [b] - 1986;   [c] - 1987;   [d] - 1988;   [e] - 1989;   [g] - 1991

Table 5.2d Stable isotopic composition of waters collected from rivers and streams in the Kenya Rifts. Results in permil with respect to SMOW.

Site Name	Site No.	Date	δ^2H	$\delta^{18}O$
Ewasongiro 1	K20	7/11/85	- 6	-1.5
Ewasongiro 2	K32	16/11/85	-12	-2.9
Oloibotort	K21	7/11/85	-22	-4.2
Kijabe Str	K27	17/11/85	-18	-4.3
Ngosorr	K40	3/4/86	-16	-4.6
Kapedo	K52	5/4/86	-13	-2.4
Bogoria SE Str	K62	19/4/86	-12	-2.8
Bogoria S Str	K63	19/4/86	-13	-3.2
Malewa	K79	4/5/86	-62	-9.0
Ndau	K141	18/9/88	-12	-3.0
Tigeri	K142	4/5/86	-38	-6.9
Tigeri	K142	18/9/88	-12	-3.0
Molo	K143	30/9/88	-11	-2.9
Arabel	K144	30/9/88	-10	-2.4
Itwa	K145	30/9/88	- 7	-2.0
Kabarmel	K146	30/9/88	- 7	-1.8
Mukutan	K147	18/9/88	+ 1	+0.6
Nginyang	K148	23/9/88	-11	-2.7
Cheptopokwo	K149	23/9/88	- 6	-1.4
Suguta 1	K206	18/9/89	+ 9	+2.5
Suguta 2	K207	18/9/89	+ 5	+1.3
Suguta 3	K208	18/9/89	+ 5	+1.4
Suguta 4	K209	18/9/89	+ 7	+2.3
Suguta trib.	K210	2/10/89	- 1	0.0
Gerau	K211	1/10/89	+ 2	+0.1
Amaya	K212	19/9/89	- 8	-1.1
Namarangule	K213	26/9/89	+10	+1.8
Naliyo	K214	26/9/89	+13	+0.3
Kerio	K245	15/6/91	+ 5	+0.8

Table 5.2e   Stable isotopic composition of waters collected from lakes in the Kenya Rifts. Results in permil with respect to SMOW

Site Name	Site No.	Date	δ^2H	$\delta^{18}O$
Magadi	K19	11/11/85	+17	+10.4
Naivasha	K24	20/11/85	+34	+ 5.6
Naivasha	K24	28/4/86	+36	+ 6.6
Naivasha	K24	23/10/90	+20	+ 2.9
Naivasha	K24	19/6/91	+22	+ 4.1
Elmenteita	K270	21/10/90	+32	+ 6.9
Nakuru	K102	/5/87	+ 8	+ 4.5
Nakuru	K102	21/10/90	+29	+ 6.5
Victoria (Homa Limeworks)	K58	7/4/86	+26	+ 4.2
Victoria (Homa Bay)	K60	7/4/86	+23	+ 4.1
Bogoria*		86	+48	+ 9.5
Baringo C	K70	20/4/86	+47	+ 8.8
Baringo C	K150	19/9/88	+21	+ 2.8
Baringo N	K216	29/9/89	+32	+ 5.3
Baringo S	K217	29/9/89	+34	+ 5.0
Baringo C	K150	5/6/91	+40	+ 7.6
Baringo C	K150	17/6/91	+42	+ 6.7
Turkana S	K215	27/9/89	+43	+ 6.8
Turkana N	K246	14/6/91	+36	+ 5.9
Turkana C	K247	14/6/91	+35	+ 5.8

*Analysis from Cioni et al (1992)

PAGE MISSING IN ORIGINAL

Table 5.2f   **Stable isotopic composition of geothermal well waters from the southern KRV.**

Geothermal well	Site No	Well-field	Sample type	$\delta^{18}O$ ‰	δ^2H ‰
Olkaria OW-2	K110	O. East	T	+2.1	+3
Olkaria OW-5	K116	O. East	T	+3.7	+18
Olkaria OW-16	K113	O. East	T	+3.1	+10
Olkaria OW-21	K604	O. East	T	+2.8	+8
Olkaria OW-22	K112	O. East	T	+2.7	+13
Olkaria OW-23	K114	O. East	T	+3.6	+13
Olkaria OW-26	K111	O. East	T	+2.6	+11
Olkaria OW-703[1]	K606	O. Northeast	T	+4.5	+34
Olkaria OW-705[1]	K610	O. Northeast	T	+3.7	+25
Olkaria OW-706[1]	K611	O. Northeast	T	+2.2	+21
Olkaria OW-715	K259	O. Northeast	T	+1.0	+4
Eburru EW-1[1]	K502	Eburru	T	-2.1	-9
Eburru EW-1[1] 1500m	K502	Eburru	D	-1.4	-4
Eburru EW-1[1] 1600m	K502	Eburru	D	-2.5	-7
Eburru EW-1[1] 1850m	K502	Eburru	D	+5.2	+10
Eburru EW-1[1] 2250m	K502	Eburru	D	0.0	-5
Eburru EW-1[1] 2400m	K502	Eburru	D	-0.9	-7

T - total fluid   D - depth sample

[1] sample collected by Kenya Power and Light Company

Table 5.2g   Stable isotopic composition and ammonia content of fumarolic steam condensates from sites in the KRV.

Site Name	Site No	Temp °C	pH	NH$_4$ mgl^{-1}	δ^{2}H ‰	δ^{18}O ‰
Suswa F12[g]	K258	94.1	4.35	0.39	-2	-3.3
Domes F15[c]	K127	92.2	-	-	-38	-5.5
Longonot F23[c]	K128	-	-	-	-49	-8.0
Olkaria OF-W[c]	K123	-	-	-	-16	-4.0
Olkaria OF-1[f]	K261	92.6	3.95	-	-4	-2.0
Olkaria OF-4[f]	K262	94.6	4.85	-	-3	-3.1
Olkaria OF-13[f]	K263	95.1	5.45	-	-6	-2.6
Olkaria OF-14[f]	K264	93.8	4.05	-	+5	-4.0
Olkaria OF-15[f]	K265	90.8	-	-	-17	-4.1
Olkaria OF-16[f]	K266	95.7	4.45	-	-3	-1.9
Olkaria OF-20[f]	K267	78.3	2.75	-	-19	-10.0
Eburru EF-1[f]	K270	-	5.75	-	-31	-8.0
Eburru EF-2[c]	K119	92.0	-	-	-37	-7.9
Eburru EF-13[c]	K120	-	-	-	-75	-13.5
Arus AR1[g]	K257	95.0	4.30	4.20	-24	-7.3
Ol Kokwe OK1[d]	K152	95.8	5.90	38.2	-18	- 3.6
Korosi KR10[d]	K153	85.5	5.60	-	-70	-10.6
Korosi KR12[d]	K154	95.7	5.05	4.0	-38	- 7.1
Korosi KR16[d]	K155	94.0	5.30	4.3	-48	- 8.8
Korosi KR18[d]	K156	96.4	-	5.2	-55	- 9.5
Korosi KR19[d]	K157	95.9	4.90	9.0	-50	- 9.0
Korosi KR21[d]	K158	90.1	6.00	6.8	-51	- 8.6
Korosi KR23[d]	K159	95.4	3.60	8.5	-33	- 6.5
Korosi KR23[e]	K159	96.0	5.70	10.6	-42	- 7.6
Korosi KR24[d]	K160	82.5	6.45	-	-48	- 8.4
Korosi KR27[d]	K172	-	-	10.2	-60	-13.2
Korosi KR32[d]	K161	91.5	6.05	-	-53	- 9.6
Korosi KR34[d]	K162	91.0	5.30	31.5	-112	-18.2
Korosi KR34[e]	K162	94.5	-	-	-99	-15.9
Paka PK1a[d]	K163	96.2	-	0.08	+ 7	- 2.3
Paka PK1a[e]	K163	95.0	4.10	0.09	+ 2	- 2.4
Paka PK1b[d]	K164	91.2	-	-	+10	- 1.2
Paka PK1c[d]	K165	91.0	-	-	+ 2	- 2.8
Paka PK3[d]	K173	-	-	2.5	-15	- 2.4
Paka PK4a[d]	K166	95.3	4.55	1.3	-14	- 4.3
Paka PK4b[d]	K167	95.5	4.50	<0.05	-18	- 4.0
Paka PK6e[d]	K174	-	-	0.34	- 5	- 2.8
Paka PK7a[d]	K168	94.0	3.90	<0.05	-13	- 3.5

Table 5.2g (contd)

Site name	Site No	Temp °C	pH	NH$_4$ mgl^{-1}	δ^2H ‰	δ^{18}O ‰
Paka PK7b[d]	K169	91.0	5.00	-	-22	- 5.2
Paka PK7c[d]	K170	91.0	5.25	-	-21	- 4.8
Paka PK7d[d]	K171	92.0	4.90	<0.15	-26	- 5.7
Paka PK7e[d]	K175	-	-	0.30	-36	- 7.1
Paka PK20a[d]	K176	-	-	3.6	-17	- 4.3
Paka PK20b[d]	K177	-	-	2.0	-17	- 4.5
Paka PK23[d]	K178	-	-	1.1	-18	- 4.9
Paka PK31[d]	K179	-	-	1.7	-21	- 5.0
Paka PK39[d]	K180	-	-	0.90	-69	-11.9
Paka PK42[d]	K181	-	-	1.5	-52	- 9.3
Paka PK49[d]	K182	-	-	0.05	-76	-13.4
Silali SL4[e]	K218	96.5	6.25	4.8	-28	- 5.5
Silali SL7[e]	K219	95.3	3.90	0.03	- 6	- 2.6
Silali SL11[e]	K220	94.4	5.05	10.3	-52	- 8.0
Silali SL14[e]	K221	95.8	4.15	1.42	-22	- 5.8
Silali SL15[e]	K222	96.6	4.20	2.22	-18	- 4.6
Silali SL16[e]	K223	96.1	4.55	0.07	-27	- 4.7
Silali SL19[e]	K224	95.7	4.70	6.54	-50	- 7.1
Silali SL22[e]	K225	92.3	4.05	0.37	-86	-11.0
Emuruang. EM7[e]	K226	90.6	4.53	0.53	-13	- 6.1
Emuruang. EM9/23[e]	K227	92.6	4.30	0.48	-10	- 5.2
Emuruang. EM9/27[e]	K228	94.7	4.75	0.70	-13	- 5.4
Emuruang. EM9/40[e]	K229	90.6	5.85	0.47	- 2	- 3.3
Emuruang. EM16/2a[e]	K230	90.0	5.60	1.35	-19	- 4.4
Emuruang. EM16/2b[e]	K231	90.4	5.00	0.66	-22	- 5.0
Emuruang. EM20a[e]	K232	96.0	4.60	1.98	-27	- 6.0
Emuruang. EM20b[e]	K233	95.6	4.85	1.89	-25	- 5.8
Emuruang. EM20c[e]	K234	92.4	5.12	2.32	-54	- 9.2
Kakorinya BR11[e]	K235	96.0	-	3.04	- 5	- 3.1
Kakorinya BR5[g]	K248	92.8	-	-	-30	-5.8
Kakorinya BR4[g]	K249	94.0	-	3.98	-19	-4.2
Kakorinya BR18[g]	K250	94.4	-	3.39	-17	-3.7
Kakorinya BR29[g]	K251	92.9	-	-	-22	-4.3
Central Island[g]	K254	97.3	-	116	+11	+0.6
Central Island[g]	K255	97.4	-	108	+17	+0.9
North Island[g]	K252	95.5	-	0.9	-18	+0.1
North Island[g]	K253	95.9	-	204	-13	+1.3

Year of sampling [c] - 1987, [d] - 1988, [e] - 1989, [f] - 1990, [g] - 1991
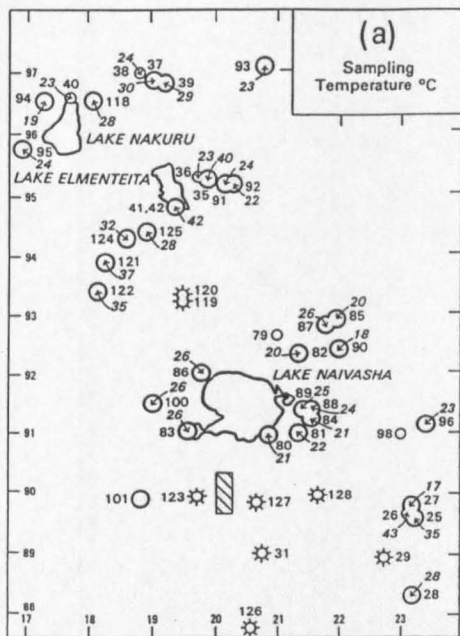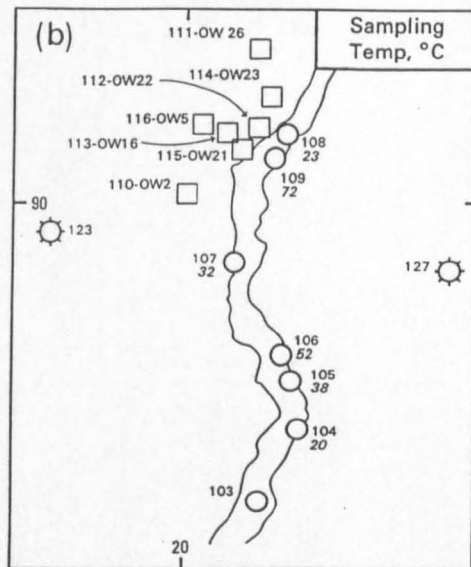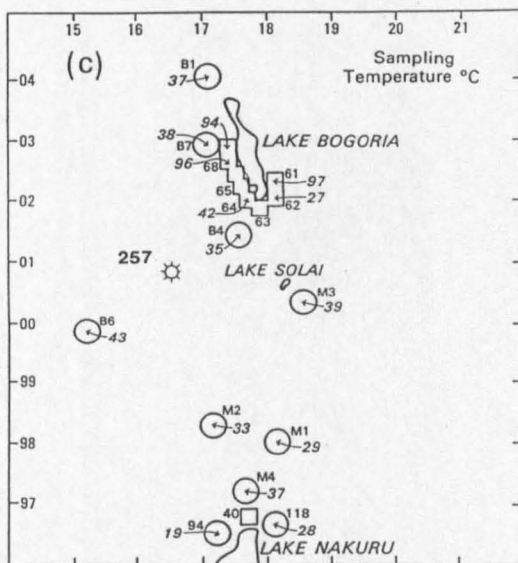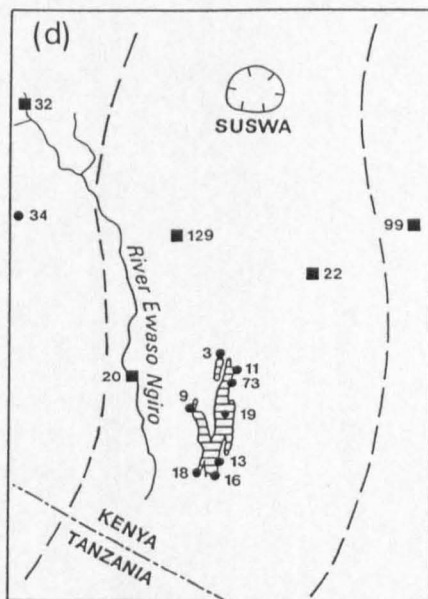
Fig 5.2   Sampling locations in the Gregory Rift. a - Naivasha-Nakuru area, b -
Olkaria East and Hell's Gate, c - Bogoria area, d - Magadi. a, b and c
also give sampling temperatures.
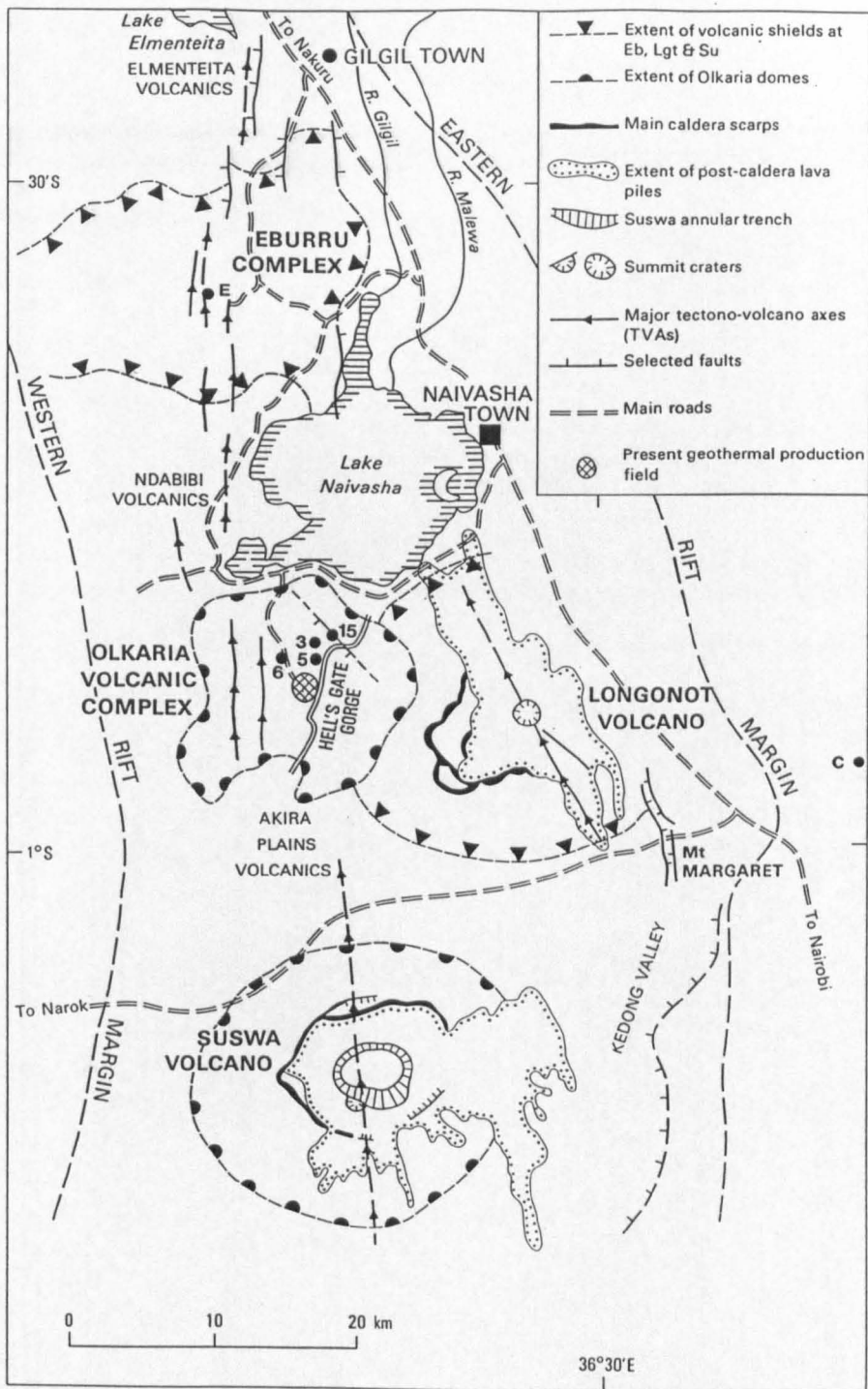
Fig 5.2 (contd) (e) the location of the Olkaria East geothermal wellfield and individual wells of the Olkaria Northeast and Eburru wellfields are shown. The numbers 3, 5, 6 and 15 refer to wells OW−703, 705, 706 and 715, while E refers to EW-1. The location of the Carbacid CO_2 borehole (C) at Kerita beyond the eastern rift escarpment is also shown.
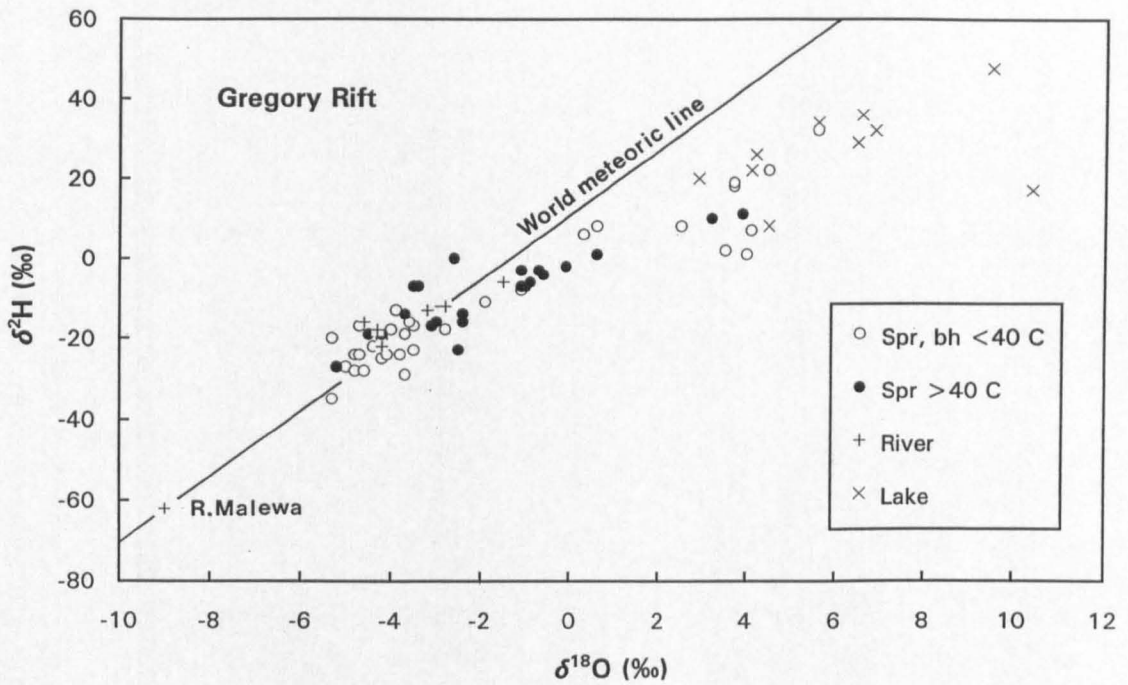
Fig 5.3   Plot of δ^2H vs $\delta^{18}O$ for ground and surface waters in the Gregory Rift, excluding geothermal well waters and fumarole steam condensates.

higher-altitude rift wall recharge, e.g. Oltepesi, RVA, Emerit, Kinangop and the ADC farm wells (K22, 25, 72, 96, 121, 122). Isotopically heavier waters are the result of evaporative concentration in one form or another, as will be explained below mainly on a surface catchment basis.

5.1.2.1 Magadi

The Magadi basin is somewhat hydrologically isolated from the remainder of the Gregory Rift by a long (~ 100 km) stretch of the valley without significant ground or surface water. Hot springs occur at many points around the lake (Fig 5.2). When these are plotted as δ^2H vs $\delta^{18}O$ (δ-diagram) in Fig 5.4, they split into two main groups relative to the cool boreholes of the region (Oltepesi and Emerit): samples more enriched in heavy isotopes from Little Magadi (K3), Northeastern and Northern Lagoons (K67, 73), and samples enriched to a lesser extent from Graham's, Bird Rock, Southwestern and Northwestern Lagoons (K13, 16, 18, 9). This suggests that the groups have different origins.

For the more depleted springs, an origin from the same kind of water as sampled in the cool boreholes is indicated, with some minor modification by evaporation, perhaps because of an element of recycling in the vicinity of the springs, which have a high TDS content (Chapter 6). The northern spring group however has a *lower* TDS content and cannot therefore be a more-evaporated version of the other group. It was suggested by Eugster (1980) that the Magadi springs in general are fed by water infiltrating from the Ewasongiro River some 20 km to the west, as it proceeds towards Lake Natron in Tanzania. Certainly, in the lower part of its course (K20) the Ewasongiro has a similar isotopic composition to the northern springs, but it is surprising that this does not also affect the composition of the northwestern spring K9, which is closer to the supposed source. It is also difficult to see how the northern and northeastern springs could be affected by a westerly source of recharge.

However, Lake Naivasha may provide a source of recharge, as this lake is known to have a large subsurface outflow (see below). This alternative would explain rather better why only the northern springs are affected, and would also account for the enriched isotopic composition but lower TDS values in this group. The aridity of the area between Naivasha and Magadi may explain why the lakewater signal has not been more attenuated by influxes of unmodified meteoric water.

Hillaire-Marcel and Casanova (1987) postulated the existence of palaeowater beneath Magadi,
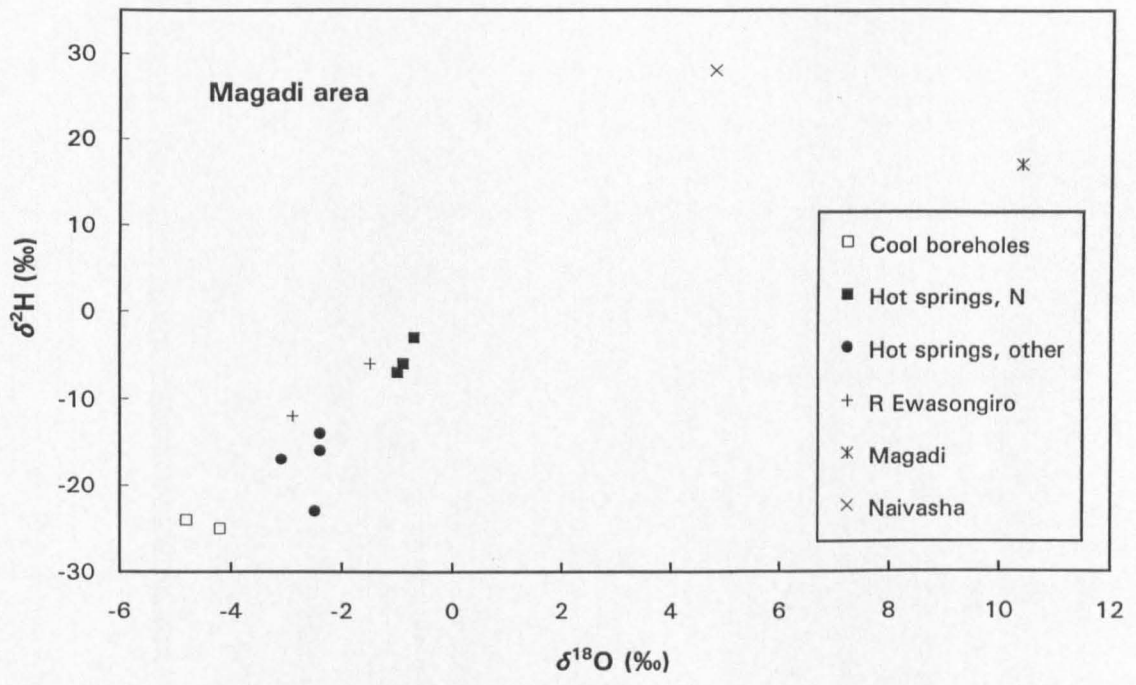
Fig 5.4   Plot of δ^2H vs $\delta^{18}O$ for waters in the Magadi area, southern Gregory Rift.

but this interpretation was based on a enveloping line highly dependent on a single analysis in one of their figures (Fig 12), and cannot be regarded as an adequate indication that a depleted water exists at depth. None of the isotopic measurements made on waters of the Magadi area by these researchers or during the present study have encountered compositions more depleted than those of present-day recharge, which might otherwise be expected if palaeowaters were a significant component in the spring circulation.

5.1.2.2   Naivasha

The Naivasha catchment has two main river inputs, the Malewa and the Gilgil. The former is more important to the maintenance of the lake. The headwaters of this river lie in the Nyandarua (Aberdare) Mountains at altitudes of up to 4000 m asl, and this no doubt accounts for the depleted stable isotopic content measured for site K79 on the river. This has important implications for an isotopic balance on the lake, which is not saline and therefore must have a subsurface outflow. Since the lake is shallow and of low volume, its isotopic composition changes with time, as inflow and evaporation fluctuate around a long-term mean. These isotopic changes are predictably reflected in lake chemistry (see 6.1.4 below).

The typical Rift-wall composition of -30‰ δ^2H, -5‰ $\delta^{18}O$ does not accord well with the isotope-altitude relationships propounded in 5.1.1 above, but these are necessarily tentative and probably more important as *relative* indicators of altitude. In the Gregory Rift unmodified meteoric water generally appears to range from -35 to about -18‰ δ^2H, an altitude difference of some 700 m. The corresponding $\delta^{18}O$ range is -5.3 to -3.5‰ $\delta^{18}O$ suggesting a difference of 600 m.

The stable isotopic content of most of the groundwater sampled in this and other parts of the Eastern Rift can be explained in terms of a mixing series between directly-recharged meteoric water and lake water. While there are many examples of waters with compositions close to the meteoric end member, there are few close to the lake end member. However, some of the wells around Naivasha are profoundly affected by lakewater, for example C4989, C567, C563, C1063 and C580 (K80, 81, 83, 86, 89). The general absence of boreholes to the north and south of the lake makes it difficult to tell directly on piezometric grounds whether or not the lake is discharging. However, the geothermal manifestations of the area provide some very strong indications that there is a significant flow away from the lake and there is not simply some local mixing of water adjacent to the lake.
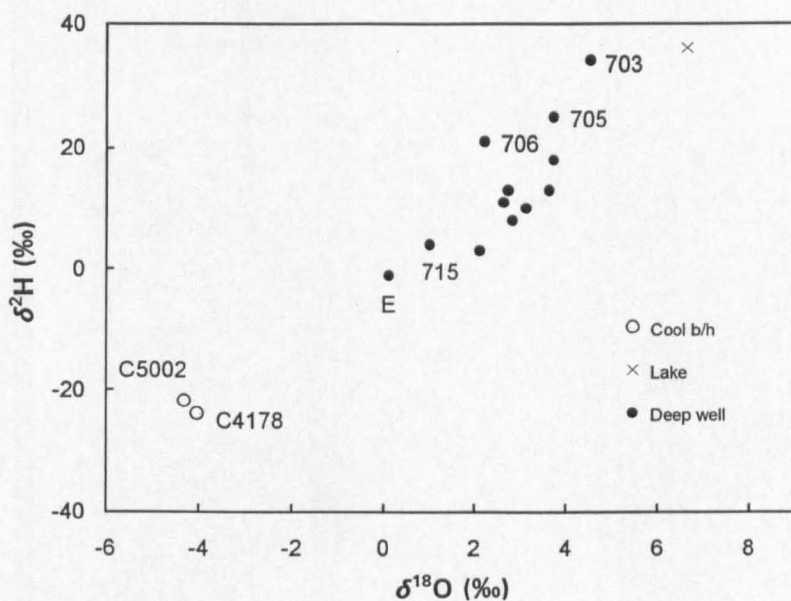
Fig 5.5   Plot of δ^2H vs $\delta^{18}O$ for Lake Naivasha and the geothermal well waters of Olkaria and Eburru. Well numbers refer to boreholes in the Olkaria Northeast wellfield. E refers to Eburru well EW-1. The identity of wells in the Olkaria East wellfield is given in Fig 5.6. Also shown are typical compositions of rift-margin waters as found in boreholes away from the vicinity of the lake.

Deep ($\sim$2000 m below ground level) geothermal waters from the Olkaria eastern and northeastern fields show lakewater contents of 70% or more, with the highest proportions in general from the northeastern field (Fig 5.2). Fig 5.5 shows a δ-plot of lake, geothermal well and typical groundwater compositions, illustrating the large range of isotopic values found in the Naivasha catchment. Importantly, there is no evidence of a significant ^{18}O-shift in the high-enthalpy waters, which could otherwise have provided a third end-member composition for possible mixing series. When fumarolic compositions are plotted on a δ-diagram together with single-stage steam separation curves (Fig 5.6), about half the samples can be related to a notional percentage of lakewater in the source. The remainder are too depleted, and have probably suffered subsurface condensation. This enables a contour plot of lakewater percentage to be produced (Fig 5.7). Up to 30% lake water can be seen at Suswa, over 30 km to the south of the lake, where it seems that lake water is brought to the surface in the hotter parts of the hydrothermal plume. However, subsurface condensation probably occurs and this means that the calculated lakewater percentages are only *minimum* figures, and that there could be a higher percentage beneath Suswa. In this way, it might be possible for some lakewater signal to be preserved even as far away as the northern end of Lake Magadi (see 5.1.2.1).

Subsurface condensation may also explain why fumarolic steam from EF-2 (Site K119) on Eburru indicates no lakewater, while results from nearby geothermal well EW-1 (K502) indicate the presence of lakewater, especially in a depth profile (Fig 5.8). In fact this profile illustrates the importance of local fissuring in permitting the influx of different water types to wells; this may be the reason why well OW-715 (K259), adjacent to the NW-trending Gorge Farm Fault, shows the reverse relationship of low lakewater in an otherwise high lakewater area (Fig 5.5).

Three studies based on river gauging and evaporation-rate measurement have given comparable results for subsurface outflow from Naivasha of 43 x 10^6 m^{3}a^{-1} (Sikes, 1935), 34 x 10^6 m^{3}a^{-1} (McCann, 1972) and 46 to 56 x 10^6 m^{3}a^{-1} (Ase et al, 1986). Panichi and Tongiorgi (1974) used the following isotopic balance equation

$$\delta_L = [-\Sigma + h\delta_v + a\delta_i(1-h)]/[h + a(1-h)] \qquad (5.8)$$

where δ_L = isotopic composition of lakewater (in permil)
Σ = fractionation factor = [(^{18}O/^{16}O)$_{vapour}$/(^{18}O/^{16}O)$_{liquid}$]-1
h = relative humidity normalised to lake temperature (as fraction of unity)
δ_v = isotopic composition of atmospheric vapour (in permil)
a = inflow rate/evaporation rate
δ_i = isotopic composition of inflow (in permil)
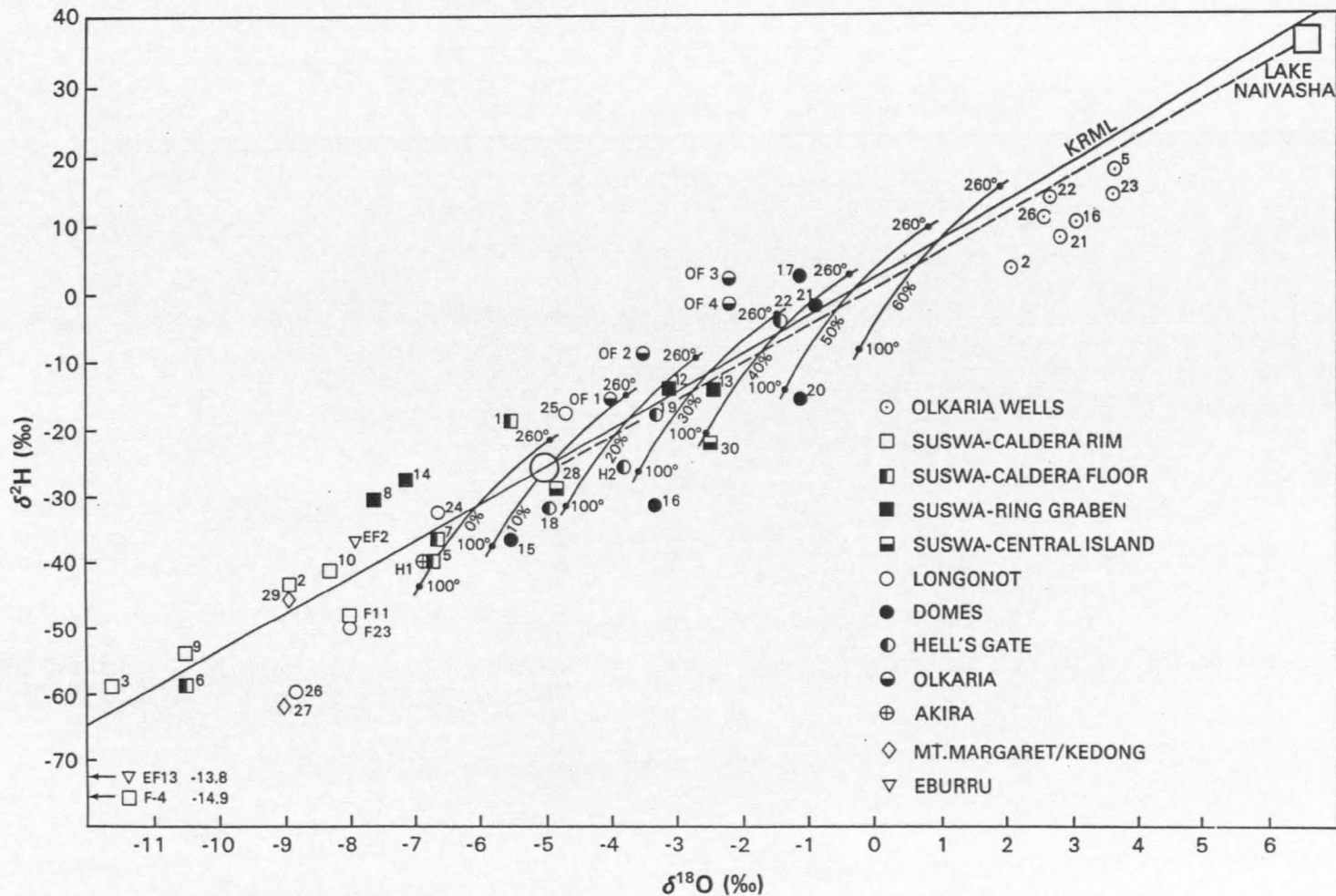
Fig 5.6   Plot of δ^2H vs $\delta^{18}O$ for the Naivasha area including Olkaria East geothermal wells and fumarolic steam condensates. Also shown are primary steam-separation curves for mixed waters with up to 60% lakewater (see text for further details).

74
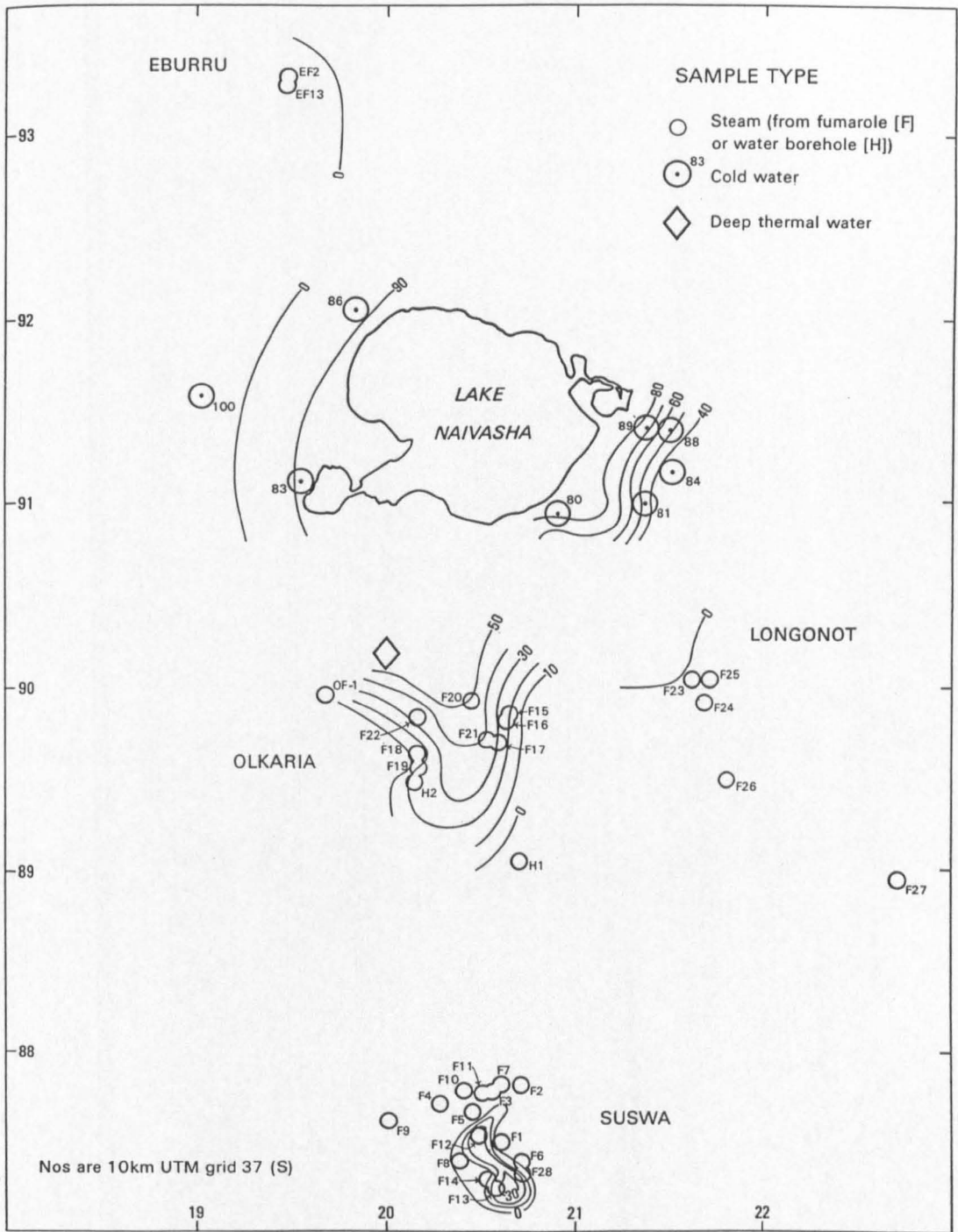
Fig 5.7   Map of contours showing percentage of lakewater in the general area of Lake Naivasha.
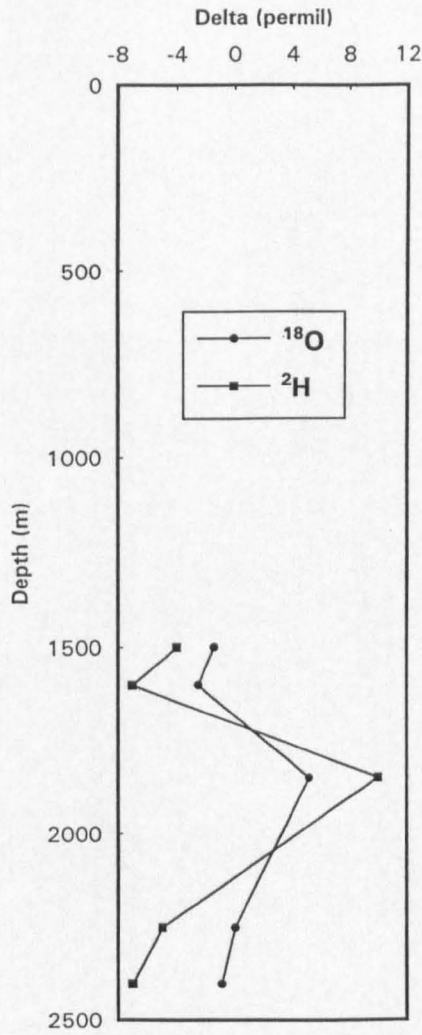
Fig 5.8   Plot of δ^2H and $\delta^{18}O$ vs depth below wellhead for depth samples extracted from Eburru geothermal well EW1.

to arrive at an averaged outflow of 250 x 10^6 m^3a^{-1}. For the calculation values of lake water and inflow, figures of $+4.6‰$ and $-4‰$ $\delta^{18}O$ were used. While the lake water value is probably a fairly good long-term average, it has been shown that the Malewa River can have a light isotopic composition ($-9‰$), and so the input is probably on average more depleted than $-4‰$. Using an inflow of $-7‰$, plus a lakewater value of $+6‰$, the ratio of inflow to evaporation lies between 1.01 and 1.15. For McCann's estimate of an evaporation of 346 x 10^6 m^3a^{-1}, and with a humidity range of 0.7-0.8, this corresponds to a recharge rate of between 4 and 52 x 10^6 m^3a^{-1} , which encompasses the physical water balance estimates.

5.1.2.3   *Elmenteita and Nakuru*

Lakes Elmenteita and Nakuru occupy what is essentially the same basin. These water bodies are very shallow, carbonate lakes with no known surface or subsurface outflow. Thus there can only be a relatively small inflow which is on average balanced by evaporation in the longer term. Apart from minor inputs from streams such as the Kariandusi (itself fed by a thermal spring) the main recharge to the lake seems to be derived from groundwater.

The warm springs (K41) at the southern end of Lake Elmenteita show evidence of about 30% water from Naivasha. However, unmixed discharge from the Eburru geothermal field is also likely to be contributing to the lake, judging by the composition of the "badlands" wells at sites K121, 122, 124 and 125. These waters have a basic rift-wall isotopic composition but their chemistry is clearly influenced by thermal processes - they contain for example high silica, lithium and bicarbonate, as well as having a high gas content (mainly CO_2) and a $^3He/^4He$ ratio similar to those found at Eburru (see Chapter 7).

Therefore the Elmenteita-Nakuru combination is fed by waters which have already suffered some preconcentration in stable isotopes and/or chemistry, which undoubtedly contributes to the enriched isotopic and chemical nature of the lakes. In parallel with this there are only limited signs of enriched water in wells to the northwest of Nakuru, implying that flow out of this basin is very small and most water is lost by evaporation.

5.1.2.4   *Bogoria*

Lake Bogoria is significantly deeper than Elmenteita and Nakuru, but resembles them in having few fresh surface water inputs or evidence of significant outflow. A sizeable input of saline waters on the edge and within the lake occurs (Glover, 1972; Geotermica Italiana, 1987). In
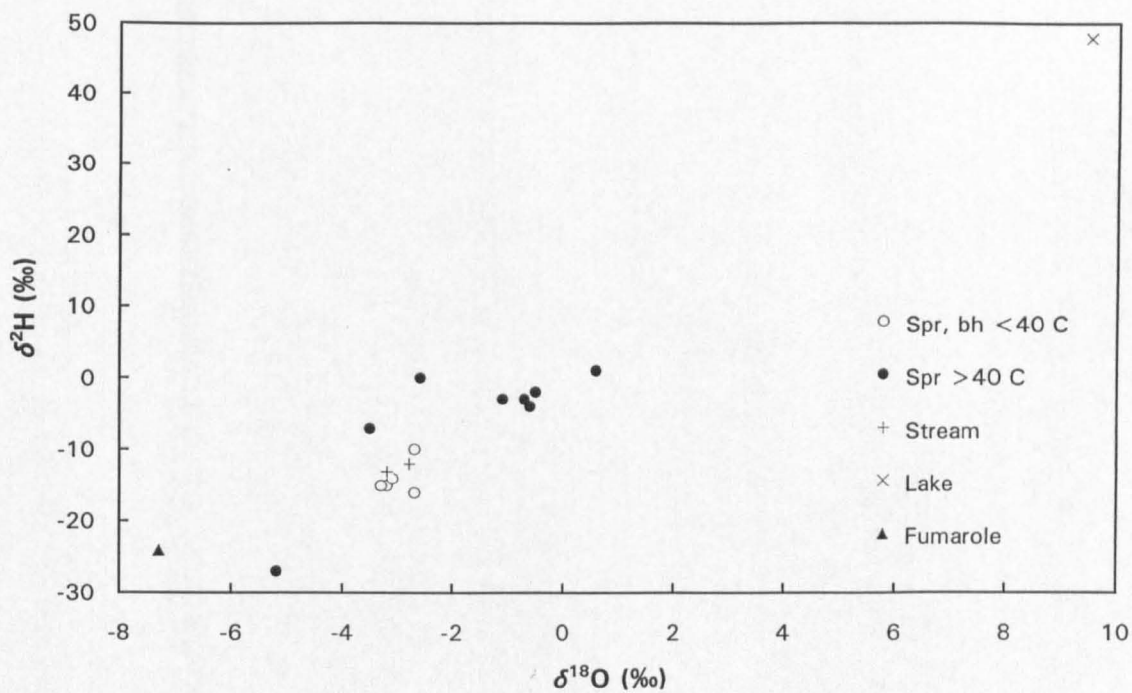
Fig 5.9   Plot of δ^2H vs $\delta^{18}O$ for waters of the Lake Bogoria area of the Gregory Rift.

the lake basin a wide variation in O and H stable isotopes is seen, ranging from unmodified rift-floor recharge through boiling springs to highly evaporated lakewater (see 5.2.1 above). Fig 5.9 shows the positions of representative waters on a δ-plot. Non-thermal or slightly thermal waters cluster around the KRV meteoric line at about -13‰ δ^2H, -2.8‰ $\delta^{18}O$ and are presumably derived from local recharge in the hills around the lake. The three boiling springs sampled have rather heavier compositions, whereas the lakewater itself is extremely enriched in heavy isotopes due to the large amount of evaporation taking place from the closed basin.

It was suggested by Glover (1972) that slightly thermal water underlying the general area reacts both with ascending steam and with lakewater, while Geotermica Italiana (1987) postulated a ternary mixing model involving local groundwater, thermal water and lakewater. The few data reported here support neither model directly. Although the three boiling springs do not all lie directly on a dilution trend between the regional cool springs and the extremely evaporated lakewater, the position of two is consistent with a process of steam loss (Fig 5.9). To this extent the contention that lakewater is involved is likely to be correct (and indeed the situation of the boiling springs on the lake shore makes this very likely), but there is no evidence that steam with a different isotopic composition is playing a part in the process. This is not to rule out the possibility of the boiling springs being the product of a complex mixing process between shallow groundwater, thermally-modified groundwater and lakewater.

The Arus fumaroles (K257), which are situated close to the Molo River, may be associated with the Bogoria hydrothermalism. The composition of the steam condensate shows that it could have come from a similar source. However, subsurface condensation may have occurred and it may be ultimately derived from a heavier groundwater more typical of the rift floor in this area.

5.1.3   Ground and surface waters in the Nyanza Rift

Fig 5.10 shows a δ-plot of waters associated with the Nyanza Rift, with sample locations shown on the inset map. The Kureswa springs (K256) are situated between the main Rift and the Nyanza, and have an isotopic composition falling on the Kericho meteoric line referred to above. Since the Bala area lies at a somewhat lower altitude, the hot springs with their more enriched composition are probably the result of local recharge on the nearby Homa Mountain, or possibly some 50 km away to the east on higher ground. Despite their geographical proximity to Lake Victoria, there is no indication that lake water is involved in the hydrothermal circulation.
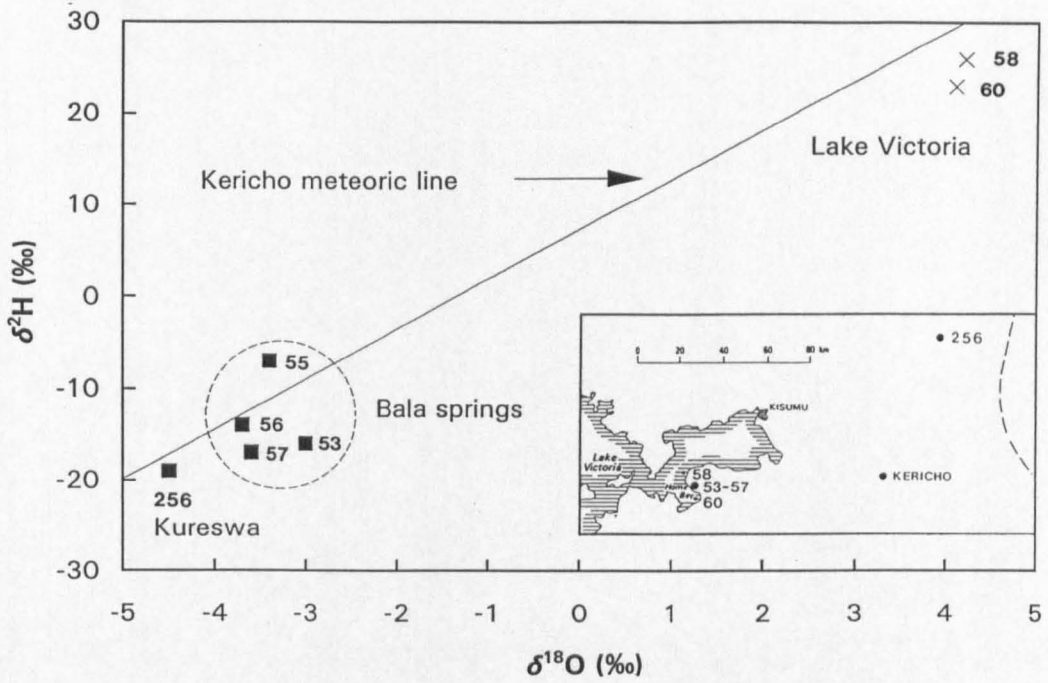
Fig 5.10 Plot of δ^2H vs $\delta^{18}O$ for waters of the Nyanza Rift area, western Kenya. Inset - location of sample sites.

5.1.4 Ground and surface waters in the Turkana Rifts

5.1.4.1 South Turkana Rift

Surface waters - This area includes the sector of the rift from Lake Baringo in the south to the Barrier volcanic complex in the north. Fig 5.11 shows a δ-plot of waters from both the Turkana Rifts, with site locations indicated on Fig 5.12. The relatively fresh Lake Baringo is fed by a network of minor rivers, whose stable isotopic compositions are not significantly affected by evaporation, except perhaps for the Mukutan (K147). While the river compositions cluster in the same area as unmodified groundwaters (see below), rivers such as the Tigeri may change their isotopic content depending on the season of the year. The waters of Lake Baringo are isotopically heavy (Table 5.2e), as a result of the combined effects of high evaporation and the shallowness of the lake. They show significant variation with time as at Naivasha, and these changes are reflected in lake water chemistry (6.1.4).

When the isotopic balance model is applied to Baringo assuming the same values as in eqn 5.8 above for fractionation factor, relative humidity and the isotopic composition of atmospheric vapour, a figure of around 150×10^6 m^3a^{-1} is obtained for underflow from the lake. The physical data obtained during a hydrological study of the area suggested a smaller underflow of 33×10^6 m^3a^{-1} when a TDS balance was used (WRAP, 1987), but using the Cl data from this study and the WRAP inflow volume, an underflow of 104×10^6 m^3a^{-1} is obtained. Clearly, whichever estimate is more correct, an underflow of at least several tens of millions of cubic metres per year is occurring.

The major river occupying the inner trough of any of the Kenya rifts, the Suguta, rises at the Kapedo hot springs and flows perennially towards the northern end of the South Turkana rift (Fig 5.12). During wet periods it is also augmented by flood waters from the Nginyang River which drains the rift floor and rift margins south of the Silali volcano. The increasing temperature and aridity towards the north raises the potential for evaporation. This is reflected in the isotopic composition of the rivers draining into the Suguta Valley from the eastern margin of the rift (Gerau, Amaya and Naliyo, K211, 212, 214), which become progressively isotopically heavier northwards. Likewise, the heaviest isotopic compositions of the Suguta occur in the north, where the river breaks down into a series of distributaries which soak into the floor of the valley or feed into the ephemeral Lake Alablab. This and Lake Logipi in the extreme north of the Suguta Valley (Fig 5.12) are in part fed by hot springs. Both are highly saline and have surface encrustations of trona round their edges; no analyses were undertaken
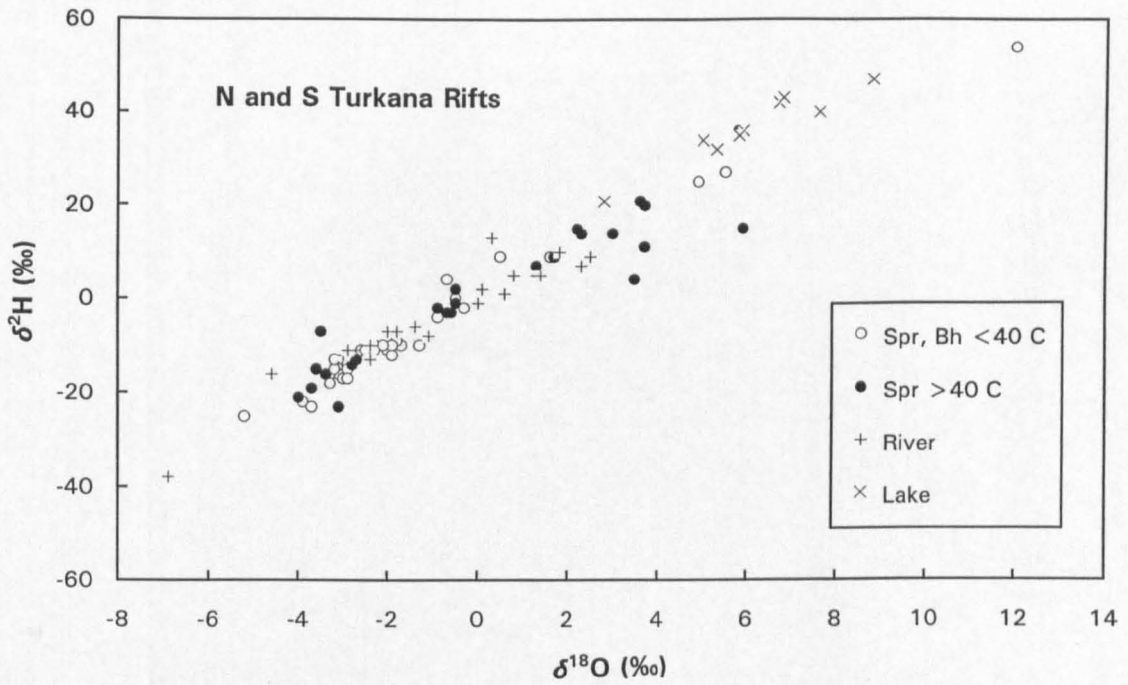
Fig 5.11   Plot of δ^2H vs $\delta^{18}O$ for ground and surface waters in the Turkana rifts of Kenya (fumarolic steam condensates not included).
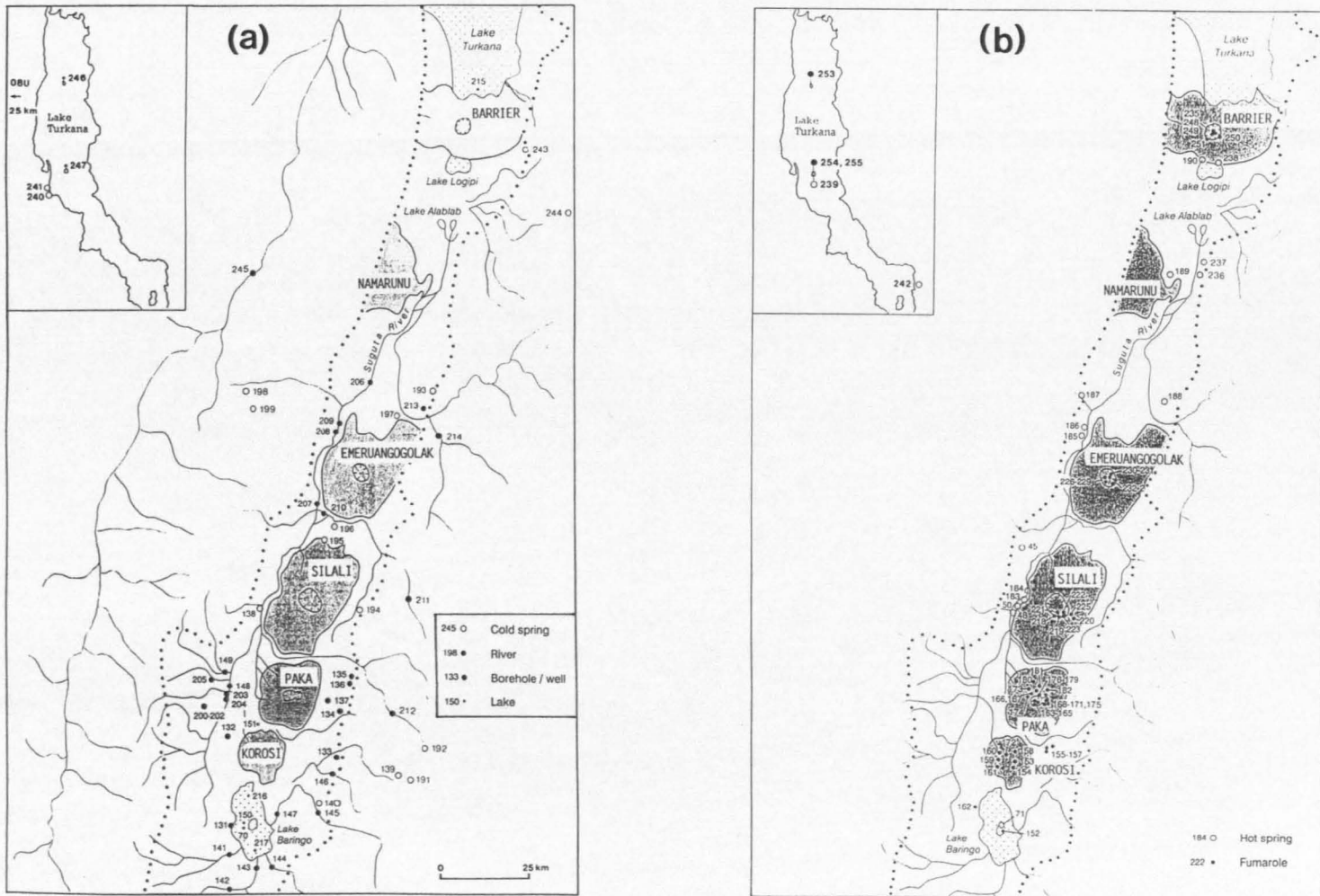
Fig 5.12   Sampling sites in the Turkana rifts. Numbers have a K prefix in text and tables. (a) ambient
and cool groundwaters, (b) thermal manifestations. Insets: sample sites of the Lake Turkana
area (scale half that of main map).

on these lakes because of their ephemeral nature.

Cool groundwaters - The isotopic composition of rift-margin groundwaters in the southeast of the area is defined by a group of springs along the eastern margin of the rift (K139, 140, 191, 192) which have δ^2H and $\delta^{18}O$ of around -16‰ and -3‰ respectively (Table 5.2b). Such values are compatible with the KRV meteoric line and, if fed into the altitude/isotope correlation developed in 6.1.1 above, give an average recharge altitude of about 1800 m. They can be compared with the rather lighter isotopic compositions (around -25‰ δ^2H, -4.5‰ $\delta^{18}O$) on the higher-altitude margins of the Gregory Rift.

As far as natural discharges of <40°C are concerned, some springs on both margins of the rift are little more than seepages. Therefore their isotopic compositions may be affected by evaporation, accounting for slightly enriched compositions at North Samburu Gates and Nasaken (K193, 199). However, the seepages at Napeiton (K198), northwest of Emuruangogolak, have similar isotopic compositions to the springs in the south-east. This similarity suggests that the isotopic composition of meteoric waters is broadly similar throughout both rift margins. Chemical indications of water-rock interaction (Chapter 6) suggest that the waters in the northwest around Napeiton may have circulated to greater depths, possibly along rift boundary faults, before rising to the surface and cooling. This would be consistent with the geological interpretation of a half-graben downfaulted to the west (Chapter 2).

In the Suguta Valley, cool waters of <40°C are uncommon, only three instances occurring on the rift floor north of Baringo. The Amakat pools (K196) between Silali and Emuruangogolak are isotopically very enriched, but TDS is low suggesting the pools consist largely of highly evaporated rainwater. The springs at Lake Kalnangi and South Nangarabat (K195 and 197) occur where water flows out from beneath the basalt lava fields along the northern periphery of Silali and Emuruangogolak respectively. Both sets of springs have similar isotopic and chemical compositions, and from their locations could be assumed to represent cooled outflow waters from the Silali and Emuruangogolak hydrothermal systems. However, their chemistry does not support this assumption (6.1.2)

Most of the sampled wells and boreholes are situated on the floor of the rift in the south of the area. These can be divided into two groups, to the east and west of the volcanic centres. The eastern group of wells (K133, 134, 135, 136 and 137, Table 5.2a) presents a coherent body of isotopic data, which indicate that, unless the waters have suffered mixing, recharge has taken

place at a lower average altitude than the rift-margin springs. This would be consistent with recharge taking place on the lower slopes of the eastern margin of the rift, or upon the floor or the volcanic centres within the inner trough, as predicted by hydrogeological indications (Allen and Darling, 1992). The chemical analyses (Table 6.4) and δ^{13}C-DIC values (see below) indicate that the eastern wells in this area contain relatively unmodified meteoric water. Even the Katangora borehole (K137), which is situated relatively close to the eastern flanks of the Paka volcano and has a slightly elevated temperature of 36°C, shows no geothermal influence other than higher-than-average F and δ^{13}C-DIC values.

The western group of wells is more variable. The Kositei and Chemolingot boreholes (K202 and 205) are similar in chemical and isotopic composition, and their isotope values suggest an origin for the water on the higher western margin of the rift. The Chesirimion and Nginyang boreholes (K132, 203 and 204) have isotopic compositions consistent with a greater contribution from rainfall on the rift floor, but are otherwise different. While Chesirimion water is similar to that from the eastern group of wells, the two Nginyang wells have very high HCO_3^- and F (Tables 5.2c and 6.4). The reasons for this are probably related to mixing between groundwater and infiltrating river water (see 5.2.1 below).

The borehole at Kampi-ya-Samaki is situated very close to the edge of Lake Baringo. By virtue of its position, it might be expected that the isotopic composition of water from the borehole could represent a time-averaged composition for lakewater. This assumption is confirmed by examining the δ^{18}O and Cl concentrations (Tables 5.2a, 5.2e and 6.4, 6.8), which show that the borehole sample (K131) and the averaged composition of lake samples collected between 1986 and 1991 are virtually identical.

Hot springs, southern - Hot springs occurring within the inner trough of the rift are not necessarily found in close proximity to the volcanic centres. They have temperatures of 40°C and over, although cooler waters which have similar chemical characteristics to hot springs are also considered with this category.

On the stable isotope plot of δ^2H vs δ^{18}O (Figure 5.13) the hot springs show a range from rift margin-like compositions (Lorusio and Kamuge, K45, 187) to compositions enriched in heavy isotopes (Ol Kokwe Island, K71 and Kageinya, K188), which must contain a proportion of evaporated water. The springs of Ol Kokwe Island have the most enriched compositions, undoubtedly due to mixing with Lake Baringo water either before or after heating. The other thermal springs, and the non-thermal springs with similar chemistry such as Kalnangi (K195)
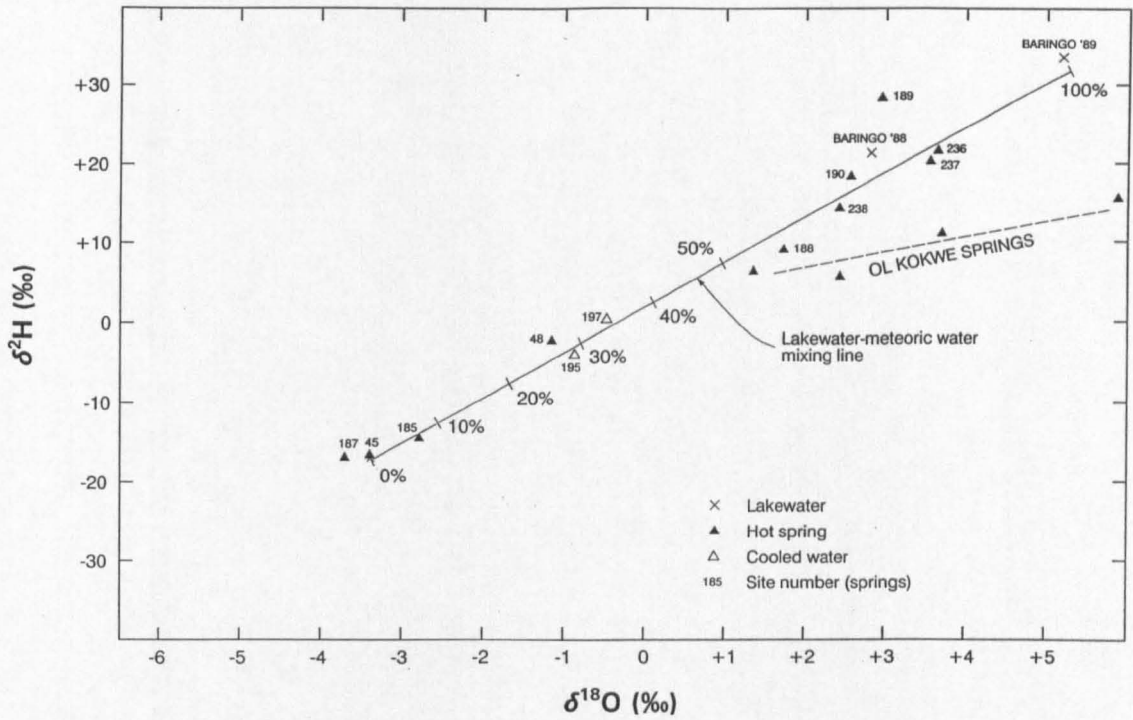
Fig 5.13   Plot of δ^2H vs $\delta^{18}O$ for hot and ?cooled waters of the South Turkana Rift, showing percentages of lakewater in the mixing series with water from the rift wall areas.

and Nangarabat (K197), may represent different amounts of mixing between subsurface outflow from Lake Baringo with meteoric water from the rift margins or from recharge on the volcanic centres, in a similar way to the mixing described in the vicinity of Lake Naivasha. The percentage markings in Figure 5.13 refer to the calculated proportion of lakewater apparently in the springs. The Kapedo hot springs (K48) have about 30% lakewater, as do the cool springs of Kalnangi and South Nangarabat (K195, 197). In contrast, hot springs situated on or close to the base of the rift margin escarpment appear to have little or no lakewater in their discharge, as for example those of Kamuge, SV3 and Lorusio (K187, 185, 45).

A plot of δ^2H versus Cl (Figure 5.14) illustrates that while all the waters have isotopic compositions within the range of a rift margin - lakewater mixing series, they can have variable chemistries that are not the result of straightforward mixing.

None of the thermal springs shows evidence of being an outflow from a high-temperature ($> 150°C$) system, except for those on Ol Kokwe Island. The other thermal springs are likely to be simply the result of deep circulation, although there may be local zones of higher heat flow which have some magmatic characteristics, such as at Lorusio with its abundant CO_2 gas and relatively high $^3He/^4He$ value (Chapter 7). As in the Gregory Rift, there is no evidence for ^{18}O-shifting on a significant scale.

Hot springs, northern - The hot springs in the Suguta Valley, such as those at Kageinya (K188), Namarunu (K189), Elboitong (K236, 237) and Logipi (K190, 238) have much higher TDS values (~ 15000 mgl^{-1}) than those further south. The Suguta Valley is the terminal drainage area for the northern half of the South Turkana Rift and as such it should have the greatest amount of salts available for recycling in thermal waters. This sump area, which terminates in the highly alkaline Lake Logipi, resembles in some ways the Magadi basin which is the corresponding terminal drainage area for the southern Gregory Rift. The springs are associated with the volcanic centres of Emuruangogolak, Namarunu and Barrier. Despite this, they do not appear to be high-temperature outflows, though the Namarunu and Logipi springs have elevated $^3He/^4He$ ratios (see Chapter 7).

Three sources of water could be contributing to these hot springs: infiltrating surface water derived from the south, meteoric water from the rift flanks, and subsurface leakage from Lake Turkana in the north. The first and second categories potentially apply to the Namarunu and Elboitong springs, while the second and third could apply to the Logipi springs. Stable isotope data offer only a partial resolution of the sources. The δ-plot of Figure 5.11 shows the
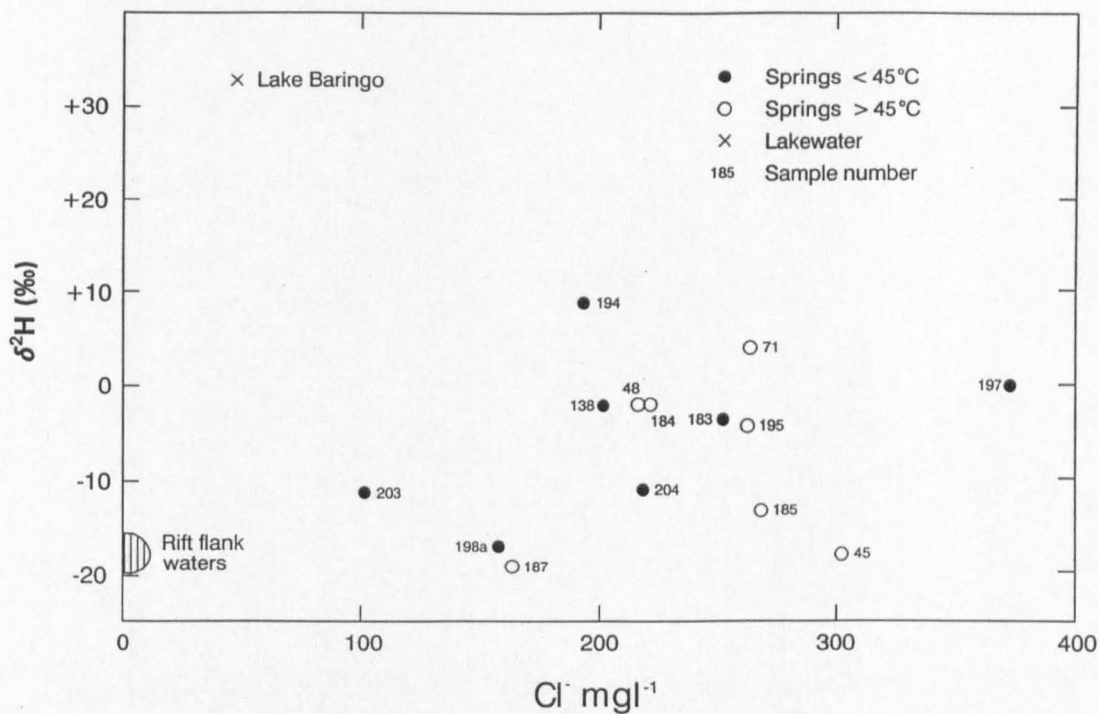
Fig 5.14   Plot of δ^2H vs Cl for selected groundwaters of the South Turkana Rift, showing that water chemistry is not the result of simple mixing processes.

compositions involved. The only obvious water source in the northern part of the Suguta Valley is the Suguta River. Samples K207-209 were taken from the river to the south, with 209 being collected nearest to Namarunu. The river waters show an evaporative trend, as would be expected for surface waters in a hot and arid area, but the hot spring samples are not aligned with this trend, suggesting that river waters do not make a major contribution to the springs. However, most recharge of groundwater may take place during the flood events to which the Suguta Valley is periodically subjected. Under these conditions the river and direct rainfall will deliver more isotopically depleted water, or at least water with a composition on or near the Rift Valley Meteoric Line, and the springs at Namarunu and Elboitong derive their waters from such a source. There is likely to be considerable recycling of water by thermal springs in this sump area, and this could result in the observed isotopic enrichments.

If, however, the analyses from sites K206-209 are indicative of the bulk of any recharge from the Suguta River, then the river could not be a major contributor to the springs. The springs might then consist of meteoric water from the rift flanks enriched by evaporation. While this is feasible for Elboitong, it is less likely for the Namarunu springs because of their position on the eastern tip of the Namarunu volcanic promontory. An alternative explanation is that underflow from Lake Baringo may be contributing to the springs, although this is impossible to prove because of evaporative effects during recycling.

In the case of the Logipi hot springs, discharge from Lake Turkana may be a component . On geochemical grounds discharge is unlikely to be significant in terms of the total lakewater budget (Yuretich and Cerling, 1983), and this is supported by the small output of the Logipi springs. Furthermore, Lake Logipi tends to shrink considerably during periods of drought, which would probably not be the case if there were significant subsurface outflow from Lake Turkana towards the Logipi area. However, isotopic considerations (Figure 5.11) show that a mixture of meteoric water and lakewater could be responsible for the observed isotopic ratios of the Logipi springs, although the exact proportions involved may be being masked by evaporative effects during recycling. While an upper limit of about 70% can be put on a lakewater contribution, the stable isotope compositions of steam from Kakorinya fumaroles suggest that 40% is a more likely figure for the actual contribution (see below). This indicates that even in this hot and arid part of the Suguta Valley there appears to be significant input of meteoric water from the rift flanks, or from recharge by rainfall on the Barrier Volcanic Complex itself. As with the Elboitong and Namarunu springs to the south, it is not possible to prove unequivocally that lakewater is involved. The springs have much the same isotopic composition, and may simply represent discharges from various points of a rather homogeneous

body of hot saline groundwater occupying the discharge area and fed mainly by meteoric waters which are then subject to evaporative enrichment. On balance, however, it would seem more likely that waters already enriched by evaporation, such as lake or river waters, must be contributing.

Fumaroles - As in the Gregory Rift, the fumaroles are relatively weak. Therefore only the strongest and hottest at each volcanic centre were sampled. O and H stable isotope data for fumarole condensates from the region between Lake Baringo and Emuruangogolak are plotted in Figure 5.15, together with data for ambient groundwaters and lakewaters. Fig 5.16 shows an expanded portion of Figure 5.15 covering the main group of fumaroles and including the hot springs of the area. Primary steam condensate curves are shown on the diagram based upon 10% steps in a rift margin-lakewater mixing series, in a similar manner to the method employed for the Naivasha area. On this basis, most of the fumaroles in the main group can be explained by primary steam separation from varying mixtures of rift margin water and lakewater, except for the PK1 series of samples from Paka (K163-165) and the EM7 and EM9 series from Emuruangogolak. The EM7 and EM9 fumaroles (K226, 227, 228, 229) of Emuruangogolak caldera are not particularly strong, and may be explained in terms of a secondary origin, such as steam heating of groundwater. In contrast, the PK1 fumaroles of Paka caldera are strong and rich in CO_2 so a secondary origin is less likely for these. Only a water that has already lost steam could have a suitable isotopic composition to provide steam with the composition of these fumaroles. However, other Paka fumaroles with more "normal" isotopic compositions could be derived by primary steam separation, such as the PK4 series (K166-167) situated just outside the main caldera to the north and the PK7 fumaroles (K168-171 and 175) located in the eastern crater.

With the exception of the strongest and hottest fumarole on the Nakaporon fault zone (KR23), the Korosi and Chepchuk fumarole condensates are isotopically depleted and cannot be directly related to the proposed groundwater-lakewater mixing series. Some Paka, Silali and Emuruangogolak fumaroles also lie in the isotopically-depleted area in Figure 5.16. These depleted compositions may be explained by subsurface steam condensation, which could have the effect of lowering the heavy isotope content of steam quite considerably. The Rayleigh process of condensation examined in Darling and Armannsson (1989) could account for quite large fractionations (see 8.2.3), particularly for weak fumaroles at a large distance from their upflow. A prime example of this is the very weak fumarole KR34 (K162) at Loruk, a considerable distance from the nearest volcanic centres of Korosi or Ol Kokwe, which has a highly depleted isotopic composition (site 34 in Figure 5.12). However, the isotopic data
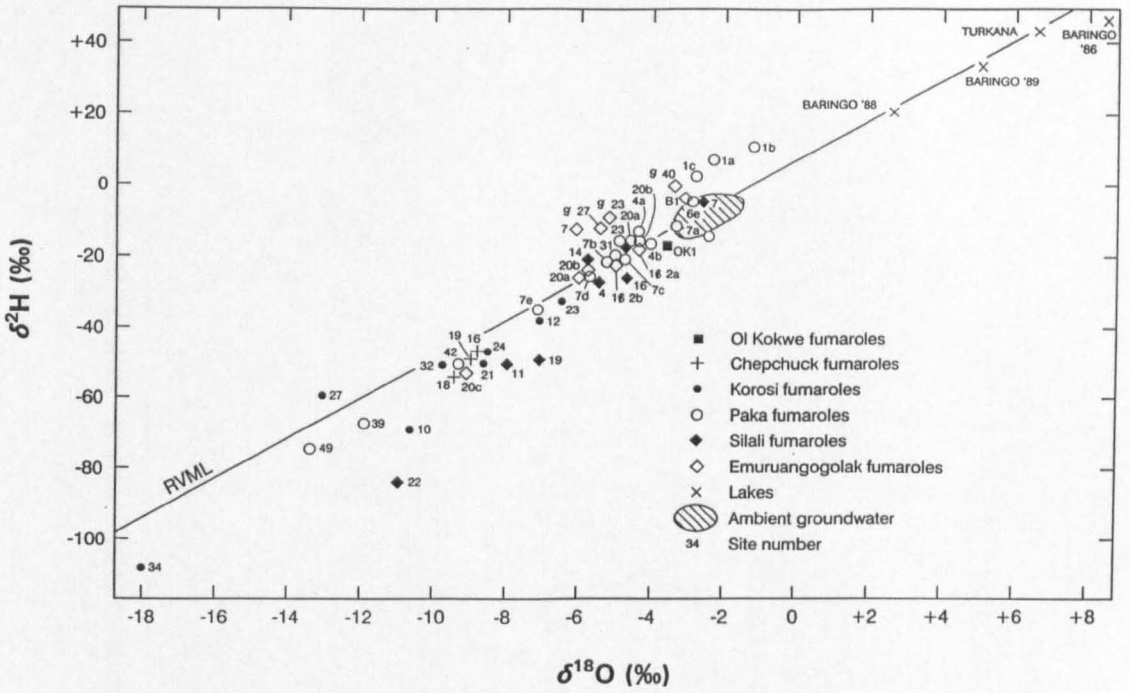
Fig 5.15   Plot of δ^2H vs $\delta^{18}O$ for South Turkana Rift waters, including fumarole condensates.
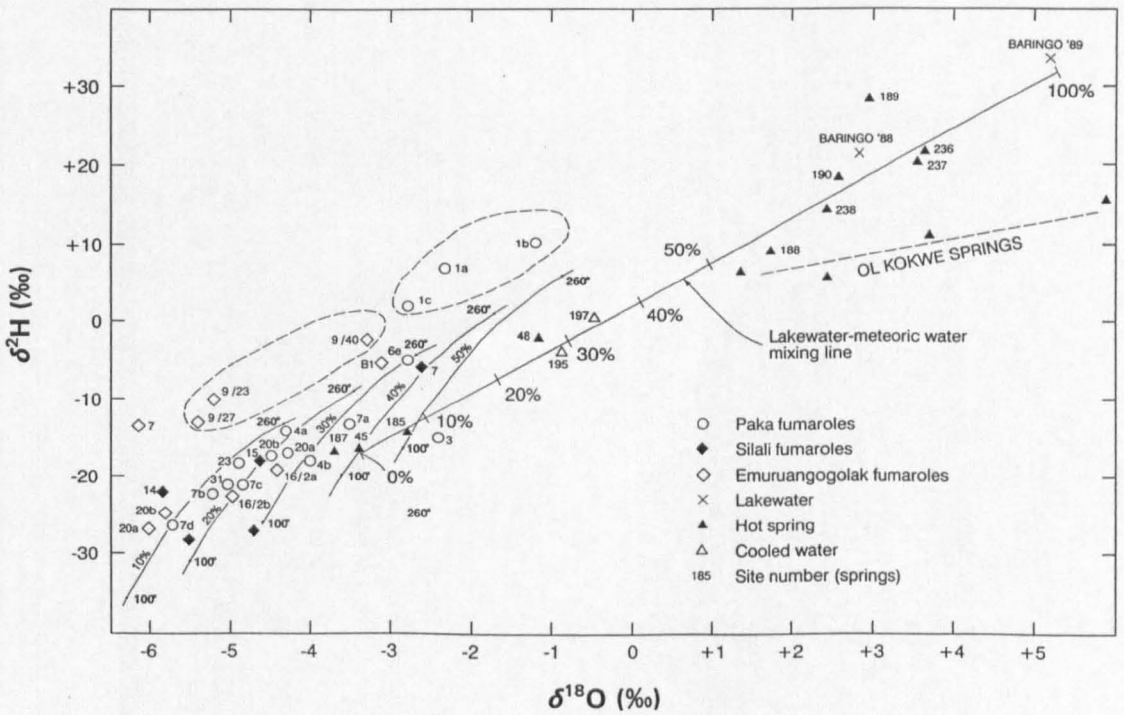
Fig 5.16   Expanded version of part of Fig 5.15.

indicate that even locally the process of subsurface condensation can operate on a significant scale. This is exemplified by significant variations in the isotopic composition of fumaroles occurring within spatially constrained groups; for example, the PK1 group (K163a-b, 164, 165) from the main caldera of Paka, the PK7 group (K168-171) from the eastern crater of Paka, and the EM9 group (K227-229) and EM20 group (K232-234) from the caldera of Emuruangogolak.

On the assumption that the most enriched fumarole condensates at each centre approximate to original, uncondensed steam compositions, Paka, Silali and Emuruangogolak have fumaroles which indicate 45%, 25% and 10% of lakewater respectively in their source reservoirs (Fig 5.16). This pattern is consistent with the progressive dilution northwards of outflow from Lake Baringo.

Alternative models for the production of fumarolic steam - Simple condensation processes and derivation of fumarole steam from a lakewater-meteoric water mixing series can explain the steam stable isotope composition measured in many fumaroles. However, other mechanisms must be briefly considered. For example, some very depleted isotopic compositions might be merely the product of an individual, depleted storm event infiltrating into a volume of hot rock and being largely or completely vaporised. However, three dissimilar fumaroles within the area were measured in separate years when weather conditions were very different. The sites include KR34, with the most depleted steam composition yet found in the Rift, and PK1, a vigorous "heavy" fumarole. Table B.4 shows that while there are variations in year-to-year compositions, these are relatively minor and therefore the basic interpretation could still be valid. This observation indicates that a second putative mechanism, reflux condensation, is also not a significant cause of isotopic variation. Such a process would work if steam condensate, which would be significantly heavier isotopically than the remaining vapour, could be re-vaporised independently. Under steady-state conditions, which have been generally assumed to apply to fumaroles and which the duplicate results of Table B.4 support, this could not happen because of the re-equilibration between the condensed water and "new" steam. Only if condensate could drain to some different volume of hot, dry rock could vaporisation of condensate take place without subsequent modification of the resulting enriched steam. It might be possible for this to occur locally, but would suggest that highly depleted fumaroles should occur relatively near to fumaroles with heavy steam. On the whole this does not occur. The most vigorous fumaroles (those least prone to modification) are usually situated within crater or caldera areas, while those further away from these presumed upflow zones show in a fairly predictable way signs of depletion due to condensation and dilution of any lakewater contribution by lighter water from meteoric sources. While this may suggest a

relatively local meteoric input it is assumed that, as is the case further south in the Rift (and indeed in most of the rest of the world), this recharge has a time-averaged composition little different from rift-flank water and therefore effectively indistinguishable from it.

Additionally, if the isotopically heavy steam fumaroles were the result of separation via a condensation process, a very low gas content would be anticipated. Instead the "heavy" fumaroles usually have relatively strong gas flows uncontaminated by air and enriched in $^3He/^4He$, a good magmatic tracer.

None of the foregoing arguments is to say that *all* isotope ratio-modifying processes act in a completely predictable manner, and it is possible that the notably anomalous compositions such as the PK1 and EM9 groups owe something to the alternative mechanisms proposed above. However, many of the measured isotopic ratios fit the simplest model and this is therefore retained for the purposes of interpretation.

5.1.4.2   *Turkana basin*

The isotopic composition of Lake Turkana is mainly governed by input from the Omo River which drains from the Ethiopian Highlands. While the lake is terminal it is by no means as saline as other closed lakes within the rift to the south, such as Bogoria, Elmenteita-Nakuru and Magadi. This is because closure only occurred relatively recently, at about 3.5 ka (Butzer et al., 1972), and the large volume of the lake has not yet permitted the development of hypersalinity. Yuretich and Cerling (1983) concluded that the chemical balance of the lake does not require major subsurface outflow from the lake to the west or south, but minor outflow could be masked by various uncertainties attending the chemical balance. Isotopic analyses (K215, 246, 247; Table 5.2e) show that the lakewater is considerably evaporated, as illustrated by the δ-plot of Figure 5.17, which also shows an analysis of the Kerio River (K245) sampled at Lokori, some 60 km upstream from the mouth, and of the Omo River measured by Craig et al. (1977). Predictably both rivers show isotopic enrichment, but since the compositions at their mouths are not known, an isotopic balance for the lake cannot be attempted.

Isotopic and chemical samples revealed no significant difference between lakewater at North and Central islands, despite their separation by 60 km. Sampling took place in June 1991, when the annual flood from the Ethiopian Highlands via the Omo would have started. However, there is no evidence of mixing in the vicinity of Central Island between waters from
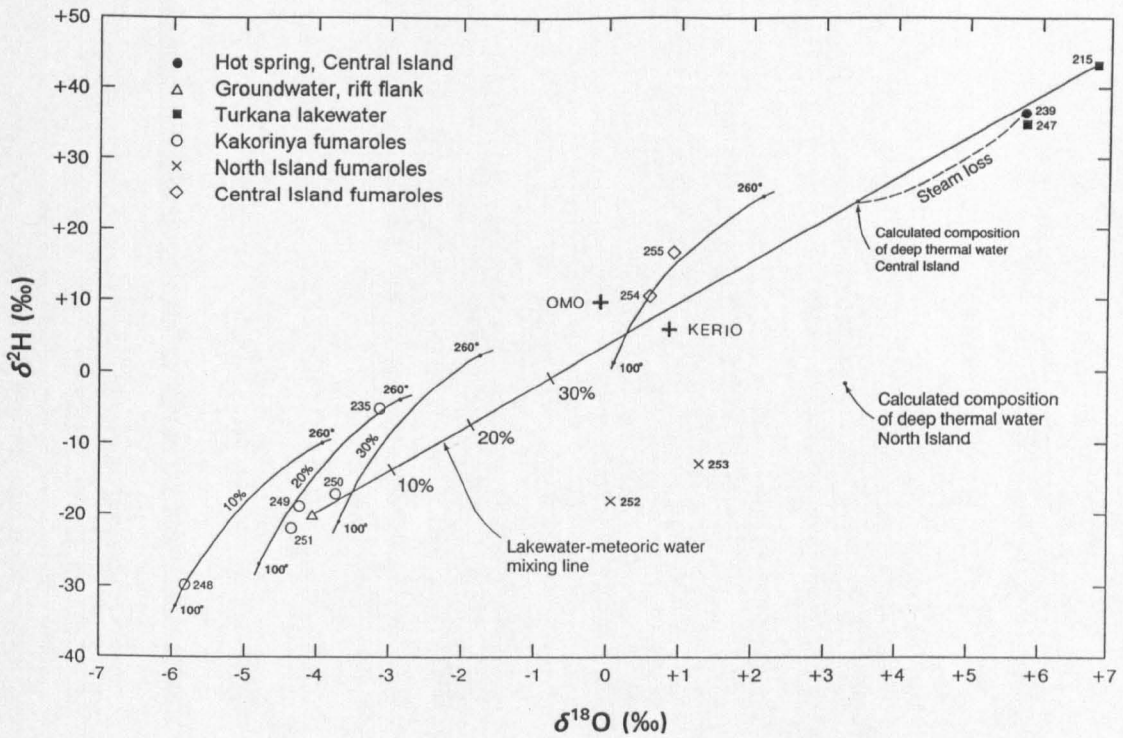
Fig 5.17   Plot of δ^2H vs $\delta^{18}O$ for fumarolic steam condensates from Kakorinya and Central and North Islands of Lake Turkana, showing the relationship with lakewater and deep thermal waters.

the south with those from the Omo as described by Yuretich and Cerling (1983).

Sample K215 from the southern end of the lake was collected in October 1989 and shows signs of chemical and isotopic enrichment. This would be expected for samples collected furthest from the main input to the lake, although the possibility of local near-shore evaporation cannot be wholly discounted. Assuming that there is minor subsurface outflow southwards from Lake Turkana into the topographically lower northern end of the Suguta Valley, the outflow will be derived from this end of the lake, and therefore the composition of K215 was used in considering the implications of such underflow in the previous section.

For groundwaters <40°C in the Turkana basin there are relatively few data. Springs on the west side of the lake at Eliye Springs (K240, 241) must be derived from a fairly low average altitude because they are relatively enriched. The similarity of the isotope ratios for the Eliye Springs with those of the Kankurdio borehole (08U), situated 30 km to the west of the lake, suggests that the springs do not derive their recharge locally.

The springs at Loyangalani (K242), on the south-east shores of Lake Turkana, which fall just within the thermal category, appear to derive their water partly from a higher-than-local altitude, but probably not exclusively from Mt Kulal to the east which rises to 3500 m and would presumably supply more depleted water. The only really hot springs found within the vicinity of Lake Turkana occur around the main crater lake of Central Island (K239). Isotopically, the spring water is of similar composition to lakewater (Figure 5.17), which is the obvious source of any thermal fluid. The implication of the isotope analyses is that little or no shift in $\delta^{18}O$ has been caused by water-rock interaction. In chemical terms, however, the spring fluid has evolved considerably from a lakewater composition, and is also unlike any of the hot springs in the northern part of the Suguta Valley. The high K and Si, and $Cl >> SO_4$ suggests high-temperature water-rock interactions, which implies that steam heating is not important. There is little doubt that this is one of the few examples in the Kenya Rift of a fluid derived from mixing with a high-temperature geothermal outflow. This is comparable to the hot springs of Ol Kokwe Island, which are situated in an analogous position in the centre of Lake Baringo (see 5.1.4.1 above).

Stable isotope data for fumarole condensates from the Barrier and Central and North Islands show that the compositions of the fumaroles of the islands are markedly different from those of the Kakorinya centre (Fig 5.17). The condensates from North Island plot significantly below the local meteoric line and are dissimilar to fumaroles in the remainder of the KRV. Such

compositions either require significant low-temperature subsurface condensation processes, which is unlikely because of the vigorous nature of these fumaroles, or are derived from a reservoir composition falling significantly off the meteoric line. Given the absence of suitable end-members for mixing, the only plausible way that such a composition could arise appears to be by an oxygen isotope shift of about 4‰ (Fig 5.17). Such shifts caused by high-temperature water-rock interaction are known from various geothermal systems around the world, but have not been found within the Eastern Rift; unequivocally geothermal water from Olkaria has a $\delta^{18}O$ shift of only about 1‰ maximum (see 5.1.2.2 above). However, in the absence of contrary evidence, it is assumed that oxygen shifting of a greater order is occurring in the North Island hydrothermal system.

The magnitude of oxygen isotope shifting is a function of the amount of water-rock contact, and relatively large shifts therefore imply that a system has low permeability or is young, or is the result of a combination of these features. Each case limits the amount of water that has passed through the rock, therefore limiting the extent to which rock and water can readjust towards isotopic equilibrium. If the assumption is made that all the rift's hydrothermal systems have roughly similar permeability, then a comparatively large $\delta^{18}O$ shift in this case implies a young hydrothermal system. Certainly there has been very recent volcanic activity on the island (Dunkley et al, 1993). A difficulty with this interpretation is that the postulated deep fluid would consist of little more than 30% lakewater.

On Central Island, however, hot springs are available to test the validity of any assumptions made from consideration of fumarole steam analyses. The composition of fumarole condensates from Central Island, while more enriched than those found elsewhere within the rift, are compatible with derivation from a lakewater source without oxygen shifting. Figure 5.17 shows the likely relationship between steam and source water based on boiling off at ~280°C and cooling of steam to the local surface boiling point. The results indicate limited dilution of lakewater, perhaps resulting from direct infiltration of rainfall on the island.

5.1.4.3   Hydrothermal sinters

Hitherto in the discussion of stable isotopes the emphasis has centred on processes occurring essentially at the present day. The existence of relict hydrothermal silica sinters on certain volcanic centres of the northern KRV provides a possible method of estimating the $\delta^{18}O$ values of palaeowaters in the area. These sinters, which have been dated by U-series methods (Sturchio et al, 1993), are found at various levels on the northern volcanic centres, and could

only have formed when hydrological base levels were significantly higher than at present. As part of the present study, the $\delta^{18}O$ composition of the sinters was measured (Table 5.3) and an equilibrium lakewater composition calculated on the basis of the following three assumptions:

1) The sinters were deposited in isotopic equilibrium with waters at 100°C: the silica-depositing springs are likely to have issued at around boiling point, because lower-temperature springs in the KRV have too little silica for significant deposition on cooling. This would imply a $\delta^{18}O_{SiO2}-\delta^{18}O_{H2O}$ fractionation of ~21‰ (Clayton et al, 1972). There is no guarantee that silica was not deposited at lower temperatures with consequent greater fractionations, but this can be validated to some extent by comparison with the stromatolitic $\delta^{18}O$ record.

2) The calculated $\delta^{18}O$ values of the depositing waters were close to the average lakewater value during the period of deposition: the extent of Holocene lake sediments shows that the depositing springs are likely to have been situated on islands or peninsulas in the lakes (Sturchio et al, 1993), and modern analogues such as Ol Kokwe Island and Central Island have springs with isotopic compositions similar to those of lakewater (see 5.1.4.1 and 2 above).

3) The depositing waters were not significantly affected by ^{18}O-shifting. There is no evidence from present-day deep geothermal waters that the ^{18}O shift exceeds ~1‰ anywhere in the Eastern Rift (except possibly for North Island).

The $\delta^{18}O$ values of lakewater thus inferred are plotted against their U-series ages, extending back to 150 ka BP in Fig 5.18. The older sinters from Arus and Chepchuk are poorly constrained for age and are not included. Also shown in Fig 5.18 are the $\delta^{18}O$ ranges for waters suggested by isotopic analyses of stromatolitic carbonate from various East African lakes (Abell et al, 1982; Hillaire-Marcel and Casanova, 1987; Tiercelin et al, 1987; Casanova and Hillaire-Marcel, 1992). A separate plot, Fig 5.19, amplifies the detail of the last 15 ka and also shows the present-day values of lakes Baringo, Bogoria, Magadi, Turkana and Manyara (Tanzania).

There is reasonable agreement between the $\delta^{18}O$ values inferred for contemporaneous sinters and stromatolites. While it is true that they come from different Rift Valley lakes, at times of high lakestands it is likely that the isotopic compositions would be similar for all the lakes: only when lakes become terminal and/or small in volume do the differentiating effects of evaporation

Table 5.3   Values of $\delta^{18}O$ for siliceous sinters from the northern KRV, with the equilibrium values for the depositing waters, assuming a temperature of 100°C.

Site	$\delta^{18}O$-SiO$_2$ ‰	$\delta^{18}O$-H$_2$O @100°C ‰	U-series age[1] ka ± 1σ
Arus-1	+21.8 ± 0.3	+0.8	350 ± 110
Korosi-1-A	+19.3 ± 0.1	-1.7	11.9 ± 0.6
Chepchuk-2-A	+20.5 ± 0.4	-0.5	350 ± 60
Chepchuk-2-B	+19.2 ± 0.1	-1.8	430 ± 120
Paka-1-A	+19.9 ± 0.1	-1.1	81 ± 5
Paka-1-B	+20.5 ± 0.1	-0.5	64 ± 4
Emuruangogolak-3-C	+23.7 ± 0.1	+2.7	29 ± 4
Emuruangogolak-3-D	+24.8 ± 0.1	+3.8	29 ± 4
Namarunu-2-A	+25.7 ± 0.1	+4.7	133 ± 11
Namarunu-2-B	+21.0 ± 0.1	0.0	≥ 380
Namarunu-2-C	+23.6 ± 0.1	+2.6	≥ 440
Barrier-1-A	+25.3 ± 0.1	+4.3	6.9 ± 0.4
Barrier-1-C	+29.7 ± 0.1	+8.7	9.3 ± 0.5
Barrier-1-F	+28.7 ± 0.1	+7.7	7.6 ± 0.3

Analyses of $\delta^{18}O$-SiO$_2$ by NERC Isotope Geosciences Laboratory

[1] Data from Sturchio et al (1993)
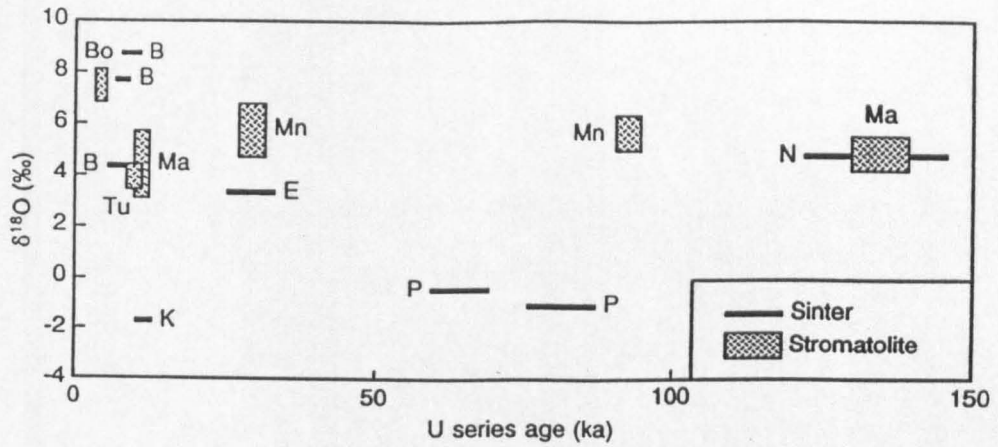
Fig 5.18   Plot of inferred $\delta^{18}O$ values of lakewaters vs U-series ages for KRV
            sinters over 0-150 ka BP.   Also shown are $\delta^{18}O$ values of
            lakewaters inferred from stromatolites (most Holocene ages from
            radiocarbon dating). Volcanic centres: B - Barrier, E - Emuruan-
            gogolak, K - Korosi, N - Namarunu, P - Paka. Lakes: Bo - Bogoria,
            Ma - Magadi, Mn - Manyara (Tanzanian rift), Tu - Turkana.
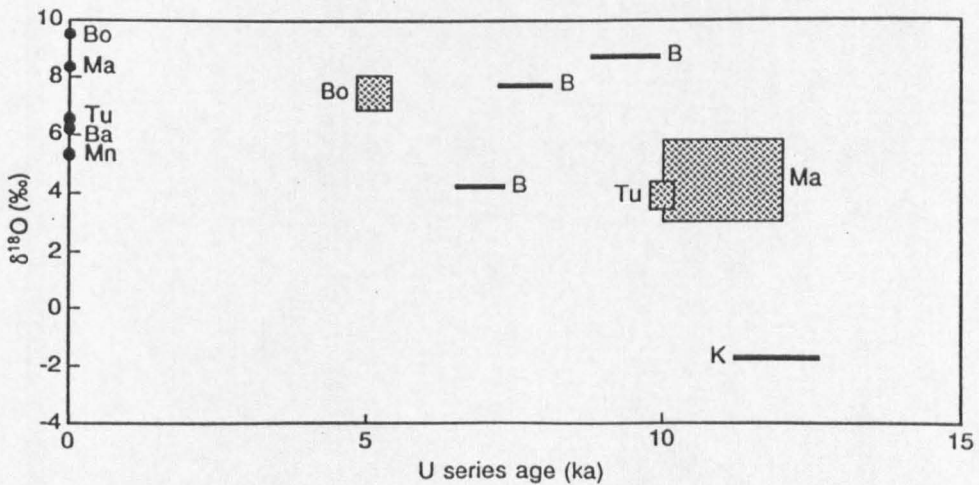
Fig 5.19   Expanded version of Fig 5.18 over the period 0-15 ka BP. Volcanic
            centres identified as before. Lakes identified as before, plus Ba -
            Baringo.

99

on isotope content become apparent.

It is significant that the more depleted $\delta^{18}O$ values inferred from the sinters are not accompanied by any stromatolite data. Presumably these periods were too cool to permit stromatolite growth. However, if isotopic equilibration between silica and water were taking place at temperatures significantly below 100°C, the inferred values for lakewater would be up to 8‰ more negative. Such low values of $\delta^{18}O$ would seem to be implausible for East African lakes even during cooler periods of the Pleistocene.

Given that the $\delta^{18}O$ values of lakewater inferred from sinters may therefore be reasonably representative, a brief interpretation of palaeoconditions can be attempted. Beyond 150 ka BP there is little detailed information about local climatic conditions, and the only high lakestand known during the period is in the Magadi-Natron basin at about 300 ka (Hillaire-Marcel and Casanova, 1987). This may correspond with the Arus and Chepchuk samples. In the period of 15-150 ka BP lake levels in East Africa generally were high from 25-35 ka and 125-145 ka. Fig 6.18 shows that the U-series dates on sinters from Emuruangogolak and Namarunu are consistent with these ages, suggesting that lakewater $\delta^{18}O$ values were similar to the present ones, though indicating somewhat cooler conditions. The Paka samples from 65-85 ka BP do not correlate with any known highstand but indicate a humid phase under significantly cooler conditions.

More is known about the last 15 ka. During this period Baringo reached its highest level at 11-12 ka BP, while the highest stand on the Suguta palaeolake has an age of 9.7 ka BP. Turkana fluctuated around a maximum level between 7.5 and 9.5 ka BP. Fig 5.19 shows that at the beginning of the Holocene the sample from Korosi, associated with the highstand of Baringo, indicates a lakewater considerably depleted in ^{18}O compared to the present. Shortly after this, however, a sinter from the Barrier shows much more enrichment in ^{18}O, although this falls over the next 2.5 ka to a value not dissimilar to today's. The implications of these results are that at the start of the Holocene the lake basins were full of isotopically depleted water, but that rapid changes in atmospheric circulation (Nicholson and Flohn, 1980), and perhaps catchment area, led to an enrichment in ^{18}O reaching a peak within 2 ka. After 9 ka BP Suguta and Turkana became separate lakes, and as Suguta dried up the sinters may have become derived primarily from Turkana lakewater. By this time the main source of Turkana was probably the Ethiopian highlands (as at present), and therefore the lake would have had an increasingly depleted composition due to the altitude effect. At about 3.5 ka BP Turkana became a closed basin (Yuretich and Cerling, 1983), and is presumably becoming more

enriched in ^{18}O with time. The same process would have begun in the much smaller Lake Bogoria at an earlier date.

5.1.5   Ground and surface waters in the Main Ethiopian Rift

The interpretation that follows is based largely on the data of Craig et al (1977) and some from Gizaw (1989) in Appendix C (Table C.1), with some original supplementary data from this study (Table 5.4). Fig 5.20 shows the location of sampling sites, while Fig 5.21 is a δ-plot of all oxygen and hydrogen stable isotope data excluding steam condensate compositions.

Despite the long-term rainfall weighted average of -1.3‰ $\delta^{18}O$, +2‰ $\delta^{2}H$ (IAEA, 1992) referred to in 5.1.1.2 above, available data for Addis Ababa give results of -4.0‰ $\delta^{18}O$, −16‰ $\delta^{2}H$ for a cool groundwater (CRA97) or -6.2‰ $\delta^{18}O$, -30‰ $\delta^{2}H$ for a hot water (E23). The difference between the waters is significant and suggests that the cold water is recharged quite locally, while the thermal water is the result of deep circulation from higher-altitude recharge. This is not an unusual situation, except that CRA97 is so different from the rainfall weighted average. The sub-thermal water of Ambo (E24), on the plateau to the west, is intermediate between the two compositions. In general, groundwaters within the MER whether thermal or otherwise also show a more depleted composition compared to rainfall in Addis Ababa. This nonetheless accords well with the typical rift-wall composition of $\sim$ -3.6‰ $\delta^{18}O$, -15‰ $\delta^{2}H$ encountered at sites such as Imba Koto, Koshe, Bodicho and Sholicha (CRA11, 14, 59, 67) in thermal and sub-thermal waters alike. There are, however, two more-depleted sites at Mojo and Jido Combol (CRA3, 17) which may contain palaeowater. There are no published ^{14}C for any MER site. Hence the residence time of these waters is unknown, and due to the absence of $\delta^{13}C$-DIC data for these particular sites it is difficult to tell whether radiocarbon dating would be compromised by volcanic CO_2 inputs (see 6.3.1 below).

Some groundwater sampling sites on the floor of the MER are clearly affected by inputs of surface waters. The influence of crater-lake water is apparent at Debre Zeit (CRA2), while the Awash River may affect the composition of the Sodere thermal springs (E16). The Southern Cross well (CRA8) between the Koka reservoir and Lake Zwai has a somewhat enriched composition, perhaps due to infiltration from the Maki River which sometimes during flood conditions flows into Koka (see 4.3.2). Some river infiltration may also reach the Maki well (CRA9). The Zwai well (CRA7) clearly abstracts water from the highly enriched Lake Zwai. Other notably enriched waters are encountered in the Adami Tulu well (CRA5), which is probably fed by the Bulbula river outflow from Zwai, and the Bekele Molla well (CRA55) at
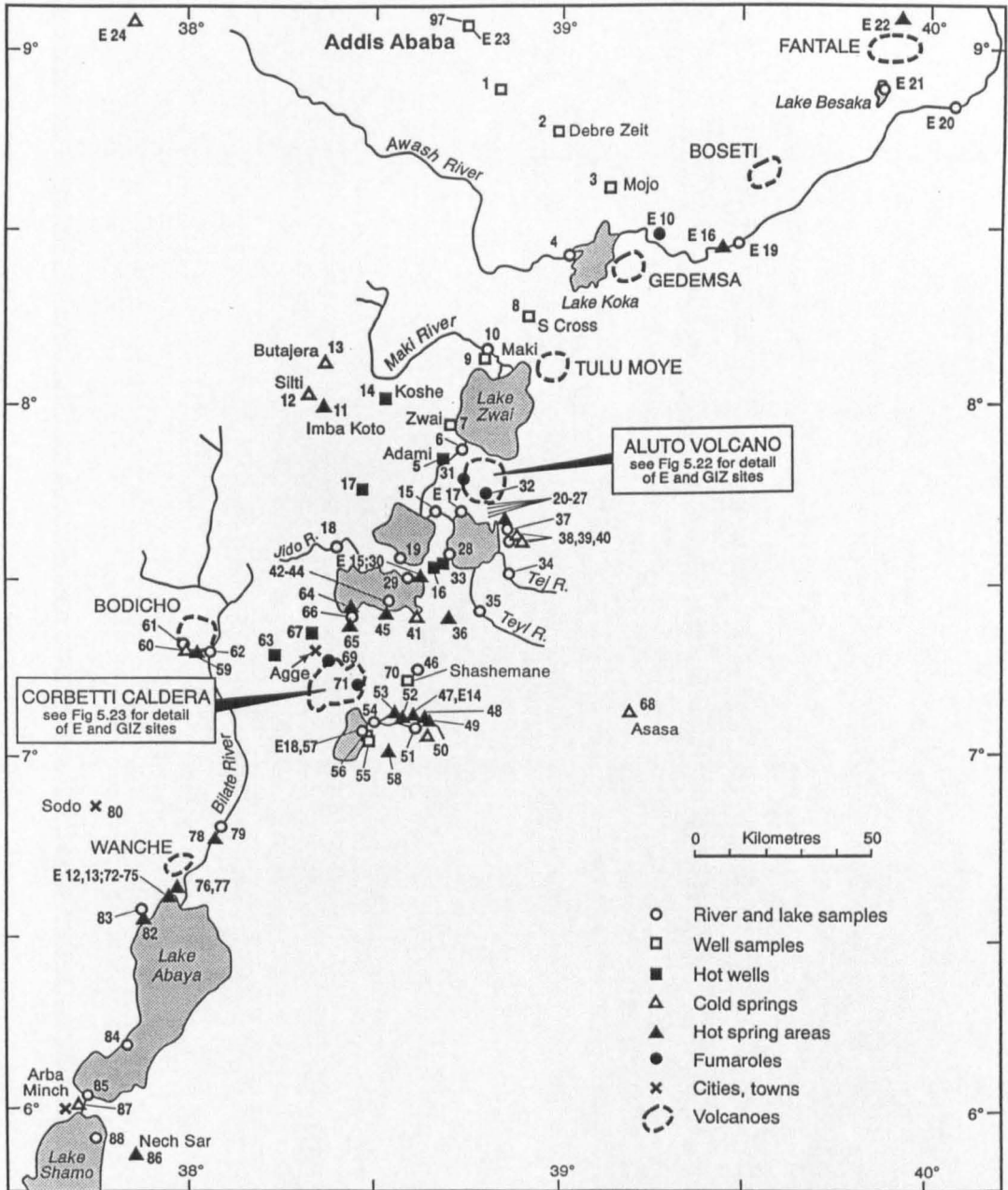
Fig 5.20   Sample sites in the Main Ethiopian Rift. Plain numbers denote the sites of Craig et al (1977). Numbers prefixed E refer to sites sampled during this study.

Table 5.4   **Stable isotopic composition of ground and surface waters collected in the MER and southern Afar during the present study.**

Site Name	Site No	Sample type	Temp °C	$\delta^{18}O$ ‰	δ^2H ‰	$\delta^{13}C_{DIC}$ ‰
Langano #2	E11	S	65	-0.2	-6	-
Abaya #6	E12	S	96	+0.1	-10	-
Abaya #7	E13	S	88	+9.7	+14	-
Wondo Genet	E14	S	65	-2.1	-11	-
Shalla #30	E15	S	96	+2.8	+12	-
Sodere	E16	S	65	-2.1	-11	-1.1
Langano	E17	L	amb	+7.5	+50	-
Awasa	E18	L	amb	+7.8	+53	-
Awash at Sodere 12/90	E19	R	amb	+1.7	+9	-
Awash at Sodere 2/95	E19	R	amb	-0.7	-1	-
Awash at Sodere 9/95	E19	R	amb	-1.1	-2	-
Awash at ANP 9/95	E20	R	amb	-1.1	0	-
Besaka Hayk	E21	L	amb	+5.8	+34	-
Awash Filwoha	E22	S	43	-2.7	-16	-5.7
Ghion, Addis Ababa	E23	S	70	-6.2	-30	-3.7
Ambo	E24	S	39	-4.8	-21	-
Asal A-3	D1	G	-	+0.9[1]	-	-
Korilli	D5	S	36	-1.3[1]	-	-
Abbe C	D6	S	75	-2.9	-23	-
Abbe N	D7	S	90	-3.7	-27	-
Plage de Ghoubet	D8	M	amb	+0.4	+3	-

G - geothermal well   L - lake   M - seawater   R - river   S - spring   amb - ambient

[1] measured at the University of Iceland

Samples collected in Dec 1990 with the following exceptions: River Awash - as dated; E22 - Feb 1995; E21, 23, 24 - Sept 1995.
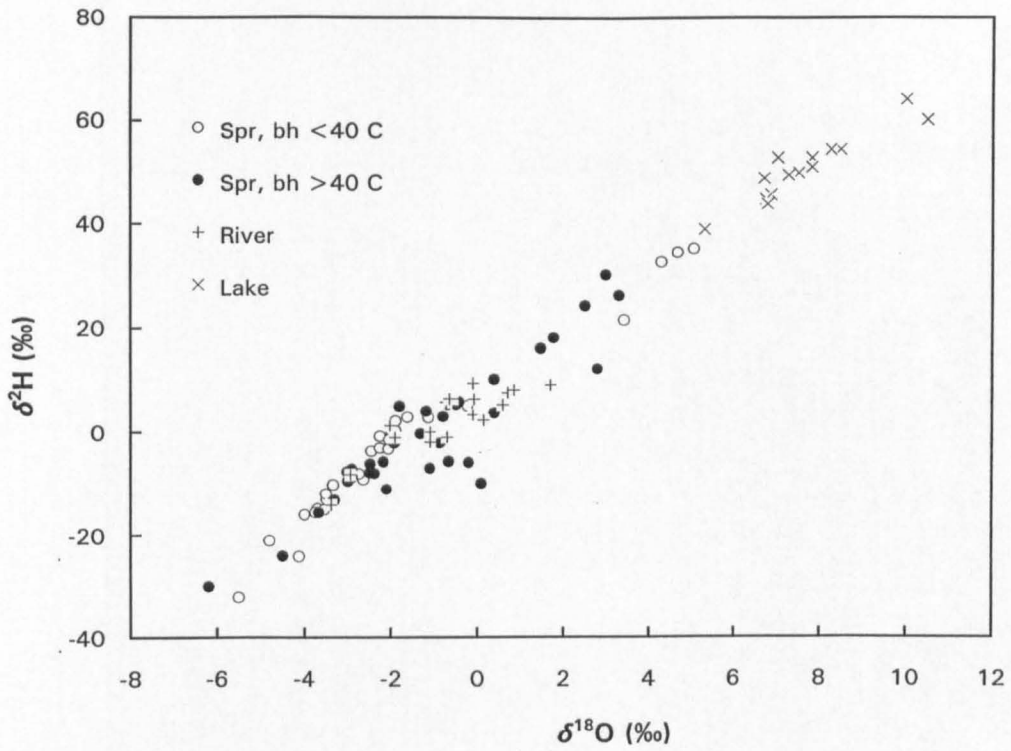
Fig 5.21   Plot of δ^2H vs $\delta^{18}O$ for waters of the MER, excluding high-temperature geothermal waters and fumarole steam condensates.

Awasa, which is situated close to the lake. Otherwise, typical rift-floor meteoric recharge seems to be of the order of $\sim$ -2.6‰ $\delta^{18}O$, -8‰ δ^2H, as seen for example in the Wondo Genet area east of Lake Awasa, and the Chokare area north of Lake Abaya. In this respect the stable isotope values are basically similar to, if slightly more enriched than, the rift-wall and rift-floor groundwaters in the South Turkana Rift of Kenya.

By analogy with the Kenya rifts and in particular the examples of Naivasha and Baringo, the question arises of the extent of underflow from the lakes of the MER. From the hydrological information in Chapter 4, potential exists for underflow from Zwai to Langano and Abiata, and from these two lakes to Shalla. Awasa too, a fresh lake without a river outlet, is likely to have a subsurface outflow. Abaya also has the potential to discharge into Shamo.

It is not clear from existing data that Zwai has a significant underflow. Reference has been made to the Adami Tulu well (CRA5) but this is probably affected by river water. Data from Craig et al (1977), Gizaw (1989) and the present study relating to the Aluto volcanic centre are plotted in Fig 5.22. The deep geothermal wells inside the complex reveal little if any mixing between water from Zwai and a typical rift-wall water. This shows that, despite a large water resource immediately to the north, firstly the Aluto hydrothermal plume must be fed laterally, presumably from the east, and secondly that there is very little ^{18}O-shifting. Fumarolic steam compositions likewise suggest a very minor lakewater compositions (assuming subsurface condensation to be minimal). Some fairly enriched isotopic compositions have been measured in the springs on the edge of Langano, but it is not clear whether these are intercepting water flowing around the outside of the complex or whether there is an element of recycling of Langano water due to convective circulation. Evidence from shallow boreholes drilled for thermal gradient measurement indicates that either there is some mixing with lakewater at higher levels near the periphery of the complex, or that the waters have been affected by steam loss.

Judging by its positive isotopic content, the Bekele Molla Hotel borehole (CRA33) on the southwest edge of Langano extracts a proportion of lakewater. At the Wildlife Conservancy borehole (CRA16) midway between Langano and Shalla, the isotopic composition is still enriched relative to rift-floor recharge. It therefore seems probable that some underflow to Shalla is occurring. It was contended by Von Damm and Edmond (1985) that the Shalla NE boiling springs (CRA30, E15) are merely recycling Shalla lakewater under hydrothermal circulation. However, the springs are depleted compared to Shalla and there must therefore be an input from elsewhere; conceivably this is a mixture of rift-floor recharge and underflow
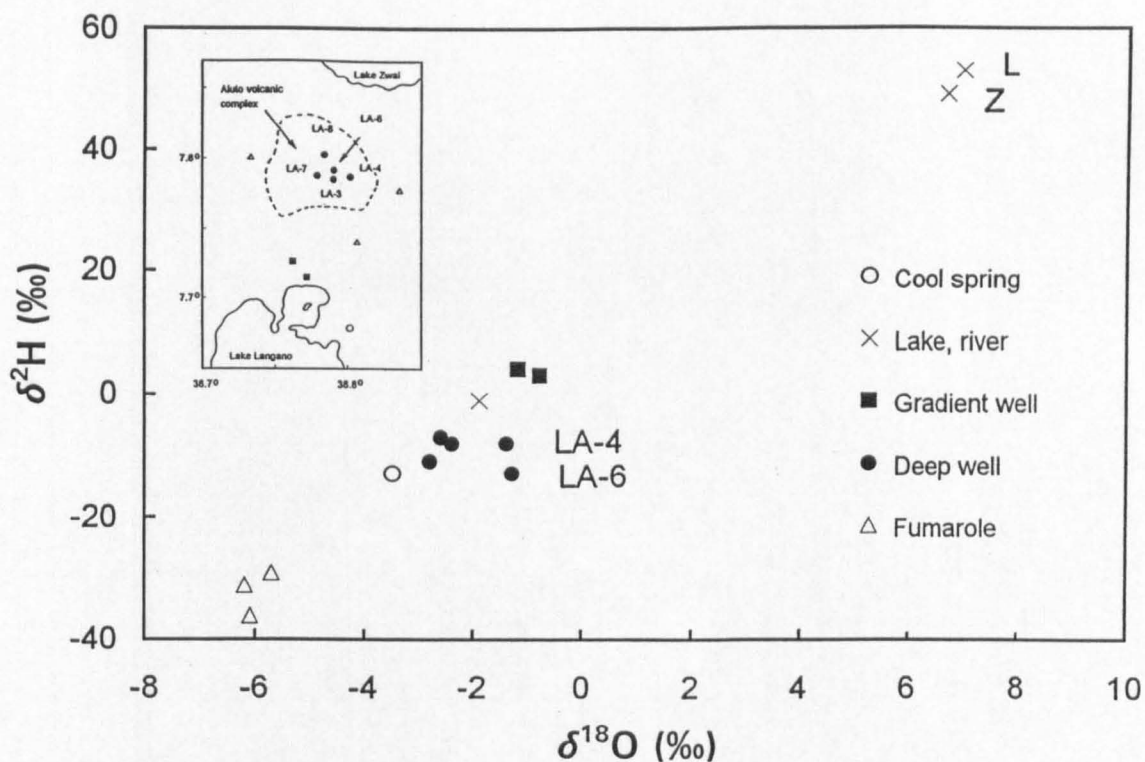
Fig 5.22   Plot of δ^2H vs $\delta^{18}O$ for waters of the Aluto area, including deep geothermal waters and fumarolic steam. Samples from geothermal wells LA-4 and LA-6 show signs of minor ^{18}O shifting. L - Langano, Z - Zwai. Well data from Gizaw (1989), lake and spring data from Craig et al (1977) and fumarole data from this study. Inset: map of the area.

from Langano. It is even more likely (on chemical grounds— Von Damm and Edmond, 1984) that underflow is occurring from Abiata to Shalla, but no isotopic data are yet available from between the lakes.

The likelihood of subsurface outflow from Awasa is confirmed by the results of isotopic analysis of groundwater and steam in the vicinity of the Corbetti caldera. Fig 5.23 shows a map of sampling sites, while the data are plotted in Fig 5.24. The samples are interpreted with respect to Awasa lakewater (E18) and rift-floor recharge as measured in the Shashemane well (CRA70). Gradient boreholes outside the caldera boundary reveal the presence of lakewater, as do the fumarolic steam samples from Borama (CRA71) and Koka (E9). Inside the caldera complex, however, neither the gradient boreholes nor steam from the Chebicha and Danshe fumaroles (E7, 8) shows any evidence of a lakewater component, even allowing for the fractionating effects of steam separation. Since Awasa is situated on a local high point on the floor of the MER, underflow may occur to the south as well, but no sample points exist to provide evidence for or against this.

In the south of the MER, at Arba Minch, many springs discharge in the same area, apparently as a result of underflow from Lake Abaya to Lake Shamo. Assuming the spring CRA87 is typical, the isotopic composition shows that if there is a component of lakewater from Abaya in the area, it has been significantly diluted by water from the rift wall, to the extent where lakewater could only amount to some 10-15% of the total.

The lakes of the MER, including the small Lake Besaka (E21) at the extreme northern end of the valley (Fig 5.20) are highly enriched in heavy isotopes, apparently more so than the lakes of the Kenya Rifts. For the shallow lakes to some extent their composition varies seasonally, as the variations for Langano and Awasa show (CRA15, 57; E17, 18). However for the extremely deep Lake Shalla fluctuations could be expected to be much smaller; this is probably the most isotopically enriched lake of significant size in the whole of the Eastern Rift.

In summary, waters of the MER behave similarly to those of the KRV in terms of their isotope hydrology to the extent that similar processes operate. The MER is shorter in length than the main KRV and because of this experiences a reduced range of climatic conditions, since altitude differentials are smaller. Also, rainfall is generally higher than in the KRV. Despite these differences, the range of isotopic results is very similar to that found for Kenya, even for the more extreme values exhibited by lakes and fumarolic steam. Perhaps the main contrast with the KRV is that stable isotopes provide no evidence of underflow beneath volcanic centres of
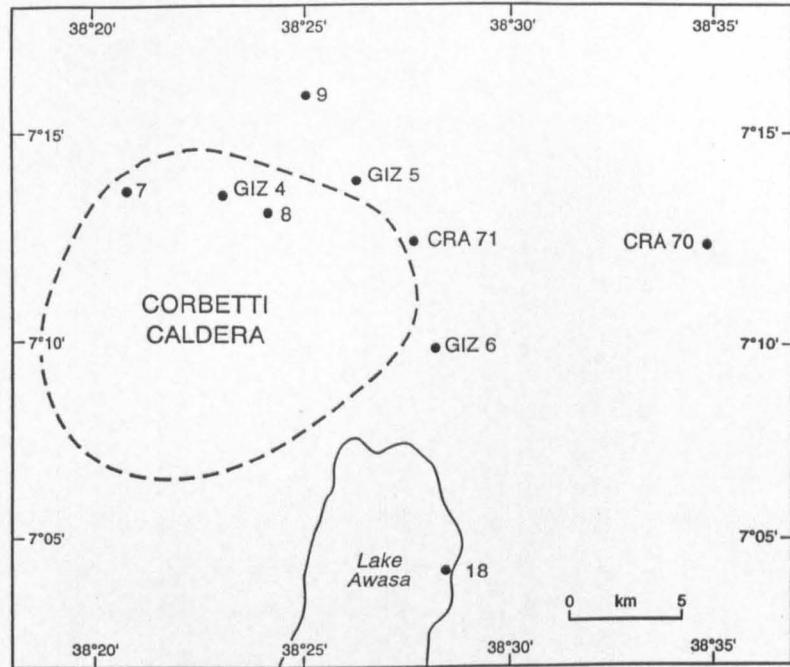
Fig 5.23   Sampling sites in the Corbetti caldera area. Plain numbers, denoting samples from this study, are referred to with E prefixes in text and tables. Prefixed numbers as follows: CRA - Craig et al (1977), and GIZ - Gizaw (1989).
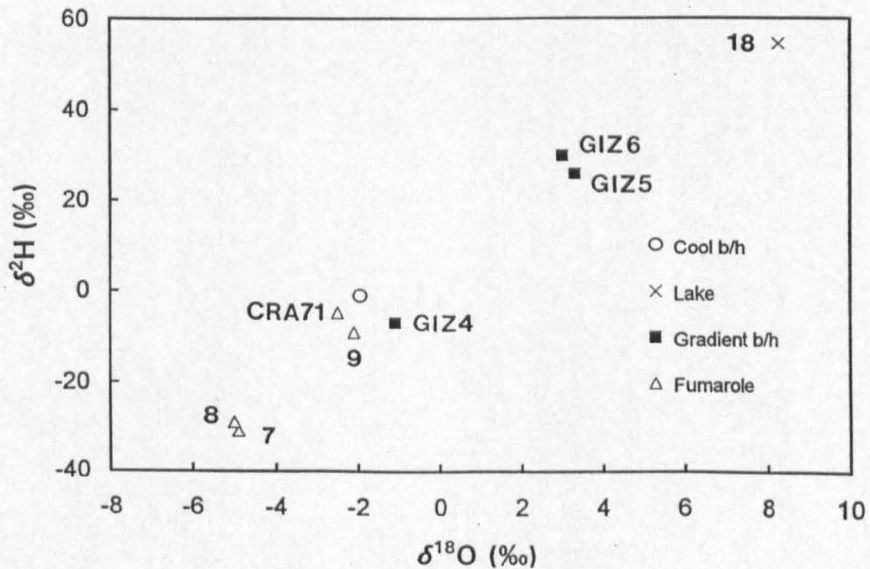
Fig 5.24   Plot of δ^2H vs $\delta^{18}O$ for waters of the Corbetti area, including gradient well waters (see numbers in Fig 5.23) and fumarolic steam. Cool borehole (CRA70) is situated in Shashemane to the east of the caldera.

the MER, whereas there appear to be several examples in the KRV.

5.1.6   Ground and surface waters in Southern Afar

A δ-plot of ground and surface waters for the area is shown in Fig 5.25, based on data from various sources summarised in Tables 5.4 and C.2 and with sample sites located on Fig 5.26. The data from the Ethiopian part (Filwoha, Meteka; E22, NC sites), albeit sparse, indicate that the recharge to these springs can be local but also sometimes more isotopically depleted than might have been expected from consideration of rift-floor recharge in the MER to the south. This depletion may be due to recharge from a higher altitude, conceivably the wetter Ethiopian Plateau to the west.   A similar mechanism of higher-altitude recharge, but from the Somalian Plateau to the south, may explain the rather depleted waters from sites in Djibouti such as Mouloud, Kourtimalay and Doubdoub (VER9, 28, FON75/1).   More local recharge is indicated for some sites, particularly nearer the coast (Oueah, PK50 and PK20; VER5, 6, 25) but also well inland at Dikhil (VER7).   It may be that the isotopically heavier samples are the product of local flood infiltration from the "oueds" (wadis) of the area, whereas the depleted samples are the result of regional recharge.   Judging by the radiocarbon values in these groundwaters (see 6.3.2 below), there is little evidence that the O and H isotopic depletions could be due to the existence of early Holocene groundwater.

The isotopic content of the Awash and Mille rivers (CRA93, 96, E20) is not compatible with the composition of Lake Abbe as reported by Fontes et al (1980).   Most unusually for an Eastern Rift lake, this has a negative δ^2H content and could not be the result of evaporative concentration of water from the Awash.   In reality, it is likely that the isotopic composition of Abbe is far more isotopically enriched than was measured, and that the sample obtained by Fontes et al was a mixture of lakewater and spring water.   (The difficulty of collecting representative samples away from springs at the edge of such shallow lakes makes this hypothesis feasible.)   A mixing of waters would remove the incompatibility between the reported isotopic value and the statement in Fontes et al (1980) that the lake consists of evaporated river water.

Consideration of the data from the Gulf of Ghoubet and the Manda springs (D8, FON76/8) supports the inference that Lake Asal, at ~ 150 m below sea level, is fed by seawater.   The composition of the lake (F76/9) does not appear to be particularly enriched by evaporation, despite ~ 3000 mm of evaporation annually, until it is realised that this represents the reversal of enrichment in δ^2H that takes place in the mother liquor as halite is deposited (Fontes et al,
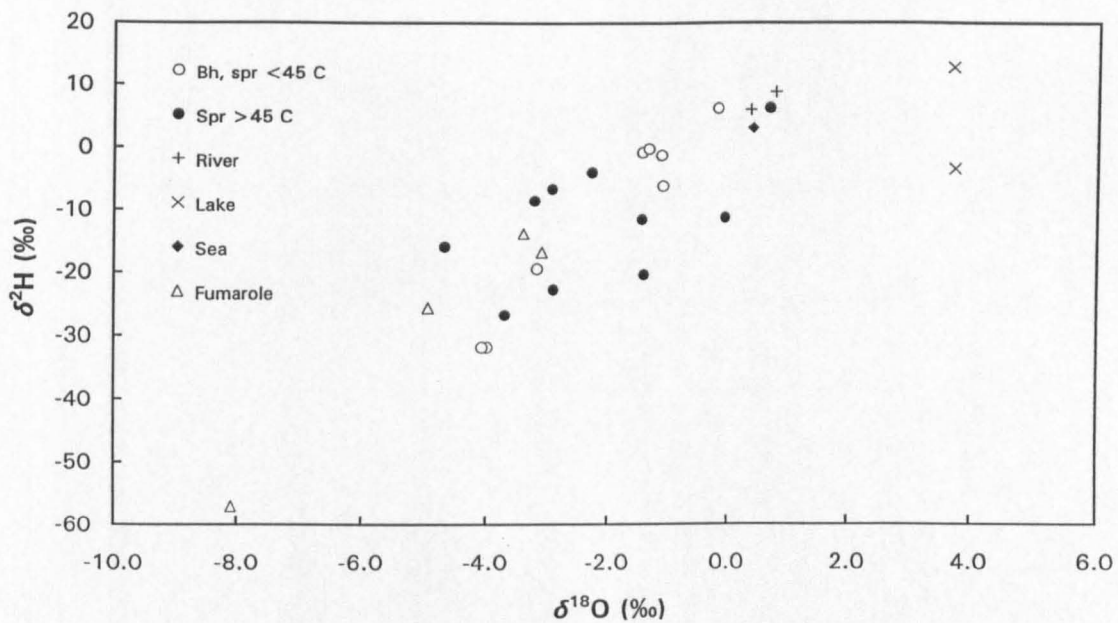
Fig 5.25   Plot of δ^2H vs $\delta^{18}O$ for waters of the Southern Afar area.
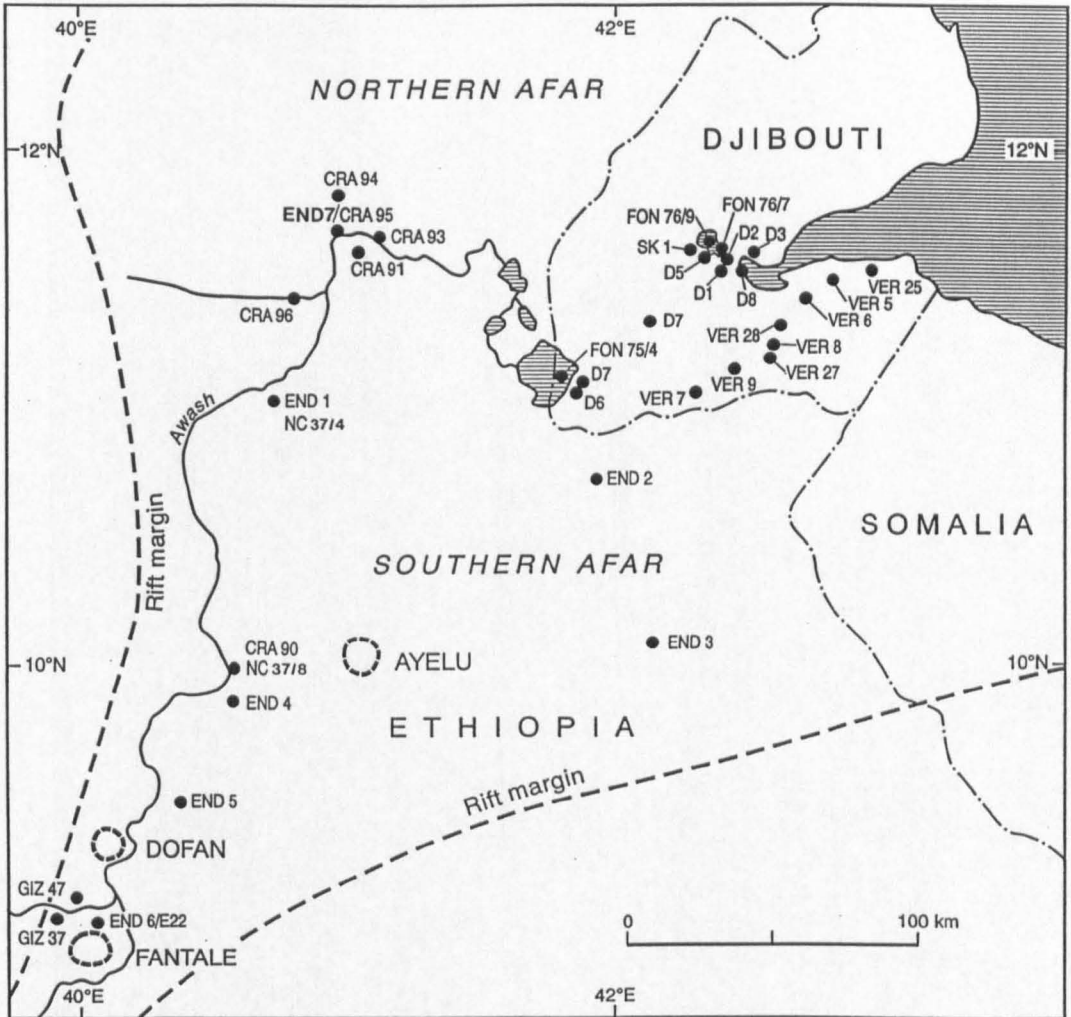
Fig 5.26   Sampling sites in Southern Afar. Plain numbers, denoting samples from
this study, are referred to with E or D prefixes in text and tables,
depending on whether they are from Ethiopia or Djibouti. Prefixed
numbers as follows: CRA - Craig et al (1977), END - Endeshaw (1988),
FON - Fontes et al (1979, 1980), NC - Schoell and Faber (1976),
S – Sanjuan et al (1990) and VER - Verhagen et al (1991).

1979). The Korilli Spring, despite its very high NaCl content, has a relatively depleted isotopic composition. This observation, together with the chemical data from Oued Kalou (see 6.3.3 below), confirms that there is some discharge of meteorically-derived water into the Asal basin in addition to the predominant seawater leakage.

The only item of isotopic data available for the deep geothermal fluid at Asal is a $\delta^{18}O$ value from Well A-3, at +0.9‰ (D1). Since seawater is the basic source of the geothermal fluid (Sanjuan et al, 1990), this is evidence against a significant ^{18}O shift.

In southern Afar, therefore, stable O and H isotopes are acting as excellent hydrological tracers as they do elsewhere in the Eastern Rift. Despite the hot and arid climate some groundwaters are as isotopically depleted as in the MER, but this is likely to be the result of infiltration on the high plateaux along the boundaries of the area rather than on the plains. More surprising is the lack of highly-enriched surface waters, although this is probably related to a scarcity of data than to any differences between Afar and elsewhere. The existence of marine evaporites (Chapter 6) means that chloride is not a reliable indicator of contemporary marine influences, and therefore stable isotopes have a particularly important role to play in unravelling the hydrogeology of the Asal basin.

5.2   Carbon stable isotopes

5.2.1   Kenya Rifts

Values of $\delta^{13}C$ for dissolved inorganic carbon (DIC) for samples from Kenya are provided in Table 5.2a-c and range from -16.5 to +0.9‰ PDB. The lighter values are typical of the dissolution of rock carbonate by soil CO_2 under open-system conditions. Accordingly, the waters with $\delta^{13}C$ values in the range -12 to -16‰ are likely to consist largely of little-modified meteoric water. Thus many of the cool well and spring waters fall in this category, but few of the hot springs. Only the barely thermal waters from Kijabe and Loyangalani (K26, 242) have $\delta^{13}C$ values more depleted than -12‰, while all other thermal waters are more enriched than -8‰. This indicates that there is a degree of water-rock interaction in most cases.

However, the amount of such interaction is not necessarily a function of sampling temperature. Some enriched $\delta^{13}C$ values are obtained in cool spring and well waters. There are different explanations for this in various cases. For example, well C567 (K81) is believed to have a contribution of around 50% from Lake Naivasha (5.1.2.2). Isotopic equilibration between the

atmosphere and the lakewater would be expected to give the lakewater a $\delta^{13}C$ value of around 0‰, and the C567 value of -0.4‰ is clearly consistent with this. In other cases, such as the springs of Kachurkolh (K194), which are not close to a lake but which have a high HCO_3 content, a different explanation is required. In this case the dissolution of bicarbonate (the term is used here to include carbonate) formed originally by hydrolysis of silicates by CO_2 might be responsible. The basis of this is the following reaction whereby feldspar reacts with water and CO_2:

$$2NaAlSi_3O_8 + 11H_2O + 2CO_2 = Al_2Si_2O_5(OH)_4 + 2Na^+ + 2HCO_3^- + 4H_4SiO_4 \qquad (5.9)$$

This could be the mechanism ultimately responsible for the $\delta^{13}C$-DIC values seen in many of the Kenya Rift groundwaters. High HCO_3 might result from *in situ* hydrolysis where groundwater flow is sufficiently slow, or the process might simply be contributing to the chemistry of lakes which periodically become desiccated (5.1.4.3), presumably accompanied by the deposition of carbonate evaporites.

Fig 5.27 shows a plot of groundwater $\delta^{13}C$-DIC values against their alkalinity expressed as HCO_3. Also shown in the figure is a model dissolution line based on the assumption that water with an initial recharge composition of 250 mgl^{-1} HCO_3 and -16‰ $\delta^{13}C$-DIC progressively acquires either evaporitic or in situ bicarbonate with a typical value of -1‰. There is no *a priori* connection with geothermal activity other than that usually the hotter waters are more effective at redissolving evaporites or at promoting silicate hydrolysis. There is no certain way of distinguishing whether near-ambient high-TDS springs like Kalnangi and South Nangarabat (K195, 197) are cooled thermal waters, or merely waters which have been in residence long enough to acquire a greater concentration of evaporites. If they are cooled waters, the plot of HCO_3 versus sampling temperature (Fig 6.5) suggests they could have cooled from temperatures of up to 65°C.

The reason why there may be an abundance of bicarbonate with a $\delta^{13}C$ of around -1‰ is related to the pervasive flux of CO_2 from the rift (see Chapter 7 below). A marine-derived calcium carbonate source can be ruled out, since there is no evidence for such deposits in the continental Eastern Rift, and little evidence of the Ca which should otherwise be present at higher concentrations in groundwaters. The $\delta^{13}C$ content of the bicarbonate may be the result of direct hydrolysis at an elevated temperature by magmatic CO_2, or the result of atmospherically equilibrated evaporites. The primary source is uncertain because both processes would tend to produce a result close to 0‰. For example, the Lorusio springs (K45)

113

deposit a travertine with a $\delta^{13}C$ of -0.4‰.

However, Fig 5.27 also shows that there are some exceptions to the dissolution model. A group of boreholes in the area north of Eburru in the Gregory Rift have magmatic indicators (e.g. high $^3He/^4He$ at K124, see Chapter 7) and may well have been perturbed by outgassing CO_2 (see also the radiocarbon data for this well in 5.3.1 below). Also, two boreholes at Nginyang in the South Turkana Rift (K203, 204) do not fall on or near the dissolution/hydrolysis trend. These sites are both close to the Nginyang River, and may be affected by mixing between groundwater and river water. This would account for the observed $\delta^{13}C$ values of around -10‰, but not for the HCO_3 concentrations, which are still high.

5.2.2   Main Ethiopian Rift

A similar situation to that of the Kenya rifts obtains for the MER. Fig 5.28 shows a plot of $\delta^{13}C$-DIC versus groundwater bicarbonate, based mostly on data from Craig et al (1977), given in Tables C.1 and E.1. The chief differences from Kenya are (a) that a slightly more enriched bicarbonate source of around 0‰ is indicated, (b) there are no HCO_3 concentrations above about 3500 mgl^{-1}, and (c) that there are no exceptions to the dissolution trend on the scale of the Nginyang wells referred to in 5.2.1 above.

The data of Craig et al (1977) reveal that the lakes of the MER have elevated, positive $\delta^{13}C$-DIC values. This accords with the amount of fractionation that would be expected relative to an atmospheric value of ~-7‰ at the kind of average temperatures encountered in the MER (around 20°C). Although they were not measured, the Kenya lakes are assumed to have similar values, and like the example cited in 5.2.1 above of borehole C567 adjacent to Lake Naivasha, a borehole near to Lake Awasa (CRA55) was found to have a high $\delta^{13}C$-DIC value. No high-HCO_3 cool springs like those of the South Turkana Rift have been reported for the MER. However, Craig et al (1977) tended to restrict their $\delta^{13}C$ analyses to hot springs.

5.2.3   Southern Afar

In southwest Afar, the Filwoha and Meteka springs resemble some of those to the south in the MER in that they have relatively high HCO_3 contents and enriched $\delta^{13}C$ values (Tables C.2 and E.2). As such, they conform reasonably well to the dissolution/hydrolysis model (Fig 5.29). However, as explored in more detail in Chapter 6, this is a transitional area for water chemistry where HCO_3 is replaced by Cl as the dominant anion. Thus, further north in the Tendaho area,
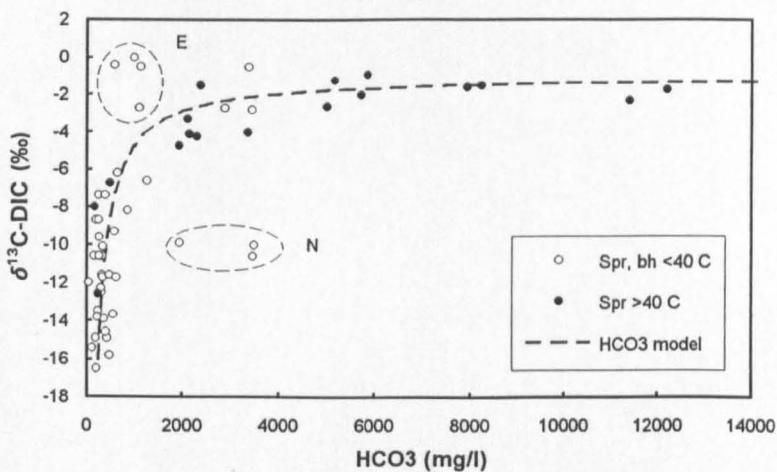
Fig 5.27 Plot of $\delta^{13}C$-DIC vs concentration of DIC as HCO_3 for the KRV. E - Eburru "badland" wells, N - Nginyang wells (see text).
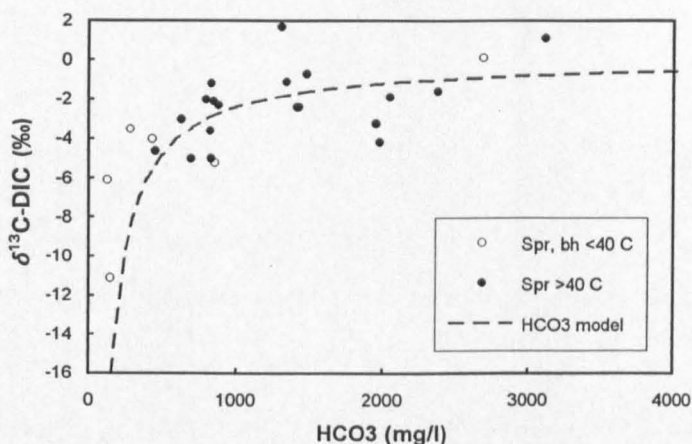
Fig 5.28 Plot of $\delta^{13}C$-DIC vs concentration of DIC as HCO_3 for the MER. Data from Craig et al (1977) and this study.
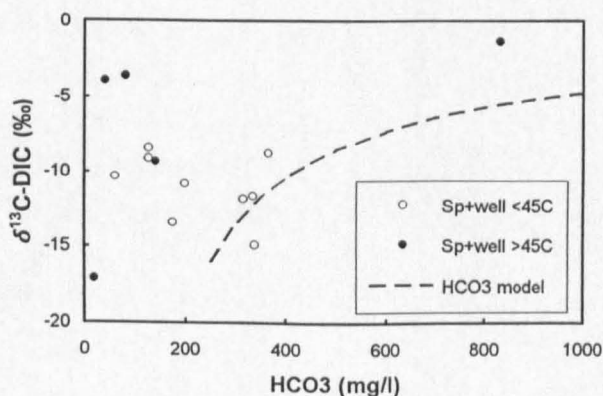
Fig 5.29 Plot of $\delta^{13}C$-DIC vs concentration of DIC as HCO_3 for southern Afar. Data from Fontes et al (1980), Verhagen et al (1991) and this study.

the Allallobeda springs and Loggia well (CRA91, 95) have elevated $\delta^{13}C$-DIC values, but very low HCO_3, and therefore do not fit a hydrolysis model. Presumably in these waters carbon is present largely in the form of CO_2 with a typically geothermal value of around -3‰, and this is controlling the measured values.

Data relating to $\delta^{13}C$-DIC from the cross-section of sites in Djibouti running eastwards from Lake Abbe, already considered for stable isotopes in 5.1.6 above, show that waters are too low in HCO_3 to be expected to follow a dissolution/hydrolysis trend (Table E.2). If the Afar data are taken as a whole, if anything there is a trend towards *lower* HCO_3 as $\delta^{13}C$ rises (Fig 5.29), for the reason given in the previous paragraph.

5.3   Radioisotopes

5.3.1   Gregory Rift

The radiocarbon (^{14}C) content of groundwater was measured at seven representative sites in the Gregory Rift (Table 5.5, Fig 5.30), in order to estimate groundwater "age" as a check on the flow rates deduced from physical modelling of groundwater movement. The uncorrected ages shown on Fig 5.30 are calculated on the basis of simple ^{14}C decay and take no account of addition of "dead" carbon to the system. In most groundwater systems this addition comes from the dissolution of rock carbonate phases by "active" CO_2 produced in the soil zone; if rock and dissolved inorganic carbon (DIC) $\delta^{13}C$ values are known or assumed, corrections to the groundwater age can be attempted. In this case these were attempted using WATEQF-ISOTOP (Reardon and Fritz, 1978).

Table 5.6 shows the results of running the correction program with two initial pH values, 5 and 8, and using two different rock carbonate $\delta^{13}C$ values, to test the effect of a range of inputs. In each case the soil zone CO_2 is assumed to have had a composition of -25‰ PDB. As has been shown in 6.2.1, rock carbonate is likely to have a $\delta^{13}C$ of about 0‰. This was used as a starting point to run the ISOTOP model. It is primarily the areas unaffected by CO_2 where radiocarbon is going to give the most useful results. However it is also here where the rock carbonate composition is not known with any certainty. Therefore, in view of the carbonatitic volcanism associated with the KRV, the model was also run with a rock carbonate value of -5‰ PDB, a typical carbonatite value (an average obtained for three carbonatite samples collected from the Homa Mountain complex). In most cases the resulting model ages are modern, irrespective of the starting conditions, as the raw ^{14}C values had suggested. The

Table 5.5   **Results of radiocarbon and tritium analysis on samples from selected sites in the southern KRV.**

Site Name	Site No	Sample type	Temp °C	^{14}C pmc ± pmc	δ^{13}C ‰PDB	^{3}H TR ± 1σ
Kijabe RVA	K25	B	35	6.2 ± 0.17	-7.4	0.09 ± 0.14
Mayers' Fm	K28	S	28	78.6 ± 0.6	-16.5	0.00 ± 0.17
Kariandusi	K35	S	39	-	-	0.34 ± 0.16
C4178 Naivasha	K82	B	20	91.4 ± 0.7	-13.5	0.05 ± 0.15
Kanyamwi Fm	K92	B	24	62.8 ± 0.6	-2.5	0.34 ± 0.16
P65 Kinangop	K96	B	23	-	-	-0.01 ± 0.14
C1404 Ndabibi	K100	B	26	86.0 ± 0.7	-10.6	0.34 ± 0.17
Kokot	K101	S	-	-	-	0.42 ± 0.15
Olkaria OW-2	K110	G	-	-	-	0.19 ± 0.14
Olkaria OW-26	K111	G	-	-	-	0.27 ± 0.14
Nakuru No 7	K118	B	28	94.7 ± 0.6	-8.7	1.64 ± 0.16
DEL Soysambu	K124	B	32	4.0 ± 0.11	-2.7	0.15 ± 0.15

B - borehole   G - geothermal well   S - spring

pmc - percent modern carbon   TR - tritium ratio (≡ TU, i.e. 1 ^{3}H per 10^{18} ^{1}H atoms)

^{14}C measured at the NERC Radiocarbon Laboratory, East Kilbride, UK.
^{3}H measured at the DSIR Institute of Nuclear Sciences, Lower Hutt, NZ.
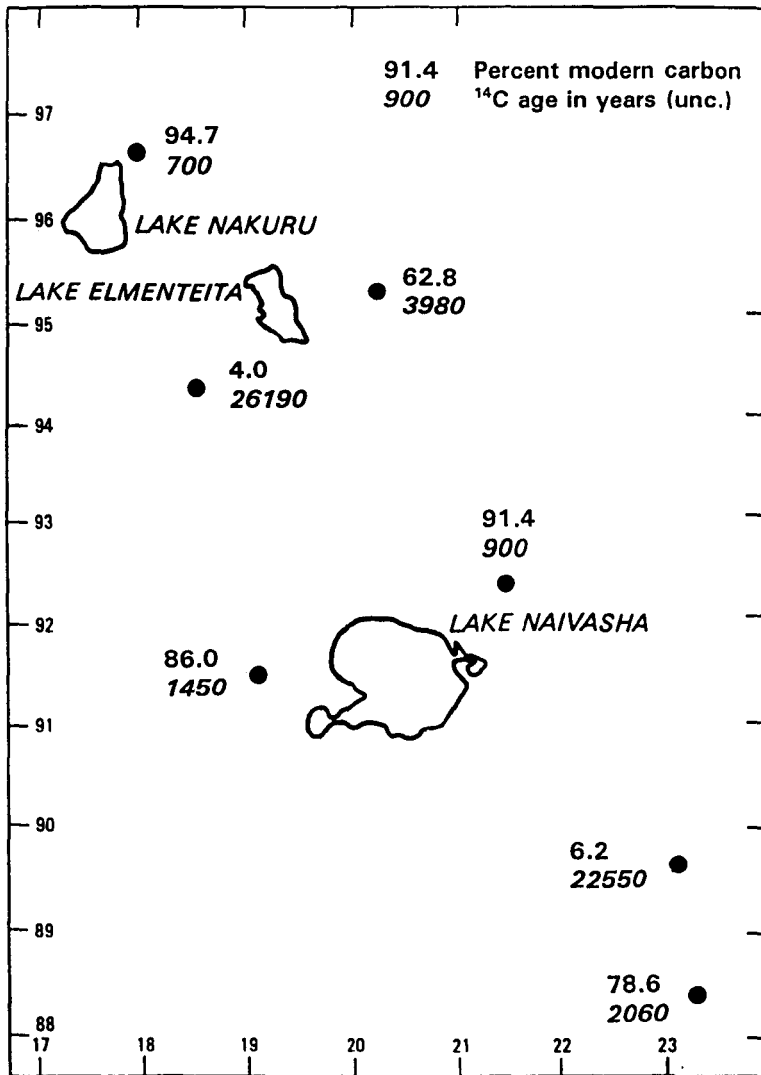
Fig 5.30   Map of radiocarbon sampling locations with pmc values and uncorrected ^{14}C ages.   See 5.3.1 for an explanation of the apparently very old groundwaters SW of Lake Elmenteita and SE of Lake Naivasha.

Table 5.6 Radiocarbon uncorrected and WATEQ-ISOTOP modelled ages for groundwaters from selected sites in the southern KRV.

Site Name	Site No	Sample type	Temp °C	^{14}C pmc	$\delta^{13}C_{DIC}$ ‰	Uncorr. age in years	^{14}C age in years			
							—$pH_I=5$—		—$pH_I=8$—	
							$\delta^{13}C_r=0$	$\delta^{13}C_r=0$	$\delta^{13}C_r=0$	$\delta^{13}C_r=0$
Kijabe RVA	K25	B	35	6.2	-7.4	22500	9136	4823	16405	8249
Mayers' Fm	K28	S	28	78.6	-16.5	2060	m	m	m	m
C4178 Naivasha	K82	B	20	91.4	-13.5	900	m	m	m	m
Kanyamwi Fm	K92	B	24	62.8	-2.5	3980	m	m	m	m
C1404 Ndabibi	K100	B	26	86.0	-10.6	1450	m	m	m	m
Nakuru No 7	K118	B	28	94.7	-8.7	700	700	m	m	m
DEL Soysambu	K124	B	32	4.0	-2.7	26190	26190	8388	m	m

B - borehole   G - geothermal well   S - spring

pH_I - assumed initial pH of open system $\delta^{13}C_r$ - assumed rock carbonate value   m - modern

two exceptions to this are from the DEL well on the Soysambu Estate and the Rift Valley Academy borehole (K124 and 25). Both these wells have a high bicarbonate content, especially the DEL well, and it is probable that the apparent ages are an artefact caused by the addition of large amounts of mantle CO_2 to the carbonate system. In reality these two waters are likely to be very much younger than the modelled ages, and by analogy with springs and wells in similar positions within the Rift, e.g. Mayers Farm and C1404 (K28, 100), are probably largely modern.

The tritium (^3H) content of groundwaters was measured at 12 representative sites in the Gregory Rift (Table 5.5). In all cases except the Nakuru No. 7 borehole (K 118), values were well below 1 TR. Records for ^3H in rainfall in the EARS and adjacent areas are not plentiful. However, in the mid-1980s, prior to the collection of the KRV water samples in 1987, a sequence of monthly collections at Addis Ababa showed a range of 4.6 to 25 TR in rainfall, with a weighted average of 9.7 TR (IAEA, 1992). Additionally, the collection station at Ndola in Zambia (the only other station in the area operating in the 1980s) measured a range of 5.2 to 12.8 TR in the early 1980s (IAEA, *ibid*). It seems unlikely that ^3H concentrations in Kenya would have been significantly different from those at the two collection stations. In the late 1960s and the 1970s tritium concentrations were higher because of increased rain-out from atmospheric thermonuclear testing.

The KRV results suggest that there is a negligible contribution from thermonuclear tritium. Accordingly, the waters must be at least 30 years old. The slightly higher ^3H figure for Lanet can be compared with the ^{14}C value which gave the youngest uncorrected age of any of the Rift samples. Possibly this is evidence of mixing between a small component of young, post-thermonuclear water and a rather older pre-bomb water.

Sites where radiocarbon and/or tritium were measured were selected on the basis of their value in identifying groundwater flow paths. Thus, radiocarbon samples were taken on the western side of the Rift floor at the Ndabibi and Soysambu estates (K100, 124), the central part of the Rift at Naivasha C4178 and Nakuru No. 7 (K82, 118) and the eastern flanks at Mayers' Farm, Kijabe RVA and Kanyamwi Farm (K28, 25, 92). Mayers Farm might, in particular, be expected to be associated with deep faulting, and Nakuru No. 7 is situated on a prominent N-S lineation on the valley floor, but neither of these sites indicates long residence times once radiocarbon corrections have been made. Conversely, tritium measurements show that in places where rapid flow might have been expected, especially perhaps at the Kokot water collection gallery (K101), water was of pre-thermonuclear age. The Olkaria geothermal well

samples (K110, 111) show that despite the proximity of the field to the lake, and the undoubted component of lakewater (see 6.1.2.2 above), transport of the lakewater even over a relatively short distance takes a significant time (a minimum of tens of years).

The radioisotope measurements therefore suggest that while there are no slow, deeply circulating groundwater flow paths playing a significant role in the hydrogeology of the Gregory Rift (with the possible exception of long-distance flow from Naivasha to Magadi), groundwater transport is by no means as rapid as the amount of secondary porosity (faulting and fissuring) might suggest. This broadly agrees with the conclusion of Allen et al (1989) concerning likely flowpaths based on physical observations (see Fig 4.3). Insofar as the Gregory Rift seems typical of the continental part of the Eastern Rift, there seems no reason to believe that the situation is significantly different in the Turkana rifts or the MER, for which there are no published data.

5.3.2 Southern Afar

Both Fontes et al (1980) and Verhagen et al (1991) give measurements of ^{14}C and ^{3}H in groundwaters of Djibouti. The main difference between Djibouti and the Gregory Rift is that ^{3}H was present at higher concentrations in some of the Djibouti wells. This led to the conclusion that waters are on the whole either pre-nuclear (e.g. the thermal waters) or post-nuclear (some of the well waters), but that none had been in residence for more than one or two thousand years. For example, Fontes et al (1980) calculated that the age of water from a typical "chimney" spring adjacent to Lake Abbe was 1.2 ka.

This interpretation is consistent with that for the Gregory Rift insofar as it indicates no scope for the existence of palaeowaters. On the other hand, the different mode of recharge to some of the wells in Djibouti (infiltration from wadi runoff) would account for the higher ^{3}H concentrations (up to 15 TR; Verhagen et al, 1991) observed in some of the boreholes considered here.

CHAPTER 6

CHEMICAL EVIDENCE
FOR WATER ORIGIN, MOVEMENT AND EVOLUTION

The conventional approach to the consideration of chemistry of the water cycle frequently adopts the sequence rainfall - surface waters - groundwaters. In the eastern rift, little or no rainfall chemistry is available for consideration. Additionally, lake water chemistry may be dominated by surface or groundwater inputs. Therefore, as for the previous chapter, lake waters will be considered after discussion of river waters and groundwaters. Similarly, water types will be treated on a geographical basis. Sample site locations are the same as for Chapter 5.

6.1   Kenya Rifts

6.1.1   Rivers and streams

The results of chemical analyses carried out during the present project are reported in Table 6.1. The physical and isotopic hydrology of these rivers has been discussed above in Chapters 4 and 5.

With two exceptions (Kerio and Suguta), the rivers of the KRV are short in length and of comparatively low volumetric flow. However, they are in some cases important sources of lake water (principally for Naivasha and Baringo). The chemical composition of all these river waters (except for the Suguta and some of its tributaries) indicates low-TDS waters, usually dominated by Na and HCO_3 but still containing relatively important amounts of K, Ca and Mg, particularly in the Baringo catchment.

In the case of the Ewasongiro, which was sampled at two different sites, there is clear evidence of evaporative concentration (backed by stable isotopic data, see 5.1.2.1) between the upstream (K32) and downstream site (K20). (By contrast, the only other river to be sampled at different points, the Suguta, showed few signs of enrichment by evaporation, but the reasons for this will be considered in more detail below.)

The Kerio, volumetrically the most important river, actually spends most of its course outside

Table 6.1   Chemical composition of waters collected from rivers and streams in the Kenya Rifts. Results in mgl[1].

Site Name	Site No.	Temp. °C	pH	Na	K	Ca	Mg	HCO$_3$	Cl	SO$_4$	Si	Li	B	F
Ewasongiro 1[a]	K20	26	8.20	59.1	16.2	16.9	4.0	193	15	10.6	49.2	<0.01	<0.04	2.3
Ewasongiro 2[a]	K32	22	7.85	23.7	11.8	8.5	1.5	78	6.9	4.6	24.8	<0.01	<0.04	1.4
Oloibotort[a]	K21	22	8.00	5.5	2.6	6.2	3.9	46	4.4	2.5	7.8	<0.01	<0.04	-
Kijabe Stream[a]	K27	17	7.05	38.9	8.0	3.6	1.3	106	10.5	5.8	31.4	<0.01	<0.04	-
Ndau[d]	K141	-	8.85	24.3	5.2	21.9	4.4	133	5.5	3.2	16.4	<0.01	<0.06	0.45
Tigeri[d]	K142	-	7.65	10.7	4.9	7.2	1.4	48.3	3.7	1.9	14.3	<0.01	<0.06	0.40
Arabel[d]	K144	-	8.55	47.1	7.4	8.0	2.7	101	37.0	1.8	13.2	<0.01	<0.06	0.52
Itwa[d]	K145	-	8.60	91.2	8.2	5.5	2.3	500	25.3	2.5	18.8	<0.01	<0.06	0.86
Kabarmel[d]	K146	-	8.05	45.4	10.0	16.8	3.9	135	26.4	8.6	18.8	<0.01	<0.06	0.35
Mukutan[d]	K147	-	8.15	79.1	9.4	15.9	3.2	222	21.3	4.1	11.0	<0.01	<0.06	1.20
Cheptopokwo[d]	K149	-	7.95	21.4	6.7	14.9	2.8	102	5.3	4.1	15.5	<0.01	<0.06	0.76
Suguta 1[e]	K206	-	-	1150	21.6	3.1	1.9	2460	288	124	31.0	-	-	44
Suguta 2[e]	K207	-	-	1030	24.0	3.9	1.9	2200	246	98.5	33.5	-	-	36
Suguta 3[e]	K208	-	-	1104	20.3	3.4	1.7	2340	267	115	34.6	-	-	90
Suguta 4[e]	K209	-	-	1093	22.4	3.8	2.1	2380	273	104	30.3	-	-	42
Suguta Trib.[e]	K210	-	-	1340	20.1	1.6	0.3	2930	350	142	30.2	-	-	47
Gerau[e]	K211	-	8.70	54	9.0	12.5	3.6	128	28.5	5.0	12.3	-	-	0.83
Amaya[e]	K212	-	-	158	8.7	7.6	2.1	389	26.0	7.2	20.7	-	-	2.1
Namarangule[e]	K213	-	8.30	-	-	-	-	-	-	-	-	-	-	-
Naliyo[e]	K214	-	8.50	65	10.4	16.5	3.0	152	16.3	15.8	9.7	-	-	0.78
Kerio[g]	K245	-	8.65	12.3	10.4	29.0	10.7	58	2.8	2.1	80.6	0.01	<0.03	0.90

Year of sampling: [a] - 1985; [b] - 1986; [c] - 1987; [d] - 1988; [e] - 1989; [g] - 1991

Analysed at BGS Wallingford by J Cook, J Trafford and K Smith

124

the inner trough of the South Turkana Rift. The Kerio Valley (Fig 1.2) is an area where fluorite is present in sufficient quantity to be mined locally, but saturation indices for the waters indicate that fluorite is well below saturation in the Kerio water and is therefore comparable to the other northern rift rivers (Table 6.2). All the northern "fresh" rivers are similar in their saturation index (SI) for the commonest minerals, being saturated or slightly oversaturated with respect to calcite and chalcedony (see Appendix D for details of SI calculation). The southern streams are also saturated with respect to chalcedony but undersaturated in calcite, most notably at Kijabe where the small stream has presumably had insufficient time to reach saturation point (Table 6.2, Fig 6.1).

For the most part, the chemical composition of streams and rivers is (as normally the case) strongly influenced by the surface geology of the catchment. However, in the case of the Suguta other factors are operating. The main source of this river is thermal springs, which have a constant output throughout the year. This ensures that the Suguta flows perennially.

The bulk of the Suguta's flow arises immediately to the west of Silali (Fig 5.12), where numerous hot springs with high TDS values (see 6.1.3 below) are diluted by seasonal contributions by the freshwater Cheptopokwo and Nginyang rivers. Further north, the only inputs to the Suguta originate from thermal or sub-thermal springs. The Gerau, Amaya and Naliyo streams, draining the eastern wall of the rift at the same latitude, terminate on the rift floor, failing to reach the Suguta in any direct way.

The ultimate source of the Suguta's high TDS composition is probably associated with evaporite dissolution or in-situ hydrolysis, discussed in 5.2.1. As noted above, the isotopic composition of the river fluctuates where there is an input of rift-flank water associated with Sites K185 and 186. Since the *chemistry* of this spring complex is similar to that of the others, there is only a subdued reflection of this input in the river chemistry.

6.1.2 Cool groundwaters

Chemical analyses of cool groundwaters ($<40^\circ$C) are reported in Tables 6.3 (springs) and 6.4 (boreholes and wells). Typically, the combined amount of Na and HCO_3 (almost invariably the dominant ions) in these waters is well below 1000 mgl^{-1}. Up to this limit, groundwaters can be regarded as the product of normal water-rock interaction under a tropical climate in volcanic terrain. Therefore they represent slightly evolved versions of the more dilute river waters considered above. Saturation indices show that groundwaters cluster around the
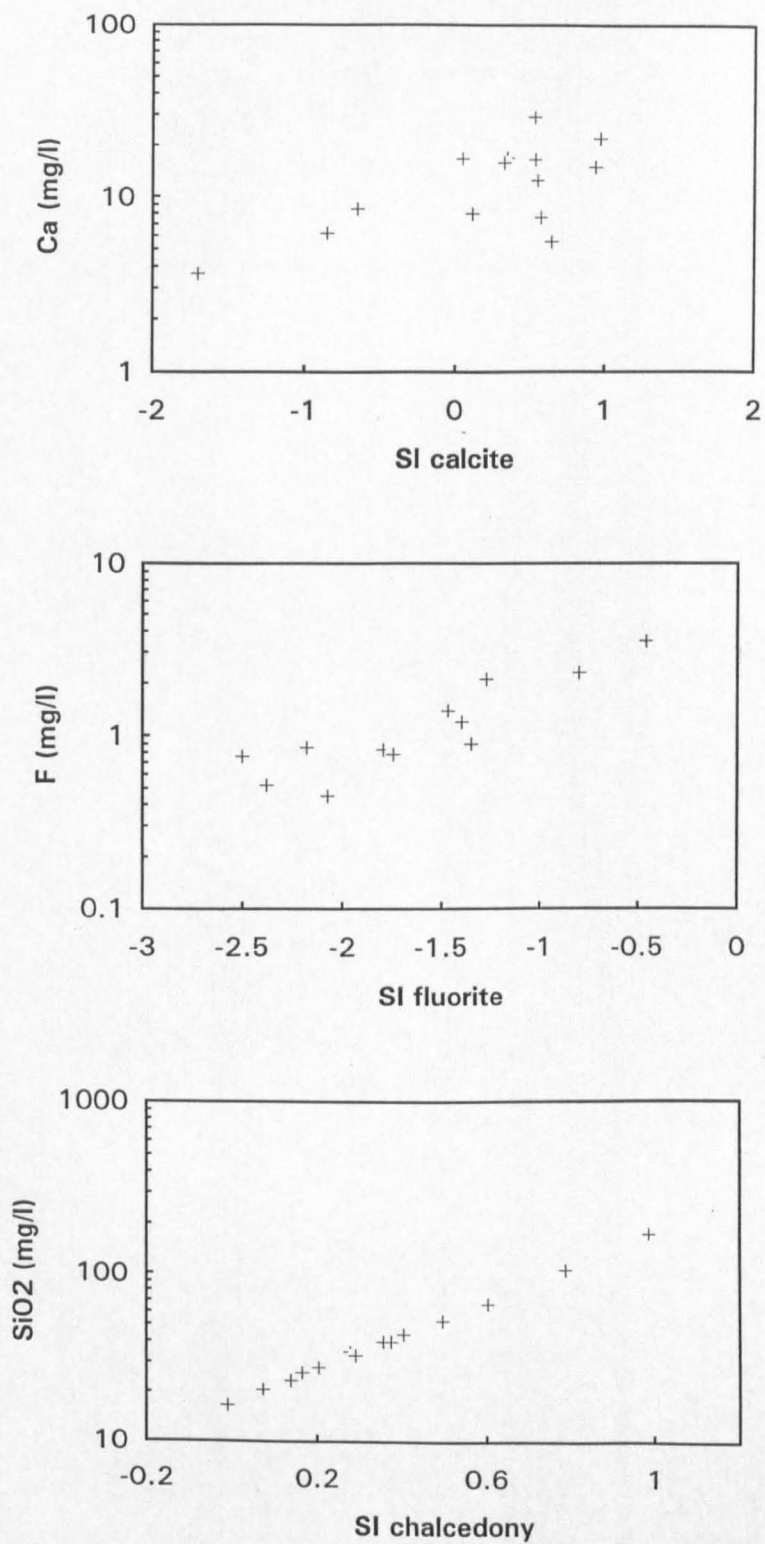
Fig 6.1   Plots of $SI_{calcite}$, $SI_{fluorite}$ and $SI_{chalcedony}$ vs Ca, F and SiO_2 for river and stream waters in the KRV.

Table 6.2   Saturation indices of surface waters in the KRV with respect to calcite, fluorite and chalcedony.

Site Name	Site No	pH	SI calc	SI fluor	SI chalc
Rivers and streams					
Ewasongiro 1	K20	8.20	0.345	-0.802	0.787
Ewasongiro 2	K32	7.85	-0.655	-1.470	0.494
Oloibotort	K21	8.00	-0.853		-0.009
Kijabe	K27	7.05	-1.701		0.601
Ndau	K141	8.85	0.967	-2.075	0.277
Tigeri	K142	7.65			
Arabel	K144	8.55	0.113	-2.383	0.203
Itwa	K145	8.60	0.647	-2.180	0.354
Kabarmel	K146	8.05	0.047	-0.462	0.372
Mukutan	K147	8.15	0.326	-1.399	0.138
Cheptopokwo	K149	7.95	0.936	-2.505	0.289
Suguta 1	K206				
Suguta 2	K207				
Suguta 3	K208				
Suguta 4	K209				
Suguta Trib	K210				
Gerau	K211	8.70	0.549	-1.798	0.164
Amaya	K212		0.571	-1.276	0.401
Naliyo	K214	8.50	0.533	-1.747	0.072
Kerio	K245	8.65	0.529	-1.351	0.985
Lakes					
Naivasha	K24	7.90	0.172		-0.258
Naivasha	K24	8.45	0.501		0.191
Naivasha	K24	7.60	-0.206		0.135
Elmenteita	K270	10.45	2.761		0.336
Nakuru	K102	10.45	3.525		0.369
Baringo	K70	8.95	1.299		0.213
Baringo	K150	9.05	1.182		0.221
Baringo	K216	8.85	1.075		0.173
Baringo	K217	8.75	0.966		0.211
Baringo	K150	8.85	1.206		0.329
Baringo	K150	8.60	0.954		0.253
Turkana	K215		1.211		0.127
Turkana	K246	9.45	1.788		0.028
Turkana	K247	9.45	1.791		-0.035
Victoria	K58	8.05	-0.584		-0.223

Table 6.3   Chemical composition of waters collected from cool springs in the Kenya Rifts.   Results in mgl^{-1}.

Site Name	Site No.	Temp. °C	pH	Na	K	Ca	Mg	HCO$_3$	Cl	SO$_4$	Si	Li	B	F
Mayers Farm[a]	K28	28	7.90	31.5	8.4	10.0	2.8	201	21	4.1	30.8	0.012	<0.035	0.7
Meroronyi[a]	K37	30	6.45	58	20	10.5	2.7	156	50	3.4	43.8	0.02	0.02	-
Chamuka[a]	K39	29	7.05	29	13	5.09	0.7	90	5.5	4.9	45.2	0.02	0.02	-
Kanyamwi Farm[b]	K91	24	7.30	23	9.0	3.67	0.7	77	2.2	1.5	38.2	0.01	0.02	-
Kokot[c]	K101	-	7.65	26	18.0	9.6	2.7	90	14.0	16	36.6	0.021	<0.02	3
Hell's Gate seep 2[c]	K104	20	-	197	7.1	0.5	0.1	305	33	22	57.0	0.11	0.04	38
Hell's Gate seep 5[c]	K107	35	-	957	31	11	0.2	-	900	419	78	1.02	0.93	-
Hell's Gate seep 6[c]	K108	23	-	379	27	10.8	1.8	713	86	64	40	0.24	0.95	48
Nginyang-Kapedo[d]	K138	36	8.30	991	21.3	2.8	2.1	2140	200	80.7	32.7	0.05	0.82	26
Churo[d]	K139	28	7.20	131	4.5	1.7	0.3	326	13.9	4.8	24.9	<0.01	<0.06	1.2
Churo[e]	K139	-	8.15	133	4.7	1.6	0.3	313	17.5	5.0	24.3	<0.01	<0.06	1.1
Ebirisat[d]	K140	38	9.00	178	1.9	0.4	<0.1	435	23.0	7.1	19.3	<0.01	<0.06	0.14
Nangarwa[e]	K191	-	8.85	153	2.4	0.5	<0.1	340	30.0	8.5	18.4	<0.01	<0.06	2.1
Amaya[e]	K192	-	8.35	142	3.0	0.8	0.1	328	20.0	7.7	15.6	<0.01	<0.06	1.9
N. Samburu Gates[e]	K193	-	8.85	638	4.7	4.9	1.2	1260	141	140	26.0	<0.01	0.53	19
Kachurkolh[e]	K194	31	9.15	1450	10.6	3.8	1.4	3370	191	126	10.0	0.61	0.06	18
Kalnangi[e]	K195	32	9.15	1040	18.0	0.5	<0.1	2880	260	102	36.0	0.16	1.04	35
Amakat[e]	K196	-	9.80	353	10.7	4.8	0.8	577	125	88	9.1	<0.01	1.09	16
S. Nangarabat[e]	K197	31	9.15	1680	24.9	0.6	0.2	3440	370	213	25.3	0.02	1.80	60
Napeiton[e]	K198a	33	7.80	351	6.2	5.1	2.6	731	65.0	47.7	29.9	0.06	0.06	14
Nasaken[e]	K199	31	7.50	104	6.6	15.6	1.6	260	15.0	16.6	28.0	0.06	0.04	7.7
Eliye[b]	K09U*	32	8.90	185	1.3	1.1	0.3	403	9.9	8.8	10.1	<0.01	0.08	-
Eliye[g]	K240	35	9.00	142	0.6	1.0	0.2	344	5.5	11.8	9.7	<0.01	0.04	2.0
Eliye N[g]	K241	37	8.75	110	0.8	1.4	0.3	267	3.5	6.5	9.0	<0.01	<0.03	2.2
Tum	K244	-	7.55	19.6	3.8	30.9	7.4	128	8.0	23.5	15.8	<0.01	<0.03	0.2

128

*UNDP analysis   Year of sampling: [a] - 1985; [b] - 1986; [c] - 1987; [d] - 1988; [e] - 1989; [g] - 1991

Analysed at BGS Wallingford by J Cook, J Trafford and K Smith

Table 6.4 Chemical composition of waters collected from boreholes and wells in the Kenya Rifts. Results in mgl[-1].

Site Name	Site No.	Temp.°C	pH	Na	K	Ca	Mg	HCO₃	Cl	SO₄	Si	Li	B	F
Oltepesi[a]	K22	-	8.80	162	15.8	8.8	1.8	390	26	10.5	38.7	0.11	0.08	20
C4635, RVA[a]	K25	35	7.95	100	7.1	0.9	0.2	251	5.0	2.1	36.2	0.011	<0.04	30
Suswa S. slope[a]	K30	-	7.90	5.1	13.4	4.6	1.3	62	6.7	2.6	6.5	<0.010	0.05	-
Emerit[a]	K72	37	9.40	544	10.7	10.9	5.9	1210	25	207	16.4	0.60	0.11	-
C4989[b]	K80	21	7.05	56	38	46.3	10.0	297	20	0.8	36.4	0.02	0.04	-
C567[b]	K81	22	7.70	212	18.7	27.5	8.3	575	30	4.9	28.3	0.03	0.06	-
C4178[b]	K82	20	7.45	75	14.0	19.1	2.1	241	7.5	4.8	37.5	0.02	0.03	-
C563[b]	K83	26	7.70	186	26	23.1	10.6	513	27	<0.5	30.4	0.07	0.09	-
C1487[b]	K84	21	7.80	275	17.0	11.2	1.8	626	60	45	31.9	0.03	0.06	-
C5002[b]	K85	20	7.95	80	15.0	13.8	1.8	238	8.2	8.7	32.4	0.02	0.02	-
C1063[b]	K86	26	7.20	122	36	52	28	480	30.5	5.8	46.5	0.05	0.06	-
C1488[b]	K87	26	7.95	177	29	10.0	0.6	476	16.8	12	36.3	0.01	0.04	-
C467[b]	K88	24	7.75	264	18.2	13.4	1.7	575	59	48	29.1	0.03	0.06	-
C580[b]	K89	25	8.20	341	17.7	18.2	2.1	740	100	22	29.0	0.07	0.08	-
C814[b]	K90	18	8.15	113	14.2	8.8	0.6	297	10.6	9.0	34.0	0.02	0.03	-
C570, Kanyamwi[b]	K92	22	7.00	24	9.4	4.0	0.7	88	2.2	1.6	38.6	0.01	0.02	-
C3784[b]	K93	23	7.45	81	29	26.3	6.1	256	39	35	44.5	0.02	0.02	-
C307[b]	K94	19	8.35	797	38	4.5	<0.7	1360	390	58	29.2	0.06	0.11	-
C1190[b]	K95	24	8.20	109	8.6	3.2	0.3	223	29.0	14	20.2	<0.01	<0.02	-
P65, Kinangop[b]	K96	23	7.00	10.9	5.9	1.7	0.6	44	0.6	1.1	34.1	0.01	0.16	-
C3955[b]	K97	23	6.65	37	17.0	6.1	1.6	124	6.8	2.3	47.6	0.01	0.02	-
C4179[b]	K99	26	7.15	98	4.6	120	48	308	100	31	29.7	<0.01	-	-
C1404, Ndabibi[c]	K100	26	6.95	64	16.0	5.7	0.9	151	13.0	12.6	47.0	0.04	<0.02	8.0
Nakuru No.7[c]	K118	28	7.00	68	15.0	12.0	1.3	187	13.0	9.5	38.0	0.02	<0.02	3.3
C431, ADC Fm[c]	K121	37	6.95	400	48	40.0	1.4	1120	14.0	9.1	59	0.53	0.05	8.9
C1798, ADC Fm[c]	K122	35	-	199	32	41.6	3.3	653	13.0	8.6	49.4	0.25	0.05	-
DEL, Soysambu[c]	K124	32	6.40	403	64	58	4.9	1100	55	17	61	0.43	0.14	13
C1990, Soysambu[c]	K125	28	7.95	386	30	13	14	989	78	22	31	0.10	0.10	9.4
C3525, Mosiro[c]	K129	-	-	187	48	38	18	686	12	8.8	43	0.09	0.03	8.4
Kampi Ya Samaki[d]	K131	-	7.70	263	21.0	18.8	16.7	727	55	22.7	31.1	0.05	0.13	43.0
Kampi Ya Samaki[a]	K131	-	8.15	227	18.5	16.0	13.9	637	46.8	11.4	29.2	0.04	0.12	-
C6364, Chesirimion[e]	K132	-	7.20	94.8	7.4	2.2	1.1	199	14.4	9.6	43.1	0.03	0.06	3.60
C6364, Chesirimion[e]	K132	34	7.10	107	7.5	2.4	1.2	235	21.0	9.5	50.4	0.04	0.07	3.5
C3437, Tangulbei[d]	K133	30	7.70	164	5.4	27.0	21.3	556	26.5	11.7	23.7	<0.01	<0.06	0.90
D7, Kokwo Toto[d]	K134	28	7.05	76.0	11.3	69.4	11.7	399	10.7	3.3	31.2	<0.01	<0.06	1.28
D4b, Orus Solar[d]	K135	28	7.00	139	10.5	37.6	12.3	483	31.7	-	27.8	<0.01	<0.06	1.40
D4a, Orus Hand[d]	K136	28	6.45	49.2	5.0	8.8	3.4	121	18.8	6.6	23.3	<0.01	<0.06	0.76
D1, Katangora[d]	K137	36	8.30	122	10.9	7.2	3.3	266	48.2	12.7	13.7	<0.01	<0.06	3.76
Napeiton[e]	K198B	37	7.60	468	8.0	7.1	4.3	855	155	77.5	28.3	0.06	0.08	14
Napeiton[a]	K198B	37	7.80	471	7.8	7.1	4.2	899	156	79.7	27.2	0.06	0.08	-
Kositei Proj[d]	K200	-	7.35	104	6.1	28.9	6.9	360	17.5	7.5	40.7	0.01	<0.06	3.1
Kositei Miss[d]	K201	-	7.25	168	6.2	26.9	7.6	478	12.5	33.9	33.0	0.04	<0.06	2.2
C6363, Kositei[d]	K202	36	8.95	224	1.8	0.8	<0.1	482	15.5	15.8	23.5	0.08	0.06	11
C3868, Nginyang Sch[e]	K203	-	-	893	4.7	1.4	1.1	1950	100	85	18.5	0.06	0.21	20
Nginyang Poly[e]	K204	36	8.40	1500	10.4	2.4	1.1	3490	218	165	18.7	0.09	0.23	44
Nginyang Poly[a]	K204	34	8.45	1500	8.1	2.03	0.9	3460	195	145	17.6	0.08	0.21	-
C3470, Chemolingot[e]	K205	38	8.35	269	3.1	2.9	0.5	614	20.5	27.1	24.1	0.04	0.06	5.4
Parkati[a]	K243	-	7.50	244	22.8	104	45.7	262	217	306	56.6	0.01	0.03	1.3
Kanukurdio[b]	K08U*	33	7.00	162	1.9	41.8	46.5	543	50	8.8	38.0	<0.01	0.09	-

* UNDP Analysis

Year of sampling: [a] - 1985; [b] - 1986; [c] - 1987; [d] - 1988; [e] - 1989; [f] - 1990; [g] - 1991

Analysed at BGS Wallingford by J Cook, J Trafford and K Smith

equilibrium range for calcite (Table 6.5, Fig 6.2), though outliers can extend to two orders of magnitude under or oversaturation. No correlation with Ca concentration is evident. The oversaturated spring waters are from high-TDS sources in the Suguta Valley. Some of these may represent cooled thermal waters. The oversaturated well waters are also high in TDS, but are found from Oltepesi (K22) in the south to Nginyang (K284) in the north.

All the spring, borehole and well waters are at least saturated with respect to chalcedony and in most cases slightly oversaturated (Fig 6.2). Sometimes this may be due to deep circulation of waters causing an increase in temperature and thereby promoting silica dissolution before the water cools again on its way to the surface. However, in most cases the waters are unlikely to have exceeded significantly their sampling temperatures, and there is if anything a *negative* correlation between silica concentration and sampling temperature (Fig 6.3). The precise origin of oversaturation therefore remains unclear. As nearly all the cool groundwaters have pH values <9, a straightforward relationship between SiO_2 concentration and saturation index would be expected, and is observed. Therefore chalcedony is probably the dominant control on SiO_2 concentration.

The behaviour of F, although only a minor element, in groundwaters of the EARS is of some interest owing to health implications: waters which would otherwise be potable are rendered harmful in some cases by high F concentrations. In the well waters there is a weak negative correlation between F and Ca (Fig 6.4), perhaps because as Ca is removed by the formation of calcite there is insufficient left to precipitate F as fluorite. However, the cool springs show no correlation. The cool waters are predominantly undersaturated or just at equilibrium with respect to fluorite (Fig 6.2). Only a few high-TDS wells are oversaturated.

In wells and springs beyond 1000 mgl^{-1} Na+HCO$_3$, other factors are likely to be contributing to chemical composition. In some cases, such as Site K138, the proximity of high-TDS springs with temperatures above 40°C strongly suggests local cooling effects. The composition of K138 is almost identical to that of the nearby K48 hot springs (Table 6.6). Dilution by cold waters can therefore be ruled out. This may also be the case for sites such as Kalnangi and South Nangarabat (K195, 197). Alternatively they could be the result of evaporite dissolution. This may be the case for two sites near the eastern wall of the rift at N Samburu Gates and Kachurkolh (K193,194), since Cl and SO$_4$ are relatively high. In some cases, however, there appears to be a contribution from high-temperature thermal fluids, which has the effect of raising Cl slightly and HCO$_3$ significantly. This occurs principally in the area north of Eburru and is represented by samples from boreholes at Sites K121, 124 and 125.

130

Table 6.5   Saturation indices of cool (<40 C) groundwaters in the KRV with respect to calcite, fluorite and chalcedony.

Site Name	Site No	Temp C	pH	SI calc	SI fluor	SI chalc
Springs						
Mayer's Farm	K28	28	7.90	-0.106	-2.073	0.555
Meroroni	K37	30	6.45	-1.628		0.690
Chamuka	K39	29	7.05	-1.574		0.696
Kanyamwi Farm	K91	24	7.30			
Kokot	K101		7.65	-0.786	-0.754	0.690
HG s2	K104	20				
HG s5	K107	35				
HG s6	K108	23				
Nginyang-Kapedo	K138	36	8.30	0.651	0.094	0.476
Churo	K139	28	7.20	-1.396	-2.420	0.464
Churo	K139		8.15			
Ebirisat	K140	38	9.00	0.016	-5.048	0.159
Nangarwa	K191		8.85	-0.310	-2.444	0.325
Amaya	K192		8.35	-0.617	-2.319	0.283
N Samburu Gates	K193		8.85	1.103	0.249	0.476
Kachurkolh	K194	31	9.15	1.716	-0.111	-0.059
Kalnangi	K195	32	9.15	0.807	-0.386	0.482
Amakat	K196		9.80			
S Nangarabat	K197	31	9.15	0.899	0.099	0.345
Napeiton	K198a	33	7.80	0.014	0.011	0.485
Nasaken	K199	31	7.50	-0.195	0.119	0.481
Eliye	K09u	32	8.90	0.287	-2.288	-0.101
Eliye	K240	35	9.00			
Eliye N	K241	37	8.75	0.117	-2.054	-0.125
Tum	K244		7.55	-0.248	-2.632	0.325
Boreholes and wells						
Oltepesi	K22		8.80	0.928		0.656
C4635, RVA	K25	35	7.95	-0.932		0.545
Suswa S Slope	K30		7.90			
Emerit	K72	37	9.40	2.144		-0.002
C4989	K80	21	7.05	-0.265		0.712
C567	K81	22	7.70	0.423		0.589
C4178	K82	20	7.45	-0.331		0.735
C563	K83	26	7.70	0.364		0.573
C1487	K84	21	7.80	0.138		0.653
C5002	K85	20	7.95	0.023		0.669
C1063	K86	26	7.20	0.176		0.759
C1488	K87	26	7.95	0.229		0.648
C467	K88	24	7.75	0.174		0.578
C580	K89	25	8.20	0.866		0.558
C814	K90	18	8.15	0.084		0.713
C570, Kanyam	K92	22	7.00	-1.814		0.725
C3784	K93	23	7.45	-0.152		0.776
C307	K94	19	8.35	0.489		0.630
C1190	K95	24	8.20	-0.336		0.413
P65, Kinangop	K96	23	7.00	-2.450		0.660
C3955	K97	23	6.65	-1.836		0.808
C4179	K99	26	7.15	0.266		0.566
C1404, Ndabibi	K100	26	6.95	-1.456	-0.186	0.766
Nakuru No 7	K118	28	7.00	-0.971	-0.665	0.651
C431, ADC Farm	K121	37	6.95	0.278	0.440	0.741
C1798, ADC Farm	K122	35				
DEL, Soysambu	K124	32	6.40	-0.195	0.967	0.812
C1990, Soysambu	K125	28	7.95	0.613	0.094	0.556
C3525, Mosiro	K129					
K.Samaki	K131		7.70	0.344	1.670	0.619
K.Samaki	K131		8.15			
Chesirimion	K132		7.20	-1.398	-1.392	0.704
Chesirimion	K132	34	7.10			
Tangulbei	K133	30	7.70	0.513	-1.568	0.419
Kokwo Toto	K134	28	7.05	0.119	-0.804	0.564
Orus Solar	K135	28	7.00			
Orus Hand	K136	28	6.45	-2.423	-2.051	0.438
Katangora	K137	36	8.30	-0.090	-0.898	0.101
Kositei Project	K200		7.35			
Kositei Mission	K201		7.25			
Kositei	K202	36	8.95	-0.728	-0.962	0.278
Nginyang School	K203					
Nginyang Poly	K204	36	8.40	0.408	-1.599	0.234
Nginyang Poly	K204	34	8.45			
Chemolingot	K205	38	8.35	-0.498	-1.068	0.321
Parkati	K243		7.50	-0.248	-0.732	0.879
Napieton	K198b	37	7.60	-0.256	0.066	0.373
Napieton	K198b	37	7.80			
Kanukurdio	K08u	33	7.00	-0.064		0.595

131
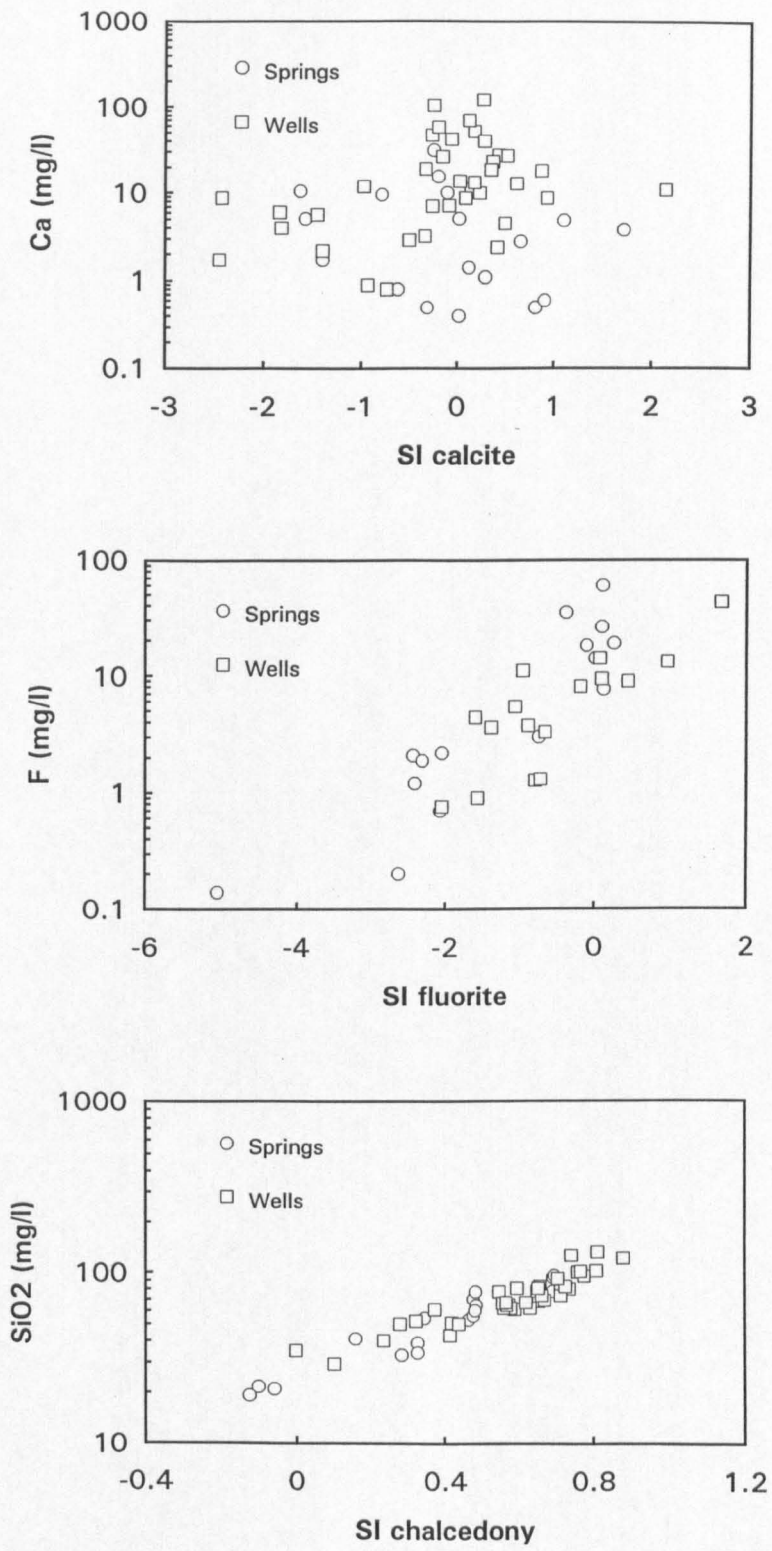
Fig 6.2   Plots of $SI_{calcite}$, $SI_{fluorite}$ and $SI_{chalcedony}$ vs Ca, F and SiO_2 for cool ($< 40°C$) groundwaters in the KRV.
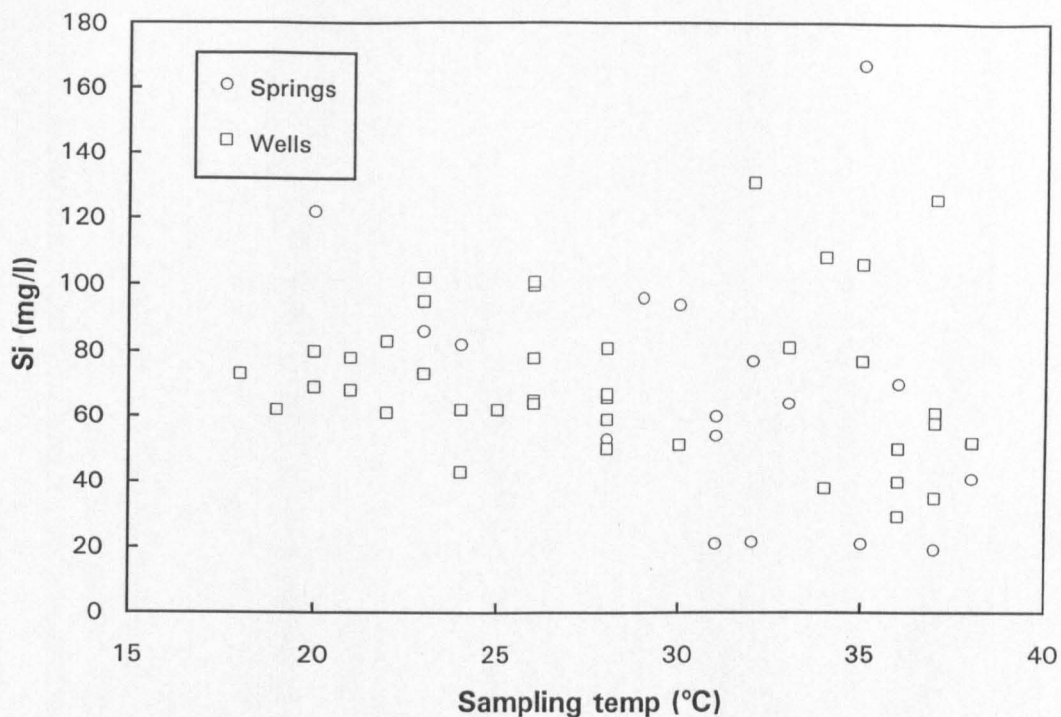
Fig 6.3　　　Plot of concentration of Si vs temperature for cool (<40ºC) groundwaters in the KRV.
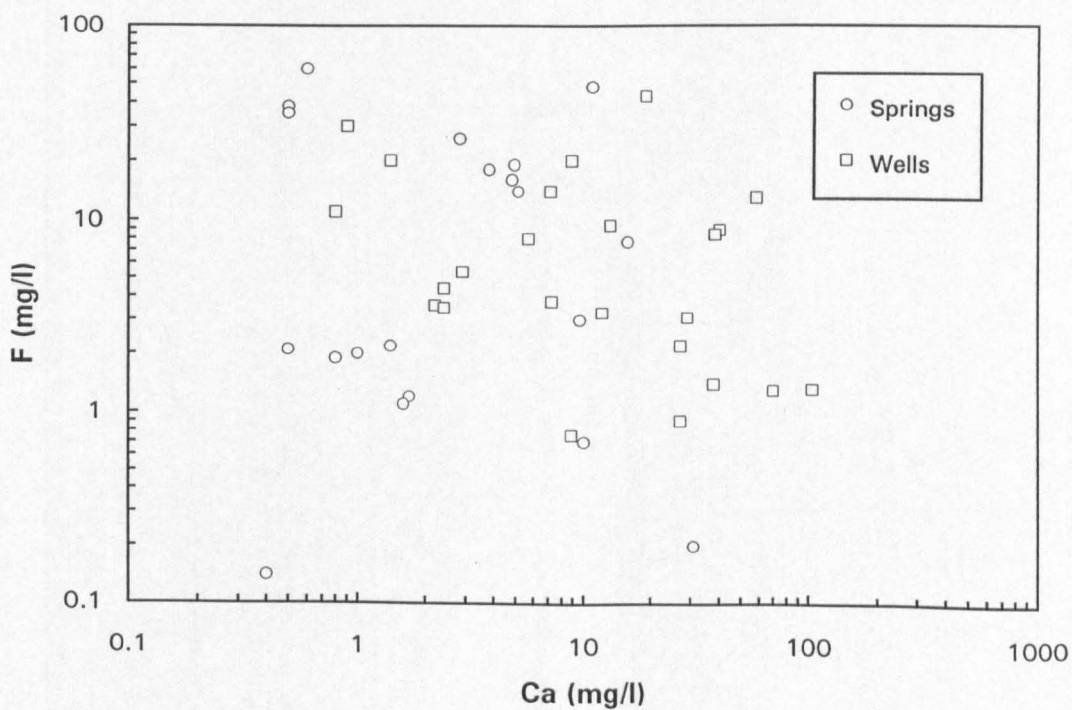
Fig 6.4　　　Plot of F vs Ca for cool (<40ºC) groundwaters in the KRV.

In a few cases, principally the seepages of the Hell's Gate/Ol Njorowa gorge south of Naivasha (Sites K104, 107 and 108), these are merely cooled versions of hotter counterparts. These seepages are either the product of fumarolic steam condensation or the result of leakage of the reservoir fluid of the nearby Olkaria geothermal field, where Cl is the dominant cation.

Some wells adjacent to lakes have a high but still "normal" TDS as a result of proximity to, and inflow from, the lakes. This applies to the Naivasha wells C4989, C567, C563, C1487, C1063, C467 and C580 (Sites K80, 81, 83, 84, 86, 88 and 89) and the Baringo well at Kampi Ya Samaki (K131), all of which have a clear lake water contribution on the basis of stable isotope measurements (see Chapter 5).

6.1.3   Hot groundwaters

During the present study in Kenya, only spring waters were found to exceed 40ºC (borehole waters were all <40ºC, with the obvious exception of the geothermal wells at Olkaria and Eburru). The chemistry of these thermal spring waters (Table 6.6) is for the most part proportionally very similar, particularly in those waters with TDS values well over 1000 mgl^{-1}. However, there is also a number of relatively dilute thermal springs which will be considered first.

Other than the steam condensate-related compositions of the Ol Kokwe Island springs (K71) and the Hell's Gate seepages (K106, 109) alluded to in the previous section, there are only four low-TDS "natural" thermal springs, at Kijabe (K26) on the eastern wall of the Gregory Rift, Majiyamoto (K34) on the rift flank to the northwest of Magadi, Kureswa (K260) on the western rift flank, and Loyangalani (K242) between Lake Turkana and Mt Kulal. All the sites are on or near the edges of the rifts concerned, and are probably the results of deep circulation promoted by rift boundary faults. The topographic situation of these springs means that dissolution of lake-related evaporites (5.2.1) is not likely. Further, indications from the concentration of elements such as Li, B and F are that contributions from magmatic heat sources can be ruled out. Compositions and concentrations are generally similar to rift-wall springs which are too cool to qualify in the "hot" category (e.g. Mayers' Farm, K128, in the Gregory Rift, and Ebirisat, K140, in the S Turkana Rift).

The high-TDS thermal springs are commonly found on the inner trough of the rift floor at some distance from the rift walls. This applies to the Magadi (K3, 9, 11, 13, 16 18), Elmenteita (K41), W Bogoria (K68), Kapedo (K48), Lorusio (K45), SV3 (K185,186) and

Table 6.6 Chemical composition of waters collected from hot springs in the Kenya Rifts. Results in mgl^{-1}

Site Name	Site No.	Temp° C	pH	Na	K	Ca	Mg	HCO₃	Cl	SO₄	Si	Li	B	F
Little Magadi[a]	K3	85	8.85	10900	185	0.5	<0.4	20400	5550	160	39.4	1.13	8.04	170
Little Magadi[a]	K3	83	8.80	11100	220	0.4	<0.1	19600	5350	151	33.0	1.30	7.83	180
Magadi NW[a]	K9	45	8.80	9640	112	0.7	<0.4	16700	4900	204	49.2	0.45	7.70	80
Magadi N[b]	K73	63	8.90	13300	240	0.5	<0.7	24900	6600	132	35.2	1.17	9.24	-
Magadi NE[a]	K11	67	8.95	11100	157	0.6	<0.4	20900	5850	134	39.0	0.78	7.83	130
Magadi E[a]	K13	40	9.55	12200	100	0.6	<0.4	23100	6400	160	23.8	0.16	6.83	-
Bird Rock[a]	K16	41	9.60	12700	109	0.7	<0.4	23800	6450	169	25.6	0.17	7.42	140
Magadi S[a]	K18	45	9.55	12300	115	0.6	<0.4	23400	6450	189	32.0	0.16	7.44	130
Hell's Gate seep 4[c]	K106	52	4.00	97	49	5.4	0.5	0	4.3	262	95	0.16	0.02	3.4
Hell's Gate seep 7[c]	K109	72	-	489	6.1	3.4	<0.1	183	370	299	68	0.33	0.30	52
Kijabe[a]	K26	43	9.05	82.5	1.4	0.2	<0.15	240	53.5	1.7	19.0	<0.01	<0.03	30
Elmenteita[a]	K41	43	9.30	1050	35	0.46	<0.1	1610	490	82	58.3	0.21	5	-
Bala[a]	K53	72	8.05	6430	108	160.0	0.4	12200	1800	1630	29.7	0.47	0.92	-
Bala[a]	K53	72	7.60	6670	111	164.0	0.4	13300	1850	1530	29.8	0.53	2.28	12.0
Kureswa[a]	K256	62	7.55	204	4.4	7.41	0.4	497	12.3	7.9	37.2	0.08	2.42	14.0
Bogoria W[b]	K68	96	8.05	1250	25.3	1.3	0.4	2760	220	63.9	50.0	0.58	0.05	55.0
Bogoria SE[a]	K262	97	9.60	4870	135	1.46	<0.10	5400	1190	97	95.4	0.35	0.51 200	0.14
Majiyamoto[a]	K34	52	7.10	33.1	13.2	21.8	8.8	135	13.5	25.1	24.3	<0.01	2.89	-
Lorusio[b]	K45	81	7.60	2150	57.0	3.0	0.2	4710	295	197	35.7	0.96	<0.04	48
Lorusio[d]	K45	82	7.45	2120	55.8	3.0	0.2	5000	300	200	33.2	0.96	0.96	-
Kapedo[b]	K48	50	8.25	988	22.0	1.6	0.6	2000	215	80.0	35.6	0.06	0.92	28
Kapedo[d]	K48a	51	8.25	1020	22.7	1.6	0.5	2140	210	83.0	33.0	0.05	0.87	27
Kapedo[e]	K48a	50	8.35	994	23.3	1.7	0.6	2110	240	83.4	36.1	0.05	0.92	0.42
Ol Kokwe Island[d]	K71a	96	6.90	22.1	4.5	1.5	0.5	121	1.4	76.1	38.3	0.02	0.88	-
Ol Kokwe Island[d]	K71b	94	9.10	832	36.0	0.5	<0.7	1960	260	40.0	87.0	0.56	<0.06	19
Ol Kokwe Island[d]	K71b	96	9.05	922	39.3	1.0	<0.1	1980	260	30.5	126	0.61	1.04	5.4
Ol Kokwe Island[d]	K71c	96	6.40	38.7	7.6	23.3	9.2	<1	6.2	1510	116	0.04	1.19	28
Kapedo Spr SL26/2[e]	K183			963	22.9	2.2	0.3	1900	250	84.9	41.0	0.07	<0.06	29
Kapedo Spr SL27/5[e]	K184	45	8.25	913	20.1	2.3	<0.1	1720	220	82.4	48.7	0.15	0.94	53
Suguta Spr SV3a[e]	K185	68	8.25	1160	12.2	1.0	<0.1	2290	250	140	54.0	0.26	0.86	46
Suguta Spr SV3b[e]	K186	64	8.30	1146	13.2	1.1	<0.1	2220	265	138	53.9	0.24	0.78	37
Kamuge Spr[e]	K187	50	7.75	925	6.9	4.2	1.3	1930	160	100	38.4	0.22	0.72	190
Kageinya Spr[e]	K188	68	9.50	5420	85.5	3.0	0.3	3350	2280	3700	81.5	0.23	0.47	140
Namarunu Spr[e]	K189	66	8.80	5500	113	0.5	0.2	5860	3200	814	26.0	<0.01	13.6	110
Logipi NW[e]	K190	61	8.30	4170	79.4	0.5	0.1	5160	3420	590	18.5	0.05	6.53	87
Elboitong S[g]	K236	95	7.10	6770	129	0.82	<0.1	7940	4400	1070	46.2	0.31	5.11	87
Elboitong N[g]	K237	92	9.00	6690	126	1.40	0.5	8240	4500	1060	58.8	0.25	6.78	87
Logipi NE[g]	K238	70	8.85	6200	120	0.48	<0.1	5720	5250	920	30.8	0.15	6.81	4.2
Central Island[g]	K239	71	7.20	1550	78.9	13.9	25.2	2480	1059	30.8	95.7	0.41	6.39	0.3
Loyangalani[g]	K242	40	7.65	89	5.0	17.3	25.6	302	40	20.8	21.4	<0.01	4.45 0.07	

Year of sampling: [a] - 1985; [b] - 1986; [c] - 1987; [d] - 1988; [e] - 1989; [g] - 1991

Analysed at BGS Wallingford by J Cook, J Trafford and K Smith

Kageinya (K188) springs. Sometimes, however, springs may be situated at the rift wall. e.g. Kamuge (K187). In the northern part of the Suguta Valley in the South Turkana Rift, the width of the valley floor decreases markedly and is partially obstructed by the Namarunu complex, in the vicinity of which the Namarunu (K189) and Elboitong (K236,237) springs occur. To the north of this, the valley is closed altogether by the Barrier volcanic complex, at whose southern foot issues the Logipi series of springs, represented by sites K190 and K238.

Despite the existence of many of these springs on the rift floor, sometimes in proximity to volcanic centres (e.g. the Kapedo and Namarunu springs), there is little evidence that they have a significant high-enthalpy component, except at Ol Kokwe (K71) and Central Island (K239) where the samples have Si contents of ~ 100 mgl^{-1} or above. Even then, both these samples have HCO$_3$/Cl molar ratios > 1, whereas deep thermal waters are frequently regarded as having ratios well below unity (i.e. anionic content dominated by Cl, see for example Ellis and Mahon, 1977), as indeed is usually the case for wells in the Olkaria geothermal field. The implication of this is that in most cases the predominant source of heat is conductive via deep circulation as for the dilute springs considered above, but with some additional chemical evolution.

It has been shown in the previous chapter from consideration of ^{13}C data that there is evidence for in situ silicate hydrolysis and/or evaporite dissolution (5.2.1). Both these processes would tend to be accelerated by hot waters, and indeed a plot of HCO$_3$ versus sampling temperature reveals a basic correlation (Fig 6.5). Also shown on this diagram are the high-TDS sub-thermal springs which may represent cooled thermal waters.

Further evaporative concentration of such waters can lead to very high TDS values of ~ 15000 mgl^{-1} in the northern Suguta Valley and ~ 40000 mgl^{-1} in the Magadi basin. Both these areas are natural discharge points, at the northern and southern ends respectively of the KRV, i.e. more or less at the limits of the Kenya dome.

Fig 6.6 shows a plot of Cl and SO$_4$ relative to alkalinity as HCO$_3$, invariably the dominant anion. The northern Suguta and Magadi samples form separate groupings away from nearly all the other rift groundwaters. However, the waters appear to have evolved in rather different ways. The Magadi waters have only slightly more Cl than the Suguta waters, and considerably less SO$_4$. Given that average temperatures and evaporation rates are similar in both areas (Allen and Darling, 1992; Allen et al, 1989), other factors must be responsible for the observed differences. Using plots of various species against chloride (Fig 6.7), which is assumed to be
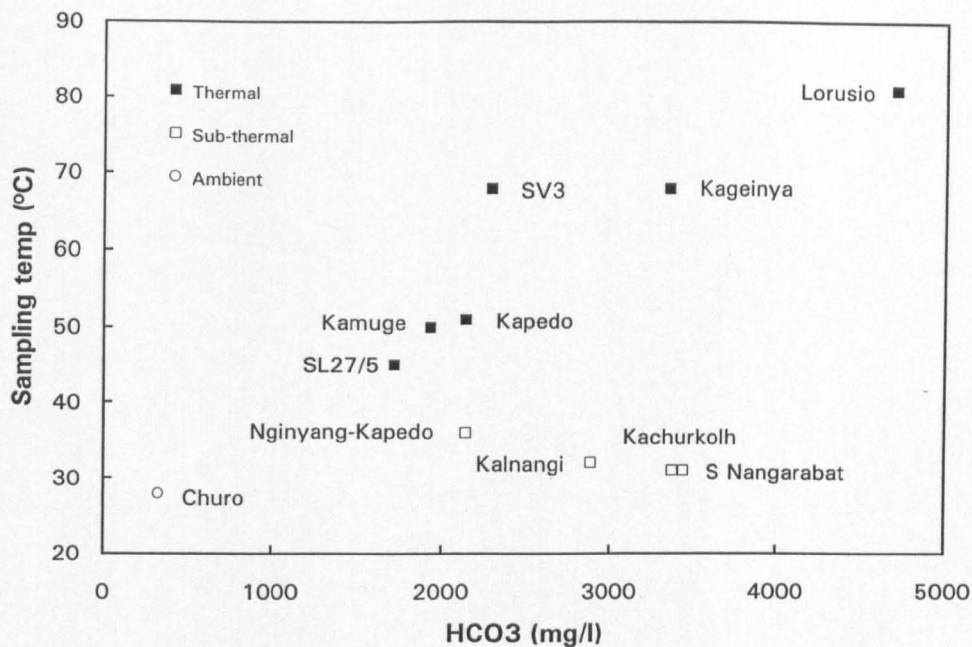
Fig 6.5   Plot of alkalinity as HCO₃ vs sampling temperature for hot (>40°C) groundwaters in the northern KRV.
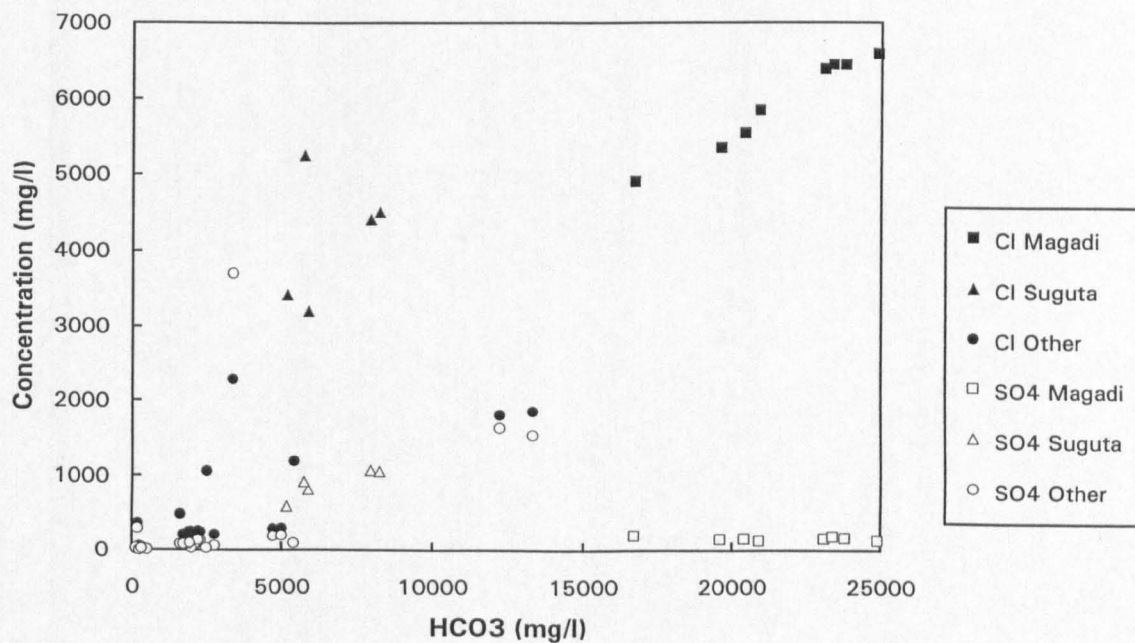
Fig 6.6   Plot of Cl and SO₄ vs alkalinity as HCO₃ for hot (>40°C) springs in the KRV.

a conservative element, some inferences can be drawn on how these waters have formed.

A plot of Na versus Cl for all KRV waters shows that simple evaporative concentration appears to be operating over several orders of magnitude. This is shown best by rivers but rather less well by dilute groundwaters, which if anything show an increase in Cl at the expense of Na when in fact the opposite would be expected as the waters start to dissolve feldspar. At the most concentrated end of the spectrum, the Suguta and Magadi springs show a slight reduction in Na relative to Cl. Since none of these waters is yet concentrated enough to deposit trona ($NaHCO_3.Na_2CO_3.2H_2O$), there is no large-scale removal of sodium.

When carbonate species (as HCO_3) are plotted against Cl, a departure from a simple evaporation line is seen which increases with rise in TDS. However, more carbonate loss is found for the Suguta than the Magadi springs, even though the TDS of the former is significantly lower than the latter. Eugster (1980), writing about Magadi, suggested that four mechanisms could potentially be responsible for removing carbonate: degassing of CO_2, alkaline earth precipitation, sodium carbonate precipitation in efflorescent crusts, and trona precipitation. It is difficult initially to see how the northern Suguta differs from the Magadi basin, but the answer may lie in the apparently greater amount of recirculation of groundwaters in the northern Suguta. The isotopic enrichment in ^{18}O and ^2H is significantly greater for the northern Suguta than for Magadi (Chapter 5), and though some of this is probably due to recharge from the already-evaporated water from the Suguta River, there are signs of still more evaporation within the terminal area. Recirculation would have the effect of precipitating carbonate crusts (which are extensive in parts of the area), thereby depleting the carbonate species in the water more than in the Magadi hot springs. This raises the question of why the Suguta springs have not reached or exceeded the Magadi springs in TDS. The relative isotopic depletion of springs at Magadi away from the northern end of the lake suggests that subsurface dissolution of evaporites dominates, and this may lead to the higher TDS values observed there. Also, the Magadi basin has been closed for much longer than the Suguta (Nyamweru, 1989).

The proposed recirculation in the northern Suguta may also be the key to the difference in sulphate depletion between the two areas. In this case, while many surface and hot and cool groundwaters conform reasonably well to an evaporative concentration trend, there is considerable SO_4 depletion at Magadi, but much less so in the northern Suguta. Bacterial action under reducing conditions has been proposed as the most likely cause of sulphate depletion in this instance (Eugster, 1980): if more recirculation is occurring in the northern Suguta, this would presumably result in a greater amount of oxygen in the system and therefore
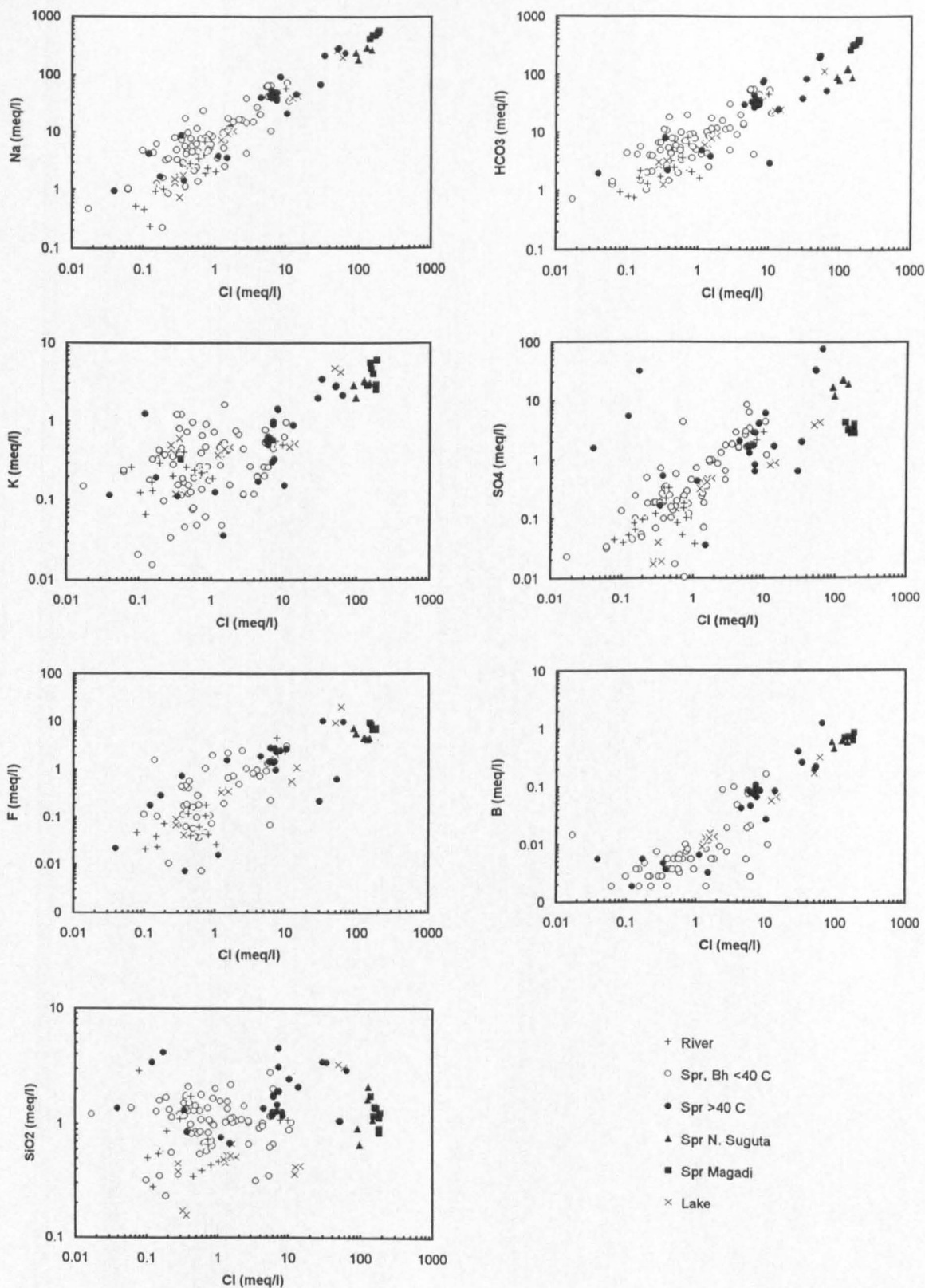
Fig 6.7   Plots of Na, HCO₃, K, B, F and SiO₂ vs Cl for waters in the KRV.

Table 6.7   Saturation indices of hot (>40 C) groundwaters in the KRV with respect to calcite, fluorite, quartz and chalcedony.

Site Name	Site No	Temp C	pH	SI calc	SI fluor	SI qtz	SI chalc
Little Magadi	K3	85	8.85	1.776	0.274	0.256	-0.017
Little Magadi	K3	83	8.82				
Magadi NW	K9	45	8.82	1.352	0.047	0.898	0.527
Magadi NE	K11	67	8.96	1.782	0.232	0.453	0.138
Magadi E	K13	40	9.56	2.120		0.455	0.070
Bird Rock	K16	41	9.58	2.235	0.599	0.459	0.077
Magadi S	K18	45	9.57	2.197	0.464	0.486	0.115
Magadi N	K73	63	8.89	1.679		0.489	0.164
Majiyamoto	K34	52	7.07	-0.445	-3.379	0.556	0.204
HG s4	K106	52	3.98				
HG s7	K109	72					
Kijabe	K26	43	9.05	-0.391	0.692	0.454	0.078
Elmenteita	K41	43	9.29	0.821		0.875	0.498
Bala	K53	72	8.06	3.081	0.506	0.400	0.097
Bala	K53	72	7.60				
Kureswa	K260	62	7.55	0.175	0.008	0.612	0.285
Bogoria W	K68	96	8.05	0.859	-0.022	0.355	0.105
Bogoria SE	K260	97	9.58	2.593	0.916	0.076	-0.173
Lorusio	K45	81	7.65				
Lorusio	K45	82	7.45	0.800	0.165	0.384	0.101
Kapedo	K48	50	8.25				
Kapedo	K48a	51	8.25	0.542	-0.227	0.680	0.325
Kapedo	K48a	50	8.35				
Ol Kokwe	K71a	96	6.90	1.641	-0.994	0.526	0.275
Ol Kokwe	K71b	94	9.10				
Ol Kokwe	K71b	96	9.05				
Ol Kokwe	K71c	96	6.40				
Kapedo SL26/2	K183						
Kapedo SL27/5	K184	45	8.25	0.597	0.037	0.923	0.552
Suguta SV3a	K185	68	8.25	0.546	-0.027	0.680	0.368
Suguta SV3b	K186	64	8.30				
Kamuge	K187	50	7.75	0.413	0.457	0.774	0.416
Kageinya	K188	68	9.50	2.114	1.135	0.511	0.199
Namarunu	K189	66	8.80	0.973	0.227	0.319	0.002
Logipi NW	K190	61	8.30	0.385	0.084	0.300	-0.030
Elboitong S	K236	95	7.10	-0.082	-0.162	0.371	0.119
Elboitong N	K237	92	9.00	2.033	0.083	0.277	0.018
Logipi NE	K238	70	8.85	1.025	-0.252	0.333	0.025
Central Island	K239	71	7.20	0.670	-1.166	0.927	0.622
Loyangalani	K242	40	7.65	0.162	-2.779	0.649	0.264
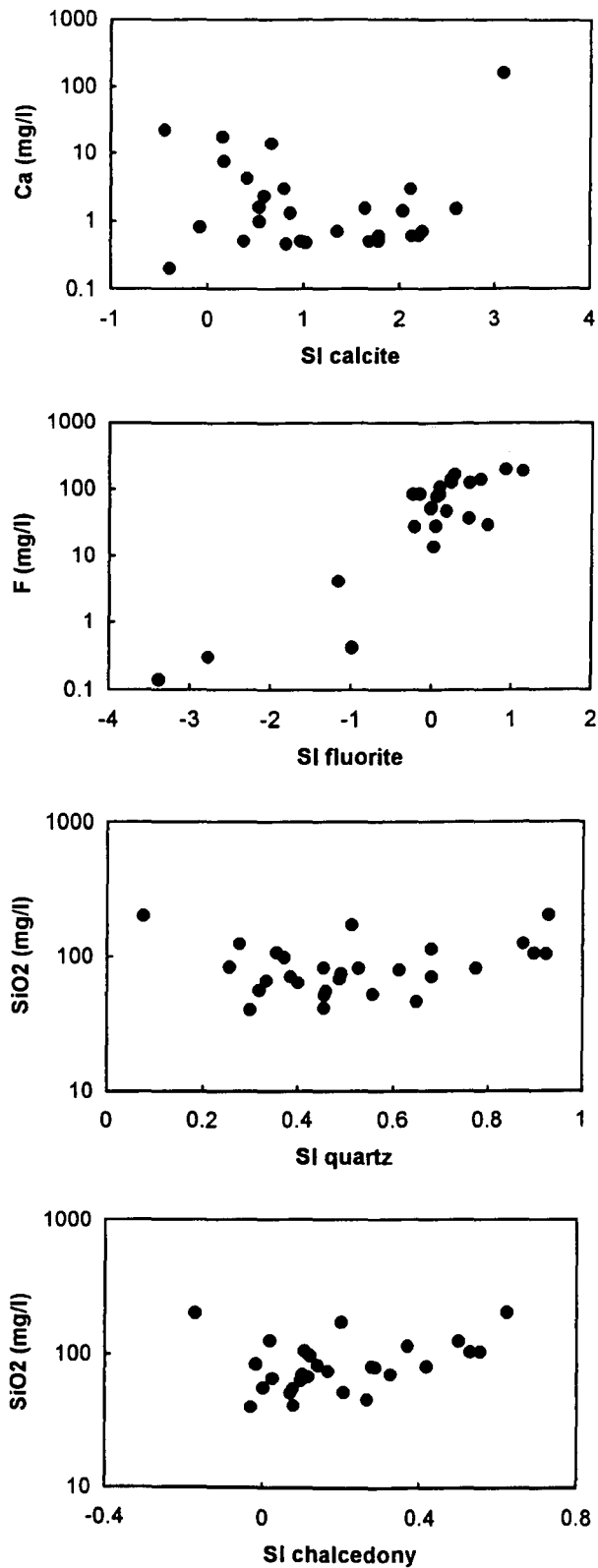
Fig 6.8   Plots of $SI_{calcite}$, $SI_{fluorite}$, SI_{quartz} and $SI_{chalcedony}$ vs Ca, F and SiO_2 for hot (>40°C) groundwaters in the KRV.

less scope for bacterial reduction to operate.

The difference between the Magadi and Suguta spring areas is not significantly reflected in the behaviour of K relative to Cl. Lower-TDS groundwaters, cool and thermal, show marked K loss due to exchange on reactive volcanic glass and silica gel surfaces (Eugster, 1980). As expected, higher-TDS springs from both terminal areas are very similar. Some similarity is also seen in the behaviour of F, of which there is much less relative to Cl. There are signs of a small F depletion for both areas, the reasons for which are not clear. There is little Ca available to precipitate CaF_2 and all hot springs are saturated with respect to calcite (Fig 6.8) even at the very low Ca concentrations measured (typically <1 mgl^{-1}). However, sufficient Ca exists to cause fluorite saturation in some cases.

A slight loss of B for the most concentrated hot springs may be due to the substitution of B for Si in silica precipitates (Jones et al, 1977). SiO_2 at lower concentrations shows little change relative to Cl, but then increases suddenly in the medium-TDS hot springs, before declining again in the Magadi and Suguta basins. At lower concentrations, silica dissolution is pH-controlled, whereas in higher-TDS waters more of an evaporative relationship is maintained. The mechanism by which SiO_2 is lost again in the Magadi and Suguta spring waters is not clear. Nearly all hot springs are at saturation with respect to chalcedony (Fig 6.8), which is probably the SiO_2-controlling phase for nearly all surface-sampled waters.

The difference between Bala (K53) and all main rift sites is its location on an eroded carbonatite complex (see 2.1.3). Although this has resulted in a carbonate concentration only exceeded by the Magadi springwaters, the main chemical difference from other waters is the relatively high Ca content (~ 160 mgl^{-1}), which is higher than any other water of the KRV. As a result, while some species when plotted against Cl show little difference between Bala and the other sites (e.g. Na, K and SiO_2), there are important differences for Ca, SO_4 and F.

In view of the high partial pressure of CO_2 at this site (0.15 bar), Ca is highly oversaturated (Table 6.7). Sulphate, shown in Fig 6.7 to have increased relative to Cl, is the only sample from the rifts to approach saturation with respect to gypsum (SI = 0.72; other samples are from 2-5 orders of magnitude undersaturated). Fluoride is greatly depleted compared to other high-TDS springs (Fig 6.8), with a loss comparable to that at Central Island (K239) where Ca is also responsible for lowering F. This explains why F is unable to reach a concentration any higher than ~ 12 mgl^{-1} at Bala.

142

6.1.4   Lakes

There are marked differences between the various lakes of the KRV (Fig 4.1), and these are discussed in general terms under section 4.1.1. Chemical anlyses are provided in Table 6.8.

The "fresh" lakes, Naivasha and Baringo, have surface inflows and important subsurface outflows. Victoria, though not a rift valley lake, can also be included in the "fresh" category; it has of course a substantial output in the form of the Nile. It is included in the discussion mainly for reference purposes.

Turkana also has a surface inflow. Because there is now no important surface or subsurface outflow, the lake is in the process of building up its TDS and alkalinity (Yuretich and Cerling, 1983).

The remaining lakes (Magadi, Elmenteita, Nakuru, Bogoria and Logipi) are all alkaline, with TDS values well in excess of 10^4 mgkg^{-1}, especially Magadi. Logipi is only an ephemeral lake and will not be further considered here.   Neither Bogoria nor Magadi was sampled for chemistry during the present study, and data from Cioni et al (1992) and Eugster (1980) have been used in the following discussion.

The chemistry of the different lake waters reflects the type of input and output, and any modifications caused by processes operating within the lake.   The simplest of these is evaporation, which initially at least results in a simple scaling-up of concentrations. Eventually as solubility limits for certain minerals are exceeded these will precipitate out, and the dissolved species ratios will change. These processes may be supplemented by diagenetic changes due to ion exchange and bacterial activity.

The water balance of Naivasha and Baringo is such that only a limited amount of evaporative enrichment is possible. However, as shown for stable isotopes in the previous chapter, these lakes are shallow, and wet-season influxes of water can have a significant effect on lake water chemistry as well. The limited scope for evaporative enrichment means that the chemistry of these lakes is in most cases explicable by simple concentration. Fig 6.7 suggests a 5-10 times concentration for Cl over river inputs, and this is accompanied reasonably linearly by increases in HCO_3, Na, K, SO_4 and F. On the other hand, SiO_2 does not follow this relationship, having already reached saturation (Fig 6.9).   The composition of Lake Victoria is always slightly depleted in the various species relative to Cl compared to the rift lakes. The origin of this

Table 6.8 Chemical composition of waters collected from lakes in the Kenya Rifts. Results in mgl^{-1}.

Site Name	Site No.	Temp °C	pH	Na	K	Ca	Mg	HCO$_3$	Cl	SO$_4$	Si	Li	B	F
Naivasha[a]	K24	-	7.90	40.7	23.8	22.3	7.8	195	13	0.9	4.4	0.01	<0.03	0.80
Naivasha[f]	K24	-	8.45	29.8	17.2	15.7	5.3	161	10.0	0.9	12.7	<0.01	<0.03	1.75
Naivasha[a]	K24	-	7.60	34.6	19.7	19.4	6.0	184	10.0	0.8	10.8	<0.01	<0.03	1.30
Elmenteita[f]	K270	-	10.45	4500	164	1.5	<0.1	7410	2100	203	86.0	0.09	3.53	390
Nakuru[f]	K102	-	10.45	5950	186	5.3	<0.1	13400	1750	182	92.0	0.03	1.87	180
Victoria E[a]	K58	-	8.05	16.9	4.7	6.4	3.3	76	11.5	1.9	4.8	0.01	0.02	-
Baringo C[b]	K70	-	8.95	241	18.8	11.2	5.2	546	65	23.0	14.5	<0.01	0.15	-
Baringo C[d]	K150	-	9.05	192	15.4	9.2	2.5	384	48.5	19.7	15.2	0.01	0.14	6.4
Baringo N[e]	K216	-	8.85	192	14.3	11.0	3.5	399	46	17.0	12.9	<0.01	0.11	7.1
Baringo S[e]	K217	-	8.75	170	14.9	11.3	3.5	375	44	15.3	13.8	<0.01	0.10	6.3
Baringo C[e]	K150	-	8.85	245	18.3	12.3	4.4	498	56.8	23.0	18.5	<0.01	0.17	6.6
Baringo C[e]	K150	-	8.60	217	17.7	12.3	4.3	495	54.8	20.1	14.9	<0.01	0.14	6.6
Turkana S[e]	K215	-	-	985	20.5	3.8	2.5	1580	515	43.3	12.0	<0.01	0.72	21
Turkana N[g]	K246	-	9.45	932	19.2	5.0	2.4	1580	446	40.0	11.8	<0.01	0.65	10
Turkana C[g]	K247	-	9.45	909	18.8	5.2	2.4	1520	436	39.3	10.2	<0.01	0.63	11

Analysed at BGS Wallingford by J Cook, J Trafford and K Smith

144
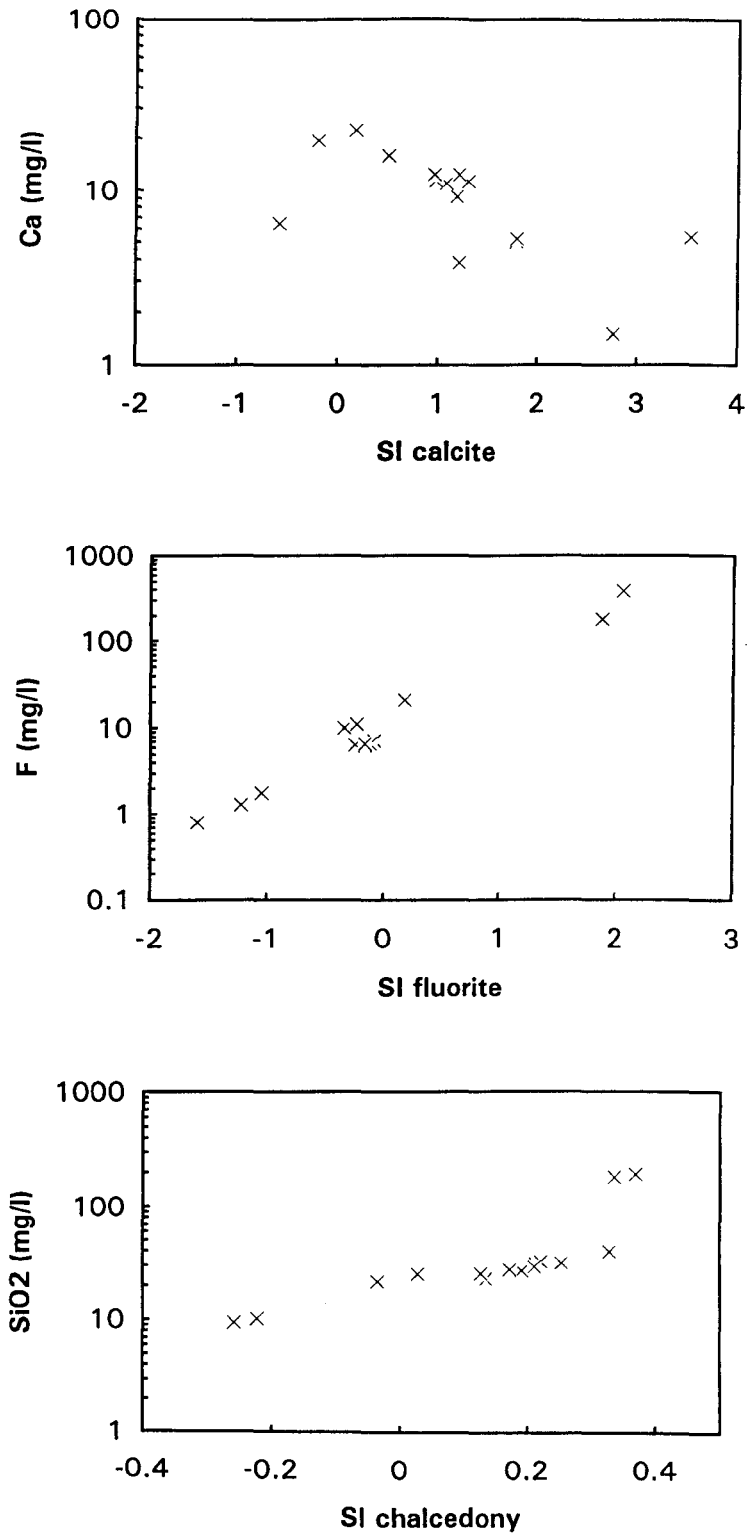
Fig 6.9 Plots of $SI_{calcite}$, $SI_{fluorite}$, SI_{quartz} and $SI_{chalcedony}$ vs Ca, F and SiO_2 for lake waters in the KRV.

"excess" chloride may be related to the extensive drainage into Victoria from river basins on Precambrian metamorphic rocks, where ions such as Na and K are less readily dissolved than from the volcanics of the rifts.

Lake Turkana, though with the next lowest TDS, is an alkaline lake with a pH of ~9. In this case there seems to be a loss of each species compared to Cl; Yuretich and Cerling (1983) discussed the various ways in which these species were removed from solution. They reached the conclusion that no subsurface outflow from the lake was necessary to explain its chemical evolution. Turkana is not therefore likely to be an important feed for Lake Logipi, although isotopic evidence does not rule out some leakage (5.1.4.1).

The Elmenteita-Nakuru combination resembles a more evaporated version of Turkana. The pair are fed largely by groundwater leakage from Naivasha, plus probably some geothermal outflow from Eburru. The recharge is assumed here to be typified by the Elmenteita hot springs (K41). The spring water has already been considerably modified from the typical Naivasha composition, being depleted relative to Cl in all species, especially K and SiO_2, presumably by exchange and saturation respectively. However, from this point the main mechanism in arriving at the lakewater composition appears to be simply evaporation, there being little loss relative to Cl except again for SiO_2 which once again has reached saturation (Fig 6.9).

The situation at Bogoria seems to be anomalous in some ways. For example, HCO_3 is not depleted relative to the dilute waters of the rift. However, the main feed to the lake is probably represented by the composition of the southeasterly boiling springs (Cioni et al, 1992), e.g. site K262. For whatever reason, this spring is not depleted in HCO_3 either, and the relationship appears to be one of simple evaporation as for Elmenteita-Nakuru. Sodium, which is much less prone to depletion in high-TDS waters anyway, is in a similar position to HCO_3, as is F also. There is a major depletion in SO_4 presumably due to sulphate reduction. For K, however, there is no depletion beyond that already observed for the spring sources around the lake. Silica maintains the usual trend of depletion, having reached saturation (Fig 6.9).

The hydrochemical evolution of Lake Magadi and its associated springs has been discussed in great detail by Eugster and co-workers (e.g. Eugster, 1970, 1980 and Jones et al, 1977). From the perspective of this study, one of the more important aspects is where the recharge to Magadi originates. On the basis of similar Na/Cl ratios, it was assumed by Eugster and others (references *ibid*) that leakage from the Ewasongiro to the west was a major contributor to the

springs feeding the lake, even though this river flows ultimately into Lake Natron. However, consideration of stable isotopic data (a technique not used during Eugster's studies) reveals that only the northern springs of the lake are as isotopically enriched as the river, raising the possibility that Naivasha water may be contributing instead of the river (6.1.2.1 and 2). Unfortunately, the chemistries of both the Ewasongiro and Lake Naivasha are very similar, and do not form a basis for source discrimination.

6.1.5   High-temperature geothermal waters

Analyses for geothermal waters from all parts of the rift are given in Table 6.9. Kenya wells have OW- (Olkaria) and EW- (Eburru) prefixes. It is not proposed to go into great detail on the evolution of these waters, but to focus more on what they can reveal about water sources. To a large extent this has already been done by isotopic methods (Chapter 5) and consideration of the chemistry is therefore of reduced importance compared to other parts of the hydrological cycle.

Concentrations of Na, K and Si are almost purely a function of system temperature, with the Na/K and SiO_2 solute geothermometers mostly agreeing fairly closely with measured temperatures (8.1.2). Li and B are relatively high, as would be expected in a high-enthalpy geothermal system. In virtually all cases at Olkaria, Cl exceeds HCO_3. This is commonly observed in the deeper parts of geothermal systems worldwide, in which bicarbonate-dominated waters are believed to arise from condensation of steam and CO_2 into shallow groundwaters (e.g. Ellis and Mahon, 1977). However, the copious outgassing of CO_2 from the whole rift system means that even the deeper fluids are sometimes considerably affected, as is the case for well EW-01 (and also all the Langano wells in Ethiopia).

The isotopic evidence that some two-thirds of the water in the eastern and northeastern wellfields at Olkaria is contributed by Naivasha can be compared with the chemical relationships. Tables 6.8 and 6.9 shows that relative to Cl there is a loss of HCO_3 and K, no change in Na and SO_4, and a gain in SiO_2, F and B in the thermal waters compared to the lake. This is largely as would be expected, insofar as HCO_3 is depleted with distance from the surface, and F and B are typical magmatic inputs. However, depletion of K is unusual in geothermal systems. At Olkaria, Na/K geothermometry gives reasonably valid results, so the relative loss of K is likely to be related to the unusual concentration of K in the lacustrine component of recharge to the system, which is then brought to equilibrium by reaction with feldspar.

Table 6.9   **Chemical composition of high-temperature geothermal waters in the Eastern Rift. Results in mg/l.**

Well	Site No	pH	Na	K	Ca	Mg	HCO3	Cl	SO4	Si	Li	B	F
OW-2	K110		584	118	0.8		57	800	30	55.1	1.09	7.14	
OW-16	K113		486	74	0.4		181	624	20.2	248	1.16	7.12	
OW-21	K115		386	53	0.2		172	390	151	262	1.05	4.78	
OW-22	K112		398	37	0.3		334	236	86	212	0.52	2.06	
OW-23	K114		311	42	0.4		183	194	34	247	0.72	2.82	
OW-26	K111		265	40	0.5		108	240	23	250	0.66	2.53	
OW-715	K259		406	86	0.5		233	480	39	312	1.67	2.73	
OW-29	(1)	8.90	579	96	0.3		180	608	27	336	1.4	7	53
OW-714	(1)	8.60	570	106			234	635	68	244	1.6	3.2	59
OW-716	(1)	9.65	624	124			83.5	899	83	296	2.3	6.2	38
		8.00											
EW-01	K502		2085	365			2501	978	160	429	2.8	2.1	279
EW-04	(1)	9.70	810	77			631	778	172	152	0.74	2.2	102
		10.00											
LA-3	E1		675	157	1	0.1	1081	310	282	259		3.4	38
LA-4	(2)	9.30	758	230	5	0.5	651	479	473	260		13	37
LA-5	(2)	9.50	1060	148	6	0.5	1518	720	168	148		6.7	28
LA-6	E2	9.00	934	150	6	0.2	1685	454	204	195		7.4	46
LA-7	(2)	9.00	684	81	8	0.9	1626	325	135	98		5.7	23
LA-8	E3	8.80	670	53	6	0.4	684	55	73	87		7.6	22
		9.10											
A-1	(3)		28520	4888	16389	24.3		78100	21.1	18.3	13.2	6.5	
A-3	D1	5.20	24900	4830	15900	24.6		70100	19.1	233		7.7	2.3
A-4	(3)	5.10	32200	5318	17511	2.4		85200	26.9		15.2	7	

OW- Olkaria   EW- Eburru   LA- Aluto-Langano   A- Asal

(1) Data from Arusei (1992)   (2) Data from Endeshaw (1988)   (3) Data from Sanjuan et al (1990)

148

6.2 Main Ethiopian Rift

Much of the data considered here is derived from Craig et al (1977), whose data are reported for reference purposes in Appendix E. All data sources are acknowledged in figure or table captions as appropriate.

6.2.1 Rivers and streams

In view of the general similarity of rock types drained by streams and rivers in both the Kenya and Ethiopian rifts, it would be expected that in the absence of complicating factors the chemistry would be proportionally similar in all cases. A comparison between the results shows that this to a large extent is the case (Tables 6.1, 6.10 and E.1). As in Kenya, the range of concentrations in the MER is for most species governed by evaporative concentration. Therefore when various species are plotted versus Cl, a simple relationship is seen for most sites (Fig 6.10). Silica, however, reaches saturation early on (Table 6.11, Fig 6.10) and is unable to rise with overall TDS.

The most chemically modified river in the region is the Bilate (CRA62, 79), which is supplemented by the discharge of hot springs (Craig et al, 1977), though not to the extent of the Suguta in Kenya. Only SO_4 shows much sign of a departure from a 1:1 relationship with Cl (Fig 6.10), and this is only a minor effect.

As in Kenya, the saturation indices for rivers in the MER reveal a range of conditions from under- to over-saturation with respect to calcite, but virtually all undersaturated for fluorite. Only Bilate 2 reaches saturation, owing to the hot spring input (Fig 6.11).

6.2.2 Cool groundwaters

Results for the MER (Tables 6.10, E.1) are generally similar to those from the KRV, though they do not reach the high TDS levels noted for some of the Kenya groundwaters. In addition, although there are fewer data, Ca exceeds Na (in mgl^{-1}) more frequently than in Kenya, a feature which was not observed for the river waters (see previous section).

As usual, HCO_3 is by far the dominant anion. While it never rises above 400 mgl^{-1} in the springs, virtually all the boreholes exceed this concentration, reaching a maximum of ~ 1100 mgl^{-1} at Debre Zeit. However, this town near the edge of the MER (a poorly defined

149

Table 6.10   Chemical composition of ground and surface waters collected in the MER and southern Afar during the present study. Results in mgl⁻¹.

Site Name	Site No	Sample Source	Temp °C	pH	Na	K	Ca	Mg	HCO₃	Cl	SO₄	Si	Li	B	F
Langano #2	E11	S	65	7.9	740	85.6	9.18	2.6	1470	464	21.9	92.2	0.532	2.66	28
Abaya #6	E12	S	96	9.5	1330	186	0.35	<0.1	2480	686	108	154.0	1.39	3.19	66
Abaya #7	E13	S	88	6.8	5.7	9.2	1.28	0.3	22	2.2	87.6	48.9	0.007	0.03	0.28
Wondo Genet	E14	S	65	7.1	173	44.5	11.1	3.5	600	23.3	<0.05	60.0	0.047	0.08	1.45
Shalla #30	E15	S	96	8.8	2190	20.0	0.60	<0.1	3460	1470	30.3	33.4	0.474	5.65	76
Sodere	E16	S	65	7.3	550	29.7	14.7	8.3	1340	140	113	52.2	0.232	1.28	7.2
Langano	E17	L	-	9.4	370	20.6	4.94	1.7	791	155	14.7	33.2	0.007	0.64	14
Awasa	E18	L	-	9.2	159	31.1	8.91	5.5	505	28.3	0.9	35.4	0.121	0.14	8.2
Asal A-3[1]	D1	G		-	292000	5030	17035	22.9	335	78425	11	237	15.3	10.1	9.8
Korilli[1]	D5	S	36	6.45	10310	464	3040	466	55	22670	253	30.3	2.18	4.2	-
Abbe C.	D6	S		8.70		14.6		<0.1	26	785	304	41.6	0.136	1.00	0.90
Abbe N.	D7	S	90	6.05	901	29.7	213	0.3	18.6	1530	323	47.9	0.290	1.55	1.14

G - geothermal well   L - lake   S - spring

[1] Analyses provided by Dr H Armannsson

Analysed at BGS Wallingford by J Cook, J Trafford and K Smith

150

Table 6.11   Saturation indices of river waters in the MER with respect to calcite, fluorite and chalcedony.

Site Name	Site No.	pH	SI calc	SI fluor	SI chalc
Rivers					
Awash	CRA4	8.20	0.827	-0.832	0.295
Maki	CRA10	8.00	0.715	-0.553	0.323
Jido	CRA18	7.10	-0.405		0.282
Tej	CRA34	7.80	-1.049	-2.259	0.300
Teyl	CRA35	7.80	-1.294	-2.050	0.112
NE Langano	CRA37	7.80	-0.092	-1.413	0.606
Melka	CRA46	7.60	0.290	-1.075	0.493
Worka	CRA51	8.10	0.460	-1.398	0.832
Imbalu	CRA61	7.60	-0.462	-1.110	0.237
Bilate 1	CRA62	8.40	0.452	-1.493	0.275
Bilate 2	CRA79	8.80	1.388	0.223	0.727
Omo	CRA81	7.75	0.263	-1.620	0.236
Humasa	CRA83	7.85	-0.194	-1.786	0.322
Lakes					
Zwai	CRA6	7.60	-0.175	-1.170	0.266
Langano	CRA15	8.80	0.759	-0.088	-0.527
Abiata	CRA19	9.60	1.854	0.826	0.673
Langano SW	CRA28	9.20	1.313	-0.100	0.504
Shalla	CRA44	9.60	2.442	2.118	0.607
Shallo	CRA54	7.70	-0.322	-0.432	0.130
Awasa	CRA57	9.15	1.654	-2.940	0.887
Chitu	CRA66	9.85			0.977
Abaya	CRA84	8.85	1.339	-0.140	0.284
Shamo	CRA88	9.05	1.314	-0.222	0.115

CRA sites: saturation indices calculated from the analyses of Craig et al (1977)

Fig 6.10   Plots of Na, HCO₃, K, SO₄, F and SiO₂ vs Cl for waters in the MER.
(Data from Craig et al, 1977, and this study.)

152

Fig 6.11   Plots of $SI_{calcite}$, $SI_{fluorite}$ and $SI_{chalcedony}$ vs Ca, F and SiO_2 for river and stream waters in the MER (calculated from the data of Craig et al, 1977, and this study).

feature in this area) is surrounded by crater lakes and, on the basis of stable isotope results, evaporated water from these is contributing to the elevated TDS observed. A relationship with lake waters is probably responsible for high TDS values at Southern Cross and Awasa (CRA8, 56) too, though not at Jido Combol (CRA17) on the basis of stable isotope data (Chapter 5).

Modification of most of these groundwaters by water-rock interaction is small and predictably follows Cl for Na, HCO_3 and F (Fig 6.10). Although there is some scatter, K seems to become depleted, while SiO_2 as usual reaches early saturation. The data for SO_4 are too scattered to draw any conclusions. Waters cluster around saturation with respect to calcite, extend from saturated to oversaturated for chalcedony, and are predominantly below saturation for fluorite (Table 6.12, Fig 6.12).

6.2.3   Hot groundwaters

Unlike the Kenya sites considered under 6.1 above, some groundwaters exceeding 40°C have been sampled from boreholes in the MER. Tables 6.10 and E.1 give the analytical data. Although they are mainly high-bicarbonate waters, values are all below the equivalent of 4500 mgl^{-1} HCO_3 and therefore never approach the high TDS spring waters of the Suguta Valley or Magadi. Some of the larger hot springs in the MER have a significant high-enthalpy component, in contrast to the situation in Kenya. In the case of the Aluto volcanic centre (Fig 5.20), springs immediately to the south on the edge of Lake Langano (Langano #1, #2, Bole Fault and Geyser Island; CRA20, E11, CRA21, 24) have high levels of SiO_2 consistent with such an origin. High-output springs north of Lake Abaya (Abaya #6, #8, #10; CRA72, 74, 75, E12) also have elevated SiO_2 concentrations, but in this case the relationship with a volcanic centre is less clear. As far as other springs are concerned, the heat source is not always obvious (Table 3.1), but none of these springs has such a clear high-enthalpy signature.

The only very dilute hot water, from Kenteri (CRA49), is associated with the eastern wall of the rift and presumably represents a deep-circulation water. (However, one of the nearby Wondo Genet springs, CRA47, is also likely from its position to be a deep-circulation water, but has a much higher TDS.) There is nothing to distinguish Kenteri from cool groundwaters of similar TDS. Otherwise, although there is some overlap, the hot springs are generally more chemically evolved than the cool waters. Plots of various species against Cl reveal a relative loss in the range 1 to 5 $meql^{-1}$ Cl. The apparent removal of Na around the 20 $meql^{-1}$ concentration level is at first sight slightly puzzling, since Na and Cl are normally highly correlated. From the concentrations and locations involved, there can be no question of Na

Table 6.12   **Saturation indices of cool (<40 C) groundwaters in the MER with respect to calcite, fluorite and chalcedony.**

Site Name	Site No.	Temp C	pH	SI calc	SI fluor	SI chalc
Springs						
Silte Tekel	CRA12	18	7.40	-0.321	0.426	0.926
Butajera	CRA13		7.20	-0.097	-1.641	0.639
Oitu	CRA27	38	7.85	0.426	-1.270	0.591
Huluka	CRA36	18	6.40	-2.219	-1.686	0.490
Sedi 1	CRA38		7.10	-1.023	-1.669	0.602
Sedi 2	CRA39		7.60	-0.099	-0.613	0.576
Sedi 3	CRA40		7.25	-0.530	-1.224	0.593
Shalla	CRA41	21	7.40	-0.743	-1.255	0.487
Saisha	CRA52	32	6.90	-0.853	-0.832	0.588
Motokawa	CRA60	35	7.40	-0.213	-1.108	0.472
Asasa	CRA68	21	7.70	-0.241	-1.446	0.451
Humasa	CRA82	35	6.90	-0.484	-1.045	0.635
Arba Minch	CRA87	17	7.60	-0.001	-1.445	0.781
Boreholes and wells						
Akaki	CRA1	21	7.60	0.600	-1.419	0.461
Debre Zeit	CRA2	26	8.20	1.204	-0.625	0.522
Mojo	CRA3	25	7.40	0.300	-1.018	0.653
Adami Tulu	CRA5	31	8.10	0.282	-0.979	0.341
Zwai Well	CRA7		7.40	0.470	-0.275	0.706
S Cross	CRA8		7.90	0.642	0.078	0.650
Maki	CRA9	25	7.80	0.715		
Koshe	CRA14	38	7.60	0.416	-1.303	0.611
Jido Combol	CRA17	34	9.00			0.591
Bek Mol Awasa	CRA55		7.40	-0.042	0.804	0.639
Awasa Bank	CRA56	32	7.80	-0.187	-0.261	0.380
Sholicha	CRA67	36	8.10	-0.363	0.026	0.534
Shashemane	CRA70		7.20	-0.753	-1.162	0.494

CRA sites: saturation indices calculated from the analyses of Craig et al (1977)
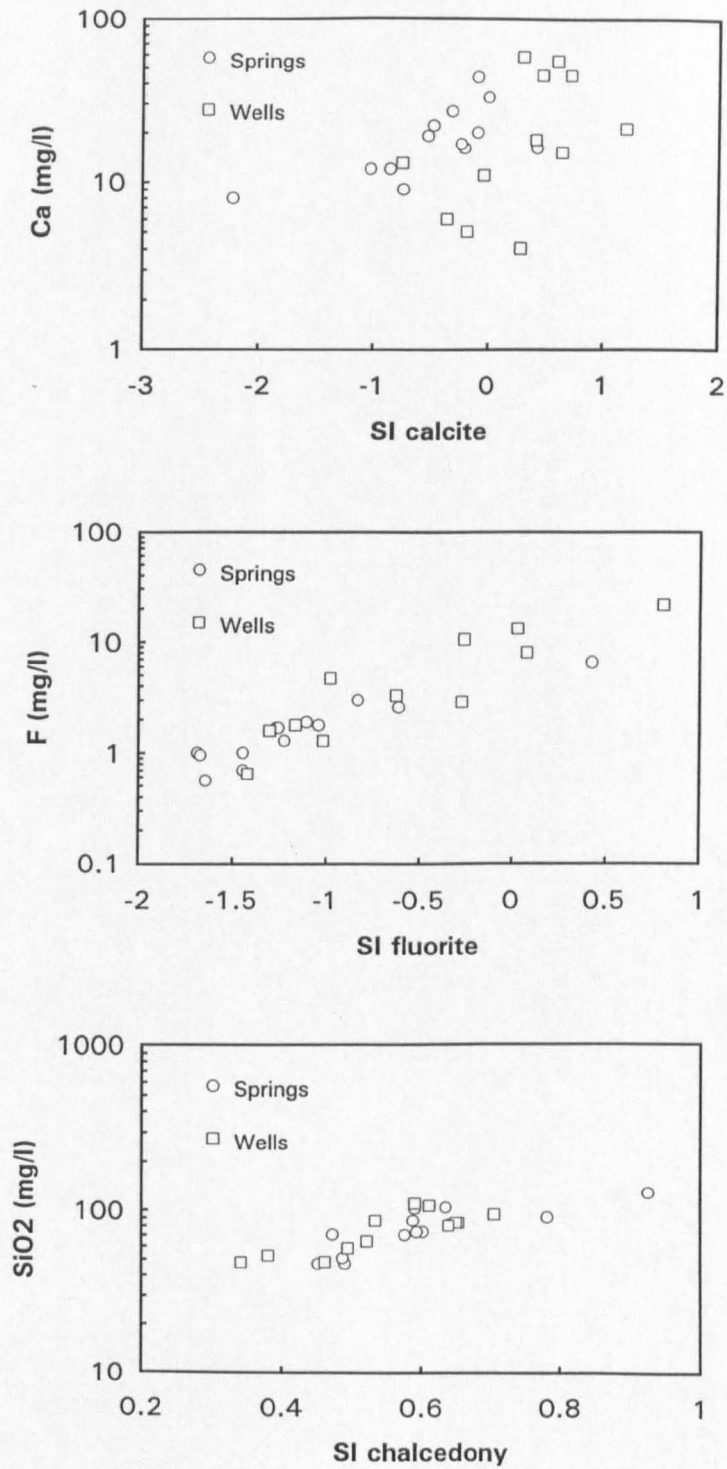
Fig 6.12   Plots of $SI_{calcite}$, $SI_{fluorite}$ and $SI_{chalcedony}$ vs Ca, F and SiO_2 for cool (< 40°C) groundwaters in the MER (calculated from the data of Craig et al, 1977, and this study).

dropping out of solution owing to carbonate deposition.

Species such as HCO_3, K and SiO_2 show a decline relative to Cl (Fig 6.10) for the reasons outlined in 6.1.3 above. However, F is normally conservative over this range but also shows a decline. If F is plotted versus Na rather than Cl, a much more linear relationship is seen (Fig 6.13). This suggests that the observed deviations in Fig 6.10 are partially (HCO_3, K) or wholly (Na, F) controlled by an increase in Cl. This is most probably due to the invasion of shallow aquifers by the relatively low HCO_3/Cl waters from high-enthalpy sources. The spring waters in the "zone of deviation" are those for which high silica has been noted (see above). This is indicated by a plot of Na/K versus Cl (Fig 6.14). If chloride is being supplemented through high-temperature water-rock interaction with the more acid volcanics, an inverse correlation with Cl should be seen, because Na/K declines with increasing temperature under the control of plagioclase feldspar. While most of the hot springs show the opposite relationship, almost all the springs in question show a good correlation with Cl.

If Cl is rising in concentration more rapidly than Na in the 1 to 5 meql^{-1} Cl zone, the question arises of how the natural ionic balance is being achieved. Possibly the somewhat variable analytical ionic balances might be a factor, but similar deviations against Cl were noted on lake water samples independently analysed by Von Damm and Edmond (1984) (see next section). In any case, HCO_3 measurement is more usually a cause of balance discrepancies. Although Li was not measured for most of these samples, unless concentrations are very much higher in the MER than in similar waters in the KRV (which Table 6.10 suggests they are not), it does not seem possible that a rise in Li could balance the Cl. This leaves pH as the only alternative source of positive ions. An input of chloride in the form of HCl should lower the pH of waters, and Table E1 shows that pH values are generally at their lowest in the 30 to 150 mgl^{-1} zone, i.e. approximately 1-5 meql^{-1} Cl. The possible significance of "excess" Cl in connection with lake water chemistry is considered in the next section.

Virtually all the hot springs are at or above calcite saturation (Table 6.13, Fig 6.15). Quartz is likely to be the controlling phase for silica only at the higher concentrations, otherwise chalcedony is a more likely control and most springs are at saturation. Most of the waters are undersaturated with respect to fluorite.

6.2.4   Lakes

The lack of significant surface water bodies in the MER to the north of the artificial Lake Koka
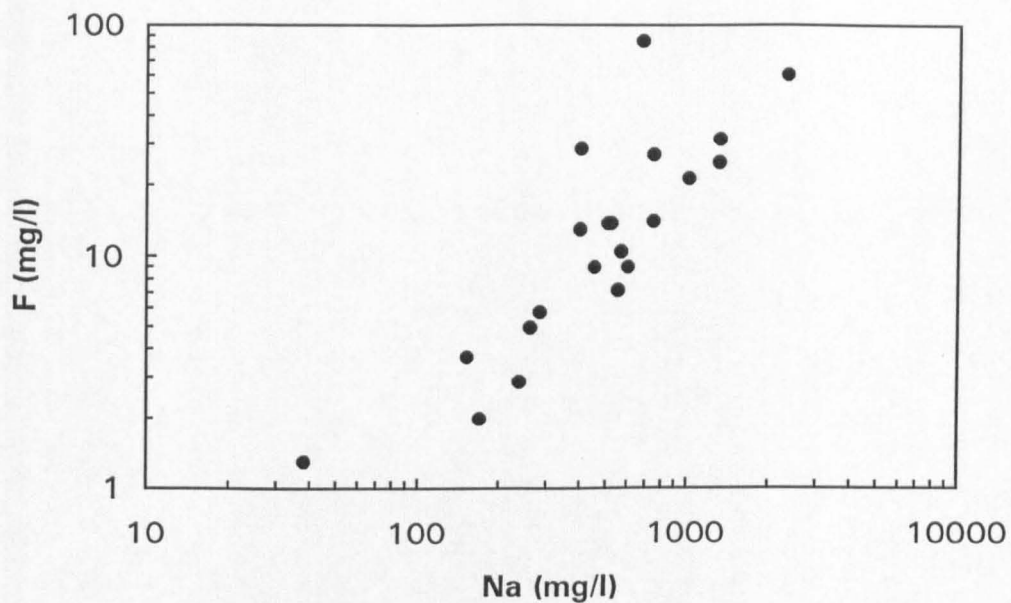
Fig 6.13   F vs Na for hot (> 40°C) groundwaters in the MER. (Data from Craig et
                al, 1977, and this study.)
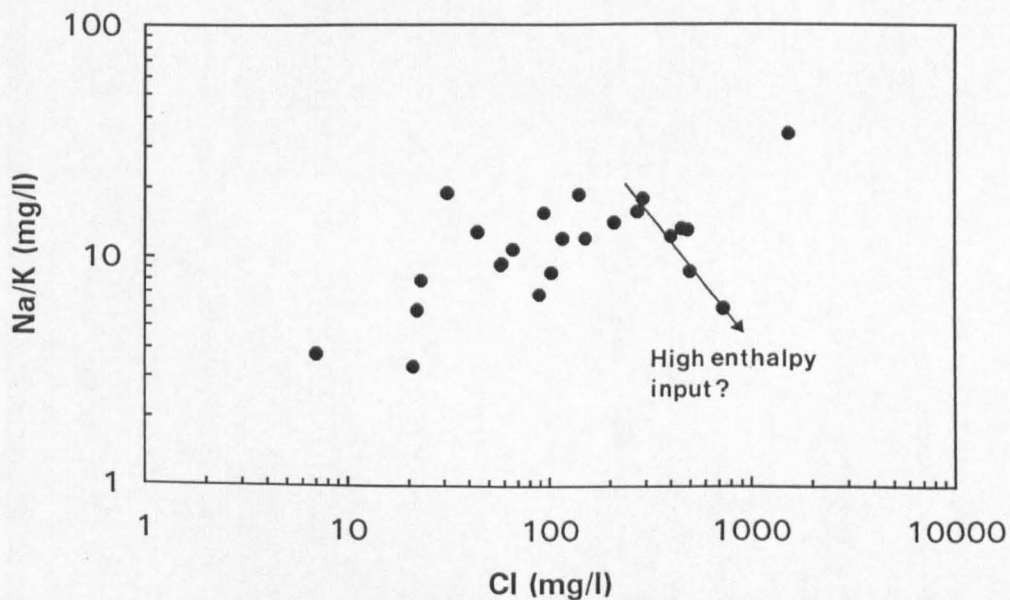
Fig 6.14   Na/K vs Cl for hot (> 40°C) groundwaters in the MER. (Data from Craig
                et al, 1977, and this study.)

Table 6.13 Saturation indices of hot (>40 C) groundwaters in the MER with respect to calcite, fluorite, quartz and chalcedony.

Site Name	Site No.	Temp C	pH	SI calc	SI fluor	SI qtz	SI chalc
Imba Koto	CRA11	49	8.50	1.294	-0.777	0.632	0.272
Wildlife Con	CRA16	46	8.20	0.345			
Langano #1	CRA20	67	7.80	1.052	0.439	0.692	0.378
Bole Fault	CRA21	92	8.80	-0.003	-2.478	0.416	0.157
Geyser Is	CRA24	97	8.80	0.145	-2.264	0.347	0.098
Shalla 30	CRA30	94	8.70	0.467	-1.199	0.193	-0.062
Bekele M well	CRA33	43	9.10	1.371			
Wondo Genet	CRA47	65	7.00	0.069	1.291	0.597	0.278
Kike	CRA48	52	7.55	0.409	-1.469	0.926	0.574
Kenteri	CRA49	69	7.40	-0.426	-2.152	0.484	0.174
Shallo	CRA53	90	8.00	0.467	-1.199	-0.008	-0.062
Graha Que	CRA58	86	7.35	0.724	-0.142	0.569	0.297
Bodicho	CRA59	89	9.20	1.242		-0.094	-0.359
W Agge	CRA63	43	7.45	0.569	-0.388	0.941	0.565
Shalla SW	CRA64	54	8.80	0.845	-0.843	0.501	0.153
Chitu	CRA65	60	7.70	0.65	-0.182	0.748	0.416
Abaya 6	CRA72	95	9.60	1.224	-1.664	-0.123	-0.375
Abaya 8	CRA74	67	6.95	0.569	-0.151	0.739	0.425
Abaya 10	CRA75	50	6.75	0.326	0.484	0.925	0.567
Chokare 15	CRA76	67	6.80	-0.035	-0.176	0.707	0.393
Chokare 16	CRA77	42	7.20	0.663	-0.548	0.956	0.577
Bilate	CRA78	51	7.60	0.463	-0.618	0.365	0.009
Nech Sar	CRA86	58	7.60	0.842	0.156	0.693	0.356
Sodere	E16	65	7.30	0.567	-0.468	0.693	0.373

CRA sites: saturation indices calculated from the analyses of Craig et al (1977)
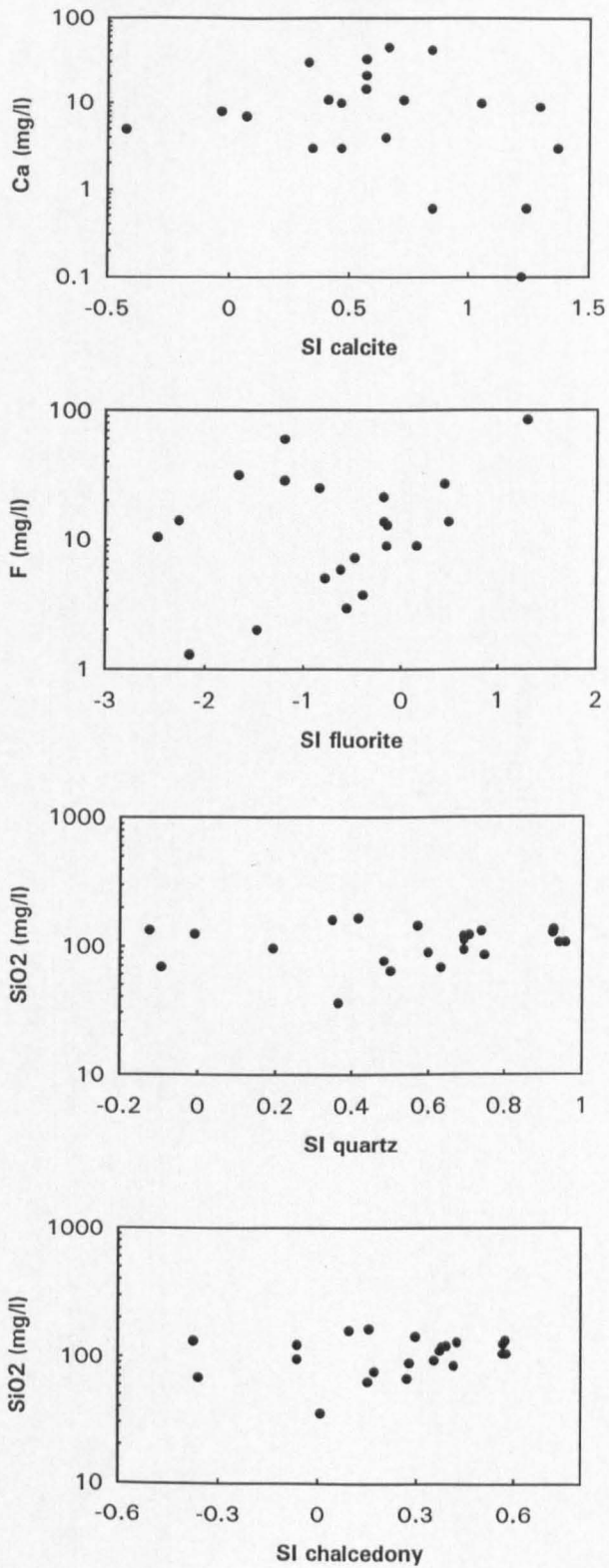
Fig 6.15   Plots of $SI_{calcite}$, $SI_{fluorite}$, SI_{quartz} and $SI_{chalcedony}$ vs Ca, F and SiO_2 for hot (>40°C) groundwaters in the MER (calculated from the data of Craig et al, 1977, and this study).

has already been mentioned. The only "natural" body, the small Lake Besaka (Fig 5.20), which appears to be expanding at present owing to a variety of anthropogenic sources, has a relatively high TDS content (~ 7000 mgl^{-1}; Gizaw, 1996) largely due to the shallow depth permitting significant evaporative enrichment, although hot springs also discharge into the northern side of the lake. While the lake fills the gap in the TDS range between Langano and the soda lakes of the central MER, its HCO_3/Cl ratio is a little higher and by implication the hydrothermal input is of less importance (see below).

However, the main interest in lakes of the MER lies southwards of the culmination of the rift floor south of Koka. The chemistry of all these lakes has been treated in some detail by Von Damm and Edmond (1984), and for Shalla specifically by Baumann et al (1975).

Fig 4.5 shows that the freshest lakes are Zwai, nearest to the culmination, Awasa, and Abaya, the largest lake of the MER in terms of surface area. Only slightly more saline are Langano and Shamo. Zwai, Langano and Abaya all have surface outflows and possibly additional subsurface leakage (see previous chapter). Shamo probably has a periodic overflow as well (4.2.1). Awasa, which has an even higher surface elevation than Zwai, must have substantial subsurface outflow to maintain its freshness, and this has been demonstrated by isotopic techniques (5.1.5). The remaining two lakes, Abiata and Shalla, are apparently terminal and are much more saline.

The chemistry of Zwai represents evaporative concentration by only a few times of the main river feeding it (Maki). Awasa, Abaya and Shamo also show a simple evaporative concentration on the basis of plots of Na and F versus Cl (Fig 6.10), though even at these relatively dilute TDSs, K and HCO_3 decline relative to Cl. As usual, SiO_2 has reached early saturation (Table 6.14, Fig 6.16).

Langano shows the first signs of a change in the Na/Cl ratio. Von Damm and Edmond (1984) interpreted this change of Na relative to Cl in terms of slight but progressive Na loss as the lakes increased in TDS. On the evidence of the data considered here there appears to be an offset between Awasa-Shamo and Langano, in the same region of the plot as the hot springs (Fig 6.10). In view of the presence of a sizeable input from hot springs on the northeastern shores of Langano, the change in Na/Cl seems to result from an input of Cl rather than a depletion of Na. Thus Cl is not a conservative species in this case; the source of this extra Cl is presumably water-rock interaction in the nearby Aluto hydrothermal plume. The Na offset is reflected to about the same extent by HCO_3 and F, confirming that an increase in Cl rather

161

Table 6.14   Saturation indices of lake waters in the MER with respect to calcite, fluorite and chalcedony.

Site Name	Site No.	pH	SI calc	SI fluor	SI chalc
Rivers					
Awash	CRA4	8.20	0.827	-0.832	0.295
Maki	CRA10	8.00	0.715	-0.553	0.323
Jido	CRA18	7.10	-0.405		0.282
Tej	CRA34	7.80	-1.049	-2.259	0.300
Teyl	CRA35	7.80	-1.294	-2.050	0.112
NE Langano	CRA37	7.80	-0.092	-1.413	0.606
Melka	CRA46	7.60	0.290	-1.075	0.493
Worka	CRA51	8.10	0.460	-1.398	0.832
Imbalu	CRA61	7.60	-0.462	-1.110	0.237
Bilate 1	CRA62	8.40	0.452	-1.493	0.275
Bilate 2	CRA79	8.80	1.388	0.223	0.727
Omo	CRA81	7.75	0.263	-1.620	0.236
Humasa	CRA83	7.85	-0.194	-1.786	0.322
Lakes					
Zwai	CRA6	7.60	-0.175	-1.170	0.266
Langano	CRA15	8.80	0.759	-0.088	-0.527
Abiata	CRA19	9.60	1.854	0.826	0.673
Langano SW	CRA28	9.20	1.313	-0.100	0.504
Shalla	CRA44	9.60	2.442	2.118	0.607
Shallo	CRA54	7.70	-0.322	-0.432	0.130
Awasa	CRA57	9.15	1.654	-2.940	0.887
Chitu	CRA66	9.85			0.977
Abaya	CRA84	8.85	1.339	-0.140	0.284
Shamo	CRA88	9.05	1.314	-0.222	0.115

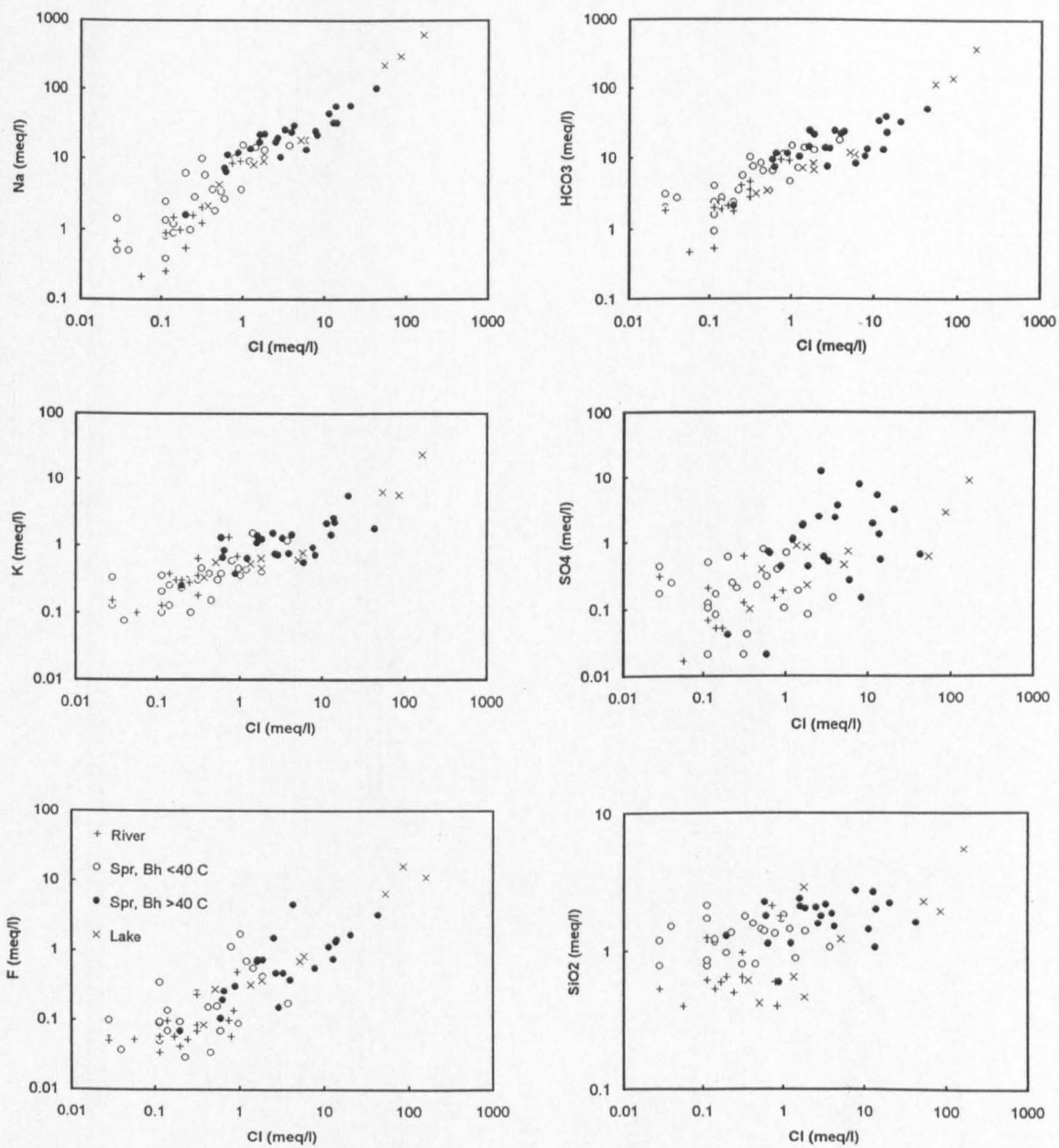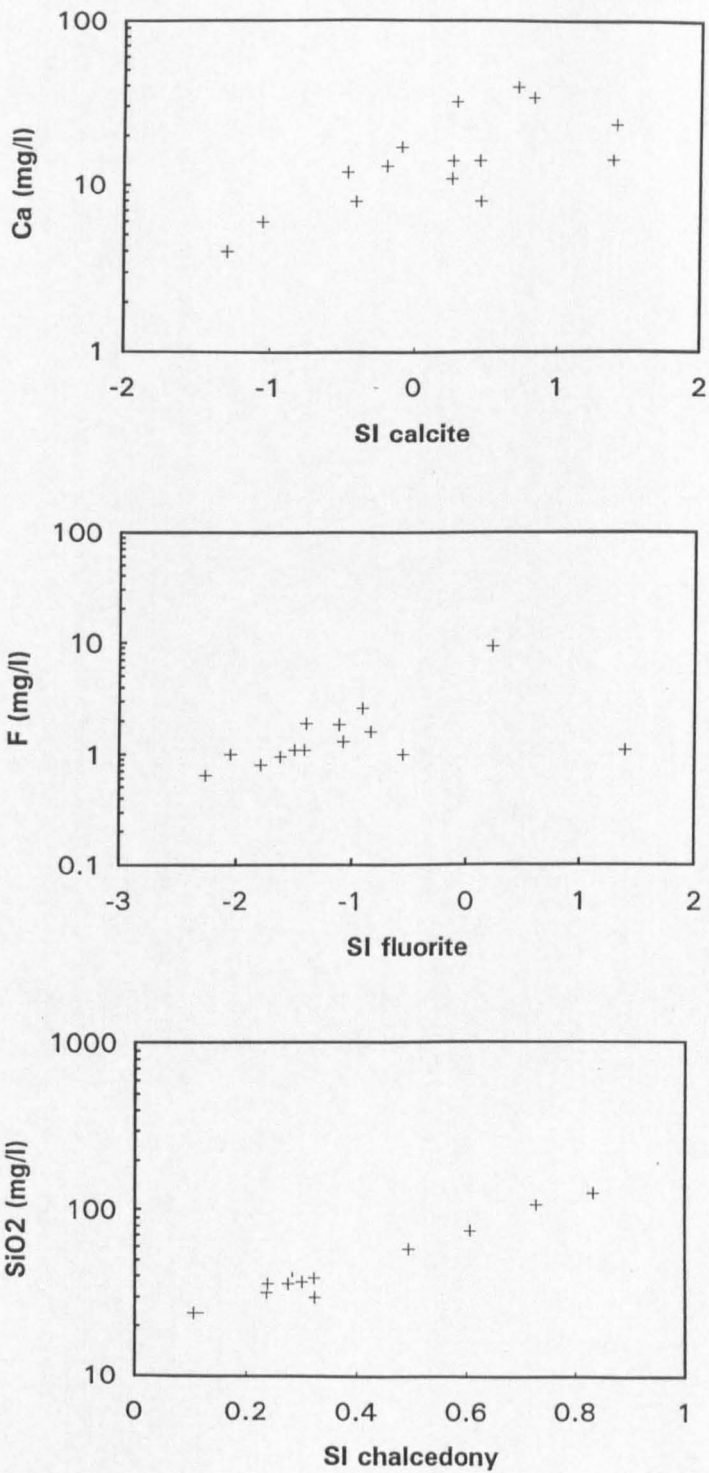CRA sites: saturation indices calculated from the analyses of Craig et al (1977)

Fig 6.16   Plots of $SI_{calcite}$, $SI_{fluorite}$ and $SI_{chalcedony}$ vs Ca, F and SiO_2 for lake waters in the MER (calculated from the data of Craig et al, 1977).

than a depletion in Na is responsible for the change. This extra input of Cl may explain why the chloride balance of Von Damm and Edmond (1984) failed to match their water balance.

After Langano, elevation of TDS appears again to be primarily controlled by evaporation. On both the data considered here and in Von Damm and Edmond (1984), the Na/Cl composition of the shallow lake Abiata is slightly depleted in Cl compared to the Langano-Shalla concentration line, perhaps because Abiata receives some water from Zwai as well as Langano. While the drowned caldera occupied by Shalla has hot spring feeds on the northeast and southwest shores, and perhaps submerged as well, these seem to be too low in discharge volume to affect the chemistry of such a deep, high-volume lake. Isotopic evidence suggests some underflow from Langano (see 5.1.5). Although the data on inflow amounts and Cl inputs to Langano were considered by Von Damm and Edmond (1984) to allow little scope for underflow, it now appears that the Cl budget of the lake is too uncertain to rule out large-scale leakage. As far as Abiata is concerned, its TDS value suggests that it is not a true terminal lake and that some flow into Shalla, surface or subsurface, may occur periodically or otherwise. The source of "extra" Cl for Shalla therefore remains unclear; there may be contributions from Langano and Abiata, but also perhaps there is an input of Cl from hydrothermalism beneath the caldera itself.

Chitu, a small crater lake south of southwest Shalla, has an extremely elevated TDS (Table E.1, Fig 6.10), though not as high as Magadi. In most respects Chitu resembles a more strongly evaporated version of Shalla, but depleted in F for reasons which are not clear. Since Chitu does not obtain its water from Shalla, but is related to the same major caldera, it provides an indication that Shalla's chemistry is largely endogenous rather than deriving substantially from leakage from Langano and Abiata.

In terms of saturation state, the lakes are at or above saturation with respect to calcite, chalcedony and fluorite (Fig 6.16), with the exception of Zwai which is below saturation in fluorite.

6.2.5 High-temperature geothermal waters

In contrast to the deep geothermal waters from Kenya, the waters of the Aluto-Langano geothermal field lying beneath the Aluto volcanic centre (Fig 5.20) usually have HCO_3 as the dominant anion rather than Cl (Table 6.9). This implies that there is even more CO_2 present at least in this part of the MER than in southern Kenya. Perhaps as an adjunct to this, SO_4 is

also considerably higher than at Olkaria, perhaps due to the oxidation of higher quantities of H_2S, which like the CO_2 is likely to be of magmatic origin.

Unlike at Olkaria and Eburru, isotopic evidence suggests that there is no large-scale feed to the Aluto system from the nearby lake (in this case Zwai, Fig 5.20). Recharge to the system may therefore have to travel a greater distance (presumably from the eastern rift wall area), and this may account for the higher TDS values encountered in the Aluto-Langano geothermal wells.

6.3   Southern Afar

Consideration of water chemistry in the Ethiopian part of the region is constrained by a general lack of data. Rather more is known about the southern Djibouti region.

6.3.1 Rivers

The only important flowing surface waters are those of the Awash and its tributaries, coming mainly from the western rift wall, such as the Kessem and Mille (Fig 2.5). Despite flowing for over 400 km between sampling points near Lake Koka and Tendaho, the TDS of the Awash changed little according to the data of Craig et al (1977) reported in Table E.2. This was in spite of inputs from the Kessem, which is affected by thermal waters from springs to the north of the Fantale volcano, and the Mille, which has a rather higher TDS. The main chemical difference between Koka and Tendaho appears to be the replacement of Ca-Na by more dominant Na, while Cl increases at the expense of HCO_3.

The Awash proceeds from Tendaho towards the southeast where it debouches into Abbe and smaller shallow lakes on or near the border between Ethiopia and Djibouti (Fig 5.26). In Djibouti itself, no important flowing surface waters exist, other than the wadis ("oueds") which carry occasional flash-flood water.

6.3.2   Groundwaters

In this region, which is closer to sea level than the MER, annual average temperatures are so high that waters of up to 45°C are considered here as "cool" (i.e. not significantly thermalised) for purposes of classification. However, this is a fairly arbitrary distinction, and as there are relatively few data all groundwaters are treated in a single section, in contrast to the MER and Kenya.

165

In the southwest of the region, immediately to the north of Fantale, two springs near the Kessem River (GIZ37, 47, Fig 5.26) represent the dilute end-member composition of groundwater in Afar (Table E.2). These waters are indistinguishable from cool spring and well waters from the MER to the south, and presumably reflect much the same kind of geochemical evolution in similar volcanic and volcaniclastic rock types. The "cool" Bilen and Filwoha springs (END5, 6) on the other hand are more highly mineralised and are beginning to show signs of the trend towards Cl-domination of the anions, which continues to its ultimate expression in the Oued Kalou springs of Djibouti (and presumably the Salt Plain of northern Afar, though this is outside the area considered in this thesis).

The geochemical relationships of the various groundwaters can be interpreted as before by plotting different species against Cl (Fig 6.17). A plot of Na versus Cl reveals that most samples fall along a trend towards the composition of seawater in the Gulf of Ghoubet. In the case of the sub-sea level Korilli and Manda springs of Lake Asal, undiluted or evaporated sea water is involved. In the remainder of cases, the springs and wells are above sea level and saline intrusion is unlikely to be involved; it is more likely that evaporites remaining from Quaternary marine incursions are responsible for the observed chemistry. Even so, there is evidence that some extra Cl has been added to the system, presumably from hydrothermal sources. This pattern of groundwater evolution is reflected by K and SO_4 versus Cl, though the data are more sparse.

A plot of HCO_3 against Cl shows that to the northeast of Hertale (END4, Fig 5.26) most groundwaters have Cl as their dominant cation. This trend continues through to the hot springs of Lake Abbe.

The hot spring waters are mostly indistinguishable from the cooler waters on the basis of chemistry. However, Mg is an exception to this. Whereas in Kenya and the MER the content of Mg is not particularly diagnostic of these two categories of groundwater, and was therefore not plotted, in Afar there is a notable distinction. Virtually all groundwaters below 45°C fall on an evolutionary trend towards seawater composition, while the hot springs show progressive Mg loss with increasing mineralisation. The tendency for Mg (and Ca) to decline in East African Rift waters due to carbonate precipitation and exchange processes has already been demonstrated. What seems to be occurring in this case is that there is limited Mg-removing capacity in the form of carbonate in the waters of Afar, except where temperatures are hot enough to promote the exchange reactions which tend to deplete Mg and Ca in hydrothermal waters.

166
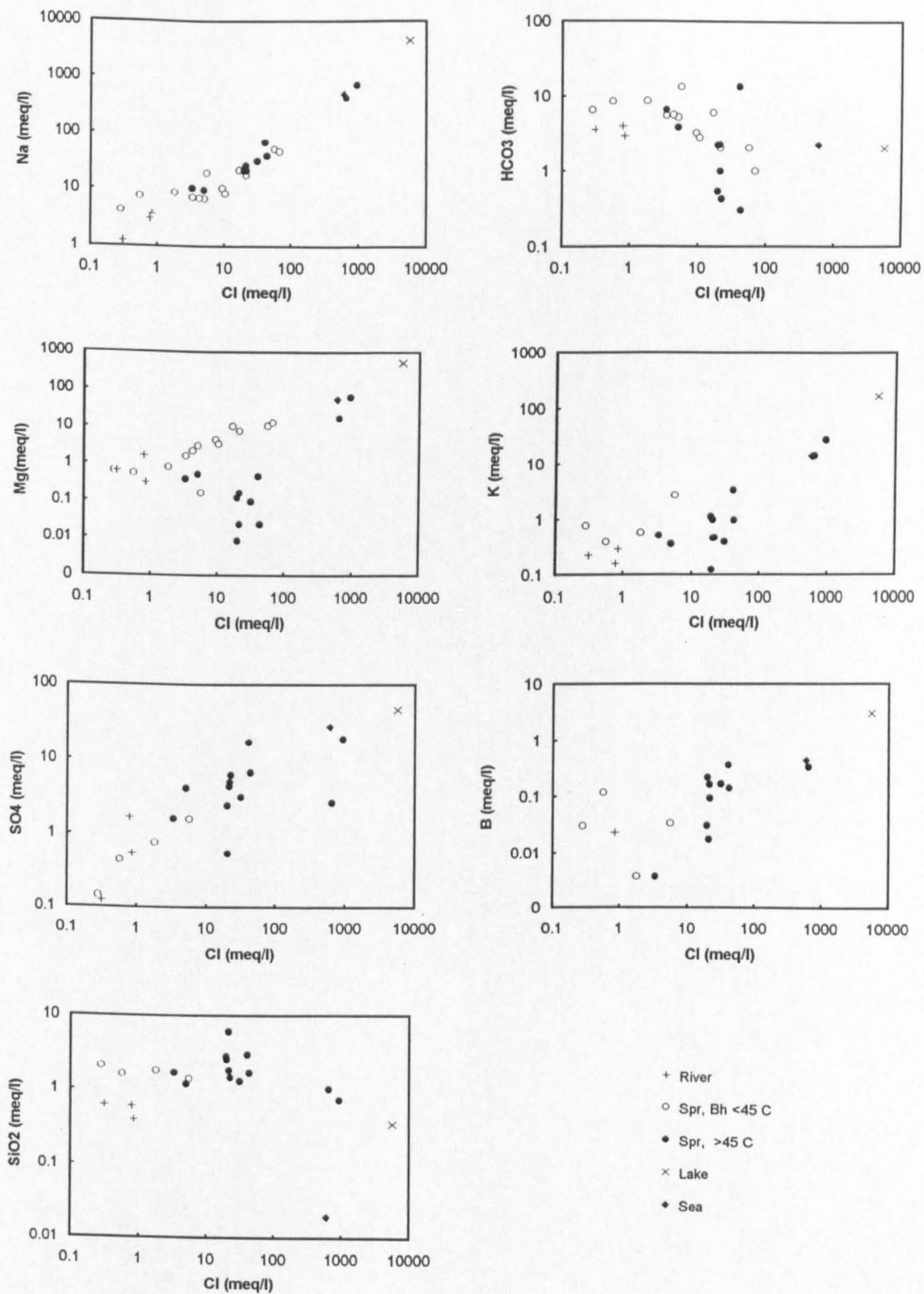
Fig 6.17   Plots of Na, HCO$_3$, Mg, K, SO$_4$, B and SiO$_2$ vs Cl for waters in southern Afar. (Data from Craig et al, 1977, Endeshaw, 1989, Fontes et al, 1979, Gizaw, 1986, Sanjuan et al, 1990 and this study.)

Predictably, most groundwaters hot or cold are at or above calcite saturation (Table 6.15, Fig 6.18). From both the chemical and geological evidence, few of the hot spring waters have a high-enthalpy component, and therefore chalcedony is likely to be the controlling phase for silica in all waters, which are at or only slightly above saturation. In view of the probable influence of marine evaporites, waters might have been expected to be nearer saturation with respect to gypsum than the continental waters to the south. This is broadly the case (Fig 6.18), though very few waters actually reach or exceed saturation, presumably because of a lack of Ca. Fluorite does not reach saturation, but is held at relatively low levels, never achieving the high concentrations seen in the MER or Kenya.

6.3.3   Lakes

There is a dearth of published information on the composition of Lake Abbe. According to Fontes et al (1980) the "brines from Lake Abbe correspond to the concentration by evaporation of waters from the River Awash". Although no data were provided in support of this statement there can be little doubt that the Awash is the major input to the lake. It is clear from the relict "chimney" structures, resulting from hot spring activity when the lake level was higher, that two different water types were mixing. The Awash is an Na-HCO$_3$ water, while the spring waters as typified by sample D6 (Table 6.10) are sufficiently high in Ca and SO$_4$ to reach well above saturation with respect to calcite and gypsum (Fig 6.18) presumably as a result of mixing in the shallow subsurface.

The other lake of the region, Asal, is only tenuously connected to the Afar groundwater regime. There is an order-of-magnitude jump in Cl between groundwater-fed hot springs in the Asal region, such as Oued Kalou (SK1, Fig 5.26), and the seawater-fed springs sustaining the lake. The lake itself is an evaporated version of the latter springs, and its salt crust is a clear sign of oversaturation with respect to halite. At around 150 m below sea level the lake is an obvious discharge area for groundwater, but the arid climate of Afar means that there is only a relatively small amount of groundwater flowing into the Asal basin in comparison to the large influx of seawater along the fissured zone of rifting between the lake and the Gulf of Ghoubet.

6.3.4   High-temperature geothermal waters

The high-temperature fluids sampled from the Asal geothermal wells are totally different to the thermal waters from the MER and Kenya (Table 6.9). Because the wells are situated within

Table 6.15   Saturation indices of ground and surface waters in southern Afar with respect to calcite, gypsum, quartz (hot springs only), chalcedony and fluorite.

SiteName	Site No	T deg C	pH	SI calc	SI gyps	SI qtz	SI chalc	SI fluor
Springs and boreholes <45C								
Kessem	G37		7.35	0.016	-3.032		0.869	-1.099
Sabire	G47		8.05	0.746	-2.676		0.751	-0.757
Bilen	END5	40	6.90	-0.214	-2.456		0.598	-0.589
Filwoha	END6	43	7.85	-0.195	-3.331		0.464	-1.145
Dikhil II	VER7	42	7.90	0.751				
Mouloud III	VER9	39	8.80	1.596				
Ali Sabieh	VER30	33	6.90	0.186				
Doubdoub	VER27	41	7.50					
Goroya	VER8	39	7.60	0.511				
Kourtimalay	VER28		7.80	0.499				
PK 50	VER6	40	8.10	0.782				
Oueah V	VER5	36	8.10	0.973				
PK 20	VER25	44	8.00	0.899				
Springs and boreholes > 45C								
Meteka	CRA90	72	7.40	0.735	-1.517	0.831	0.528	-1.036
Allallobeda	CRA91	79	8.00	0.517	-1.668	0.509	0.222	-2.117
Tendaho	END7	95	7.00	-0.743	-2.572	0.522	0.269	-2.249
Teo	END1	73	7.60	0.298	-1.683	1.118	0.818	-1.739
Danab	END2	93	7.75	0.671	-1.882	0.576	0.319	-1.431
Waruf	END3	50	7.30	0.013	-1.663	0.681	0.324	-2.27
Hertale	END4	49	7.35	-0.277	-2.609	0.837	0.477	-1.696
Korilli	SAS1	80			-0.896	0.341	0.056	
Manda	SAS3	45	7.05		-0.435	0.599	0.228	
Oued Kalou	SK1	74			-1.601	0.486	0.188	
Abbe C	DO6	75	8.70	1.355	3.837	0.422	0.126	
Abbe N	DO7	90	6.05	-1.195	-0.846	0.43	0.167	-1.181
Rivers								
Awash	CRA4		8.20	0.827	-3.007		0.295	-0.832
Awash 2	CRA93		8.20	0.254	-2.487		0.106	-0.906
Mille	CRA96		8.95	1.412	-2.134		0.238	1.39

Saturation indices calculated from the following data sources:
CRA - Craig et al (1977), D - this study, END - Endeshaw (1988), G - Gizaw (1986),
SAS and SK - Sanjuan et al (1990), VER - Verhagen et al (1991)
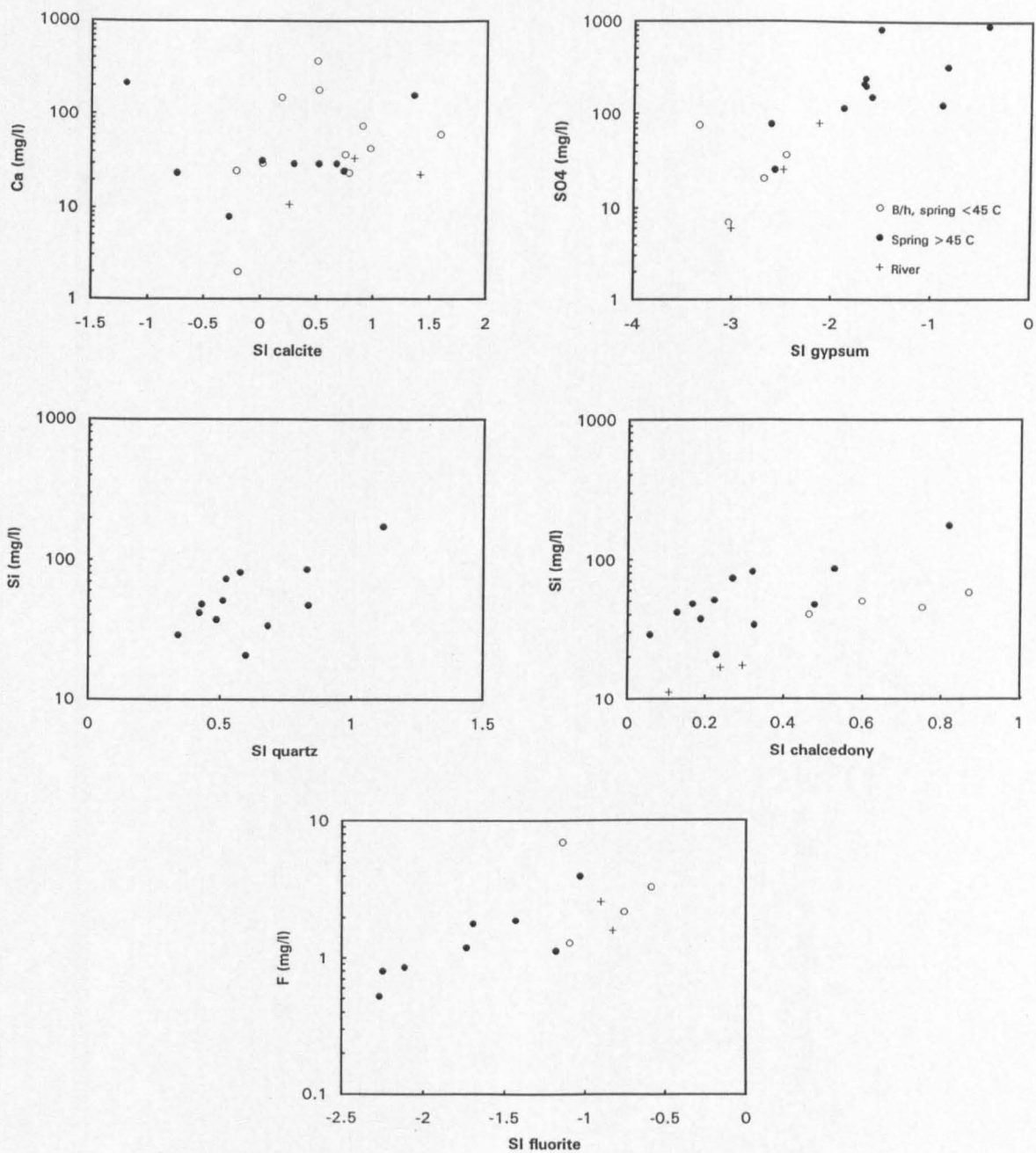
Fig 6.18   Plots of $SI_{calcite}$, SI_{gypsum}, $SI_{fluorite}$, SI_{quartz} and $SI_{chalcedony}$ vs Ca, SO_4, F and SiO_2 for river and groundwaters in southern Afar (calculated from the data of Craig et al, 1977, Endeshaw, 1989, Fontes et al, 1979, Gizaw, 1986, Sanjuan et al, 1990 and this study.)

or on the edge of the magmatically active zone of rifting where seawater is percolating through to Lake Asal (Fig 5.26), the fluid consists basically of seawater, though this has been concentrated some three times in terms of Na and Cl, while Ca has been considerably raised and SO_4 very much reduced. This was attributed by Sanjuan et al (1990) to reaction with basalt at high temperature, coupled with the effects of evaporative concentration. The consistency of Br/Cl ratios between the sea and other waters seemed to rule out the possibility of evaporite dissolution.

CHAPTER 7

CHEMICAL AND ISOTOPIC EVIDENCE
FOR GAS ORIGIN, MOVEMENT AND EVOLUTION

Major gases, and carbon isotope values were measured for a variety of sites in Kenya, Ethiopia and Djibouti (Table 7.1). Noble gas measurements were restricted to the Gregory Rift (Table 7.2), although helium isotope ratios were measured on samples from representative sites throughout the areas (Table 7.3). Higher hydrocarbon "trace" gases were measured at nearly all sites (Tables 7.4-7.6). Sample locations are as previously shown (Figs 5.2, 5.12, 5.20, 5.26).

7.1   Major Gases

7.1.1   Nitrogen, oxygen and argon

Fumaroles in the EARS as a whole are not generally very vigorous features and in addition are not always easy to sample. The presence of O_2 represents atmospheric "contamination" at a late stage either by near-surface entrainment from air which has penetrated porous rock, or conceivably from dissolved air in shallow perched water bodies. While some N_2 is also due to contamination at or near the point of sampling, there are cases where there is clearly an original component in the emanating gases, though this is likely to be ultimately derived from the atmosphere also. When the ratios N_2/Ar and $^{40}Ar/^{36}Ar$ (Table 7.2) are plotted against each other (Fig 7.1) most samples reveal evidence of air equilibration with water (N_2/Ar ~40). Samples with higher ratios indicate at least a component of direct air contamination not involving solution processes. However, all of these samples are dispersed along a trend coincident with the $^{40}Ar/^{36}Ar$ ratio of air, except for the Nyanza Rift sample from Bala (K53) which has a higher value. This particular case is presumed to be due to excess Ar produced by radiogenic decay of ^{40}K; the $^{40}Ar/^{36}Ar$ ratio of 846 is some three times higher than the atmospheric value of 296 (Nier, 1950) (Fig 7.1).

For some fumaroles, particularly in the MER and Djibouti, the presence of large amounts of air is obvious from the high percentages of N_2 and O_2+Ar present in the gases. This was a particular problem in terrain with a high degree of fissuring and fracturing, which presumably allows air to penetrate to significant depths below surface.

Table 7.1 Gas and carbon stable isotope analyses of gas phase samples collected from the Eastern Rift.

Area Site	Site No.	Sample Source	Sampling Temp. °C	CO₂ mmole/kg	CO₂	N₂	O₂ + Ar	H₂	H₂S	CH₄	$\delta^{13}C_{CO_2}$	$\delta^{13}C_{CH_4}$
							per cent				% PDB	
Suswa												
F-3	K126	F	93	851	10.2	71.3	18.5	<0.001	<0.01	0.0003	nd	nd
F-12	K258	F	94	1364	16.5	66.4	16.5	0.001	0.03	0.087	-3.0	-25.0
F-28[1]	K501	F	92	3720	97.4	0.27	<0.1	0.92	<0.01	1.40	-3.7	nd
Longonot												
F-23	K128	F	90	9382	77.4	16.2	4.0	1.7	0.01	0.75	-4.0	nd
Mt. Margaret[1]	K29	F	86	12561	95.2	4.6	<0.1	<0.001	<0.01	0.18	-1.7	nd
Olkaria/Domes												
OF-n[2]	.	F	91(7)	.	84.3(7)	10.9(7)	2.7(7)	1.54(7)	0.10(3)	0.58(7)	-3.8(7)	-26.5(6)
OW-n[2]	.	G	.	118(9)	81.0(9)	0.9(9)	<0.1(9)	9.4(9)	7.9(9)	0.76(9)	-2.6(2)	-27.2(11)
H-1[1]	K31	C	95	61	99.0	<0.1	<0.1	0.11	<0.01	0.77	-2.1	nd
F-15	K127	F	92	631[1]	17.4	64.5	18.0	<0.001	<0.01	0.13	-3.0	nd
Eburru												
EF2	K119	F	92	.	78.9	11.7	3.1	1.7	.	4.6	-2.3	nd
EW1	K502	G	.	272	97.4	0.34	<0.1	0.09	1.18	0.99	nd	-23.2
Menengai-Bogoria												
MN1	K260	F	76	.	4.55	78.3	17.2	<0.001	.	0.033	-6.9	nd
Arus	K257	F	95	2561	99.5	0.17	<0.1	0.004	<0.01	0.35	-4.3	-28.1
Ol Kokwe-Korosi												
OK1	K152	F	96	1254	88.8	9.8	0.10	0.79	0.23	0.32	-3.5	-18.3
KR12	K154	F	96	753	42.7	46.6	10.3	<0.001	0.15	0.21	-4.3	nd
KR18	K156	F	96	1178	96.2	1.9	0.30	<0.001	0.03	1.5	-3.9	-24.5
KR19	K157	F	96	1494	97.4	1.0	0.05	<0.001	0.05	1.3	-3.9	-23.4
KR23	K159	F	96	1420	16.3	65.1	18.2	0.40	<0.01	0.015	-6.2	-19.7
KR34	K162	F	92	1580	85.0	11.7	2.8	0.006	0.01	0.44	-4.6	-29.6
Paka												
PK1	K163	F	96	450	83.1	11.3	3.4	<0.001	0.74	1.5	-2.9	-24.9
PK4	K166	F	95	215	91.7	2.1	0.61	4.1	0.19	1.3	-3.4	-27.8
PK7	K168	F	94	684	67.0	30.2	0.61	0.92	0.38	0.85	-2.7	-22.2
Silali												
SL7	K219	F	95	336	97.7	0.34	0.09	0.87·	0.70	0.25	-3.8	-23.0
SL14	K221	F	96	377	98.2	0.29	0.05	0.65	0.60	0.25	-3.7	-24.3
SL15	K222	F	97	142	98.0	0.22	0.06	0.93	0.58	0.24	-3.9	-25.0
SL19	K224	F	96	5273	77.5	16.8	4.4	<0.001	0.24	1.1	-4.6	nd
SL22	K225	F	92	5591	69.4	24.4	5.9	<0.001	0.08	0.17	-3.6	-21.7
Lorusio	K45	S	81	.	83.6	13.3	2.3	0.79	.	0.11	-2.6[3]	-28.3
Emuruangogolak												
EM9	K228	F	95	2272	28.8	57.0	13.4	0.001	0.15	0.64	-4.7	-20.7
EM20	K232	F	96	1545	58.0	32.5	7.9	0.002	1.1	0.51	-4.0	-22.5
Kageinya	K188	S	68	.	<0.1	97.5	1.1	0.003	.	1.41	nd	-31.8
Namarunu												
Elboitong	K236	S	95	.	99.0	0.64	0.37	<0.001	.	0.011	-2.2[3]	-28.3
Barrier												
KK1	K235	F	96	208	17.1	64.8	18.0	0.008	0.02	0.044	-3.3	-26.3
Turkana Islands												
North	K253	F	96	3070	89.0	8.6	1.2	0.053	0.008	1.12	-5.4	-28.4
Central	K255	F	97	857	92.5	0.56	<0.1	1.85	4.2	0.89	-3.8	-30.9
W. of main KRV												
Bala	K53	F	72	.	89.6	9.86	<0.1	0.21	.	0.28	-2.0[3]	-26.8
Kureswa	K256	S	62	.	2.9	95.6	0.6	<0.001	.	0.82	-7.1[3]	-27.5
E. of main KRV												
Carbacid Co.	K237	C	amb	.	98.4	0.35	<0.1	0.001	.	1.24	-2.4	-20.5
Meru/Chogoria	K503	M	amb	.	37.5	nd	nd	<0.001	.	0.006	-3.5	nd
Southern MER												
Abaya #7	E13	S	88	.	17.6	64.2	18.2	0.001	.	0.0042	-3.2	-18.0
Chebicha	E7	F	80	379	0.55	77.4	22.1	<0.001	<0.001	0.0065	-8.7	-29.9
Danshe	E8	F	90	4162	6.3	73.0	20.7	<0.001	0.001	0.032	-7.1	-30.7
Koka	E9	F	94	491	99.8	<0.1	<0.1	0.003	0.013	0.17	-3.5	-28.6
Northern MER												
Shalla #30	E15	S	96	.	14.8	65.3	17.9	<0.001	.	2.0	+0.8	-21.9
LA-3	E1	G	.	425	98.3	<0.1	<0.1	0.16	0.34	1.2	-4.7	-28.5
LA-6	E2	G	.	384	98.7	<0.1	<0.1	0.22	0.89	0.16	-3.9	-27.0
Bobessa	E4	F	.	559	48.7	39.8	11.4	<0.001	0.049	0.14	-4.1	-25.7
Gebiba	E5	F	93	187	99.4	0.22	0.04	0.011	0.053	0.32	-4.1	-25.7
Auto	E6	F	90	5802	3.1	76.0	20.9	<0.001	<0.001	0.017	-7.5	.
Boku	E10	F	73	.	2.3	76.1	21.6	0.002	.	0.016	-10.7	-24.0
Djibouti												
Abbe N	D7	S	.	.	0.45	83.8	15.3	<0.001	.	0.48	.	-29.3
Garrabays	D4	F	.	8.6	0.33	78.1	21.6	<0.001	<0.001	0.0077	-9.8	-31.1
Asal A-3	D1	G	.	510	99.1	0.29	0.04	0.25	0.23	0.16	-3.0	-25.9
Asal (A5)	D2	F	.	454	9.1	70.8	20.1	0.037	0.003	0.0009	-5.7	-32.1
N Ghoubet	D3	F	.	27.2	16.5	65.0	18.4	0.10	0.061	0.023	-3.1	-17.0

Sample Sources: C - dry borehole; F - fumarole; G - geothermal well; M - mofette; S - spring

[1] Data for whole gas analysis or specific measurement from Armannsson (1987).
[2] OF-n and OW-n refer respectively to averages for typical Olkaria fumaroles and geothermal wells; numbers in brackets refer to the number of samples averaged (full data in Darling and Talbot, 1991).
[3] Corrected to total inorganic carbon balance.

174

Table 7.2 Noble gas analyses from selected sites in the southern KRV, including N_2/Ar and ^{40}Ar/^{36}Ar ratios.

Site No.	Locality	Sample Source	Sampling Temp. °C	Ne x 10^{-7}	Ar x 10^{-4}	Kr x 10^{-8}	Xe x 10^{-8}	N_2/Ar	^{40}Ar/^{36}Ar
Dissolved Phase									
K25	Kijabe RVA	B	35	1.64	2.60	5.98	0.86	37.8	294.1
K28	Mayer's Farm	S	28	1.47	2.25	4.97	0.70	39.9	294.1
K35	Kariandusi	S	39	1.43	1.94	4.16	0.58	49.8	295.4
K82	C4178 Naivasha	B	21	2.47	3.38	7.09	0.97	42.4	296.4
K92	Kanyamwi Farm	B	27	1.64	2.60	5.87	0.84	39.3	294.9
K96	P65 Kinangop	B	21	1.67	2.83	6.42	0.91	39.1	296.8
K100	C1404 Ndabibi	B	21	1.47	2.11	4.53	0.62	57.9	297.6
K118	Nakuru No 7	B	28	1.53	2.29	5.03	0.69	40.2	293.7
K124	Soysambu DEL	B	32	0.87	1.05	2.12	0.30	35.2	297.0
Gaseous Phase									
K53	Bala	S	72	3.65	30.9	22.4	3.09	22.5	846.0
K110	Olkaria OW2	G	.	0.15	0.10	0.15	.	43.2	304.4
K119	Eburru EF2	F	92	0.30	0:35	0.75	0.11	23.2	303.4
K123	Olkaria W	F	92	0.21	0.26	0.53	0.10	35.2	261.4
K126	Suswa F-3	F	93	74.9	34.5	43.1	3.64	87.8	293.1
K127	Domes F-15	F	92	61.8	30.9	35.6	3.27	88.0	291.3
K128	Longonot F-23	F	90	28.4	12.0	14.0	1.45	77.8	278.7

Sample sources: B · borehole; F · fumarole; G · geothermal well; S · spring

Gas concentrations in cm^3 (STP)/g water or cm^3/cm^3 total gas as appropriate.

175

Table 7.3   Helium isotope data, ratios with respect to air and carbon dioxide to helium ratios.

Site Name	Site No.	Sample Source	Temp °C	^{3}He x10^{-12}	^{4}He x10^{-6}	He/Ne	R/R$_A$ corr	C/^{3}He x10^9	C/^{4}He x10^3
Dissolved phase									
Kijabe RVA	K26	B	35	0.97	0.54	43	0.9	-	-
Kariandusi	K35	S	39	0.49	0.12	1	3.0	-	-
Kapedo	K48	S	50	38	7.0	1	3.9	-	-
Bogoria	K68	S	96	2.3	0.45	11	3.8	-	-
Kanyamwi Fm	K91	B	27	0.19	0.11	2	1.3	-	-
Ndabibi C1404	K100	B	32	-	-	0.39	0.9	-	-
Nakuru No 7	K118	B	28	-	-	0.22	1.0	-	-
DEL	K124	B	32	13	2.9	32	6.5	-	-
SV3	K185	S	68	7.7	1.2	18	4.6	-	-
Namarunu	K189	S	66	6.5	.65	4	7.1	-	-
Logipi NW	K190	S	61	3.9	.43	22	6.5	-	-
Logipi NE	K238	S	70	6.8	0.76	13	6.4	-	-
Sodere	E16	S	65	87	3.9	41	16.0	-	-
Abbe C	D6	S	75	146	28	0.27	1.8	-	-
Abbe N	D7	S	90	197	18	14	7.8	-	-
Korilli	D5	S	36	0.38	0.05	0.63	5.5	-	-
Gaseous phase									
Lorusio	K45	S	81	120	17	15	5.0	7.0	49
Bala	K53	S	72	5950	2900	72	1.5	0.15	0.3
Olkaria OW-2	K111	G	-	210	27	33	5.7	1.9	15
Olkaria OW-26	K112	G	-	180	23	37	5.8	2.7	21
Olkaria OW-16[1]	K113	G	-	-	-	2	5.8	-	-
Eburru EF-2	K119	F	92	100	12	24	6.3	7.9	66
Olkaria West	K123	F	92	32	4.1	75	5.6	23	180
Suswa F-3	K126	F	93	16	7.3	93	1.6	6.4	14
Domes F-15	K127	F	92	2.1	0.52	92	2.9	83	335
Longonot F-23	K128	F	90	280	30	92	6.7	2.8	26
Ol Kokwe	K152	F	96	21	3.1	35	4.9	42	14
Korosi KR12	K154	F	96	99	18	2	3.9	4.3	24
Korosi KR19	K157	F	96	260	74	7	2.5	3.8	13
Korosi KR23	K159	F	96	65	30	1	1.6	2.5	5.4
Korosi KR34	K162	F	92	200	46	5	3.2	4.3	19
Paka PK1	K163	F	96	350	32	2	7.9	2.4	26
Paka PK4	K166	F	95	290	34	21	6.2	3.2	27
Paka PK7	K168	F	94	420	83	7	3.6	1.6	8.1
Silali SL7	K219	F	95	230	21	30	7.5	4.2	46
Silali SL14	K221	F	96	320	29	31	8.0	3.1	34
Silali SL22	K225	F	92	310	28	35	7.9	2.2	24
Emuruang EM9	K228	F	95	16	2.7	1	4.2	18	107
Emuruang EM20	K232	F	96	130	15	3	6.0	4.5	39
Barrier BR11	K235	F	96	56	12	1	3.3	3.1	14
Arus[1]	K251	F	95	-	-	71	4.5	-	-
Eburru EW-1[1]	K261	G	-	-	-	22	6.7	-	-
Aluto LA-3	E1	G	-	179	11	75	11.5	5.5	90
Aluto LA-6	E2	G	-	693	47	270	10.5	1.4	21
Bobessa	E4	F	-	186	15	0.73	9.1	2.6	32
Gebiba	E7	F	93	-	-	90	6.3	-	-
Koka	E9	F	94	434	24	223	12.9	2.3	42
Abaya #7	E13	S	88	113	4.6	0.30	1.6	1.6	39
Shalla #30	E15	S	96	518	34	2.3	11.0	29	44
Asal A-3	D1	G	-	448	26	38	12.3	2.2	38
Nord Ghoubet	D3	F	-	447	29	0.80	11.0	37	570

[1] Data used by permission of Unocal Geothermal Division

He measurements carried out by E Griesshaber at Cambridge University (for Kenya) and GSF, Munich (for Ethiopia and Djibouti), unless otherwise indicated.

Table 7.4   Composition of light hydrocarbons in gases from geothermal wells in the Eastern Rift.

Site Name	Site No.	T_{res} °C	CH_4 %	C_2H_6	C_3H_8	C_4H_{10} ppmv	C_5H_{12}	C_6	CO_2/CH_4	$\delta^{13}C_{CH4}$	$\delta^{13}C_{CO2}$ ‰
Olkaria OW-2	K110	313	0.67	7.0	<1	-	-	-	127[4]	-	-2.7
Olkaria OW-10	K117	306	2.2	11	0.13	<0.01	-	-	30	-28.1	-
Olkaria OW-11[1]	K601	310	1.1	1.4	0.04	<0.01	<0.01	<0.01	72	-28.4	-
Olkaria OW-12[1]	K602	308	0.46	2.1	0.02	<0.01	<0.01	<0.01	195	-27.0	-
Olkaria OW-19[1]	K603	311	1.7	3.7	0.05	<0.01	<0.01	<0.01	40	-26.4	-
Olkaria OW-21	K604	273	0.46	2.9	0.67	<0.01	<0.01	<0.01	188	-	-
Olkaria OW-22	K112	249	0.43	13	0.60	0.07	<0.01	<0.01	181	-27.3	-
Olkaria OW-23	K114	255	0.26	14	0.66	<0.01	<0.01	<0.01	296	-27.3	-
Olkaria OW-25[1]	K605	264	0.44	3.6	0.06	0.07	<0.01	<0.01	180	-27.3	-
Olkaria OW-26	K111	245	0.18	9.5	<1	-	-	-	492[4]	-	-2.4
Olkaria OW-703[1]	K606	300	0.069	1.9	0.04	<0.01	-	-	1442	-21.1	-
Olkaria OW-710[1]	K607	282	0.12	3.3	0.15	<0.01	<0.01	<0.01	815	-27.7	-
Olkaria OW-711[1]	K608	287	0.18	9.3	0.76	0.12	<0.01	<0.01	543	-29.0	-
Olkaria OW-713[1]	K609	297	0.38	10	0.71	0.32	<0.01	1.5	220	-29.1	-
Olkaria OW-715	K259	289	0.42	13	0.86	0.70	0.51	14.7	216	-18.5	-
Eburru EW-1[1]	K502	329	0.99	2.7	0.08	<0.01	<0.01	<0.01	98	-23.2	-
Langano LA-3	E1	298	1.2	2.3	0.08	0.04	<0.01	10	82	-28.5	-4.7
Langano LA-6	E2	309	0.16	3.5	0.43	0.32	<0.01	18	617	-27.0	-3.9
Langano LA-8[2]	E3	254	0.69	21	25	6.6	1.6	-	142	-22.0	-
Asal A3[3]	D1	264	0.16	7.3	3.0	1.9	1.0	16	619	-25.9	-3.0

T_{res} - Reservoir temperature, average of Na/K and SiO_2 geothermometers of FOURNIER (1989).

[1,2,3] Samples collected by Z W Muna and M K Arusei, B Gizaw, and H Armannsson respectively.
[4] Based on CO_2 data from ARNORSSON et al (1990)

Table 7.5 Composition of light hydrocarbons in gases from predominantly fumarolic sources in the Eastern Rift.

Site Name	Site No.	Sampling Temp °C	CH$_4$ %	C$_2$H$_6$	C$_3$H$_8$	C$_4$H$_{10}$ ppmv	C$_5$H$_{12}$	C$_6$	CO$_2$/CH$_4$	δ^{13}C$_{CH4}$ ‰	δ^{13}C$_{CO2}$
Suswa F-7[1]	K504	94	0.45	0.68	<1	·	·	·	55	·	·
Suswa F-12	K258	94	0.087	0.40	0.1	0.22	<0.1	<0.1	190	-25.0	-3.0
Suswa F-28[1]	K501	92	1.4	3.4	<1	·	·	·	70	·	-3.7
Carbacid CO$_2$[2]	K237	amb	1.2	190	58	24	8.9	3.9	79	-20.5	-2.4
Longonot F-23	K128	90	0.75	1	<1	·	·	·	103	·	-4.0
Mt Marg. F-27[1]	K29	85	0.18	1	<1	·	·	·	529	·	-1.7
Domes F-15	K127	92	0.13	2.5	<1	·	·	·	134	·	-3.0
Akira H-1[1,2]	K31	95	0.77	2.9	<1	·	·	·	129	·	-2.1
Olkaria OF1	K261	93	0.61	18	10	1.7	1.6	54	157	-28.8	-3.4
Olkaria OF4	K262	95	0.15	5.5	<0.1	<0.1	0.4	30	156	-27.2	-5.6
Olkaria OF13	K263	95	0.49	13	6	<0.1	<0.1	<0.1	169	-26.5	-4.0
Olkaria OF14	K264	94	0.38	74	1.1	<0.1	<0.1	<0.1	222	-26.0	-3.2
Olkaria OF15	K265	91	0.24	5.4	<0.1	0.9	0.2	99	287	-26.7	-4.5
Olkaria OF16	K266	96	1.60	5.5	<0.1	7.6	0.2	562	56	-26.7	-5.0
Olkaria OF20	K267	78	0.034	0.06	<0.1	<0.1	<0.1	<0.1	2770	-24.5	-3.6
Olkaria OFW	K123	-	0.37	11	<1	·	·	·	201	·	-2.8
Eburru EF2	K119	92	4.6	5.0	<1	·	·	·	17	·	-2.3
Arus AR1	K257	95	0.35	6.4	1.2	0.4	<0.1	24	284	-28.1	-4.3
Ol Kokwe OK1	K152	96	0.32	20	4	<1	·	·	278	-18.3	-3.5
Korosi KR12	K154	96	0.21	8	3	<1	·	·	203	·	-4.3
Korosi KR18	K156	96	1.5	340	130	43	·	·	64	-24.5	-3.9
Korosi KR19	K157	96	1.3	290	130	26	·	·	75	-23.4	-3.9
Korosi KR23	K158	96	0.015	9	0.8	0.2	<0.1	·	1090	-19.7	-6.2
Korosi KR34	K162	92	0.44	98	16	17	12	21	192	-29.6	-4.6
Paka PK1	K163	96	1.5	1.0	<0.1	<0.1	·	·	55	-24.9	-2.9
Paka PK4	K166	95	1.3	1.0	<0.1	<0.1	·	·	71	-27.8	-3.4
Paka PK7	K168	94	0.85	38	14	6	·	·	79	-22.2	-2.7
Silali SL7	K219	95	0.25	0.7	<0.1	<0.1	·	·	391	-23.0	-3.8
Silali SL11	K220	94	0.48	18	4	<0.1	·	·	108	-24.3	·
Silali SL14	K221	96	0.25	0.6	0.1	<0.1	·	·	393	-24.3	-3.7
Silali SL15	K222	97	0.24	1.0	0.1	<0.1	·	·	408	-25.0	-3.9
Silali SL16	K223	96	0.026	0.3	0.2	<0.1	·	·	1000	-23.5	-4.7
Silali SL19	K224	96	1.1	0.5	<0.1	<0.1	·	·	70	·	-4.6
Silali SL22	K225	92	0.17	0.6	0.1	<0.1	·	·	408	-21.7	-3.6
Emuruang. EM9	K228	95	0.64	20	2.0	<0.1	·	·	45	-20.7	-4.7
Emuruang. EM20	K232	96	0.51	0.1	<0.1	<0.1	·	·	114	-22.5	-4.0
Barrier BR4	K249	94	0.023	0.84	<0.1	<0.1	<0.1	32	301	-24.4	-5.7
Barrier BR5	K248	93	0.014	0.23	<0.1	<0.1	<0.1	12	257	-26.0	-1.8
Barrier BR11	K235	96	0.044	0.1	<0.1	<0.1	·	·	389	-26.3	-3.3
Barrier BR18	K250	94	0.020	6.3	<0.1	<0.1	<0.1	<0.1	441	-25.8	-6.0
Barrier BR29	K251	93	0.064	1.2	0.17	<0.1	<0.1	<0.1	79	-26.6	-4.0
Central Is CI1	K254	97	0.90	45	11	4.9	2.8	140	104	-32.2	-4.3
Central Is CI2	K255	97	0.89	46	9.4	3.7	3.7	134	97	-30.9	-3.8
North Is NI1	K252	96	0.47	29	5.5	0.7	0.7	75	84	-28.2	-5.2
North Is NI2	K253	96	1.1	80	10	1.1	0.7	35	79	-28.4	-5.4
Corb. Chebicha	E7	80	0.0065	0.09	1.9	<0.01	<0.01	<0.01	141	-29.9	-8.7
Corb. Danshe	E8	90	0.032	1.3	0.11	0.05	<0.01	<0.01	197	-30.7	-7.1
Corbetti Koka	E9	94	0.17	140	58	28	10	22	587	-28.6	-3.5
Aluto Bobessa	E4	-	0.14	6.0	0.16	<0.01	<0.01	<0.01	348	-25.7	-4.1
Aluto Gebiba	E5	93	0.32	11	3.3	3.2	1.7	5.5	311	-25.7	-4.1
Aluto Auto	E6	90	0.017	1.8	0.47	<0.01	<0.01	<0.01	182	·	-7.5
Gedemsa Boku	E10	73	0.016	0.11	<0.1	<0.1	<0.1	<0.1	144	-24.0	-10.7
Garrabays	D4	-	0.0077	0.24	0.02	<0.01	<0.01	<0.01	43	-31.1	-9.8
Asal	D2	-	0.0009	0.02	<0.01	<0.01	<0.01	<0.01	10460	-32.1	-5.7
N. Ghoubet	D3	-	0.023	1.6	0.14	0.43	<0.01	<0.01	717	-17.0	-3.1

[1] sample collected by H Armannsson
[2] dry borehole - all other samples from fumaroles

178

Table 7.6 Composition of light hydrocarbons in gases from hot spring sources in the Eastern Rift.

Site Name	Site No.	Sampling Temp °C	CH₄ %	C₂H₆	C₃H₈	C₄H₁₀ ppmv	C₅H₁₂	C₆	CO₂/CH₄	$\delta^{13}C_{CH4}$ ‰	$\delta^{13}C_{TIC}$
Abaya #7	E13	88	0.0042	1.9	0.07	1.2	<0.1	<0.1	4190	-18.0	-3.7
Little Magadi	K3	85	9.1	320	100	<10	<10	-	63	-	-3.3
Bala	K53	72	0.28	5.3	0.17	<0.1	<0.1	-	320	-26.8	-2.0
Kureswa	K260	62	0.82	16	0.8	0.4	<0.1	<0.1	3.5	-27.5	-7.1
Bogoria SE	K256	97	0.33	26	1.4	4.7	13	<0.1	11	-	-1.5
Lorusio	K45	81	0.045	8.5	1.4	0.8	<0.1	3.1	7600	-28.3	-2.6
Kageinya	K188	68	1.41	280	120	33	<0.1	-	-	-31.8	-4.0
Namarunu	K189	66	0.013	1.0	<0.1	<0.1	<0.1	-	954	-	-0.9
Elboitong S	K236	95	0.011	1.1	0.06	<0.01	<0.01	19	9000	-28.3	-2.2
Logipi NW	K190	61	0.14	28.0	<0.1	<0.1	<0.1	-	11	-	-1.2
Logipi NE	K238	70	0.33	4.1	-	8.3	14	<0.1	20	-	-2.0
Shalla #30	E15	96	2.0	8.5	2.5	0.71	<0.1	<0.1	7.4	-21.9	+1.1 [2]
Abbe N	D7	90	0.48	35	10	3.1	0.32	6.0	0.9	-29.3	-17.1 [3]

$\delta^{13}C_{TIC}$ refers to the bulk ^{13}C composition of the CO_2-HCO_3-CO_3 system

[2] value calculated from CRAIG et al (1977)
[3] value calculated from FONTES et al (1980)

7.1.2   Carbon dioxide and methane

Oxidised carbon is represented by CO_2 and the chemically equilibrated forms of HCO_3^- and CO_3^{2-}. When atmospheric contamination (as indicated by the amount of O_2) is low or absent, CO_2 is almost always by far the most abundant fumarolic gas on a steam-free basis, with concentrations often in excess of 90%. In the KRV, the largest dataset, highly consisten values of $\delta^{13}C$-CO_2 were obtained from 32 fumaroles, wells and seeps (Table 7.1), with an average of -3.7‰, a standard deviation of 1.1‰ , and a total range from -1.7 to -7.1‰ . These comparatively consistent results were not produced solely from recently-active centres; examples from Bala (K53, Miocene carbonatite), Kureswa (K256, a travertine-depositing area west of the Rift proper), the Kerita CO_2 well (K237, on the eastern Rift shoulder) and from mofettes at Meru (K503 on the eastern flanks of Mt Kenya some 130 km to the east of the KRV) all fall within a restricted range.

In the MER, if the most air-contaminated fumaroles (E6, 7, 8, 10) are disregarded, a similar average $\delta^{13}C$-CO_2 of -3.9‰ is obtained. The number of sites in Djibouti is too small to calculate an average.

Reduced carbon is principally represented by CH_4 (higher alkanes are treated in 8.3 below). Even in the least air-contaminated fumaroles, CH_4 is rarely present at more than 1% by volume of the gas phase. Results of $\delta^{13}C$-CH_4 analysis are given in Table 7.1. As with CO_2 these are quite consistent for the Kenya Rifts (28 sites, average -25.2‰, standard deviation 3.4‰, range -18.3 to -31.8‰), despite the variety of site types from which samples were collected. The average in the MER is very similar at -26.0‰, with a standard deviation of 3.9‰ and a range from -18 to -30.7‰. On the basis of the number of samples involved, no statistical difference between the KRV and the MER can be discerned. The few data from Djibouti fall within or very close to the range seen in the continental EARS. The more extreme $\delta^{13}C$-CH_4 values in all the rifts tend to have been obtained on low-CH_4 samples, due probably to poorer measurement precisions (Appendix B). Exceptions to this are the samples from Central Island (K254, 255).

7.1.3   Hydrogen and hydrogen sulphide

Hydrogen and H_2S concentrations are generally lower in fumarolic gases of the EARS than is typical of other hydrothermal systems. This is probably mainly due to the considerable depth of geothermal reservoirs in the rather arid areas concerned, which allows abundant scope for
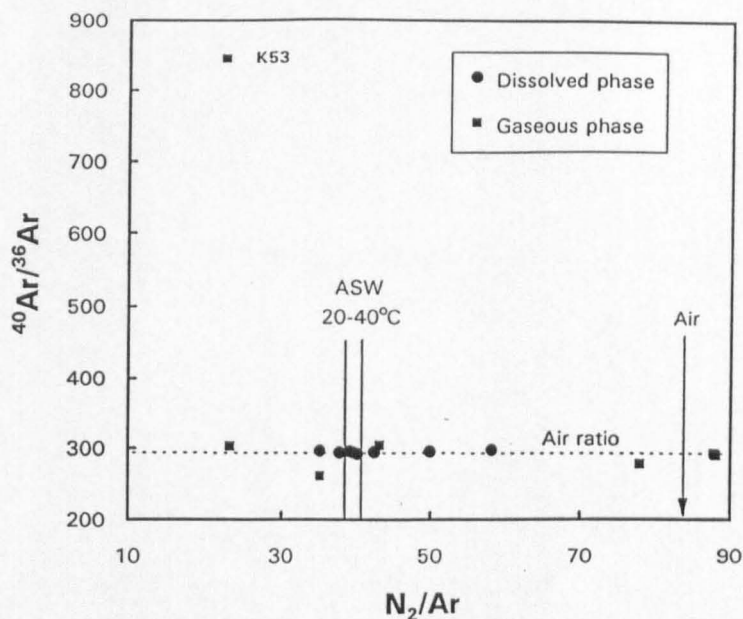
Fig 7.1   Plot of $^{40}Ar/^{36}Ar$ vs N_2/Ar for water and gas samples from representative sites in the Gregory Rift. The $^{40}Ar/^{36}Ar$ for air is shown, together with atmospheric and air-saturated (ASW) values of N_2/Ar.
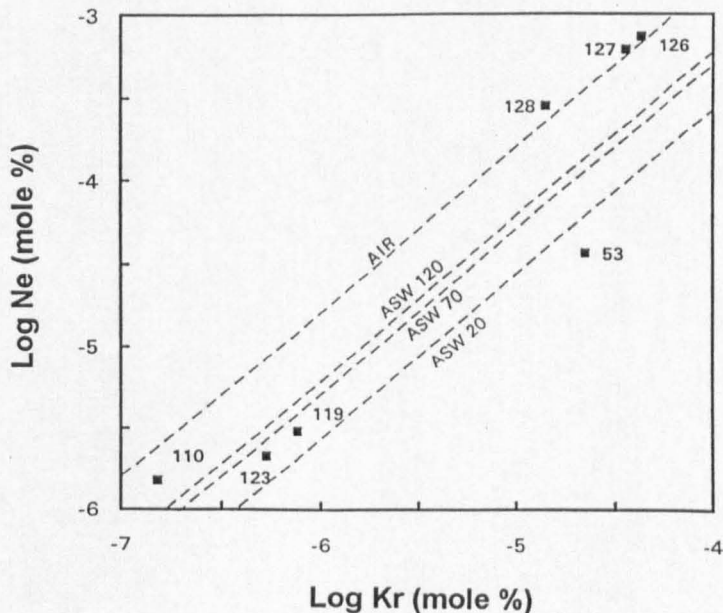
Fig 7.2   Plot of Ne vs Kr for gas phase samples from representative sites in the Gregory Rift (site numbers have K prefixes in text and tables). Also shown are the air ratio line (AIR) and the ASW ratio lines for 20, 70, and 120°C (ASW 20, 70 and 120) based on the data of Wilhelm et al (1977) and Potter and Clynne (1978).

181

these gases to react with wallrock or become oxidised during passage to the surface. This is demonstrated by a comparison of gas analyses from the Olkaria well (OW-n) and fumarole (OF-n) averages, and also a comparison of the less numerous wells and fumaroles at Aluto-Langano (Table 7.1). The fumarole gases are depleted in H_2 and H_2S compared to the deep fluids which are brought rapidly to the surface by the geothermal wells. Gas chromatographic analysis of some of the more sulphur-rich gas samples was undertaken to test for forms other than H_2S such as COS and CS_2. These could not be detected at ppm level in the total gas, implying that there is little or no reaction between the S and carbon phases. The only H_2 isotope analyses available, for Central Island sites K254 and 255 with δ^2H-H_2 values of -490 and -513‰ respectively, are consistent with high temperature equilibrium between H_2 and H_2O (Arnason, 1977).

7.2   Noble Gases

7.2.1   Neon, krypton and xenon

The noble gases Ne, Kr and Xe are normally almost wholly derived from the atmosphere. Table 7.2 gives analyses for waters and gases of the southern KRV. The results, where they indicate that samples have not re-equilibrated with air at or near the point of discharge, may be used to infer various physical processes. In the case of waters, this centres largely on estimation of recharge temperatures. These can be calculated from knowledge of noble gas contents in the sampled groundwaters (Andrews and Lee, 1979). The presence of "excess" air (i.e. entrained air bubbles dissolving as hydrostatic head increases with depth of recharge) can be corrected for by the notional subtraction of small amounts of air from the analysed contents until the best agreement of temperatures between the remaining gases is obtained. The estimated recharge temperature is, however, dependent on altitude of recharge because of changes in atmospheric pressure with elevation (recharge under different climatic conditions can be ruled out on the basis of the radioisotope evidence in Chapter 5). The maximum relief above the rift floor in the Gregory Rift is some 2000 m, and therefore significant pressure differences are possible. The altitude of recharge of the individual springs and boreholes sampled may in principle be deduced by comparison of the derived recharge temperature with the mean annual temperature for the assumed altitude of recharge. Table 7.7 gives the results of computations for various altitudes of recharge until, for suitable individual sites, the estimated recharge temperature agrees with the mean annual air temperature.

The results show that in about half the cases no sensible agreement between temperatures can

Table 7.7 **Results of using noble gas concentrations to infer recharge altitude by comparison of expected and modelled recharge temperatures.**

	DISCHARGE				RECHARGE			
Site No.	Locality	Sample Source	Sampling Temp °C	Sampling Altitude masl	Altitude masl	Anticipated Temp °C	Modelled Temp °C	Inference
K25	Kijabe RVA	B	35	2500	4000 2000 1750	5 17 19	10.0±0.3 17.6±1.0 18.5±1.1	Recharge probably local with some gas loss
K28	Mayer's Farm	S	28	2100	4000 3000 2000 1500	5 10 17 21	16.5±0.4 20.2±0.7 24.4±1.1 27.9±2.2	Re-equilibration with air near discharge
K35	Kariandusi	S	39	2300	2500 1500 1000	13 21 24	30.2±1.7 34.9±2.2 39.1±3.4	Re-equilibration with air near discharge
K82	C4178 Naivasha	B	21	1900	3500 3000	7 10	12.3±0.3 10.0±0.8	Recharge at around 3000 m
K92	Kanyamwi Farm	B	27	2300	3000 2500 2000 1750	10 13 17 19	14.3±0.3 16.2±0.6 18.1±0.8 19.2±0.9	Recharge probably local with some gas loss
K96	P65 Kinangop	B	21	2600	4000 3000 2750	5 10 11.5	7.6±0.6 11.0±0.3 12.0±0.3	Recharge in the range 2750-3000 m
K100	C1404 Ndabibi	B	21	2100	2000 1500	17 21	28.7±1.1 31.2±1.3	Re-equilibration with air near discharge
K118	Nakuru No. 7	B	28	2000	3000 1000	10 24	20.3±0.4 30.2±2.1	Re-equilibration with air near discharge
K124	Soysambu DEL	B	32	1900	cannot be modelled			Dilution of noble gas concentrations by deep gases

183

be reached, and it is inferred that re-equilibration with air must have taken place at some point. Sometimes, as at K25, the indicated altitude is lower than the site itself and suggests partial loss of dissolved gas. Only for K82 is a large difference in altitude indicated. Site K124 has significantly smaller quantities of noble gases in solution (except He) than the other sites; outflow from the Eburru geothermal field probably affects this area (Arusei, 1992) and atmospherically-derived gases are likely to have been diluted by high concentrations of CO_2 and He.

Information about free gases is obtained from a log plot of Ne vs Kr (Fig 7.2). Some fumaroles (K126 and 127) show ratios close to that of air, suggesting air entrapment or contamination which is confirmed by the analyses in Table 7.1 (the position of K128 on the plot is more problematical because of much lower air contamination as indicated in Table 7.1). Noble gases in these fumaroles can therefore reveal little about conditions at depth. In the case of fumaroles K119 and K123 equilibrium with water at a somewhat higher temperature than that of average recharge (~25°C) suggests that perched aquifers may be causing gases to re-equilibrate at lower than geothermal reservoir temperatures. Higher equilibration temperatures are marked by a tendency towards air-like ratios (though not quantities) for the noble gases (e.g. Potter and Clynne, 1978). This explains the position of the geothermal well OW2 (K110) on the plot. Conversely, the carbonatite complex spring (K53) at Bala in the Nyanza rift has a composition suggesting equilibrium with recharge at cooler than normal temperatures, but this is inconsistent with the O and H stable isotope ratios (5.1.3 above). Possibly noble gas ratios have been perturbed in this water by the same factors which have led to the exceptionally high He content (Table 7.3).

It is assumed that as for radiocarbon and tritium (5.3 above), the results from the Gregory Rift will be typical of the MER.

7.2.2   Helium

Amounts of He in the gases of the EARS are almost uniformly low (Table 7.3). There is no significant correlation between concentration of He and other geothermal parameters, as has also been noted elsewhere (Griesshaber et al, 1992; Poreda et al, 1992). Only when $^3He/^4He$ isotope ratios are considered does a pattern emerge. These are normally expressed as R/R_A, i.e. the ratio in the sample divided by the ratio in air (see Appendix B). The highest $^3He/^4He$ values, with R/R_A from approximately 5.5 to 8 in the KRV, and up to 16 in the MER, are generally found in close association with the late-Quaternary volcanic centres of the

Eastern Rift.

For gaseous sources it may be noted that for the KRV a plot of CO_2 percentage vs neon-corrected $^3He/^4He$ as R/R_A indicates that highest ratios are only obtained when CO_2 exceeds 50% of the gas phase (Fig 7.3). Below this figure the presence of air-derived gases appears to perturb the $^3He/^4He$ ratio to the extent that corrections based on the Ne content cannot alone restore the "true" $^3He/^4He$ value. While this is difficult to prove conclusively, samples with <50% CO_2 have been largely excluded from further discussion of the helium isotope data. In the MER and Afar, the very high $^3He/^4He$ background makes this air contamination less apparent.

Examination of the data in Table 7.3 shows that where there is more than one helium isotope analysis for an individual volcanic centre, there is usually fair agreement between the results. Whether the results are from Craig et al (1977), Marty et al (1993), Unocal Corporation (unpublished) or the present study, in most cases where the same location has been sampled similar $^3He/^4He$ results have been obtained (the relevant data are assembled in Table 7.8). For example in the Gregory Rift, four very similar $^3He/^4He$ values of 5.7 ± 0.1 reported as R/R_A have been obtained from the Olkaria geothermal area, while in the South Turkana Rift the Silali caldera provided three sites with R/R_A values averaging 7.8 ± 0.3. The Olkaria, Eburru, Langano and Asal $^3He/^4He$ data, apart from demonstrating consistency within individual volcanic centres, also show that similar He isotope data can be obtained from surface fumarolic and deep (~2000 m) geothermal well sources, thereby giving confidence that under suitable conditions the results obtained from fumaroles elsewhere in the Eastern Rift are genuinely representative of deep fluids (though it the agreement is rather less good between the wells and fumaroles in the MER and in Afar than it is in the KRV).

Table 7.3 shows that ratios of $CO_2/^3He$ (effectively total-$C/^3He$) for many sites are close to the MORB average of 2 x 10^9 (Marty, 1992). The only site with a significantly lower ratio is Bala in the Nyanza Rift, where He concentrations are extremely high. A few sites have significantly higher values, for reasons to be discussed below. In general, however, neither $C/^3He$ nor $C/^4He$ ratios reveal any differences between the upper and lower mantle sources which are assumed to be contributing to gases in different parts of the EARS.
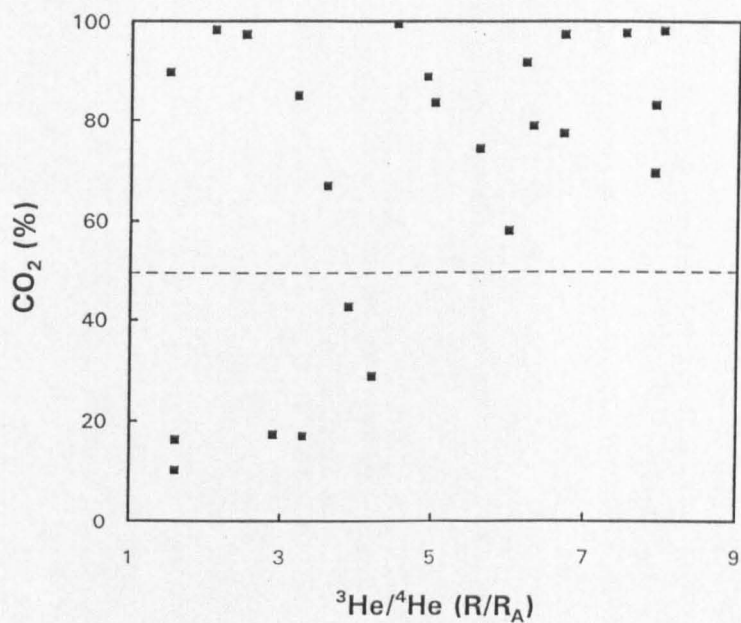
Fig 7.3   Plot of CO_2 percentage vs He isotope ratio for gaseous sources in the KRV (cutoff line indicates that samples with $<50\%$ CO_2 may not be giving a representative $^3He/^4He$ value).

Table 7.8   Helium isotope ratios measured on the same or adjacent sites, to demonstrate consistency within areas and between laboratories.

| Site Name | Site No | Sample type | This research | | | Craig et al (1977) SIO |
			U Camb	Unocal	GSF	
Olkaria						
OF-W	K123	Fumarole	5.6	-	-	-
OW2	K111	Well	5.7	-	-	-
OW16	K113	Well	-	5.8	-	-
OW26	K112	Well	5.8	-	-	-
Eburru						
EF-2	K119	Fumarole	6.3	-	-	-
EW 1	K261	Well	-	6.7	-	-
Barrier						
Logipi NW	K190	Spring	6.5	-	-	-
Logipi NE	K238	Spring	-	-	6.4	-
Corbetti						
Koka	E9	Fumarole	-	-	12.9	-
Doredimtu	CRA69	Fumarole	-	-	-	12.2
Shalla						
Spring #30	E15/CRA30	Spring	-	-	11.0	10.0
Aluto						
Gebiba	E5	Fumarole	-	-	6.3	-
Aluto #18	CRA32	Fumarole	-	-	-	7.4
Bobessa	E4	Fumarole	-	-	9.1	-
LA-3	E1	Well	-	-	11.5	-
LA-6	E2	Well	-	-	10.5	-
Asal						
N Ghoubet	D3	Fumarole	-	-	11.0	-
A-3	D1	Well	-	-	12.3	-

Laboratories: U Camb - University of Cambridge; Unocal - at McMaster University; GSF − Gesellschaft fur Strahlen, Munich; SIO - Scripps Institute of Oceanography.

7.3   Higher Hydrocarbons

When plotted as ratios against CH_4 (Fig 7.4), the hydrocarbons have a distribution largely similar to those from hydrothermal systems elsewhere in the world (Darling, in rev.). There appears from Tables 7.4 and 7.5 to be no predictable relationship with the amount of CO_2, which is normally the dominant gas.

Isomeric ratios for C_4 and C_5 and ratios of benzene to hexane (Table 7.9) are on the whole typical of those found worldwide (Darling, in rev.). Major departures may be due as much to the difficulties of measurement at very low concentrations as to real variations.

The composition of hydrocarbon gases from geothermal wells in Kenya, Ethiopia and Djibouti is shown in Fig 7.4. The results show that C_1/C_2 ratios are all in excess of 100. The generally low concentrations of hydrocarbons in these high-temperature reservoirs made butane, pentane and C_6 unmeasurable in many cases. However, where C_6 could be measured, concentrations similar to ethane were obtained. These gases therefore showed characteristics of other hydrothermal hydrocarbon gases elsewhere (high C_1/C_2, high relative concentrations of C_6) considered in Darling (in rev.). Carbon isotope ratios in CH_4 (Table 7.4) are also similar to those found in other geothermal wells.

Fumarolic gases show similar characteristics (Fig 7.4), though C_1/C_2 ratios cover a wider range, particularly in the 10-100 category. This wider variation probably results from the greater range of geothermal temperatures sampled via fumaroles compared to the restricted, usually 200-300°C range of producing geothermal wells. High-enthalpy springs are included in this category.

The general paucity of hydrothermal hydrocarbon gases in the Eastern Rift together with their relatively enriched $\delta^{13}C$-CH_4 values accords with the view that there is little sedimentation. There is however some limited evidence from North and Central Islands in Lake Turkana (K252-255) that the sediments there may be contributing hydrocarbons. The islands are strong hydrothermal centres, or more accurately centres which are exposed much nearer to hydrological base level than most of the others. The $\delta^{13}C$-CH_4 values from Central Island are particularly depleted in comparison to the strongest centres (Paka, Silali) of the northern Kenya Rift to the south (Table 7.5). However, it is not clear whether this difference is attributable to the presence of lake sediments, or in some way related to variation in reservoir-surface distance between the island and valley centres, since CH_4 molar concentrations comparable with those of the islands were measured in some of the Paka and Silali fumaroles.
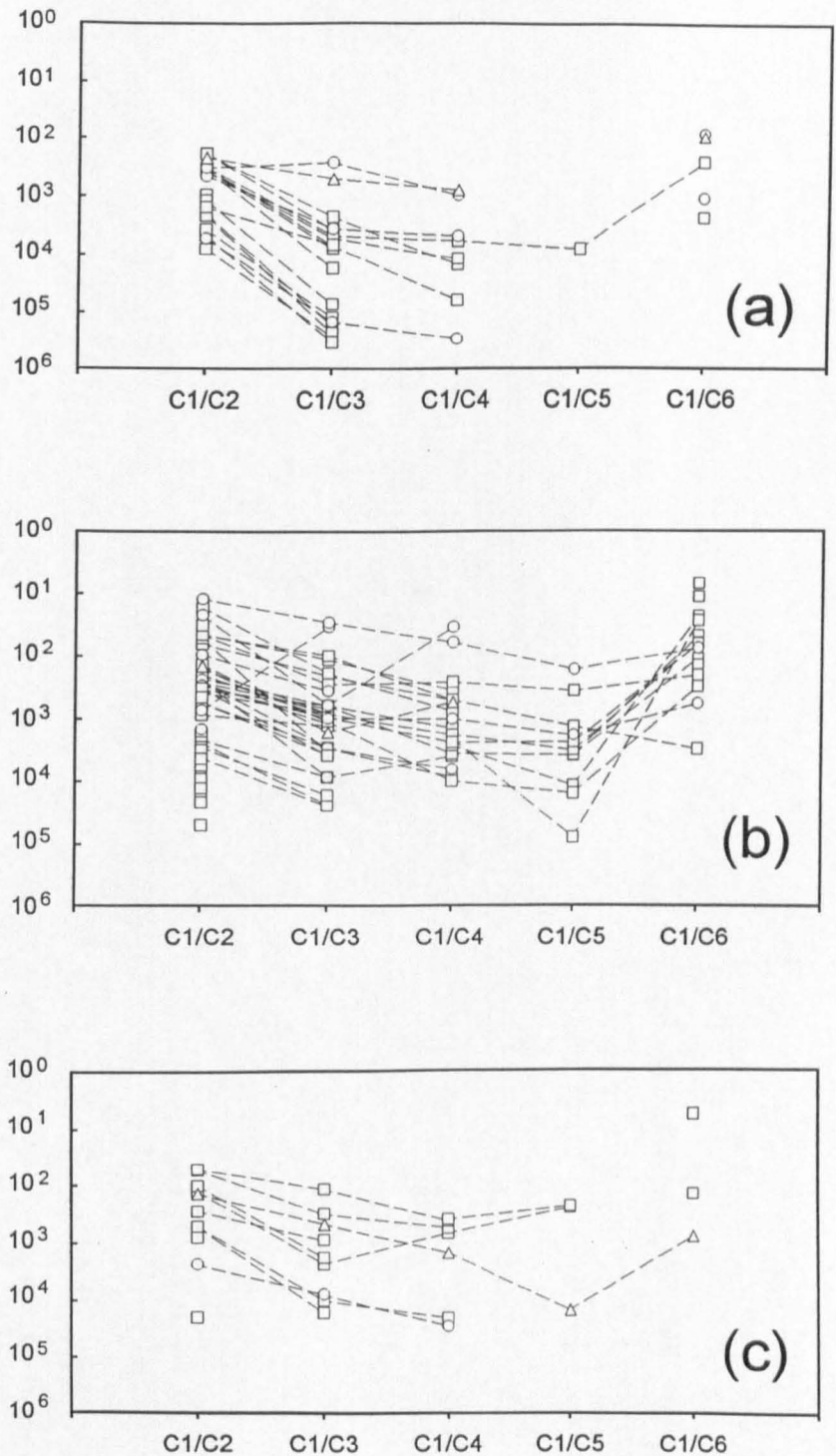
Fig 7.4   Plots to characterise the hydrocarbon gas contents of samples as molar ratios relative to methane: i.e. ethane (C_1/C_2), propane (C_1/C_3), butane (C_1/C_4), pentane (C_1/C_5) and undifferentiated C_6 (C_1/C_6). (a) geothermal wells, (b) fumaroles, (c) springs. □ - Kenya, ○ - Ethiopia, △ - Djibouti

189

Table 7.9   Isomeric ratios for butane and pentane and ratios of benzene to hexane for hydrothermal gases from various sources in the Eastern Rift. The signs ' > ' and ' < ' denote cases where hexane and benzene respectively are below detection limit.

Site Name	Site No.	nC_4/iC_4	nC_5/iC_5	ben/hex
FUMAROLES				
Suswa F-12	K258	-	-	<0.003
Carbacid Co.	K237	2.0	0.85	0.50
Olkaria OF1	K261	1.5	-	0.32
Olkaria OF4	K262	-	-	>300
Olkaria OF15	K265	10	3.2	>990
Olkaria OF16	K266	-	-	>5600
Arus AR1	K257	13	6.3	2.1
Korosi KR18	K156	2.6	-	-
Korosi KR19	K157	2.5	-	-
Korosi KR23	K158	1.0	-	-
Korosi KR34	K162	3.3	2.3	1.5
Paka PK7	K168	1.1	-	-
Barrier KK2	K248	-	-	<0.009
Barrier KK3	K249	-	-	<0.003
Central Is CI1	K254	4.7	3.1	4.6
Central Is CI2	K255	4.5	2.1	3.3
North Is NI2	K253	3.7	2.0	3.2
Corbetti Koka	E9	2.6	10	0.46
Aluto Gebiba	E5	1.3	24	5.4
Nord Ghoubet	D3	1.8	-	-
GEOTHERMAL WELLS				
Olkaria OW-713	K608	-	-	>15
Olkaria OW-715	K259	-	2.0	>7500
Langano LA-3	E1	3.0	-	1.8
Langano LA-6	E2	-	-	15
Langano LA-8	E3	0.78	0.88	-
Asal A3	D1	0.86	1.5	19
SPRINGS				
Bogoria SE	K260	-	0.36	-
Lorusio	K45	2.9	-	>31
Kageinya	K188	0.57	-	-
Elboitong S	K236	-	-	0.19
Abaya #7	E13	1.0	-	-
Shalla #30	E15	2.2	-	-
Abbe N	D7	0.55	1.0	>60
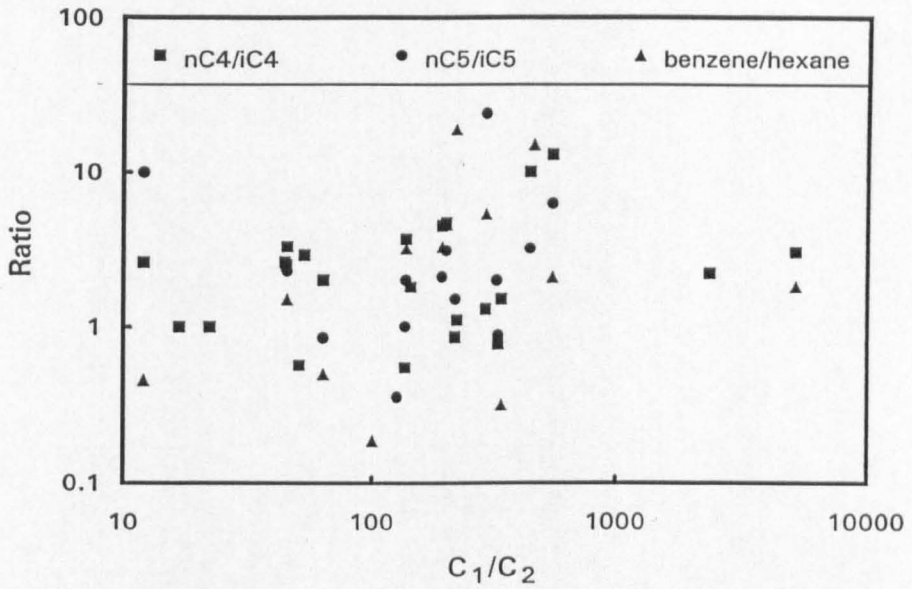
Fig 7.5   Ratios of nC_4/iC_4, nC_5/iC_5 and benzene/hexane in hydrothermal hydrocarbons of the Eastern Rift (all sample types), showing a tendency for ratios to increase with rise in methane/ethane (C_1/C_2) ratio.

It has been noted that hydrothermal gases tend to have higher normal/iso ratios for butane and pentane than sedimentary natural gases, and also that C_1/C_2 tended to increase with system temperature (Darling, in rev.). In Fig 7.5, isomeric data from geothermal wells, fumaroles and springs in the Eastern Rift are plotted against C_1/C_2. ($<$ and $>$ values result from benzene and hexane respectively being below detection, and are not plotted.) Rather general tendencies are shown towards increases in normal/iso ratio for butane and pentane together with an increase in benzene/hexane, as C_1/C_2 rises.

7.4   Origins of Gases

The gaseous emanations of the Eastern Rift must be derived from three source types: the atmosphere, the crust and the mantle. For the purposes of considering their origin it is convenient to divide the gases into these subgroups, which are described below.

7.4.1   Gases derived from the atmosphere

The amount of original N_2 in fumarolic and borehole gases is almost uniformly low, once the effects of any atmospheric contamination are discounted (Table 7.1). In the absence of any $^{15}N/^{14}N$ data, it is assumed that all N_2 has been ultimately derived from atmospheric sources (although a "deep" component with a $\delta^{15}N$ of -10 to -15‰ was assumed for the Oldoinyo Lengai volcano in the northern Tanzanian Rift by Javoy et al, 1989). The evidence of $^{40}Ar/^{36}Ar$ makes it likely that in virtually all cases, argon too has an ultimately atmospheric source. Although the $^{40}Ar/^{36}Ar$ data reported here are all from fluids in the KRV south of the equator, very similar results were obtained from trapped Ar during the dating of volcanic rocks from Silali. These ratios ranged from 275-315 (Smith et al, 1995), and tend to confirm that there is very little radiogenic gas production in the main KRV. Similarly in Djibouti, Marty et al (1993) measured $^{40}Ar/^{36}Ar$ in rocks and found generally air-like values, even when there was a high $^4He/^3He$ ratio.

It is also assumed that Ne, Kr and Xe are almost wholly derived from atmospheric sources and therefore that their concentrations may (when uncontaminated) permit tracing of hydrological processes in the subsurface. He isotope results, on the other hand, suggest that only a proportion of helium is atmospherically-derived.

7.4.2   Gases derived from the crust

While it has been demonstrated that most Ar is atmospheric in origin, the sample at Bala (K53) in the Nyanza rift contains crustally produced ^{40}Ar. A possible interpretation of this is that the thermal groundwater at Bala is in residence for significantly longer than similar groundwaters in the main KRV, but differences in mineralogy between the two areas may also contribute. The igneous rocks of the main KRV are predominantly intermediate-peralkaline in type (comendites, trachytes and phonolites) while Bala is situated on the site of the Homa Mountain carbonatite complex.   Carbonatites commonly contain higher concentrations of radiogenic elements than intermediate rocks (Mariano, 1989). However, some volcanic rocks in the main KRV have higher concentrations of radioelements than others, notably in the southern Rift at Olkaria (Clarke et al, 1990), without appearing to perturb the atmospheric $^{40}Ar/^{36}Ar$ signature in gases and water. The high $^{40}Ar/^{36}Ar$ ratio at Bala may therefore be related to the dominance of mineral alteration over mineral diffusion as a release mechanism for ^{40}Ar (Andrews, 1992) rather than high radioactivity; carbonate minerals would be more susceptible to alteration than the silicates of the main KRV.

Despite the high concentration of He at Bala, the He isotope ratio suggests a balance between mantle and crustal sources.   This could be the result of mantle He trapped during the emplacement of the carbonatite being supplemented before release by in-bred ^{4}He.

However, some doubt about the source of Ar and He at Bala is raised by the results of measurements on the Maji Moto Springs of Tanzania, which lie about 150 km to the south of the Homa area and 110 km east of Lake Victoria. These springs are probably not connected with carbonatitic volcanism, but are found near the edge of a metagabbro associated with acid pseudoporphyries. James (1967) noted that the springs had an extremely high He content (up to 17.9% of the gas phase), and a $^{40}Ar/^{36}Ar$ ratio of approximately 800, little different from the ratio of 846 at Bala.   However, CO_2 did not dominate the gas phase at Maji Moto, amounting to only some 0.2%. This suggests for Bala that while the source of CO_2 is probably the carbonatite, the high concentration of He may be a result of leakage from the Precambrian rocks of the area. A mass-balance approach to investigating this is however not possible due to a lack of $^{3}He/^{4}He$ data for the Tanzanian springs.

The high flux of CO_2 from the EARS and its environs cannot be derived predominantly from atmospheric or soil zone sources, and this is borne out by the generally consistent $\delta^{13}C$-CO_2 values (Table 7.1). The average value of -3.6‰ is unrepresentative of atmospheric ($\sim$-7‰)

or soil zone ($\sim$ -16 to -26‰) sources, though a few air-contaminated fumaroles such as K159, 260, E6-8, 10, D2, 4 have more depleted values which may indicate the influence of atmospheric CO_2 or bacterially produced CO_2 from the soil zone.

It is also unlikely that the CO_2 from most sites is crustally derived. Mechanisms such as decarbonation of marine limestones have been postulated as sources of CO_2 with near-zero $\delta^{13}C$ values (e.g. in Truesdell and Hulston, 1980). While no such limestones exist in the continental rift, there are carbonate evaporites in places, and carbonatites are known from the wider region. Nevertheless, the sheer amount of CO_2 outgassing suggests that oxidised carbon must be predominately derived from a mantle reservoir. This is supported by most of the $C/^3He$ ratios in Table 7.3.

However, there are a few sites in the KRV where $C/^3He$ is significantly higher than MORB-like values. This is illustrated by Fig 7.6a, which shows a plot of helium isotope ratios versus $C/^3He$ values. Points representing fumaroles at Olkaria (K123) and Ol Kokwe Island (K152), and the Kerita CO_2 well (K237) lie on what appears to be a single trend away from the MORB zone. Fig 7.6(b) shows this to be a partial coincidence; while in each case there are indications of the influence of crustal He, the CO_2 well is clearly differentiated from the fumarole sites by its $\delta^{13}C-CO_2$ value. The ^{13}C data suggest that there is a minor crustal contribution of organically derived "light" CO_2 at Olkaria and Ol Kokwe. This is not shown by the deep geothermal wells at Olkaria. Therefore a comparatively near-surface addition is indicated in that particular case. The Carbacid Company well at Kerita, however, appears to derive its "extra" CO_2 from an inorganic crustal "heavy" source. The well is situated on the rift flanks, almost adjacent to the highest elevation of the rift floor, where carbonate evaporite source rocks are unlikely to have formed. Possibly the CO_2 is derived from decomposition of carbonatites. Though none are exposed in the area, Miocene carbonatites are well developed to the west and south of the region, and may possibly be present at depth in parts of the KRV. The data under consideration here suggest that if present they are very localised.

Unlike most oxidised carbon, reduced carbon probably does have a predominantly crustal source in the Eastern Rift. A lack of detectable alkene compounds is an indication that methane is unlikely to have been formed by abiogenic synthesis (Gunter and Musgrave, 1971). While the presence of H_2 in most hydrothermal systems might be thought to rule out the survival of such unsaturated hydrocarbons, they have been detected in certain geothermal fields elsewhere, e.g. by Giggenbach and Glover (1992) and Capaccioni et al (1993), albeit at low concentrations. On the other hand, the presence of sometimes relatively abundant C_{2+}

194
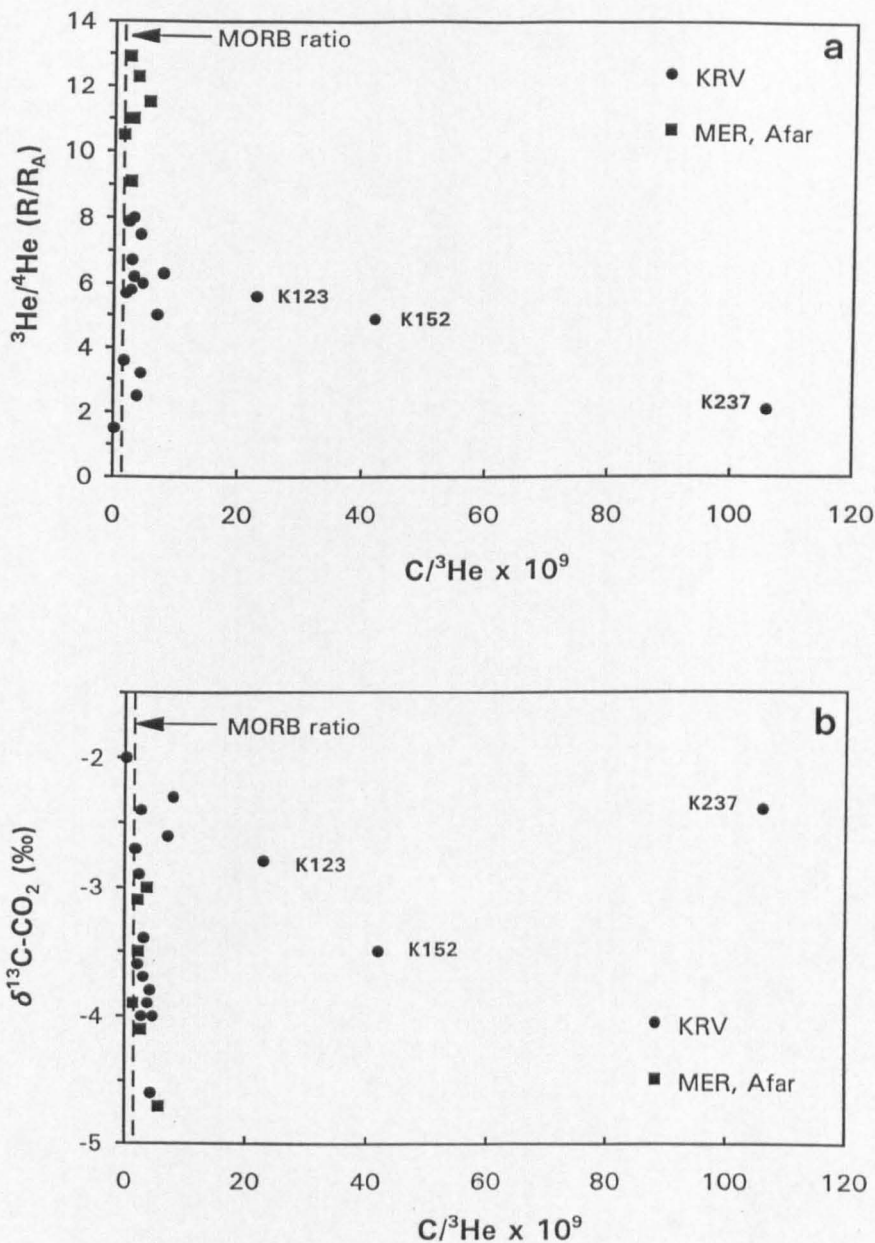
Fig 7.6   (a) Plot of $^3He/^4He$ vs $C/^3He$ for gaseous sources in the Eastern Rift (KRV
          samples < 50% CO_2 excluded). Most samples plot around the MORB ratio
          of 2×10^9, but a few KRV sites have values suggesting a crustal
          contribution of CO_2 (site numbers for these are shown). (b) Plot of $\delta^{13}C$-
          CO_2 vs $C/^3He$. One outlying site appears to receive a contribution from a
          different crustal source of CO_2 from the others.

compounds probably rules out production by bacterial methanogenesis, which tends to produce CH_4 and very little else. A thermogenic (thermocatalytic) decomposition of organic matter seems the most likely source of hydrocarbon production.

Such an origin would tend to be confirmed by the $\delta^{13}C$-CH_4 results (Table 7.1). The average of -25.6‰ is typical of carbon in terrestrial and lacustrine plant matter (e.g. Deines, 1980) and also of geothermal methane in many other areas. In geothermal fields hosted at least partly in sedimentary rocks, suitable organic precursors have often been identified (for example, coal at Cerro Prieto, Mexico; Des Marais et al, 1988). The Eastern Rift does not possess sedimentary sequences of great thickness. However, lacustrine deposits may provide a source of suitable organic compounds. Either these are invaded episodically in places by hot fluids, or dissolved organic compounds may be drawn into hydrothermal plumes. In each case geothermal heat will cause degradation of the organic compounds into hydrocarbon gases. The spread of $\delta^{13}C$-CH_4 values may reflect the degree of thermal maturity reached locally, or possibly an approach to isotopic equilibrium with CO_2, though calculated $\Delta^{13}C$ temperatures are nearly always improbably high for the hydrothermal systems concerned. It does not appear to be due to inputs of abiogenic mantle CH_4 (see next section).

A correlation between log (C_1/C_{2+}) and temperature has been observed for the Eastern Rift (Chapter 8), and it is concluded that when organic compounds are drawn into hydrothermal plumes, progressive degradation to CH_4 takes place with rising temperature. This suggests that hydrocarbon generation is taking place at shallow levels in the crust where suitable conditions prevail. That the temperature need not be high is confirmed not only by petroleum research literature (e.g. Simoneit, 1990) but also by the results from relatively low-temperature spring systems such as Bala, Kureswa, Shalla and Abbe (K53, 256, E15, D7), with solute geothermometer temperatures of <100°C, and the Kerita CO_2 well on the rift flank (K237). While long heating times would be required at such temperatures, there are indications that KRV hydrothermal systems are in general long-lived. There is for example no evidence for a significant ^{18}O-shift in the deep thermal waters at Olkaria (5.1.2.2 above), which suggests that a large amount of water has already passed through the system. Also, the work of Sturchio et al (1993) on the dating of hydrothermal sinters in the northern KRV (5.1.4.3 above) testifies to the longevity of hydrothermal activity.

During the thermal cracking of organic matter H_2S may be produced, especially in areas with carbonate evaporite sequences (Tissot and Welte, 1984) such as are found in parts of the KRV. While the H_2S in volcanic rock-hosted hydrothermal systems seems likely to be largely mantle-

derived (indicated by the SO_2 commonly emitted from active volcanoes), a small crustal contribution might therefore be possible in the KRV (though as mentioned earlier, no COS or CS_2 was detected).

Hydrogen is at low or undetectable concentrations except in geothermal wells. Probably production takes place in the upper part of the crust by dissociation of water buffered by minerals such as chlorite or epidote (Giggenbach, 1980). It is also quite possible that some H_2 is produced by redox reactions between water and the steel lining of the wells. As stated earlier, stable isotope analyses indicate high temperature equilibrium between H_2 and water, and therefore cannot be used to diagnose ultimate origin.

7.4.3 Gases derived from the mantle

Notwithstanding the few exceptions, there is only one significant source of CO_2, which must be mantle-derived (Fig 7.6). The occurrence of carbonatite at Bala and south of the KRV at Oldoinyo Lengai demonstrates that CO_2-rich fluids have been ascending from the upper mantle in the region since at least Miocene times. A more negative average with $\delta^{13}C$-CO_2 of -5 to $-8‰$ is generally associated with such a source, but fractionations between magma and exsolved gas of 1-2‰ for carbonate (the main dissolved species in melts; Ohmoto and Rye, 1979) and up to 4‰ for graphite, put the Eastern Rift $\delta^{13}C$ values well within range of outgassing from MORB-type magmas. A minor problem associated with the assumption that the observed $\delta^{13}C$-CO_2 values are the result of isotopic fractionation of mantle CO_2 is that unless fresh magma were entering volcanic systems in a fairly continuous manner, a decrease in $\delta^{13}C$-CO_2 would be noted with time (Friedman et al, 1987). It is highly unlikely that all Eastern Rift volcanic centres would be at the same stage in such a cycle and therefore the similarity in $\delta^{13}C$-CO_2 values may not arise solely in this way. However, to the south of the KRV, the active Oldoinyo Lengai volcano gave average $\delta^{13}C$-CO_2 values of -2.6 ‰ and $^3He/^4He$ values of 7.6 R/R_A, similar to the fumaroles of the northern KRV (Javoy et al, 1989). The implication of this is that significant differences in the CO_2 fractionation stage between centres do not occur, or are masked by other processes over the timescales involved (i.e. late-Quaternary to present day).

Although a predominantly crustal origin is indicated for reduced carbon, inputs from mantle sources cannot wholly be discounted on isotope evidence alone. While the $\delta^{13}C$ range of supposed abiogenic mantle CH_4 is not very well constrained, it is believed to be of the order of -15 to -18 ‰ (Welhan and Craig, 1983) and would thus not be easily distinguishable from

thermogenic CH_4. However, a plot of $\delta^{13}C$-CH_4 versus $^3He/^4He$ as R/R_A (Fig 7.7) shows no well-defined trend that might indicate mixing between crustal and mantle CH_4 reservoirs, in either of the helium isotope zones (see below).

The sulphur in H_2S, an important constituent of geothermal well gases but not normally of surface manifestations as explained above, is assumed here in the absence of S isotope data to be largely derived from magmatic sources in the upper mantle (though see earlier remarks about possible crustal production from evaporitic sources). A relatively low concentration of H_2S was reported even from Oldoinyo Lengai by Javoy et al (1989), suggesting that the KRV and perhaps the Eastern Rift in general is a low-S province.

The $^3He/^4He$ results from the KRV are similar to those obtained from MORB (Mid-Ocean Ridge Basalt) sources. This indicates an important upper mantle contribution to the He content of fumarolic gases in Kenya. By contrast, the results from Ethiopia and Afar are indicative of a lower mantle source, possessing a typical "hotspot" signature (Lupton, 1983). Taken in conjunction with generally lower R/R_A values from the few sites on or towards the rift flanks (usually springs rather than gaseous sources), this suggests that magmatic melts rather than deep normal or listric rift boundary faults are the most important conduit by which mantle He reaches the surface even in an area with relatively thin crust. Similar observations were made in connection with the continental rifting in western Europe (Griesshaber et al, 1992). However, as much or even more mantle He may be released via major boundary faults, but is more difficult to identify because of dilution effects.

There is no correlation between He isotopes and carbon species. However, there is a relationship between $^3He/^4He$ and the non-isotopic parameter log ($CH_4/\Sigma C_{2-4}$) for KRV fumarole and borehole gases from Longonot to Silali, with a correlation coefficient of $r^2 = 0.75$ (Fig 7.8). The reason for this relationship is not clear. A mixing series based on crustal thermogenic CH_4 with a relatively high C_{2+} content with a "pure" abiogenic mantle methane could be invoked to explain the relationship, but would tend to result in a linear rather than logarithmic correlation (i.e. a curve on Fig 7.8). It would also receive no confirmation from the $\delta^{13}C$-CH_4 results. A relationship between geothermal reservoir temperatures and log CH_4/C_{2+} has already been mentioned, so the correlation may simply arise because $^3He/^4He$ is a proxy for temperature. Crustally produced ^4He can be ruled out as a cause of variation on the evidence of the $^{40}Ar/^{36}Ar$ data considered above. It is likely, after all, that sampling points overlying the hottest parts of hydrothermal plumes will tend to have the highest mantle He contents and therefore probably the highest $^3He/^4He$ ratios. This agrees with the link between
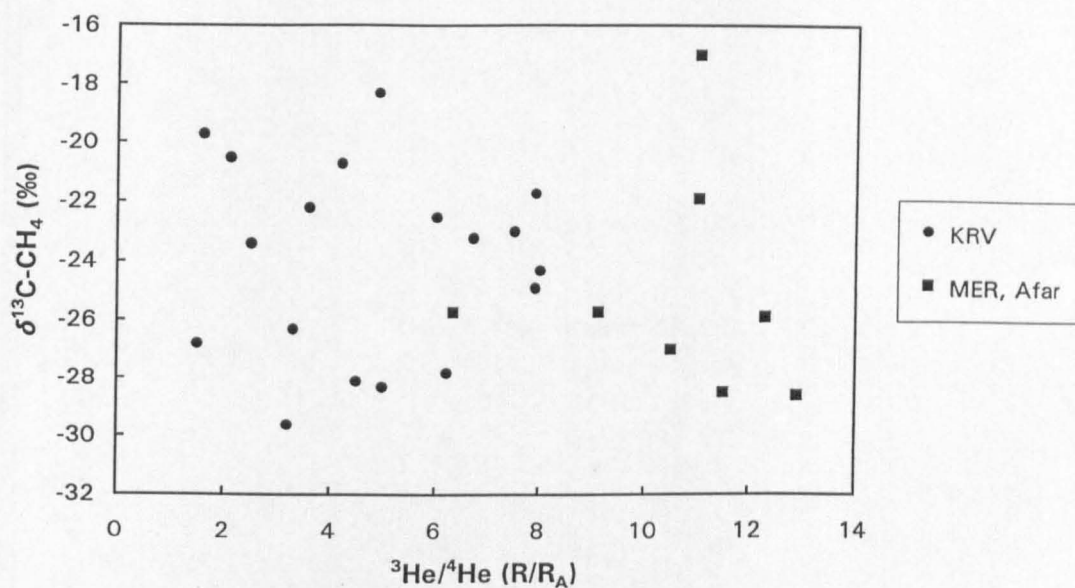
Fig 7.7   Plot of $\delta^{13}C\text{-}CH_4$ vs $^3He/^4He$ for gaseous sources in the Eastern Rift.
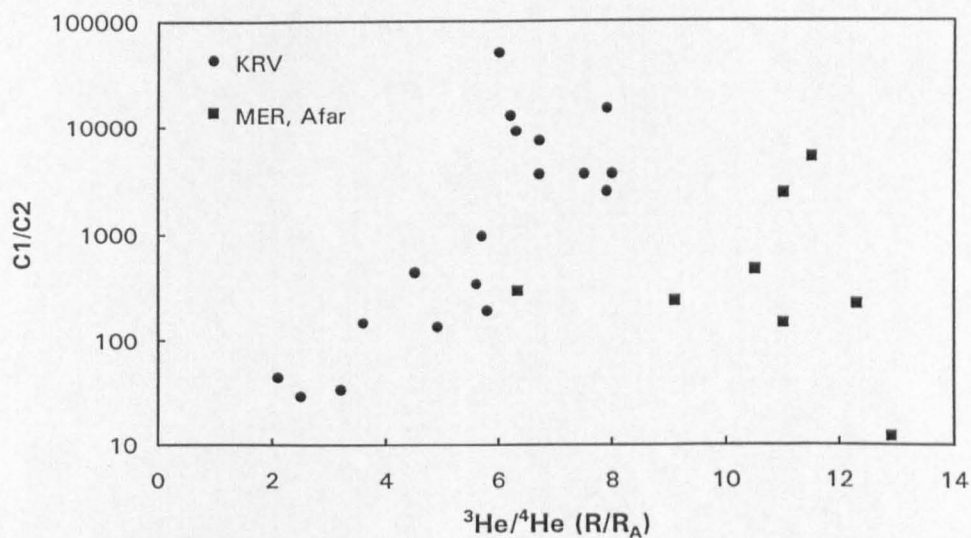
Fig 7.8   Plot of methane/ethane (C_1/C_2) ratio vs $^3He/^4He$ as R/R_A for Eastern Rift
           hydrothermal gases. Samples are divided into upper mantle (Kenya) and
           lower mantle hotspot (MER and Southern Afar) types.

high ^{3}He and heat flow proposed by Mamyrin and Tolstikhin (1984), but only because both heat and ^{3}He are magmatically derived in the KRV; in other cases no clear link has emerged (e.g. Oxburgh and O'Nions, 1987). Nevertheless the consistency of the relationship for many different volcanic centres, plus the Kerita CO_2 well in the eastern rift flank, suggests that there may be more to the relationship than a simple temperature/^{3}He correlation.

In the MER and Afar the available data are too sparse to examine properly whether a similar relationship holds for the hotspot region.

Most of the above remarks refer to He in the gas phase from fumarolic outlets situated above active hydrothermal systems. By contrast, He in the dissolved phase can apparently retain its isotope ratio at some distance from the supposed hydrothermal source. A high ^{3}He/^{4}He value was for instance found in sub-thermal groundwater of the Elmenteita area (site K124, north of the Eburru volcanic centre, Fig 8.1) which may contain a proportion of outflow from the Eburru hydrothermal plume (Allen et al, 1989). In the northern KRV, high ^{3}He/^{4}He ratios have been found in thermal water associated with the Namarunu centre. However, this centre is for the most part much older than Eburru and no longer has any surface fumaroles. The springs do not give high solute geothermometer temperatures (Chapter 9), although there are some young ($<$10 ka) basalts in close proximity (Dunkley et al, 1993). The Elmenteita area also has prominent basaltic activity of similar age (Clarke et al, 1990) and the high ^{3}He/^{4}He ratios in both areas may be associated with flushing by water of these basalts. A similar process was proposed for rhyolites in parts of the MER by Craig et al (1977). The existence of the highest ^{3}He/^{4}He yet measured on a fluid sample from the EARS at Sodere (E16), an upfaulted rhyolite block, may be further evidence. The possibility of such leaching of He from rocks raises the question of whether gas-phase fumarolic He is wholly "new" or whether at least some is coming by a similar process from previously erupted or intruded volcanic rocks. However, as Marty et al (1993a) pointed out, the consistency of C/^{3}He in fumarolic gases from various hotspot areas suggests that leaching is not important, as this would tend to affect the proportions of the CO_2 and He. The case for rock leaching is in any case certainly not proved. For example, Hilton et al (1990, 1995) assumed that the cause of extremely high ^{3}He/^{4}He ratios in northwest Iceland, away from the zone of active rifting, was due to the addition of basaltic melt to the crust, in quantities too small to reach the surface, rather than leaching.

The ^{3}He/^{4}He results for the KRV do not show any evidence that high R/R_A values are associated with the centre of the Kenya dome adjacent to the Nyanza Rift (see 2.1.2 above). Admittedly, the fumaroles of Menengai are so weak and air-diluted that satisfactory He isotope
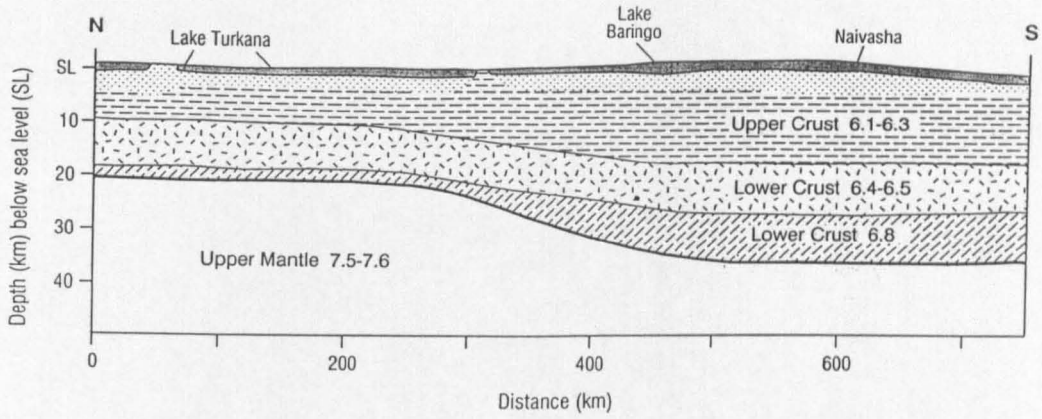
Fig 7.9   Schematic velocity model for the axial profile along the KRV (after Keller et al, 1992). He isotope values may be inversely correlated with crustal thickness.

samples are impossible to obtain, but if there were particularly high ratios in the vicinity these should have been detectable at Arus (K257) where air-free samples are obtainable. Instead of a possible "bullseye" distribution of $^3He/^4He$, the data suggest that there may be a rise in $^3He/^4He$ *peak* values from south to north in the KRV. A crude illustration of this is that R/R_A values >7 are only found northwards from Paka. This could simply be an artefact of sampling, but it is likely that at least one of the wells or fumaroles in the southern KRV would have provided a similar result if equally high R/R_A values were present in the south. Such a rise in $^3He/^4He$ may have structural and volcanogenic implications. For example it might be related to the northerly crustal thinning identified by geophysical studies, which commences at around the latitude of the equator and reaches a minimum in the Silali - Emeruangogolak area, as depicted in Fig 7.9.

The He isotope data also reveal the extent of the influence of lower mantle He in Ethiopia and Djibouti. While the work of Craig et al (1977) and Marty et al (1993) had already established the outlines of this, the present work has filled in some of the detail and gaps. In the MER, Craig et al found really high $^3He/^4He$ (10-14 R/R_A) only round the Shalla-Corbetti area and in the Tendaho area, plus the rhyolite locality mentioned above (Graha Que). In Djibouti similarly high $^3He/^4He$ values were measured in rocks from the north of the country and dredged from the Gulf of Tadjoura. This raised the question of whether there were "hotspots within the hotspot", and if so, what the implications for fluid transport were. The results presented here show that high $^3He/^4He$ is more uniform than previously revealed, ratios >10 R/R_A being found in association with the Aluto volcanic centre, midway between the Lakes and Afar (at Sodere), and at the Asal spreading centre. The results from the "chimney" springs of Lake Abbe, which coincides with the supposed centre of the Afar mantle plume, do not have hotspot signatures. However, they are not part of a CO_2-rich hydrothermal system and are therefore assumed to be the product of a comparatively isolated shallow circulation. This serves to illustrate the importance of CO_2 as a carrier gas for the transport of mantle He. Even so, the result from D7 would be high by MORB standards and clearly represents leakage of mantle gas into the shallow system.

CHAPTER 8

FLUID GEOTHERMOMETRY

The geothermometry of fluids is an important aspect of the geochemistry of thermal areas, particularly those that have not been investigated by deep drilling. It relies on the fact (or at least the belief) that certain, highly temperature-dependent reactions are primarily responsible for the concentration of particular species in the dissolved or gaseous phases, and that these concentrations are not significantly altered during passage to the surface. This chapter is divided into consideration of solute and gas geothermometry. The geothermometry equations to which it refers are provided in Appendix F.

8.1   Solute geothermometry

8.1.1   Ambient and thermal groudwaters

The use of cation and silica-based geothermometers is based on the assumption that chemical equilibrium is obtained between water and rock at elevated temperatures (e.g. Fournier, 1981). In high-enthalpy geothermal fields worldwide, the geothermometers have been quite successful when compared to measured temperatures at depth. This also applies within certain limits to the deep wells of the Eastern Rift (8.1.2 below). However, application of these geothermometers to the thermal springs of the Eastern Rift is constrained because at least some of the dissolved solids in these waters appears to have been acquired by processes other than water-rock interaction in its more limited sense: e.g. by silicate hydrolysis, or evaporative concentration/modification. Thus, for example, the Na/K ratio in waters may not be strictly the product of equilibrium with feldspar at a particular temperature. Also, the geothermometers based on the various forms of dissolved silica may be distorted by the effects of pH on silica solubility (and this is in addition to any difficulties in deciding which form of the mineral may be controlling SiO_2 solubility).

The calculated temperatures in Table 8.1 must therefore be treated with considerable reservation. For example, Na/K may not be reliably temperature-dependent below ~ 150°C; also, it is not certain which silica phase is in control. The data show that Na/K temperatures are often very high, implausibly so when sampling temperatures are in the lower parts of the 40-100°C band. This suggests that there is insufficient depletion in K compared to that decreed by equilibrium with feldspar: either the initial water ratios are unusual (as some of the lake

Table 8.1 Solute geothermometer temperatures in °C for groundwaters of the Eastern Rift, based on the equations of Fournier (1989) for sodium/potassium (T Na/K), quartz (T qtz), quartz with maximum steam separation (T qtz-a), and chalcedony (T chalc).

Location	Site	Temp C	pH	T Na/k	T qtz	T qtz-a	T chalc
Hot springs							
Little Magadi	K3	85	8.85	101	128	125	100
Little Magadi	K3	83	8.82	109	119	117	90
Magadi NW	K9	45	8.82	83	140	135	114
Magadi NE	K11	67	8.96	92	127	124	99
Magadi E	K13	40	9.56	68	103	103	73
Bird Rock	K16	41	9.58	70	106	106	77
Magadi S	K18	45	9.57	73	117	115	88
Magadi N	K73	63	8.89	104	122	120	93
Majiyamoto	K34	52	7.07	373	104	104	74
HG s4	K106	52	3.98	411	181	169	160
HG s7	K109	72		86	159	151	135
Kijabe	K26	43	9.05	101	93	95	62
Elmenteita	K41	43	9.29	138	150	143	125
Bala	K53	72	8.06	100	114	113	85
Bala	K53	72	7.60	100	114	113	85
Kureswa	K260	62	7.55	113	125	122	97
Bogoria W	K68	96	8.05	110	141	136	115
Bogoria SE	K260	97	9.58	127	181	169	160
Lorusio	K45	81	7.65	125	122	120	94
Lorusio	K45	82	7.45	124	119	117	90
Kapedo	K48	50	8.25	115	122	120	94
Kapedo	K48a	51	8.25	115	119	117	90
Kapedo	K48a	50	8.35	118	123	121	95
Ol Kokwe	K71a	96	6.90	287.	126	124	99
Ol Kokwe	K71b	94	9.10	154	175	164	153
Ol Kokwe	K71b	96	9.05	153	201	185	184
Ol Kokwe	K71c	96	6.40	283	195	180	176
Kapedo SL26/2	K183			119	130	127	103
Kapedo SL27/5	K184	45	8.25	114	139	135	113
Suguta SV3a	K185	68	8.25	78	145	139	119
Suguta SV3b	K186	64	8.30	83	145	139	119
Kamuge	K187	50	7.75	64	126	124	99
Kageinya	K188	68	9.50	97	171	161	148
Namarunu	K189	66	8.80	111	107	107	78
Logipi NW	K190	61	8.30	107	92	94	61
Elboitong S	K236	95	7.10	107	137	132	110
Elboitong N	K237	92	9.00	106	151	144	125
Logipi NE	K238	70	8.85	108	115	114	86
Central Island	K239	71	7.20	165	182	170	161
Loyangalani	K242	40	7.65	172	98	99	68
Springs							
Mayer's Farm	K28	28	7.90	318			86
Meroroni	K37	30	6.45	352			107
Chamuka	K39	29	7.05	391			108
Kanyamwi Farm	K91	24	7.30	371			99
Kokot	K101		7.65	468			96
HG s2	K104	20		143			123
HG s5	K107	35		136			145
HG s6	K108	23		190			101
Nginyang-Kapedo	K138	36	8.30	113			90
Churo	K139	28	7.20	140			75
Churo	K139		8.15	142			74
Ebirisat	K140	38	9.00	79			62
Nangarwa	K191		8.85	97			60
Amaya	K192		8.35	112			52
N Samburu Gates	K193		8.85	63			78
Kachurkolh	K194	31	9.15	63			33
Kalnangi	K195	32	9.15	102			95
Amakat	K196		9.80	132			29
S Nangarabat	K197	31	9.15	94			76
Napelton	K198a	33	7.80	103			85
Nasaken	K199	31	7.50	181			81
Eliye	K09u	32	8.90	62			34
Eliye	K240	35	9.00	42			33
Eliye N	K241	37	8.75	63			30
Tum	K244		7.55	281			54

Table 8.1 (contd)

Site name	Site no	Temp	pH	T Na/K	T qtz	T qtz-a	T chalc
Boreholes and wells							
Oltepesi	K22		8.80	215			99
C4635, RVA	K25	35	7.95	189			95
Suswa S Slope	K30		7.90	871			18
Emerit	K72	37	9.40	108			55
C4989	K80	21	7.05	464			96
C567	K81	22	7.70	206			82
C4178	K82	20	7.45	277			97
C563	K83	26	7.70	247			86
C1487	K84	21	7.80	179			88
C5002	K85	20	7.95	278			89
C1063	K86	26	7.20	331			110
C1488	K87	26	7.95	263			96
C467	K88	24	7.75	187			83
C580	K89	25	8.20	167			83
C814	K90	18	8.15	237			92
C570, Kanyam	K92	22	7.00	371			99
C3784	K93	23	7.45	358			107
C307	K94	19	8.35	161			83
C1190	K95	24	8.20	197			64
P65, Kinangop	K96	23	7.00	422			92
C3955	K97	23	6.65	395			112
C4179	K99	26	7.15	159			85
C1404, Ndabibi	K100	26	6.95	311			111
Nakuru No 7	K118	28	7.00	296			98
C431, ADC Farm	K121	37	6.95	233			125
C1798, ADC Farm	K122	35		261			114
DEL, Soysambu	K124	32	6.40	260			128
C1990, Soysambu	K125	28	7.95	196			86
C3525, Mosiro	K129			314			105
K.Samaki	K131		7.70	198			87
K.Samaki	K131		8.15	200			83
Chesirimion	K132		7.20	197			105
Chesirimion	K132	34	7.10	188			115
Tangulbei	K133	30	7.70	137			73
Kokwo Toto	K134	28	7.05	254			87
Orus Solar	K135	28	7.00	194			80
Orus Hand	K136	28	6.45	218			72
Katangora	K137	36	8.30	208			47
Kositei Project	K200		7.35	175			102
Kositei Mission	K201		7.25	144			90
Kositei	K202	36	8.95	67			72
Nginyang School	K203			50			61
Nginyang Poly	K204	36	8.40	61			61
Nginyang Poly	K204	34	8.45	51			59
Chemolingot	K205	38	8.35	83			74
Parkati	K243		7.50	211			123
Napiton	K198b	37	7.60	101			82
Napiton	K198b	37	7.80	100			79
Kanukurdio	K08u	33	7.00	83			98

Table 8.1 (contd)

Site name	Site no	Temp	pH	T Na/K	T qtz	T qtz-a	T chalc
Hot springs							
Imba Koto	CRA11	49	8.50	238	117	115	88
Wildlife Con	CRA16	46	8.20	189			
Langano #1	CRA20	67	7.80	230	148	141	122
Bole Fault	CRA21	92	8.80	181	167	158	144
Geyser Is	CRA24	97	8.80	194	165	156	142
Shalla 30	CRA30	94	8.70	131	135	131	108
Bekele M well	CRA33	43	9.10	172			
Wondo Genet	CRA47	65	7.00	201	131	128	104
Kike	CRA48	52	7.55	334	155	147	130
Kenteri	CRA49	69	7.40	317	123	121	95
Shallo	CRA53	90	8.00	253	150	143	124
Graha Que	CRA58	86	7.35	224	158	150	134
Bodicho	CRA59	89	9.20	197	117	116	88
W Agge	CRA63	43	7.45	268	141	136	115
Shalla SW	CRA64	54	8.80	195	114	113	85
Chitu	CRA65	60	7.70	200	129	126	101
Abaya 6	CRA72	95	9.60	266	154	147	129
Abaya 8	CRA74	67	6.95	202	153	146	128
Abaya 10	CRA75	50	6.75	223	151	144	126
Chokare 15	CRA76	67	6.80	211	149	142	123
Chokare 16	CRA77	42	7.20	231	141	136	115
Bilate	CRA78	51	7.60	168	87	90	56
Nech Sar	CRA86	58	7.60	182	134	130	107
Sodere	E16	65	7.30	169	143	138	117
Springs							
Silte Tekel	CRA12	18	7.40	374			126
Butajera	CRA13		7.20	416			98
Oitu	CRA27	38	7.85	291			112
Huluka	CRA36	18	6.40	427			69
Sedi 1	CRA38		7.10	290			92
Sedi 2	CRA39		7.60	357			90
Sedi 3	CRA40		7.25	305			92
Shalla	CRA41	21	7.40	237			73
Saisha	CRA52	32	6.90	254			101
Motokawa	CRA60	35	7.40	372			90
Asasa	CRA68	21	7.70	380			69
Humasa	CRA82	35	6.90	306			112
Arba Minch	CRA87	17	7.60	311			104
Boreholes and wells							
Akaki	CRA1	21	7.60	247			70
Debre Zeit	CRA2	26	8.20	239			85
Mojo	CRA3	25	7.40	305			99
Adami Tulu	CRA5	31	8.10	167			70
Zwai Well	CRA7		7.40	271			107
S Cross	CRA8		7.90	166			99
Maki	CRA9	25	7.80	176			
Koshe	CRA14	38	7.60	243			114
Jido Combol	CRA17	34	9.00	147			116
Bek Mol Awasa	CRA55		7.40	216			97
Awasa Bank	CRA56	32	7.80	271			75
Sholicha	CRA67	36	8.10	200			101
Shashemane	CRA70		7.20	179			79

Table 8.1 (contd)

Site Name	Site No	T deg C	pH	T Na/K	T qtz	T qtz-a	T chalc
Hot springs							
Meteka	CRA90	72	7.40	185	174	164	152
Allallobeda	CRA91	79	8.00	117	142	137	116
Tendaho	END7	95	7.00	65	164	155	140
Teo	END1	73	7.60	164	227	206	214
Danab	END2	93	7.75	185	171	161	149
Waruf	END3	50	7.30	166	120	118	92
Hertale	END4	49	7.35	185	138	133	111
Korilli	SAS1	80		154	112	111	83
Manda	SAS3	45	7.05	165	96	98	66
Oued Kalou	SK1	74		100	125	122	97
Abbe C	DO6	75	8.70	131	131	127	103
Abbe N	DO7	90	6.05	137	139	134	112
Springs and boreholes							
Kessem	GIZ37		7.35	312			124
Sabire	GIZ47		8.05	189			108
Bilen	END5	40	6.90	208			115
Filwoha	END6	43	7.85	278			101

waters are), or there may be an aluminosilicate source of extra K.

Silica temperatures are much more constrained for the most part. However, whether they accurately reflect subsurface temperatures is questionable. It is likely that below 150°C chalcedony rather than quartz is the main control on silica solubility, and indeed the saturation index data considered in Chapter 6 support this. However, if the chalcedony geothermometer temperatures for hot springs are compared with those calculated for cool springs, there is a very considerable overlap (Fig 8.1). It is highly unlikely that all rift groundwaters have been thermalised. For example, in cases such as Kokot (K101), Kampi Ya Samaki (K131) and Bekelle Molla Awasa (CRA 55) it is virtually certain that the waters are recharged very close by, yet chalcedony temperatures of 87-97°C are indicated.

This calls into question the application of solute geothermometry except in very specific cases where other evidence suggests a high-enthalpy component. The various lines of evidence considered so far concerning hydrogeology in the Eastern Rift suggest that there is little interaction, and conseqently mixing, between thermal sources. Therefore in most cases thermal dilution can probably be ruled out. Further, it is unlikely that a water emerging at a spring at a temperature of, say, 50°C has cooled conductively from a significantly higher temperature, especially at relatively high flow rates. This leads to the conclusion that in most cases the temperature of sampling is only slightly less (perhaps by 10-20°C) than the maximum temperature achieved during deep circulation.

It is assumed here for the EARS that under ordinary circumstances only springs at or close to boiling point (i.e. >90°C) are likely to contain a high-enthalpy (>150°C) component. Even then, not all of these boiling springs will necessarily have a high-enthalpy component; Elboitong (K236, 237), Shalla #30 (CRA 30, E15) and the Abbe chimney springs (D7) do not appear to have connections with such systems. This leaves very few examples of spring systems which do apparently have a high-enthalpy component: Bogoria, Ol Kokwe and Central Island in the KRV (Central Island is an exception because its sampling temperature has been affected by lake water dilution), Abaya and the northern shores of Langano in the MER, and Meteka, Teo and Tendaho in Afar.

If the geothermometry of these systems is considered, a more consistent picture of conditions at depth is obtained. These are systems in which the Na/K and quartz geothermometers are likely to be applicable; since most are visibly boiling, the adiabatic version is the most appropriate form of the quartz geothermometer. In the KRV, at Bogoria SE (K260), the hottest
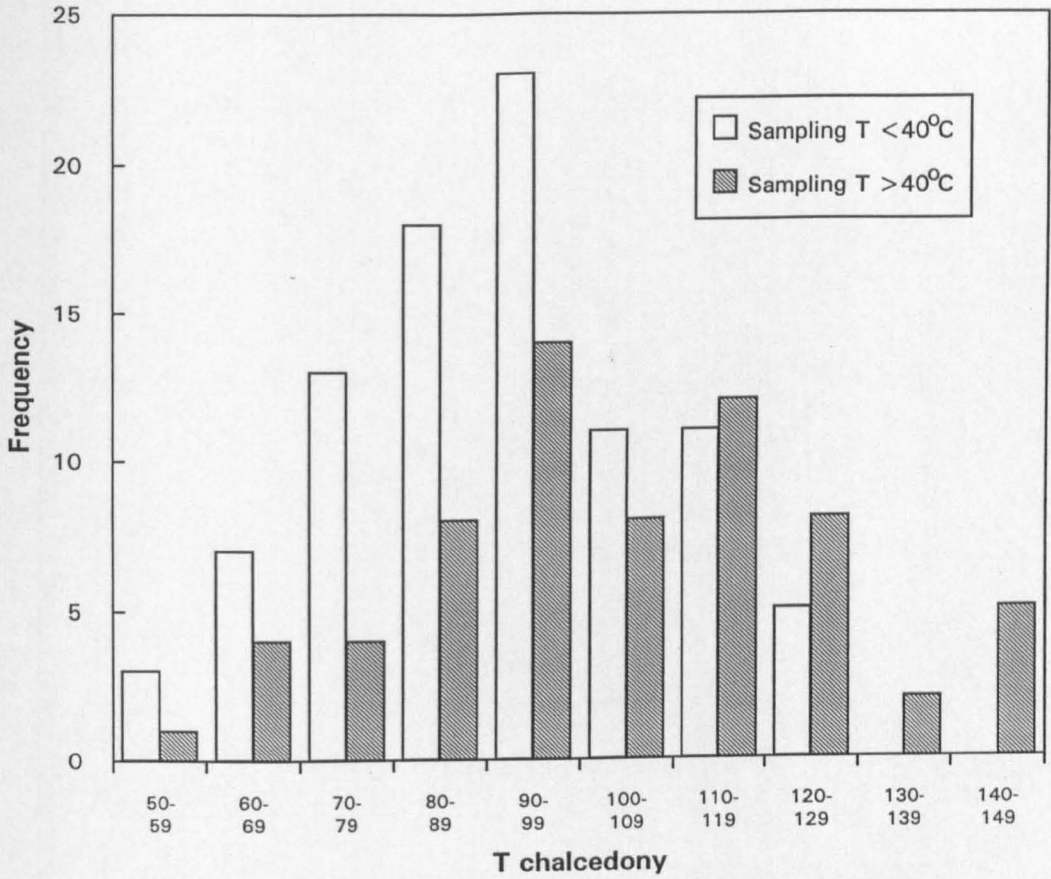
Fig 8.1 Histogram of chalcedony solute temperatures (°C) for cool and hot groundwaters in the Eastern Rift.

part of the system, $T_{Na/K}$ gives 127°C but $T_{quartz-a}$ 169°C; the latter seems the more likely temperature considering the vigour of the system. The disparity may be due to mixing effects between deep thermal water and cool water from the rift wall which is immediately adjacent. At Ol Kokwe (K71b), $T_{Na/K}$ averages 154°C and $T_{quartz-a}$ 175°C. For Central Island (K239), $T_{Na/K}$ gives 165°C while T_{quartz} (the adiabatic version is not appropriate in this case) gives 182°C. In the MER, the vigorously boiling springs of Abaya give $T_{Na/K}$ of 202-266°C and $T_{quartz-a}$ of 144-147°C. The North Langano springs (CRA 21 and 24) have $T_{Na/K}$ values of 181 and 194°C and $T_{quartz-a}$ temperatures of 158 and 156°C. In both cases the more consistent quartz values suggest that this geothermometer is giving the "truest" result, though the close association (at least at Aluto-Langano) with known geothermal system temperatures in the range 250-350°C means that the $T_{Na/K}$ values cannot be wholly disregarded. They may be retaining evidence of a high-enthalpy component which the more rapidly-equilibrating quartz geothermometer has lost. In Afar, Meteka, Teo and Tendaho (CRA 90, END1, 7) have $T_{Na/K}$ values of 164-185°C (the Na/K temperature of 65°C has been disregarded) and the $T_{quartz-a}$ values 155-206°C.

8.1.2 Geothermal wells

In the deep geothermal wells, processes like mixing with shallow groundwater or different kinds of cooling (conductive, adiabatic) should be much less important than for the ambient and thermal groundwaters (8.1.1). The available data suggest that up to a point this is indeed the case.

Fig 8.2 shows a plot of $T_{Na/K}$ and $T_{quartz-lt}$ (the 250+°C version of Fournier, 1989) versus the maximum measured well temperature from wells at Olkaria East, West and Northeast, Eburru, Aluto-Langano, and Asal, based on data from Gizaw (1993), Glover (1972), Muna (1984) and Zan et al (1990). While about half the data points fall within ±30°C of the 1:1 line, there are also some considerable outliers. In around half these cases, both geothermometers are reading low. This leads to the conclusion that the maximum measured temperature is unrepresentative of the bulk reservoir temperature as indicated by the geothermometers. On the other hand, where calculated solute temperatures are too high, the quartz geothermometer alone is usually responsible. The quartz geothermometer reacts more quickly to changes in temperature than the Na/K (Fournier, 1981), so its behaviour in these cases appears to be anomalous.

There are insufficient data from the MER and Afar to reveal any differences between them and the Olkaria-Eburru area. Taken as a whole, the performance of the geothermometers is probably about as good as it is for most other geothermal fields worldwide, suggesting that the

210
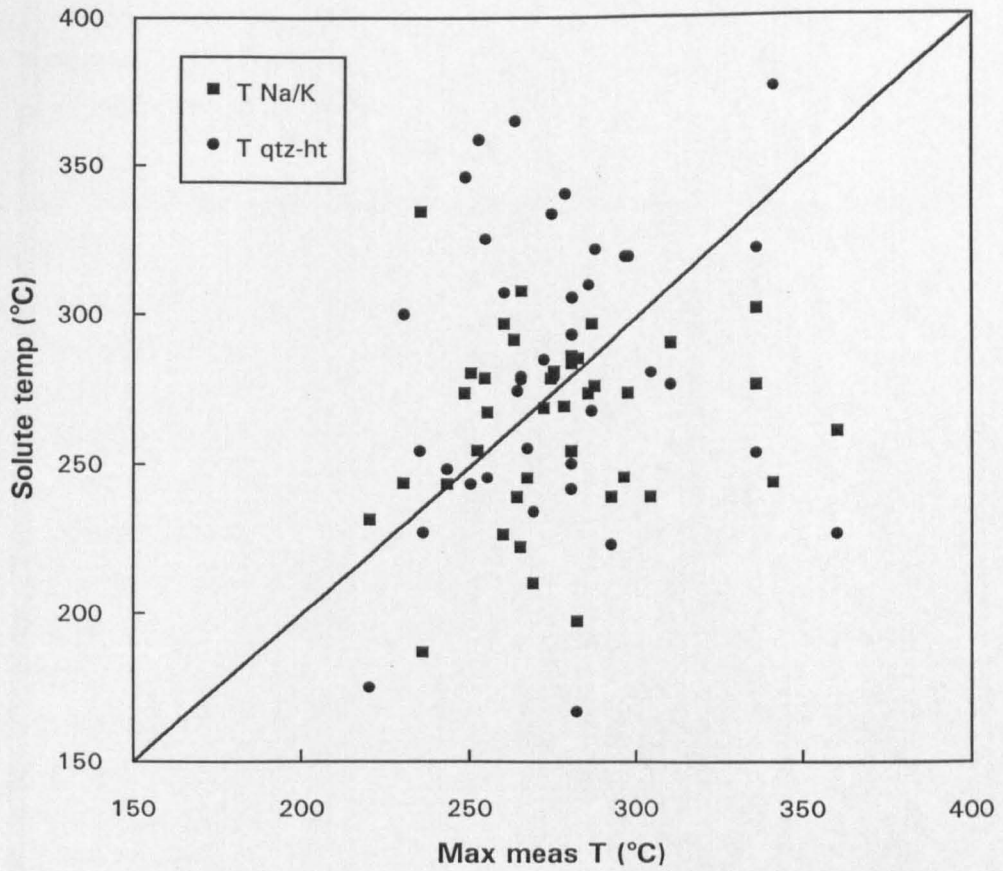
Fig 8.2   Plot of the Na/K and quartz (high temp. version) geothermometers of Fournier (1989) applied to geothermal wells in the Eastern Rift vs maximum measured well temperature.

usual mineral controls apply in the high-enthalpy systems of the Eastern Rift.

8.2   Gas Geothermometry

Gas geothermometry is a much less proven method of estimating reliable temperatures in the subsurface; there is simply not the same body of evidence worldwide that exists for the solute geothermometers.   Despite this, because there are so few high-enthalpy springs in the Eastern Rift (owing to the generally low groundwater levels) some reliance has to be placed on gas methods, especially during reconnaissance studies.

8.2.1   Assessment of existing gas geothermometers

In order to test gas geothermometry for the Eastern Rift, a selection of published equations were applied to the geothermal wells in Kenya, Ethiopia and Djibouti.   Figure 8.3 shows results for individual wells based on the geothermometers of Arnorsson and Gunnlaugsson (1985) and D'Amore and Panichi (1980).   These require various permutations of CO_2, H_2 and H_2S, based on the assumption that certain gas-mineral equilibria are operating (Arnorsson and Gunnlaugsson), or empirically on all the above gases plus CH_4 (D'Amore and Panichi).   The results from these geothermometers vary in consistency, with some showing wide scatter (eg CO_2 and D'Amore-Panichi), while one (H_2S) appears to have a good relationship with temperature but is displaced from the predicted line.   It may be that in the EARS the required mineralogical controls are not always operating (e.g. there could be a lack of calcite to control CO_2 concentrations), or (as referred to above) that many of the wells receive inputs from more than one horizon and that some gas geothermometers adjust to lower temperatures more rapidly than others.   A further complication is provided by the chlorinity of well waters, because most of the geothermometers of Arnorsson and Gunnlaugsson (1985) are provided in <500 and >500 mgkg^{-1} Cl versions.   It is unclear at Olkaria whether an original <500 mgkg^{-1} Cl upflow water becomes more saline owing to steam separation, or whether a >500 mgkg^{-1} Cl upflow becomes less saline owing to dilution by low-salinity meteoric waters.   Accordingly, geothermometers for individual wells have been applied in the correct version for the chlorinity of the well (data from Muna, 1984 and KPLC records).   This feature is responsible for most of the lower temperature values given at Olkaria and Aluto-Langano by some of the geothermometers (though not the CO_2 or D'Amore-Panichi equations).
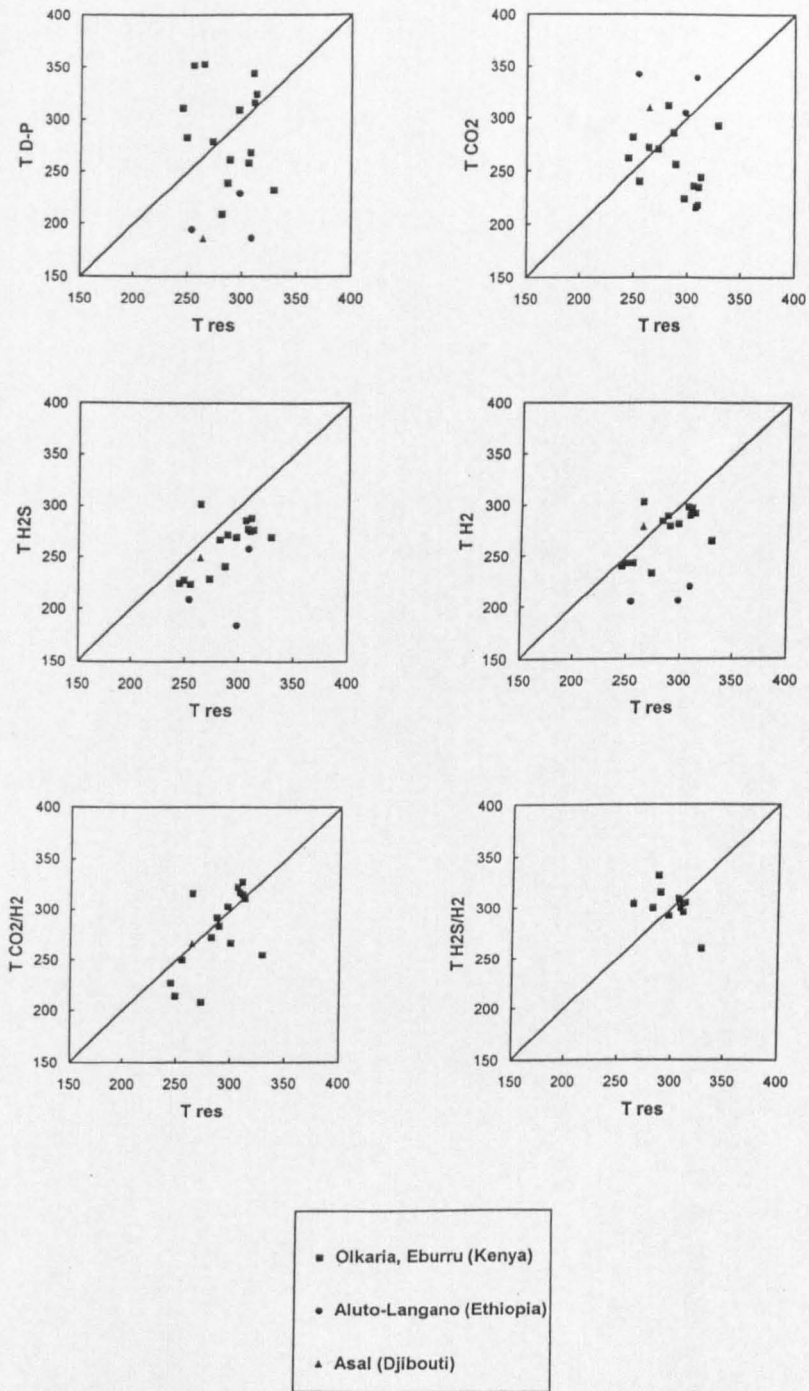
Fig 8.3 Plot of the gas geothermometers of D'Amore and Panichi (1980), and Arnorsson and Gunnlaugsson (1985) vs reservoir temperatures (based on the average of $T_{Na/K}$ and $T_{quartz-ht}$ geothermometer temperatures) in geothermal wells of the Eastern Rift.

8.2.2   An alternative gas geothermometer

The work of Darling (in rev.) on hydrocarbon gases in hydrothermal systems worldwide suggests that the ratio of methane to higher hydrocarbons may have a geothermometric function. Effectively this can be represented by CH_4/C_2H_6, since C_1/C_2 is a good approximation for C_1/C_{2+}. Geothermal wells at Olkaria, Eburru, Aluto-Langano and Asal were used to calibrate such a C_1/C_2 geothermometer for the Eastern Rift. The only drawback to this was that most producing wells are extracting from reservoirs in the fairly restricted range of 250-300+°C, and therefore to extend the range towards lower temperatures, results from the only high-gas content springs apparently related to high enthalpy sources (i.e. above ~150°C) have been included in Fig 8.4. This shows C_1/C_2 plotted against reservoir temperature, itself calculated from the average of the Na/K and quartz geothermometers in Fournier (1989). (The reason for using this average as a means of assessing reservoir temperature is because it is common for geothermal wells to receive feeds from several levels conceivably with differing temperatures. The averaging of a relatively slowly equilibrating geothermometer [Na/K] with a more rapidly equilibrating one [quartz] represents a compromise solution to the problem of assigning a single "reservoir temperature" value to a given well for this particular application.)

Superimposed on the plot of Fig 8.4 is the empirical C_1/C_2 geothermometric line developed on the basis of results worldwide (Darling, in rev.). While about three-quarters of the data points fall within 50°C, and about half within 30°C of the line, most fall on the higher-temperature side of the line and that therefore a better fit could be obtained by a modified line. A curve suitable for the range ~160-360°C was chosen, with the form

$$t = 454.8 - (586.4/R) + (281.4/R^2) \qquad (9.1)$$

where t is the temperature in °C, and R is log (C_1/C_2). The plotted points fit the curve with a standard deviation of 20.5°C and an average deviation of 17.1°C.

When the C_1/C_2 geothermometer is applied to fumaroles in and around the drilled geothermal fields, some assessment of its performance can be made by comparing the calculated temperatures with the known solute geothermometer temperatures of the nearer wells. At Olkaria, most fumaroles are situated along the Ololbutot fault zone (Fig 8.5). The C_1/C_2 geothermometer could only be calibrated against wells in the presently-producing eastern and northeastern wellfields, the nearer wells of which are shown in Fig 8.5. Despite this, agreement between fumarole results and well solute temperatures in and around the fault zone

214
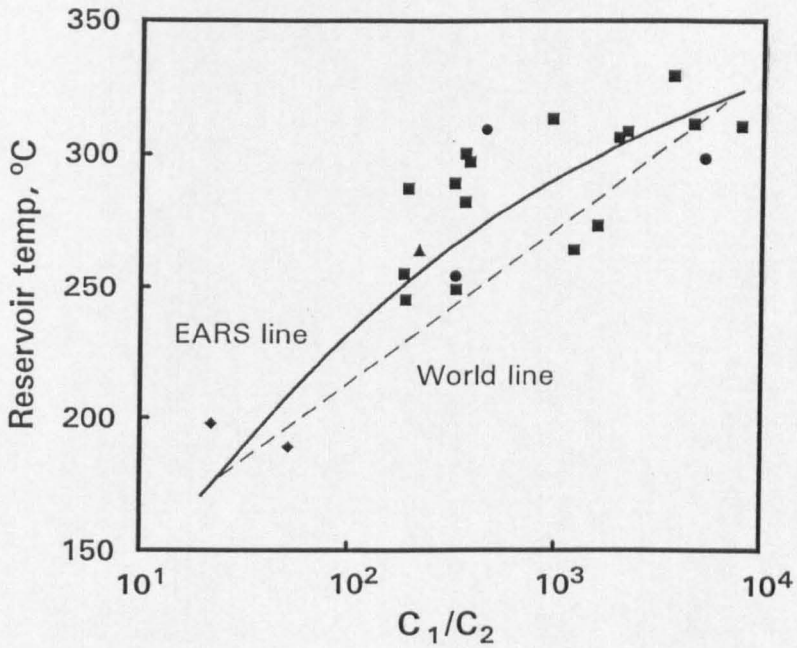
Fig 8.4　　　　Plot of reservoir temperatures (based on the average of $T_{Na/K}$ and $T_{quartz-ht}$ geothermometer temperatures) vs CH_4/C_2H_6 ("C_1/C_2") for geothermal wells of the Eastern Rift (symbols as for Fig 8.3, plus diamonds for high-enthalpy spring gases). The proposed C_1/C_2 geothermometer is derived from the EARS curve, while the straight-line regression is based on the world data in Darling (in rev.).
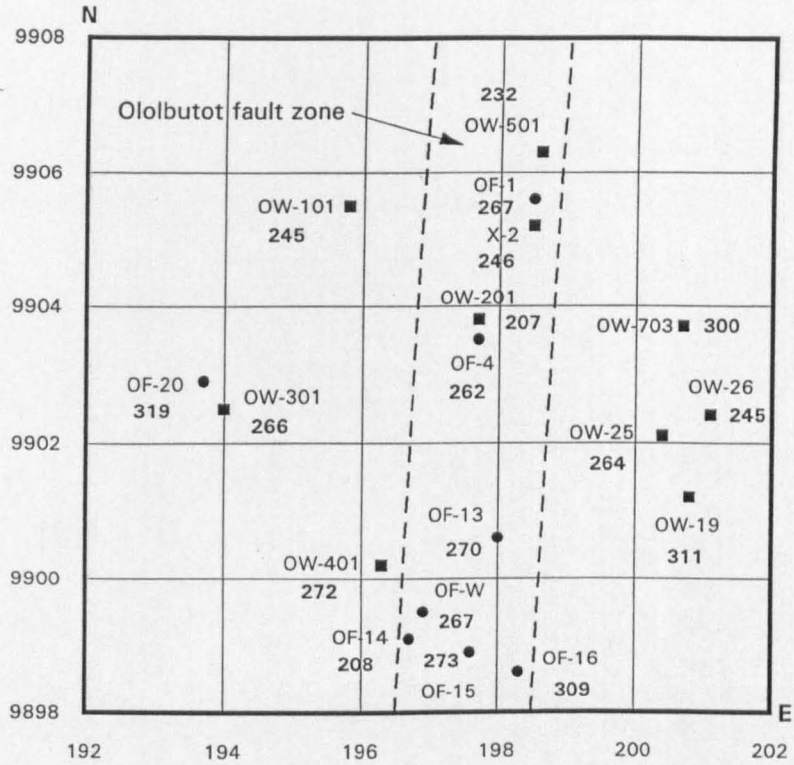
Fig 8.5   Map showing the area around the Ololbutot fault zone of the Olkaria geothermal area, Kenya. 2 km grid squares are shown based on the UTM grid. Well (OW-) and fumarole (OF-) identifiers are shown, together with temperatures (in bold) calculated by solute geothermometry (average of $T_{Na/K}$ and $T_{quartz-ht}$) for the wells, and the methane/ethane geothermometer for the fumaroles.

is generally good, although there is a bias towards higher temperatures from the fumaroles. This is seen in more extreme form for the isolated western fumarole OF-20, adjacent to well OW-301, the solute temperature of which is 53°C lower than that of the fumarole. This may have been due to OF-20 having by some way the lowest measured CH_4 and C_2H_6 contents in the whole Olkaria area, possibly affecting the accuracy of the ratio. However, a maximum measured temperature of 299°C was noted for this well (Haukwa, 1984), which would reduce the discrepancy to only 20°C.

To compare the C_1/C_2 geothermometry results for Olkaria with those of the other gas geothermometers, Fig 8.6 shows a plot of results versus grid northing for fumaroles and wells within the fault zone and up to 2 km outside it. While there are no well data for the southern few kilometres of the fault zone, it has been shown (7.2.1) that the fumarole OF-W had a $^3He/^4He$ value very similar to those of wells in the eastern and northeastern wellfields, implying that magmatic heat sources were as active. Therefore temperatures might perhaps be as high at depth in the southern part of the fault zone as in the presently-producing wellfields. With the exception of the C_1/C_2 geothermometer, the gas geothermometers generally perform variably compared to the range covered by well solute temperatures (approximately 200-300°C) (Fig 8.6). Apart from C_1/C_2, the best-performing geothermometers are H_2S, H_2 and CO_2/H_2, though the first of these tends to be restricted to the lower part of the envelope and the others to the upper part. Also, H_2S and H_2 suffer from the disadvantage that they are not always detectable in fumaroles. Other geothermometers tend to give excessively high temperatures, sometimes CO_2, but more notably $\Delta^{13}C$ (Panichi et al, 1975, included here to show that this geothermometer is inappropriate for the Eastern Rift), or implausibly low (the D'Amore-Panichi geothermometer). In the case of the geothermometers of Arnorsson and Gunnlaugsson (1985), it was noted by the authors themselves that the "correct" versions are not always easy to apply because of the chlorinity restriction mentioned above. However, it seems that at Olkaria Cl contents are generally above 500 $mgkg^{-1}$ and from the local well evidence (albeit limited) are likely to be so in the Ololbutot zone (Muna, 1984), and therefore these geothermometer versions have been used. Had the other versions been used many temperature results would have been low, especially those of the H_2S geothermometer.

In Ethiopia, the Aluto-Langano wellfield is situated within the Aluto volcanic complex (Fig 8.7). Only fumaroles outside the complex were sampled, there being little surface activity within the complex. Outflow from the Aluto hydrothermal system is believed to take place to the south, towards Lake Langano where several hot or boiling springs discharge near the shore. The C_1/C_2 temperature calculated for the Gebiba fumarole fits the progression from ~300°C
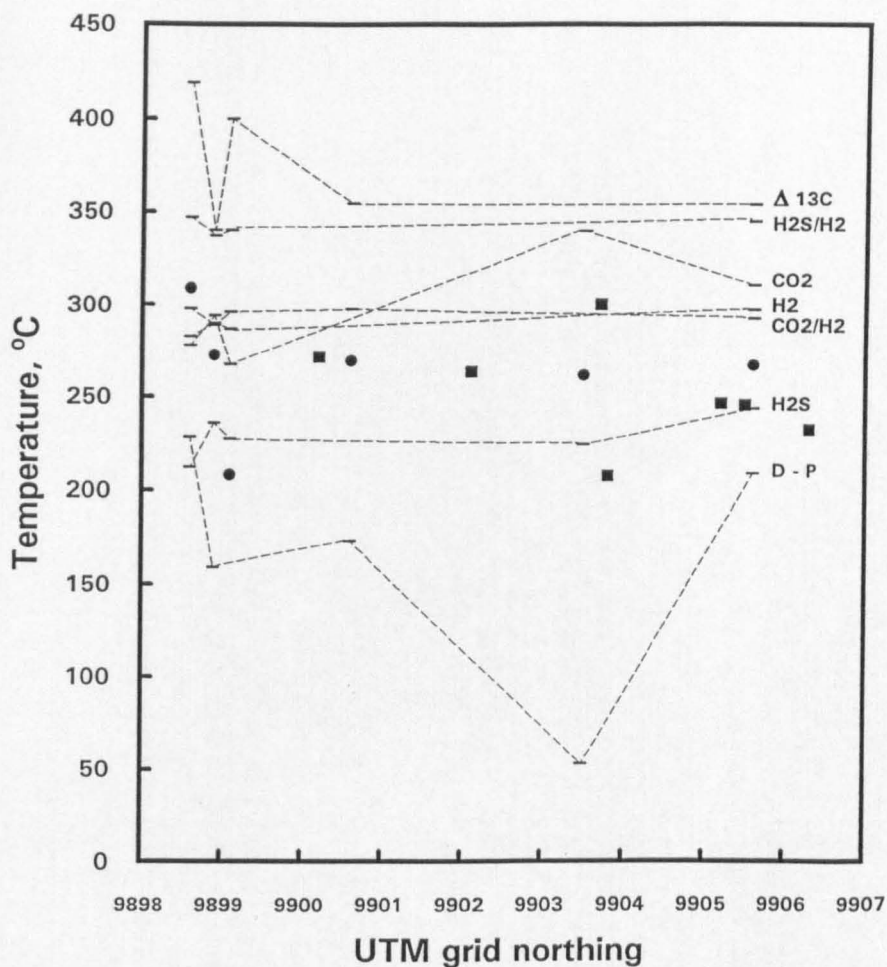
Fig 8.6   Comparison of gas geothermometer results from S to N along the Ololbutot fault zone, Olkaria. Well solute temperatures (■) and fumarole C_1/C_2 temperatures (●) are indicated. Other gas geothermometers are represented as dashes joined by dotted lines. Based on the geothermometers of Panichi et al (1975), D'Amore and Panichi (1980), and Arnorsson and Gunnlaugsson (1985).

218
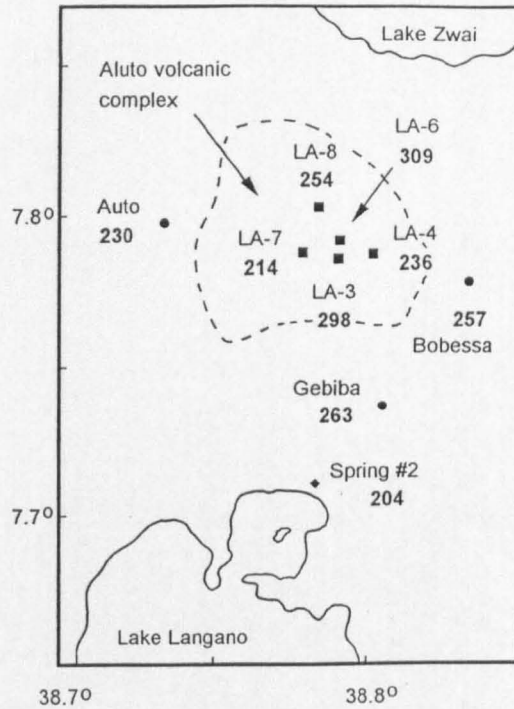
Fig 8.7 Map of the Aluto-Langano geothermal area, Ethiopia. Well (LA-) and fumarole and spring (name) identifiers are shown, together with temperatures (in bold) calculated from solute geothermometry for the wells and spring, and the C_1/C_2 geothermometer for the fumaroles.
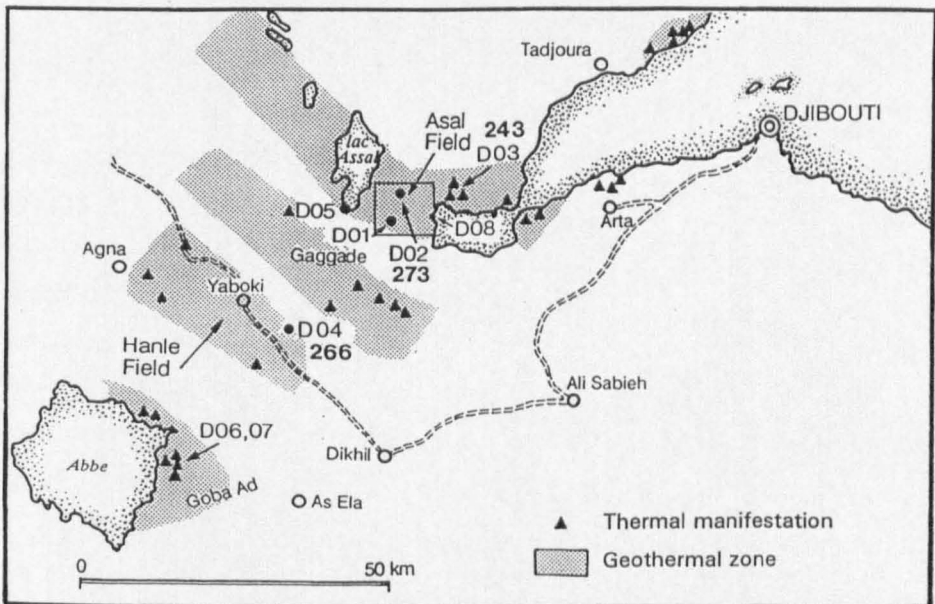
Fig 8.8 Map of the Asal area, Djibouti. Figure adapted from Khaireh (1989). Temperatures shown are derived from the methane/ethane geothermometer.

solute temperatures in the south-central part of the wellfield to a solute temperature of $\sim 200\,°C$ at Spring #2. The fumaroles at Bobessa and Auto, although somewhat nearer the complex than Gebiba, have lower C_1/C_2 temperatures, presumably because they are not situated above zones of outflow. Because of the absence of detectable H_2 in any of the area's fumaroles except for Gebiba (Glover, 1976), few of the conventional geothermometers can be calculated for purposes of comparison. Temperatures given by CO_2 are higher than would be expected, while H_2S temperatures are too low if it is assumed that reservoir Cl values are < 500 mgl^{-1} for most of the wellfield (Gizaw, 1989).

At Asal in Djibouti (Fig 8.8), a fumarole (D2) close to the centre of the active rift zone gave a temperature of $273\,°C$, rather higher than the solute temperature for well A-3, which is situated on the periphery of the rift zone. A-5, the nearest well to D2, gave *measured* upper and lower reservoir temperatures of 190 and $355\,°C$ respectively (Zan et al, 1990). The other gas geothermometers (D'Amore and Panichi, 1980; Arnorsson and Gunnlaugsson, 1985) function well in Djibouti in spite of, or possibly because of, the very high salinity of the thermal fluid, which consists basically of concentrated seawater (see 5.1.6 and 6.3.5 above).

Further inland, a fumarole (D4) adjacent to a 2000 m deep test well gave a C_1/C_2 temperature of $266\,°C$, whereas the maximum measured well temperature was only $120\,°C$ even at the bottom of the drillhole. The only other gas geothermometer which could be applied to this fumarole was that for CO_2, which gave a temperature of $148\,°C$, in better agreement with the well temperature.

Outside the wellfields there are few independent data with which to compare temperatures calculated from fumarolic gas data. In this case the only comparison available is the probable temperature distribution. Figure 8.9 shows histograms of the different geothermometers calculated from the same dataset, with results from the dual-salinity versions plotted separately because of a general lack of information on likely Cl values. Although the higher Cl versions of some geothermometers often give comparable results, the distribution of C_1/C_2 temperatures is the most consistent and realistic on the reasonable assumption that most high-enthalpy reservoirs will have temperatures around the 250-300°C range, as they do in the wellfields. The C_1/C_2 temperatures also accord with other geochemical and geological indications (Darling and Talbot, 1991; Dunkley et al, 1993). The evidence from the wellfield fumaroles suggests that the C_1/C_2 geothermometer may at times give results that are higher than the actual temperatures, but that this tendency is in most cases only slight.
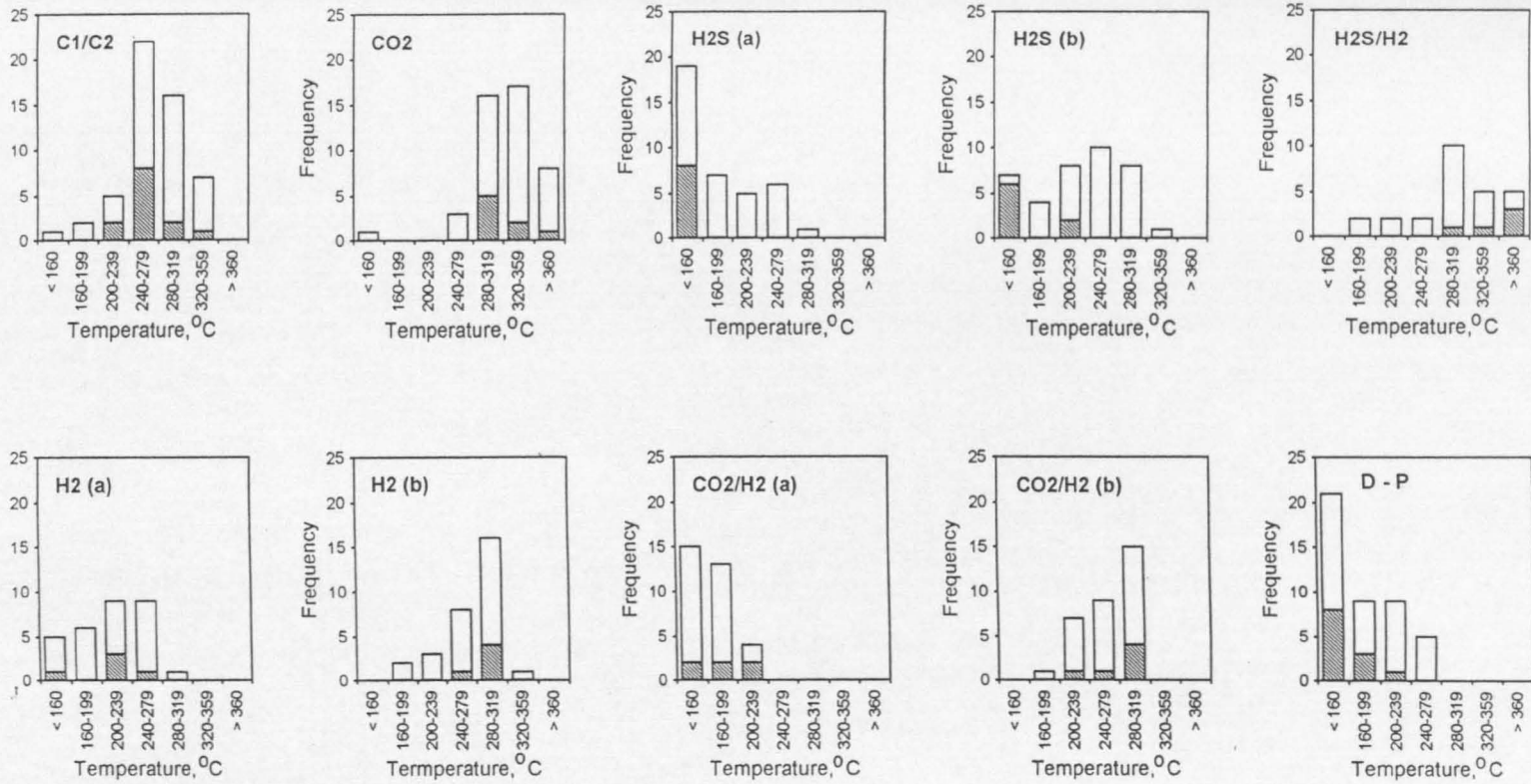
Fig 8.9   Histograms for various gas geothermometers applied to fumaroles of the Eastern Rift. Shaded and blank areas represent cumulatively wellfield and non-wellfield fumaroles respectively. Based on data from this research and Glover (1972, 1976). Gas geothermometers as previously used. Where two versions of the Arnorsson and Gunnlaugsson geothermometers exist, both have been used because of uncertainty about subsurface conditions.

There are three basic reasons why the conventional gas geothermometers may sometimes be failing in Kenya and Ethiopia. Firstly, subsurface steam condensation is known from stable isotopic data to be common in the Rift (Darling et al, 1990; Allen and Darling, 1992), and this would affect the gas geothermometers based on concentration relative to steam. Secondly, the lighter gases will tend to diffuse out of fumarolic conduits: this would affect the H_2 concentration and ratio geothermometers the most. Thirdly, there is ample scope for reaction between gases and wall rocks because there is a thick unsaturated zone to traverse. This may account for the very low concentrations of H_2S observed in fumarolic gases in the continental Eastern Rift. The advantage of the C_1/C_2 geothermometer appears to be that the gases are relatively unaffected by the above processes, and furthermore are easy to detect down to very low concentrations by simple GC methods. An additional advantage is that, unlike the geothermometers considered above, there is no need to know or make assumptions regarding the concentration of chloride or pCO_2 in reservoirs, and also it is not necessary to know concentrations of gases relative to steam.

8.2.3 Correction of gas geothermometers using stable isotopes

While subsurface steam condensation is but one of several processes which can affect gas concentrations (see above), it is the only one which can in principle be quantified. The use of stable isotopic techniques rather than the internal gas comparison techniques of Arnorsson and Gunnlaugsson (1985) allows correction to be made to some of the geothermometers.

In cases where there is subsurface condensation of steam which is travelling towards a fumarole, apparent concentrations of gas relative to steam will increase and therefore elevate the geothermometry temperatures. If the isotopic composition of the reservoir before boiling is known or can be inferred, some estimate of the degree of condensation suffered by the steam at each fumarole can be attempted. It is assumed that all fumarole steam is the result of single-stage (maximum-fractionating) separation. In some cases steam isotope composition will fall on or near the single-stage temperature curve, indicating little or no condensation. However, in other cases steam may be considerably more depleted in heavy isotopes due to their preferential dropout during condensation. It is assumed for present purposes that such highly-depleted steam can be related to the original water composition by a Rayleigh-type relationship, as proposed in Darling and Armannsson (1989). The equation is

$$(1000 + \delta_r)/(1000 + \delta_i) = f^{\alpha-1} \qquad (9.2)$$

222

where δ_r = isotopic composition of steam remaining after condensation

δ_i = initial isotopic composition of the steam

f = fraction of steam remaining

α = relevant fractionation factor for a particular temperature.

This relationship can be used to calculate the fraction of steam which has dropped out by condensation. Gas concentrations can then be adjusted and the new geothermometric temperatures calculated. Fig 8.10 shows the effects of assuming that a particular gas concentration is the product of varying amounts of steam loss. Depending on the amount of condensation taking place, a given measured concentration could represent a significant temperature range, particularly for CO_2. While no allowance has been made for loss of CO_2 into the condensate, solubility of CO_2 in the range 100-200°C (the most likely temperature range) is at its lowest (Ellis and Mahon, 1977). In practice, a small amount of gas loss into condensate would have the effect of slightly counteracting the tendency towards erroneously high temperatures.

One problem in using such a correction is that the isotopic composition of the deep water may not be known with any certainty. However there is sometimes evidence from other sources as to what it may be. Another problem is that the processes producing the final steam and gas mixture may be more complicated than the simple condensation-after-single-stage-separation model would suggest. Nevertheless, Fig 8.11 shows the basis of attempts to correct apparently condensed fumarole gas samples by use of the isotope technique in different areas of the Rift system where it appears to be feasible. The isotopic composition of steam undergoing progressive condensation is predicted by use of the Rayleigh equation. Radiating lines are temperature-controlled, while the parallel lines represent the fraction of original steam remaining at various stages in the condensation process. Estimated starting compositions for the deep fluid and resulting single stage steam are shown in each case. The position of individual fumaroles on the plot is then translated to an uncondensed steam fraction term. The results are then used to recalculate the conventional gas geothermometers and are given in Table 8.2. Clearly only the concentration geothermometers can be modified by these techniques.

In the Suswa area, CO_2 temperatures generally over 300°C (Armannsson, 1987) are lowered to the 270-300°C range. To the north, in the Olkaria area, condensation does not appear to be a major factor and no correction has been applied. Not enough is known about deep thermal water in the Menengai-Bogoria area to attempt any isotopic correction. However, north of
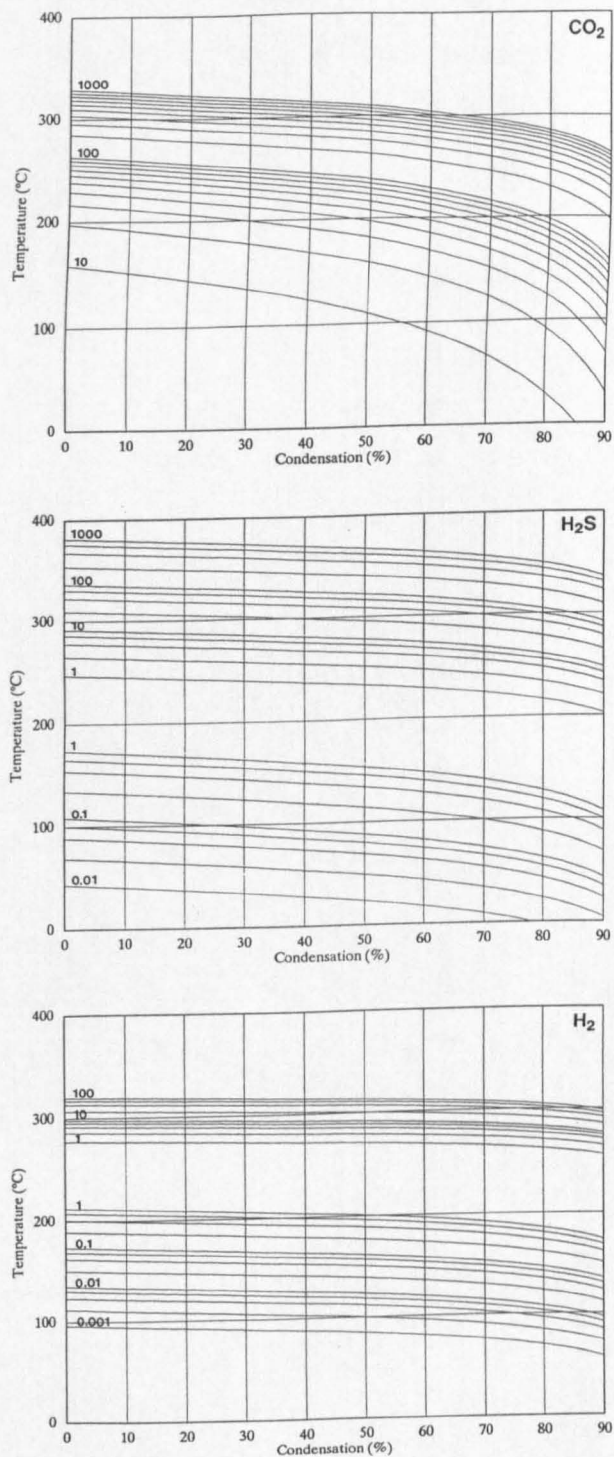
Fig 8.10   The effect of steam condensation on calculated temperatures for the CO_2, H_2S and H_2 geothermometers of Arnorsson and Gunnlaugsson (1985). Gas concentrations indicated on plots are in mmole gas per kg steam. Both versions of the H_2S and H_2 geothermometers are shown.
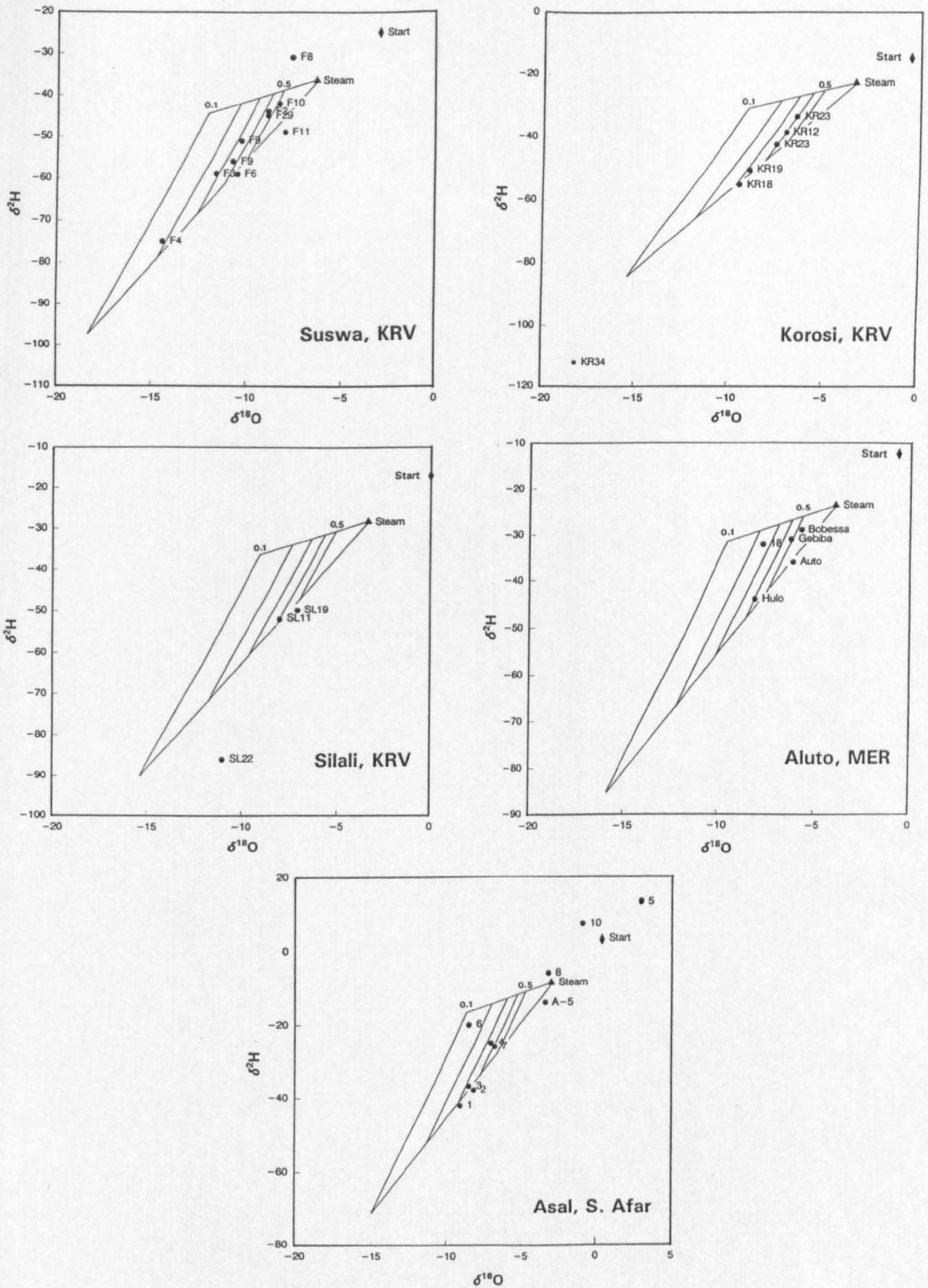
Fig 8.11 δ-plots with calculated steam condensate fields superimposed on measured fumarole compositions for sites in the Eastern Rift. The parallel lines represent the fraction of original steam remaining after condensation. F numbers for Suswa refer to the isotopic data of Armannsson (1987). Plain numbers for Asal refer to the isotopic data of Geotermica Italiana (1987b).

Table 8.2   Results of stable isotopic correction of condensation effects on geothermometer temperatures for selected fumaroles in the KRV, MER and southern Afar (temperatures in °C). Raw data sources as referred to below.

Fumarole	CO$_2$ init	CO$_2$ corr	H$_2$S init	H$_2$S corr	H$_2$ init	H$_2$ corr	H$_2$S init	H$_2$S corr	H$_2$ init	H$_2$ corr
			— Cl > 500 mgl^{-1} —				— Cl < 500 mgl^{-1} —			
Kenya										
F-2[a]	312	290								
F-3[a]	324	289								
F-4[a]	335	288								
F-6[a]	292	269								
F-9[a] (ave.)	330	301								
F-10[a]	294	275								
KR12[b]	321	296	267	249			202	176		
KR18[b]	333	302	227	205			145	113		
KR19[b]	340	308	242	219			167	134		
KR23[b]	339	313	210	192	245	237	120	94	153	138
SL11[b]	299	272	325	308			287	262		
SL19[b]	384	358	301	287	238	232	252	232	140	129
Ethiopia										
Bobessa[c]	313	297	236	224			157	140		
Gebiba[c]	282	259	202	188	242	235	108	87	147	135
Auto[c]	388	379	201	196			106	100		
18[d]	289	242	234	206			154	114		
Hulo[d] (ave.)	281	251	232	214			152	126		
Djibouti										
G2[e]	178	116			232	224			130	114
G4[e]	256	215			247	238			158	140
G6[e]	238	129			244	225			150	116
G7[e]	217	170			247	239			157	142

F - Suswa; KR - Korosi; SL - Silali; G - Fiale

init - initial geothermometric temperature; corr - geothermometric temperature after correction of gas concentration by isotopic method.

a - Armannsson (1987); b - Dunkley et al (1993); c - Gizaw (1989) and Darling and Talbot (1991); d - Glover (1976) and Craig et al. (1977); e - Geotermica Italiana Srl (1987b)

Lake Baringo the correction has been applied to certain fumaroles on Korosi and Silali. The CO_2 temperatures on Korosi, previously far higher than any supporting evidence would suggest, are reduced, though are still around 300°C. (KR34, the most condensed steam sampled in the Rift so far, has not been corrected because its extremely depleted composition may be the result of multi-stage modification). The "correct" (<500 mgl^{-1} Cl) H_2S geothermometer gives amended results which are rather low. The results from Silali fumarole SL11 are more convincing, but the already highly varied temperatures from SL19 outside the caldera do not become easier to interpret.

In Ethiopia the corrections can be applied to some of the fumaroles of the Aluto complex, where there is evidence from the geothermal wells for the deep water isotopic composition. Maximum effects are seen at the No. 18 fumarole (Glover, 1976) where CO_2 temperature is reduced by 47°C. At Corbetti and Tendaho there are insufficient data to define a starting composition and corrections have not been attempted.

In the rift zone of Djibouti some of the fumaroles at Asal show evidence of condensation. However the CO_2 geothermometer did not give the usual high values even before correction, and the recalculated temperatures now appear to be too low in some cases. Corrections to the H_2 geothermometer are considerably smaller and more in line with what is known about geothermal reservoir temperatures at Asal.

Although condensation corrections based on stable isotope evidence can be applied in several rift localities, they are not usually sufficient in scale to correct the apparently most wayward of the geothermometers (usually the CO_2 version). In a sense this is not unexpected; it has already been demonstrated that the CO_2 geothermometer does not work well in the continental Eastern Rift, even when sampled in geothermal wells where condensation cannot be playing a major role. Also, condensation must usually be indicative of long and tortuous paths for steam and gas before they reach the surface, thus giving time for the unquantifiable effects of diffusion and reaction to occur.

The use of condensation corrections for geothermometry therefore seems to be of only marginal importance to exploration in the Eastern Rift. Their application has not led to a fundamental re-interpretation of geothermal potential in any area and their use is probably best restricted to particular local circumstances.

PAGE MISSING IN ORIGINAL

CHAPTER 9

SUMMARY AND CONCLUSIONS

The previous chapters have attempted to show largely from a geochemical standpoint the sometimes complex way in which the fluids of the Eastern Rift behave and interact. The purpose of this chapter is to draw together this information, to identify the extent to which the objectives of this study have been achieved, and to identify subject areas that may be worthy of further investigation.

9.1   Synthesis

Fluids in the crust of the Eastern Rift can be considered under the four headings of atmospheric inputs, mantle inputs, inputs from the crust itself, and structural considerations.

9.1.1   Atmospheric inputs

The primary atmospheric input is of course rainwater, whether directly infiltrated or recharged via rivers, lakes or seawater. At the most basic level, the amount of surface water can be correlated with the amount of rainfall, but there are additional implications. In the Eastern Rift, the MER has the highest rainfall (with the minor exception of the Nyanza Rift). This has resulted not only in a relative abundance of surface water, but also higher groundwater levels in general. This in turn has given rise to greater spring activity in the MER than elsewhere, and also to the readily identifiable discharge of high-enthalpy fluids, in contrast to the very minor examples of the KRV. As important, in terms of geochemical processes, is the lack of arid discharge areas in the MER where evaporative enrichment of waters can take place on the scale of Magadi or the northern Suguta Valley. Therefore very high TDS values and the accompanying deposition of evaporites are not presently seen in the MER.

The amount of recharge in southern Afar is very low and the climate very hot. However, there seems to have been little opportunity for evaporative recycling of carbonate to have taken place. Instead, the chemistry of groundwaters in Afar appears to result from the legacy of Quaternary marine incursions, leading to domination of the anions by chloride. The ultimate expression of this is Lake Asal which, although situated in a arid area, is a sizeable lake because of the constant marine input. Accordingly the lake exhibits halite deposition.

Oxygen and hydrogen isotopes in rainwater may be modified after precipitation, primarily by surface evaporation. The lakes of the MER seem to be slightly more enriched isotopically than those of the KRV. This may reflect a combination of factors such as lower altitudes and different relative humidity in the MER compared to the KRV. However, the effect may be more apparent than real, because the lakes may have been sampled at different stages in their seasonal cycles (the time-series data from Naivasha and Baringo show how compositions can vary).

The limited tritium data, all from the Gregory Rift, indicate that groundwater flowpaths give rise to residence times of a minimum of a few tens of years. Whether this would be the case in the somewhat wider MER remains to be determined, but the background level of ^{3}H is probably now so low that it would be difficult to separate very recent from moderately old recharge. In Afar, tritium data led to much the same conclusions as for the KRV.

Other atmospheric inputs include $^{14}CO_2$ and the noble gases. The radiocarbon data, where unaffected by inputs from "dead" mantle CO_2, confirm the tritium picture of relatively young circulation, both in the KRV and Djibouti. The noble gases can also be important as tracers, though of physical processes such as recharge temperature or subsurface modifications. While they have only been studied in the southern KRV, they clearly have the potential to play a similar role in the other rifts.

9.1.2 Mantle inputs

Helium isotopes indicate that there are different source regions for volcanism: lower mantle in Afar and the MER due to the influence of the Afar "hotspot", and upper mantle ("MORB") in the KRV, where updoming is much more local and has been produced by a much less deep-rooted minor plume. (There is a link here with hydrology, since the greater rainfall in the MER is largely a consequence of the Ethiopian Plateau's higher elevation, which is due to its plume origin.) The ubiquitous carbon dioxide in the Eastern Rift has a predominantly mantle origin. Whether all the CO_2 is of upper mantle origin in the Eastern Rift, or whether it is supplemented by CO_2 from the lower mantle in the MER and Afar remains an open question. If it is supplemented, a greater flux of CO_2 per unit area might be expected in the hotspot area. There is no real evidence that this is so, except perhaps that the deep geothermal wells of Aluto-Langano have very high HCO_3/Cl ratios compared to geothermal fields elsewhere, including Olkaria-Eburru. Despite the clear mantle origin of CO_2 beneath the rifts, CO_2-rich gas sources are also known outside the MER (e.g. at Ambo) and the KRV (e.g. the gas seeps

at Meru in the Mount Kenya area). In the latter case, the $\delta^{13}C$ signature is very similar to those in the KRV, despite the considerably thicker crust away from the Rift.

Whatever its exact source, as the primary agent for the widespread silicate hydrolysis assumed to occur in the Eastern Rift, CO_2 has a major influence on groundwater chemistry.

9.1.3   Crustal inputs

Gaseous inputs from the crust are only minor in quantity and influence. In Afar, the MER and the main KRV, they are more or less restricted to the hydrocarbon gases. Although usually very low in concentration, these may have a role in geothermometry, and may also have other implications (for example, the hydrocarbon spectrum appears to be similar whether the source water is fresh or marine). In the Nyanza Rift, the presence of carbonatites leads to generation of additional crustal gases, i.e. ^{40}Ar, ^4He and CO_2. However, the carbonatites from which these gases are produced will themselves have had a mantle origin in the relatively recent past (Miocene-Pliocene).

Chemical inputs to the water circulating through the crust mainly take the form of the products of *in situ* silicate hydrolysis or dissolution of evaporites, the latter being ultimately a product of the former. However, it is difficult to tell which is presently dominant since they have a similar outcome. To a large extent, the principal chemical characteristics of groundwater in the whole of the continental Eastern Rift are a product of this interaction: high Na, HCO_3 and F, and low Ca. The very highest concentrations are likely to be caused by evaporative enrichment when such waters reach the surface. At least some of the evaporating water at present originates from recirculation, as in the northern Suguta Valley of the KRV, but sometimes re-dissolution takes place with almost unmodified meteoric water, as at Magadi. The only area where silicate hydrolysis is apparently unimportant is in Afar, where it may be being masked by the acquisition of residual halite.

9.1.4   Structure

Rift structure has a varying effect on the geochemistry of rift fluids. At the simplest level, the surface expression of rift-floor structures may lead to the formation of lakes which promote evaporative enrichment of contributing ground and surface waters. This occurs at various scales: for example Lake Chitu in the MER, which owes its existence to a small volcanic crater, or the northern Suguta Valley and Magadi in the KRV, which are low-lying discharge

areas at or near the northern and southern extremities of the Kenya Dome.

The existence of "grid faulting" (faulting parallel or sub-parallel to the sides of the rifts) on the rift floors may be affecting groundwater chemical quality by preventing mixing between regional water flows (largely driven by recharge from the rift walls) and the high-temperature hydrothermal cells that exist beneath most of the volcanic centres of the inner trough areas of the various rifts. Insofar as groundwater geochemistry is able to provide information relating to physical hydrogeology, it supports the rather minor hydrogeological differences between the half-grabens of the KRV (especially in the South Turkana Rift) and the true graben of the MER.

The major faults at rift boundaries are obviously a factor to be taken into account when considering fluid geochemistry. They are likely to provide an effective conduit for infiltrating waters, promoting their circulation to considerable depth with the consequent acquisition of heat from the enhanced geothermal gradients common to the rift areas. Thus many low-enthalpy hot springs are encountered near the edge of the KRV and MER. (In Afar this effect is largely missing, though local hydrothermal circulation still produces some hot springs.) Despite the heating, water-rock interaction does not always seem to be particularly marked: sites such as Kureswa and Majiyamoto in the KRV and Kenteri in the MER demonstrate this. Most other rift-side springs are however more chemically evolved. This may well be due to fluxes of CO_2 up the faults promoting silicate hydrolysis. If this is so, however, there seems to be rather little ^{3}He involved. In both the KRV and MER, ^{3}He/^{4}He values decline away from the central volcanic structures. This makes it appear that although CO_2 may be ubiquitous in the Eastern Rift (and possibly some distance outside it), it is only through magmatic action that ^{3}He is readily transported to the surface. This indicates that rift-boundary faults are probably normal rather than listric: the latter would be expected to transport helium from the central volcanoes rather more identifiably. This agrees with the conclusions of geophysical work in the KRV, that rift-boundary faults are of steep normal type.

9.2   Specific achievements of the present research

In addition to the broad overview that this research was intended to include, Chapter 1 made reference to five particular areas where more specific aims were stated. New observations, methods and concepts in the realisation of these aims are now considered.

Groundwater flow - Stable isotopes are highly effective tracers of groundwater origin and have

worked particularly well in the Eastern Rift. However, the novel element of their use in this research has been the attempt to use the stable isotopic ratios in fumarolic steam to calculate the ratios in deep underlying thermal groundwaters in areas where no spring or borehole waters exist. While it was only possible to validate the method to any extent in the vicinity of Olkaria in the southern KRV, the results in general had a realistic distribution. Coupled with this is the indication that there may be axial groundwater flow over considerable distances in the KRV.

Groundwater chemistry - The high bicarbonate concentrations in Eastern Rift waters have been attributed to a hydrolysis/evaporite dissolution mechanism on the basis of carbon stable isotope ratios. Although the carbonate lake of Magadi has received considerable attention from a chemical viewpoint, it had received little isotopic study before the present research. It is possible to rule out certain suggestions for the origin of high-TDS conditions, for example that evaporation at or near the ground surface during transport of solutes towards the lake is presently a major factor. Conversely, for the previously uninvestigated Suguta Valley area towards the other end of the KRV, isotopic and chemical differences from Magadi suggest that such evaporation *has* played an important role.

Palaeohydrology - While the existence of hydrothermal siliceous sinters of various Quaternary ages is unequivocal evidence of higher water levels in the past, the use of their oxygen isotope values to infer palaeo-$\delta^{18}O$ values in the hydrological cycle, while novel, cannot be regarded as infallible considering the assumptions necessary. Nevertheless, in the absence of suitable confined aquifers the technique remains the only way of estimating the isotopic content of palaeowaters during cooler climatic episodes. This could help the calibration of general circulation models (GCMs), which appear to be most vulnerable in low-latitude regions.

Outgassing - The CO_2 of the EARS undoubtedly originates in the underlying mantle, but carbon stable isotope ratios show that it is not totally restricted to the rift area. The CO_2 is rather heavier in ^{13}C than what is conventionally regarded as the mantle signature, but typical of geothermal areas elsewhere. The general lack of sedimentary precursors in the EARS suggests that the putative metamorphosis of limestones frequently invoked to explain $\delta^{13}C$ values in other geothermal areas is unnecessary. The use of helium isotope ratios has confirmed the belief that the large Ethiopian Plateau and the smaller Kenya Dome have different mantle reservoirs. In the previously unexplored northern KRV, signs of a relationship between He isotope ratio and crustal thickness have been detected. Results also suggest that He transport is related to magmatic outgassing, in common with other rift areas.

Geothermal applications - Stable isotopic techniques have been highly effective in showing where geothermal systems are being supplied predominantly by surface water (e.g. Olkaria, southern KRV) or by groundwater (e.g. Aluto-Langano in the MER). This kind of information has an important part to play in the effective management of water and energy resources. For geothermometry, solute methods have been found to be unreliable in the KRV, and of relatively little use in the MER, except where geothermal wells already exist for sampling purposes. The alternative, gas geothermometry, is also unsatisfactory for exploration, except in Djibouti. The idea of applying "corrections" to geothermometry temperatures elsewhere in the Eastern Rift using O and H stable isotope systematics, while original, has not been especially useful in practical terms. However, a new geothermometer using the concept of hydrocarbon breakdown has been proposed for the Eastern Rift on the basis of research into minor gases.

Some of the research carried out during this study has been published or is in the process of publication. Details are given in Appendix G.

9.3   Areas of further research

Some of these are of more immediate applicability than others, and so are divided into practical and theoretical categories.

9.3.1   Practical

The trace element content of waters in the Eastern Rift has not been investigated to any significant extent. Apart from possibly permitting further insights into hydrogeology generally, such as revealing greater detail about flowpaths and aquifer units, this topic could have important implications for the health of local communities. For example, some of the more primitive rift communities rely on condensed fumarolic steam for water supply, and it seems likely that this could contain excesses or deficiencies in certain elements.

In the drilled geothermal areas, oxygen isotope studies of hydrothermal systems based on the analysis of solid phases would complement the existing mineralogical information to provide a better understanding of system maturity and exploitation trends, and hence estimation of energy reserves.

9.3.2 Theoretical

A more detailed study of oxygen isotopes in siliceous sinters, particularly in the MER, might have palaeoclimatic applications, though further U-series dating would be required to provide a time-frame. The possible existence of palaeowater in the northern MER could also be investigated.

The study of sulphur stable isotopes in gases and dissolved sulphate would promote a better understanding of the sulphur cycle in the Eastern Rift: whether it is very largely magmatic, or whether there is an atmospheric or other input of any significance. Strontium and boron isotope ratios might also have an application, but probably not to the extent they do in other hydrothermal areas where there are the possibilities of important inputs from marine or sedimentary sources.

Opportunities for noble gas studies are far from exhausted as far as the Eastern Rift and its surroundings are concerned. While coverage of ^{3}He/^{4}He is reasonably adequate in the KRV, it is much more patchy in the MER and Southern Afar. Even in Kenya questions remain regarding the relationship of ^{3}He/^{4}He to crustal thickness and about the amount of He flux up the major rift boundary faults. Also, there are as yet no published He isotope data for the potentially interesting area of northern Afar, where the Erta Ale volcano is currently active, or for that matter outside the Ethiopian Rift at sites with CO_2 outgassing such as Ambo on the Ethiopian Plateau. Helium isotope studies might also help to resolve the relationships of off-axis volcanism (e.g. Kilimanjaro, Chyulu Hills, Mount Kenya and Mount Elgon) to the Rift. The effect of the buried Cretaceous Anza Graben on fluid fluxes from the mantle in the North Turkana area between the Kenya and Ethiopian domes might also be amenable to investigation using He isotope techniques.

Noble gas isotope ratios other than helium, i.e. those of argon, neon, krypton and xenon, would be of interest if applied to the hotspot area of the MER and Afar, but in most circumstances would probably have to be analysed on gases trapped in rocks to avoid uncorrectable dilution by atmospheric noble gases.

9.4   Concluding remarks

This study has provided a timely account of crustal fluids in a major portion of the East African Rift System. In particular it has shown the value of isotopic techniques for investigating a wide

range of processes. The work provides the first supporting evidence for the concept of long-distance axial flow in rift valleys, and extends the pre-existing knowledge of phenomena ranging from high-bicarbonate waters to geothermal systems to rift structure. While much more undoubtedly remains to be discovered about rift fluids in East Africa, it is hoped that the present study will form a useful foundation for such work in the future.

REFERENCES

Abell P I, Awramik S M, Osborne R H, Tomellini S (1982) Pleistocene lacustrine stromatolites from Lake Turkana, Kenya: morphology, stratigraphy and stable isotopes *Sedimentary Geology* **32**, 1-26

Allen D J and Darling W G (1982) Geothermics and hydrogeology of the Kenya Rift Valley between Lake Baringo and Lake Turkana. *British Geological Survey Research Report*, SD/92/1.

Allen D J, Darling W G and Burgess W G (1989) Geothermics and hydrogeology of the southern part of the Kenya Rift Valley with emphasis on the Magadi-Nakuru area. *British Geological Survey Research Report*, SD/89/1.

Andrews J N (1992) Mechanisms for noble gas dissolution by groundwaters. In *Isotopes of Noble Gases as Tracers in Environmental Studies*, IAEA, 87-110.

Andrews J N and Lee D J (1979) Inert gases in groundwater from the Bunter Sandstone of England as indicators of age and palaeoclimatic trends. *Journal of Hydrology* **41**, 232-252.

Armannsson H (1987) Studies on the Geochemistry of Steam in the Suswa and Longonot Geothermal Areas and Water in the Lake Magadi, Kedong Valley and Lake Turkana Areas, Rift Valley, Kenya. *UNDP Technical Report* for Project KEN/82/002.

Arnason B (1977) The hydrogen-water isotope thermometer applied to geothermal areas in Iceland. *Geothermics* **5**, 75-80.

Arnorsson, S and Gunnlaugsson, E (1985)   New gas geothermometers for geothermal exploration - calibration and application. *Geochimica et Cosmochimica Acta* **49**, 1307-1325.

Arnorsson S, Bjornsson S, Muna Z W and Bwire-Ojiambo S (1990) The use of gas chemistry to evaluate boiling processes and initial steam fractions in geothermal reservoirs with an example from the Olkaria field, Kenya. *Geothermics* **19**, 497-514.

Arusei M K (1992) Hydrochemistry of Olkaria and Eburru geothermal fields, Kenyan Rift Valley. In *Water-Rock Interaction*, (eds Y K Kharaka and A S Maest), Balkema, 1261-1265.

Ase L E, Sembo K and Per S (1986) Studies of Lake Naivasha, Kenya, and its drainage area. University of Stockholm Report STOU-NG 63.

Baker B H, Mohr P A and Williams L A J (1972) Geology of the Eastern Rift System of Africa. *Geological Society of America Special Paper* **136**, 67pp.

Baumann A, Forstner U and Rohde R. (1975) Lake Shalla: water chemistry, mineralogy and geochemistry of sediments in an Ethiopian Rift lake. *Geologische Rundschau* **64**, 593-609.

Bodvarrsson S, Pruess K, Stefansson V, Bjornsson S and Ojiambo S B (1987) East Olkaria geothermal field, Kenya. 1: History match with production and pressure data decline. *Journal of Geophysical Research* **92**, B1, 521-539

Bosch B, Deschamps J, Leleu M, Lopoukhine M, Marcel A and Vilbert C (1977) The geothermal zone of Lake Asal (TFAI). Geochemical and experimental studies. *Geothermics* **5**, 166-175.

BRGM (Bureau de Recherches Geologiques et Minières) (1983) Construction d'un modéle synthétique du champ géothermique d'Asal. *Rapport du BRGM* 82 SGN 951 GTH.

Butzer K W (1971) Recent history of an Ethiopian delta, the Omo River and the level of Lake Turkana. *Research Papers of the Department of Geography, University of Chicago* **1361**, 184pp.

Butzer K W, Isaac G L, Richardson J L and Washbourn-Kamau C (1972) Radiocarbon dating of East African lake levels. *Science* **175**, 1069-1076.

Calmbach L (1994) *Hydrowin V3.0* (groundwater chemical equilibria programs for personal computer). Institut de Mineralogie, Universite de Lausanne.

Capaccioni B, Martini M, Mangani F, Giannini L, Nappi G and Prato F (1993) Light hydrocarbons in gas emissions from volcanic areas and geothermal fields. *Geochemical Journal* **27**, 7-17.

Casanova J and Hillaire-Marcel C (1992) Chronology and palaeohydrology of late Quaternary high lake levels in the Manyara basin (Tanzania) from isotopic data (^{18}O, ^{13}C, ^{14}C, Th/U) on fossil stromatolites. *Quaternary Research* **38**, 205-226.

Chernet T (1988) *Hydrogeological Map of Ethiopia*. Ethiopian Institute of Geological Surveys, Addis Ababa.

Cioni R, Fanelli G, Guidi M, Kinyariro J K and Marini L (1992) Lake Bogoria hot springs (Kenya): geochemical features and geothermal implications. *Journal of Volcanology and Geothermal Research* **50**, 231-246.

Clarke M C G and Roberts B (1986) Carbonated melilites and calcitized alkalicarbonatites from Homa Mountain, western Kenya: a reinterpretation. *Geological Magazine* **123**, 683-692.

Clarke M C G, Woodhall D G, Allen D J and Darling W G (1990) Geological, volcanological and hydrogeological controls on the occurrence of geothermal activity in the area surrounding Lake Naivasha, Kenya. *Ministry of Energy Report*, Nairobi.

Clayton R N, O'Neil J R and Mayeda T K (1972) Oxygen isotope exchange between quartz and water. *Journal of Geophysical Research* **77**, 3057-3067.

Coleman R G (1993) *Geologic Evolution of the Red Sea*. Clarendon Press, 186pp.

Coleman M L, Shepherd T J, Durham J J, Rouse J E and Moore G R (1982) Reduction of water with zinc for hydrogen isotope analysis. *Analytical Chemistry* **54**, 993-995.

Craig H (1961) Isotopic variations in meteoric waters. *Science* **133**, 1702-1703.

Craig H, Lupton J E and Horowitz R M (1977) Isotopic Geochemistry and Hydrology of Geothermal Waters in the Ethiopian Rift Valley. *Scripps Institute of Oceanography Report* 77-14.

D'Amore F and Panichi C (1980) Evaluation of deep temperatures in hydrothermal systems by a new gas geothermometer. *Geochimica et Cosmochimica Acta* **44**, 549-556.

Darling W G (in revision) Hydrothermal hydrocarbon gases: 1, Genesis and geothermometry. *Applied Geochemistry*.

Darling W G and Armannsson H (1989) Stable isotopic aspects of fluid flow in the Krafla, Namafjall and Theistareykir geothermal systems of northeast Iceland. *Chemical Geology* **76**, 197-213.

Darling W G and Lardner A J (1985) The effect of altitude on the stable isotopic compositions in the Balquhidder research catchments. *British Geological Survey Hydrogeology Group Stable Isotope Technical Report* 27.

Darling W G and Talbot J C (1991) Evaluation and development of gas geothermometry for geothermal exploration in the East African Rift System. *British Geological Survey Technical Report* WD/91/72.

Darling W G, Allen D J and Armannsson H (1990) Indirect detection of subsurface outflow from a Rift Valley Lake. *Journal of Hydrology* **113**, 297-305.

Davies G R, Norry M J and Jones P W (1994) Spatial and temporal variations in the geochemistry of the Ethiopian flood basalts province. In *Abstracts of the 8th International Conference on Geochronology, Cosmochronology and Isotope Geology* (Eds M A Lanphere, G B Dalrymple and B D Turrin). United States Geological Survey Circular 1107, 75.

Deines P (1980) The isotopic composition of reduced organic carbon. In *Handbook of Environmental Isotope Geochemistry, Vol. 1: The Terrestrial Environment, A*, (eds P Fritz and J C Fontes), Elsevier, 329-406.

Des Marais D J, Stallard M L, Nehring N L and Truesdell A H (1988) Carbon isotope geochemistry of hydrocarbons in the Cerro Prieto geothermal field, Baja California Norte, Mexico. *Chemical Geology* **71**, 159-167.

Dunkley P N, Smith M, Allen D J and Darling W G (1993) The geothermal activity and geology of the northern sector of the Kenya Rift Valley. *British Geological Survey Research Report* SC/93/1.

ELC-Electroconsult and Geotermica Italiana Srl 1986 Geothermal Reconnaissance Study of Selected Sites of the Ethiopian Rift System. Second Interim Report to EIGS.

Ellis A J and Mahon W A J (1977) *Chemistry and Geothermal Systems,* Academic Press.

Endeshaw A (1988) Current status (1987) of geothermal exploration in Ethiopia. *Geothermics* **17**, 477-488.

Endeshaw A and Belaineh M (1990) Status of geothermal energy in Ethiopia. *Geothermal Resources Council Transactions* **14**, 47-53.

Epstein S and Mayeda T (1953) Variations of the O^{18} content of waters from natural sources. *Geochimica et Cosmochimica Acta* **4**, 213-223.

Eugster H P (1970) Chemistry and origin of the brines of Lake Magadi, Kenya. *Mineralogic Society of America Special Paper* **33**, 215-235.

Eugster H P (1980) Lake Magadi, Kenya, and its precursors. In *Developments in Sedimentology: 28, Hypersaline Brines and Evaporitic Environments.* (Ed A Nissenbaum). Elsevier, 195-232.

Fontes J C, Florkowski T, Pouchan P and Zuppi G M (1979) Preliminary isotopic study of Lake Asal system (Republic of Djibouti). In *Isotopic Lake Studies*, IAEA, 163-174.

Fontes J C, Pouchan P, Saliege J F and Zuppi G M (1980) Environmental isotope study of groundwater systems in the Republic of Djibouti. In *Arid Zone Hydrology*, IAEA, 237-262.

241

Fournier R.O. (1981) Application of water geochemistry to geothermal exploration and reservoir engineering. In *Geothermal Systems: Principles and Case Histories* (ed L L Rybach and L G P Muffler). John Wiley & Sons Ltd, Chapter 4, pp 109-143.

Fournier R O (1989) Lectures on Geochemical Interpretation of Hydrothermal Water. Report 10/89, UNU Geothermal Training Programme, Orkustofnun, Iceland.

Friedman I, Gleason J and Jackson T (1987) Variation of $\delta^{13}C$ in fumarolic gases from Kilauea Volcano. In *Volcanism in Hawaii*, (eds R S Decker, T L White and P H Stauffer), United States Geolological Survey Professional Paper 1350.

Geotermica Italiana Srl (1987a) Geothermal Reconnaissance Survey in the Menengai-Bogoria Area of the Kenya Rift Valley. Report TCD CON 7/85 for UNDP Project KEN 82/002.

Geotermica Italiana Srl (1987b) Geochemistry of North Ghoubbat Asal Region. Report to ISERST.

Giggenbach W F (1980) Geothermal gas equilibria. *Geochimica et Cosmochimica Acta* **44**, 2021-2032.

Giggenbach W F and Glover R B (1992) Tectonic regime and major processes governing the chemistry of water and gas discharges from the Rotorua geothermal field, New Zealand. *Geothermics* **21**, 121-140.

Gizaw B (1986) Southern Afar Geothermal Reconnaissance Study: Fantale area, Ethiopian Rift Valley. Preliminary geochemical report, Ethiopian Institute of Geological Surveys.

Gizaw B (1989) *Geochemical Investigation of the Aluto-Langano Geothermal Field, Ethiopian Rift Valley*. M Phil Thesis (unpublished) University of Leeds.

Gizaw B (1993) Aluto-Langano geothermal field, Ethiopian Rift Valley: physical characteristics and the effects of gas on well performance. *Geothermics* **22**, 101-116.

Gizaw B (1996) The origin of bicarbonate and fluoride in waters of the Main Ethiopian Rift Valley. *Journal of African Earth Sciences* **22**, 391-402.

Glover R B (1972) Chemical characteristics of water and steam discharges in the Rift Valley of Kenya. *UNDP Technical Report.*

Glover R B (1976) Geochemical investigations in the Lakes District and Afar of Ethiopia. *DSIR Chemistry Division Report*, Wairakei, N.Z.

Green V W, Achauer U and Meyer R P (1991) A three-dimensional seismic image of the crust and upper mantle beneath the Kenya Rift. *Nature* **354**, 199-203.

Griesshaber E, O'Nions R K and Oxburgh E R (1992) Helium and carbon isotope systematics in crustal fluids from the Eifel, the Rhine Graben and the Black Forest, FRG. *Chemical Geology* **99**, 213-235.

Gunter B D and Musgrave B C (1971) New evidence on the origin of methane in hydrothermal gases. *Geochimica et Cosmochimica Acta* **35**, 113-118.

Haukwa C B (1986) Interpretation of well measurements for exploration areas and reservoir changes in Olkaria East Field. *Kenya Power and Light Co Technical Report.*

Henry W J, Mechie J, Maguire P K H, Khan M A, Prodehl C, Keller G R and Patel J (1990) A seismic investigation of the Kenya Rift Valley. *Geophysics Journal International* **100**, 199-203.

Hillaire-Marcel C and Casanova J (1987) Isotopic hydrology and palaeohydrology of the Magadi (Kenya) - Natron (Tanzania) basin during the late Quaternary. *Palaeogeography, Palaeoclimatology and Palaeoecology* **58**, 155-181.

Hilton D R, Gronvold K, O'Nions R K and Oxburgh E R (1990) Regional distribution of ^{3}He anomalies in the Icelandic crust. *Chemical Geology* **88**, 53-67.

Hilton D R, Gronvold K, Sveinbjornsdottir A E and Hammerschmidt K (1995) Mapping the Icelandic Hotspot: a helium isotope study utilising off-axis geothermal fluids. *Eos* **76**, No 46, F709.

IAEA (International Atomic Energy Agency) (1971) Environmental isotope data No 3: world survey of isotope concentration in precipitation (1966-1967). *IAEA Technical Reports Series* **129**.

IAEA (International Atomic Energy Agency) (1973) Environmental isotope data No 4: world survey of isotope concentration in precipitation (1966-1967). *IAEA Technical Reports Series* **147**.

IAEA (International Atomic Energy Agency) (1992) *Statistical Treatment of Isotopes in Precipitation*, IAEA, Vienna.

James T C (1967) Thermal springs in Tanzania. *Transactions of the Institute of Mining and Metallurgy* **76**, B2-18.

Javoy M, Pineau F, Staudacher T, Cheminee J L and Kraft M (1989) Mantle volatiles sampled from a continental rift: the 1988 eruption of Oldoinyo Lengai (Tanzania). *Terra* abstracts **1**, 324.

Jones B F, Eugster H P and Rettig S L (1977) Hydrochemistry of the Lake Magadi basin, Kenya. *Geochimica et Cosmochemica Acta* **44**, 53-72.

Keller R G, Braile L W, Davis P M, Meyer R P and Mooney W D (1992) Kenya Rift International Seismic Project 1989-90 experiment. *Eos* **73**, 345-351.

Keller R G and 12 co-authors (1994) The East African Rift System in the light of KRISP 90. *Tectonophysics* **236**, 465-483.

Khaireh A E (1989) Borehole Geology of Well Asal-5, Asal Geothermal Field, Djibouti. Report 6/89, UNU Geothermal Training Programme, Orkustofnun, Iceland.

Lepine J C and Hirn A (1992) Seismotectonics in the Republic of Djibouti, linking the Afar Depression and the Gulf of Aden. *Tectonophysics* **209**, 65-86.

Lupton J E (1983) Terrestrial inert gases: isotope tracer studies and clues to primordial components in the mantle. *Annual Reviews of Earth and Planetary Science* **11**, 371-414.

Lyon G L and Hulston J R (1984) Carbon and hydrogen isotope composition of New Zealand geothermal gases. *Geochimica et Cosmochimica Acta* **48**, 1161-1171.

Macdonald R (1994) Petrological evidence regarding the evolution of the Kenya Rift Valley. *Tectonophysics* **236**, 373-390.

Mamyrin B A and Tolstikhin I N (1984) *Helium Isotopes in Nature*, Developments in Geochemistry 3, Elsevier.

Mariano A N (1989) Nature of economic mineralisation in carbonatites and related rocks. In *Carbonatites - Genesis and Evolution* (ed K Bell), Unwin Hyman, 149-176.

Marty B (1992) Volcanic fluxes of volatiles: Preliminary estimates based on rare gas and major volatile calibration. In *Isotopes of Noble Gases as Tracers in Environmental Studies*, IAEA, 295-301.

Marty B, Appora I, Barrat J A, Deniel C, Vellutini P and Vidal P (1993) He, Ar, Sr, Nd and Pb isotopes in volcanic rocks from Afar: Evidence for a primitive mantle component and constraints on magmatic sources. *Geochemical Journal* **27**, 219-228.

McCann D L (1974) Hydrogeologic Investigation of the Rift Valley Catchments. *UNDP Technical Report*.

Meyer W, Pilger A, Rosler A and Stets J (1975) Tectonic evolution of the northern part of the Main Ethiopian Rift in southern Ethiopia. In *Afar Depression of Ethiopia* (Eds A Pilger and A Rosler), Schweizerbart, 352-362.

Mohr P (1963) *The Geology of Ethiopia*. University College of Addis Ababa Press.

Mohr P (1967) The Ethiopian Rift System. *Bulletin of the Geophysical Observatory of Addis Ababa* **11**, 1-65.

Mohr P (1978) Afar. *Annual Reviews in Earth and Planetary Science* **6**, 145-172.

Morgan, P (1973) *Terrestrial heat flow studies in Cyprus and Kenya*. PhD thesis (unpublished), Imperial College, London, UK.

Muna Z W (1984) An attempt to build a reservoir model from the chemistry of well discharges in the Olkaria field. *Kenya Power and Light Co Technical Report.*

Nicholson S E and Flohn H (1980) African environmental and climatic changes in the general atmospheric circulation in the late Pleistocene and Holocene. *Climate Change* **2**, 313-348.

Nier A O (1950) A redetermination of the relative abundances of the isotopes of carbon, nitrogen, oxygen, argon and potassium. *Physics Review* **77**, 789.

Nyamweru C (1989) New evidence for the former extent of the Nile drainage system. *Geographical Journal* **155**, 179-188.

Ohmoto H and Rye R O (1979) Carbon and sulfur in ore bodies. In *Hydrothermal Ore Deposits* (ed H L Barnes), Wiley, 509-567.

Olsen K H and Morgan P (1995) Introduction: Progress in understanding continental rifts. Chapter 1 in *Continental Rifts: Evolution, Structure, Tectonics*, (Ed K H Olsen), Developments in Geotectonics 25, Elsevier, 3-26.

Oxburgh E R and O'Nions R K (1987) Helium loss, tectonics and the terrestrial heat budget. *Science* **237**, 1583-1588.

Panichi C and Tongiorgi E (1974). Isotopic study of the hot water and steam samples of the Rift Valley, Kenya. *United Nations Development Programme Report*, 56pp

Panichi, C, Ferrara, G C and Gonfiantini, R (1975) Isotope geochemistry in the Lardarello geothermal field. *Geothermics* **5**, 81-88.

Pickford M (1982) The tectonics, volcanics and sediments of the Nyanza Rift Valley, Kenya. *Zeitschrift Geomorphologie* **42**, 1-33.

Poreda R J, Craig H, Arnorsson S and Welhan J A (1992) Helium isotopes in Icelandic geothermal systems: 1. ^{3}He, gas chemistry, and ^{13}C relationships. *Geochimica et Cosmochimica Acta* **56**, 4221-4228.

Potter R W and Clynne M A (1978) The solubility of the noble gases He, Ne, Ar, Kr and Xe in water up to the critical point. *Journal of Solution Chemistry* **7**, 837-844.

Reardon E J and Fritz P E (1978) Computer modellimg of groundwater ^{13}C and ^{14}C isotope compositions. *Journal of Hydrology* **36**, 201-224.

Rosendahl B R (1987) Architecture of continental rifts with special reference to east Africa. *Annual Reviews of Earth and Planetary Science* **15**, 445-503.

Sanjuan B, Michard G and Michard A (1990) Origine des substances dissoutes dans les eaux des sources thermales et des forages de la region Asal-Ghoubbet (Republique de Djibouti). *Journal of Volcanology and Geothermal Research* **43**, 333-352.

Schoell M and Faber E (1976) Survey on the isotopic composition of waters from NE Africa. *Geologische Jahrbuch* **D17**, 197-213.

Sikes H L (1935) Notes on the hydrology of Lake Naivasha. *Journal of the East Africa and Uganda Natural History Society* **13**, 74-89.

Smith M (1994) Stratigraphic and structural constraints on mechanisms of active rifting in the Gregory Rift, Kenya. *Tectonophysics* **236**, 3-22.

Smith M and Mosley P N (1993) Crustal heterogeneity and basement influence on the development of the Kenya Rift, East Africa. *Tectonics* **12**, 591-606.

Smith M, Dunkley P N, Deino A, Williams L A J and McCall G J H (1995) Geochronology, stratigraphy and structural evolution of Silali volcano, Gregory Rift, Kenya. *Journal of the Geological Society of London* **152**, 297-310.

Street F A (1979) *Late Quaternary Lakes in the Ziway-Shalla Basin, Southern Ethiopia*. PhD Thesis (unpublished), Cambridge University, 493pp.

Sturchio N C, Dunkley P N and Smith M (1993) Climate-driven variations in the geothermal activity in the northern Kenya Rift Valley. *Nature* **362**, 233-234.

Tiercelin J J, Vincens A and 26 co-authors (1987) Le demi-graben de Baringo-Bogoria, Rift Gregory, Kenya: 30,000 ans d'histoire hydrologique et sedimentaire. *Bulletin Centres de Recherche d'Exploration-Productiom Elf Aquitane* **II**, 249-540.

Tissot B P and Welte D H (1984) *Petroleum Formation and Occurrence*, Springer-Verlag, 699 pp.

Truesdell A H and Jones B F (1974) WATEQ, a computer program for calculating chemical equilibria of natural waters. *United States Geological Survey Journal of Research* **2**, 233-248.

Truesdell A H and Hulston J (1980) Isotopic evidence on environments of geothermal systems. In *Handbook of Environmental Isotope Geochemistry, Vol. 1: The Terrestrial Environment, A,* (eds P Fritz and J C Fontes), Elsevier, 179-226.

Verhagen B T, Geyh M A, Frohlich K and Wirth K (1991) Djibouti (Chapter 7). In *Isotope Hydrological Methods for the Quantitative Evaluation of Ground Water Resources in Arid and Semi-arid Areas: Development of a Methodology.* Federal Institute of Geosciences and Mineral Resources, Hanover, 89-104.

Von Damm K L and Edmond J M (1984) Reverse weathering in the closed-basin lakes of the Ethiopian Rift. *American Journal of Science* **284**, 835-862.

Welhan J A and Craig H (1983) Methane, hydrogen and helium in hydrothermal fluids at 21°N on the East Pacific Rise. In *Hydrothermal Processes in Seafloor Spreading Centres*, (eds P A Rona, K Boström, L Laubier and K L Smith), Plenum Press, 391-409.

Wheildon J, Morgan P, Williamson K H, Evans T R and Swanberg C A (1994) Heat flow in the Kenya rift zone. *Tectonophysics* **236**, 131-149.

Wilhelm E, Battino R and Wilcock R J (1977) Low-pressure solubility of gases in liquid water. *Chemical Reviews* **77**, 219-262.

Wolde B (1989) Cenozoic volcanism and rift development in Ethiopia. *Journal of African Earth Sciences* **8**, 99-105.

WoldeGabriel G, Aronson J L and Walter R C (1990) Geology, geochronology and rift basin development in the central sector of the Main Ethiopian rift. *Geological Society of America Bulletin* **102**, 439-458.

WRAP (Water Resource Assessment Project) (1987) Water resource assessment study in Baringo District. Water Resource Assessment Division Report, Ministry of Water Development, Kenya.

Wright E P and Gunston H (eds) (1988) The Chyulu Hills water resources study, Kenya: 1984-1987. *British Geological Survey Technical Report* WD/88/5C.

Yuretich R F and Cerling T E (1983) Hydrogeochemistry of Lake Turkana, Kenya: Mass balance and mineral reactions in an alkaline lake. *Geochimica et Cosmochimica Acta* **47**, 1099-1109.

Zan L, Gianelli G, Passerini P, Troisi L and Haga O A (1990) Geothermal exploration in the Republic of Djibouti: thermal and geological data of the Hanle and Asal areas. *Geothermics* **19**, 561-582.

APPENDIX A

Research and survey work of relevance to fluid geochemical studies in the Eastern Rift

Table A.1   Investigating teams and sources of fluid geochemical data for the Eastern Rift.

Country/locality (State Organisation)	"Normal" gases	C_2-C_5 HCs	Carbon isotopes	Helium isotopes	Hydro-chemistry
Kenya (MERD, KPLC)					
Magadi, Bala	BGS[1,14]	BGS[1,14]	BGS[14]	BGS[1]	BGS[1]
Suswa-Longonot-Domes	UNDP[2] BGS[1]	BGS[1]	BGS[1]	BGS[1] ?SIO	BGS[1]
Olkaria-Eburru	UNDP[3] KPLC[5] BGS[1,14]	BGS[14]	UNDP[3] BGS[14]	BGS[1]	UNDP[4] BGS[1] KPLC[16]
Menengai-Bogoria	UNDP[3] GIS[6] BGS[14,15]	BGS[15]	BGS[15]	BGS[15]	GIS[6]
Baringo-Turkana	BGS[7]	BGS[7]	BGS[7]	BGS[7,u]	BGS[7]
Ethiopia (EIGS)					
Abaya-Langano	UNDP[8] SIO[9] EIGS[10] BGS[14]	BGS[14]	SIO[9] BGS[14]	SIO[9] BGS[u]	EIGS/SIO[9]
Sodere-Tendaho	UNDP[8] SIO[9] ELC[11]	-	SIO[9]	SIO[9] BGS[u]	EIGS/SIO[9]
Djibouti (ISERST, EDD)					
Asal-Abbe	BRGM[12] GIS[13] BGS[14]	BGS[14]	?BRGM BGS[u]	BGS[u]	BMZ[17]

"Normal" gases - CO_2, CH_4, H_2, H_2S, N_2 HCs - hydrocarbons

BGS	British Geological Survey
BRGM	Bureau de Recherches Geologiques et Minières
BMZ	Bundesministerium fur Wirtschaftliche Zusammenarbeit
EDD	Electricité de Djibouti
EIGS	Ethiopian Institute of Geological Surveys
ELC	ELC Electroconsult
GIS	Geotermica Italiana Srl
ISERST	Institut Superieur d'Etudes et de Recherches Scientifiques
KPLC	Kenya Power and Light Company
MERD	Ministry of Energy and Regional Development
SIO	Scripps Institute of Oceanography
UNDP	United Nations Development Programme

1. Allen et al (1989)
2. Armannsson (1987)
3. Glover (1972)
4. McCann (1974)
5. Muna (1984)
6. Geotermica Italiana Srl (1987a)
7. Dunkley et al (1993)
8. Glover (1976)
9. Craig et al (1977)

10. Endeshaw (1988)
11. ELC Electroconsult and Geotermica Italiana Srl (1986)
12. BRGM (1983)
13. Geotermica Italiana Srl (1987b)
14. Darling and Talbot (1991)
15. Darling et al (1995)
16. Arusei (1992)
17. Verhagen et al (1991)
u. Unpublished data

APPENDIX B

Sampling and Analysis

B.1   Sampling and field measurements

B.1.1   Water

Water was sampled from boreholes, ambient and thermal springs, rivers and lakes. Samples for chemical analysis were filtered at 0.45μ pore size under wellhead or syringe pressure. Two 30-ml plastic tubes were collected for each sample, one acidified to a pH of >2 with concentrated HCl or HNO_3 to stabilise cations, and the other unacidified for the analysis of anions. For hot springs a third plastic tube was filled with a 1:10 mixture of sample with deionised water, to enable high silica contents to be analysed without problems arising from silica precipitation on cooling.

Samples for oxygen ($\delta^{18}O$) and hydrogen (δ^2H) stable isotope analysis were collected without treatment into 28-ml McCartney glass bottles with neoprene-lined caps. Waters for isotopic measurement of dissolved inorganic carbon ($\delta^{13}C$-DIC) were collected in 250-ml glass bottles and usually precipitated in the field with alkaline $BaCl_2$ solution.

Samples for tritium (^3H) analysis were collected in 500-ml glass bottles, while sampling for radiocarbon (^{14}C) analysis of the DIC fraction entailed the collection of two 60-litre aspirators unless there was a high DIC content, in which case one was sufficient. Field precipitation with alkaline $BaCl_2$ was carried out, with $FeSO_4$ added to accelerate flocculation where necessary. The resulting pairs of carbonate precipitates were subsequently bulked together in 2.5-litre polythene bottles.

For the analysis of noble gases water samples were collected (from boreholes and springs only) in tubes of soft-annealed copper, sealed at each end by swage clamps. Care was taken to exclude atmospheric contamination as far as possible. In the case of springs this meant trying to intercept the inflow of water as early as possible, and passing it through the copper tube by use of a hand pump *via* a conical flask, similar to the sampling methods for gases shown in Fig B.1a below.

B.1.2   Gas

Gas phase samples (including steam where present) were collected from geothermal wells, fumaroles, bubbling springs, mofettes and a CO_2 production borehole. From wells and fumaroles, usually two samples were collected: one as a free gas sample in a glass tube, and one over concentrated NaOH solution in a pre-evacuated glass flask to collect CO_2 and H_2S (if present) and thereby to allow the determination of gas/water ratio. A schematic of the collection process is shown in Fig B.1b. Free gases were taken from the steam source in a

doubly-terminated glass tube via a stainless steel or copper condensing coil. The coil was immersed in cooling water or, where transport of sufficient water was impractical, was wrapped in lint which was kept moist (the latent heat required to evaporate water makes a highly effective cooling mechanism). An arrangement of two tubes was generally used (Fig B.1b), the first being used to trap condensed water before being upended to fill the second

(Fig B.1b). This process caused the first tube to fill with gas, whenever possible by a combination of gravity drainage and gas pressure alone to minimise the possibility of air contamination. However, weaker fumaroles required some assistance from a hand pump. The water collected during the process was sub-sampled for stable isotope and sometimes chemical analysis. For determination of gas/water ratio samples were collected directly from the steam source into pre-evacuated singly-terminated flasks containing 50 ml of 40% NaOH (Fig B.1c).

Gases from warm and hot springs were collected in a variety of ways depending on the nature of individual springs. For very gassy springs, such as Lorusio (K45) and particularly Bala (K53), a method similar to Fig B.1b was used. For cooler, less gassy springs a method resembling Fig B.1c was employed, except that NaOH was not used.

In all cases where gases were collected, great care was taken to purge all atmospheric gases from the various tubes and vessels involved.

B.1.3 Field measurements

Measurements of pH, temperature and alkalinity (as HCO_3^-) were made at the time of sampling. For pH determinations, samples and buffers were measured at similar temperatures using a Kane-May KM7002 meter with Orion electrodes. Buffers of pH 4, 7 and 9 were used depending on sample source (condensed steam tended to be acid, while many spring sources were alkaline). Temperatures were measured by thermocouple probes or mercury-in-glass thermometers. Alkalinity was determined by titration on a Hach kit, or titration on a standard burette using either an indicator or pH electrode to mark the end point.

B.2 Analysis

B.2.1 Water chemistry

Chemical analysis was carried out at BGS Wallingford using atomic emission spectrophotometry for all species except for halides, which were analysed by automated colorimetry, and alkalinity, which was measured by electronic titrimetry when field measurement had no been carried out. Ionic balances were in most cases within $\pm$ 5%. The precision of analyses is indicated by the significant figures quoted in the various tables of results in Chapter 6.

B.2.2 Water isotopes

Stable isotopes of oxygen, hydrogen and carbon were measured at BGS Wallingford on a VG-602E dual-analyser dynamic mass spectrometer. Preparation methods were isotopic equilibration with CO_2 for $\delta^{18}O$ (Epstein and Mayeda, 1953), reduction with zinc for δ^2H (Coleman et al, 1982), and liberation of CO_2 from precipitated $BaCO_3$ using anhydrous H_3PO_4 for $\delta^{13}C$-DIC. Full details of preparation techniques are given in Darling et al, 1982). Analytical precisions for $\delta^{18}O$, δ^2H and $\delta^{13}C$-DIC were estimated to be ±0.2, ±2 and ±0.3‰ respectively for preparation and analysis of "normal" samples. Some samples with high total
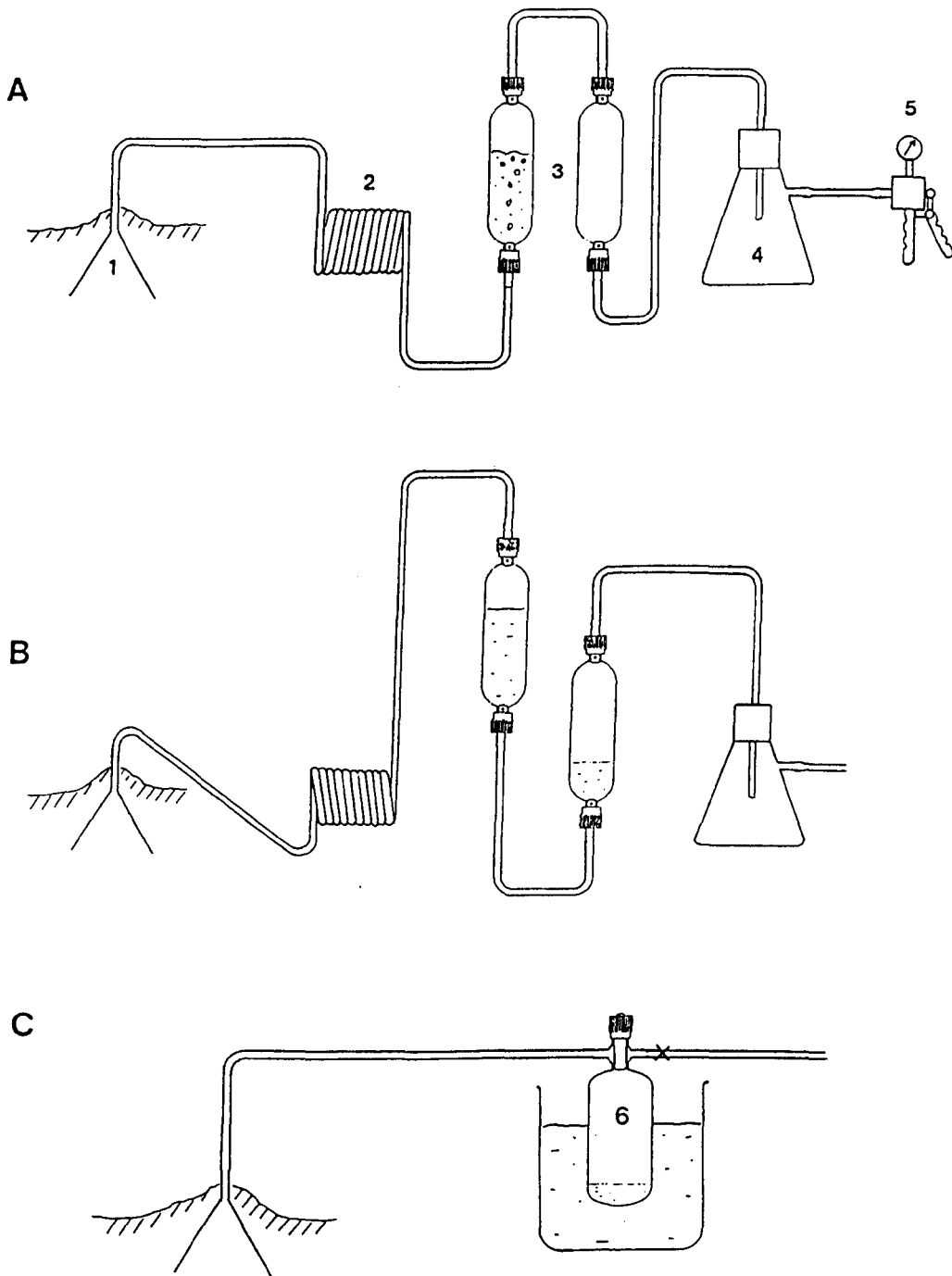
Fig B.1a-c Collection techniques for geothermal gases in the Eastern Rift. (a) steam condensate is collected in first tube by pumping. (b) condensate is transferred to second tube by gravity, leaving gas sample in first tube. (c) collection of separate combined steam and gas sample into NaOH solution. (1 - collecting funnel, 2 - condensing coil, 3 - glass gas tubes, 4 - water trap, 5 - hand pump, 6 - flask containing 50 ml of 40% NaOH.)

dissolved solids (TDS) caused analytical difficulties which are described in B.5 below.

Radiocarbon measurements were made at the Natural Environment Research Council's Radiocarbon Laboratory at East Kilbride by radioactive counting of benzene produced from CO_2 liberated from the $BaCO_3$ precipitate collected in the field. Tritium analyses were made by the DSIR Institute of Nuclear Sciences in New Zealand, using a preparation process of pre-distillation and electrolytic enrichment, and analysis by liquid scintillation counting. Measurement precisions for ^{14}C and ^3H are given in the results tables in Chapter 5.

B.2.3 Gas chemistry

Analysis of gases other than H_2S and NH_3 was carried out at BGS Wallingford by packed-column chromatography, using Porapak and MS5A columns and thermal conductivity (TCD) and flame ionisation (FID) signal detection output to a chart recorder or integrator. CO_2 and H_2S concentrations in steam were determined by titration of the NaOH condensate. Analytical precisions varied over the period of investigations, partly owing to use of different equipment at various times and also the nature of the samples (i.e. free gas or condensate residue). The precisions are indicated by the significant figures quoted in the results tables in Chapter 7.

Noble gas (argon, neon, krypton and xenon) concentrations were analysed using isotope dilution techniques on an Kratos MS10S static mass spectrometer at the University of Bath following preparation by removal of water with a cold trap, adsorption of N_2 onto a titanium getter at 800°C, and selective separation on charcoal traps. N_2/Ar was measured on samples to which no tracer additions were made.

B.2.4 Gas isotopes

The analysis of $\delta^{13}C$ in gases was carried out at BGS Wallingford using the free gas samples for CO_2, and (usually) the residual gases overlying NaOH condensates for CH_4. CO_2 gas was prepared for mass spectrometry by freezing in liquid nitrogen (LN_2, -196°C) and pumping off the non-condensable gases, followed by the freezing out of water vapour at -60°C. Methane was first converted to CO_2 by passing it over CuO at 850°C, then dried as for CO_2. When methane in free gas samples was analysed, separation from existing CO_2 was effected by LN_2, supplemented by a Carbosorb-filled U-tube as an additional precaution. Reproducibility of $\delta^{13}C$ analysis including sampling and preparation steps is estimated to be within ± 0.2‰ for CO_2 and ± 0.5‰ for CH_4.

Hydrogen concentrations were almost always too low to make isotopic analysis feasible. However, in a few cases this was done by passing the NaOH condensate residual gases over copper metal at 400°C. Reproducibility is estimated to be within ± 10‰.

Measurement of $^{40}Ar/^{36}Ar$ was carried out on undiluted samples of Ar (otherwise as prepared in B.2.3 above) on the MS10S mass spectrometer at the University of Bath. Helium isotope measurements were made on VG-3000 static mass spectrometers at the University of Cambridge and the Gesellschaft fur Strahlung Institute at Neuherburg, Munich. Preparation

involved the removal of reactive gases by a combination of cold traps and zirconium-aluminium getters, and trapping of Ar, Kr and Xe onto activated charcoal. Measurement precisions for $^{40}Ar/^{36}Ar$ averaged $\pm 2\%$. Precisions for $^3He/^4He$ and He/Ne are estimated to be $\pm 1\%$ and $\pm 10\%$ respectively.

B.2.5 Analytical problems

While relatively few difficulties were encountered with the majority of samples, there were certain problem areas. Firstly, some waters had very high alkalinities (up to around 11,000 mgl^{-1} HCO_3 equivalent in some cases). While this did not appear to affect ionic balances to any significant degree, even when using laboratory-measured alkalinity values, it made the analysis of $\delta^{18}O$ difficult because the equilibration technique requires a water pH < 4 to avoid chemical absorption of CO_2. For normal samples, the addition of a drop of 50% HNO_3 is sufficient to give an appropriate pH, but some of the alkaline samples needed several ml of the acid. Analyses were corrected by measuring the $\delta^{18}O$ content of the acid and carrying out a simple mass-balance correction using the $\delta^{18}O$ measured for the acid. (An alternative method would have been to acidify with anhydrous H_3PO_4, which would have required no correction). The addition of varying amounts of HNO_3 meant that $\delta^{18}O$ precisions might exceed the $\pm 0.2\%o$ quoted above for routine determinations.

The analysis of trace gases (H_2, H_2S and hydrocarbons) was not in itself a problem, though detection limits varied with the equipment used. However, the analysis of $\delta^{13}C\text{-}CH_4$ was sometimes difficult owing to very low concentrations. At methane concentrations below 0.1% molar, precision of $\delta^{13}C\text{-}CH_4$ measurement may exceed the $\pm 0.5\%o$ quoted above.

The analysis of noble gases was compromised if there was significant atmospheric contamination. This might be due to entrained air in fumaroles or difficulties in excluding air from spring samples. For noble gas concentrations, air contamination is fairly easily detected because the ratios resulting from solution in water are different from their ratios in air. For helium isotope ratios, the ratio of He/Ne is used as an index of atmospheric contamination because unlike He, virtually all Ne is atmospherically derived. Accordingly, the results of noble gas analyses have to be interpreted with regard to the indicated atmospheric component.

B.3   Results

This section is concerned with the way in which analytical results are expressed, rather than the results themselves, which are given in the chapters to which they are most relevant.

B.3.1   Water chemistry

Apart from pH, all analyses are quoted in terms of milligrams per litre (mgl^{-1}). Strictly, at high salinities (e.g. at Magadi, Kenya or Asal, Djibouti) this is more correctly described as $mgkg^{-1}$. Some plots use the data converted to millimoles or milliequivalents to make particular points.

B.3.2   Water isotopes

Oxygen ($^{18}O/^{16}O$) hydrogen ($^2H/^1H$) and carbon ($^{13}C/^{12}C$) isotope ratios are expressed as $\delta-$values (in permil, ‰) in the following way:

$$\delta = [(R_{sample}/\ R_{std}) - 1] \times 10^3 \tag{B.1}$$

where $R = {^{18}O/^{16}O}$, $^2H/^1H$ or $^{13}C/^{12}C$ as appropriate, and the standard is SMOW (Standard Mean Ocean Water) for oxygen and hydrogen, and PDB (Pee Dee Belemnite) for carbon. Radiocarbon values are given in pmc (percent modern radiocarbon in the sample). Tritium values are expressed in TR (formerly TU), where 1TR is defined as 1 atom of ^3H in 10^{18} atoms of hydrogen.

B.3.3   Gas chemistry

Reactive gas (H_2, CO_2, N_2, O_2+Ar, CH_4 and C_{2+}) analyses are expressed on a dry-gas basis in mole percent (or, if present at low concentrations) as parts per million by volume (ppmv). When the concentration of gas in fumaroles is expressed relative to steam+gas, the units used are millimoles gas per kilogram steam (mmolekg^{-1}). Thus, providing the concentration of one or more gases in the steam is known, it is simple to convert between the two systems. CO_2 and H_2S in NaOH condensates were converted from mgl^{-1} in the condensate to mmolekg^{-1} in the original steam via a knowledge of the mass of steam condensed (i.e. the condensation vessel was weighed before and after sampling).

Noble gases (Ar, Ne, Kr, Xe and He) are expressed in the free phase as cm^3/cm^3 total gas, while in the dissolved phase as cm^3 STP/g water.

B.3.4   Gas isotopes

Carbon stable isotope analyses of CO_2 and CH_4 are expressed in permil as in eqn B.1 above. Argon isotope ratios are reported simply as $^{40}Ar/^{36}Ar$. Helium isotope ratios are presented in the form of sample ratio, corrected on the basis of Ne content for atmospheric contamination, relative to the ratio in air according to the following equations:

$$R/R_A = [(R_M/R_A)X - 1]/(X - 1) \tag{B.2}$$

where $R_A = {^3He/^4He}$ in the atmosphere
$\quad\quad R_M = {^3He/^4He}$ measured in the sample
$\quad\quad X = [(He/Ne)_{sample}\ \beta Ne]/[(He/Ne)_{air}\ \beta He]$

The terms βNe and βHe refer to the Bunsen solubility coefficients for He and Ne at appropriate temperature and pressure. For gas phase samples the β terms were not used.

B.4   Sequential sample analyses as indices of consistency

Some sites in Kenya were sampled more than once, with gaps of a year or more in between. Such samples can ideally provide a test of analytical consistency in the longer term, on the assumption that the source chemistry remains constant (though in reality this is not invariably the case).

B.4.1   Water chemistry and stable isotopes

Table B.1 gives the year and chemical analyses for sequential samples taken from springs and boreholes in the Gregory, South Turkana and Nyanza Rifts. The samples are listed in order of rising TDS content, which is broadly correlated with source temperature. For six out of the ten sites, agreement between the analyses is consistently good from low to very high TDS. In the four cases where agreement is less good, the differences lie in a consistent direction. In three of these cases, inputs of surface waters are implicated: the Ol Kokwe Island spring and the water supply well at Kampi Ya Samaki are both likely to be affected by the seasonal changes in composition known to affect the water of Lake Baringo, the latter particularly so from the evidence of the highly enriched stable isotope contents. The Nginyang Polytechnic well is considered on the grounds of its ^{13}C-DIC content and proximity to the Nginyang River to be a mixture of river and groundwater which may also be affected by seasonal changes. The reason for discrepancies at the fourth exception, Chesirimion, is less obvious (although changes in the turbidity of the water were noticed) but again the differences are in a consistent direction. It is highly unlikely in any of the four cases that laboratory dilutions could have been a cause of discrepancies, since the differences occur across anions and cations irrespective of the analytical methods used.

Samples from some of these sites were also analysed for stable isotope contents (Table B.2). Most of the δ^2H and δ^{18}O values are the same within analytical error. Discrepancies in δ^{18}O occur for two of the anomalous sites mentioned above, Kampi Ya Samaki and Nginyang Polytechnic. For Kampi Ya Samaki, the difference is consistent with the slight freshening with time of the well water, implying that the lake water had latterly a fresher, less evaporitically enriched composition. At the Nginyang well, the change in H and O isotopes also agrees with the slight freshening observed. By contrast, the Chesirimion waters show an enrichment in these isotopes, consistent with the change in time from a lower to higher TDS. This may also be the reason for the observed change in δ^{13}C-DIC, though in none of the cases is the agreement between sequential δ^{13}C values particularly good, for reasons that are not clear.

B.4.2   Gas chemistry and isotopes

Only two fumarole sites were sampled twice for gas chemistry (Table B.3). Korosi KR 23, a low-CO_2 fumarole, gave relatively consistent results. Paka PK 1 fumarole gave superficially very different results. However, on the assumption that virtually all of the N_2 and $O_2 + Ar$ is the result of air contamination, the amounts of CO_2 and CH_4 on an air-free basis are similar on both occasions. Therefore, while the air derived gases at KR 23 are likely to be entrained in the ground, the influx of air at PK 1 in 1989 is more probably due to a problem at the time

Table B.1   Results for sites in the KRV sampled on more than one occasion.   Results in mgl⁻¹.

Site	No	Year	T°C	pH	Na	K	Ca	Mg	HCO₃	Cl	SO₄	Si	Li	B	F
Chesirimion	K132	1988	-	7.2	94.8	7.4	2.2	1.1	199	14.4	9.6	43.1	0.03	0.06	3.6
		1989	34	7.1	107	7.5	2.4	1.2	235	21.0	9.5	50.4	0.04	0.07	3.5
Churo	K139	1988	28	7.2	131	4.5	1.7	0.3	326	13.9	4.8	24.9	<0.01	<0.06	1.2
		1989	-	8.2	133	4.7	1.6	0.3	313	17.5	5.0	24.3	<0.01	<0.06	1.1
Kampi Ya	K131	1988	-	7.7	263	21.0	18.8	16.7	727	55	22.7	31.1	0.05	0.13	43
Samaki		1991	-	8.2	227	18.5	16.0	13.9	637	47	11.4	29.2	0.04	0.12	-
Napeiton	K198	1989	37	7.6	468	8.0	7.1	4.3	855	155	77.5	28.3	0.06	0.08	14
		1991	37	7.8	471	7.8	7.1	4.2	899	156	79.7	27.2	0.06	0.08	-
Nginyang	K204	1989	36	8.4	1500	10.4	2.4	1.1	3490	218	165	18.7	0.09	0.23	44
Polytechnic		1991	34	8.5	1500	8.1	2.0	0.9	3460	195	145	17.6	0.08	0.21	-
Ol Kokwe Is	K71	1986	94	9.1	832	36.0	0.5	<0.7	1960	260	40.0	87.0	0.56	1.04	-
		1988	96	9.1	922	39.3	1.0	<0.1	1980	260	30.5	126	0.61	1.19	19
Kapedo	K48	1986	50	8.3	988	22.0	1.6	0.6	2000	215	80.0	35.6	0.06	0.87	-
		1988	51	8.3	1020	22.7	1.6	0.5	2140	210	83.0	33.0	0.05	0.92	28
		1989	50	8.4	994	23.3	1.7	0.6	2110	240	83.4	36.1	0.05	0.88	27
Lorusio	K45	1986	81	7.7	2150	57.0	3.0	0.2	4710	295	197	35.7	0.96	0.96	-
		1988	82	7.5	2120	55.8	3.0	0.2	5000	300	200	33.2	0.96	0.92	48
Bala	K53	1986	72	-	6430	108	160	0.4	12200	1800	1630	29.7	0.47	2.28	-
		1989	72	7.6	6670	111	164	0.4	13300	1850	1530	29.8	0.53	2.42	12.0
Little	K3	1985	85	-	10900	185	0.5	<0.4	20400	5550	160	39.4	1.13	8.04	170
Magadi		1989	83	8.8	11100	220	0.4	<0.1	19600	5350	151	33.0	1.30	7.83	180

Table B.2   Results for sites in the KRV sampled on more than one occasion: water stable isotopes in permil.

Site	No	Year	δ^2H ‰	$\delta^{18}O$ ‰	$\delta^{13}C_{DIC}$ ‰
Chesirimion	K132	1988	-11	-2.6	-14.9
		1989	-10	-2.3	-13.8
Churo	K139	1988	-15	-3.0	-11.6
		1989	-15	-3.1	-12.5
Kampi Ya Samaki	K131	1988	+27	+5.5	-
		1991	+25	+4.9	-
Nginyang Poly	K204	1989	-11	-2.3	-10.0
		1991	-12	-2.8	-10.6
Kapedo	K48	1988	+2	-0.5	-4.1
		1989	-2	-0.9	-3.3
Lorusio	K45	1988	-16	-3.4	-
		1991	-15	-3.6	-
Little Magadi	K3	1985	-6	-0.9	-
		1989	-3	-0.7	-

Table B.3   Results for sites in the KRV sampled on more than one occasion: gas chemistry (mole percent).

Site	No	Year	CO_2 %	CH_4 %	N_2 %	O_2+Ar %
Korosi KR 23	K159	1988	16.1	0.015	65.1	18.2
		1989	14.3	0.024	66.9	18.8
Paka PK 1	K163	1988	83.8	1.5	11.3	3.4
		1989	30.0	0.45	55.4	14.2

Table B.4   Results for sites in the KRV sampled on more than one occasion: gas and steam stable isotopes (permil).

Site	No	Year	δ^2H-H_2O ‰ SMOW	$\delta^{18}O$-H_2O ‰ SMOW	$\delta^{13}C$-CO_2 ‰ PDB	$\delta^{13}C$-CH_4 ‰ PDB
Korosi KR 23	K159	1988	-33	-6.5	-6.3	-
		1989	-42	-7.6	-6.1	-
Korosi KR 34	K162	1988	-112	-18.2	-4.3	-
		1991	-99	-15.9	-	-27.6
Paka PK 1	K163	1988	+7	-2.3	-2.9	-24.9
		1989	+2	-2.4	-3.2	-24.0

of sampling.

It might be expected that carbon isotope ratios in the original hydrothermal gases would be more consistent than the gas concentrations, and therefore a better test of analytical reproducibility. This is reflected in the results of Table B.4, where the sequential $\delta^{13}C$ values are within the overall analytical errors. However, the H and O isotope content of fumarolic steam is more likely to have been affected by preceding rainfall events. On the evidence of Table B.4, this appears to have affected the fumaroles in inverse proportion to their strength, with the greatest discrepancy seen in the weakest fumarole (the isolated Korosi KR 34), and the least at the relatively strong PK 1 fumarole.

APPENDIX C

Stable isotopic analyses carried out previous to this study, but used in the interpretation

Table C.1 Stable isotopic data for waters of the MER. Data sources: CRA - Craig et al (1977), E - this study, GIZ - Gizaw (1989). Results in permil with respect to SMOW for O and H, and PDB for C.

SPRS <40C		T deg C	$\delta^{18}O$	δ^2H	$\delta^{13}C_{DIC}$
Silte Tebel	CRA12	18	-2.4	-4	
Butajera	CRA13		-2.3	-3	
Oitu	CRA27	38	-3.5	-13	
Huluka	CRA36	18	-1.9	2	
Sedi 1	CRA38		-3.5	-12	
Sedi 2	CRA39		-3.3	-10	
Sedi 3	CRA40		-3.3	-10	
Shalla	CRA41	21	-1.6	3	
Kenteri	CRA50		-2.1	-3	
Saisha	CRA52	32	-1.9	0	
Motokoma	CRA60	35	-3.7	-15	
Asasa	CRA68	21	-2.3	-1	
Arba Minch	CRA87	17	-2.0	0	
Ambo	E24	39	-4.8	-21	
BH + WELLS <40C					
Akaki	CRA1	21	-2.6	-9	
Debre Zeit	CRA1	26	3.4	21	
Mojo	CRA3	25	-5.5	-32	
Adami Tulu	CRA5	31	4.3	33	
Zwai Well	CRA7		5.0	35	
S Cross	CRA8		-0.2	5	
Maki	CRA9	25	-2.7	-8	
Koshe	CRA14	38	-3.5	-15	
Jido Combol	CRA17	34	-4.1	-24	
Bek Mol Awasa	CRA55		4.7	34	
Awasa Bank	CRA56	32	-1.2	3	
Sholicha	CRA67	36	-3.7	-16	
Shashemane	CRA70		-2.1	-1	
US Embassy	CRA97	24	-4.0	-16	
SPRS + BH > 40C					
Imba Koto	CRA11	49	-3.7	-16	
Wildlife Con	CRA16	46	-0.5	5	
Langano #1	CRA20	67	-1.3	0	-2.4
Langano #2	E11	65	-0.2	-6	
Bole Fault	CRA21	92	-0.9	-2	-1.7
Geyser Is	CRA24	97	0.4	4	-2.0
Shalla 30	CRA30	94	2.5	24	1.1
Shalla 30	E15	96	2.8	12	
Bekele M well	CRA33	43	0.4	10	-3.6
Wondo Genet	CRA47	65	-2.4	-8	-2.4
Wondo Genet	E14	65	-2.1	-11	
Kike	CRA48	52	-2.5	-6	
Kenteri	CRA49	69	-3.0	-8	
Shallo	CRA53	90	-0.4	6	-2.1
Graha Que	CRA58	86	-0.7	5	-2.3
Bodicho	CRA59	89	-3.3	-13	-3.0
W Agge	CRA63	43	-4.5	-24	
Shalla SW	CRA64	54	1.8	18	-1.6
Chitu	CRA65	60	1.5	16	-1.9
Abaya 6	CRA72	95	-0.7	-6	
Abaya 6	E12	96	0.1	-10	-4.2
Abaya 8	CRA74	67	-2.9	-9	
Abaya 10	CRA75	50	-2.5	-8	-0.7
Chokare 15	CRA76	67	-3.0	-9	1.7
Chokare 16	CRA77	42	-2.9	-7	-1.2
Bilate	CRA78	51	-2.2	-6	-5.0
Nech Sar	CRA86	58	-1.9	-2	-4.6
Sodere	E16	65	-2.1	-11	-1.1
CTG-2	GIZ4	94	-1.1	-7	-1.9
CTG-3	GIZ5	91	3.3	26	-5.4
CTG-7	GIZ6	73	3.0	30	-3.3
LTG-30	GIZ8		-1.2	4	-5.6
LTG-32	GIZ9		-0.8	3	-1.8
Ghion	E23	70	-6.2	-30	

Table C.1 (Contd)

RIVERS + STRS		$\delta^{18}O$	δ^2H	$\delta^{13}C_{DIC}$
Awash (<Koka) '76	CRA4	-0.1	3	
Awash (Sodere) '90	E19	1.7	9	
Awash (Sodere) 2/95	E19	-0.7	-1	
Awash (Sodere) 9/95	E19	-1.1	-2	
Awash (NP) 9/95	E20	-1.1	0	
Maki '76	CRA10	0.7	8	
Jido'76	CRA18	0.6	5	
Tej '76	CRA34	-0.7	6	
Muluka '88	GIZ1	-1.9	-1	
Teyl '76	CRA35	-0.6	6	
NE Langano '76	CRA37	-2.9	-8	
Melka '76	CRA46	-0.7	6	
Worka '76	CRA51	-2.0	1	
Ibala '76	CRA61	-3.4	-14	
Bilate 1 '76	CRA62	0.9	8	
Bilate 2 '76	CRA79	0.1	2	
Omo '76	CRA81	-0.1	9	
Humasa '76	CRA83	-0.1	6	
LAKES				
Besaka '95	E21	5.8	34	
Zwai '76	CRA6	5.3	39	
Zwai '88	GIZ3	6.7	49	
Langano '76	CRA15	6.9	46	
Langano '88	GIZ2	7.0	53	
Langano '90	E17	7.5	50	
Langano SW '76	CRA28	6.7	45	0.2
Abiata '76	CRA19	10.0	64	-3.8
Shalla '76	CRA44	8.5	55	2.8
Shallo '76	CRA54	6.8	44	
Awasa '76	CRA57	8.3	55	8.3
Awasa '90	E18	7.8	53	
Chitu '76	CRA66	10.5	60	5.5
Abaya '76	CRA84	7.3	50	0.7
Shamo '76	CRA88	7.8	51	
FUM. STEAM COND.				
Aluto 18	CRA32	-7.7	-32	
Aluto 26	CRA31	-8.1	-44	
Bobessa	E4	-5.7	-29	
Gebiba	E5	-6.2	-31	
Auto	E6	-6.1	-36	
Borama	CRA71	-2.5	-5	
Chebicha	E7	-4.9	-31	
Danshe	E8	-5.0	-29	
Koka	E9	-2.1	-9	

Table C.2   Stable isotopic data for the waters of southern Afar. Data sources: CRA − Craig et al (1977), E and D - this study, FON - Fontes et al (1979, 1980), NC - Schoell and Faber (1976), VER - Verhagen et al (1991). Results in permil with respect to SMOW for O and H, and PDB for C.

SPRS + BH > 45C		T deg C	$\delta^{18}O$	δ^2H	$\delta^{13}C_{DIC}$
Meteka	NC37/11/5		-2.3	-4	
Meteka	NC37/8/10	50	-2.9	-7	
Meteka	NC37/8/15	49	-3.2	-9	
Meteka	NC37/8/23	84	-4.7	-16	
Allallobeda	CRA90	79	-1.4	-21	
Teo	NC37/4/16	73	-0.1	-12	
Korilli	FON76/7	80	-1.4	-12	-3.9
Manda	FON76/8	45	0.7	6	-9.3
Abbe C	D6	75	-2.9	-23	
Abbe N	D7	90	-3.7	-27	-17.1
SPRS, WELLS <45C					
Loggia	CRA95		-0.2	6	
Filwoha	E22	43	-2.7	-16	
Dikhil II	VER7	42	-1 4	-1	-11.8
Mouloud III	VER9	39	-4.0	-32	-10.8
Doubdoub	FON75/1	41	-4.1	-32	-9.1
Goroya	VER8	39	-3.2	-20	-8.4
Kourtimalay	VER28		-4.1	-32	-10.3
PK 50	VER6	40	-1.1	-2	-11.6
Oueah V	VER5	36	-1.1	-7	-14.9
PK 20	VER25	44	-1.3	-1	-13.4
RIVERS + STRS					
Awash 2	CRA93		0.4	6	
Mille	CRA96		0.8	9	
LAKES					
Abbe	FON75/4		3.7	-4	
Asal	SS3	32	3.7	13	0.6
SEA					
Ghoubet	D8		0.4	3	
FUM. STEAM COND.					
Airobera	CRA94		-4.9	-26	
Asal-5	D2		-3.4	-14	
N Ghoubet	D3		-3.1	-17	
Garrabays	D4		-8.1	-57	

APPENDIX D

Calculation of Saturation Index (SI)

Calculation of Saturation Index (SI) of solutions with respect to minerals

Saturation index is defined as follows:

$$SI = Log(Q/K)$$

where Q is the activity quotient (or ionic activity product) and K the equilibrium constant (or solubility product) for the mineral and temperature concerned. Positive and negative values denote oversaturation and undersaturation of the water with respect to the mineral in question. (However, it should be pointed out that saturation with respect to any particular mineral does not prove that the mineral is controlling the concentration of a given species, or even that the mineral is actually present in the rock at all.)

Speciation-saturation programs use extended versions of the Debye-Hückel equation to calculate iteratively the activities in multi-component systems. Some programs (e.g. WATEQ, Trusedell and Jones, 1974) use a more comprehensive list of component equations than others. The program used for this study, included in HYDROWIN V3.0 (Calmbach, 1994) takes into account a relatively restricted series of components, but where tested against WATEQ gave similar results. Table D.1 provides a comparison between the two programs for groundwaters in the Gregory Rift over a range of TDS values and sampling temperatures:

Table D.1   Comparison of SI values for a range of Gregory Rift groundwaters calculated by HYDROWIN and WATEQ.

Sample No	Temp °C	TDS mgl^{-1}	$SI_{calcite}$		$SI_{chalcedony}$	
			Hydrowin	WATEQ	Hydrowin	WATEQ
K25	35	440	-0.932	-1.001	+0.545	+0.516
K26	43	430	-0.391	-0.482	+0.078	+0.032
K28	28	310	-0.106	-0.165	+0.555	+0.526
K37	30	350	-1.628	-1.659	+0.690	+0.660
K39	29	200	-1.574	-1.611	+0.696	+0.684
K85	20	400	+0.023	-0.052	+0.669	+0.637
K88	24	1010	+0.174	+0.091	+0.578	+0.548
K94	19	2690	+0.489	+0.301	+0.630	+0.607
K121	37	1700	+0.278	+0.163	+0.741	+0.714
K124	32	1780	-0.195	-0.298	+0.812	+0.779

The Table shows that HYDROWIN values of SI are consistently close to WATEQ values. The HYDROWIN saturation program is intended for general-purpose use and will tend to overestimate the saturation state of the higher-TDS and thermal waters, though not sufficiently to affect the conclusions drawn in Chapter 6.

APPENDIX E

Chemical analyses carried out previous to this study, but used in the interpretation

Table E.1 Chemical data for waters of the MER. Data source: Craig et al (1977). Results in mgl^{-1}.

RIVERS + STRS		T deg C	pH	Na	K	Ca	Mg	HCO3	Cl	SO4	Si	B	F
Awash	CRA4		8.2	29	7	34	8	216	11	6	17.3		1.6
Maki	CRA10		8	37	11	39	12	250	8.6		14		1
Jido	CRA18		7.1	47	25	8	5	170	11		18.2	0.84	4.4
Tej	CRA34		7.8	6	5	6	3	33	4	3.3	17.3		0.65
Teyl	CRA35		7.8	5	4	4	3	29	2	0.8	11.2		1
NE Langano	CRA37		7.8	21	5	17	4	122	4	10	35		1.1
Melka	CRA46		7.6	48	14	32	14	281	11	30	27.1		1.3
Worka	CRA51		8.1	200	52	8	5	567	26	7	59.3		1.9
Imbalu	CRA61		7.6	35	15	12	4	116	5	2.5	14.9		1.85
Bilate 1	CRA62		8.4	23	12	14	4	129	6	2.5	16.8		1.1
Bilate 2	CRA79		8.8	213	27	14	2	451	33	9	49.9		9.3
Omo	CRA81		7.75	16	6	14	6	112	1	15	14.9	0.1	0.95
Humasa	CRA83		7.85	13	12	13	3	109	7		18.2		0.8
SPRS <40C													
Silte Tekel	CRA12	18	7.4	20	8	27	0.1	145	4	1	59.7	0.19	6.6
Butajera	CRA13		7.2	23	12	44	9	211	8	12	37.8		0.56
Oitu	CRA27	38	7.85	85	18	16	9	281	34	5	47.6		1.7
Huluka	CRA36	18	6.4	9	5	8	1	57	4	5.8	21.9		1
Sedi 1	CRA38		7.1	19	4	12	2	98	4	5	34.1		0.95
Sedi 2	CRA39		7.6	28	10	20	4	166	5	8	32.7		2.6
Sedi 3	CRA40		7.25	21	5	19	5	142	5	4	34		1.3
Shalla	CRA41	21	7.4	32	4	9	3	146	4		23.8		1.7
Saisha	CRA52	32	6.9	80	12	12	4	210	19	38	40.1		3
Motokoma	CRA60	35	7.4	33	13	16	8	190	1	21	33.1		1.9
Asasa	CRA68	21	7.7	12	5	17	7	124	1	8.2	21.9		1
Humasa	CRA82	35	6.9	58	14	22	9	244	4	24	48.1		1.8
Arba Minch	CRA87	17	7.6	12	3	33	8	168	1.4	12	42		0.7
BH + WELLS <40C													
Akaki	CRA1	21	7.6	43	6	55	22	396	16	11	22.4	0.39	0.65
Debre Zeit	CRA2	26	8.2	360	46	21	52	1098	133	7	29.9	1.7	3.3
Mojo	CRA3	25	7.4	63	15	58	13	394	21	15	38.7		1.3
Adami Tulu	CRA5	31	8.1	230	12	4	1	620	11	1	22.4	0.1	4.7
Zwai Well	CRA7		7.4	85	15	45	25	512	15		43.9	0.2	2.9
S Cross	CRA8		7.9	310	16	15	4	781	66	4	38.7	0.05	8
Maki	CRA9	25	7.8	67	4	45	18	342	9	10			
Koshe	CRA14	38	7.6	135	18	18	5	456	12	2	49.5		1.6
Jido Combol	CRA17	34	9	365	14			908	36	33	50.9		32.5
Bek Mol Awasa	CRA55		7.4	233	23	11	19	688	28	19	37.3		21.3
Awasa Bank	CRA56	32	7.8	335	59	5	14	853	51	9	24.7	0.1	10.5
Sholicha	CRA67	36	8.1	210	17	6	1	432	43	52	40.1	0.54	13
Shashemane	CRA70		7.2	145	9	13	2	146	7	29	27.1	0.1	1.8

SPRS + BH > 40C		T deg C	pH	Na	K	Ca	Mg	HCO3	Cl	SO4	Si	B	F
Imba Koto	CRA11	49	8.5	260	33	9	2	699	23	33	31.7	0.2	5
Wildlife Con	CRA16	46	8.2	310	22	3	0.1	512	209	13			
Langano #1	CRA20	67	7.8	745	86	10	3	1411	500	26	56	2.8	26.9
Bole Fault	CRA21	92	8.8	565	36	0.1	0.1	651	273	375	77	3	10.5
Geyser Is	CRA24	97	8.8	743	56	0.1	0.1	793	455	255	75	3.4	14
Shalla 30	CRA30	94	8.7	2340	69	0.1	0.1	3116	1526	31	45	6.9	60
Bek Mol well	CRA33	43	9.1	500	28	3	0.1	822	291	7			
Wondo Genet	CRA47	65	7	675	56	7	4	1424	151	177	42	0.84	85
Kike	CRA48	52	7.55	170	51	11	5	570	21	1	63	0.2	2
Kenteri	CRA49	69	7.4	38	10	5	4	130	7	2	36	0.1	1.3
Shallo	CRA53	90	8	400	59	3	0.1	847	89	118	58	0.1	28.7
Graha Que	CRA58	86	7.35	397	43	11	5	879	57	86	67	1.1	13
Bodicho	CRA59	89	9.2	320	25	0.6	0.1	629	44	54	32		
W Agge	CRA63	43	7.45	152	26	33	2	451	22	35	50	0.05	3.7
Shalla SW	CRA64	54	8.8	1310	100	0.6	0.1	2373	485	63	30	1.1	25
Chitu	CRA65	60	7.7	1010	82	4	15	2051	400	92	40	1.1	21.4
Abaya 6	CRA72	95	9.6	1320	222	0.1	0.1	1979	730	152	62.5	2.5	31.5
Abaya 8	CRA74	67	6.95	600	50	21	8	1476	116	25	61		9
Abaya 10	CRA75	50	6.75	505	54	30	16	1474	58	89	59	0.54	13.7
Chokare 15	CRA76	67	6.8	518	48	8	5	1302	66	21	57		13.7
Chokare 16	CRA77	42	7.2	238	28	45	48	832	102	29	50		2.9
Bilate	CRA78	51	7.6	283	15	10	2	695	31	21	16.8		5.8
Nech Sar	CRA86	58	7.6	450	29	42	2	452	94	602	44		9
LAKES													
Zwai '76	CRA6		7.6	50	13	15	5	189	13	4.8	17.2	0.25	1.6
Langano '76	CRA15		8.8	425	30	3	2	676	202	35	2.8	0.25	15.3
Abiata '76	CRA19		9.6	5000	250	1	0.6	7025	1896	29	63.9	6.3	120
Langano SW '76	CRA28		9.2	423	24	4	1	718	180	22	34	0.82	13
Shalla '76	CRA44		9.6	6800	225	3.4	1.5	8467	3030	137	54.1	24.4	300
Shallo '76	CRA54		7.7	99	22	8	5	210	18	19	11.7		5.3
Awasa '76	CRA57		9.15	213	25	13	10	499	64	40	80.3		
Chitu '76	CRA66		9.85	14100	938			23000	5680	433	155	11.4	208
Abaya '76	CRA84		8.85	188	21	14	3	437	48	43	18.2	0.1	6.1
Shamo '76	CRA88		9.05	265	18	9	15	567	65	11	13		7

Table E.2   Chemical data for the waters of southern Afar. Data sources: BOS - Bosch et al (1975), CRA - Craig et al (1977), D - this study, END - Endeshaw (1989), FON - Fontes et al (1979, 1980), GIZ - Gizaw (1986), SA, SK and SS - Sanjuan et al (1990), VER - Verhagen et al (1991). Results in mgl[-1].

SPRS + BH > 45C		T deg C	pH	Na	K	Ca	Mg	HCO3	Cl	SO4	Si	Li	B	F
Meteka	CRA90	72	7.4	1555	105	25	6	830	1454	828	86		4	4
Allallobeda	CRA91	79	8	610	14	30	2	61	759	242	51	0.35	1.8	0.85
Tendaho	END7	95	7	506	3.9	24	0.1	33	710	26	73	0.55	2.4	0.8
Teo	END1	73	7.6	600	30	30	0.3	140	746	211	174	0.55	0.19	1.2
Danab	END2	93	7.75	520	35	30	1.5	137	699	116	82	1.1	0.33	1.9
Waruf	END3	50	7.3	219	11.2	32	6.8	234	178	200	34			0.52
Hertale	END4	49	7.35	238	16	8	5	403	118	78	47	0.03	0.04	1.8
Korilli	SAS1	80		10500	450	1540	225		22720	126	29	2.6	3.7	
Manda	SAS3	45	7.05	16400	835	1100	810		33370	910	20.7	1.587		
Oued Kalou	SK1	74		735	12.3	64	1.2		1120	152	37.3	0.05	1.84	
Abbe C	D06	75	8.7	493	14.6	157	<0.1	26	785	304	41.6	0.136	1	0.9
Abbe N	D07	90	6.05	901	29.7	213	0.3	18.6	1530	323	47.9	0.29	1.55	1.14
SPRS, WELLS <45C														
Kessem	GIZ37		7.35	95	24	30	8	390	10	7	58	0.04	0.32	1.3
Sabire	GIZ47		8.05	170	12	25	7	531	20	21	45	0.01	1.3	2.2
Bilen	END5	40	6.9	200	18	25	10	537	64	37	50	0.02	0.04	3.3
Filwoha	END6	43	7.85	450	85	2	2	824	197	76	40	0.01	0.36	7
Dikhil II	VER7	42	7.9	155		37	40	315	180					
Mouloud III	VER9	39	8.8	236		61	58	198	329					
Ali Sabieh	VER30	33	6.9	508		148	127	364	595					
Doubdoub	VER27	41	7.5	405		118	98	126	764					
Goroya	VER8	39	7.6	1180		180	132	126	1990					
Kourtimalay	VER28		7.8	1080		368	165	61	2420					
PK 50	VER6	40	8.1	165		24	21	334	120					
Oueah V	VER5	36	8.1	158		43	29	337	150					
PK 20	VER25	44	8	190		75	45	174	363					
RIVERS + STRS														
Awash	CRA4		8.2	29	7	34	8	216	11	6	17.3			1.6
Awash 2	CRA93		8.2	84	9	11	4	180	30	26	11.2		0.25	2.6
Mille	CRA96		8.95	70	5	23	21	243	28	80	16.8			1.1
LAKES	AFAR													
Asal	SS3/BOS2	32	7	101200	5160	1340	6270	125.1	199200	2200	79.3	5.5	32.3	
SEA	AFAR													
Ghoubet	SG1/BOS3			11430	440	205	700	140.3	21100	1320	0.56	2.6	4.8	

E3

Geothermometer equations used in Chapter 8

Table F.1   Solute geothermometer equations (from Fournier, 1989).

1.   Silica (quartz) - no steam loss:

$$t°C = (1309/5.19 - \log SiO_2) - 273.15$$

2.   Silica (quartz) - high-temperature version for geothermal wells:

$$t°C = C_1 + C_2S + C_3S^2 + C_4S^3 + C_5 \log S$$

where S = concentration of SiO_2 in mgl^{-1}
C_1 = -4.220 x 10^1
C_2 = 2.883 x 10^{-1}
C_3 = -3.669 x 10^{-4}
C_4 = 3.167 x 10^{-7}
C_5 = 7.703 x 10^1

3.   Silica (quartz) - maximum steam loss at 100°C:

$$t°C = (1522/5.75 - \log SiO_2) - 273.15$$

4.   Silica (chalcedony):

$$t°C = (1032/4.69 - \log SiO_2) - 273.15$$

5.   Sodium/Potassium:

$$t°C = (1217/1.483 + \log [Na/K]) - 273.15$$

Table F.2   Gas geothermometry temperature functions

(a)   <u>Arnorsson and Gunnlaugsson (1985):</u>

CO_2 $t°C = -44.1 + 269.25Q - 76.88Q^2 + 9.52Q^3$ Applicability: universal

---

H_2S	$t°C = +246.7 + 44.81Q$	Applicability: all waters
H_2	$t°C = +277.2 + 20.99Q$	above 300°C and waters
CO_2/H_2	$t°C = +341.7 - 28.57R$	in the range 200-300°C if
H_2S/H_2	$t°C = +304.1 - 39.48R$	chloride > 500 mgl^{-1}

H_2S	$t°C = +173.2 + 65.04Q$	Applicability: all waters below 300°C
H_2	$t°C = +212.2 + 38.59Q$	and waters in the range 200-300°C if
CO_2/H_2	$t°C = +311.7 - 66.72R$	chloride < 500 mgl^{-1}

---

where Q = log gas concentration in mmoles per kg of steam, R = log gas ratio

(b)   <u>D'Amore and Panichi (1980):</u>

      $t°C = (24775/\alpha + \beta + 36.05) - 273$

where $\alpha = 2log(CH_4/CO_2) - 6log(H_2/CO_2) - 3log(H_2S/CO_2)$

       $\beta = -7log\ pCO_2$

       $pCO_2 = 0.1$ if $CO_2 < 75\%$
       $pCO_2 = 1.0$ if $CO_2 > 75\%$
       $pCO_2 = 10$ if $CO_2 > 75\%$ and $CH_4 > 2H_2$ and $H_2S > 2H_2$

When H_2, H_2S or CH_4 are absent, a vol % of ≤ 0.001 should be used

(c)   <u>Panichi et al (1975):</u>

      $1000\ ln\alpha = -9.01 + (15.30 \times 10^3T^{-1}) + (2.361 \times 10^6T^{-2})$

where $\alpha = (^{13}C/^{12}C)_{CO2}/(^{13}C/^{12}C)_{CH4}$

nb: $1000\ ln\alpha \simeq \delta^{13}C_{CO2} - \delta^{13}C_{CH4}$

APPENDIX G

Journal and symposium publications arising from this research

[3]

INDIRECT DETECTION OF SUBSURFACE OUTFLOW FROM A RIFT VALLEY LAKE

W.G. DARLING[1], D.J. ALLEN[1] and H. ARMANNSSON[2]

[1]*British Geological Survey, Maclean Building, Wallingford, Oxfordshire OX10 8BB (U.K.)*
[2]*Orkustofnun (National Energy Authority), Grensasvegur 9, 108 Reykjavik (Iceland)*

ABSTRACT

Darling, W.G., Allen, D.J. and Armannsson, H., 1990. Indirect detection of subsurface outflow from a rift valley lake. J. Hydrol., 113:297–305.

Naivasha, highest of the Kenya (Gregory) Rift Valley lakes, has no surface outlet. However, unlike other Rift lakes it has not become saline despite high potential evaporation rates, which indicates that there must be some subsurface drainage. The fate of this outflow has been the subject of speculation for many years, especially during the general decline in lake water level during the 1980's. Particularly to the south of the lake, there are few opportunities to obtain information from direct groundwater sampling. However, the stable isotopic composition of fumarole steam from late Quaternary volcanic centres in the area has been used to infer groundwater composition. Using a simple mixing model between Rift-flank groundwater and highly-evaporated lakewater, this has enabled subsurface water flow to be contoured by its lakewater content. By this method, outflow can still be detected some 30 km to the south of the lake. Stable isotope data also confirm that much of the steam used by the local Olkaria geothermal power station is derived from lakewater, though simple balance considerations show that steam use cannot alone be responsible for the fall in lake level observed during the 1980's.

INTRODUCTION

The falling surface level of Lake Naivasha during the 1980's has prompted research into the hydrogeology of the lake and its environs (Åse et al., 1986; Anon., 1988). In this respect calculations of the lake's water balance are important. At Naivasha rainfall averages 608 mm yr^{-1} (Anon., 1966), but low relative humidity and an average daily maximum temperature of 25°C combine to cause annual potential evaporation of 1500–1900 mm yr^{-1} (Åse et al., 1986), far in excess of rainfall. The lake appears to be fed chiefly by the perennial Malewa and Gilgil rivers, which collect runoff from the Nyandarua (Aberdare) Mountains and their foothills to the northeast of the lake, and which discharge into a papyrus swamp forming part of the lake. Three studies based on river gauging and evaporation-rate measurement have given comparable results for subsurface outflow of 43×10^6 m^3 yr^{-1} (Sikes, 1935), 34×10^6 m^3 yr^{-1} (McCann, 1972) and $46–56 \times 10^6$ m^3 yr^{-1} (Åse et al., 1986). These are likely to be un-
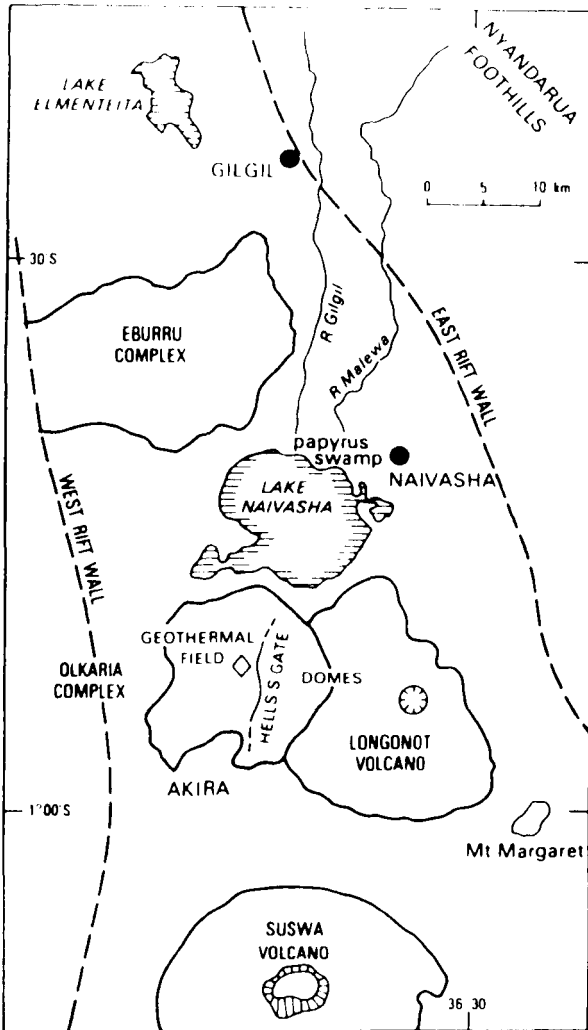
Fig. 1. Physical features of the Lake Naivasha section of the Kenya Rift Valley, showing the relative position of the lake and the various volcanic complexes on which fumaroles are situated. The culmination of the Rift floor occurs in the Naivasha area.

derestimates, as not all inflows could be gauged, but suggest that substantial outflow is occurring.

Lake Naivasha lies at some 2000 m.a.s.l. on the culmination of the Kenya Rift Valley, which arches from north to south (Fig. 1). Because of this, ground-water flow away from the lake is potentially possible in both these directions. It is tentatively concluded from well-water level data that between 50 and 90% of lake outflow is directed towards the south, but data are sparse and cease within a few km of the lake (Allen et al., 1989). Although the presence of
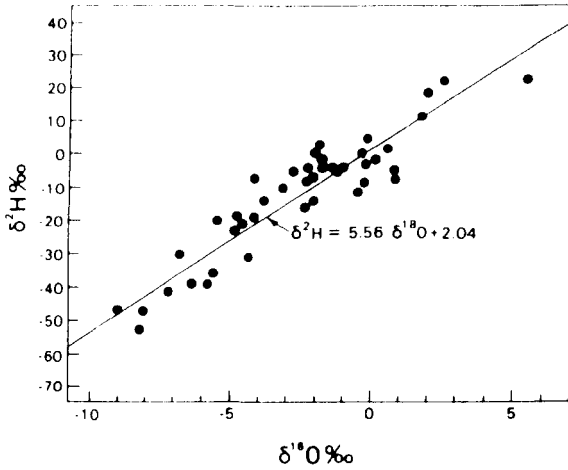
Fig. 2. Stable isotope crossplot of rainwater sampled at Rift Valley meteorological stations from 2°S to 2½°N.
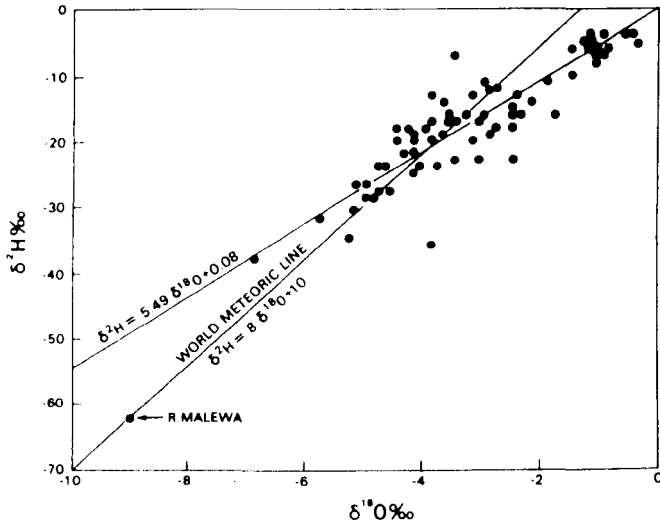
Fig. 3. Stable isotope crossplot of unmodified Rift Valley groundwater collected from wells and springs. The regression shows a close similarity to that of rainfall in Fig. 2. The River Malewa contains depleted water from the Nyandarua Mountains which lies on the world meteoric line.
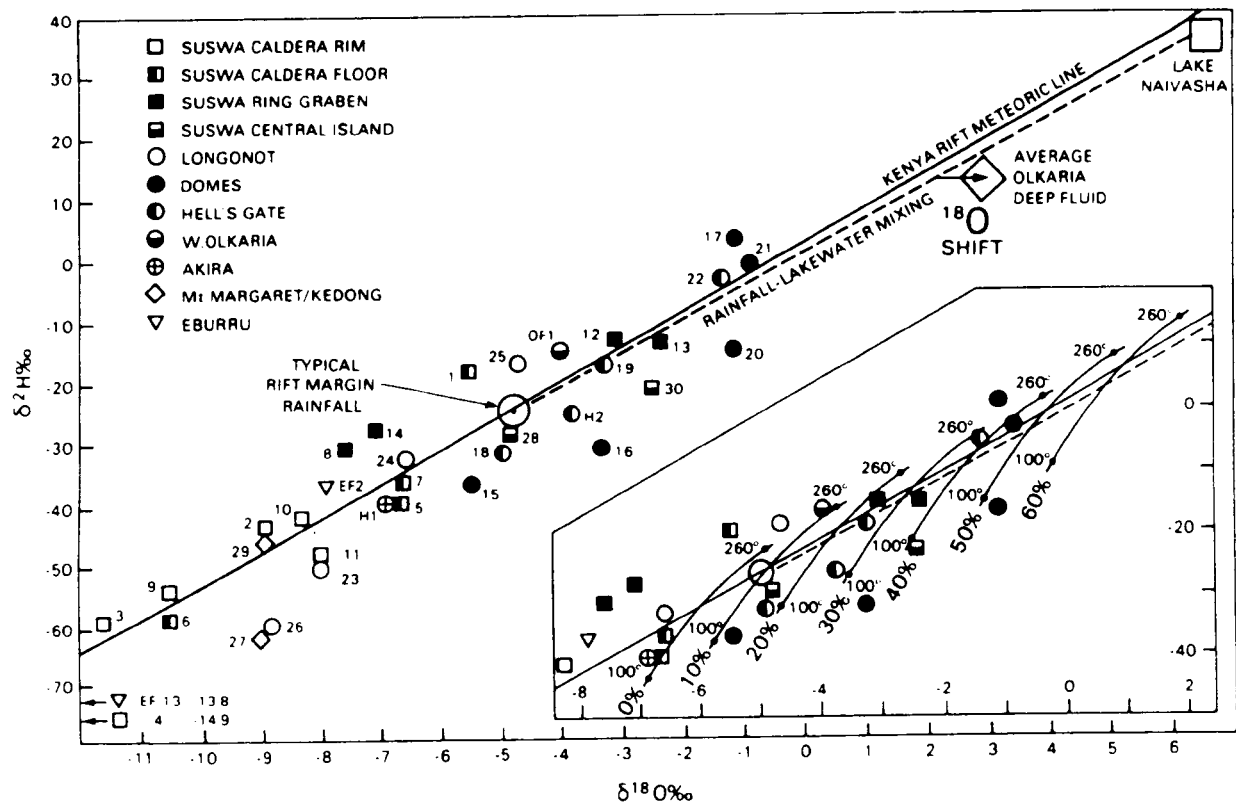
Fig. 4. Stable isotope crossplot of condensed steam from fumaroles of the Naivasha region shown in relation to the Kenya Rift meteoric line. Fumarole numbers refer to geographical location as shown in Fig. 5. Also shown are the values of average Rift margin rainfall, Olkaria deep thermal fluid, and Naivasha lakewater. Inset: the central portion of the plot with lines superimposed showing the theoretical composition of steam derived over a range of temperatures from groundwater containing various percentages of lakewater.

which is close to the rainfall line. While this may be partly coincidental, as the regression is biased by isotopically heavier groundwaters from the lower and hotter Magadi area to the south, the rainfall regression seems likely to be representative since a similar one was observed for 35 samples of rainfall from the Chyulu Hills in southeast Kenya:

$$\delta^2 H \; = \; 5.68\,\delta^{18}O \; + \; 6.04 \qquad (r^2 \; = \; 0.89)$$

(B.G.S., unpubl. data). However, there is limited evidence from the composition of the River Malewa (Fig. 3) which drains the 3900 m Nyandarua Mountains that a slope nearer 8 may obtain at higher altitudes. The reason may be that the Nyanduruas are high enough to interact with airflow above the sub-tropical inversion (Vincent et al., 1979). The difference is of some significance, since much of Lake Naivasha's inflow is delivered by the River Malewa. Attempts to estimate lake outflow using isotopic balance techniques are highly dependent on the input value used (Panichi and Tongiorgi, 1974; Allen et al., 1989).

Rainfall on the Rift flanks in the Naivasha area results in groundwater with typical values of $-25‰\ \delta^2 H$, $-4.8‰\ \delta^{18}O$ (Allen et al., 1989). These figures are at the depleted end of the range of values shown in Fig. 3 because the Naivasha area is situated on the highest point of the Rift. Analysis of water level data (Allen et al., 1989) shows that flows must be directed towards Lake Naivasha from the east and west Rift flanks, and therefore groundwater with these average values is likely to mix eventually in most proportions with evaporated outflow water from Lake Naivasha, which possesses values of the order of $+36‰\ \delta^2 H$, $+6.6‰\ \delta^{18}O$. A $\delta^2 H$ vs. $\delta^{18}O$ crossplot (Fig. 4) shows such a mixing line between 100% lakewater and 100% Rift-flank water with a positive horizontal displacement of $1‰\ \delta^{18}O$ to allow for a small amount of isotopic exchange between water and rock. This figure is based on the average of analyses of deep geothermal fluid from six wells in the East Olkaria geothermal field (Fig. 1). In addition the crossplot shows the Rift Valley meteoric line as a reference.

Isotopic compositions of fumarole steam condensates are also shown in Fig. 4. It is assumed that the steam sampled in many of the fumaroles is the product of single-stage separation from a high-temperature geothermal fluid; such a process is known to occur in other geothermal areas (Giggenbach and Stewart, 1982). Lines have therefore been superimposed on the inset to Fig. 4 to show the theoretical consequences of single-stage steam separation between 100°C (local surface boiling point is actually around 93°C) and 260°C (a typical local geothermal reservoir temperature (Armannsson, 1987; Bodvarsson et al., 1987)) from various mixtures of lakewater and Rift-flank water. It is apparent that more than half of the data points fall on or near the theoretical lines; these points together with well-water data have been used to construct a contour map of lakewater influence (Fig. 5), insofar as this is possible in what must be a complex three-dimensional groundwater system. Data points more negative than the theoretical lines are presumed to represent a zero lakewater contribu-
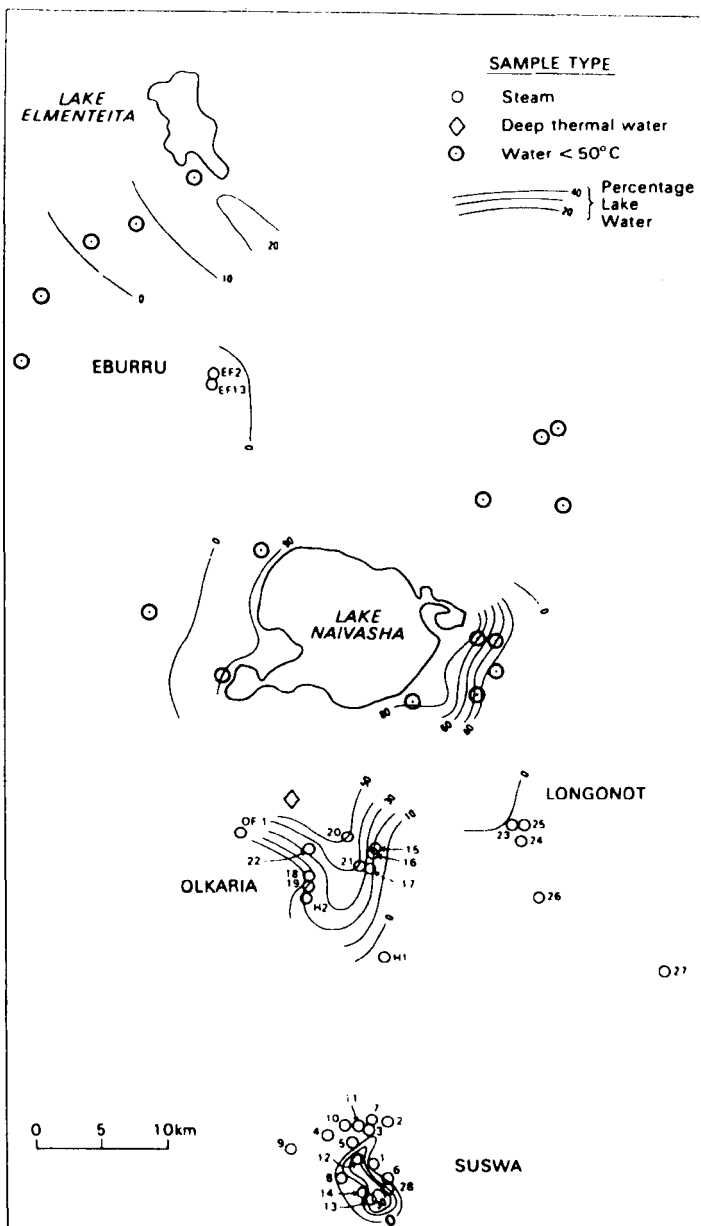
Fig. 5. Contour map of percentage of lakewater in the groundwater system of the Naivasha region, based on the isotopic content of fumarole steam and water from wells and springs.

tion, the more remote examples being probably the results of steam condensation below surface, a process considered by Darling and Armannsson (1989).

The contour map (Fig. 5) demonstrates a tendency for the proportion of lakewater to diminish with increasing distance from Lake Naivasha, as would be expected. However some volcanic centres (Eburru, Longonot and Mount Margaret) show little or no evidence of lakewater, indicating that subsurface outflow is restricted to certain zones. At Suswa only the fumaroles at or near the centre of the volcanic complex appear to contain a substantial proportion of lakewater. This suggests that beneath Suswa, outflow is at a depth such that only the hotter parts of geothermal convective cells can bring it to the surface (though depth and extent of rock fracturing must also be a key factor). Very little is known about the hydrogeological conditions between the Olkaria–Longonot area and Suswa. Two boreholes drilled about 10 km south of the Olkaria–Longonot area struck steam at around 200 m, and a borehole drilled 20 km further south proved to be dry to 250 m. It is apparent therefore that groundwater in the Suswa area is unlikely to be present in the upper 200 m.

Lake Magadi, to the south, forms a natural sump for drainage in the southern Kenya Rift. It is presumed that much of the outflow from Lake Naivasha terminates there. There is however little prospect of detecting it at this distance (100 km) because of excessive dilution by Rift-flank waters.

North of Lake Naivasha the groundwater table lies at a much shallower depth, which should facilitate detection of outflow. The scarcity of wells makes this speculative, but the few in the Elmenteita area (Fig. 5) suggest that the lakewater is generally more diluted than below parts of Suswa, which is slightly further away from Naivasha. This would indicate a smaller amount of flow to the north of the lake.

Since 1981, the Olkaria geothermal power station has used steam produced from a fluid which appears from present isotopic evidence to be 60–70% lakewater (Fig. 4), thus confirming a persistent local speculation as expressed in Smith (1988). To what extent this means an additional discharge from the lake rather than merely a diversion of outflow is difficult to tell from existing data, but based on recent production history (Bodvarsson et al., 1987) it represents at worst an anthropogenic increase in outflow of some $2 \times 10^6 \, m^3 \, yr^{-1}$. This would be a small fraction of the estimated total discharge, and Olkaria power station therefore cannot be implicated in the decline of lake level. Apart from climatic considerations, irrigation for the prolific agricultural activity in the area is a more plausible cause of water loss from the lake.

CONCLUSIONS

The interpretation of stable-isotope measurements presented here supports the tentative hydrogeological model, based on sparse well data, of considerable southerly outflow from Lake Naivasha supplemented by lesser northerly outflow. The stable isotope data further suggest that the northerly outflow is confined to the area between Eburru and Gilgil and the southerly outflow

between Olkaria and Longonot (Fig. 1), with a considerable depth to water table beneath Suswa. Though much of the steam at Olkaria must ultimately be derived from lakewater, there is no evidence that extraction has had any effect on lake level.

NOTE ADDED IN PROOF

Samples from recent deep (> 2000 m) drilling on the eastern end of Eburru indicate up to 20% lakewater at depth. Further drilling may reveal its rate of decline towards the west.

REFERENCES

Allen, D.J., Darling, W.G. and Burgess, W.G., 1989. Geothermics and hydrogeology of the southern part of the Kenya Rift Valley. Brit. Geol. Surv., Rep. SD/89/1, 67 pp.
Anon., 1966. Monthly and annual rainfall in Kenya during the 30 years 1931–1960. Rep. East. Afr. Meteorol. Dep., 172 pp.
Anon., 1988. Kenya's Lake Naivasha on the way down. World Water, April, 5.
Armannsson, H., 1987. Geochemistry of steam in the Suswa and Longonot geothermal areas. Rep. U.N.D.P., 26 pp.
Åse, L.E., Sernbo, K. and Syren, P., 1986. Studies on Lake Naivasha, Kenya, and its drainage area. Univ. Stockholm, Rep. STOU–NG 63, 75 pp.
Bodvarsson, G.S., Pruess, K., Stefansson, V., Bjornsson, S. and Ojiambo, S.B., 1987. East Olkaria geothermal field, Kenya: 1: History match with production and pressure data decline. J. Geophys. Res., 92: 521–539.
Coleman, M., Shepherd, T.J., Durham, J.J., Rouse, J.E. and Moore, G.R., 1982. Reduction of water with zinc for hydrogen isotope analysis. Anal. Chem., 54: 993–995.
Darling, W.G. and Armannsson, H., 1989. Stable isotopic aspects of fluid flow in the Krafla, Namafjall and Theistareykir geothermal systems of N.E. Iceland. Chem. Geol., 76: 197–213.
Giggenbach, W.F. and Stewart, M.K., 1982. Processes controlling the isotopic composition of steam and water discharges from steam vents and steam-heated pools in geothermal areas. Geothermics, 11: 71–80.
McCann, D.L., 1972. A preliminary hydrogeologic evaluation of the long-term yield of catchments related to the geothermal prospect areas in the Rift Valley of Kenya. Rep. U.N.D.P., 23 pp.
Panichi, C. and Tongiorgi, E., 1974. Isotopic study of the hot water and steam samples of the Rift Valley, Kenya. Rep. U.N.D.P., 30 pp.

Sikes, H.L., 1935. Notes on the hydrology of Lake Naivasha. J. East Afr. Uganda Nat. Hist. Soc., 13: 74 89.

Smith, A., 1988. The Great Rift: Africa's Changing Valley. BBC Books, London, 224 pp.

Vincent, C.E., Davies, T.D. and Beresford, A.K.C., 1979. Recent changes in the level of Lake Naivasha, Kenya, as an indicator of equatorial westerlies over East Africa. Clim. Change, 2: 175 189.

ISOTOPE TECHNIQUES
IN THE STUDY OF
PAST AND CURRENT
ENVIRONMENTAL CHANGES
IN THE HYDROSPHERE
AND THE ATMOSPHERE

OXYGEN ISOTOPES IN RELICT SINTERS AS A
PALAEOINDICATOR OF RIFT VALLEY CLIMATE

W.G. Darling, D.J. Allen, B. Spiro

555-559

OXYGEN ISOTOPES IN RELICT SINTERS
AS A PALAEOINDICATOR OF RIFT VALLEY CLIMATE

W.G. DARLING, D.J. ALLEN
British Geological Survey,
Wallingford, Oxfordshire

B. SPIRO
NERC Isotope Geosciences Laboratory,
Keyworth, Nottinghamshire

United Kingdom

1. INTRODUCTION

There is good isotopic evidence for recharge under wetter and cooler climatic conditions during the later Quaternary from many sites across North Africa and to a lesser extent southern Africa [1]. However, in equatorial Africa the absence of suitable aquifers has prevented direct isotopic analysis of such palaeowaters. The only stable isotope information concerning palaeowaters has come indirectly from the study of stromatolites in the Rift Valley lakes [2–5]. Various factors affect the ^{18}O content of stromatolites; hence, inference of the possible isotopic composition of the water in which they grew is difficult; in addition, rather special conditions are necessary for their growth. As a result, not all high lakestands are represented by stromatolitic deposits [5].

Sinters (deposits of amorphous silica normally formed at or near ground surface) are found at various elevations on dormant volcanoes in the northern Kenya Rift. Present day groundwater levels are low, and the sinters could only have been formed during past pluvial episodes when the hydrological base levels were significantly higher. These sinters have been dated by U series methods to ages from 7 ka to over 500 ka BP [6]. The ^{18}O contents of these sinters were measured as a possible alternative way of providing information on palaeo-lakewater isotope contents.

2. ASSUMPTIONS

As a working hypothesis, three assumptions were made about the sinters. First, the sinters were deposited in isotopic equilibrium with waters at 100°C. Silica depositing springs are likely to have issued at around boiling point (lower tempera-

ture springs in the Rift Valley have too little silica for significant deposition on cooling), which would imply a $\delta^{18}O_{SiO_2}-\delta^{18}O_{H_2O}$ fractionation of $\sim 21\permil$ [7]. There is, however, no guarantee that silica was not deposited at lower temperatures during cooling; the only real test of this assumption is comparison, where possible, with the stromatolitic record. Secondly, the calculated $\delta^{18}O$ values of the depositing waters were close to the average lakewater value during the period of deposition. The extent of Holocene lake sediment deposits [6] shows that the depositing springs are likely to have been situated on islands or peninsulas in the palaeolakes; modern analogues such as Ol Kokwe Island, Lake Baringo, and Central Island, Lake Turkana, have springs with isotopic compositions similar to those of lakewater. Thirdly, the depositing waters were not significantly affected by ^{18}O shifting. There is no evidence from present day deep geothermal waters that the ^{18}O shift exceeds $1\permil$ anywhere in the Rift Valley [8, 9].

3. RESULTS

The inferred $\delta^{18}O$ contents of depositing waters are shown in Fig. 1, plotted against their U series ages [6], extending back in time to 150 ka BP. Older sinters were measured for oxygen isotopes and gave a relatively restricted range of inferred $\delta^{18}O$ values for waters of -1.8 to $+2.6\permil$, but their ages were rather poorly constrained between 250 ka and 500 ka BP; they are not shown here.
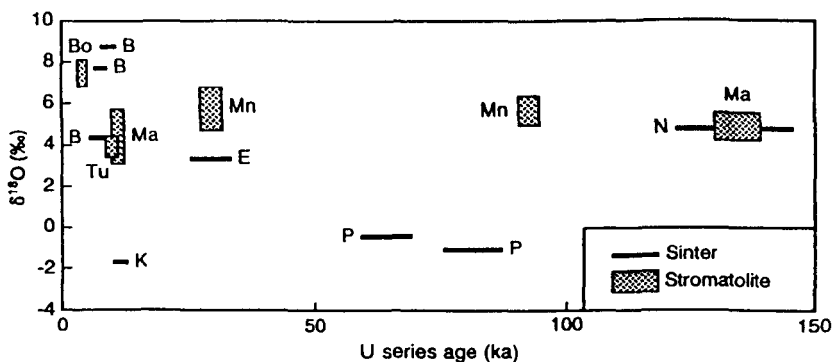
FIG. 1. Plot of inferred $\delta^{18}O$ values of lakewaters versus U series ages [6] for sinters over 0-150 ka BP. Also shown are $\delta^{18}O$ values of lakewaters inferred from stromatolites [2-5]. Volcanic centres: B = Barrier, E = Emuruangogolak, K = Korosi, N = Namarunu, P = Paka. Lakes: Bo = Bogoria, Ma = Magadi, Mn = Manyara, Tu = Turkana.
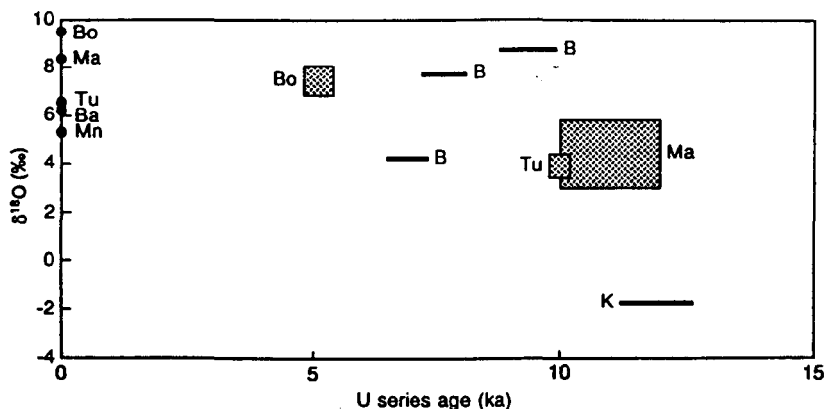
FIG. 2. *Expanded version of Fig. 1 over the period 0–15 ka BP. Volcanic centres as identified before. Lakes identified as before plus Ba = Baringo.*

Also shown in Fig. 1 are the $\delta^{18}O$ ranges for waters suggested by isotope analyses of stromatolitic carbonate from various East African lakes [2–5]. A separate plot (Fig. 2) amplifies the rather crowded detail of the last 15 ka and also shows the present day values of lakes Baringo, Bogoria, Magadi, Manyara and Turkana.

4. INTERPRETATION

The results are first used to test the assumptions made above concerning the composition of depositing waters. There is reasonable agreement between the $\delta^{18}O$ values for lakewater inferred from contemporaneous sinters and stromatolites (Figs 1 and 2). Admittedly, they may come from different Rift Valley lakes, but at times of high lakestands it is likely that the isotopic compositions would be similar for all the lakes. Only when lakes become terminal and small in volume does the effect of evaporation on isotope content become apparent. For example, stromatolite $\delta^{18}O$ evidence from Lake Bogoria at ~5 ka BP shows a trend towards the highly enriched values of the present day.

It is probably significant that the more depleted $\delta^{18}O$ values inferred from sinters are not accompanied by any stromatolite data (Fig. 1 and the > 150 ka data referred to above). Presumably these periods were too cool to permit stromatolite growth. However, if isotopic equilibration between silica and water were taking

place at temperatures significantly below the boiling point the inferred $\delta^{18}O$ values for lakewater would be 4-8°/oo more negative. Such low values of $\delta^{18}O$ would seem to be implausible for East African lakes even during the Pleistocene.

Given that the $\delta^{18}O$ values for lakewater inferred from sinters may therefore be reasonably reliable, a brief interpretation of palaeoconditions can be attempted. Beyond 150 ka BP there is little detailed information about local climatic conditions, and the only high lakestand known during the period is that of the Magadi-Natron basin at about 300 ka BP [3]. This probably corresponds to the samples mentioned earlier. In the period of 15-150 ka lake levels in East Africa generally were high from 25-35 ka and 125-145 ka BP. Figure 1 shows that the U series dates on sinters from Emuruangogolak and Namarunu are consistent with these ages, suggesting that lakewater $\delta^{18}O$ values were not dissimilar to the present ones, though indicating somewhat cooler conditions. The Paka samples from 60 to 85 ka do not correlate with any known highstands but indicate a humid phase under significantly cooler conditions.

More is known about the last 15 ka. During this period Lake Baringo reached its highest level at 11-12 ka, while the highest stand on the Suguta palaeolake has an age of 9.7 ka BP. Lake Turkana fluctuated around a maximum level between 7.5 and 9.5 ka BP. Figure 2 shows that at the beginning of the Holocene the sample from Korosi (associated with the highstand of Lake Baringo) indicates a lakewater considerably depleted in ^{18}O compared to the present. Shortly after this, however, a sinter from the Barrier shows much more enrichment in ^{18}O, although this falls over the next 2.5 ka to a value not dissimilar from today's. The implications of these results are that at the start of the Holocene the lake basins were full of isotopically depleted water, but that rapid changes in atmospheric circulation [10] and perhaps catchment led to an enrichment in ^{18}O reaching a peak within 2 ka. After 9 ka BP lakes Suguta and Turkana became separate [11] and, as Lake Suguta dried up, the sinters may have been derived primarily from Turkana lakewater. By this time the main source of Turkana water was probably the Ethiopian Highlands (as at present), and therefore the lake would have had an increasingly depleted composition. At about 3.5 ka BP Turkana became a closed basin [12] and is presumably becoming more enriched in ^{18}O with time. The same process would have begun in the much smaller Lake Bogoria at an earlier date.

5. CONCLUSIONS

Lakewater $\delta^{18}O$ values inferred from the measurement of hydrothermal siliceous sinters are generally supported by available evidence from stromatolites. This suggests that sinters can play a useful role in constraining palaeoclimatic and palaeohydrological reconstructions during the late Quaternary of the East African Rift Valley, particularly during the cooler episodes.

REFERENCES

[1] BATH, A.H., "Stable isotopic evidence for palaeo-recharge conditions of ground-water", Palaeoclimates and Palaeowaters: A Collection of Environmental Isotope Studies (Proc. Advisory Group Mtg, Vienna, 1980), IAEA, Vienna (1983) 169.

[2] ABELL, P.I., AWRAMIK, S.M., OSBORNE, R.H., TOMELLINI, S., Plio-Pleistocene lacustrine stromatolites from Lake Turkana, Kenya: morphology, stratigraphy and stable isotopes, Sediment. Geol. **32** (1982) 1.

[3] HILLAIRE-MARCEL, C., CASANOVA, J., Isotopic hydrology and palaeohydrology of the Magadi (Kenya)-Natron (Tanzania) basin during the late Quaternary, Palaeogeogr. Palaeoclimatol. Palaeoecol. **58** (1987) 155.

[4] TIERCELIN, J.-J., et al., Le demi-graben de Baringo-Bogoria, Rift Gregory, Kenya: 30000 ans d'histoire hydrologique et sédimentaire, Bull. Centres Rech. Explor. Prod. Elf-Aquitaine **11** (1987) 249.

[5] CASANOVA, J., HILLAIRE-MARCEL, C., Chronology and palaeohydrology of late Quaternary high lake levels in the Manyara basin (Tanzania) from isotopic data (^{18}O, ^{13}C, ^{14}C, Th/U) on fossil stromatolites, Quat. Res. **38** (1992) 205.

[6] STURCHIO, N.C., DUNKLEY, P.N., SMITH, M., Climate-driven variations in geothermal activity in the Northern Kenya Rift Valley, Nature (London) **362** (1993) 233.

[7] CLAYTON, R.N., O'NEIL, J.R., MAYEDA, T.K., Oxygen isotope exchange between quartz and water, J. Geophys. Res. **77** (1972) 3057.

[8] DARLING, W.G., ALLEN, D.J., ARMANNSSON, H., Indirect detection of subsurface outflow from a Rift Valley lake, J. Hydrol. **11** (1990) 297.

[9] CRAIG, H., LUPTON, J.E., HOROWITZ, R.M., Isotopic Geochemistry and Hydrology of Geothermal Waters in the Ethiopian Rift Valley, Rep. 77-14, Scripps Inst. Oceanogr. (1977).

[10] NICHOLSON, S.E., FLOHN, H., African environmental and climatic changes and the general atmospheric circulation in late Pleistocene and Holocene, Clim. Change **2** (1980) 313.

[11] TRUCKLE, P.H., Geology and late Cainozoic lake sediments of the Suguta Trough, Kenya, Nature (London) **263** (1976) 380.

[12] YURETICH, R.F., CERLING, T.E., Hydrogeochemistry of Lake Turkana, Kenya: mass balance and mineral reactions in an alkaline lake, Geochim. Cosmochim. Acta **47** (1983) 1099.

Water-Rock
Interaction

Edited by
YOUSIF K. KHARAKA & ANN S. MAEST
U.S. Geological Survey, Menlo Park, California, USA

OFFPRINT

Hydrocarbon gas ratio geothermometry in the East African Rift System

W.G. Darling & J.C.Talbot
British Geological Survey, Wallingford, UK

ABSTRACT: A gas geothermometer based on the ratio of methane to ethane (C_1/C_2) has been developed for use in geothermal exploration in the East African Rift System. The geothermometer was calibrated using data from geothermal wells in Kenya, Ethiopia and Djibouti. It appears to be robust, apparently not suffering to the same extent the problems (condensation, diffusion, reactivity) which beset the conventional ratio and concentration geothermometers using CO_2, H_2 and H_2S. It is postulated that a mixture of hydrocarbons is produced at $\leq 100°C$ from dissolved or sedimentary organic matter. When these gases enter the hotter parts of hydrothermal plumes, breakdown to CH_4 increases almost logarithmically with temperature. Independent evidence that C_1/C_2 is predictably temperature-dependent comes from a good correlation with $^3He/^4He$. Both ratios are likely to reach a maximum where temperature conditions are hottest. Sparse C_1/C_2 data from hydrothermal systems elsewhere in the world suggest that the methane/ethane geothermometer may have a wider application.

1 INTRODUCTION

The East African Rift System (Fig 1) contains many areas of geothermal activity, usually found in association with late-Quaternary volcanic centres. The generally rather arid nature of Rift climates has resulted in groundwater levels often a considerable distance below surface, and consequently few areas of natural discharge. The use of conventional cation and silica geothermometry is therefore seldom possible. Fumarolic discharges of steam and gas are however fairly common, and in most areas offer the only key to underground temperatures. Various gas geothermometers have been proposed, but their application to the comparatively weak fumaroles of the Rift is frequently inappropriate because the more reactive gases tend to disappear while traversing the often large distance from reservoir boil-off to the surface, and because subsurface condensation of steam changes the gas-water ratio (Armannsson, 1987).
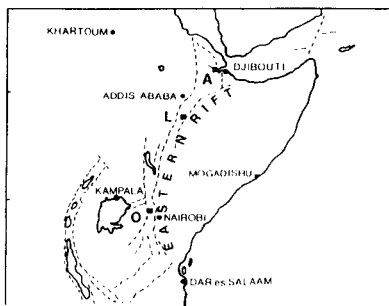

Fig 1. The East African Rift System. O, L and A refer to the Olkaria-Eburru, Langano and Asal geothermal fields respectively.

The ideal gas geothermometer would: (a) be based on a ratio, which would be much less affected by condensation than a concentration geothermometer, (b) use similar gases, which would be relatively immune to differentiation by diffusion, (c) use comparatively unreactive gases, which would not be consumed during

passage to the surface, and (d) use gases which can be detected down to low concentrations that could be measured even in weak or air-contaminated fumaroles.

During geothermal exploration in the Kenya Rift, it became apparent that the ratio between methane and ethane might provide a basis for geothermometry (Darling and Talbot, 1991).

2 RESULTS

To calibrate the putative C_1/C_2 geothermometer, gases were collected from geothermal wells at Olkaria and Eburru (Kenya), Langano (Ethiopia) and Asal (Djibouti). Results were supplemented by sampling from two localities where fumaroles could be sampled close to related boiling springs, and one outgassing hot spring.

Values of log CH_4/C_2H_6 are plotted against reservoir solute temperatures in Fig 2. A curve with a correlation coefficient of $r^2 = 0.64$ can be fitted to the data according to the following equation where R represents log C_1/C_2:

$$t°C = 454.8 - (586.4/R) + (281.4/R^2)$$

The plotted points fit the curve with a standard deviation of 27°C. The preponderance of data points from geothermal wells means that the curve is adequately constrained in the 200-300°C range, but less well so at lower temperatures. The curve is intended to be used with values of C_1/C_2 from 10^1 to 10^5, which is the approximate limit of detection, and which correspond to a temperature range of 150-350°C.
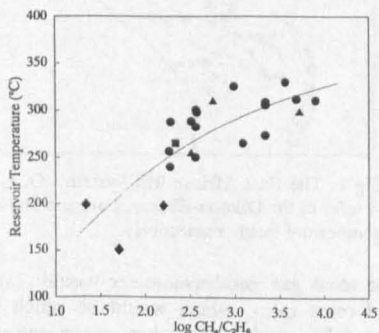
Fig 2. Log CH_4/C_2H_6 plotted versus reservoir solute temperature for geothermal wells at Olkaria (circles), Langano (triangles) and Asal (square). Diamonds represent springs.

3 APPLICATION

The histograms in Fig 3 show the C_1/C_2 geothermometer applied to fumaroles (some within the wellfields and some in unrelated areas) in Kenya, Ethiopia and Djibouti. In addition other geothermometers are shown for the same data set: the empirical equation of D'Amore and Panichi (1980), and the CO_2, H_2S, H_2 and CO_2/H_2 equations of Arnorsson and Gunnlaugsson (1985). These latter equations come in two different versions according to salinity and temperature of the underlying reservoir, and the appropriate version has been used for each fumarole plotted (details in Darling and Talbot, 1991). Some of the geothermometers give results above or below any feasible temperature range and these are omitted from the figures. Given that geothermal reservoir temperatures are commonly in the range 200-300°C, the methane/ethane geothermometer gives a likely distribution of results. CO_2 temperatures are almost uniformly high, and the others low or very low.

4 DISCUSSION

Unlike most other gas geothermometers, the methane/ethane geothermometer seems unlikely to be dependent on gas-mineral equilibria. Carbon stable isotope values for methane in the Rift are nearly all within the -30 to -20‰ range (Darling and Griesshaber, 1990), which suggests that the hydrocarbon gases are produced thermogenically. Abundant petroleum industry literature testifies that hydrocarbon production can begin at temperatures <100°C, and it is considered here that mixtures relatively rich in C_{2+} alkanes are produced from dissolved or sedimentary organic material in the warm outer regions of hydrothermal plumes. If these mixtures are drawn into the hotter parts of the plume, progressive breakdown of the C_{2+} alkanes occurs resulting in an almost logarithmic increase in C_1/C_2 with temperature.

Evidence that breakdown to CH_4 will increase with temperature is shown in Fig 4. This is based on the lignite pyrolysis experiments of Des Marais et al (1988) and clearly indicates a rise in log C_1/C_2 with temperature. Conditions in geothermal systems are very different from laboratory experiments, but independent evidence that there is a relationship between
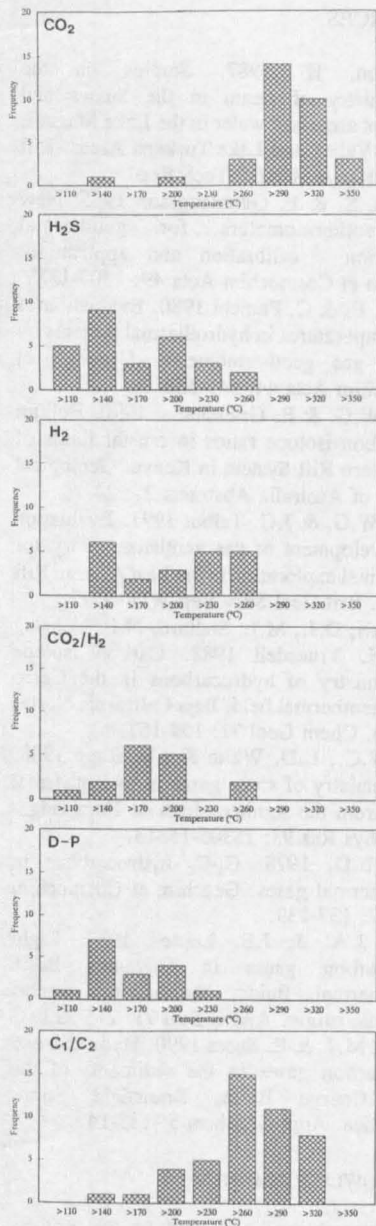
C_1/C_2 and temperature is provided by helium isotope ratios. Fig 5 shows the correlation between C_1/C_2 and $^3He/^4He$ for various fumaroles and wells from Olkaria in the southern Rift to Silali in the northern Rift of Kenya. In the absence of complicating factors, the highest helium R_A values will be found overlying the hottest parts of hydrothermal plumes where magmatic influences are largest. Clearly these are also the zones where greatest thermal breakdown could be expected.

5 APPLICABILITY ELSEWHERE

There appear to be few localities worldwide where both C_1/C_2 values and reservoir temperatures are known and therefore the
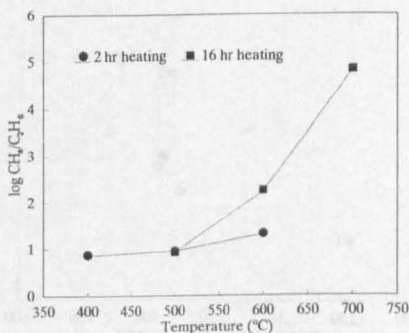
Fig 4. The lignite pyrolysis experiments of Des Marais et al (1988) plotted as log CH_4/C_2H_6 versus heating temperature.
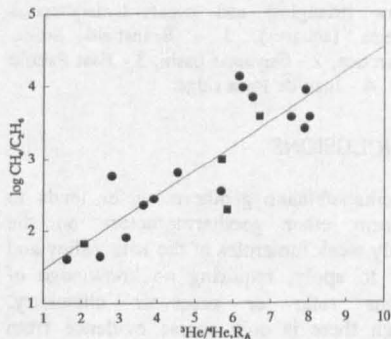
Fig 5. Plot of log CH_4/C_2H_6 versus $^3He/^4He$ (units R_A) for fumarole (circles) and well (squares) samples in the Kenya Rift.

Fig 3. Histograms of the C_1/C_2 geothermometer and other published geothermometers on the same data set. (D-P is the D'Amore-Panichi geothermometer).

1443

Miles, Douglas L. (ed.)   90 6191 970 3
Water rock interaction (WRI-6) – *Proceedings of the 6th international symposium, Malvern, UK, 3 – 8 August 1989*
1989, 25 cm, 838 pp., Hfl.150 / $85.00 / £47
Interactions between water & rock affect many vital aspects of everyday life. Geochemical reactions are all around us on the surface of the earth, in the atmosphere & beneath our feet. Scientific understanding of such natural processes has a bearing on topics including: the quality of the water we drink; the waste we produce & its disposal; what happens to acid rain; the search for new raw materials; the development of traditional sources of energy such as oil, coal, & gas; and the search for alternative sources of energy such as geothermal power. 199 papers.

Franciss, Fernando Olavo   90 6191 550 3
Soil and rock hydraulics – *Fundamentals, numerical methods and techniques of electrical analogs*
1985, 23 cm, 184 pp., Hfl.150 / $85.00 / £47
A textbook for geologists, mining & civil engineers. Soil & rock hydraulics describes mathematically the physical phenomena related to water seepage through soil & rock masses.

Kolkman, P.A., J. Lindenberg & K.W. Pilarczyk (eds.)
Modelling soil-water-structure interactions – *Proceedings of the international symposium, Delft, 29.08–02.09.1988*
1988, 25 cm, 514 pp., Hfl.150 / $85.00 / £47   90 6191 815 4
Topics on soil-water-structure interactions: General introduction of the processes & screening of the fields of interaction; Different ways of computation modelling & scale modelling; Use & usefulness of models for the designer. Topics on interactions: Wave & current induced behaviour of the seabed; Local scour; Behaviour & stability of block revetments & filter layers; Wave impact loads & behaviour of asphalt revetments; Piles, platforms, piers & gravity structures; Sand suppletion & flow slides; Breakwaters, dams & walls; Dynamics of slender structures & shock-induced wave propagation. Miscellaneous.

                                                          90 6191 632 1
Geotechnical and geohydrological aspects of waste management – *Proceedings of the 8th annual symposium on geotechnical and geohydrological aspects of waste management, Fort Collins, 5–7 February 1986*
1986, 23 cm, 570 pp., Hfl.185 / $99.00 / £58
Groundwater & surface hydrology; Geochemical transport; Geotechnical design; Reclamation & design aspects; Regulations & public concerns; Groundwater & other case histories.

Sargand, Shad M., Gayle F. Mitchell & John Owen Hurd (eds.)
Structural performance of flexible pipes – *Proceedings of the first national conference, Columbus, Ohio, 21 – 23 October 1990*
1990, 25 cm, 176 pp., Hfl.95 / $50.00 / £30   90 6191 165 6
Pipe deflections: A redeemable asset; Rib-stiffened soil-steel structures; Field measurements & analysis of a large diameter flexible culvert; Application of deep corrugated, box-culvert with corrugated plate reinforcement; Spiral rib metal pipe structural performance limits; etc.

Appelo, C.A.J. & D. Postma   90 5410 105 9
Geochemistry, groundwater and pollution
1992, 25 cm, c.500 pp., Hfl.140 / $78.00 / £44
Groundwater geochemistry is an interdisciplinary science concerned with the chemistry in the subsurface environment. Because it is the interaction with minerals in aquifers that ultimately determines the composition of groundwaters, this book emphasizes on water-mineral interactions as well as on the mineralogical and chemical compositions of rocks in aquifers. Introduction to groundwater geochemistry; From rainwater to groundwater; Solutions, minerals and equilibria; Carbonate reactions; Ion exchange and absorption; Silicate weathering; Redox processes; Transport in aquifers; etc.

Lee, J. H.W. & Y. K. Cheung (eds.)   90 5410 038 9
Environmental hydraulics – *Proceedings of the international symposium on environmental hydraulics, Hong Kong, 16 – 18 December 1991*
1991, 25 cm, 1500 pp., 2 vols., Hfl.225 / $120.00 / £69
The scientific management of water resources requires an understanding of hydraulic and hydrologic processes. The need to understand and predict the impact of pollutant discharges of engineering works on the water environment has provided an impetus to the development of hydraulics in the past three decades. In recent years, environmental hydraulic problems have been assuming increasing importance in many Southeast Asian countries and cities, including China and Hong Kong. The proceedings contains a collection of keynote and invited papers together with contributions selected for presentation at the symposium. The papers summarize recent advances and practical applications in themes that include: Mixing of wastewater effluent discharges; sea outfall design; hydrodynamic and water quality modelling; environmental management; flood hydraulics and hydrology; hydraulics of wastewater collection and treatment systems. Editors: University of Hong Kong.

Usmen, Mumtaz A. & Y. B. Acar (eds.)   90 5410 055 9
Environmental geotechnology – *Proceedings of the Mediterranean conference on environmental geotechnology, Cesme, Turkey, 25 – 27 May 1992*
1992, 25 cm, 600 pp., Hfl.140 / $78.00 / £44
Topics: Characterization of wastes; risk assessments techniques; fundamentals of experimental and theoretical modelling of contaminant transport; determination of model parameters; soil waste interactions which influence performance; design and anlysis schemes for passive containment systems; available and emerging active systems; performance assessment methods; use of amended wastes in earth structures; monitoring schemes; etc.

Balasubramaniam, A. S., et al. (eds.)   90 6191 785 9
Environmental geotechnics and problematic soils and rocks
Proceedings of an international symposium, Bangkok, December 1985
1988, 25 cm, 576 pp., Hfl.225 / $125.00 / £70
Geotechnical control & envrionmental protection; Environmental geotechnical aspects of major infra-structure projects; Environmental geotechnical aspects of natural hazards; Wastes & their use; Problematic soils & rocks.

Pergamon

0016-7037(95)00145-X

The origin of hydrothermal and other gases in the Kenya Rift Valley

W. G. DARLING,[1] E. GRIESSHABER,[2] J. N. ANDREWS,[3,*] H. ARMANNSSON,[4] and R. K. O'NIONS[5]

[1]British Geological Survey, Maclean Building, Wallingford, OX10 8BB, UK
[2]Max-Planck Institut für Chemie, Saarstrasse 23, D-55020 Mainz, Germany
[3]Postgraduate Research Institute for Sedimentology, University of Reading, Reading RG6 2AB, UK
[4]National Energy Authority, Grensásvegur 9, 108-Reykjavik, Iceland
[5]Department of Earth Sciences, Cambridge University, Cambridge CB2 3EQ, UK

Abstract—The Kenya Rift Valley (KRV) is part of a major continental rift system from which much outgassing is presently occurring. Previous research on gases in the KRV has tended to concentrate on their geothermal implications; the present paper is an attempt to broaden the interpretation by consideration of new data including helium and carbon isotope analyses from a wide cross-section of sites. In order to do this, gases have been divided into categories dependent on origin. N_2 and noble gases are for the most part atmospherically derived, although their relative concentrations may be altered from ASW ratios by various physical processes. Reduced carbon (CH_4 and homologues) appears to be exclusively derived from the shallow crust, with thermogenic $\delta^{13}C$ values averaging $-25\permil$ PDB for CH_4. H_2 is likely also to be crustally formed. CO_2, generally a dominant constituent, has a narrow $\delta^{13}C$ range averaging $-3.7\permil$ PDB, and is likely to be derived with little modification from the upper mantle. Consideration of the ratio $C/^3He$ supports this view in most cases. Sulphur probably also originates there. Ratios of $^3He/^4He$ reach a MORB-like maximum of 8.0 R/R_A and provide the best indication of an upper mantle source of gases beneath the KRV. A correlation between $^3He/^4He$ and the hydrocarbon parameter $\log(C_1/\Sigma C_{2-4})$ appears to be primarily temperature related. The highest $^3He/^4He$ ratios in spring waters are associated with basalts, perhaps because of the leaching of basalt glasses. There may be a structural control on $^3He/^4He$ ratios in the KRV as a whole.

INTRODUCTION

The Kenya Rift Valley is part of the extensive East African Rift System, which "defines a diffuse plate boundary within Africa and is often regarded as an example of the early stage of continental breakup" (Daly et al., 1989). The term Kenya Rift Valley (KRV) is used here to denote the Gregory and Turkana rift zones, plus the Nyanza rift unit (Rosendahl, 1987). In terms of geography, coverage in this paper extends from the Suswa volcano in the south to Lake Turkana in the north and from the Mt. Kenya area in the east to Lake Victoria in the west (Fig. 1).

The KRV is part of the East African Rift System and is a good example of a major continental rift structure, with a typical width of 60–80 km and a depth of about 1 km. The KRV is situated on a broad domal uplift with a thin (20–35 km) crust which abruptly thickens beyond the rift margins (Achauer et al., 1992). The rifting process has resulted in extensive Tertiary to Quaternary volcanism. Considerable outgassing is presently taking place and has probably been doing so in one form or another for at least 20 Ma (Bailey, 1980). In contrast to the largely nonvolcanic Western Rift, stretching from Uganda in the north to Malawi in the south, the Eastern Rift is characterised by numerous late-quaternary eruptive centres which are generally situated on or close to the rift axis. Only Oldoinyo Lengai in northern Tanzania is currently active, but many eruptive centres are dormant and support convective hydrothermal systems. The KRV forms about one-third of the Eastern Rift. Outgassing in the KRV occurs via fumaroles (steam jets) on the volcanic centres, and also by emissions from dry boreholes and seeps within the KRV proper and beyond.

Documentation of this activity commenced with detailed geological survey work in the 1950s and 1960s (Mason, 1967; McCall, 1967), and the gases themselves have been studied from the time geothermal exploration commenced in the 1970s. These studies (Glover, 1972; Armannsson, 1987; Geotermica Italiana, 1987) have been mostly concerned with the assessment of subsurface temperatures and flowpaths in connection with prospective geothermal development. A more comprehensive isotopic study of gases in the KRV was started with the British Geological Survey's regional exploration work in the southern and northern parts of the KRV (Allen et al., 1989; Allen and Darling, 1992).

This contribution presents a detailed study of gases from the KRV including carbon and helium isotope ratios and noble gas concentrations in gas and water samples. The aim is to gain further insights into the nature and mechanisms of outgassing in this part of the rift system in the belief that these may have applicability to a broad range of geological and related topics.

SAMPLING AND ANALYSIS

Samples of gas were taken from a variety of natural sources. An inverted conical funnel immersed in water was used for springs while a clay seal was used for fumaroles and gas seeps. Details of these methods are provided in Darling and Talbot (1991). Additional samples from geothermal, water, and dry wells were collected direct from the wellhead thus minimising the risk of air contamination.

Aliquots intended for major gas analysis (CO_2, H_2S, H_2, N_2, O_2, CH_4, and higher hydrocarbons, on an H_2O-free basis) were collected
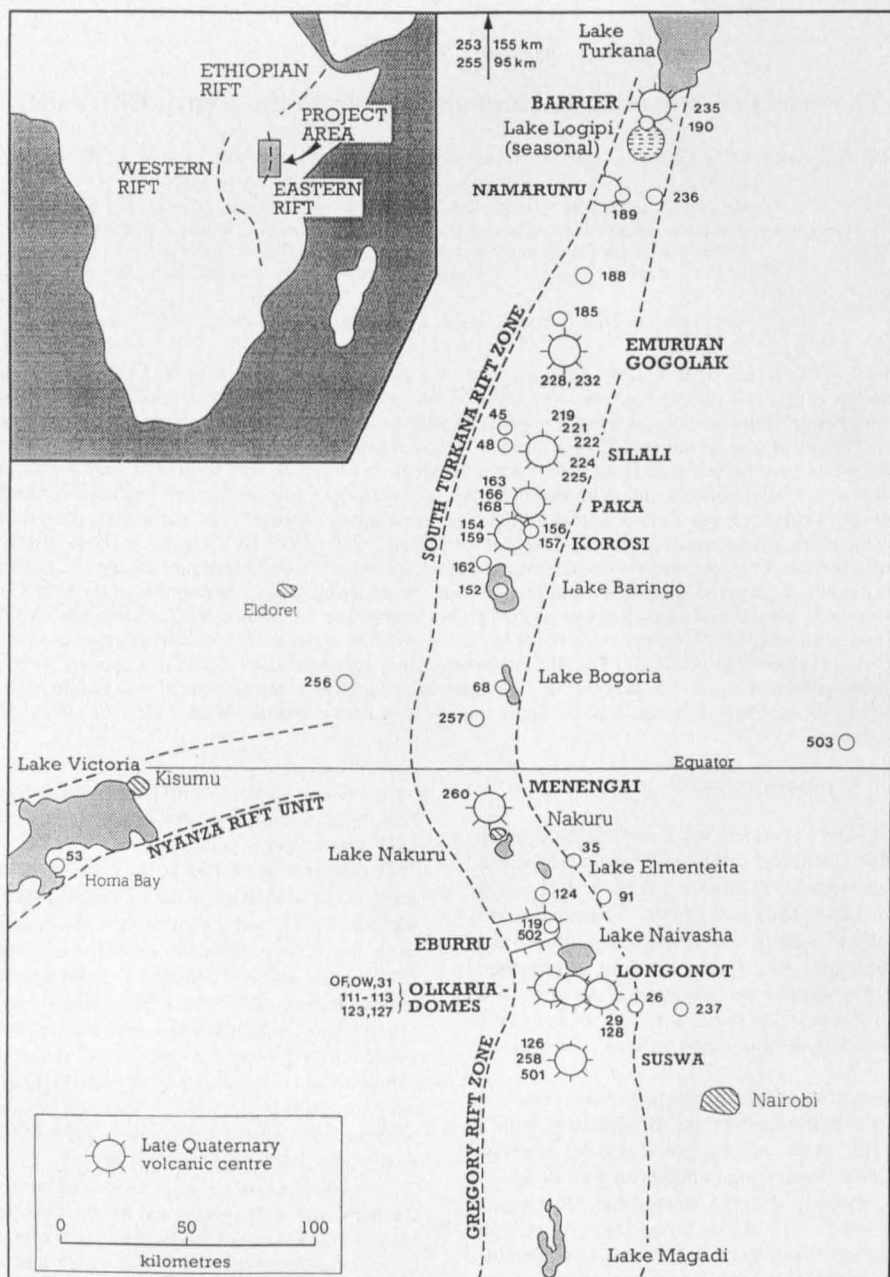

FIG. 1. Map of the KRV showing the disposition of late-Quaternary volcanic centres and location of sampling sites (site numbers are given a K prefix in text and tables).

into glass vessels, which were either untreated, or evacuated and containing a 40% NaOH solution to absorb CO_2 and H_2S. Samples for noble gas analysis (He, Ne, Ar, Kr, and Xe) were collected into tubes of annealed copper which were sealed by swage clamps.

Analysis of major gases was carried out at BGS Wallingford by standard techniques of chromatography and titrimetry. Carbon stable isotope ratios of CO_2 and CH_4 (after oxidation to CO_2 by CuO at 850°C) were measured on a VG-602E mass spectrometer. Noble gas abundances were analysed at Bath University on an Kratos MS-10S

mass spectrometer, while helium isotope ratios were measured at the University of Cambridge on a VG-3000 mass spectrometer using the procedures of Hooker et al. (1985).

RESULTS

General

Locations for which a range of analytical results are available are shown in Fig. 1. Abundances of major gases together

with carbon isotope ratios of CO_2 and CH_4 were obtained for a majority of these sites and are reported in Table 1. Gas concentrations are reported in mole percent while isotope ratios are reported in the following form:

$$\delta^{13}C = [(R_{sample}/R_{std}) - 1] \times 10^3, \qquad (1)$$

where R_{sample} is the $^{13}C/^{12}C$ ratio of the sample (CO_2 or CH_4) and R_{std} is the $^{13}C/^{12}C$ ratio of the PDB standard. Reproducibility of $\delta^{13}C$ analysis including sampling and preparation steps is estimated to be within $\pm0.2\%o$ for CO_2 and $\pm0.5\%o$ for CH_4.

Noble gas samples were taken from a smaller number of representative sites in the southern part of the KRV (Table 2) and were determined to a precision of $\pm1\%$. Reproducibility of N_2/Ar averaged at $\pm2\%$. Helium isotope ratios are presented in Table 3 in the form of sample ratio, corrected on the basis of Ne content for atmospheric contamination, relative to the ratio in air according to the following equation:

$$R/R_A = [(R_M/R_A)X - 1]/(X - 1), \qquad (2)$$

where $R_A = {}^3He/{}^4He$ in the atmosphere, $R_M = {}^3He/{}^4He$ measured in the sample, and $X = [(He/Ne)_{sample}\beta Ne]/[(He/Ne)_{air}\beta He]$.

The terms βNe and βHe refer to the Bunsen solubility coefficients for He and Ne at appropriate temperature and pressure. For gas phase samples the β terms were not used. Reproducibilities for measurements of $^3He/^4He$ and He/Ne were $\pm1\%$ and $\pm10\%$, respectively.

Nitrogen, Oxygen, and Argon

Fumaroles in the KRV are not generally very vigorous features and in addition are not always easy to sample. The presence of O_2 represents atmospheric contamination at a late stage either by near-surface entrainment of air which has penetrated porous rock, or conceivably from dissolved air in shallow perched water bodies. While some N_2 is also due to contamination at or near the point of sampling, there are cases where there is clearly an original component in the emanating gases, though this is likely to be ultimately derived from the atmosphere also. When the ratios N_2/Ar and $^{40}Ar/^{36}Ar$ (Table 2) are plotted against each other (Fig. 2) most samples reveal evidence of air equilibration with water ($N_2/Ar \sim 40$). Samples with higher ratios indicate at least a component of direct air contamination not involving solution processes. However, all of these samples are dispersed along a trend coincident with the $^{40}Ar/^{36}Ar$ ratio of air, except for the Nyanza Rift sample from Bala (K53) which has a higher value. This particular case is presumed to be due to excess Ar produced by radiogenic decay of ^{40}K; the $^{40}Ar/^{36}Ar$ ratio of 846 is some three times higher than the atmospheric value of 296 (Fig. 2).

Carbon Dioxide, Methane, and Higher Alkanes

Oxidised carbon is represented by CO_2 and the chemically equilibrated forms of HCO_3^- and $(CO_3)^{2-}$. When atmospheric contamination (as indicated by the amount of O_2) is low or absent, CO_2 is almost always by far the most abundant fumarolic gas (on a steam-free basis) with concentrations often in excess of 90%. Highly consistent $\delta^{13}C$-CO_2 values were obtained from thirty-two fumaroles, wells, and seeps (Table 1), with an average of $-3.7\%o$ and a standard deviation of $1.1\%o$, though with a total range from -1.7 to $-7.1\%o$. These comparatively consistent results were not produced solely from recently active centres; examples from Bala (K53, Miocene carbonatite), Kureswa (K256, a travertine-depositing area west of the Rift proper), the Kerita CO_2 well (K237, on the eastern rift shoulder), and from mofettes at Meru (K503 on the eastern flanks of Mt. Kenya some 130 km from the KRV) all fall within a restricted range.

Reduced carbon is represented by CH_4 and higher alkanes sometimes detectable up to C_6H_{14}, plus benzene (C_6H_6), though only C_2 to C_4 are reported here. Even in the least air-contaminated fumaroles, CH_4 is rarely present at more than 1% by volume of the gas phase, with the accompanying higher homologues always a factor of 10^2 or 10^3 lower in concentration (see Table 1). No alkene compounds were detected.

Results of $\delta^{13}C$-CH_4 analysis are given in Table 1. As with CO_2 these are quite consistent (twenty-eight sites, average $-25.2\%o$, standard deviation $3.4\%o$, range -18.3 to $-31.8\%o$), despite the variety of site types from which samples were collected.

Hydrogen and Hydrogen Sulphide

Hydrogen and H_2S concentrations are generally lower in fumarolic gases of the KRV than is typical of other hydrothermal systems. This is probably mainly due to the often considerable depth of geothermal reservoirs in the rather arid KRV, which allows abundant scope for these gases to react with wallrock or become oxidised during passage to the surface. This is demonstrated by a comparison of gas analyses from the Olkaria well (OW-n) and fumarole (OF-n) averages in Table 1. The fumarole gases are depleted in H_2 and H_2S compared to the deep fluids which are brought rapidly to the surface by the geothermal wells. Gas chromatographic analysis of some of the more S-rich gas samples was undertaken to test for forms other than H_2S, such as COS and CS_2. These could not be detected at parts per million level in the total gas, implying that there is little or no reaction between the S and carbon phases. The few H_2 isotope analyses available (not reported here) are, at δ^2H values of around $-500\%o$, consistent with high temperature equilibrium between H_2 and H_2O (Arnason, 1977).

Neon, Krypton, and Xenon

The noble gases neon, krypton, and xenon are normally almost wholly derived from the atmosphere. Table 2 gives analyses for waters and gases of the southern KRV. The results, where they indicate that samples have not re-equilibrated with air at or near the point of discharge, may be used to infer various physical processes.

A plot of xenon vs. krypton for wells and springs (Fig. 3) demonstrates that most waters appear to have suffered little modification (confirming other geochemical indicators) and have in at least half the cases retained ratios reflecting their recharge temperatures (which in the case of sites like K96 are likely to be at considerable altitude, though perhaps not quite as cool as the plot suggests; however, if there is "excess" gas

Table 1. Gas and carbon stable isotope analyses of gas phase samples collected mainly within the KRV (refer to Fig. 1 for sample locations).

Area Locality	Sample No.	Sample Source	Sampling Temp. °C	CO_2 mmole/kg	CO_2	N_2	$O_2 + Ar$	H_2	H_2S	CH_4	C_2H_6	C_3H_8	C_4H_{10}	$\delta^{13}C_{CO_2}$	$\delta^{13}C_{CH_4}$
							per cent					ppmv		‰ PDB	
Suswa															
F-3	K126	F	93	851	10.2	71.3	18.5	<0.001	<0.01	0.0003	<1	<1	<1	nd	nd
F-12	K258	F	94	1364	16.5	66.4	16.5	0.001	0.03	0.087	0.4	0.1	0.2	-3.0	-25.0
F-28[1]	K501	F	92	3720	97.4	0.27	<0.1	0.92	<0.01	1.40	3.4	<1	<1	-3.7	nd
Longonot															
F-23	K128	F	90	9382	77.4	16.2	4.0	1.7	0.01	0.75	1.0	<1	<1	-4.0	nd
Mt. Margaret[1]	K29	F	86	12561	95.2	4.6	<0.1	<0.001	<0.01	0.18	1.0	<1	<1	-1.7	nd
Olkaria/Domes															
OF-n[2]	-	F	91(7)	-	84.3(7)	10.9(7)	2.7(7)	1.54(7)	0.10(3)	0.58(7)	18(7)	2.5(7)	0.2(7)	-3.8(7)	-26.5(6)
OW-n[2]	-	G	na	118(9)	81.0(9)	0.9(9)	<0.1(9)	9.4(9)	7.9(9)	0.76(9)	9.9(9)	0.4(9)	<0.1(9)	-2.6(2)	-27.2(11)
H-1[1]	K31	C	95	61	99.0	<0.1	<0.1	0.11	<0.01	0.77	29	nd	nd	-2.1	nd
F-15	K127	F	92	631[1]	17.4	64.5	18.0	<0.001	<0.01	0.13	2.5	<1	<1	-3.0	nd
Eburru															
EF2	K119	F	92	nd	78.9	11.7	3.1	1.7	nd	4.6	5.0	<1	<1	-2.3	nd
EW1	K502	G	na	272	97.4	0.34	<0.1	0.09	1.18	0.99	2.7	0.1	<0.1	nd	-23.2
Menengai-Bogoria															
MN1	K260	F	76	nd	4.55	78.3	17.2	<0.001	nd	0.033	<0.1	<0.1	<0.1	-6.9	nd
Arus	K257	F	95	2561	99.5	0.17	<0.1	0.004	<0.01	0.35	6.4	1.2	0.4	-4.3	-28.1
Ol Kokwe-Korosi															
OK1	K152	F	96	1254	88.8	9.8	0.10	0.79	0.23	0.32	20	4	<0.1	-3.5	-18.3
KR12	K154	F	96	753	42.7	46.6	10.3	<0.001	0.15	0.21	8	3	<0.1	-4.3	nd
KR18	K156	F	96	1178	96.2	1.9	0.30	<0.001	0.03	1.5	340	130	43	-3.9	-24.5
KR19	K157	F	96	1494	97.4	1.0	0.05	<0.001	0.05	1.3	290	130	26	-3.9	-23.4
KR23	K159	F	96	1420	16.3	65.1	18.2	0.40	<0.01	0.015	9	0.8	0.2	-6.2	-19.7
KR34	K162	F	92	1580	85.0	11.7	2.8	0.006	0.01	0.44	98	16	17	-4.6	-29.6
Paka															
PK1	K163	F	96	450	83.1	11.3	3.4	<0.001	0.74	1.5	1.0	<0.1	<0.1	-2.9	-24.9
PK4	K166	F	95	215	91.7	2.1	0.61	4.1	0.19	1.3	1.0	<0.1	<0.1	-3.4	-27.8
PK7	K168	F	94	684	67.0	30.2	0.61	0.92	0.38	0.85	39	14	6	-2.7	-22.2
Silali															
SL7	K219	F	95	336	97.7	0.34	0.09	0.87	0.70	0.25	0.7	<0.1	<0.1	-3.8	-23.0
SL14	K221	F	96	377	98.2	0.29	0.05	0.65	0.60	0.25	0.6	0.1	<0.1	-3.7	-24.3
SL15	K222	F	97	142	98.0	0.22	0.06	0.93	0.58	0.24	1.0	0.1	<0.1	-3.9	-25.0
SL19	K224	F	96	5273	77.5	16.8	4.4	<0.001	0.24	1.1	0.5	<0.1	<0.1	-4.6	nd
SL22	K225	F	92	5591	69.4	24.4	5.9	<0.001	0.08	0.17	0.6	0.1	<0.1	-3.6	-21.7
Lorusio	K45	S	81	na	83.6	13.3	2.3	0.79	nd	0.11	1.0	<0.1	<0.1	-2.6[3]	-28.3
Emuruangogolak															
EM9	K228	F	95	2272	28.8	57.0	13.4	0.001	0.15	0.64	2.0	<0.1	<0.1	-4.7	-20.7
EM20	K232	F	96	1545	58.0	32.5	7.9	0.002	1.1	0.51	0.1	<0.1	<0.1	-4.0	-22.5
Kageinya	K188	S	68	na	<0.1	97.5	1.1	0.003	nd	1.41	280	120	33	nd	-31.8
Namarunu															
Elboitong	K236	S	95	na	99.0	0.64	0.37	<0.001	nd	0.011	1.1	0.1	<0.1	-2.2[3]	-28.3
Barrier															
KK1	K235	F	96	208	17.1	64.8	18.0	0.008	0.02	0.044	0.1	<0.1	<0.1	-3.3	-26.3
Turkana Islands															
North	K253	F	96	3070	89.0	8.6	1.2	0.053	0.008	1.12	80	10	1.1	-5.4	-28.4
Central	K255	F	97	857	92.5	0.56	<0.1	1.85	4.2	0.89	46	9.4	3.7	-3.8	-30.9
W. of Rift															
Bala	K53	F	72	na	89.6	9.86	<0.1	0.21	nd	0.28	5.3	0.17	<0.1	-2.0[3]	-26.8
Kureswa	K256	S	62	na	2.9	95.6	0.6	0.001	nd	0.82	16	0.8	0.4	-7.1[3]	-27.5
E. of Rift															
Carbacid Co.	K237	C	amb	na	98.4	0.35	<0.1	0.001	nd	1.24	190	52	21	-2.4	-20.5
Meru/Chogoria	K503	M	amb	na	37.5	nd	nd	<0.001	nd	0.006	<0.1	nd	nd	-3.5	nd

Sample Sources: C - dry borehole; F - fumarole; G - geothermal well; M - mofette; S - spring
nd - not determined   na - not applicable

[1] Data for whole gas analysis or specific measurement from ARMANNSSON (1987).
[2] OF-n and OW-n refer respectively to averages for typical Olkaria fumaroles and geothermal wells; numbers in brackets refer to the number of samples averaged (full data in DARLING and TALBOT, 1991)
[3] Corrected to total inorganic carbon balance.

Table 2. Noble gas analyses from selected sites in the southern KRV.

Site No.	Locality	Sample Source	Sampling Temp. C	Ne x 10^{-7}	Ar x 10^{-4}	Kr x 10^{-8}	Xe x 10^{-8}	N_2/Ar	^{40}Ar/^{36}Ar
Dissolved Phase									
K25	Kijabe RVA	B	35	1.64	2.60	5.98	0.86	37.8	294.1
K28	Mayer's Farm	S	28	1.47	2.25	4.97	0.70	39.9	294.1
K35	Kariandusi	S	39	1.43	1.94	4.16	0.58	49.8	295.4
K82	C4178 Naivasha	B	21	2.47	3.38	7.09	0.97	42.4	296.4
K92	Kanyamwi Farm	B	27	1.64	2.60	5.87	0.84	39.3	294.9
K96	P65 Kinangop	B	21	1.67	2.83	6.42	0.91	39.1	296.8
K100	C1404 Ndabibi	B	21	1.47	2.11	4.53	0.62	57.9	297.6
K118	Nakuru No 7	B	28	1.53	2.29	5.03	0.69	40.2	293.7
K124	Soysambu DEL	B	32	0.87	1.05	2.12	0.30	35.2	297.0
Gaseous Phase									
K53	Bala	S	72	3.65	30.9	22.4	3.09	22.5	846.0
K110	Olkaria OW2	G	-	0.15	0.10	0.15	-	43.2	304.4
K119	Eburru EF2	F	92	0.30	0.35	0.75	0.11	23.2	303.4
K123	Olkaria W	F	92	0.21	0.26	0.53	0.10	35.2	261.4
K126	Suswa F-3	F	93	74.9	34.5	43.1	3.64	87.8	293.1
K127	Domes F-15	F	92	61.8	30.9	35.6	3.27	88.0	291.3
K128	Longonot F-23	F	90	28.4	12.0	14.0	1.45	77.8	278.7

Sample sources: B - borehole; F - fumarole; G - geothermal well; S - spring

Gas concentrations in cm^3 (STP)/g water or cm^3/cm^3 total gas as appropriate.

it is unlikely to be due to air contamination on the evidence of Fig. 3). Other sites such as K35 and K118 show evidence of the Xe/Kr ratio tending towards those corresponding to sampling temperatures or even, in the case of K100, having re-equilibrated at a higher temperature than this. Site K124 is a borehole with high CO_2 and He to which outflow from the Eburru geothermal field probably contributes (Arusei, 1992), and this may be a factor behind the anomalous Xe/Kr ratio.

Information about free gases is obtained from a log plot of Ne vs. Kr (Fig. 4). Some fumaroles (K126 and 127) show ratios close to that of air, suggesting air entrapment or contamination which is confirmed by the analyses in Table 1 (the position of K128 on the plot is more problematical because of much lower air contamination as indicated in Table 1). Noble gases in these fumaroles can therefore reveal little about conditions at depth. In the case of fumaroles K119 and K123 equilibrium with water at a somewhat higher temperature than that of average recharge (~25°C) suggests that perched aquifers may be causing gases to re-equilibrate at lower than geothermal reservoir temperatures. Higher equilibration temperatures are marked by a tendency towards air-like ratios (though not quantities) for the noble gases (e.g., Potter and Clynne, 1978) which explains the position of the geothermal well OW2 (K110) on the plot. Conversely the carbonatite complex spring (K53) at Bala in the Nyanza rift has a composition suggesting equilibrium with recharge at cooler than normal temperatures. This, however, receives no support from oxygen and hydrogen stable isotope ratios (Allen et al., 1989). Possibly noble gas ratios have been perturbed in this water by the same factors which have led to the exceptionally high He content (Table 3).

Helium

Amounts of helium in crustal gases of the KRV are almost uniformly low (Table 3). There appears to be no particular

correlation between concentration of He and other geothermal parameters, as has also been noted in the Ethiopian Rift (Craig et al., 1977) and indeed elsewhere (Griesshaber et al., 1992; Poreda et al., 1992). Only when ^{3}He/^{4}He isotope ratios are considered does a pattern emerge. The highest ^{3}He/^{4}He values, with R/R_A from approximately 5.5 to 8, are generally found in close association with the late-Quaternary volcanic centres of the KRV (Table 3, Fig. 1).

For gaseous sources it may be noted that a plot of CO_2 percentage vs. Ne-corrected ^{3}He/^{4}He as R/R_A indicates that highest ratios are only obtained when CO_2 exceeds 50% of the gas phase (Fig. 5). Below this figure the presence of air-derived gases appears to perturb the ^{3}He/^{4}He ratio to the extent that corrections based on the neon content cannot alone restore the "true" ^{3}He/^{4}He value. While this is difficult to prove conclusively, samples with <50% CO_2 have been largely excluded from further discussion of the helium isotope data.

Examination of the data in Table 3 show that where there is more than one helium isotope analysis for an individual volcanic centre, there is usually fair agreement between the results. For example in the south, four very similar ^{3}He/^{4}He values of 5.7 ± 0.1 reported as R/R_A have been obtained from the Olkaria geothermal area, while in the north the Silali caldera provided three sites with R/R_A values averaging 7.8 ± 0.3. The Olkaria and Eburru ^{3}He/^{4}He data apart from demonstrating consistency within individual volcanic centres (and, happily, between laboratories) also show that similar helium isotope data can be obtained from surface fumarolic and deep (~2000 m) geothermal well sources, thereby giving confidence that under suitable conditions the results obtained from fumaroles elsewhere in the KRV are genuinely representative of deep fluids.

Table 3 shows that ratios of C/^{3}He (effectively CO_2/^{3}He) for many sites are close to the MORB average of 2 × 10^9 (Marty, 1992). The only site with a significantly lower ratio

Table 3.   Helium isotope data, ratios with respect to air and carbon dioxide to mantle helium ratios.

Site No.	Locality	Sample Source	Sampling Temp. °C	^{3}He x10^{-12}	^{4}He x10^{-6}	He/Ne	R/R$_A$	C/^{3}He x10^9
Dissolved Phase								
K26	Kijabe RVA	B	35	0.97	0.54	43	0.9	-
K35	Kariandusi	S	39	0.49	0.12	1	3.0	-
K48	Kapedo	S	50	38	7.0	1	3.9	-
K68	Bogoria	S	96	2.3	0.45	11	3.8	-
K91	Kanyamwi Farm	B	27	0.19	0.11	2	1.3	-
K124	Soysambu DEL	B	32	13	2.9	32	6.5	-
K185	SV3	S	68	7.7	1.2	18	4.6	-
K189	Namarunu	S	66	6.5	0.65	4	7.1	-
K190	Logipi	S	61	3.9	0.43	22	6.5	-
Gaseous Phase								
K45	Lorusio	S	81	120	17	15	5.0	7.0
K53	Bala	S	72	5950	2900	72	1.5	0.15
K111	Olkaria OW2	G	-	210	27	33	5.7	1.9
K112	Olkaria OW26	G	-	180	23	37	5.8	2.7
K113	Olkaria OW16	G	-	-	-	2*	5.8*	-
K119	Eburru EF2	F	92	100	12	24	6.3	7.9
K123	Olkaria W	F	92	32	4.1	75	5.6	23
K126	Suswa F-3	F	93	16	7.3	93	1.6	6.4
K127	Domes F-15	F	92	2.1	0.52	92	2.9	83
K128	Longonot F-23	F	90	280	30	92	6.7	2.8
K152	Ol Kokwe	F	96	21	3.1	35	4.9	42
K154	Korosi KR12	F	96	99	18	2	3.9	4.3
K157	Korosi KR19	F	96	260	74	7	2.5	3.8
K159	Korosi KR23	F	96	65	30	1	1.6	2.5
K162	Korosi KR34	F	92	200	46	5	3.2	4.3
K163	Paka PK1	F	96	350	32	2	7.9	2.4
K166	Paka PK4	F	95	290	34	21	6.2	3.2
K168	Paka PK7	F	94	420	83	7	3.6	1.6
K219	Silali SL7	F	95	230	21	30	7.5	4.2
K221	Silali SL14	F	96	320	29	31	8.0	3.1
K225	Silali SL22	F	92	310	28	35	7.9	2.2
K228	Emuruangogolak EM9	F	95	16	2.7	1	4.2	18
K232	Emuruangogolak EM20	F	96	130	15	3	6.0	4.5
K235	Barrier KK1	F	96	56	12	1	3.3	3.1
K237	Carbacid Co.	C	amb	9.3	3.2	82	2.1	106
K251	Arus	F	95	-	-	71*	4.5*	
K261	Eburru EW1	G	-	-	-	22*	6.7*	

Sample sources: B - water borehole; C - dry borehole; F - fumarole; G - geothermal well; S - spring.

He concentrations in cm^3 He(STP)/g water or cm^3 He/cm^3 total gas as appropriate.

R/R$_A$ - ^{3}He/^{4}He ratio relative to that of air (1.4 x 10^{-6}; MAMYRIN and TOLSTIKHIN, 1984)) corrected for contamination on the basis of Ne content.

* Data of the Unocal Geothermal Division.

is Bala in the branching Nyanza rift unit, where He concentrations are extremely high. A few sites have significantly higher values, for reasons to be discussed below.

DISCUSSION

The gaseous emanations of the KRV must be derived from one or more of the three principal sources: the atmosphere, the crust, and the mantle. For the purposes of considering their origin it is convenient to divide the gases into these subgroups which are described below.

Gases Derived from the Atmosphere

Once the effects of any atmospheric contamination are discounted, it is seen that the amount of original N_2 in fumarolic and borehole gases is almost uniformly low (Table 1). In the absence of any $^{15}N/^{14}N$ data, it is assumed that all N_2 has been ultimately derived from atmospheric sources (although a "deep" component with a $\delta^{15}N$ of -10 to $-15‰$ was as-

sumed for Oldoinyo Lengai by Javoy et al., 1989). The evidence of $^{40}Ar/^{36}Ar$ makes it likely that in virtually all cases argon too has, ultimately, an atmospheric source. Although the $^{40}Ar/^{36}Ar$ data reported here are all from fluids in the KRV south of the equator, very similar results were obtained from trapped Ar during the dating of volcanic rocks from Silali (location, Fig. 1). These ratios ranged from 275–315 (Smith et al., 1995), and tend to confirm that there is very little radiogenic gas production in the main KRV.

It is also assumed that neon, krypton, and xenon are almost wholly derived from atmospheric sources and therefore that their concentrations may (when uncontaminated) permit tracing of hydrological processes in the subsurface. Helium isotope results, on the other hand, suggest that only a proportion of helium is atmospherically-derived.

Gases Derived from the Crust

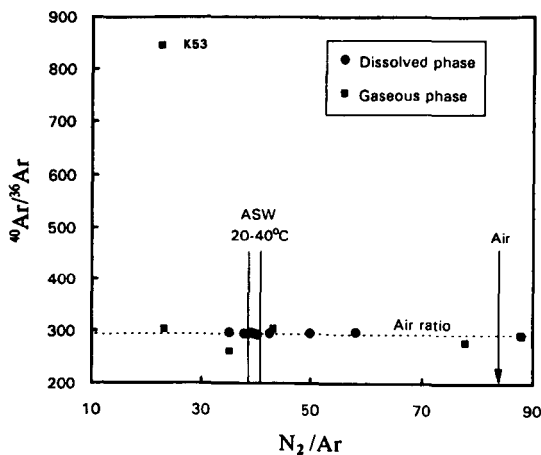While it has been demonstrated that most argon is atmospheric in origin, the sample at Bala (K53) in the Nyanza rift

FIG. 2. Plot of $^{40}Ar/^{36}Ar$ vs. N_2/Ar for water and gas samples from representative sites in the southern KRV. The $^{40}Ar/^{36}Ar$ value for air is shown, together with atmospheric and air-saturated water (ASW) values of N_2/Ar.
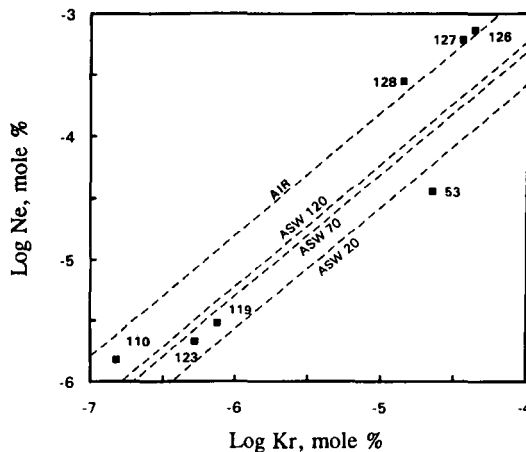

FIG. 4. Log plot of Ne vs. Kr for gas phase samples from representative localities (site numbers as shown) in the southern KRV. Also shown are the air ratio line (AIR) and the ASW ratio lines for 20, 70, and 120°C (ASW 20, 70, and 120) based on the data of Wilhelm et al. (1977) and Potter and Clynne (1978).

contains crustally produced ^{40}Ar. A possible interpretation of this is that thermal groundwater at Bala is in residence for significantly longer than similar groundwaters in the main KRV, but differences in mineralogy between the two areas may also contribute. The igneous rocks of the main KRV are predominantly intermediate-peralkaline in type (comendites, trachytes, and phonolites) while Bala is situated on the site of the Homa Mountain carbonatite complex. Carbonatites commonly contain higher concentrations of radiogenic elements than intermediate rocks (Mariano, 1989). However, some volcanic rocks in the main KRV have higher concentrations of radioelements than others, notably in the southern Rift at Olkaria (Clarke et al., 1990), without appearing to perturb the atmospheric $^{40}Ar/^{36}Ar$ signature in gases and wa-

ter. The high $^{40}Ar/^{36}Ar$ ratio at Bala is therefore probably related to the dominance of mineral alteration over mineral diffusion as a release mechanism for ^{40}Ar (Andrews, 1992) rather than high radioactivity; carbonate minerals would be more susceptible to alteration than the silicates of the main KRV.

Despite the high concentration of helium at Bala, the helium isotope ratio suggests a balance of sorts between mantle and crustal sources. Conceivably this could be the result of mantle helium trapped during the emplacement of the carbonatite being supplemented before release by inbred ^4He.

It is inconceivable that the high flux of CO_2 from the KRV and its environs could be derived predominantly from atmospheric or soil zone sources, and this is borne out by the gen-

FIG. 3. Plot of Xe vs. Kr for wells and springs from representative localities (site numbers as shown) in the southern KRV (data corrected for sampling altitude). ASW ratios corresponding to various temperatures are also shown (data of Wilhelm et al., 1977).
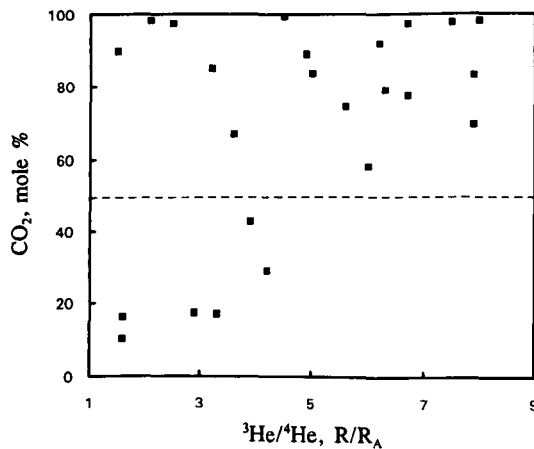
FIG. 5. Plot of CO_2 percentage vs. helium isotope ratio for gaseous sources in the KRV (cutoff line indicates that samples with <50% CO_2 may not be giving a representative $^3He/^4He$ value).

erally consistent $\delta^{13}C$-CO_2 values (Table 1). The average
value of $-3.6‰$ is unrepresentative of atmospheric ($\sim -7‰$)
or soil zone (~ -16 to $-26‰$) sources, though a few air-
contaminated fumaroles such as K159 and K260 have more
depleted values which may indicate a proportion of bacterially
produced CO_2 from the soil zone.

It is also unlikely that the CO_2 from most sites is crustally
derived. Mechanisms such as decarbonation of marine lime-
stones have been postulated as sources of CO_2 with near-zero
$\delta^{13}C$ values (e.g., in Truesdell and Hulston, 1980); while no
such limestones exist in the KRV, there are carbonate evap-
orites in places, and carbonatites are known from the wider
region. Nevertheless, the sheer amount of CO_2 outgassing
suggests that oxidised carbon must be predominantly derived
from a mantle reservoir, and this is supported by most of the
$C/^3He$ ratios in Table 3.

However, there are a few sites where $C/^3He$ is significantly
higher than MORB-like values. This is illustrated by Fig. 6a,
which shows a plot of helium isotope ratios vs. $C/^3He$ values.
Points representing fumaroles at Olkaria (K123) and Ol
Kokwe Island (K152), and the Kerita CO_2 well (K237) lie
on what appears to be a single trend away from the MORB
zone. Figure 6b shows this to be a partial coincidence; while
in each case there are indications of the influence of crustal
helium, the CO_2 well is clearly differentiated from the fu-
marole sites by its $\delta^{13}C$-CO_2 value. The ^{13}C data suggest that
there is a minor crustal contribution of organically derived
CO_2 at Olkaria and Ol Kokwe. This is not shown by the deep
geothermal wells at Olkaria and therefore implies a compar-
atively near-surface addition, at least in that particular case.
The Carbacid Company well at Kerita, however, appears to
derive its "extra" CO_2 from an inorganic crustal source. The
well is situated on the rift flanks, almost adjacent to the high-
est elevation of the rift floor, where carbonate evaporites are
unlikely ever to have formed. Possibly the CO_2 is derived
from decomposition of carbonatites; though none are exposed
in the area, Miocene carbonatites are well developed to the
west and south of the region, and may possibly be present at
depth in parts of the KRV. The data under consideration here
suggest that if present they are very localised.

Unlike most oxidised carbon, reduced carbon probably has
a predominantly crustal source in the KRV. A lack of detect-
able alkene compounds is an indication that methane is un-
likely to have been formed by abiogenic synthesis (Gunter
and Musgrave, 1971); while the presence of H_2 in most hy-
drothermal systems might be thought to rule out the survival
of such unsaturated hydrocarbons, they have been detected in
certain geothermal fields elsewhere, e.g., by Giggenbach and
Glover (1992) and Capaccioni et al. (1993), albeit at low
concentrations. On the other hand, the presence of sometimes
relatively abundant C_{2+} compounds probably rules out pro-
duction by bacterial methanogenesis which tends to produce
CH_4 and very little else. A thermogenic (thermocatalytic) de-
composition of organic matter seems the most likely source
of hydrocarbon production.

Such an origin would tend to be confirmed by the $\delta^{13}C$-
CH_4 results (Table 1). The average of $-25.2‰$ is typical of
carbon in terrestrial and lacustrine plant matter (e.g., Deines,
1980) and also of geothermal methane in many other areas.
In geothermal fields hosted at least partly in sedimentary
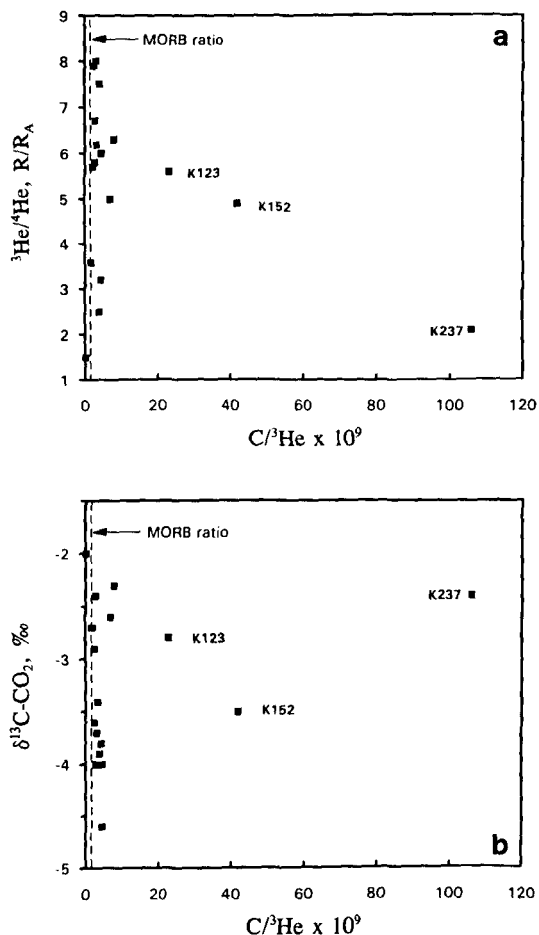
FIG. 6. (a) Plot of helium isotope ratio as R/R_A vs. $C/^3He$ for gas-
eous sources in the KRV (samples $< 50\%$ CO_2 excluded). Most
samples plot around the MORB ratio of 2×10^9, but a few sites have
values suggesting a crustal contribution of CO_2 (site numbers for
these are shown). (b) Plot of $\delta^{13}C$-CO_2 vs. $C/^3He$. One outlying site
appears to receive a contribution from a different crustal source of
CO_2 than the others.

rocks, suitable organic precursors have often been identified
(for example, coal at Cerro Prieto, Mexico; Des Marais et al.,
1988). The KRV does not possess sedimentary sequences of
great thickness, but lacustrine deposits may provide a source
of suitable organic compounds. Either these are invaded epi-
sodically in places by hot fluids, or dissolved organic com-
pounds may be drawn into hydrothermal plumes. In each case
geothermal heat will cause degradation of the organic com-
pounds into hydrocarbon gases. The spread of $\delta^{13}C$-CH_4 val-
ues may reflect the degree of thermal maturity reached locally,
or possibly an approach to isotopic equilibrium with CO_2,
though calculated $\Delta^{13}C$ temperatures are nearly always im-
probably high for the hydrothermal systems concerned. It
does not appear to be due to inputs of abiogenic mantle CH_4
(see next section).

A correlation between log (C_1/C_{2+}) and temperature has
been observed for the East African Rift System in general

(Darling, 1995; Darling and Talbot, 1991, 1992), and it is concluded that when organic compounds are drawn into hydrothermal plumes, progressive degradation to CH_4 takes place with rising temperature. This suggests that hydrocarbon generation is taking place at shallow levels in the crust where suitable conditions prevail. That the temperature need not be high is confirmed not only by petroleum research literature (e.g., Simoneit, 1990) but also by the results from relatively low-temperature systems such as Bala and Kureswa (K53, K256), with solute geothermometer temperatures of $< 100°C$, and the Kerita CO_2 well on the rift flank (K237). While long heating times would be required at such temperatures, there are indications that KRV hydrothermal systems are in general long lived. There is for example at Olkaria no evidence for a significant ^{18}O-shift in the deep thermal waters (Darling et al., 1990) which suggests that a large amount of water has already passed through the system. Also, the work of Sturchio et al. (1993) on the dating of hydrothermal sinters in the northern KRV testifies to the longevity of hydrothermal activity.

During the thermal cracking of organic matter, H_2S may be produced, especially in areas with carbonate evaporite sequences (Tissot and Welte, 1984) such as are found in parts of the KRV (Allen and Darling, 1992). While the H_2S in volcanic areas is generally considered to be mantle derived, a small crustal contribution might therefore be possible in the KRV (though as mentioned earlier, no COS or CS_2 was detected).

Hydrogen where detectable is at low concentrations except in geothermal wells. It is probable that production takes place in the upper part of the crust by dissociation of water buffered by minerals such as chlorite or epidote (Giggenbach, 1980). As stated earlier, stable isotope analyses indicate high temperature equilibrium between H_2 and water, and therefore cannot be used to diagnose ultimate origin.

Gases Derived From the Mantle

The plots in Fig. 6 show that, notwithstanding the few exceptions, there is only one significant source of CO_2, which must be mantle-derived. The occurrence of carbonatite at Bala and south of the KRV at Oldoinyo Lengai demonstrates that CO_2-rich fluids have been ascending from the upper mantle in the region since at least Miocene times. A more negative average with $\delta^{13}C$-CO_2 of -5 to $-8‰$ is generally associated with such a source, but fractionations between magma and exsolved gas of $1-2‰$ for carbonate (the main dissolved species in melts; Ohmoto and Rye, 1979) and up to $4‰$ for graphite put the KRV $\delta^{13}C$ values well within range of outgassing from MORB-type magmas. A minor problem associated with the assumption that the observed $\delta^{13}C$-CO_2 values are the result of isotopic fractionation of mantle CO_2 is that unless fresh magma were entering volcanic systems in a fairly continuous manner, a decrease in $\delta^{13}C$-CO_2 would be noted with time (Friedman et al., 1987). It is highly unlikely that all KRV volcanic centres would be at the same stage in such a cycle and therefore the similarity in $\delta^{13}C$-CO_2 values may not arise solely in this way. However, to the south of the KRV, Oldoinyo Lengai gave average $\delta^{13}C$-CO_2 values of $-2.6‰$ and $^3He/^4He$ values of $7.6 R/R_A$, similar to the fumaroles of the northern KRV (Javoy et al., 1989). The implication of

this is that over the timescales involved (i.e., late-Quaternary to present-day) significant differences in the CO_2 fractionation stage between centres do not occur, or are masked by other processes.

For reduced carbon, although a predominantly crustal origin is indicated, inputs from mantle sources cannot wholly be discounted on carbon isotope evidence alone. Although the $\delta^{13}C$ range of supposed abiogenic mantle CH_4 is not very well constrained, it is believed to be of the order of -15 to $-18‰$ (Welhan and Craig, 1983) and would thus not be easily distinguishable from thermogenic CH_4. However, a plot of $\delta^{13}C$-CH_4 vs. $^3He/^4He$ as R/R_A (Fig. 7) shows no well-defined trend that might indicate mixing between crustal and mantle CH_4 reservoirs.

The sulphur in H_2S, an important constituent of geothermal well gases but not normally seen in surface manifestations as explained above, is assumed here in the absence of sulphur isotope data to be largely derived from magmatic sources and therefore by implication the upper mantle (though see earlier remarks about possible crustal production from evaporitic sources). A relatively low concentration of H_2S was reported even from the active Oldoinyo Lengai volcano by Javoy et al. (1989), suggesting that the KRV in general is a low-S province.

The $^3He/^4He$ results of this study are similar to those obtained from MORB sources (Lupton, 1983) and undoubtedly indicate an important upper mantle contribution to the helium content of fumarolic gases in the KRV. Taken in conjunction with generally lower R/R_A values from the few sites on or towards the rift flanks (usually springs rather than gaseous sources), this suggests that magmatic melts rather than deep normal or listric rift boundary faults are the most important conduit by which mantle helium reaches the surface even in an area with relatively thin crust. Similar observations were made in connection with the continental rifting in western Europe (Griesshaber et al., 1992). However, it cannot yet be altogether ruled out that as much or even more mantle helium is released via major boundary faults, but is more difficult to identify because of dilution effects.
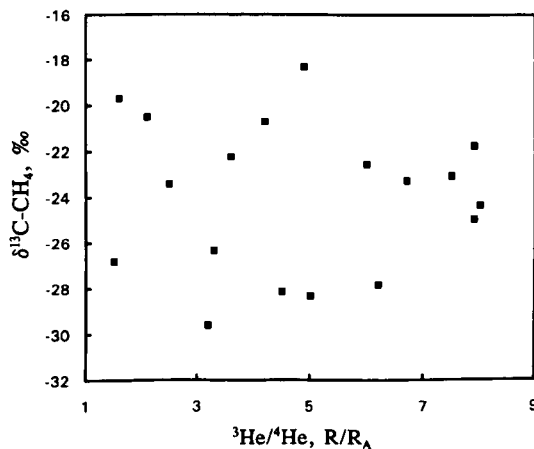

FIG. 7. Plot of $\delta^{13}C$-CH_4 vs. helium isotope ratio for gaseous sources in the KRV, showing no evidence of a mixing trend involving a mantle methane component (samples $< 50\%$ CO_2 excluded).

While there are no correlations between helium isotopes and carbon species, there is for fumarole and borehole gases from Longonot to Silali an apparent relationship between ^{3}He/^{4}He and the non-isotopic parameter log ($CH_4/\Sigma C_{2-4}$) with a correlation coefficient of $r^2 = 0.75$ (Fig. 8). The reason for such a relationship is not immediately clear; a mixing series based on crustal thermogenic CH_4 with a relatively high C_{2+} content with a "pure" abiogenic mantle methane could possibly be invoked to explain the relationship, but would tend to result in a linear rather than logarithmic correlation (i.e., a curve on Fig. 8). It would also receive no confirmation from the δ^{13}C-CH_4 results. A relationship between geothermal reservoir temperatures and log CH_4/C_{2+} has already been mentioned, so the correlation may simply arise because ^{3}He/^{4}He is a proxy for temperature (crustally produced ^{4}He can be ruled out as a cause of variation on the evidence of the ^{40}Ar/^{36}Ar data considered above). It is likely, after all, that sampling points overlying the hottest parts of hydrothermal plumes will tend to have the highest mantle helium contents and therefore probably the highest ^{3}He/^{4}He ratios. This agrees with the link between high ^{3}He and heat flow proposed by Mamyrin and Tolstikhin (1984), but only because both heat and ^{3}He are magmatically derived in the KRV; in other cases no clear link has emerged (e.g., Oxburgh and O'Nions, 1987). Nevertheless, the consistency of the relationship for many different volcanic centres, plus the Kerita CO_2 well on the eastern rift flank, suggests that there may be more to the relationship than a simple temperature/^{3}He correlation.

Most of the above remarks refer to helium in the gas phase from fumarolic outlets situated above active hydrothermal systems. By contrast, helium in the dissolved phase can apparently retain its isotope ratio at some distance from the supposed hydrothermal source. A high ^{3}He/^{4}He value was for instance found in sub-thermal groundwater of the Elmenteita area (site K124, north of the Eburru volcanic centre, Fig. 1) which has been presumed to contain a proportion of outflow from the Eburru hydrothermal plume (Allen et al., 1989). In the northern KRV high ^{3}He/^{4}He ratios have also been found in thermal water associated with the Namarunu centre (Fig. 1). However, this centre is for the most part much older than Eburru and no longer has any surface fumaroles. The springs do not give high solute geothermometer temperatures, although there are some young (< 10 ka) basalts in close proximity (Dunkley et al., 1993). The Elmenteita area also has prominent basaltic activity of similar age (Clarke et al., 1990) and it is possible that the high ^{3}He/^{4}He ratios in both areas are associated with flushing by water of these basalts (as proposed in the context of parts of the Ethiopian Rift by Craig et al., 1977). The possibility of such leaching of helium from basalt glasses raises the question of whether fumarolic helium is wholly "new" or whether at least some is coming by a similar process from previously erupted or intruded volcanic rocks. There is no simple answer to this, but in geological terms all the mantle helium must be "recent" because of the Quaternary age of volcanism in the inner trough of the KRV.

The data in Table 3 suggest that there may be a rise in ^{3}He/^{4}He peak values from south to north in the KRV. A crude illustration of this is that R/R_A values > 7 are only found northwards from Paka (location, Fig 1). (This could simply be an artefact of sampling, but it is likely that at least one of
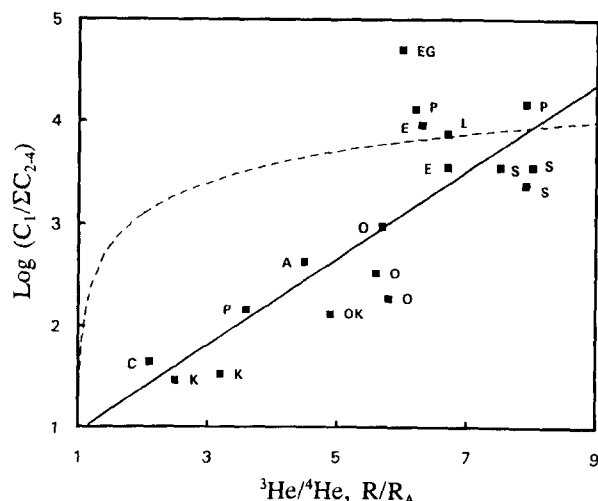

FIG. 8. Plot of log [$CH_4/(C_2H_6 + C_3H_8 + C_4H_{10})$] vs. helium isotope ratio for gaseous sources in the KRV (samples < 50% CO_2 excluded). The regression line based on all points except EG is shown. The curved line represents a theoretical mixing relationship between crustal and putative mantle methane. Site abbreviations—A: Arus; C: Carbacid; E: Eburru; EG: Emuruangogolak; K: Korosi; L: Longonot; O: Olkaria; OK: Ol Kokwe; P: Paka; S: Silali.

the wells or fumaroles in the southern KRV would have provided a similar result if equally high R/R_A values were present in the south). Such a rise in ^{3}He/^{4}He may have structural and volcanogenic implications (e.g., it might be related to the northerly crustal thinning commencing at around the latitude of the equator and reaching a minimum in the Silali-Emuruangogolak area according to Achauer et al., 1992), but it is proposed to consider these in more detail for a greater part of the Eastern Rift in a future paper. At this stage it may simply be noted that peak ^{3}He/^{4}He values are typical of an upper mantle source in contrast to the lower mantle source suggested by He isotope data from parts of the Ethiopian Rift, where values of up to 14R/R_A were measured by Craig et al. (1977).

SUMMARY AND CONCLUSIONS

Because of the position of the KRV as a thermal province situated on an extensive length of crustal thinning above a domal uplift, outgassing consists of a complex mixture of gases from different sources.

In almost all situations, N_2 and noble gases (apart from helium) are derived from atmospheric sources, though their ratios may have been altered by dissolution and boiling processes. The residence time of groundwaters (thermal or otherwise) in the main KRV appears too short to allow the acquisition of significant amounts of radiogenic argon or helium.

Methane and higher hydrocarbons appear to be the main products of the crust itself, and are probably generated relatively close to the surface by the action of hot fluids on organic compounds. Hydrogen is most likely to result from the dissociation of crustal water, though a mantle contribution cannot be ruled out on isotopic grounds because of rapid reequilibration between H_2 and meteoric water at hydrothermal temperatures.

Transport of mantle elements such as sulphur and helium to the surface is likely to depend on a significant carrier phase,

presumably CO_2 as suggested by $C/^3He$ ratios. Carbon isotope data indicate a single major source for CO_2 though original mantle signatures have been overprinted by fractionation during magmatic processes, and there is some $C/^3He$ evidence for minor crustal production. In terms of quantity there is little helium at KRV sampling sites, but abundant evidence for MORB-like isotope ratios particularly along the generally axial line of recent volcanic centres. An apparent rise in peak $^3He/^4He$ from south to north along the KRV may be structurally controlled. There is also a correlation with log C_1/C_{2-4}, which may be acting as a proxy for hydrothermal system temperatures, leading to the possibility in this area at least of a relationship between $^3He/^4He$ and heat flow. In the dissolved phase, high values of $^3He/^4He$ are found in basalt groundwaters quite far from areas of overt outgassing. Either helium can be carried some distance in dissolved form with little or no change in $^3He/^4He$ ratio, or subrecent basalts form an effective trap for helium which is then leached out relatively slowly to groundwater. By contrast, most helium outgassed from fumaroles is likely to be derived more or less directly from underlying melts.

None of the evidence gathered in the KRV conflicts with gas measurements made at the currently active Oldoinyo Lengai carbonatite volcano to the south in Tanzania, and there is no evidence of "hotspot" helium isotope ratios such as those associated with plume-driven updoming in the Main Ethiopian Rift to the north of the KRV.

This paper has shown that the study of gases in the KRV has potentially a broad range of applications ranging from hydrogeological (e.g., groundwater recharge and residence) through geothermal (e.g., identification of heat sources) to geological (e.g., elucidation of gross rift structure). Results so far suggest that future research might profitably concentrate on noble gas isotope systematics, greater knowledge of the role of rift-flank faults as conduits for fluid movement, and comparison with products of outgassing in Tertiary or Quaternary volcanic areas beyond the immediate confines of the KRV (e.g., in the Mt. Kenya, Kilimanjaro, and Chyulu areas) which might provide more information on the nature of updoming associated with rifting in Kenya.

REFERENCES

Achauer U., Maguire P. K. H., Mechie J., Green W. V., and the KRISP WORKING GROUP (1992) Some remarks on the structure and geodynamics of the Kenya Rift. *Tectonophysics* **213,** 257–268.

Allen D. J. and Darling W. G. (1992) Geothermics and hydrogeology of the Kenya Rift Valley between Lake Baringo and Lake Turkana. *British Geol. Surv. Res. Rep. SD/92/1.*

Allen D. J., Darling W. G., and Burgess W. G. (1989) Geothermics and hydrogeology of the southern part of the Kenya Rift Valley. *British Geol. Surv. Res. Rep. SD/89/1.*

Andrews J. N. (1992) Mechanisms for noble gas dissolution by groundwaters. In *Isotopes of Noble Gases as Tracers in Environmental Studies,* pp. 87–110. IAEA.

Armannsson H. (1987) Studies on the geochemistry of steam in the Suswa and Longonot areas. *U.N. Dev. Prog. Tech. Rep.*

Arnason B. (1977) The hydrogen-water isotope thermometer applied to geothermal areas in Iceland. *Geothermics* **5,** 75–80.

Arusei M. K. (1992) Hydrochemistry of Olkaria and Eburru geothermal fields, Kenyan Rift Valley. In *Water-Rock Interaction* (ed. Y. K. Kharaka and A. S. Maest), pp. 1261–1265. Balkema.

Bailey D. K. (1980) Volcanism, Earth degassing and replenished lithosphere mantle. *Phil. Trans. Roy. Soc. London* **A297,** 309–322.

Capaccioni B., Martini M., Mangani F., Giannini L., Nappi G., and Prato F. (1993) Light hydrocarbons in gas emissions from volcanic areas and geothermal fields. *Geochem. J.* **27,** 7–17.

Clarke M. C. G., Woodhall D. G., Allen D. J., and Darling W. G. (1990) Geological, volcanological and hydrogeological controls on the occurrence of geothermal activity in the area surrounding Lake Naivasha, Kenya. *Ministry of Energy Rep.*

Craig H., Lupton J. E., and Horowitz R. M. (1977) Isotope geochemistry and hydrology of geothermal waters in the Ethiopian Rift Valley. *Scripps Inst. Oceanog. Rep. 77-14.*

Daly M. C., Chorowicz J., and Fairhead J. D. (1989) Rift basin evolution in Africa: The influence of reactivated steep basement shear zones. In *Inversion Tectonics* (ed. M. A. Cooper and G. D. Williams); *Spec. Publ. Geol. Soc. London* **44,** 309–334.

Darling W. G. (1995) Hydrothermal hydrocarbon gases: 2, Application in the East African Rift System. *Appl. Geochem.* (submitted).

Darling W. G. and Talbot J. C. (1991) Evaluation and development of gas geothermometry for geothermal exploration in the East African Rift System. *British Geol. Surv. Tech. Rep. WD/91/72.*

Darling W. G. and Talbot J. C. (1992) Hydrocarbon gas ratio geothermometry in the East African Rift System. In *Water-Rock Interaction* (ed. Y. K. Kharaka and A. S. Maest), pp. 1441–1444. Balkema.

Darling W. G., Allen D. J., and Armannsson H. (1990) Indirect detection of outflow from a Rift Valley lake. *J. Hydrol.* **113,** 297–305.

Deines P. (1980) The isotopic composition of reduced organic carbon. In *Handbook of Environmental Isotope Geochemistry, Vol. 1: The Terrestrial Environment, A* (ed. P. Fritz and J. C. Fontes), pp. 329–406. Elsevier.

Des Marais D. J., Stallard M. L., Nehring N. L., and Truesdell A. H. (1988) Carbon isotope geochemistry of hydrocarbons in the Cerro Prieto geothermal field, Baja California Norte, Mexico. *Chem. Geol.* **71,** 159–167.

Dunkley P. N., Smith M., Allen D. J., and Darling W. G. (1993) The geothermal activity and geology of the northern sector of the Kenya Rift Valley. *British Geol. Surv. Res. Rep. SC/93/1.*

Friedman I., Gleason J., and Jackson T. (1987) Variation of $\delta^{13}C$ in fumarolic gases from Kilauea Volcano. In *Volcanism in Hawaii* (ed. R. S. Decker et al.); *USGS Prof. Paper 1350.*

Geotermica Italiana (1987) Geothermal reconnaissance survey in the Menengai-Bogoria area of the Kenya Rift Valley. *U.N. Dev. Prog. Rep. TCD CON 7/85.*

Giggenbach W. F. (1980) Geothermal gas equilibria. *Geochim. Cosmochim. Acta* **44,** 2021–2032.

Giggenbach W. F. and Glover R. B. (1992). Tectonic regime and major processes governing the chemistry of water and gas discharges from the Rotorua geothermal field, New Zealand. *Geothermics* **21,** 121–140.

Glover R. B. (1972) Chemical characteristics of water and steam discharges in the Rift Valley of Kenya. *U.N. Dev. Prog. Tech. Rep.*

Griesshaber E., O'Nions R. K., and Oxburgh E. R. (1992) Helium and carbon isotope systematics in crustal fluids from the Eifel, the Rhine Graben and the Black Forest, FRG. *Chem. Geol.* **99**, 213–235.

Gunter B. D. and Musgrave B. C. (1971) New evidence on the origin of methane in hydrothermal gases. *Geochim. Cosmochim. Acta* **35**, 113–118.

Hooker P. J., Bertrami R., Lombardi S., O'Nions R. K., and Oxburgh, E. R. (1985) Helium-3 anomalies and crust-mantle interactions in Italy. *Geochim. Cosmochim. Acta* **49**, 2505–2514.

Javoy M., Pineau F., Staudacher T., Cheminee J. L., and Kraft M. (1989) Mantle volatiles sampled from a continental rift: The 1988 eruption of Oldoinyo Lengai (Tanzania). *Terra Abstracts* **1**, 324.

Lupton J. E. (1983) Terrestrial inert gases: Isotope tracer studies and clues to primordial components in the mantle. *Annu. Rev. Earth Planet. Sci.* **11**, 371–414.

Mamyrin B. A. and Tolstikhin I. N. (1984) *Helium Isotopes in Nature, Developments in Geochemistry 3.* Elsevier.

Mariano A. N. (1989) Nature of economic mineralisation in carbonatites and related rocks. In *Carbonatites—Genesis and Evolution* (ed. K Bell), pp. 149–176. Unwin Hyman.

Marty B. (1992) Volcanic fluxes of volatiles: Preliminary estimates based on rare gas and major volatile calibration. In *Isotopes of Noble Gases as Tracers in Environmental Studies*, pp. 295–301. IAEA.

Mason J. E. (1967) Geothermal occurrences and investigations in the central Rift valley, Kenya. *Dept. of Mines and Geology Rep.*

McCall G. J. H. (1967) Geology of the Nakuru—Thomson's Falls—Lake Hannington area. *Geol. Surv. Kenya Rep. 78.*

Ohmoto H. and Rye R. O. (1979) Carbon and sulfur in ore bodies. In *Hydrothermal Ore Deposits* (ed. H. L. Barnes), pp. 509–567. Wiley.

Oxburgh E. R. and O'Nions R. K. (1987) Helium loss, tectonics and the terrestrial heat budget. *Science* **237**, 1583–1588.

Poreda R. J., Craig H., Arnorsson S., and Welhan J. A. (1992) Helium isotopes in Icelandic geothermal systems: 1. ^{3}He, gas chemistry, and $\delta^{13}C$ relationships. *Geochim. Cosmochim. Acta* **56**, 4221–4228.

Potter R. W. and Clynne M. A. (1978) The solubility of the noble gases He, Ne, Ar, Kr and Xe in water up to the critical point. *J. Soln. Chem.* **7**, 837–844.

Rosendahl B. R. (1987) Architecture of continental rifts with special reference to east Africa. *Annu. Rev. Earth Planet. Sci.* **15**, 445–503.

Simoneit B. R. T. (1990) Petroleum generation, an easy and widespread process in hydrothermal systems: an overview. *Appl. Geochem.* **5**, 3–15.

Smith M., Dunkley P. N., Deino A., Williams L. A. J., and McCall G. J. H. (1995) Geochronology, stratigraphy and structural evolution of Silali volcano, Gregory Rift, Kenya. *J. Geol. Soc., London* **152**, 297–310.

Sturchio N. C., Dunkley P. N., and Smith M. (1993) Climate-driven variations in geothermal activity in the northern Kenya rift valley. *Nature* **362**, 233–234.

Tissot B. P. and Welte D. H. (1984) *Petroleum Formation and Occurrence.* Springer-Verlag.

Truesdell A. H. and Hulston J. (1980) Isotopic evidence on environments of geothermal systems. In *Handbook of Environmental Isotope Geochemistry. Vol. 1: The Terrestrial Environment, A* (ed. P. Fritz and J. C. Fontes), pp. 179–226. Elsevier.

Welhan J. A. and Craig H. (1983) Methane, hydrogen and helium in hydrothermal fluids at 21°N on the East Pacific Rise. In *Hydrothermal Processes in Seafloor Spreading Centres* (ed. P. A. Rona et al.), pp. 391–409. Plenum Press.

Wilhelm E., Battino R., and Wilcock R. J. (1977) Low-pressure solubility of gases in liquid water. *Chem. Rev.* **77**, 219–262.

PII: S0899-5362(96)00026-7

Lake-groundwater relationships and fluid-rock interaction in the East African Rift Valley: isotopic evidence

W. GEORGE DARLING[1], BERHANU GIZAW[2] and MUSA K. ARUSEI[3]

[1]British Geological Survey, Wallingford, OX10 8BB, UK
[2]Ethiopian Institute of Geological Surveys, PO Box 40069, Addis Ababa, Ethiopia
[3]Moi University, PO Box 3900, Eldoret, Kenya

Abstract - The assessment of water resources in the Rift Valley environment is important for population, agriculture and energy-related issues and depends on a good understanding of the relationship between freshwater lakes and regional groundwater. This can be hampered by the amount of fluid-rock interaction which occurs throughout the rift, obscuring original hydrochemical signatures. However, O and H stable isotope ratios can be used as tracers of infiltration over sometimes considerable distances, while showing that the volcanic edifices of the rift floor have varying effects on groundwater flow patterns. Specific cases from Kenya and Ethiopia are considered, including Lakes Naivasha, Baringo, Awasa and Zwai.

In addition to their physical tracing role, stable isotopes can reveal information about processes of fluid-rock interaction. The general lack of O isotope shifting in rift hydrothermal systems suggests a high water:rock ratio, with the implication that these systems are mature. Carbon isotope studies on the predominantly bicarbonate waters of the rift show how they evolve from dilute meteoric recharge to highly alkaline waters, via the widespread silicate hydrolysis promoted by the flux of mantle carbon dioxide which occurs in most parts of the rift. There appears to be only minor differences in the C cycle between Kenya and Ethiopia.

Résumé - L'évaluation des ressources en eau dans un milieu tel que celui de la Rift Valley est importante pour les populations, l'agriculture et les problèmes en rapport avec l'énergie. Elle sous-entend une bonne compréhension des relations existant entre lacs d'eau douce et nappes phréatiques régionales. Celle-ci peut être entravée par l'importance des interactions roche-fluide à travers le Rift, effaçant les signatures hydrochimiques originelles. Toutefois, les rapports des isotopes stables de O et H peuvent être utilisés comme traceurs d'infiltration sur des distances parfois considérables. Il apparaît ainsi que les édifices volcaniques du fond du Rift ont des effets variables sur les modèles de flux de nappes phréatiques. Des cas particuliers du Kenya et de l'Éthiopie sont examinés, comprenant les lacs Naivasha, Baringo, Awasa et Zwai.

Hormis leur rôle de traceur physique, les isotopes stables peuvent révéler des informations sur les processus d'interaction roche-fluide. L'absence généralisée de migration des isotopes O dans les systèmes hydrothermaux de rift suggère un rapport roche-eau élevé, impliquant qu'il s'agit de systèmes matures. Des études isotopiques du carbone effectuées sur les eaux essentiellement bicarbonatées du Rift montrent leur évolution depuis une recharge par des eaux météoriques banales jusqu'à des eaux hautement alcalines, en passant par une hydrolyse de silicate fréquente, favorisée par un flux de gaz carbonique mantellique présent dans la plupart des régions du Rift. Il apparaît que les différences dans le cycle du C entre le Kenya et l'Éthiopie ne sont que mineures.

INTRODUCTION

Hydrochemistry often provides an effective way of discriminating between different groundwater sources and assessing the amount of any mixing between them. Typical examples of this would be coastal intrusion by sea water or, on a smaller scale, the interaction between landfill contamination plumes and the regional aquifer. However, in situations where a large amount of fluid-rock interaction is occurring, the original chemical characteristics of one or more of the end members of any mixing may be obscured, making it difficult or impossible to ascribe water origins or the amount of mixing.

One area where there is an abundance of such fluid-rock interaction is the East African Rift system. In this area, the effective management of groundwater resources is important not only for potable water supply and agriculture, but also in connection with the exploitation of geothermal energy. Each use requires a good understanding of water movement in the subsurface, but conventional hydrochemical techniques are not always easy to apply in the Rift environment. Oxygen and H stable isotopes, on the other hand, are ideally suited to this environment because of the amount of interaction between ground and surface waters. This mainly takes the form of infiltration from lakes to groundwater, where
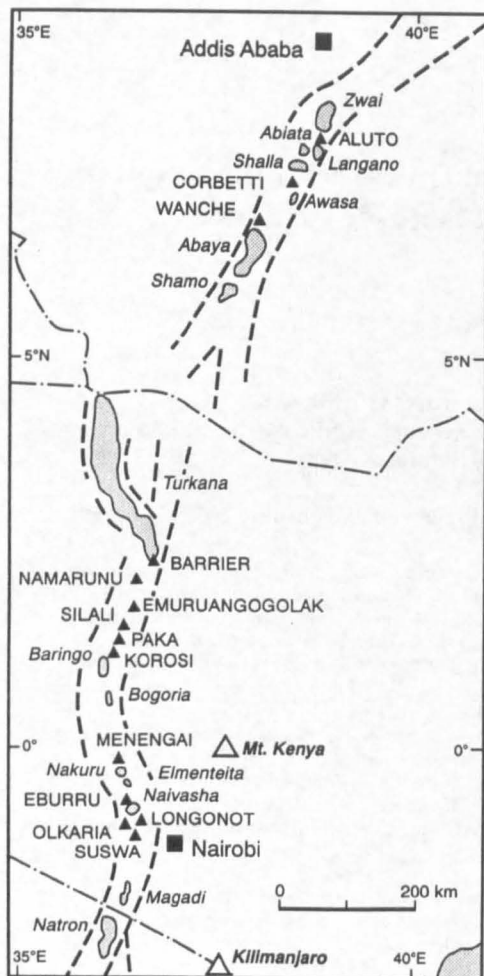
Figure 1. Lakes (italics) and Late Quaternary volcanic centres (upper case) of the East African Rift Valley in Kenya and Ethiopia.

the characteristic isotopic signature imparted by surface evaporation makes a highly effective tracer of subsequent flow into the regional aquifer system.

Stable isotopes can act as chemical as well as physical tracers. Nearly all the waters in the Rift Valley are of the Na-HCO₃ type, in certain cases reaching very high concentrations. The study of C isotope ratios in these waters helps to explain their origin and evolution.

This paper presents some new stable isotopic data for the East African Rift Valley from Kenya and Ethiopia. The main focus for O and H isotopes is on the freshwater lakes of the Rift Valley, while carbon isotopes are considered on a more regional scale.

SAMPLING AND ANALYSIS

Water samples for O and H stable isotopic analysis were collected from springs, boreholes, geothermal wells and boreholes drilled for temperature gradient studies. They were stored in 28 ml glass bottles with rubber-lined metal caps (McCartney type) prior to

analysis. Samples of water for analysis of C stable isotopes were collected in 250 ml glass bottles, in which the dissolved inorganic carbon (DIC) was precipitated by treatment with alkaline $BaCl_2$. The resulting precipitates were washed with deionized water and dried.

Samples were prepared for $^{18}O/^{16}O$ and $^{2}H/^{1}H$ analysis by the methods of Epstein and Mayeda (1953) and Coleman *et al.* (1982), respectively. For $^{13}C/^{12}C$, dissolution of the dried $BaCO_3$ precipitates with anhydrous H_3PO_4 was used to yield CO_2 gas for analysis. Isotope ratio measurements were carried out on VG 602E and Optima mass spectrometers at the British Geological Survey, Wallingford.

LAKE-GROUNDWATER RELATIONSHIPS

One of the features of the Kenya Rift Valley (KRV) and the Main Ethiopian Rift (MER) is the chain of lakes occupying the valley floors (Fig. 1). The existence of these lakes is at least partly due to the numerous Late Quaternary central volcanic structures, which often separate the lakes from each other (Fig. 1). The relationships between these lakes and regional groundwaters vary considerably, with the result that the lakes range from fresh to highly alkaline in their chemistry. Because the highly alkaline lakes are discharge areas, their relationships with regional waters are fairly clear and of less significance in terms of groundwater resource management. In the case of the fresher lakes, however, and particularly where there is no surface egress, relationships with the groundwater are not so apparent but of much more importance to the assessment of resources. The cases considered here are concerned with this type of lake.

Lake Naivasha area, Kenya

Lake Naivasha (Figs 1 and 2) has been suspected for at least 60 years of significant subsurface leakage (Sikes, 1935). Most attempts at assessing its water balance have arrived at an annual loss of tens of millions of cubic metres to the subsurface. Owing to its situation on the culmination on the floor of the updomed KRV, the potential exists for leakage to occur in both northerly and southerly directions. Darling *et al.* (1990) used stable isotopic techniques to show that lake water appeared to be detectable at least 30 km to the south at the Suswa volcano (Fig. 2). The new data presented here have been obtained from deep (~2000 m) wells drilled in the Olkaria and Eburru geothermal fields to the southwest and northwest of the lake, respectively (Fig. 2).

It has been considered for some time that the currently-producing Olkaria East wellfield might be obtaining at least some of its water from Naivasha. Darling *et al.* (1990) showed that the reservoir fluid could be explained by a 2:1 mixture of lake water with unmodified meteoric recharge from the rift wall area. Logically, therefore, it would be expected that the newer
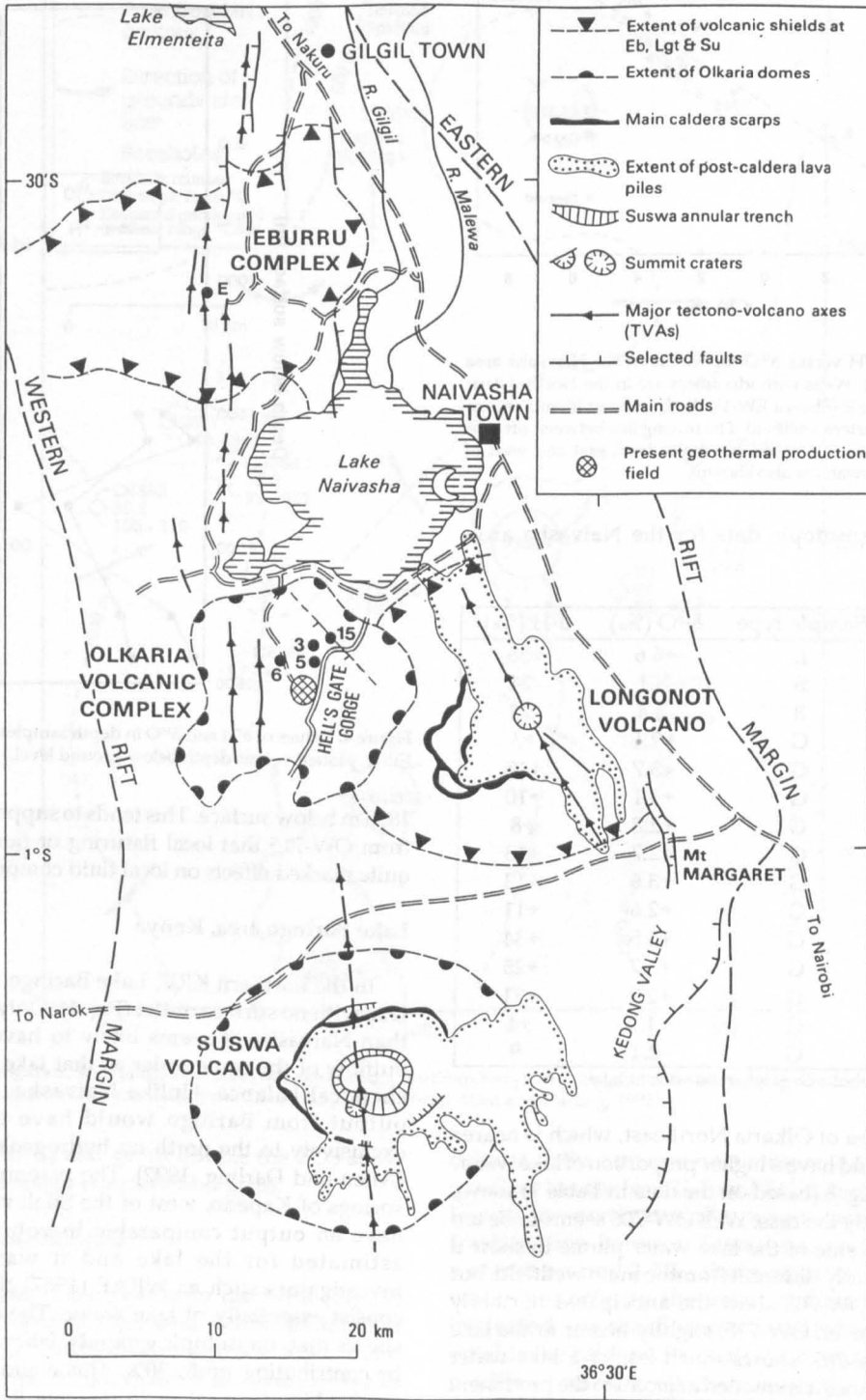
Figure 2. Lake Naivasha and the Eburru, Olkaria, Longonot and Suswa volcanic centres, southern Kenya. The location of the Olkaria East geothermal wellfield and individual wells of the Olkaria Northeast and Eburru wellfields are shown. The numbers 3, 5, 6 and 15 refer to wells OW-703, 705, 706 and 715, while E refers to EW-1.
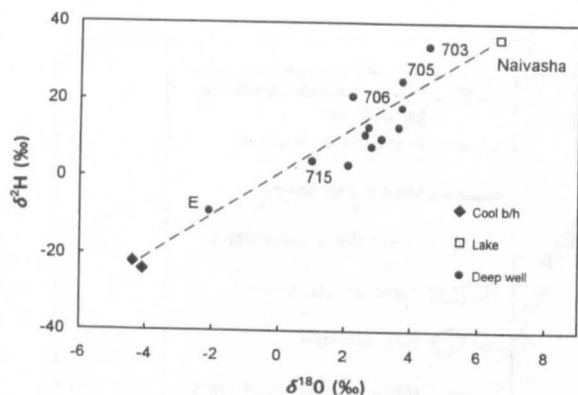
Figure 3. Plot of δ²H versus δ¹⁸O for waters in the Naivasha area (data from Table 1). Wells with identifiers are in the Northeastern wellfield, except for E (Eburru EW-1). Wells without identifiers are in the producing Eastern wellfield. The mixing line between rift side recharge (represented by typical boreholes from east and west of Naivasha) and lakewater is also shown.

Table 1. Stable isotopic data for the Naivasha area, Kenya

Site	Sample type	$\delta^{18}O$ (‰)	$\delta^{2}H$ (‰)
Naivasha	L	+6.6	+36
C4178	B	-4.1	-24
C5002	B	-4.4	-22
OW-2	G	+2.1	+3
OW-5	G	+3.7	+18
OW-16	G	+3.1	+10
OW-21	G	+2.8	+8
OW-22	G	+2.7	+13
OW-23	G	+3.6	+13
OW-26	G	+2.6	+11
OW-703	G	+4.5	+34
OW-705	G	+3.7	+25
OW-706	G	+2.2	+21
OW-715	G	+1.0	+4
EW-1	G	-2.1	-9

B: supply borehole; G: geothermal well; L: lake.

exploration area of Olkaria Northeast, which is nearer to the lake, would have a higher proportion of lake water. The δ-plot of Fig. 3 (based on the data in Table 1) shows that this is partly the case. Well OW-706 seems to be too far to the west side of the lake water plume to show a result significantly different from the main wellfield, but OW-705 and OW-703 show the anticipated northerly increase. However, OW-715, slightly nearer to the lake even than OW-703, shows much less of a lake water contribution. Since it is situated adjacent to the prominent northwest trending Gorge Farm fault, the well may be affected by a large input of meteoric water.

Isotopic evidence from the Eburru well EW-1 (Figs 2 and 3, Table 1) shows that lake water also passes beneath the Eburru volcanic ridge. When sample data from EW-1 are plotted against depth (Fig. 4), a peak is seen at
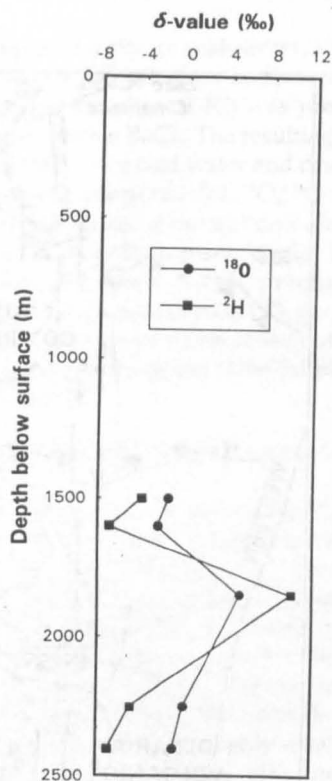

Figure 4. Values of δ²H and δ¹⁸O in depth samples from Eburru well EW-1, plotted versus depth below ground level.

1850 m below surface. This tends to support the evidence from OW-715 that local fissuring or faulting can have quite marked effects on local fluid compositions.

Lake Baringo area, Kenya

In the northern KRV, Lake Baringo is a freshwater lake with no surface outlet (Fig. 1). Only slightly larger than Naivasha, it seems likely to have a subsurface outflow of the same order as that lake to preserve its chemical balance. Unlike Naivasha, however, any output from Baringo would have to be directed exclusively to the north on hydrogeological grounds (Allen and Darling, 1992). The perennial hot (~50°C) springs of Kapedo, west of the Silali volcano (Fig. 5), have an output comparable in volume to the loss estimated for the lake and it was the view of investigators such as WRAP (1987) that the springs consist essentially of lake water. The δ-plot of Fig. 6 shows that, on isotopic grounds, lakewater could only be contributing up to 30%. This could not have been resolved by chemical measurements; the total dissolved solids (TDS) content at Kapedo is far higher than those of the lake or rift-wall source water represented by borehole C3470 (Allen and Darling, 1992). This also applies to the Lorusio hot springs some 10 km to the north of Kapedo (Fig. 5). These springs, with a higher
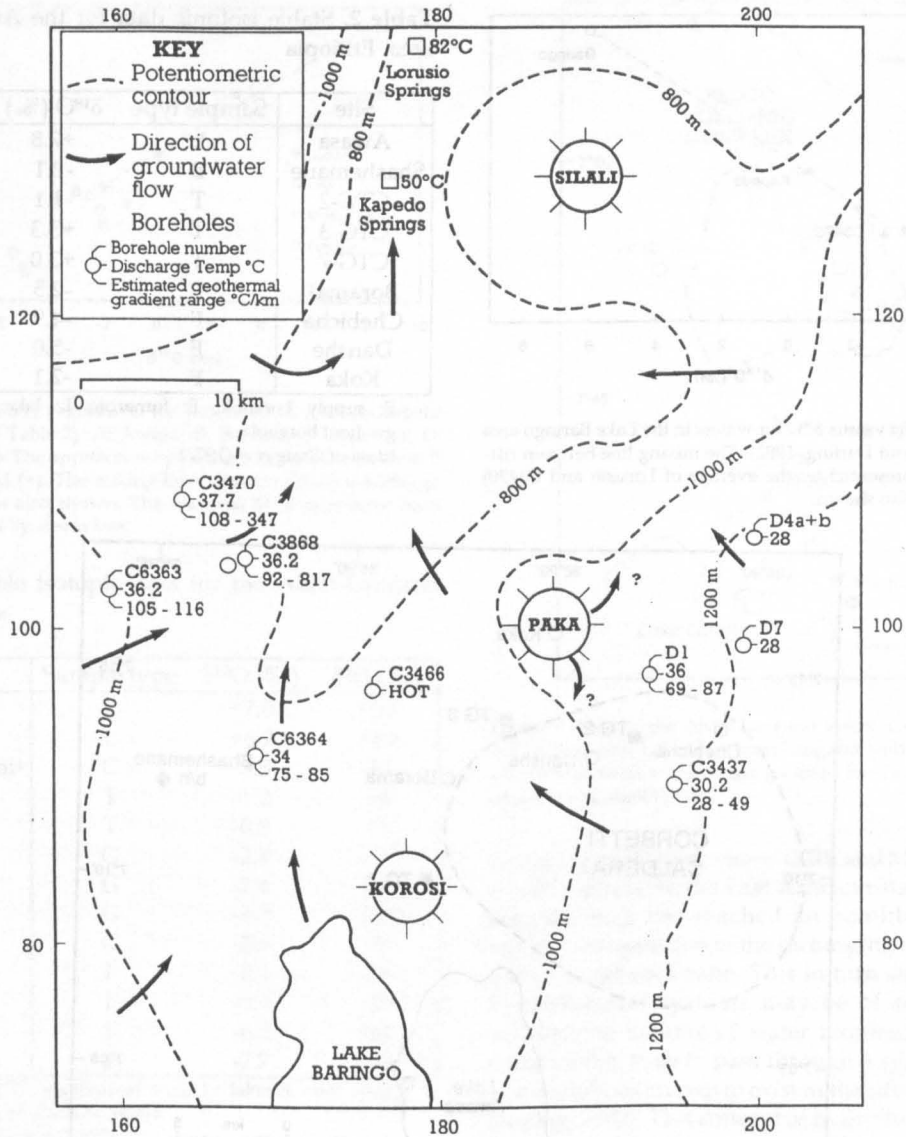
Figure 5. Map of the area north of Lake Baringo, northern Kenya, showing groundwater potentiometric contours and schematic flow directions (adapted from Allen and Darling, 1992).

temperature (~80°C) and about double the TDS show no sign of a lake water component (Fig. 6).

Lake Awasa area, Ethiopia

The freshwater Lake Awasa in the MER (Fig. 1) is also similar in size to Naivasha. While no detailed estimates of its subsurface outflow have been published, it seems likely to be of the same order as Naivasha. Table 2 gives relevant stable isotope data for the area, including some steam condensate values obtained from fumaroles associated with the nearby Corbetti caldera (Fig. 7). The δ-plot in Fig. 8 shows strong evidence that there is a northward flow from Awasa with around 50% lakewater outside the

caldera to the east and northeast at the temperature-gradient boreholes TG-7 and TG-3, but considerably less to the north at Koka, where, assuming a $\delta^{18}O$ fractionation between fumarolic steam and parent water of around 2-3‰, there might be ~20-30% lake water underlying the area. A similar amount is indicated for the Borama fumarole immediately outside the caldera. By contrast, it appears that there is little or no lake water beneath the caldera, even allowing for the possibility of steam heating or subsurface steam condensation, making the parent water in the caldera appear somewhat more isotopically depleted than it actually is. The Corbetti caldera is a much better-defined ring structure than the Olkaria or Eburru eruptive centres and may
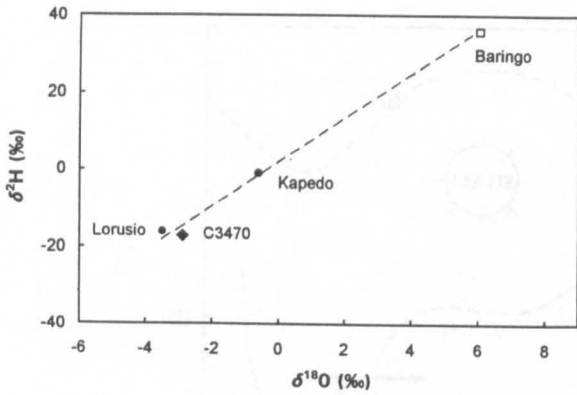
Figure 6. Plot of δ^2H versus $\delta^{18}O$ for waters in the Lake Baringo area (data from Allen and Darling, 1992). The mixing line between rift-side recharge (represented by the average of Lorusio and C3470) and lakewater is also shown.

Table 2. Stable isotopic data for the Awasa-Corbetti area, Ethiopia

Site	Sample type	$\delta^{18}O$ (‰)	δ^2H (‰)
Awasa	L	+7.8	+53
Shashemane[1]	B	-2.1	-1
CTG-2	T	-1.1	-7
CTG-3	T	+3.3	+26
CTG-7	T	+3.0	+30
Borama[1]	F	-2.5	-5
Chebicha	F	-4.9	-31
Danshe	F	-5.0	-29
Koka	F	-2.1	-9

B: supply borehole; F: fumarole; L: lake; T: temperature gradient borehole.
[1]data of Craig et al.(1977).
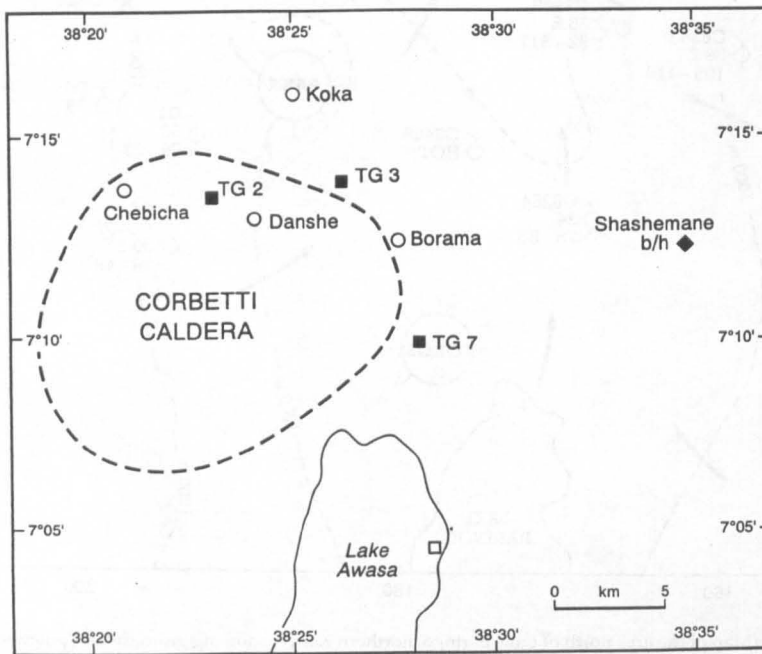
Figure 7. Map of the Awasa-Corbetti area, Ethiopia, showing the location of temperature gradient (TG) boreholes, fumaroles, groundwater and lakewater sampling sites.

therefore form a more significant barrier to the passage of lakewater into the hydrothermal plumes beneath the volcanoes within the caldera.

Zwai-Langano area, Ethiopia

The Aluto volcanic centre between Lakes Zwai and Langano (Fig. 1) has a ring-like structure intermediate in definition between those of Corbetti and Olkaria. Unlike Corbetti, it has the advantage of deep geothermal wells drilled within the complex (the Aluto-Langano geothermal field) from which fluid samples were obtained. In addition, there are fumarolic areas and

temperature gradient boreholes which also yielded samples. Stable isotope values are given in Table 3.

The difference in altitude between Lake Zwai at ~1636 m and Lake Langano at ~1582 m above sea level provides potential for subsurface leakage southward between the lakes, conceivably beneath Aluto (Fig. 9). However, the δ-plot in Fig. 10 reveals that the lake water content beneath the centre cannot exceed 10%, with the deep wells having values much more similar to the rift-side isotopic composition than to the highly-evaporated and isotopically enriched water of Zwai. The small shifts in $\delta^{18}O$ shown by wells LA-4 and LA-6 may be due to water-mineral exchange, but at least some of the isotopic

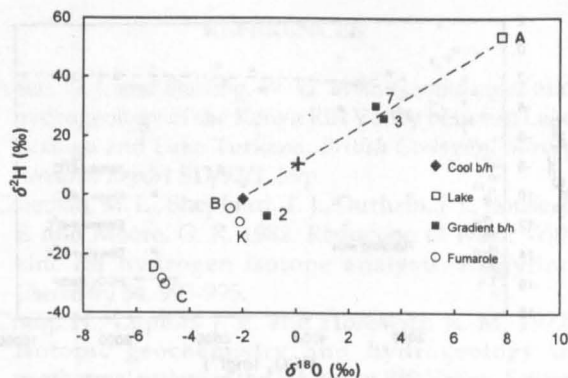Figure 8. Plot of δ^2H versus $\delta^{18}O$ for waters in the Awasa-Corbetti area (data from Table 2). A: Awasa; B: Borama; C: Chebicha; D: Danshe; K: Koka. The approximate position of the parent water of B and K is marked (+). The mixing line between rift-floor recharge and lakewater is also shown. The water in TG-2 may have been slightly enriched by steam loss.

Table 3. Stable isotopic data for the Aluto-Langano area, Ethiopia

Site	Sample type	$\delta^{18}O$ (‰)	δ^2H (‰)
Langano	L	+7.0	+53
Zwai	L	+6.7	+49
E Escarpment[1]	C	-3.5	-13
LTG-30	T	-1.2	+4
LTG-32	T	-0.8	+3
LA-3	G	-2.8	-11
LA-4	G	-1.4	-8
LA-6	G	-1.3	-13
LA-8	G	-2.6	-7
Auto	F	-6.1	-36
Bobessa	F	-5.7	-29
Gebiba	F	-6.2	-31
Aluto 18[1]	F	-7.7	-32

F: fumarole; G: geothermal well; L: lake; S: cool spring; T: temperature gradient borehole.
[1]data of Craig et al. (1977).

enrichment in LA-4 is likely to be due to the effects of steam separation within the reservoir. This implies that Lake Zwai plays little or no part in the Aluto hydrothermal circulation, an important conclusion regarding the assessment of geothermal resources.

The greater amount of lake water (~20%) indicated by the two temperature gradient wells south of the Aluto-Langano wellfield may be indicating a flow around the complex, presumably on the western side. All hydrogeological indications are that flow in this area takes place towards Lake Langano and therefore, despite their situation close to the lake, they seem unlikely to be deriving a significant amount of water from it.

FLUID-ROCK INTERACTION

It is apparent from the examples considered above that the significant enrichments in $\delta^{18}O$ sometimes
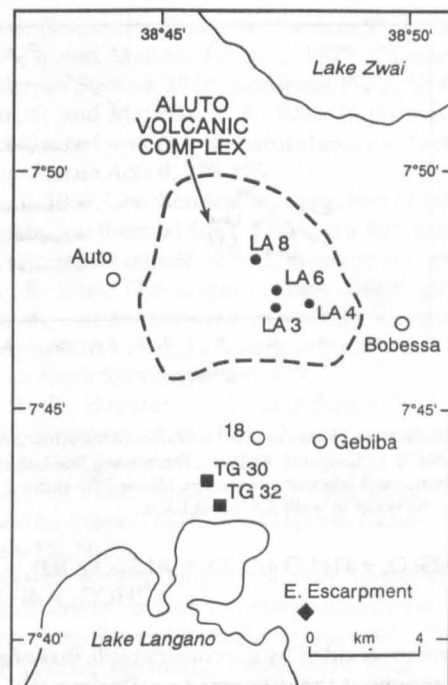

Figure 9. Map of the Aluto-Langano volcanic complex, Ethiopia, situated between Lakes Zwai and Langano, showing the location of geothermal wells, temperature gradient boreholes, fumaroles and cool spring sampling sites.

found in geothermal waters (Ellis and Mahon, 1977) are small or absent in the East African rifts. This indicates that the rock has reached an equilibrium with the isotopic composition of the recharging water, implying a high water:rock ratio. This in turn suggests that the hydrothermal systems may be of some antiquity because the volume of water required would take a considerable time to pass through a system at the low permeabilities known to exist in the rifts (e.g. Allen and Darling, 1992). This concept of hydrothermal longevity is supported by the existence of high-level hot spring sinter deposits associated with Quaternary pluvials in both the MER and KRV (Gizaw, 1989; Darling et al., 1993; Sturchio et al., 1993).

The effects of fluid-rock interaction are more easily discerned when the $\delta^{13}C$ content of dissolved inorganic carbon (DIC) is considered. Figure 11 shows a plot of $\delta^{13}C_{DIC}$ versus DIC, expressed as HCO_3^-, for groundwaters in the KRV and MER. The more depleted $\delta^{13}C$ values are typical of the dissolution of rock carbonate by soil CO_2 under open-system conditions and accordingly these waters are likely to consist of little-modified meteoric water. Many of the cooler well and spring waters fall into this category, but few of the hot springs.

The very high HCO_3 concentrations seen in most of the thermal waters are undoubtedly the product of silicate hydrolysis. The basis of this is the following reaction, whereby feldspar reacts with water and CO_2:
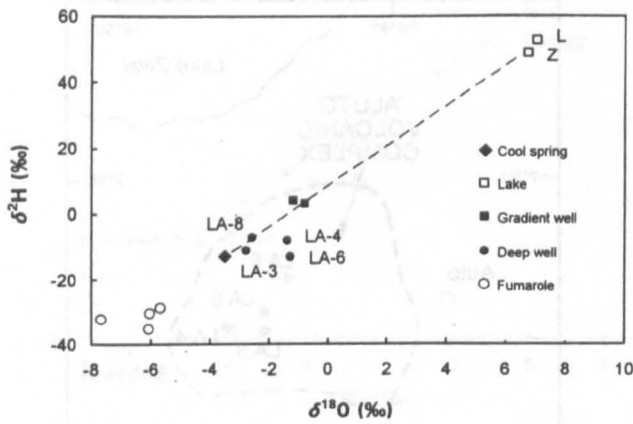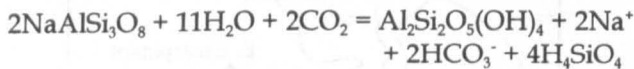
Figure 10. Plot of δ^2H versus $\delta^{18}O$ for waters of the Aluto area (data from Table 3). L: Langano; Z: Zwai. The mixing line between rift-side recharge and lakewater is shown. Minor $\delta^{18}O$ shifting may be affecting the water in wells LA-4 and LA-6.

Figure 11. Plot of $\delta^{13}C_{DIC}$ versus bicarbonate as HCO_3 for cool (<40°C) and hot (>40°C) groundwaters in the KRV and MER. The model line shows the expected trend for bicarbonate uptake (see text). Most data are from Allen and Darling (1992) for the KRV and Craig *et al.* (1977) for the MER.

$$2NaAlSi_3O_8 + 11H_2O + 2CO_2 = Al_2Si_2O_5(OH)_4 + 2Na^+ + 2HCO_3^- + 4H_4SiO_4$$

This process is aided by the considerable flux of mantle CO_2 throughout the rift areas (e.g. Darling *et al.*, 1995; Gizaw, 1996). High concentrations of HCO_3 might result from *in situ* hydrolysis, where groundwater flow is sufficiently slow, or the process might simply have contributed to the chemistry of lakes, which periodically became desiccated, accompanied by the deposition of carbonate evaporites (Lake Magadi in the southern KRV represents an extreme case of this; e.g. Jones *et al.*, 1977). Whether the primary or secondary process is responsible for the results from individual sites cannot be easily identified. Both would give rise to DIC with a composition of around 0‰ $\delta^{13}C$ (marine carbonate, which would also give rise to a similar value, can be ruled out because there has been no marine transgression within the KRV or MER.)

The evolutionary trend depicted in Fig. 11 assumes that water with an initial post-recharge composition of 250 mg l^{-1} HCO_3 and -16‰ $\delta^{13}C_{DIC}$ progressively acquires either evaporitic or *in situ* bicarbonate with a typical value of -1‰. There is not necessarily a direct connection with hydrothermal activity, other than that usually the hotter waters are more effective at promoting hydrolysis or at redissolving evaporites. In the MER, a slightly heavier bicarbonate source of around 0‰ is indicated, presumably as the result of a slightly different balance of processes.

While bicarbonate uptake can explain reasonably well the $\delta^{13}C$ content of most rift groundwaters, there is an exceptional case from the KRV north of Lake Baringo, where samples from two boreholes at Nginyang (C3868 and an un-numbered adjacent well, Fig. 5) plot away from the trend (Fig. 11). The boreholes are both close to the Nginyang River, so the anomaly may be due to leakage from the river. However, while such dilution could account for the observed $\delta^{13}C$ values of around

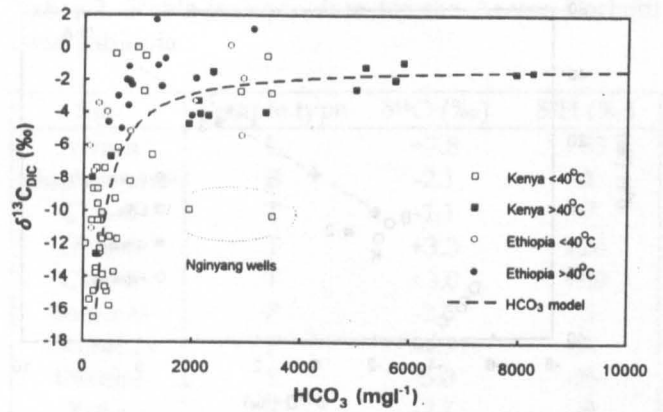10‰, it does not explain why the DIC concentrations remain so elevated.

CONCLUSIONS

Previously, subsurface leakage from the fresher Rift lakes was only demonstrable within the vicinity of the lakes from borehole water levels and hydrochemistry. Stable isotopic techniques have shown that the influence of this leakage can be traced for much greater distances. Differences between individual areas in Kenya and Ethiopia illustrate the importance of using O and H isotopes as a routine part of hydrogeological surveying. This would greatly assist the production of reliable hydrogeological maps, which are essential for good water resource management strategies, whether applied to population, agricultural or geothermal development.

The scant evidence for hydrothermal O isotope shifting is a sign of geothermal system longevity and therefore of some importance to studies of system maturity. By contrast, evidence from C stable isotopes indicates that the vast majority of rift groundwaters, hot or cold, follow a predictable trend of bicarbonate uptake as a result of fluid-rock interaction in the form of silicate hydrolysis. This trend can be followed from dilute, post recharge conditions to highly evolved alkaline groundwaters. However, the extent to which recycling may occur via carbonate evaporites remains unknown.

REFERENCES

Allen, D. J. and Darling, W. G. 1992. Geothermics and hydrogeology of the Kenya Rift Valley between Lake Baringo and Lake Turkana. *British Geological Survey Research Report* **SD/92/1**. 39p.

Coleman, M. L., Shepherd, T. J., Durham, J. J., Rouse, J. E. and Moore, G. R. 1982. Reduction of water with zinc for hydrogen isotope analysis. *Analytical Chemistry* **54**, 993-995.

Craig, H., Lupton, J. E. and Horowitz, R. M. 1977. Isotopic geochemistry and hydrogeology of geothermal waters in the Ethiopian Rift Valley. *Scripps Institute Oceanography Report* **77-14**, 140p.

Darling, W. G., Allen, D. J. and Armannsson, H. 1990. Indirect detection of outflow from a Rift Valley Lake. *Journal Hydrology* **113**, 297-305.

Darling, W. G., Allen, D. J. and Spiro, B. 1993. Oxygen isotopes in relict sinters as a palaeoindicator of Rift Valley climate. In: *Isotope Techniques in the Study of Past and Current Environmental Changes in the Hydrosphere and the Atmosphere*. Proceedings Symposium IAEA, Vienna, 555-559.

Darling, W. G., Griesshaber, E., Andrews, J. N., Armannsson, H. and O'Nions, R. K. 1995. The origin of hydrothermal and other gases in the Kenya Rift Valley. *Geochimica Cosmochimica Acta* **59**, 2501-2512.

Ellis, A. J. and Mahon, W. A. J. 1977. *Chemistry and Geothermal Systems*. 392p. Academic Press, New York.

Epstein, S. and Mayeda, T. K. 1953. Variations of the O^{18} content of waters from natural sources. *Geochimica Cosmochimica Acta* **4**, 213-223.

Gizaw, B. 1989. Geochemical investigation of the Aluto Langano geothermal field, Ethiopian Rift Valley. *M. Phil. dissertation unpubl.* 237p. University of Leeds, UK.

Gizaw, B. 1996. The origin of high bicarbonate and fluoride concentrations in waters of the Main Ethiopian Rift Valley, East African Rift system. *Journal African Earth Sciences* **22**, 391-402.

Jones, B. F., Eugster, H. P. and Rettig, S. L. 1977. Hydrochemistry of the Lake Magadi basin, Kenya. *Geochimica Cosmochimica Acta* **44**, 53-72.

Sikes, H. L. 1935. Notes on the hydrology of Lake Naivasha. *Journal East Africa Uganda Natural History Society* **13**, 74-89.

Sturchio, N. C., Dunkley, P. N. and Smith, M. 1993. Climate-driven variations in the geothermal activity in the northern Kenya Rift Valley. *Nature* **362**, 233-234.

WRAP (Water Resource Assessment Project) 1987. Water resource assessment study in Baringo District. *Water Research Assessment Division Report*. Ministry of Water Development, Nairobi, Kenya. 43p.